B. K. Vainshtein

Fundamentals of Crystals

Symmetry, and Methods of Structural Crystallography

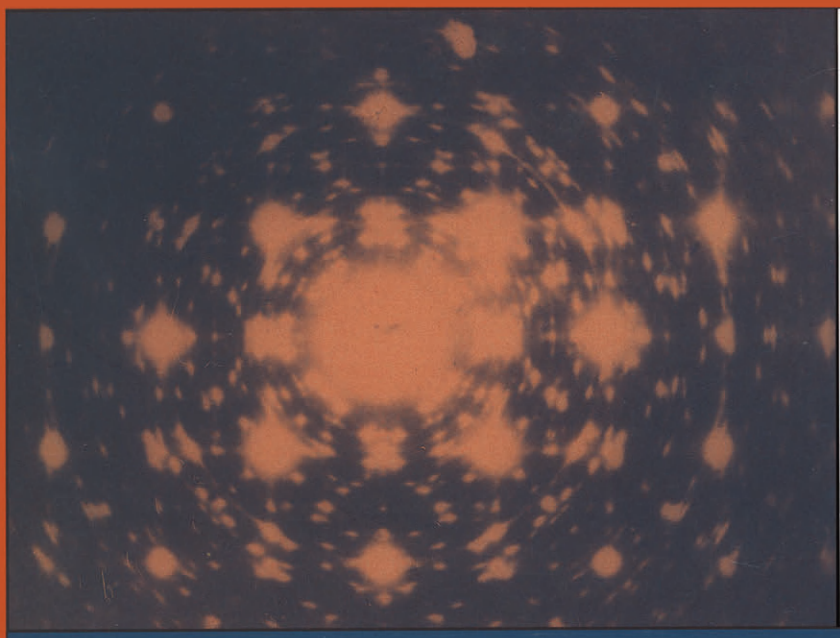

MODERN CRYSTALLOGRAPHY 1

Springer-Verlag Berlin Heidelberg GmbH

Modern Crystallography 1

Springer-Verlag Berlin Heidelberg GmbH

Modern Crystallography

Volume 1:
Fundamentals of Crystals
Symmetry, and Methods of Structural Crystallography

Volume 2:
Structure of Crystals

Volume 3:
Crystal Growth

Volume 4:
Physical Properties of Crystals

Boris K. Vainsthein

Fundamentals of Crystals

Symmetry, and Methods of Structural Crystallography

Second, Enlarged Edition

With 330 Figures and 4 Plates in Color

Springer

Professor Dr. *Boris K. Vainsthein*
Institute of Crystallography, Russian Academy of Sciences, Leninsky prospect 59,
117333 Moscow, Russia

2nd enlarged Edition 1994
Corr. Printing 1996

ISBN 978-3-642-08153-8

Cip-data applied for
Die Deutsche Bibliothek - CIP-Einheitsaufnahme
Modern crystallography : [in 4 vol.]/[ed. board: B.K. Vainsthein (ed.-in-chief)] ...

Einheitssacht.: Sovremennaja kristallografija <engl.>
NE: Vajnštejn, Boris K. [Hrsg.]; EST
Vol. 1. Vajnštejn, Boris K.: Fundamentals of crystals.-2., enl. ed., 2. print. - 1996
Vajnštejn, Boris K.:
Fundamentals of crystals : symmetry and methods of structural crystallography / Boris K. Vainshtein. - 2., enl. ed., 2. print.

(Modern crystallography ; Vol. 1)
1. Aufl. u.d.T.: Vajnštejn, Boris K.: Symmetry of crystals, methods of structural crystallography
ISBN 978-3-642-08153-8 ISBN 978-3-662-02975-6 (eBook)
DOI 10.1007/978-3-662-02975-6
This work is subject to copyright. All rights are reserved, whether the whole or part of the material is concerned, specifically the rights of translation, reprinting, reuse of illustrations, recitation, broadcasting, reproduction on microfilm or in other ways, and storage in data banks. Duplication of this publication or parts thereof is permitted only under the provisions of the German Copyright Law of September 9, 1965, in its current version, and permission for use must always be obtained from Springer-Verlag Berlin Heidelberg GmbH. Violations are liable for prosecution act under German Copyright Law.

© Springer-Verlag Berlin Heidelberg 1981 and 1994
Originally published by Springer-Verlag Berlin Heidelberg New York in 1994
Softcover reprint of the hardcover 2nd edition 1994

The use of general descriptive names, registered names, trademarks, etc. in this publication does not imply, even in the absence of a specific statement, that such names are exempt from the relevant protective laws and regulations and therefore free for general use.

Typesetting: Macmillan India Ltd, Bangalore, India; Offsetprinting: Saladruck, Berlin

SPIN:10488250 54/3020-5 4 3 2 1 - Printed on acid -free paper

Modern Crystallography

in Four Volumes*

1 *Fundamentals of Crystals*
Symmetry, and Methods of Structural Crystallography

2 *Structure of Crystals*

3 *Crystal Growth*

4 *Physical Properties of Crystals*

Editorial Board:
B. K. Vainshtein (Editor-in-Chief) A. A. Chernov L. A. Shuvalov

Foreword

Crystallography – the science of crystals – has undergone many changes in the course of its development. Although crystals have intrigued mankind since ancient times, crystallography as an independent branch of science began to take shape only in the 17th–18th centuries, when the principal laws governing crystal habits were found, and the birefringence of light in crystals was discovered. From its very origin crystallography was intimately connected with mineralogy, whose most perfect objects of investigation were crystals. Later, crystallography became associated more closely with chemistry, because it was apparent that the habit depends directly on the composition of crystals and can only be explained on the basis of atomic-molecular concepts. In the 20th century crystallography also became more oriented towards physics, which found an ever-increasing number of new optical, electrical, and mechanical phenomena inherent in crystals. Mathematical methods began to be used in crystallography, particularly the theory of symmetry (which achieved its classical completion in space-group theory at the end of the 19th century) and the calculus of tensors (for crystal physics).

* English editions have originally been published in Springer Series in Solid-State Sciences , Vols. 15 (I), 21 (II), 36 (III) and 37 (IV).

Early in this century, the newly discovered x-ray diffraction by crystals caused a complete change in crystallography and in the whole science of the atomic structure of matter, thus giving a new impetus to the development of solid-state physics. Crystallographic methods, primarily x-ray diffraction analysis, penetrated into materials sciences, molecular physics, and chemistry, and also into may other branches of science. Later, electron and neutron diffraction structure analyses became important since they not only complement x-ray data, but also supply new information on the atomic and the real structure of crystals. Electron microscopy and other modern methods of investigating matter – optical, electronic paramagnetic, nuclear magnetic, and other resonance techniques – yield a large amount of information on the atomic, electronic, and real crystal structures.

Crystal physics has also undergone vigorous development. Many remarkable phenomena have been discovered in crystals and then found various practical applications.

Other important factors promoting the development of crystallography were the elaboration of the theory of crystal growth (which brought crystallography closer to thermodynamics and physical chemistry) and the development of the various methods of growing synthetic crystals dictated by practical needs. Man-made crystals became increasingly important for physical investigations, and they rapidly invaded technology. The production of synthetic crystals made a tremendous impact on the traditional branches: the mechanical treatment of materials, precision instrument making, and the jewelry industry. Later it considerably influenced the development of such vital branches of science and industry as radiotechnics and electronics, semiconductor and quantum electronics, optics, including nonlinear optics, acoustics, etc. The search for crystals with valuable physical properties, study of their structure, and development of new techniques for their synthesis constitute one of the basic lines of contemporary science and are important factors of progress in technology.

The investigation of the structure, growth, and properties of crystals should be regarded as a single problem. These three intimately connected aspects of modern crystallography complement each other. The study, not only of the ideal atomic structure, but also of the real defect structure of crystals makes it possible to conduct a purposeful search for new crystals with valuable properties and to improve the technology of their synthesis by using various techniques for controlling their composition and real structure. The theory of real crystals and the physics of crystals are based on their atomic structure as well as on the theoretical and experimental investigations of elementary and macroscopic processes of crystal growth. This approach to the problem of the structure, growth, and properties of crystals has an enormous number of aspects, and determines the features of modern crystallography.

The branches of crystallography and their relation to adjacent fields can be represented as a diagram showing a system of interpenetrating branches which have no strict boundaries. The arrows show the relationship between the branches, indicating which branch influences the activity of the other, although, in fact, they are usually interdependent.

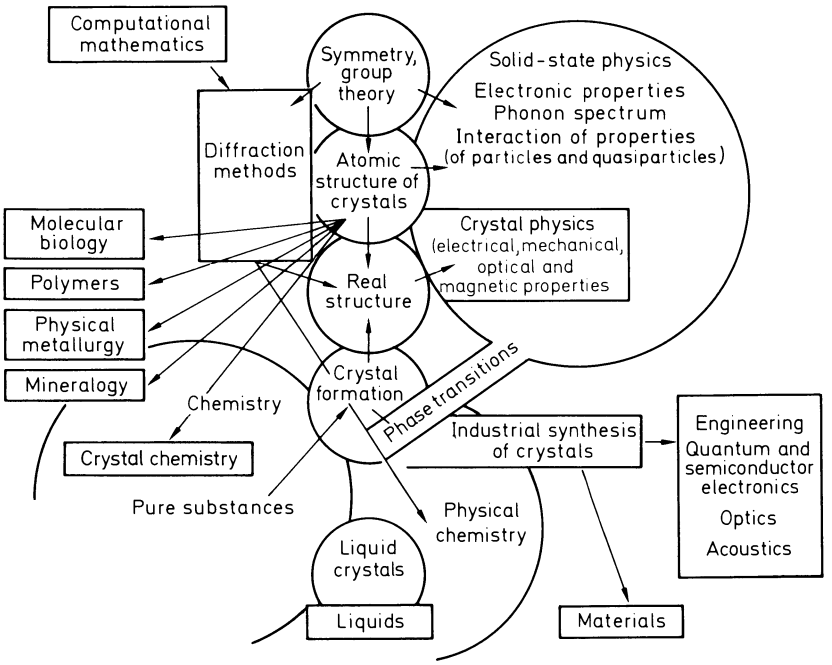

Branches of crystallography and its relation to other sciences

Crystallography proper occupies the central part of the diagram. It includes the theory of symmetry, the investigation of the structure of crystals (together with diffraction methods and crystal chemistry), and the study of the real structure of crystals, their growth and synthesis, and crystal physics.

The theoretical basis of crystallography in the theory of symmetry, which has been intensively developed in recent years.

The study of the atomic structure has been extended to extremely complicated crystals containing hundreds and thousands of atoms in the unit cell. The investigation of the real structure of crystals with various disturbances of the ideal crystal lattices has been gaining in importance. At the same time, the general approach to the atomic structure of matter and the similarity of the various diffraction techniques make crystallography a science not only of the structure of crystals themselves, but also of the condensed state in general.

The specific applications of crystallographic theories and methods allow the utilization of structural crystallography in physical metallurgy, materials science, mineralogy, organic chemistry, polymer chemistry, molecular biology, and the investigation of amorphous solids, liquids and gases. Experimental and theoretical investigations of crystal growth and nucleation processes and their development draw on advances in chemistry and physical chemistry and, in turn, contribute to these areas of science.

Crystal physics deals mainly with the electrical, optical, and mechanical properties of crystals closely related to their structure and symmetry, and

adjoins solid-state physics, which concentrates its attention on the analysis of laws defining the general physical properties of crystals and the energy spectra of crystal lattices.

The first two volumes are devoted to the structure of crystals, and the last two, to the growth of crystals and their physical properties. The contributors present the material in such a way that the reader can find the basic information on all important problems of crystallography. Due to the limitation in space the exposition of some sections is concise, otherwise many chapters would have become separate monographs. Fortunately, such books on a number of crystallographic subjects are already available.

The purpose of such an approach is to describe all the branches of crystallography in their interrelation, thus presenting crystallography as a unified science to elucidate the physical meaning of the unity and variety of crystal structures. The physico-chemical processes and the phenomena taking place in the course of crystal growth and in the crystals themselves are described, from a crystallographic point of view, and the relationship of properties of crystals with their structure and conditions of growth is elucidated.

This four-volume edition is intended for researchers working in the fields of crystallography, physics, chemistry, and mineralogy, for scientists studying the structure, properties, and formation of various materials, for engineers and those engaged in materials science and technology, particularly in the synthesis of crystals and their use in various technical devices. We hope that this work will also be useful for undergraduate and graduate students at universities and institutions of technology studying crystallography, solid-state physics, and related subjects.

Modern Crystallography has been written by a large group of researchers from the Institute of Crystallography of the USSR Academy of Sciences, who benefited from the assistance and advice of many other colleagues. The English edition of all four volumes of *Modern Crystallography* is being published almost simultaneously with the Russian edition. The contributors have included in the English edition some of the most recent data. In several instances some additions and improvements have been made.

B. K. Vainshtein

Foreword to the Second Editions

The 4-volume treatment *Modern Crystallography* was first published in the early eighties. Crystallography is centuries-old, and its basic concepts and laws are well established. However, the rapid progress in all the branches of science at the end of our century cannot by-pass crystallography. Our knowledge on the atomic structure of matter, on the formation and growth of crystals and their physical properties are becoming ever deeper, and the experimental methods are being constantly improved. Therefore, to justify the series title – *Modern Crystallography* – we had to enrich the treatment and complement it with new data.

Most of the First Edition has largely has been preserved, but several sections were up-dated, the text somewhere improved and complemented with some new illustrations. At the same time, numerous new results that could not be neglected have been summarized in the updating chapter concluding each volume. Indeed, we could not leave out quasicrystals, the high-temperature superconductors, discovered in the eighties, the development in molecular-beam epitaxy, surface melting, improper ferroelectrics, incommensurate phases, and many other topics. We have also presented several novel techniques which became widely used in crystallography – e. g., tunneling microscopy, EXAFS, position-sensitive detectors for x-rays, etc. The list of references has also been revised and supplied with new publications.

The Second Editions of *Modern Crystallography* were prepared mainly by the contributors of the first editions. In addition, we have been assisted by other colleagues with their notes, new figures and references. We take this opportunity to sincerely thank all of them.

B. K. Vainshtein, A. A. Chernov, L. A. Shuvalov

Preface to Modern Crystallography 1

Modern Crystallography 1 describes the general characteristics of the crystalline state of matter, considers crystal symmetry, and describes the methods for investigating the crystal structure.

The introductory chapter deals with the basic concepts of crystallography and the characteristics of the crystalline state of matter. It studies macroscopic features of a crystalline substance: homogeneity, anisotropy, and symmetry of properties; it also considers crystal habit, the basic regularities of the microscopic atomic structure of crystals, and differences between the structures of crystals and of other condensed media.

Chapter 2, which encompasses almost half of the volume, is devoted to a systematic presentation of the symmetry of crystals. The theory of symmetry penetrates all the crystallography, and without it one can neither study nor understand the structure and properties of crystals. The axiomatics of the theory of symmetry is given with group theory as its foundation; the basic concepts are treated geometrically. Point one-dimensional, plane, and space groups are considered, as well as generalizations of symmetry – antisymmetry and color symmetry.

Chapter 3 treats the theory of the geometric description of crystal habit and the geometric theory of a crystal lattice.

Chapter 4 is devoted to experimental methods for studying the atomic structure of crystals. Main attention is given to x-ray diffraction analysis, which is the most important tool for studying structures. This chapter discusses the general diffraction theory, experimental technique, and the fundamentals of the theory and methods of using diffraction analysis to determine the atomic structures of crystals.

The chapter also describes two other related methods – electron and neutron diffraction structure analysis, their specifics, potentialities, and limitations. It gives a brief exposition of other new methods for analysis of the structure of matter: Mössbauer diffraction and channeling particles in crystals. The final section covers electron microscopy.

Almost all of the volume was written by B. K. Vainshtein, Chapter 3 in co-operation with M. O. Kliya, and Section 4.3, with Z. G. Pinsker; Sections 4.5 and 4.6 were prepared by D. M. Kheiker. Many essential suggestions for presenting the material of Chapter 2 were made by V. A. Koptsik, who coauthored Sections 2.6.6 and 2.9. A number of valuable comments and

refinements were introduced by R. V. Galiulin. The author expresses his sincere gratitude to these colleagues. He also thanks L. A. Feigin, V. V. Udalova, L. I. Man, and many others who helped with the manuscript, the compilation of literature, and the preparation of the figures.

The crystallographic literature is enormous. In this volume and the following ones the references are divided into two categories. The Bibliography consists of basic monographs, review articles, and important original papers relating to the subject of the volume. The References consist of publications on separate special problems touched upon in the text, and also the works from which illustrations were borrowed. We also list the basic crystallographic journals and periodicals. Some original photographs were made available specially for this edition. Their authors are acknowledged in the captions. The author thanks all of them sincerely, as well as those who kindly gave permission for reproduction of pictures from their original papers or books.

Moscow, December 1980 *B. K. Vainshtein*

Preface to the Second Edition

Fundamentals of Crystals, Symmetry, and Methods of Structural Crystallography represents the second edition of the original text of *Modern Crystallography 1.* It is supplied with new data on the principles of the structure of the crystalline state and methods of its investigation. Several chapters have been revised and supplemented with new material. Two sections of Chapter 4 have been substantially revised:

4.8 *Electron Diffraction* written by B. K. Vainshtein and B. B. Zvyagin,
4.9 *Electron Microscopy* written by B. K. Vainshtein, N. A. Kiselev, and M. B. Sherman,
4.10 *Scanning Tunneling Microscopy* (a new section) written by L. M. Blinov.

We have also prepared a new, additional chapter reviewing important crystallographic achievements and methods developed in recent years. This chapter 5 consists of five sections:

5.1 *Quasicrystals* written by V. E. Dmitrienko and B. K. Vainshtein,
5.2 *Incommensurately Modulated Structures* written by V. E. Dmitrienko,
5.3 *Development of Experimental Technique of X-Ray Structure Analysis* by D. M. Kheiker and B. K. Vainshtein,
5.4 *X-Ray Studies of Crystal Surface* by A. Yu. Kazimirov,
5.5 *Methods for the Analysis of Powder Diffraction Patterns* by A. A. Loshmanov,
5.6 *EXAFS Spectroscopy* by A. N. Popov.

The author would like to express his sincere gratitude to V. V. Udalova, I. L. Tolstova, L. I. Man, L. A. Antonova for the great amount of technical work they have done in the preparation of the present volume.

Moscow, November 1993 *B. K. Vainshtein*

Contents

1. Crystalline State

1.1 Macroscopic Characteristics of Crystals 1
1.1.1 Crystals and Crystalline Matter 1
1.1.2 Homogeneity of a Crystalline Substance 5
1.1.3 Anisotropy of a Crystalline Substance 6
1.1.4 Symmetry 9
1.1.5 Crystal Habit 11
1.2 Microstructure of a Crystalline Substance 12
1.2.1 Space Lattice 12
1.2.2 Experimental Evidence for the Existence of the Crystal Lattice 15
1.2.3 Reasons for the Microperiodicity Principle 18
1.3 Structures with Distortions of the Three-Dimensional Periodicity. Quasicrystals 23
1.4 Structural Characteristics of Condensed Phases 24

2. Fundamentals of the Theory of Symmetry

2.1 The Concept of Symmetry 28
2.1.1 Definition of Symmetry 28
2.1.2 Symmetry Operations 29
2.2 Space Transformations 31
2.2.1 Space, an Object in It, Points of Space 31
2.2.2 Basic Isometric Transformations of Space 32
2.2.3 Analytical Expression for Symmetry Transformations 39
2.2.4 Relationships and Differences Between Operations of the First and Second Kind 41
2.3 Fundamentals of Group Theory 44
2.3.1 Interaction of Operations 44
2.3.2 Group Axioms 44
2.3.3 Principal Properties of Groups 46
2.3.4 Cyclic Groups, Generators 47
2.3.5 Subgroup 48
2.3.6 Cosets, Conjugates, Classes, Expansion with Respect to a Subgroup 48
2.3.7 Group Products 49
2.3.8 Group Representations 51

2.4 Types of Symmetry Groups and Their Properties 53
2.4.1 Homogeneity, Inhomogeneity, and Discreteness of Space 53
2.4.2 Types of Symmetry Groups and Their Periodicity 55
2.4.3 One-Dimensional Groups G^1 57
2.4.4 Two-Dimensional Groups G^2 58
2.4.5 Crystallographic Groups 60
2.4.6 Three-Dimensional Groups G^3 61
2.5 Geometric Properties of Symmetry Groups 64
2.5.1 Symmetry Elements 64
2.5.2 Summary and Nomenclature of Symmetry Elements... 66
2.5.3 Polarity 71
2.5.4 Regular Point Systems 71
2.5.5 Independent Region 73
2.5.6 Description of a Symmetric Object by Groups of Permutations 77
2.5.7 Enantiomorphism 79
2.6 Point Symmetry Groups 82
2.6.1 Description and Representation of Point Groups 82
2.6.2 On Derivation of Three-Dimensional Point Groups G_0^3 84
2.6.3 Point Group Families 86
2.6.4 Classification of Point Groups 95
2.6.5 Isomorphism of Groups K 100
2.6.6 Representations of Point Groups K 101
2.6.7 Group Representations and Proper Functions 106
2.7 Symmetry Groups G_1^2, G_2^2, G_1^3, G_2^3 107
2.7.1 Symmetry Groups G_1^2 of Borders 107
2.7.2 Plane Twice-Periodic Groups G_2^2 108
2.7.3 Cylindrical (Helical) Groups G_1^3 110
2.7.4 Layer Groups G_2^3 116
2.8 Space Groups of Symmetry 120
2.8.1 Three-Dimensional Lattice 120
2.8.2 Syngonies 122
2.8.3 Bravais Groups 123
2.8.4 Homomorphism of Space and Point Groups 129
2.8.5 Geometric Rules for Performing Operations and for Mutual Orientation of Symmetry Elements in Groups Φ 130
2.8.6 Principles of Derivation of Space Groups. Symmorphous Groups Φ_s 131
2.8.7 Nonsymmorphous Groups Φ_n 135
2.8.8 Number of Fedorov Groups 138
2.8.9 Nomenclature of Fedorov Groups 139
2.8.10 Subgroups of Fedorov Groups 144

2.8.11 Regular Point Systems of Space Groups 145
2.8.12 Relationship Between the Chemical Formula of a Crystal and Its Space Symmetry 146
2.8.13 Local Condition of Space Symmetry 147
2.8.14 Division of Space 149
2.8.15 Irreducible Representations of Groups Φ 155
2.9 Generalized Symmetry 156
2.9.1 On the Extension of the Symmetry Concept 156
2.9.2 Antisymmetry and Color Symmetry 157
2.9.3 Antisymmetry Point Groups 159
2.9.4 Point Groups of Color Symmetry 168
2.9.5 Space and Other Groups of Antisymmetry and Color Symmetry 171
2.9.6 Symmetry of Similarity 175
2.9.7 Partial Symmetry 177
2.9.8 Statistical Symmetry. Groupoids 177

3. Geometry of the Crystalline Polyhedron and Lattice
3.1 Basic Laws of Geometric Crystallography 179
3.1.1 Law of Constancy of Angles 179
3.1.2 Law of Rational Parameters. Lattice 180
3.2 Crystalline Polyhedron 182
3.2.1 Ideal Shape. Bundle of Normals and Edges 182
3.2.2 Simple Forms 183
3.2.3 Distribution of Simple Forms Among Classes 189
3.2.4 Holohedry and Hemihedry 192
3.2.5 Combinations of Simple Forms 192
3.2.6 The Zone Law 193
3.3 Goniometry 194
3.3.1 Crystal Setting 194
3.3.2 Experimental Technique of Goniometry 198
3.3.3 Goniometric Calculations 200
3.4 Lattice Geometry 205
3.4.1 Straight Lines and Planes of the Lattice 205
3.4.2 Properties of Planes 206
3.4.3 Reciprocal Lattice 208
3.5 Lattice Transformations 212
3.5.1 Transformation of Coordinates and Indices in the Atomic and Reciprocal Lattices 212
3.5.2 Reduction Algorithm 216
3.5.3 Computation of Angles and Distances in Crystals 219

4. Structure Analysis of Crystals
4.1 Fundamentals of Diffraction Theory 222
4.1.1 Wave Interference 222

4.1.2 Scattering Amplitude 224
4.1.3 Electron Density Distribution. Fourier Integral 226
4.1.4 Atomic Amplitude 227
4.1.5 The Temperature Factor 231
4.2 Diffraction from Crystals 234
4.2.1 Laue Conditions. Reciprocal Lattice 234
4.2.2 Size of Reciprocal Lattice Nodes 237
4.2.3 Reflection Sphere 239
4.2.4 Structure Amplitude 241
4.2.5 Intensity of Reflections. 242
4.2.6 Thermal Diffusion Scattering 244
4.2.7 Symmetry of the Diffraction Pattern and Its Relation to the Point Symmetry of the Crystal 244
4.2.8 Manifestation of Space-Symmetry of a Crystal in a Diffraction Pattern. Extinctions 245
4.3 Intensity of Scattering by a Single Crystal. Kinematic and Dynamic Theories 252
4.3.1 Kinematic Theory 252
4.3.2 Integrated Intensity of Reflection in Kinematic Scattering 253
4.3.3 Principles of Dynamic Theory 256
4.3.4 Darwin's Treatment 257
4.3.5 Laue–Ewald Treatment 258
4.3.6 Dynamic Scattering in an Absorbing Crystal. Borrmann Effect 262
4.3.7 Experimental Investigations and Applications of Dynamic Scattering 266
4.4. Scattering by Noncrystalline Substances 271
4.4.1 General Expression for Intensity of Scattering. Function of Interatomic Distances 271
4.4.2 Spherically Symmetric Systems: Gas, Liquid, and Amorphous Substances 272
4.4.3 Systems with Cylindrical Symmetry: Polymers and Liquid Crystals 274
4.4.4 Small-Angle Scattering 276
4.5 Experimental Technique of X-Ray Structure Analysis of Single Crystals 278
4.5.1 Generation and Properties of X-Rays 278
4.5.2 Interaction of X-Rays with a Substance 282
4.5.3 Recording of X-Rays 283
4.5.4 Stages of X-Ray Structure Analysis of Single Crystals . . 284
4.5.5 Laue Method 285
4.5.6 Crystal Rotation and Oscillation Methods 287
4.5.7 Moving Crystal and Film Techniques 291

4.5.8 X-Ray Diffractometers for Investigating Single Crystals ... 295
4.5.9 Diffractometric Determination of the Crystal Orientation, Unit Cell, and Intensities ... 297
4.6 X-Ray Investigation of Polycrystalline Materials ... 299
4.6.1 Potentialities of the Method ... 299
4.6.2 Cameras for Polycrystalline Specimens ... 300
4.6.3 Indexing of Debye Photographs and Intensity of Their Lines ... 303
4.6.4 Diffractometry of Polycrystalline Specimens ... 304
4.6.5 Phase Analysis ... 305
4.6.6 Investigation of Textures ... 305
4.6.7 Determination of the Sizes of Crystals and Internal Stresses ... 307
4.7 Determination of the Atomic Structure of Crystals ... 307
4.7.1 Preliminary Data on the Structure ... 307
4.7.2 Fourier Synthesis. Phase Problem ... 308
4.7.3 The Trial and Error Method. Reliability Factor ... 312
4.7.4 The Patterson Interatomic-Distance Function ... 313
4.7.5 Heavy-Atom Method ... 319
4.7.6 Direct Methods ... 321
4.7.7 "Statistical-Thermodynamical" Approach to the Crystal Structure Determination ... 325
4.7.8 Nonlocal-Search Method ... 327
4.7.9 Determination of the Absolute Configuration ... 330
4.7.10 Structure Refinement ... 331
4.7.11 Difference Fourier Syntheses ... 332
4.7.12 Automation of the Structure Analysis ... 334
4.8 Electron Diffraction ... 335
4.8.1 Features of the Method ... 335
4.8.2 Experimental Technique ... 336
4.8.3 Electron Diffraction Structure Analysis ... 338
4.8.4 Dynamic Scattering of Electrons ... 349
4.8.5 Special Methods of Electron Diffraction ... 350
4.8.6 Low-Energy Electron Diffraction (LEED) ... 355
4.9 Electron Microscopy ... 357
4.9.1 The Features of the Methods ... 357
4.9.2 Transmission Electron Microscopy ... 358
4.9.3 HREM Imaging of Atomic Structure of Crystals ... 368
4.9.4 EM in Molecular Biology. Experimental Technique ... 374
4.9.5 Processing of the Images of Biomolecules. 3D Reconstruction ... 376
4.9.6 Two-Dimensional Biocrystals ... 381
4.9.7 TEM of Single Bioparticles ... 382

4.9.8 Scanning Electron Microscopy (SEM) of Solids. 383
4.10 Scanning Tunneling Microscopy 385
4.10.1 Principle of Operation 385
4.10.2 Basic Construction of an STM 387
4.10.3 Specific Features of Scanning Tunneling Microscopy. . . 388
4.10.4 Atomic Force Microscope 389
4.10.5 Several Examples of Surface Images 390
4.11 Neutron Diffraction. Mössbauer Diffraction, and Scattering of Nuclear Particles in Crystals 392
4.11.1 Principles and Techniques of the Neutron Diffraction Method 392
4.11.2 Investigation of the Atomic Structure 394
4.11.3 Investigation of the Magnetic Structure 397
4.11.4 Other Possibilities Offered by the Neutron-Diffraction Method 400
4.11.5 Diffraction of Mössbauer Radiation 401
4.11.6 Particle Channeling and the Shadow Effect. 403

5. New Developments in Crystallography and its Methods
5.1 Quasicrystals 405
5.1.1 The Discovery of Quasicrystals 405
5.1.2 The Non-Traditional Symmetry of Aperiodic Objects . . 407
5.1.3 The One-Dimensional Quasicrystal (d = 1, N = 2) 409
5.1.4 Fourier Transform of Quasiperiodic Sequences 410
5.1.5 Two-Dimensional Quasicrystals and Their Symmetry (d = 2, N = 3, 4, 5, . . .). 412
5.1.6 Three-Dimensional Quasicrystals (d = 3, N = 4, 5, 6, . . .) 415
5.1.7 Structure Analysis of Quasicrystals 419
5.1.8 Order and Disorder in the Structure of Quasicrystals . . 424
5.2 Incommensurately Modulated Structures. 427
5.3 Development of Experimental Technique for X-Ray Structure Analysis. 427
5.3.1 Powerful Sources of X-Ray Radiation 427
5.3.2 The Synchrotron Radiation Sources 429
5.3.3 Characteristics of Synchrotron Radiation 429
5.3.4 The Primary SR Beam 431
5.3.5 Laue Method for Crystallographic Data Acquisition from Single Crystals 431
5.3.6 Some Results Obtained with Synchrotron Radiation Sources 432
5.3.7 Diffractometers with Two-Dimensional Position-Sensitive Detectors 433
5.4 X-Ray Studies of Crystal Surface 438
5.4.1 Surface Diffraction 440

5.4.2 The Method of X-Ray Standing Waves 443
5.5 Methods for Analysis of Powder Diffraction Patterns 446
5.6 EXAFS Spectroscopy 451
5.6.1 The Fundamentals of the EXAFS Theory 451
5.6.2 Structure Information Extracted from EXAFS Spectra 452
5.6.3 Experimental Methods and Apparatus 454

References 455

Bibliography 467

Subject Index 475

1. Crystalline State

The crystalline state of a substance is characterized by a time-invariant, regular three-dimensionally periodic arrangement of atoms in space. This determines all the features of the macro- and microscopic characteristics and physical properties of crystals. In this introductory chapter we shall deal with the principles of the atomic structure of crystals and of their habit, the possibility of macroscopic description of the properties on the basis of the conceptions of the anisotropy, and the symmetry of a crystalline substance. We shall also consider the thermodynamical reasons for the appearance of the crystalline state and for the differences between its structure and that of other condensed media: liquids, polymers, and liquid crystals.

1.1 Macroscopic Characteristics of Crystals

1.1.1 Crystals and Crystalline Matter

Crystals are solids which exhibit an ordered, three-dimensionally periodic spatial atomic structure and therefore have, under definite conditions of formation, the shape of polyhedra. Such are the natural crystals of minerals arising from processes that occur in the earth's crust (Fig 1.1) or synthetic crystals grown in laboratory (Figs. 1.2, 3).

The crystalline state is the thermodynamically equilibrium state of a solid. Under given thermodynamic conditions, to each solid phase of a fixed chemical composition there corresponds one definite crystalline structure. The existence of natural plane faces on a crystal is the most expressive external feature of a crystalline substance. This external feature, however, is but one of the macroscopic manifestations of its specific atomic structure. A crystal may not be polyhedral in shape (Fig. 1.2, crystals 9–14), but, like a fragment of any crystal, it possesses a number of macroscopic physical properties, which permit distinguishing it from an amorphous solid.

At the same time a great many natural and synthetic solids – minerals, various chemical compounds, metals and alloys, etc. – are polycrystalline, i.e., are aggregates of randomly oriented small crystals, which are usually of different sizes and irregular shapes; they are often called crystallites, or crystal

Fig. 1.1. Collection of natural crystals.
(1) halite NaCl; (2) calcite $CaCO_3$; (3) beryl $Be_3Al_2[Si_6O_{18}]$; (4) vorobievite, a pink variety of beryl; (5) emerald, a bright-green variety of beryl; (6) pyrite FeS_2; (7) quartz SiO_2; (8) amazonstone $K[AlSi_3O_8]$; (9) antimonite Sb_2S_3; (10) rubellite $(Na,Ca)(Mg,Al)_6[Si_6Al_3B_3(O,OH)_{30}]$; (11) topaz $Al_2(SiO_4)(F,OH)_2$; (12) Brazilian topaz; (13) diopside $CaMg[Si_2O_6]$; (14) fluorite CaF_2; (15) hematite Fe_2O_3; (16) celestine $SrSO_4$

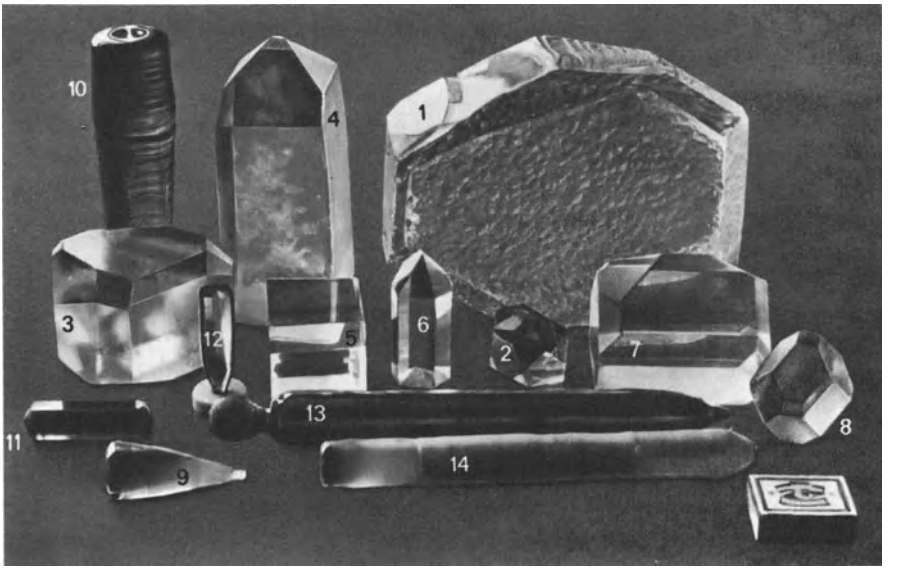

Fig. 1.2. Collection of synthetic single crystals.
(1, 2) quartz SiO_2; (3) triglycinesulphate $(NH_2CH_2COOH)_3H_2SO_4$; (4) potassium dihydrophosphate KH_2PO_4; (5) lithium fluoride LiF; (6) lithium iodate $LiIO_3$; (7) α-iodic acid α-HIO_3; (8) potash alum $KAl(SO_4)_3 \cdot 12H_2O$; (9) ruby Al_2O_3 + 0.05%Cr grown for the watch industry as a "bull"; (10) laser ruby Al_2O_3 + 0.05%Cr; (11) garnet $Y_3Al_5O_{12}$; (12) lithium niobate $LiNbO_3$; (13) silicon Si; (14) sapphire Al_2O_3

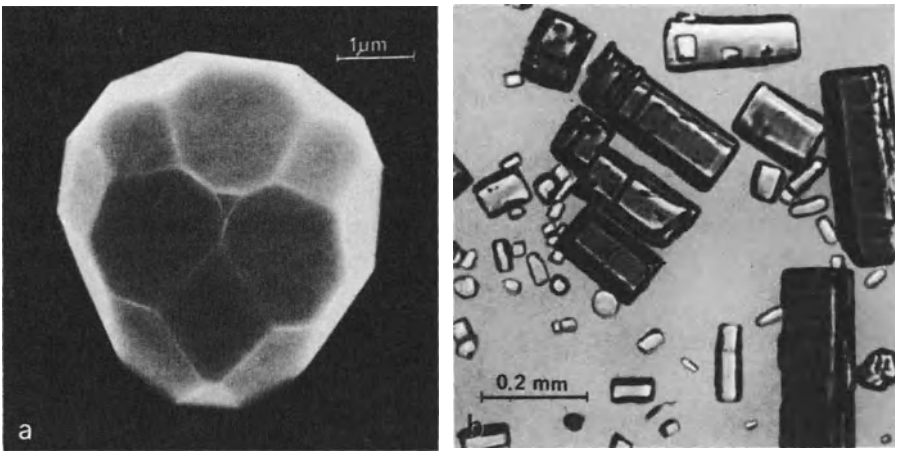

Fig. 1.3a,b. Small single crystals.
(a) germanium (courtesy of E. I. Givargizov); **(b)** protein catalase [1.1]

grains (Fig. 1.4). Sometimes crystallites show some preferred orientation, and then specimens are said to have a texture. The properties of polycrystals and textures naturally depend on those of the small crystals of which they are formed, on the size and mutual arrangement of these crystals, and on the interaction forces between them. Individual large crystals are usually called single crystals to distinguish them from polycrystals.

The principal macroscopic features of crystalline matter (substances in the crystalline state) result from the three-dimensionally periodic atomic structure

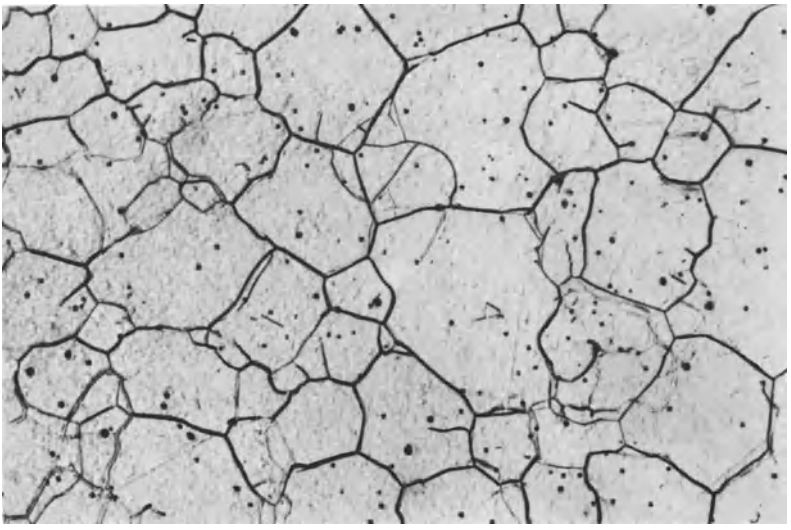

Fig. 1.4. Polished section of an austenite polycrystal (× 160)

of crystals. Such most general macroscopic properties are the homogeneity, anisotropy, and symmetry of the crystalline substance. In discussing these general and specific macroscopic physical properties of a crystal we abstract ourselves from its microscopic inhomogeneity, from the three-dimensional periodicity of the atomic structure and its microdefects (Fig. 1.5), which permits us to regard a crystal as a continuous homogeneous media.

The motions of the atoms of a substance in the crystalline state also find their macroscopic expression. The atoms in a crystal experience thermal vibrations, which are enhanced with increasing temperature; this substantially affects the physical properties of the crystal. At certain temperatures the thermal vibrations become so large that they lead to phase transitions in the solid state or to melting. The phase state naturally depends on the external pressure as well. The properties of a crystal also depend on its electrons, i.e., on the electron energy spectrum, interaction of electrons with phonons, etc.

Even under conditions of ideal thermodynamic equilibrium a crystal exhibits point defects, except them other structural imperfections such as: dislocations, blocks, and domains are practically always present in real crystals (Fig. 1.5b,c). Under actual conditions of formation, growth, and "life" of crystals one always observes local deviations of the composition and structure from the ideal, various nonequilibrium submicroscopic defects, inclusions, etc. In analyzing the concepts of macroscopic homogeneity, anisotropy, and symmetry of a crystal we ignore the kinetic phenomena and structural defects and consider the time-average spatial structure of the crystal.

Some properties of crystals have little sensitivity to the structural defects, and can largely be regarded from the standpoint of an "ideal" or "idealized" model of a crystal. But many properties depend to a greater or lesser extent on the structural defects, and then consideration of the physical properties requires

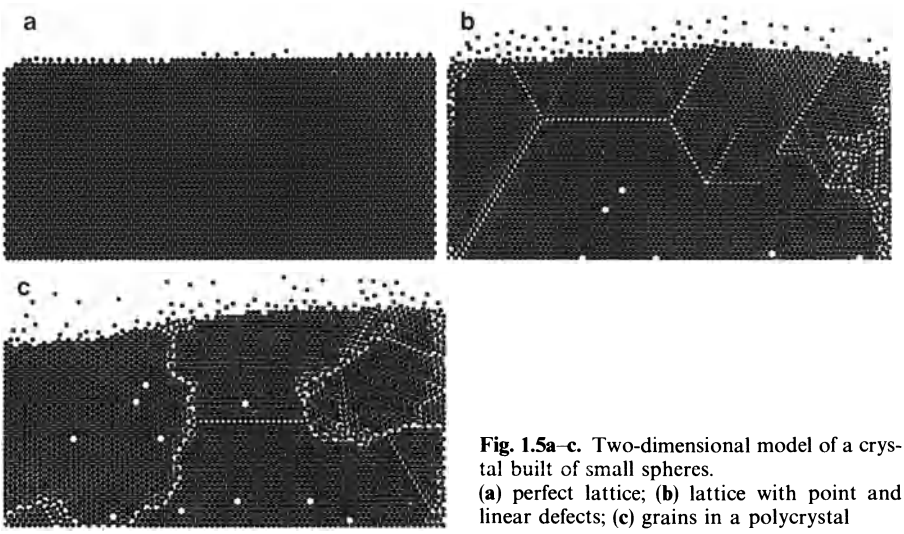

Fig. 1.5a–c. Two-dimensional model of a crystal built of small spheres.
(a) perfect lattice; **(b)** lattice with point and linear defects; **(c)** grains in a polycrystal

taking into account precisely these imperfections, i.e., the real structure of the crystal.

Note that the very existence of the surface of a crystal affects its properties, particularly if the crystal is small. Some properties of a bulk single crystal at and near its surface differ substantially from those inside the crystal. Therefore in describing certain features of a crystalline substance it is customary to ignore the existence of the boundaries and to assume the crystal to be infinitely extended. And conversely, in other cases it is precisely the boundaries of the crystalline substance that are the focus of attention, although their specific features actually stem from its "internal" properties.

1.1.2 Homogeneity of a Crystalline Substance

The term "macroscopic homogeneity" is taken to mean that all the properties of a crystalline substance are identical in any of its parts. No matter where in a single crystal we cut out from an identically oriented specimen of some shape and size (Fig. 1.6), its properties – physical (optical, mechanical, thermal, etc.), physicochemical (solubility of the surface, adsorption of some substances or other on it), and others – will be identical.

The properties of a crystal may be expressed by a scalar (e.g., heat capacity, density), a vector (e.g., polarization), or in the general case, a tensor (e.g., elasticity).

The very notion of macroscopic measurement of a property implies that the experimenter deals with lengths L, surfaces S, and volumes V of a crystal that the discrete atomic structure and microperiodicity cease to manifest themselves, i.e., when $L \gg a$, $S \gg a^2$, $V \gg a^3$ (a being the largest period of the crystal lattice). For most crystals $a \approx 10$Å[1]. In practically all measurements of macroproperties the specimens have such sizes L that the requirement $L \gg a$ is obviously met.

From the condition of homogeneity of a crystalline substance follows the constancy of its chemical composition and phase state throughout the volume.

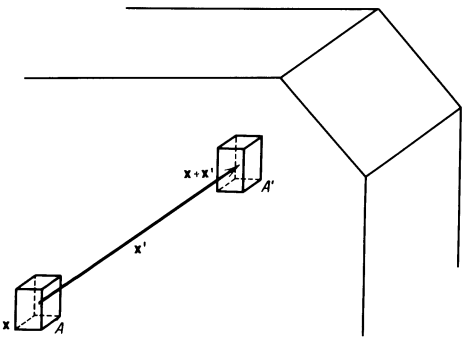

Fig. 1.6. Identity of properties in volumes A and A'

[1] 1 Å (Angstrom unit) = 10^{-8}cm = 0.1 nm (nanometer).

No matter what microregion of a perfect crystal is chosen for sampling (provided its volume is not less than V), the chemical analysis of the specimen will yield the same result. Speaking of measuring any property F of a crystal – scalar, vectorial, or tensorial – we imply that it is carried out with fixed thermodynamic parameters: pressure p, temperature T, and, in the general case, under specific external conditions. Thus, the term crystalline homogeneity means invariance of any property F in passing from measurement at a point $\boldsymbol{x}(x_1, x_2, x_3)$ to any other point $\boldsymbol{x} + \boldsymbol{x}'(x_1 + x'_1, x_2 + x'_2, x_3 + x'_3)$:

$$F(\boldsymbol{x}) = F(\boldsymbol{x} + \boldsymbol{x}'), \tag{1.1}$$

provided the above-formulated condition $L \gg a$ is fulfilled. In other words, homogeneity is the invariance of the properties with respect to an arbitrary translation of the origin in the crystalline substance. Exceptions are the surface and the adjacent layer, as mentioned above.

The concept of macroscopic homogeneity makes it possible to regard a crystalline substance as a *continuum.* This approach is extremely important in crystallography, because it enables one to give phenomenological descriptions of many physical properties of crystals without the use of the concepts of their discrete atomic structure. This notion can be extended and used in reference to a real crystal. Then, lengths $L \gg b$, areas $S \gg b^2$, and volumes $V \gg b^3$ greater than in the perfect crystal should be considered, b being the average distance between defects. This permits the influence of the defects to be averaged out. In many cases this approach can be used to advantage in explaining and describing the properties of a real crystal.

At present, the concept of homogeneity of real crystals is not only employed in the theory of crystallography, but also has an important practical significance. It is nearly always the basic criterion of the quality of synthetic crystals, be they optical, semiconducting, ferroelectric, etc. The particular characteristics of the homogeneity required in relation to impurities, blocks, dislocations, etc., are taken into consideration, depending on the technical application of the crystal.

It is worth noting that modern crystallography has at its disposal a wealth of methods for local microanalysis of composition and structural defects with a resolution of up to several angstroms. Thus it is possible to pass over from the averaged description of homogeneity under the condition $L \gg b$ to the local description of inhomogeneities with lengths $L < b$.

The concept of macroscopic homogeneity as defined above is applicable not only to crystals, but also to liquids, amorphous bodies, and gases. The characteristics of a crystalline substance and its distinction from the other states is evident when considering its anisotropy.

1.1.3 Anisotropy of a Crystalline Substance

We have already noted that certain properties of crystals are scalar, i.e., direction independent. At the same time many properties, such as thermal con-

ductivity, dielectric and magnetic susceptibility, refractive indices, and others essentially depend on the direction along which they are measured. If both the effects exerted on a crystal and the reaction being measured are vectorial (for instance, the electric field strength or induction), then the property describing their relationship (the dielectric constant in our example) is a tensor. This term encompasses both vector-tensor and tensor-tensor properties.

If a property of a substance does not depend on the direction, or, to put it differently, if the description of this property is independent of any orientation of the frame of reference, then the substance is said to be isotropic with respect to this property. Thus, liquids and gases are isotropic with respect to all properties, whereas crystals are isotropic with respect to some properties only. On the other hand, if properties are direction dependent, their description depends on the orientation of the frame of reference, and this dependence is called *anisotropy*. All the crystals without exception are anisotropic with respect to at least some of their properties.

Anisotropy manifests itself in the very habit of many crystals, for instance, in their elongated or plate shape. It is vividly expressed in the mechanical properties, e.g., in cleavage, which is the ability of some crystals to split readily along certain planes. Deformation of crystals is also direction dependent (Figs. 1.7 and 1.8).

In accordance with the principle of macroscopic homogeneity (1) we can refer a property F to an arbitrary point. Choosing now some (any) origin, we can describe anisotropy, in the simplest case, as the orientation dependence of the property F, i.e., its dependence on the direction $\boldsymbol{n}$ along which the property is measured:

$$F(\boldsymbol{n}_1) \neq F(\boldsymbol{n}_2) \,. \tag{1.2}$$

A conventional technique in studying the anisotropy of crystal properties is carving out differently oriented specimens, say columns, parallel to the direction

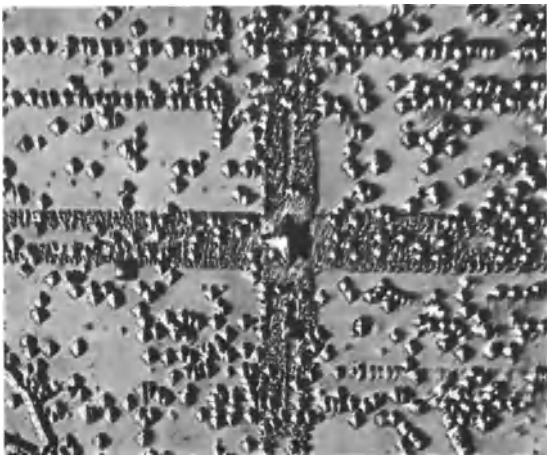

Fig. 1.7. Picture of propagation of deformation (revealed by etching) along (100) plane of a PbS crystal from an impact of a diamond indentor (× 320) [1.2]

n under study, or plates normal to it, and measuring the properties along this direction.

A pictorial description of the anisotropy of some properties is provided by the construction of indicatrice surfaces (Figs. 1.8, 9) whose radius vector length corresponds to the value of the property F being measured. Here, the variation

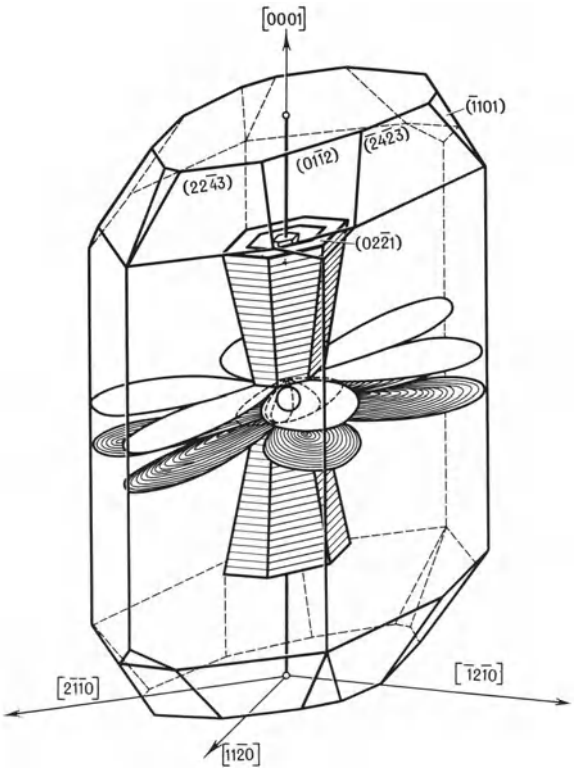

Fig. 1.8. Configuration of a space dislocation rosette arising from a local stress source in the bulk of a crystal of corundum α-Al_2O_3 at 1600°C [1.3]

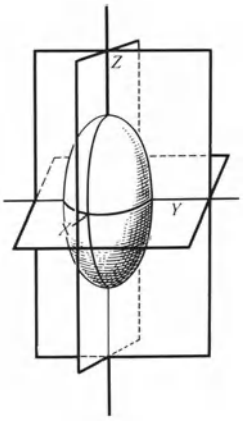

Fig. 1.9. General form of the Fresnel ellipsoid

of F in relation to the scalar (e.g., thermodynamic) parameters can be represented as a family of such surfaces for different values of these parameters. It is possible to investigate the anisotropy of properties under various external effects, e.g., under tensile stress or an applied electric field, and to establish the influence of these factors on such properties as deformation and polarization.

We note that anisotropy is not a property of crystals only. It occurs in crystal textures and exists in liquid crystals, and in natural and synthetic polymer substances. The anisotropy of these substances, as in crystals, is fundamentally determined by their molecular structure and does not necessarily require a difference in all properties in all directions. On the contrary, F may be equal for some different, continuously changing or discrete directions. This equality is in fact a manifestation of the symmetry of crystals. We shall now proceed to consider this extremely important phenomenon.

1.1.4 Symmetry

The concept of symmetry – one of the most general fundamental concepts of physics and natural science as a whole – permeates all of crystallography and lies at its basis. Symmetry is the most general law inherent in the structure and properties of a crystalline substance; it is sometimes said to be the property of properties of crystals.

To clarify the concept of symmetry we consider some examples. Figure 1.10 depicts the ideal shape of a quartz crystal. Its habit is such that it can be brought into self-coincidence by a rotation through 120° about the vertical axis 3. Such a motion appears to change nothing, although it has in fact occurred. Indeed, the essence of symmetry lies in the possibility of performing a transformation of an object, which brings it into self-coincidence in a new position. This can be formulated alternatively as the possibility of transforming the system of the coordinates of an object (in this particular case it corresponds to a rotation through 120°) so that it is described with respect to the new system precisely as it was with respect to the original one.

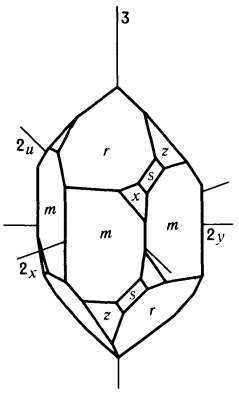

Fig. 1.10. The ideal shape of a quartz crystal and its symmetry axes

The shape of crystals, their structure, and their properties can be described by functions depending on coordinates and/or directions. Figure 1.9 portrays the Fresnel ellipsoid for a biaxial crystal. Such an ellipsoid is brought into self-coincidence on reflection in any of the coordinate planes. In each octant the function F, describing the velocities of light propagation in a crystal, has continuously changing values. However, its values at certain points of the surface in each of the octants, namely at points differing in sign of any coordinate, are equal to each other: $F(x, y, z) = F(\bar{x}, y, z) = \ldots = F(\bar{x}, \bar{y}, \bar{z})$.

Thus, a finite symmetric object in three-dimensional space is an object which can be brought into self-coincidence by rotations and/or reflections.

From the above, we can see that it is not the particular values of the function F describing an object or some of its properties which are essential, but, rather, the existence of certain relationships between them with respect to which F is invariant. In the general form this can be stated as follows. The function F is symmetric if it is invariant under a transformation of all or some of its variables. Let $\boldsymbol{x}(x_1, \ldots, x_m)$ be arguments of function F, and $\boldsymbol{x}'(x'_1, \ldots, x'_m)$, and $\boldsymbol{x}^{(n)}(x_1^{(n)}, \ldots, x_m^{(n)})$, the transformed arguments of this function. Then the relationships

$$F(\boldsymbol{x}) = F(\boldsymbol{x}') = \ldots = F(\boldsymbol{x}^{(n)}) \tag{1.3}$$

are the conditions of symmetry (invariance) of the function F.

An object (or a function describing it) can often be characterized by several distinct transformations or, in other words, symmetry operations. For instance, a quartz crystal (Fig. 1.10) is brought into self-coincidence not only on rotation through 120° about the vertical axis, but also on any of the rotations through 180° about three horizontal axes 2_x, 2_y, 2_u. The set of all symmetry transformations of any object is a *group* from the mathematical point of view. Symmetry transformations may also be such that the arguments change infinitesimally; then the group contains an infinite number of operations.

When studying the symmetry of an object, we must clearly realize what kind of symmetry we are considering – of which properties and according to which features (which are described by the appropriate variables) an object may have different symmetries and be described by different symmetry groups with respect to different properties and at different levels of consideration – macroscopic or microscopic, purely geometric or physical, in a static or dynamic state. There is then a hierarchy of the corresponding symmetry groups.

The concepts of crystalline homogeneity and anisotropy can be formulated from the viewpoint of symmetry. Homogeneity – the independence of the properties of a crystalline substance from the choice of the measuring point – is, as far as symmetry is concerned, invariance with respect to an arbitrary translation of the crystal structure. The anisotropy of crystals – the direction dependence of the properties – manifests itself within the framework of symmetry: the functions describing the properties are themselves symmetric.

Thus, a crystalline substance can be defined, according to its macroscopic features, as a homogeneous anisotropic symmetry medium.

1.1.5 Crystal Habit

In addition to the "internal" properties of homogeneity and anisotropy a crystalline substance possesses one more, most visual macroscopic property: in the course of growth under equilibrium conditions crystals acquire a natural shape of polyhedra with plane faces (see Figs. 1.1–3). Similar regular surfaces also appear in processes opposite to growth, namely in dissolution or evaporation of crystals (Fig 1.11).

In considering this macroscopic property we pass over from a crystalline substance as a continuum to a crystalline individual, a finite body built up from this substance. An important part here is played by the interaction of the crystal surface with the environment in which this crystal was formed or to which it was transferred.

We note that the polyhedral faces of single crystals satisfy the requirements of homogeneity, anisotropy, and symmetry, but are not completely determined by these principles. The formation of faces is also a manifestation of the regular atomic structure of crystalline matter.

The first law of crystal habit is the law of constancy of angle: the angle between the corresponding faces of crystals of a given substance is constant and characteristic of these crystals. The law was first formulated in 1669 by the Danish scientist N. Stenon, who used quartz and hematite crystals as examples. The validity of this law for the crystals of all substances was established much later, in 1783, by the French scientist J. B. Romé de Lisle.

In 1784 the French crystallographer Abbé R.-J. Haüy deduced the second principal law of crystal habit, the law of rational parameters. Certain edges of a crystal are chosen for its three coordinate axes according to certain rules.

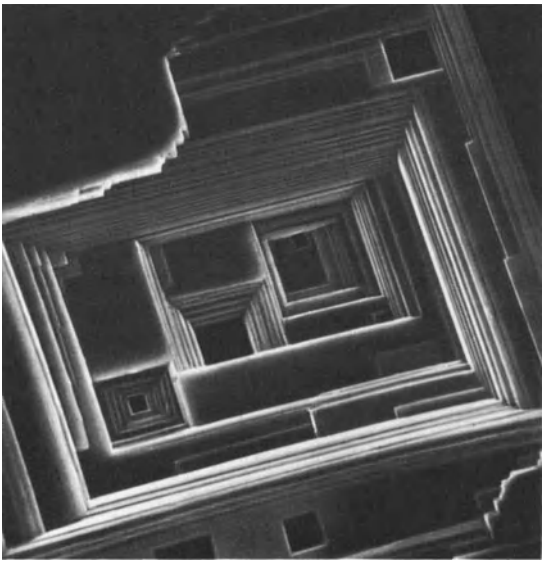

Fig. 1.11. Evaporation figures on the surface of an EuTe alloy ($\times 1520$) [1.4]

Measurements show that the intercepts on the axis cut off by the crystal faces can be expressed as integral multiples of certain axial units. But the existence of axial units in three directions immediately suggests the three-dimensional microperiodicity of the structure of crystals, and the existence of a lattice in them, which fact determines the habit and the other macroscopic properties of crystals.

We have considered the general macroscopic characteristics of a crystalline substance. A remarkable historical fact is that the combination of these characteristics led crystallographers, even before the advent of modern methods for studying the atomic structure, to the conclusion that the microstructure of crystals is characterized by a three-dimensional spatial periodicity of the packing of their constituent microparticles.

1.2 Microstructure of a Crystalline Substance

1.2.1 Space Lattice

The idea that the shape of crystals can be attributed to regular packing of infinitesimal spherical or ellipsoidal particles was first suggested independently by W. H. Wollaston, R. Hooke, H. Huygens, and M. V. Lomonosov. Lomonosov gave considerable time and attention to the phenomena of solution and crystallization of salts; he studied and classified crystals of minerals. In his thesis "Dissertation de generatione et natura nitri" (1749) he gave the scheme of arrangement of basic particles of matter – corpuscles (Fig. 1.12) and wrote: "If we assume that saltpeter particles thus arranged have a spherical shape, to which the finest natural bodies piling together tend in most cases, it will be very easy to explain why saltpeter grows into hexagonal crystals".

An explanation of the existence of diverse faces on crystals was given by R.-J. Haüy on the basis of the law of rational parameters. As we have seen, according to this law the microstructure of crystals is periodic and is characterized by axial units of periodicity a, b, c. The ratio between these units can be found by measuring the interfacial angles. The axial units – unitary edges – may serve to construct a unit parallelepiped. Haüy assumed that the "molecules" of a crystal have this form. In the phenomenon of cleavage, he perceived a physical argument in favor of the existence of such microparallelepipeds. For instance,

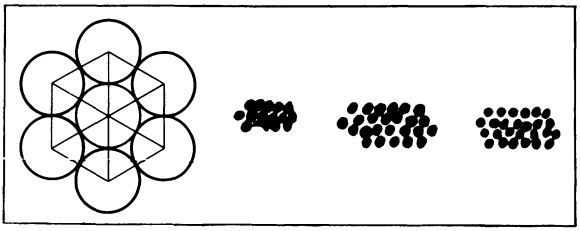

Fig. 1.12. Structure of saltpeter crystals [1.5]

calcite splits readily along the coordinate rhombohedral faces. By crushing calcite into smaller and smaller rhombohedra, reasoned Haüy, one can obtain infinitesimal elementary figures of this shape. It is easy to see that they can fill the space completely and can thus build a crystal bounded by coordinate faces. All the other faces can be constructed as steps with different numbers of molecules in them (Fig. 1.13). The "microroughness" of noncoordinate faces is of no consequence here, because it is unobservable macroscopically.

The principle of this theory was the fundamental notion of three-dimensional spatial periodicity of the arrangement of particles in a crystal. The deduction that the structure consists of polyhedra filling space completely was physically erroneous. But it gave an impetus to the development of some important formal geometric concepts in crystallography.

Indeed, a polyhedral or any other "shape" of the microparticles constituting a crystal is not essential for the explanation of the laws of geometric crystallography. The only essential element is the fact that the arrangement of any such particles obeys the law of three-dimensional repetition, i.e., spatial periodicity. This gave rise to the concept of a three-dimensional lattice of crystals, whose simplest geometric image is the three-dimensionally periodic point system (Fig. 1.14). The unit parallelepiped (unit cell), whose three-dimensional repetition forms the entire crystalline structure, may contain various numbers of atoms – from one to millions, and the arrangement of the atoms in the unit cell may itself be characterized by some symmetry or other.

It should be emphasized that the space lattice is not simply a system of nodes at which, say, some atoms or molecules are situated. It is the geometric image of symmetry operations of discrete transfers – translations. We shall explain this using as an example a two-dimensional wall-paper pattern (Fig. 1.15a) and the

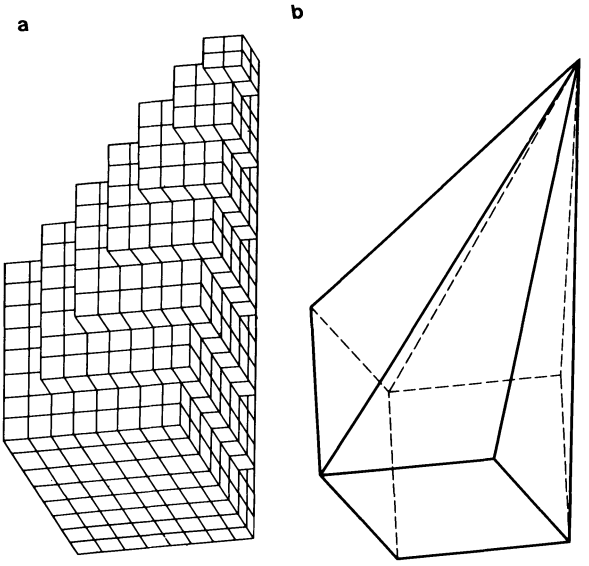

Fig. 1.13a,b. Building up a crystal from "parallelepipedal molecules" (**a**) and the formation of noncoordinate faces (**b**) [1.6]

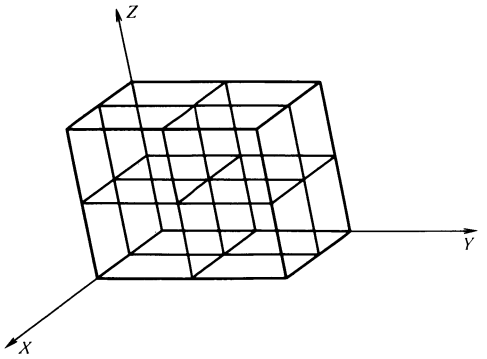

Fig. 1.14. Space lattice

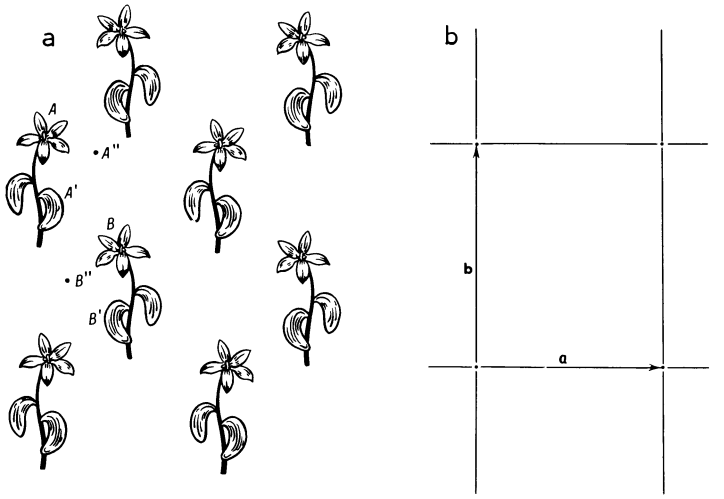

Fig. 1.15a,b. Two-dimensionally periodic pattern (**a**) and the corresponding two-dimensional lattice – a system of parallel translations (**b**)

corresponding lattice with periods a and b (Fig. 1.15b). Figure 1.15a has no selected points, but if we place a lattice positioned parallel to it at any one of them, for instance at the center of a flower, or at the edge of the leaf A', or the point A'' in the empty space between the flowers, it will in each case locate points which are identical, equal physically and geometrically in the sense of environment.

A three-dimensionally periodic space point system, when "superimposed" on a crystal structure, will likewise identify symmetrically equal points – be they the centers of atoms of the same or a different sort or any point between the atoms, etc. Therefore a crystal is sometimes said to be "in a lattice state".

Naturally, the symmetry of a crystalline substance is not restricted to translational symmetry and may be much more diversified. Figure 1.15a in-

cludes other flowers B, which are symmetric to the first A (to any point A there corresponds a symmetrically equal point B), but A and B are not related by the translations shown in Fig. 1.15b. However all the points B, as well as all the points A, are related to each other by these translations.

The term "lattice", which is widely used in the literature on crystallography, solid-state physics, and other fields of science, deserves some elaboration. In the strict sense the term "crystal lattice" actually coincides with the term "space lattice" and implies three-dimensional periodicity inherent in the atomic structure of crystals in general. We shall also use it mostly in this sense. At the same time the authors of many papers and books attach a broader meaning to this term, using it to define crystalline structure in general. For instance, they speak of lattice energy, of lattice dynamics, of the lattice as the structure of some chemical compound: "the crystal lattice of diamond . . . , of rock salt". One must clearly realize the difference between these interpretations. In describing the atomic structure of compounds and their modifications we shall use the term "crystalline structure".

1.2.2 Experimental Evidence for the Existence of the Crystal Lattice

The law of rational parameters and the development of the concepts of atomistics leave no room for doubt that crystals are three-dimensionally periodic arrangements of atoms. The possible groups of symmetry of the atomic structures of crystals – the 230 space groups – were derived theoretically by E. S. Fedorov and A. Schönflies in 1890. But the first direct proof of the existence of space lattices was given by the phenomenon of x-ray diffraction of crystals, discovered by M. Laue, W. Friedrich, and P. Knipping in 1912.

The nature of these rays was not known at the time. Laue assumed that x-rays were electromagnetic waves with a wavelength many times less than that of visible light. On the other hand, from chemical data, information on molar volumes, etc., it was clear that the interatomic distances in condensed systems were approximately several angstrom and, possibly, of the magnitudes of the order of a wavelength of x-rays. If crystals were indeed three-dimensionally periodic structures, they must represent a natural three-dimensional diffraction lattice for x-rays analogous to optical diffraction gratings. Experiment confirmed this assumption remarkably. Figure 1.16 shows the result of one of the first experiments by Laue, Friedrich, and Knipping. Shortly after that W. H. Bragg in England and, independently, G. V. Wulff in Russia derived the fundamental equation for the reflection of x-rays from crystals. In 1913–1914 W. H. Bragg and W. L. Bragg performed the first structure determinations of NaCl, Cu, diamond, etc., on the basis of x-ray experimental data, using the models of atomic packings proposed by W. Barlow (Fig. 1.17).

Today the atomic structures of more than a hundred thousand of inorganic and organic compounds have been determined by means of x-ray structure analysis and by electron and neutron diffraction methods.

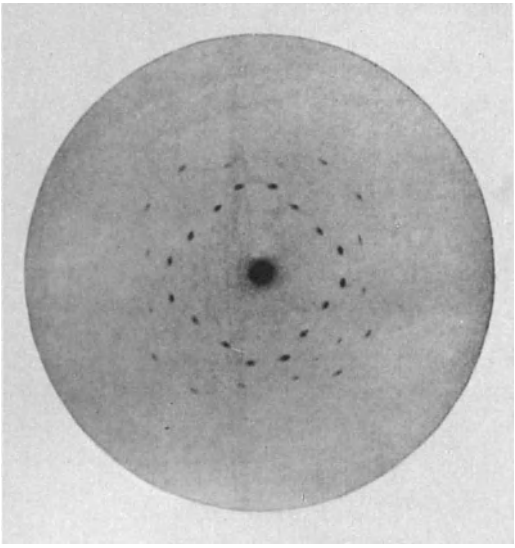

Fig. 1.16. One of the first x-ray patterns of Laue, Friedrich, and Knipping (zinc blende) [1.7]

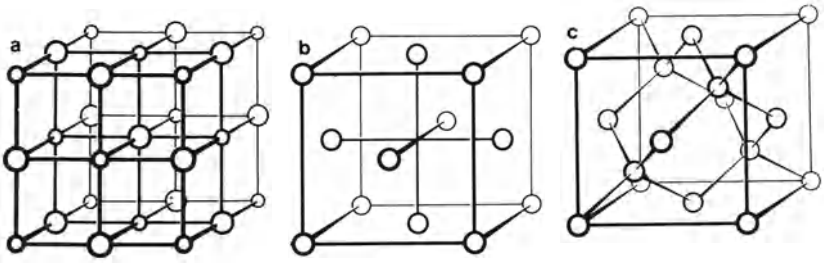

Fig. 1.17a–c. Structure of rock salt (**a**), copper (**b**), and diamond (**c**)

Electron microscopy makes it possible to observe directly the arrangements of molecules or atoms in crystal structures and the packing of large particles in different crystal faces (Fig. 1.18).

Individual atoms in the simplest crystal structures of metals may be directly visualized by the method of field emission microscopy. These kinds of pictures (Fig. 1.19) show the packing of atoms in different faces and the steplike structure of the faces.

Thus the hypothesis of the three-dimensional periodicity of atomic arrangement in crystals has now become a familiar fact of physical knowledge, which serves as a basis for all concepts of crystals and the starting point of solid-state theory.

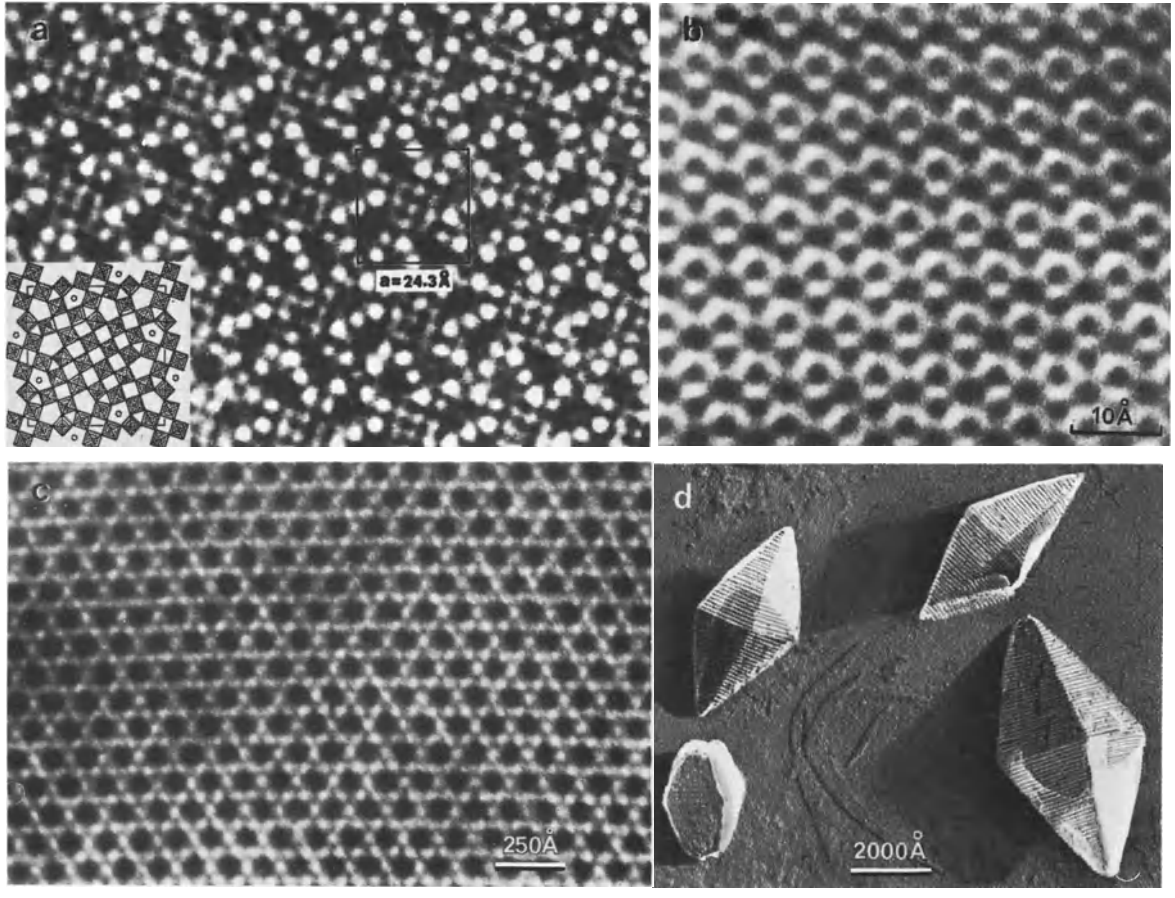

Fig. 1.18a–d. Electron micrographs of the structure of some crystals.
(a) structure of complex oxide $2Nb_2O_5 \cdot 7WO_3$. Projection of the unit cell is shown on electron micrograph. Shaded squares in the scheme represent MeO_6-octahedra [1.12]; **(b)** the structure of yttrium-aluminum garnet $Y_3Al_5O_{12}$ in projection onto the plane (111) [1.8]; **(c)** protein catalase (the packing of the molecules is visible) [1.1]; **(d)** individual crystals of protein from Bacillus thuringiensis [1.9]

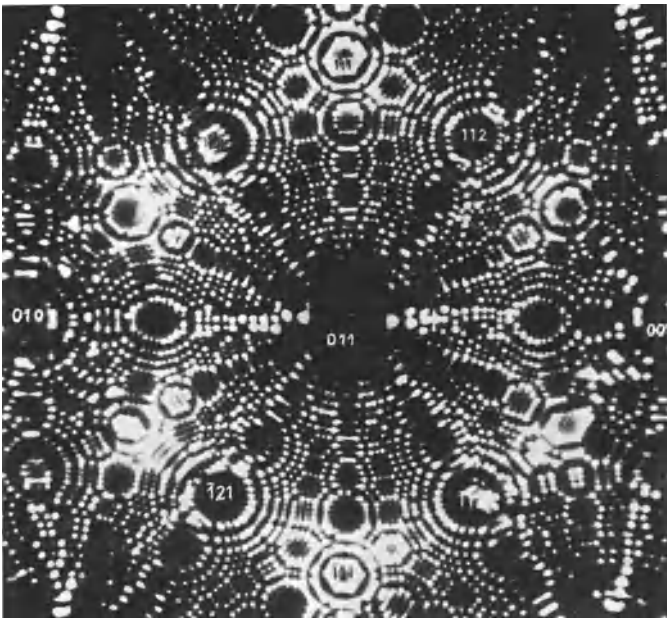

Fig. 1.19. Arrangement of atoms on the surface of a tungsten crystal needle point obtained by the ionic field emission method [1.10]

1.2.3 Reasons for the Microperiodicity Principle

What are the physical causes of the fact that the structure of a solid in the crystalline state is always characterized by three-dimensional periodicity?

In the first place, crystals (and liquids also) are condensed systems, where atoms "touch" each other. Such systems are formed because interaction forces between atoms at distances of over 3–4 Å are those of attraction. The potential energy of interaction $U(r)$ between atoms for all types of chemical bonds is described by a curve, whose shape is given in Fig. 1.20; its minimum lies within

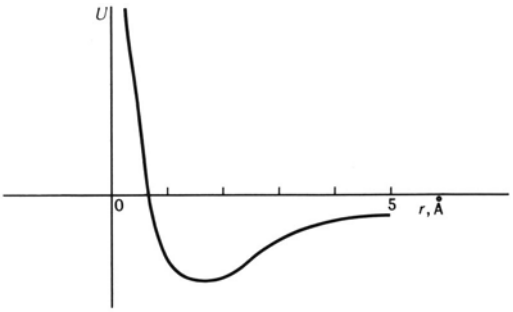

Fig. 1.20. Curve of the potential energy of atomic interaction

the range of interatomic distances from 1.5 to 3.5 Å. At distances of 1–2 Å attraction is changed for vigorous repulsion.

On the other hand, the atoms in a crystal are in the state of thermal vibration. The kinetic energy of vibration of particles with a mass m is equal to $p^2/2m$, where p is the momentum. If this energy exceeds $U(r)$, the bonding forces will be overcome. Thus the condition for the existence of a condensed system, a crystal in particular, can be written as

$$p^2/2m < U(r). \tag{1.4}$$

Condition (1.4) also holds for a liquid. But in the transition from a crystal to a liquid the nature of the order of the atoms changes sharply, because with increasing momenta the average interatomic distances also increase, and the atoms are found more and more often far from the minimum of the curve $U(r)$. In a liquid, some preferred mutual configurations of atoms are formed statistically, but they are destroyed all the time by thermal motion; ordering is lower the higher is the temperature. At 0 K when only zero vibrations of the atoms exist, all the phases are crystalline, with the exception of helium, a most quantum liquid. It is obvious that in a solid the amplitude of vibrations of the atoms is less than the interatomic distance, otherwise they would dominate over the processes of free redistribution – atom migrations – which are characteristic of the liquid state, but which may also exist in crystals as fluctuations.

In the presence of an external pressure, phase states shift towards condensation and crystallization, and substances whose atomic interaction is described by $U(r)$ without a minimum may crystallize. The effect of the pressure is similar to an increase in attraction forces and opposite to the temperature effect.

The simplest approach to the explanation of the periodicity of the atomic structure of crystals consists in consideration of close packings of particles. Strong repulsion at short distances can be interpreted as "mutual nonpenetration" of atoms, so that they can be thought of as rigid spheres ("hard balls"), and the attraction forces can be replaced by an overall effect which brings the spheres closer together, for instance, in the gravity field. Two-dimensional models of this kind (see Fig. 1.5a) yield a regular doubly periodic structure – a planar close packing of spheres. Hence the minimum of the potential energy in the simple case of equal mutually attracted spheres is equivalent to the geometric condition of their closest packing, and in the two-dimensional case such packing exhibits two-dimensional periodicity.

Three-dimensional close packing is obtained by placing two-dimensional close-packed layers upon each another so that the spheres of the next layer fit into the voids between the spheres of the preceding layer. An infinite number of different arrangements of the structure of successive layers is possible. Some of them are periodic in the third direction, i.e., they actually simulate a three-dimensionally periodic structure, while others show no such periodicity. Thus, the principle of the closest packing of identical spheres does not necessarily result in three-dimensional periodicity, although it does admit of it.

In the general form, the problem of finding an equilibrium configuration of a large number of n particles (for a crystal, $n \to \infty$) is the subject of thermodynamics and statistical mechanics.

The free energy F of a system of particles depends on its internal energy U and the entropy part TS (T is the absolute temperature and S, the entropy)

$$F = U - TS. \tag{1.5}$$

The minimum of F corresponds to the most stable state of the system and determines its configuration. A system of n particles is characterized by $6n$ parameters (coordinates and momenta) and by the interaction potentials, which define the internal energy U. In the lowest energy state, at absolute zero, $F = U$, and the state is determined by the minimum of the internal energy, which depends exclusively on coordinates.

The great diversity of forces acting between atoms and the enormous variety of crystalline structures, many of which consist of several sorts of atoms in complicated quantitative ratios, suggest that three-dimensional periodicity in the solid state must be predetermined by most general factors, and its formation is a law of nature.

This can be explained by proceeding from the fact that the minimum of energy of a system as a whole corresponds to that of its constituent parts, due account being taken of their interaction. The state of the system at $T = 0$ then must be unique.

Let us consider the equilibrium system of a very large ("infinitely large") number of uniformly mixed atoms of chemical composition corresponding to a certain compound. We select from the entire volume of this system some small finite volume A, all the atoms of the system being represented in it in the appropriate ratios. Since interatomic forces are mostly short range, the configuration corresponding to the minimum of the energy will be achieved in the volume A, which is comparable with the total volume of the atoms of one or several "chemical formula units" of the given substance.

If we select a volume A' according to the same conditions at a different arbitrary site, the same atomic arrangement must be achieved in A', because only this arrangement corresponds to the minimum of energy. The positions of the atoms in A' must be identical to those in A, not only relative to the atoms of these volumes themselves, but also relative to the entire system as a whole; in particular, the positions of the atoms in volume A' must be identical with respect to the atoms in volume A, and vice versa. In fact, it is sufficient to say that volume A' contains a point which is identical in all respects to some point in volume A, and that there will be an infinite number of such points, because A' can be chosen at infinitely many different positions.

We now see that there is a geometric equivalent of the physical requirement of minimum of energy of the system: the system must be homogeneous and symmetric. That is, certain minimum groups of atoms can all be transformed into one another by symmetry operations, which also must transform the whole

system into itself. Since the number of atoms in a system is infinite, this is possible only when there exist symmetry operations of infinite order, i.e., when they can reproduce indefinitely a certain minimum groups of atoms.

Symmetry operations of infinite order are infinitely small displacements or infinitely small rotations. Atoms or their groups, however, are of definite size, and therefore such operations are inapplicable to them. In other words, the geometric condition of symmetric equivalence in a system containing an infinite number of particles must include the concept of discreteness i.e., of the atomism of crystalline substance, since not all the points of the substance are identical. Thus, points of different atoms or points of the center and the periphery of the same atom are not equivalent.

A symmetry operation of infinite order which ensures discreteness is an operation of discrete, infinitely repeating transfers – translations. Then since the condensed system under review extends in all the three dimensions, it will be three-dimensionally periodic, i.e., crystalline.

The lowest energy state at $T = 0$, which actually is a lattice, is unique. Indeed, according to the third principle of thermodynamics the entropy $S = 0$ at $T = 0$, and the state at $T = 0$ is unique, because $S = \ln N$ (N being the number of states).

Thus, the thermodynamic principle of the minimum of energy of a system consisting of an infinite number of particles can be realized only within the framework of the principle of symmetry and specifically within the framework of three-dimensionally periodic translational symmetry. When $T > 0$ (1.5) receives a contribution from the term TS, and the number of states increases with T. But the principle of translational symmetry ensures the minimum of (1.5) up to certain temperatures, because the atoms vibrate about the equilibrium positions. Here, their thermal motions are interdependent, and their vibrations are realized in the form of plane waves, which are, from the quantum-mechanical point of view, quasi-particles of excitation, phonons. A crystal is characterized by the energy spectrum of elementary excitations. With increasing temperature the excitation level of a crystal depends on the number of quasi-particles in a definite energy state. Accordingly, the energy spectrum has phonon, electron, and other branches.

Consequently, the concept of an ensemble of attracting particles, despite the thermal motion, helps one to understand the origin of three-dimensional periodicity, which simultaneously imparts to the thermal motion itself the specific nature of "lattice" vibrations.

As the temperature increases, the thermal motion disturbs lattice more and more, the possible result being a phase transition into a different structure or melting according to condition (1.4).

Thus, the principle of microhomogeneity of a crystalline substance includes both the principle of symmetry (a crystalline substance contains an infinite number of symmetrically equal points) and the principle of discreteness (not all the points of a crystalline substance are identical). These principles are realized

simultaneously only within the framework of three-dimensional translational symmetry (see Sects. 2.4 and 2.8).

Hence also follows the principle of macroscopic homogeneity. Indeed, macroscopic phenomena and measurements, for instance optical ones, when the wavelength exceeds the lattice periods many times over, or mechanical ones, when the result depends on interaction of a large number of atoms in the specimen, affect a crystal volume containing an enormous number of unit cells; averaging occurs then, as a result of which it is possible to regard a crystalline substance as a continuum.

From the nonequivalence of directions in a space lattice follows the macroscopic principle of anisotropy. Finally, microsymmetry finds its macroscopic expression in the symmetry of the habit of crystals and their properties.

Lastly, we note that the energy gain of three-dimensional periodicity is so great that the lattice "tolerates" most diversified defects – point, linear, etc. (see Fig. 1.5b), even macroinclusions.

The trend towards condensation and crystallization is also observed at a deeper level of organization of a substance. The arrangement of nucleons in nuclei is ordered. Astrophysicists believe the crust of neutron stars to be made of a superdense packing of ^{56}Fe nuclei into a cubic face-centered lattice. Here, quantum-mechanical consideration is necessary, of course – as well, incidentally, as for certain atomic crystals, for instance, "quantum" crystals of solid helium existing near $T = 0$ K and at pressures above 25 bar.

Crystalline structures are defined as systems with a "long-range order". Indeed, knowing the structure of the crystal unit cell we also know, by virtue of three-dimensional periodicity (see Fig. 1.14), how atoms are positioned in any other unit cell and also the mutual arrangement of the atoms of the entire structure, that is of each of its atoms with respect to any other atom spaced at any distance from it.

The crystal lattice contains theoretically an infinite, and practically a very large number of atoms. However, during crystal nucleation, a small number of atoms first gather together. The question arises whether these configurations of a small number of atoms are identical to the configurations of these same atoms in a lattice, under the same conditions of thermodynamics and interaction with the environment. This evidently is not necessarily so in the general case. Energy calculations and some experimental data show that for an ensemble of a small number of atoms the equilibrium configurations may be different from those in a crystal; in particular, they may possess an icosahedral symmetry, which is forbidden in a lattice. Besides, the distances between neighboring pairs of atoms in molecules and in ensembles of a small number of atoms are, as a rule, shorter than in a lattice. This means that the crystal lattice can arise only if there is a sufficient number (of about several tens) of atoms or molecules of a given substance.

1.3 Structures with Distortions of the Three-Dimensional Periodicity. Quasicrystals

Due to the influence of different kinetic factors, the nonequilibrium growth condition and distortions of the ideal composition, etc., the three-dimensional periodicity is not completely fulfilled in some structures. These are, for example, commensurate and incommensurate modulated structures, in which the unit cell size in one, two or three directions gradually changes with a large superperiod. The superperiod can be a multiple of the true period – commensurate modulated structures, or not multiple – incommensurate modulated structures. The superperiod can change under external influences like, e.g., an electrical field.

Some structures, for example SiC, are formed by layers alternating in different order. Layer silicates are built of regularly positioned, two-dimensional rigid networks (2 or 3 kinds are possible) of atoms. Such stable atomic configurations (which can also be one dimensional) are, in a general case, called "modules", and the arising structures "modulated". If there is a uniform alternation of modules in the crystal, such a structure is called a "polytype". Structures both with a regular pattern of modules or their random alternation exist (see also Sect. 5.2).

A new kind of solid possessing distinct 3-d order but without true 3-d periodicity, are quasicrystals. They were discovered in 1984 by *Schechtman, et al.* in an $Al_{86}Mn_{14}$ [1.11], and after that in some other alloys.

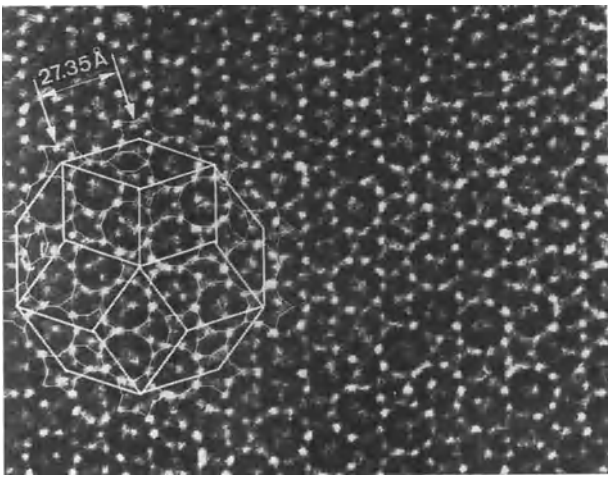

Fig. 1.21. HREM micrograph of the Al-Fe-Cu material of icosahedral structure oriented following a 5-fold zone axis. Projection of the Penrose tiling of 3D-space is shown [1.12]

To the amazement of crystallographers and physicists it was observed that quasicrystals possess icosahedral – with 5-fold axes – symmetry, incompatible with the crystalline lattice (Fig. 1.21). This caused them to recall the geometrical investigation by Penrose of two-dimensional tilings of the plane by two systems of rhombs with the resulting 5-fold symmetry. These ideas were later generalized for the 3-dimensional case. Quasicrystalline, short-range icosahedral order forbids spatial periodicity, but determines a specific spatial quasiperiodicity. Therefore in quasicrystals there is no translation invariance observed in true crystals, but it is possible to describe the structure at long-range distances. The long-range orientational order is also preserved, i.e. neighboring sets of atoms are similarly oriented throughout the whole space (Sect. 5.1).

Evidently the appearance of quasicrystals can be explained by the very strong local interactions between the atoms forming the structure. It makes a true long-range order and, consequently, the three-dimensional periodicity to be non-existent.

1.4 Structural Characteristics of Condensed Phases

We shall now consider the main principles of the structures of condensed phases in general, some of which, such as amorphous solids and many polymer substances, have no space lattices. Indeed, if we assert that the equilibrium state of a solid is a crystalline state, how can we explain the existence of amorphous and glassy bodies?[2]

The answer is simple enough: the amorphous state is not an equilibrium one; it results from kinetic factors and is equivalent to the liquid state from the structural point of view. But this is a supercooled liquid of tremendous viscosity, so that the relaxation times – rearrangement into an equilibrium crystalline structure due to diffusive thermal displacements of atoms – are very large, and often practically infinite. Transition processes for instance the phenomenon of "devitrification", i.e., crystallization of certain glasses, can occasionally be observed.

Liquids and amorphous bodies have no long-range order. At the same time they have a statistical short-range order (Fig. 1.22a). If we take any one of the atoms of such a system, the arrangement of atoms around it can be characterized by the radial-distribution function $W(r)$ (Fig. 1.22b). This function determines the probability of encounter with an atom of a certain type which is at

[2] The terms "amorphous" and "glassy" bodies are equivalent from the structural point of view, although the term "glasses" in its historical connotation is applied to amorphous bodies of high hardness. One point of view has it that glasses are polycrystalline bodies consisting of very fine crystals, possibly of various coexisting phases.

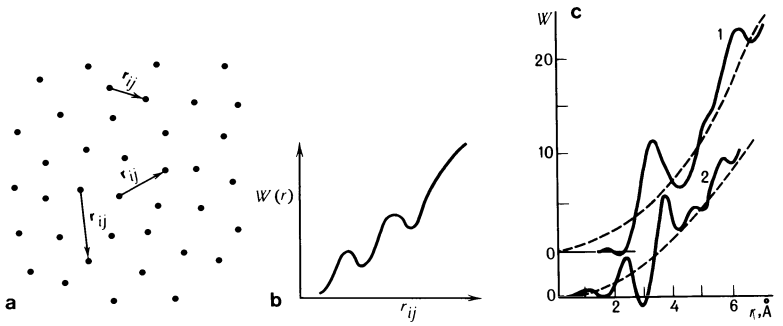

Fig. 1.22a–c. The radial-distribution function.
(**a**) Two-dimensional scheme of atomic arrangement; (**b**) frequency of appearance of certain interatomic distances; (**c**) experimental curves $W(r)$ for liquid tin (*1*) and amorphous selenium (*2*). The dashed line denotes the distribution of the average atomic density, i.e., function $W(r)$ in the absence of a short-range order [1.13]

a distance r from the one under consideration; in particular, it depends on the number of the nearest neighbors and the distance to them. Statistically, the number of first and second nearest neighbors does not necessarily have to be integral; the interatomic distances are not strictly fixed, and the maxima of the distribution functions indicate only most commonly occurring distances (Fig. 1.22c). This does not contradict the fact that within the statistical framework of the short-range order the mutual configurations of atoms in a liquid may be constant to some extent and in some cases close to those in the crystalline structure.

In amorphous solids the statistical short-range order is considered with respect to the space; in liquids, it is considered with respect to both space and time, because in liquids atoms continuously move over distances exceeding the interatomic ones. In amorphous bodies, too, the atoms naturally experience thermal motion, which largely occurs around fixed positions, as in a crystal.

Note that statistically (from a macroscopic point of view) amorphous bodies and liquids are isotropic.

There are substances which are intermediate, with respect to structure, between crystalline and amorphous bodies. These are polymer substances, which consist of long-chain molecules, and liquid crystals. Molecules of polymer substances are built up of stable atomic groups – monomer units linked together into a chain by covalent bonds. If all the units are identical, the molecule possesses strict periodicity in one direction. If the units are nonequivalent, for instance because of various kinds of side radicals, the one-dimensional periodicity is only approximate. When chain molecules are packed in polymer substances the molecules naturally tend to line up parallel to each other. The great length of polymer molecules, the possibility of their entanglement, twisting, and so on, hinder the ordering and crystallization of polymer substances. Therefore, together with equilibrium crystalline structures, polymer substances exhibit various types of ordering, which are sometimes called paracrystalline. The order

in this case is lower than the perfect order in crystals, but higher than the order in liquids. In distinction to amorphous bodies and liquids, polymers may be anisotropic because of the parallelism of stacking.

A remarkable class of substances which strictly correspond to the thermodynamic concept of a phase and exhibit an ordering intermediate between crystalline and liquid (this is also reflected in their name) are *liquid crystals*, or mesomorphic phases. Liquid crystals are fluid, like ordinary liquids, but they are anisotropic. They have a definite temperature range of existence above which they "melt" into an isotropic liquid and below which they crystallize. The properties and structures of liquid crystals are largely determined by the fact that the molecules of the substances of which they are composed have elongated shapes. Two basic types of structure of liquid crystals are known: nematic and

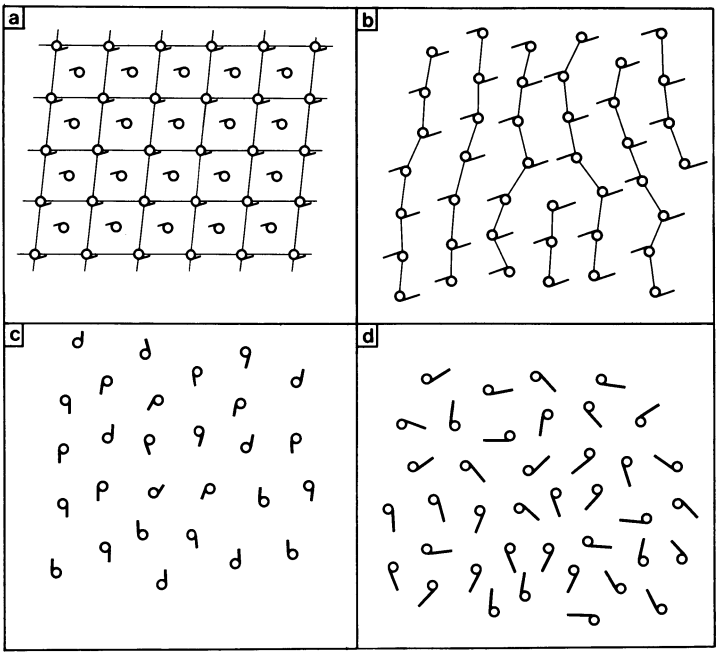

Fig. 1.23a–d. Basic types of condensed systems.
(a) crystal. Atoms, or asymmetric atomic groups, or molecules, are arranged periodically in three dimensions; within the unit cell the atoms or atomic groups are related by operations of non-translational crystallographic symmetry. The system has a long-range order in all directions;
(b) polymer. Along the chain, the atomic groups (molecules) are arranged exactly or approximately periodically and may also be related by other symmetry operations. There is one-dimensional long-range order along the chain. Only short-range order, to some degree or other, is observed in the arrangement of the monomers of neighboring chains;
(c) liquid crystal. Only short-range order exists in the arrangement of the molecular centers; the order is anisotropic, the long molecular axes show an approximately parallel orientation. Statistically the system is cylindrically symmetric;
(d) liquid and amorphous solids. Only an isotropic short-range order exists in the arrangement of the molecular (atomic) centers; the molecules are randomly oriented. The system is statistically spherically symmetric

smectic. In the former, the characteristic of ordering is the parallel arrangement of the molecules, and in the latter, in addition, the molecules are grouped into layers.

The structure of liquid crystals can be described in terms of the concept of statistical translational symmetry.

Thus, apart from the two main types of condensed state – solid (crystalline) and liquid – different states with an intermediate character of atomic order are realized in nature. Figure 1.23 is a schematic representation of the structure of the basic types of condensed systems.

The gradations in the diversified physical properties of condensed systems correspond to the degree of their internal ordering, the highest of which – the space lattice – predetermines all the remarkable features of the crystalline state.

2. Fundamentals of the Theory of Symmetry

Crystals, crystalline substances, are objects in three-dimensional space. Therefore the classical theory of symmetry of crystals is the theory of symmetric transformations of three-dimensional space into itself which are subject to restrictions imposed by the existence of the crystal lattice.

At the same time the theory of symmetry has a wider significance and application. The atoms and molecules, plants, animals, and man himself, man-made machines, and many objects of art are symmetric. Many laws of nature possess symmetry in a certain sense.

It should be mentioned that despite such diverse, extensive manifestations of symmetry in nature and its universality, the theory of symmetry was basically developed and received its logical refinement in crystallography. At the same time, the development of physics in the 20th century deepened the concept of symmetry and expanded its field of application. New extensions of the symmetry concept originated in crystallography itself; in connection with the consideration of certain classes of objects, biological in particular, the theory of noncrystallographic symmetry was developed and applied.

2.1 The Concept of Symmetry

2.1.1 Definition of Symmetry

In view of the above we shall consider the theory of symmetry from a somewhat wider platform than the classical crystallographic standpoint, while giving our principal attention to crystallographic symmetry. In certain problems of crystallography and solid-state physics, such as diffraction theory, it is necessary to introduce functions which are not defined in real three-dimensional space, but which depend on different kinds of variables. For the latter, however, it is possible to introduce formally special spaces of some appropriate dimension. In quantum-mechanical problems, or when considering tensors, and in many other cases, some variables may change not continuously, but take two or more discrete values. For these spaces and functions, definite symmetry regularities also occur.

We have already dwelt on the concept of symmetry. Any object – a geometric figure, a crystal, some function – can be subjected, as a whole, to certain

transformations in the space of the variables describing it. For instance, a geometric object in three-dimensional space can be rotated, displaced, or reflected, but the distance between any pair of points in it remains unchanged. If the object is brought into self-coincidence, is transformed into itself as a result of such a transformation, i.e., if it is invariant to this transformation, it is *symmetric*, and this transformation is a *symmetry transformation*. To emphasize that a transformation converts an object into itself, while the structure of space remains unchanged, such a transformation is called automorphous. A transformation of an object into itself implies that its parts located at one site will coincide, after the transformation, with parts located at another site. This means that the object has (can be divided into) equal parts. Hence the word symmetry, which is the Greek ($\sigma\nu\mu\mu\varepsilon\tau\rho\iota\alpha$) for commensurability.

Here we see a different approach to the definition of symmetry, namely proceeding from the existence of equal parts in the object[1], which are themselves nonsymmetric (asymmetric) in the general case. The equal parts must be mutually positioned not in an arbitrary, but in a regular, manner so that they can be converted into each other by a certain transformation. The two approaches are equivalent.

The very concept of the equality of the properties, parts, or structure requires establishing in what respect, by what features, and at what level the equality is considered. For instance, parts of the object may be geometrically equal, but differ in some physical property, and so on. One can find an adequate mathematical description of this within the framework of the theory of symmetry.

Thus, to put it concisely, symmetry is invariance of objects under some of their transformations in the space of the variables describing them.

This is, of course, not the only definition of symmetry, although it is perhaps the most general one. *Fedorov* [2.1] stated: "symmetry is the property of geometric figures to repeat their parts, or, more precisely, it is the property of figures in different positions to bring them into coincidence with the figure in the initial positions". The statement mentions the repetition, i.e., equality, of parts, while the second part of the formulation actually expresses the principal idea of invariance of an object under transformation.

We shall now consider symmetric transformations in more detail and see how many of them exist and how they are interrelated.

2.1.2 Symmetry Operations

As mentioned before, in considering symmetry in the geometric sense, transformations of the coordinates of the object's space are implied. In a broad sense, symmetry is also considered with respect to any other variables describing the given object. If there are m variables altogether, the region of their variation can

[1] The concept of equality in the theory of symmetry satisfies the general mathematical definition of equivalence, i.e., it includes the conditions of: 1) identity: $a = a$; 2) reflexivity: if $a = b$, then $b = a$; and 3) transitivity: if $a = b$ and $b = c$, then $a = c$.

be regarded as a space of m dimensions with the coordinates of a point in it $x_1, \ldots, x_i, \ldots, x_m$.

The set of coordinates will be denoted by $\boldsymbol{x}$. They may have either identical meanings (as in the three Cartesian coordinates) or distinct ones (for instance, some may mean distances, others angles, while still others, some physical parameters).

Let an operation g perform a certain transformation of the coordinates $\boldsymbol{x}$ of space

$$g[x_1, x_2, \ldots, x_m] = x'_1, x'_2, \ldots, x'_m; \; g[\boldsymbol{x}] = \boldsymbol{x}'. \tag{2.1}$$

We call F a symmetric object (function, figure) and g, a symmetry operation or transformation, provided F does not change when g acts on the initial variables,

$$\begin{aligned} &F(x_1, \ldots, x_m) = F\,(g[x_1, \ldots, x_m]) = F(x'_1, \ldots, x'_m), \\ &F(\boldsymbol{x}) = F[g(\boldsymbol{x})] = F(\boldsymbol{x}'). \end{aligned} \tag{2.2}$$

The formulation (2.1) implies that a method exists for obtaining each variable x'_i from the set of variables x_i. The transformation g may then act on all the variables x_i on which the given function depends, or just on some of them.

For each symmetry transformation g(2.1), which transforms points $\boldsymbol{x}$ to $\boldsymbol{x}'$, there is an inverse transformation g^{-1}, which transforms points $\boldsymbol{x}'$ back to $\boldsymbol{x}$,

$$g^{-1}[\boldsymbol{x}'] = \boldsymbol{x}, \tag{2.3}$$

which, according to (2.2), is also a symmetry transformation.

The identity: transformation $g = e$, which leaves all the variables unaltered, $x_i = x'_i$ is also a symmetry operation according to (2.2).

An object may have several symmetry operations g_i. Two or more consecutively performed identical or different symmetry operations also constitute a symmetry operation according to (2.1,2). Relationships can be established between operations g_i irrespective of their geometric or other meaning. As we shall see below, the set of symmetry operations of a given object is a *group* from the mathematical standpoint.

The theory of symmetry considers both aspects of the problem – the particular meaning of the operations and the general group relations between them.

It should be emphasized that symmetry transformations (2.1, 2) have two equivalent interpretations: as a change in the coordinate system with the object remaining unmoved, or, conversely, as a change in the position of the points of the object in a fixed coordinate system. The formulation (2.1) corresponds to a change in the position of the object's points, the coordinates x_i and x'_i are measured in the system of fixed axes $\boldsymbol{X}(X_1, \ldots, X_m)$. To the first case, there corresponds the transformation of the coordinate system $\boldsymbol{X}$ into $\boldsymbol{X}'$, while the object (all its points) remains unmoved. It is easy to see that the operation of transformation of the coordinate system is $g^{-1}[\boldsymbol{X}] = \boldsymbol{X}'$, i.e., it is inverse to the operation (2.1) of transformation of the object's points $g[\boldsymbol{x}] = \boldsymbol{x}'$. Naturally, it is possible to assume that the initial operation is the transformation of the axes; then the inverse operation is the transformation of the coordinates of the points.

These two interpretations can also be distinguished in the description and perception of symmetry. In one case the object is perceived as static and self-equilibrated. The observer applies a certain measure (coordinate system) to it in different positions, and the object proves identical with respect to these applications. The physical meaning of symmetry consists precisely of this internal equilibrium. In the other case the observer does not move the measure, but he can transform the object, bringing it into self-coincidence. With this approach symmetry operations are more visual, because they can be related to the displacements or other processes the object experiences as a result of the symmetry transformation. Crystallographers often take advantage of this, manipulating all kinds of models. It should be borne in mind, of course, that the "transformation process" itself, although visual enough, is not essential for the understanding of symmetry: the important point is what was "before" and what happened "after" the transformation, i.e., it is the final result that is important.

In this connection we must mention still another essential aspect of description of symmetry. Upon transformation, a symmetric object is indistinguishable from the object in its original position. Then how do we establish the possibility of such a transformation? This is exactly where we need the above-mentioned "external measure". The object must be regarded in relation to the physical or geometric conditions external to it, to its coordinate system, with respect to which their difference can be established for the internally equal parts of the object. A crystallographer with a model in his hands at first marks mentally one of its parts relative to himself and then, bringing the model into self-coincidence in the new position, checks that another part is equal to the first. But the internal, physical content of symmetry as self-equality with respect to some features and properties remains the fundamental principle.

Let us now turn to the geometric properties of symmetry operations.

2.2 Space Transformations

2.2.1 Space, an Object in It, Points of Space

Symmetry operations act on all the coordinates x_i of a space. The object may be finite, occupying part of this space, or it may be infinite, occupying the entire space. It is convenient to speak of symmetry transformation of the whole space into itself, in which a finite or infinite object described by the function, F, is transformed into itself.

The points $\boldsymbol{x}$ and $\boldsymbol{x}'$, which are transformed one into another under a symmetry transformation $g[\boldsymbol{x}]$ (2.1), will be called symmetrically equal points. We denote as "figures" any sets of points: discrete finite or infinite sets, or continuous manifolds – straight or curved lines, segments, various closed or open planes, surfaces, or volumes. Figures will be called symmetrically equal if all the corresponding points of these manifolds are transformed into each other by the specific rule $g[\boldsymbol{x}] = \boldsymbol{x}'$ (and hence $g^{-1}[\boldsymbol{x}'] = \boldsymbol{x}$).

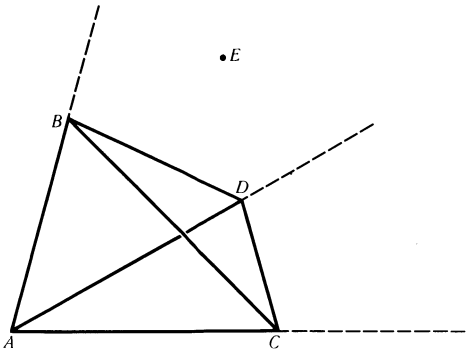

Fig. 2.1. Asymmetric tetrahedron as a label of point A and a coordinate reference for any point E

Symmetry transformations which leave the metric properties of the space unaltered are called isometric. Under these transformations the space is not stretched or twisted, i.e., it is an undeformable whole, so that the distances between any pair of points remain unchanged upon transformation.

Any transformation of an "empty" space is a symmetry transformation. But such an "empty" space has no features by which one can judge whether a transformation has been performed in it. Therefore, when speaking of transformation of a space we imply that it has certain labels which indicate that the space has brought itself into self-coincidence by some transformation or other. In studying concrete objects, crystals in particular, the "physical labels" are the objects themselves or any of their characteristics F: the shape (habit), properties expressed by one function or another, the atomic structure, etc., to which some coordinate system can be assigned.

No point, straight line, or plane (or any number of points lying on them) can serve as a label, because they may remain unmoved in some symmetry transformations. A label rigidly connected with a three-dimensional space may consist of four noncoplanar points A, B, C, and D (Fig. 2.1), the distances between which are different; or of an asymmetric (i.e., having no symmetry) tetrahedron formed by joining these points. Any three edges of this tetrahedron issuing from a common vertex may be regarded as reference axes (with the corresponding axial units). Thus, any point of space E has definite coordinates with respect to these axes, and the space as a whole is uniquely related to such a tetrahedron.

2.2.2 Basic Isometric Transformations of Space

We shall show that any transformation of a space which leaves its metric intact can be reduced to translation (which is parallel transfer), rotation and reflection[2], or to a certain combination of these transformations.

[2] The contents of these elementary operations are clear; their exact definition will be given in Sect. 2.2.3.

To prove this, it will suffice to bring an asymmetric label of space – a tetrahedron – into self-coincidence. Suppose we have two such tetrahedra: $ABCD$ and $A'B'C'D'$, equal to one another, which implies the respective equality of the lengths of all the six edges $AB = A'B'$, etc., and let these tetrahedra be placed anywhere and in any position (Fig. 2.2a). Each point of space can be brought into coincidence with any other point by translation. So we bring points A' and A into coincidence, and the tetrahedron $A'B'C'D'$ will be shifted parallel to itself (Fig. 2.2b). Now, rotating point B' about A, we bring it into coincidence with B (Fig. 2.2c), and rotating then C' about AB, we bring it into coincidence with C (Fig. 2.2d). Point B' could also be brought into coincidence with B, and C' with C simultaneously by rotating the tetrahedron about line q, which is the line of intersection of the planes of triangles $A'B'C'$ and ABC (Fig. 2.2b). In some way or other, triangles $A'B'C'$ and ABC are now brought into coincidence by motions. Distances AD, BD, and CD, $A'D'$, $B'D'$, and $C'D'$ are equal respectively; hence, if the points A, B, C are fixed, only two positions are possible for point D': either coincidence with point D or a position mirror-equal to it with respect to plane ABC (Fig. 2.2d). In the former case the result has already been obtained, and it is obvious that the transformation of the tetrahedron and of the space rigidly connected with it was reduced to motion. In the latter case the result, i.e., the coincidence of the tetrahedra (and of the space), is achieved by an additional operation of reflection of point D' in plane ABC.

These two possibilities correspond to two cases of equality of the initial asymmetric tetrahedra – coincidental or, in other words, *congruent* equality, and *mirror* equality. As to the transformation of space, it satisfies the definition of

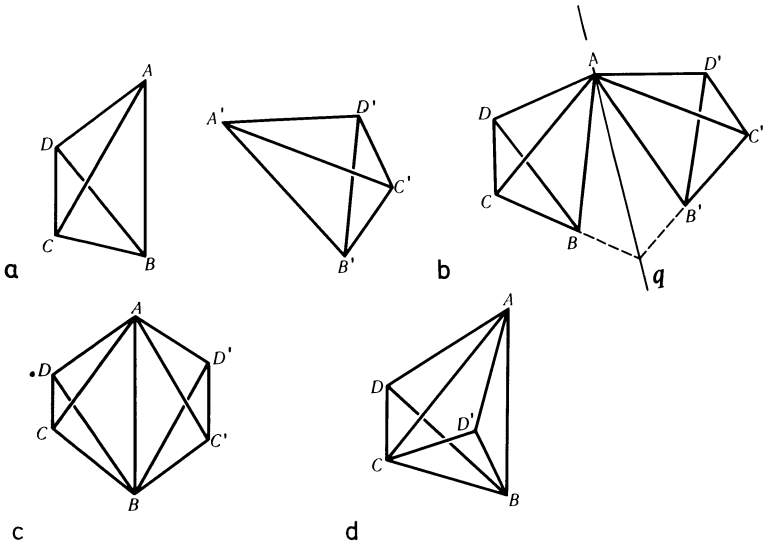

Fig. 2.2a–d. Identical tetrahedra (**a**), brought into coincidence by successive translations (**b**), a rotation (**c**), and a reflection (**d**)

symmetry transformation in both cases. Thus the concept of symmetric equality of figures includes the notion of their congruent and/or mirror equality. Transformations of translation and rotation and their combinations are called transformations of the *first kind*, or *proper motions*, or just *motions*. Transformations which include reflections are called transformations of the *second kind*, or *improper motions*.

When a space or an object contained in it is brought into self-coincidence, the symmetrically equal points are also brought into coincidence. Here it would be appropriate to elaborate on the concept of the point in crystallography and in the theory of symmetry which does not coincide with that in mathematics. We have seen that a point can serve as a label of space, which indicates its orientation when considered together with its environment, and the minimum label of such an environment is three neighboring points which make up an asymmetric tetrahedron together with it. Such a point is called "crystallographic". In distinction to this, a mathematical point x, y, z has no orientation characteristics, but has a maximum symmetry itself: it can be rotated about any axis or reflected in any plane passing through the point at hand, and it remains the same point. Crystallographic points, however, may be (and we shall call them so sometimes) parallel, rotated, or reflected.

The symmetric equality of points in any object can be explained as follows. We select any point in such an object and "view" the object as a whole and all of its parts from this point; then we "view" the object from any point symmetrically equal to it. By virtue of invariance condition (2.2) the pictures will be indistinguishable upon transformation (2.1). This emphasizes the fact that equal points and their sets – parts of symmetric objects – are equal not only in the sense that they can be brought into coincidence by symmetry operations, but also that each of these points or parts is positioned geometrically equally with respect to the set of all the others, i.e., to the object as a whole. During such observations from different symmetrically equal points, however, the observer has either to shift or to turn, maybe upside down, or even "be reflected".

Let us now revert to space transformations and demonstrate the following: any transformation of the first kind is either a translation or a simple or a screw rotation of the space about some axis.

We shall first prove that any motion of a plane which brings it into self-coincidence is either a rotation about one of its points or a translation (Chasles' theorem). We consider two points A and A' together with their two-dimensional asymmetric labels – triangles ABC and $A'B'C'$ (Fig. 2.3). Point A' can evidently be transferred to A by rotating it about any point lying on a perpendicular erected from the midpoint of AA'. We select a point O such that the angle of rotation α about it is equal to the angle between the lines AB and $A'B'$. This actually is the desired point, the Chasles center. If $AB \| A'B'$, then O lies at infinity and the triangles are brought into coincidence by translation.

Consider now two congruent tetrahedra $ABCD$ and $A'B'C'D'$ in three-dimensional space, which are positioned in any way whatsoever (Fig. 2.4). As can be seen from Fig. 2.4, they can be brought into coincidence by transferring

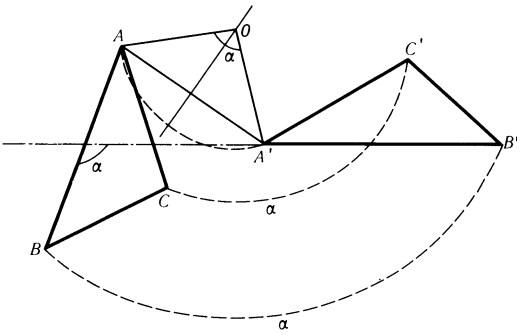

Fig. 2.3. To the derivation of the Chasles theorem

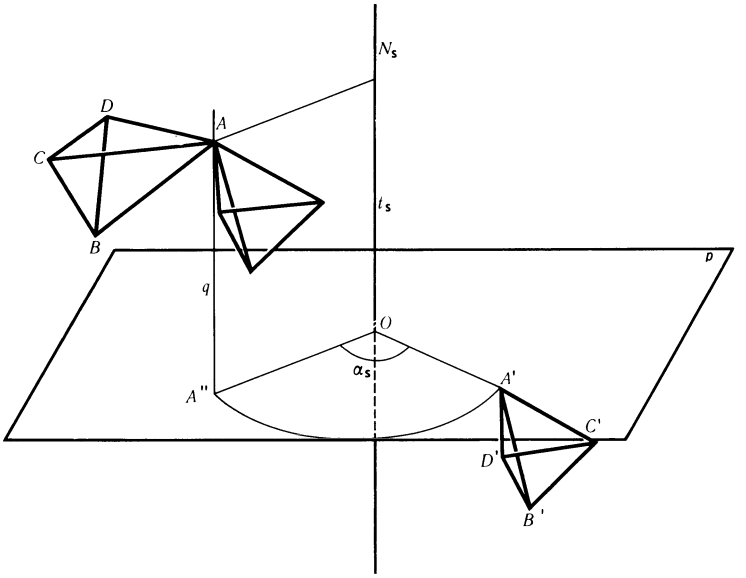

Fig. 2.4. General case of motion (first-kind operation): screw motion about axis N_s (bringing into coincidence arbitrarily positioned tetrahedra $A'B'C'D'$ and $ABCD$)

the second tetrahedron along the vector $A'A$ and rotating it about some axis q. Such a motion, which consists of a translation and a rotation, is called a *screw rotation.* Let us draw a plane p in Fig. 2.4 through A' perpendicularly to axis q; their intersection yields point A''. The Chasles centre O will be found in plane p and will transfer A' to A''; a straight line through it passing parallel to q is the axis of screw rotation N_s with a translational component $t_s = AA''$ and an angular component α_s. If $\alpha_s = 0$, the motion reduces to a translation, and if $t_s = 0$, it reduces to a simple rotation. Thus, a screw rotation (helical motion) is the most general transformation of the first kind, while translations and rotations can be regarded as its particular cases. On the other hand, a screw motion can be decomposed into a rotation and a translation.

We shall now show that any operation of the second kind can be represented as a mirror-rotation operation. Referring to Fig. 2.2 we saw that mirror-equal tetrahedra can be brought into coincidence by a translation, a rotation, and a reflection, and the translation and the rotation axes and the reflection plane were oriented arbitrarily relative to each other. We shall demonstrate that this set of operations can be replaced by a rotation about some definite axis[3] $\tilde{N}_\alpha$ and a reflection in plane m perpendicular to this axis (Fig. 2.5). This operation is called a mirror rotation.

The arrangement of mirror-equal tetrahedra T and T' with respect to $\tilde{N}_\alpha$ and m is as follows: m intersects $\tilde{N}_\alpha$ at a point O such that the distances from any corresponding points (A and A', etc.) to m are equal. By reflecting T' in m we obtain tetrahedron T'', which is congruently equal to T and positioned at the same height, and the projections of T' and T'' onto m coincide and are equal to

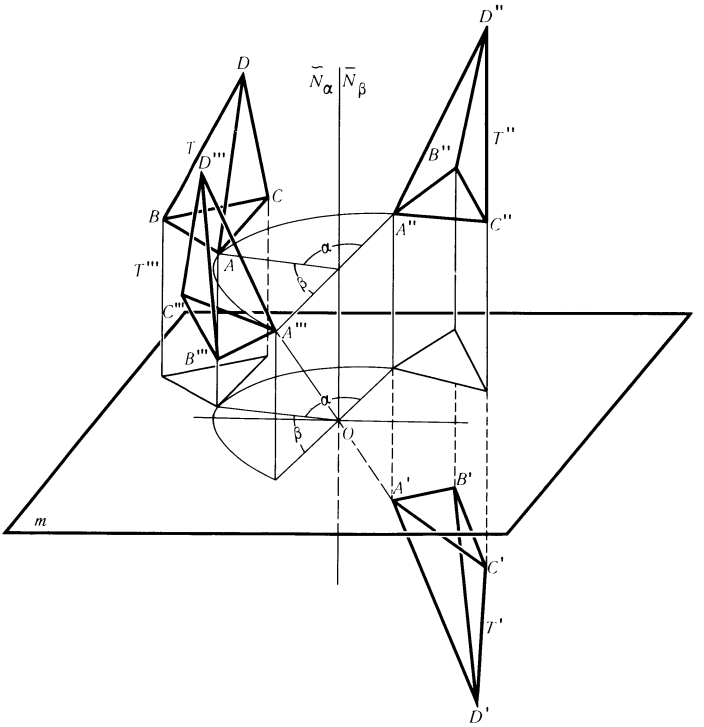

Fig. 2.5. General case of a second-kind operation: a mirror rotation about axis $\tilde{N}_\alpha$ (the same operation – inversion rotation about axis $\tilde{N}_\beta$)

[3] We shall denote symmetry operations and the respective geometric forms – symmetry elements (i.e., axes, planes, etc.) – by identical symbols; for instance, $\tilde{N}_\alpha$ is both an operation of rotation and a rotation axis, m is both a reflection and the plane in which it occurs. Whenever operations have to be distinguished from symmetry elements, special mention will be made.

the projection of T. If we rotate T'' about $\tilde{N}_\alpha$ through angle α, T'' will coincide with T, which is in the final analysis a mirror rotation of T' to T.

Special cases of mirror rotation are simply a reflection in plane m ($\alpha = 0$) (Fig. 2.6a) and a glide reflection a, when $\tilde{N}_\alpha$ is at infinity, and a rotation through α transforms into a translation t along a straight line, parallel to m (Fig. 2.6b).

At $\alpha = \pi$, we have another special case of mirror rotation – *inversion* (denoted by $\bar{1}$) or transformation with respect to the center of symmetry (Fig. 2.6c). This transformation is characterized by the fact that all the lines passing through the center of symmetry O are transformed into themselves, but "reverse" their directions (vectors $\boldsymbol{r}$ are transformed into $-\boldsymbol{r}$), while all the other lines or planes are transformed into lines or planes parallel to themselves and

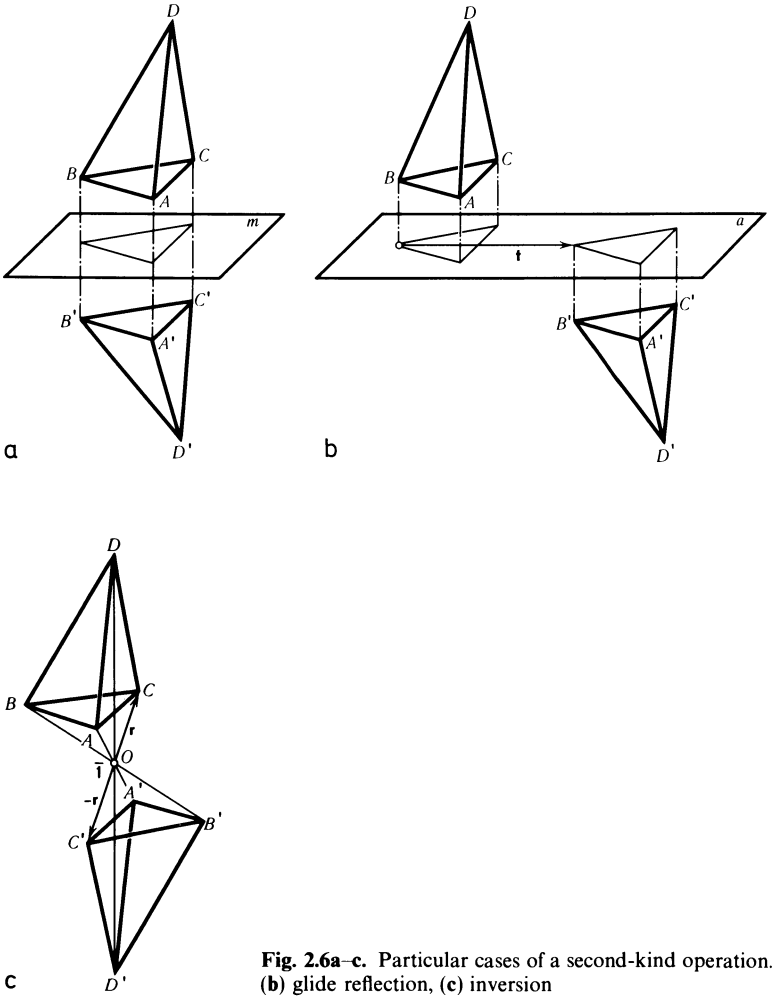

Fig. 2.6a–c. Particular cases of a second-kind operation. (**a**) reflection, (**b**) glide reflection, (**c**) inversion

situated at the same distance from O, but oriented (if we place asymmetric labels on them) oppositely, i.e., they become antiparallel.

Reverting to the general case of mirror rotation, it should be stressed that just as the screw-rotation axis N_s can be chosen in a unique way in the operation of screw displacement for two arbitrarily positioned congruently equal tetrahedra, so for arbitrarily positioned mirror-equal tetrahedra the mirror-rotation axis $\tilde{N}_\alpha$, together with the plane m perpendicular to it is also unique. An exception is inversion $\bar{1}$: any choice of axis $\tilde{N}_\pi$ and a plane m perpendicular to it, which pass through the center of symmetry, yields the same transformation.

The unique position of $\tilde{N}_\alpha$ and m can, in the general case, be found by the construction shown in Fig. 2.7, which is analogous to that of Fig. 2.4 for N_s (cf. Fig. 2.5). At first we must obtain from T' through inversion a tetrahedron T'''' in such a way that T'''' (which is congruent to T') coincides with T through some point, say C. This enables us to construct axis q. Then we construct plane m perpendicular to q and equidistant from the corresponding points of tetrahedra T and T'. From the projections of T and T' onto m we find the Chasles center O on this plane and erect from it the desired axis $\tilde{N}_\alpha$ parallel to q.

Mirror-rotation operations can be represented as operations of *inversion rotations* $\bar{N}_\beta$ (Fig 2.5). Let us perform inversion $\bar{1} = \tilde{N}_\pi$ of tetrahedron T' at point O, which will yield tetrahedron T'''. This operation differs from mirror rotation $\tilde{N}_\alpha$ by an angle $\beta = \alpha - \pi$. Rotate T''' to T through this angle. Thus we obtain the operation of inversion rotation $\bar{N}$, which is equivalent to the mirror rotation of $\tilde{N}_\alpha = \bar{N}_{\alpha-\pi}$. Symmetry theory uses both types of operation.

Thus, the most general operation of the first kind is a screw rotation, and its particular cases are a rotation and a translation. The most general operation of

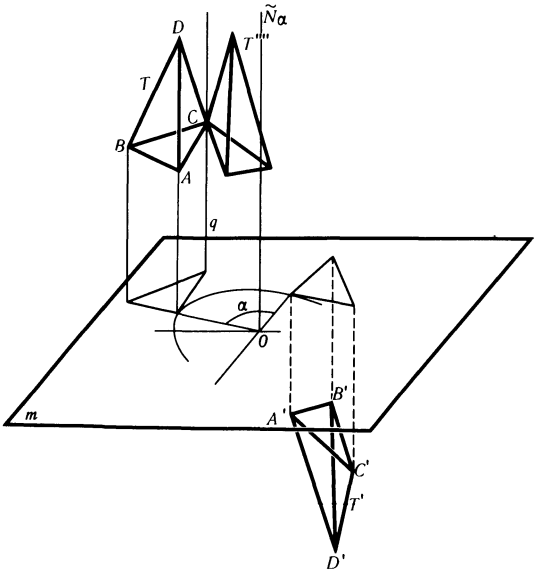

Fig. 2.7. Finding the axis of a mirror (or inversion) rotation

the second kind is a mirror (or inversion) rotation, its particular cases being a reflection, an inversion, and a glide reflection.

These transformations, as we shall see below, are symmetry operations of finite figures only at definite values of their angular components α (namely when $\alpha = 2\pi/n$, n being an integer).

Operations of simple and mirror rotations (and the particular cases of the latter, namely a reflection and an inversion) leave upon the transformation at least one point of space unmoved (invariant); axis N or $\tilde{N}$ passes through it. This point is called a singular[4] point and the operations are called point symmetry operations.

If several differently oriented rotation axes pass through the special point, the set of rotations of the space about them, which transforms this point into itself, will be called rotations, and the set of point symmetry operations of the second kind, improper rotations. Thus, under a symmetry transformation the singular point does not change its position in space, but being considered a crystallographic point it can be rotated and/or reflected into itself.

Operations of translation, screw rotation, and glide reflection contain a translational component; they displace all the points of space, and there are no special points in this case.

2.2.3 Analytical Expression for Symmetry Transformations

Let us choose in space a Cartesian system of coordinates X_1, X_2, X_3 – a right handed system, i.e., such that if we look from the end of axis X_3, a rotation from X_1 to X_2 will be an counterclockwise rotation (Fig. 2.8). The symmetry transformations $g[\boldsymbol{x}]$ of three-dimensional space are described by the following linear equations:

$$\begin{aligned} \boldsymbol{x}' &= g\,[\boldsymbol{x}], \\ x'_1 &= a_{11}x_1 + a_{12}x_2 + a_{13}x_3 + a_1, \\ x'_2 &= a_{21}x_1 + a_{22}x_2 + a_{23}x_3 + a_2, \\ x'_3 &= a_{31}x_1 + a_{32}x_2 + a_{33}x_3 + a_3, \end{aligned} \tag{2.4}$$

which are written in a matrix form

$$x'_i = (a_{ij})\, x_j + a_i \quad (i, j = 1, 2, 3), \tag{2.5}$$

where

$$(a_{ij}) = \begin{bmatrix} a_{11} & a_{12} & a_{13} \\ a_{21} & a_{22} & a_{23} \\ a_{31} & a_{32} & a_{33} \end{bmatrix} = D, \tag{2.6}$$

or in the operator form

$$\boldsymbol{x}' = D\boldsymbol{x} + \boldsymbol{t}. \tag{2.7}$$

[4] The term "special" is also used.

Matrix D describes point symmetry transformations, i.e., simple or mirror rotations, and t is a translation, which is given by components a_i.

We know that a symmetry transformation can also be regarded as a transformation of a reference system X_j into X'_i, the transformation of the point coordinates and the axis transformation being mutually inverse. Therefore the matrix of the transformation of axes (a'_{ij}) will be transposed with respect to (2.6), i.e., it will be the matrix of (a_{ji}), while the values a_{ij} are cosines of the angles between the transformed X'_i and the initial X_j axes. The values a_{ij} satisfy the orthogonality relationships

$$\sum_{j=1,2,3} a_{ij}\, a_{kj} = \begin{cases} 1, & i = k, \\ 0, & i \neq k, \end{cases} \tag{2.8}$$

where only three of them are independent.

The condition of isometricity, i.e., the constancy of the distance between the points under symmetry transformations, has the form

$$|\boldsymbol{x} - \boldsymbol{y}| = \sqrt{(x_1 - y_1)^2 + (x_2 - y_2)^2 + (x_3 - y_3)^2} = |\boldsymbol{x}' - \boldsymbol{y}'|. \tag{2.9}$$

It also ensures the preservation of the angles between the transformed lines or planes. If an isometric transformation is a point transformation, i.e., if it includes no translations, it is called orthogonal. It follows from (2.9) that the determinant of matrix D (2.7) is always equal to $+1$ or -1, i.e.,

$$|D| = |a_{ij}| = \pm 1. \tag{2.10}$$

Let us now consider a concrete form of relations (2.4–7) for the principal space transformations.

A parallel translation implies displacement of all the points $\boldsymbol{x}$ of space in the same direction by the same vector

$$\boldsymbol{x}' = \boldsymbol{x} + \boldsymbol{t}, \quad a_{ii} = 1, \quad a_{ij} = 0 \quad \text{for} \quad i \neq j, \text{ at least one of } a_i \neq 0. \tag{2.11}$$

A rotation of space is the same angular displacement of each of its points relative to the rotation axis. If we choose axis X_3 and, looking from its end at the origin, measure the angles in an counterclockwise direction (Fig. 2.8), then in rotation through angle α in cylindrical coordinates r, φ, x_3

$$r' = r, \quad x'_3 = x_3, \quad \varphi' + \alpha \tag{2.12}$$

and in Cartesian coordinates

$$x'_1 = r\cos\alpha, \quad x'_2 = r\sin\alpha, \quad \varphi' = \varphi + \alpha, \tag{2.13}$$

so that matrix (2.6) has the form

$$\begin{bmatrix} \cos\alpha & -\sin\alpha & 0 \\ \sin\alpha & \cos\alpha & 0 \\ 0 & 0 & 1 \end{bmatrix}. \tag{2.14}$$

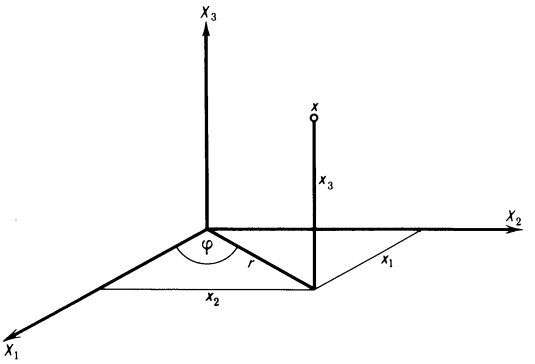

Fig. 2.8. Right-handed system of Cartesian and cylindrical coordinates

A mirror reflection in plane m transfers each point x to a point lying on the other side of this plane, equidistant from it, and situated on the same perpendicular to it. If plane m is plane $X_1\ X_2$, then

$$a_{11} = 1, \quad a_{22} = 1, \quad a_{33} = -1, \quad a_{ij} = 0 \quad \text{for} \quad i \neq j. \tag{2.15}$$

For any mirror rotation about X_3 the matrix will be the same as (2.14), but $a_{33} = -1$. For inversion all $a_{ii} = -1$, $a_{ij} = 0$ for $i \neq j$.

Operations of the first kind – motions – will be denoted by g^{I}, and those of the second kind – improper motions – by g^{II}.

2.2.4 Relationships and Differences Between Operations of the First and Second Kind

Matrices of operations of the first kind g^{I} have a determinant (2.10) equal to +1

$$|a_{ij}|_{g^{\mathrm{I}}} = +1. \tag{2.16}$$

Successive performance (product) of any number q of such operations $g_1^{\mathrm{I}} g_2^{\mathrm{I}} \ldots g_q^{\mathrm{I}} = g_r$ has a determinant

$$|a_{ij}|_{g_r} = (+1)^q = +1. \tag{2.17}$$

Hence the product of any number of operations of the first kind is always an operation of the first kind: $g_r = g_r^{\mathrm{I}}$, i.e., a product of motions is always a motion.

For operations g^{II} of the second kind the determinant (2.10) is always equal to -1,

$$|a_{ij}|\, g^{\mathrm{II}} = -1. \tag{2.18}$$

Comparing (2.17) and (2.18), we can see that no operation of the second kind g^{II} can be obtained by any combination of motions g^{I}. Indeed, by moving an asymmetric figure – a tetrahedron – it is possible to bring it into coincidence only with a congruently equal tetrahedron, but not with a mirror-equal one; the latter would require an operation of the second kind.

A sequence of q operations of the second kind $g_1^{II} g_2^{II} \ldots g_q^{II} = g_r$ has a determinant

$$|a_{ij}|_{g_r} = (-1)q = \begin{cases} +1 & \text{for } q = 2n: \quad g_r^{even} = g^{I}, \quad (2.19) \\ -1 & \text{for } q = 2n+1: \quad g_r^{odd} = g^{II}. \quad (2.20) \end{cases}$$

Consequently, a product of an even number of operations of the second kind g^{II} (2.19) is an operation of the first kind g^{I}. On the other hand, an odd number of such operations g^{II} (2.20) is an operation of the second kind g^{II}, which is not reducible to motions.

The operation of motion g^{I} will always remain such but the result of its action can also be represented as the result of a simultaneous action of an even number of operations g^{II} (2.19).

There are the following simple theorems, which illustrate the above conclusions.

Theorem I. The line of intersection of two planes m and m' at an angle $\alpha/2$ is a rotation axis N_α. Indeed, taking this axis to be perpendicular to the drawing, we can see from Fig. 2.9a that the reflection in m transforms figure T to its mirror reflection T', and the reflection in m' gives a figure T'' congruent to T and rotated through angle α.

Theorem II. Translation t can be obtained by two reflections in planes m spaced by $t/2$, parallel to one another and perpendicular to the translation axis (Fig. 2.9b).

Theorem III (Euler's theorem). A rotation about two intersecting axes N_{α_1} and N_{α_2} is equivalent to a rotation about a third axis N_{α_3}, their resultant (Fig. 2.10). Let us draw a plane m through axes N_{α_1} and N_{α_2}. By Theorem I we replace the action of N_{α_1} by that of planes m and m', the angle between which is equal to $\alpha_1/2$. Similarly, we draw a plane m'' through axis N_{α_2} at an angle $\alpha_2/2$ to m. The successive reflections here are as follows: A in m' gives A', A' in m gives A'' (this is equivalent to a rotation of N_{α_1}). A'', again in m, yields the same A', A' in m'' gives A''' (this is equivalent to N_{α_2}). A''' is congruent to A and rotated about N_{α_3}, which is the line of intersection of planes m' and m''. The rotation angle α_3 is a doubled angle between m' and m'' (note that in the general case several resultant axes may be obtained).

Thus, as we have seen, operations of the first kind can be reduced to an even number of those of the second kind. Of course, the operations of first kind exist and can be introduced irrespective of the operations of the second kind. At the same time it follows from the foregoing that any symmetry operation can be represented as the result of one or more operations of the second kind – mirror reflections.

The existence of the two types of symmetric equality – congruent and mirror – is a fundamental property of our space and of all physical objects, and it plays an important role in crystallography.

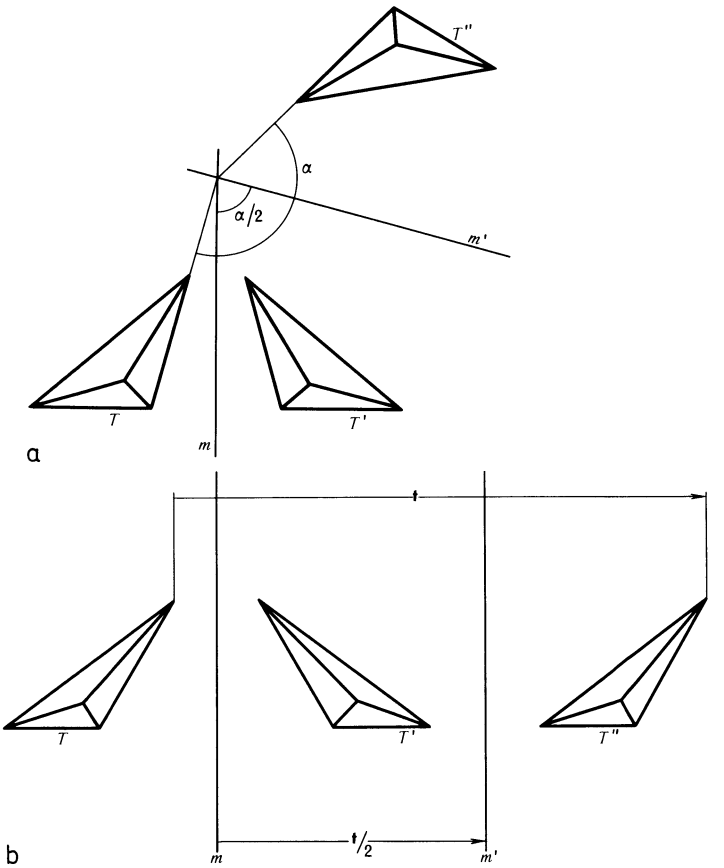

Fig. 2.9a,b. Motion operation as the result of successive reflections in two planes m and m'. (**a**) rotation (planes m and m' intersect, the line of intersection is the rotation axis); (**b**) translation (planes m and m' are parallel)

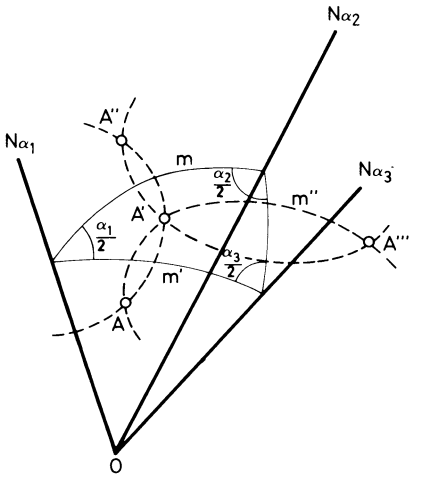

Fig. 2.10. The derivation of Euler's theorem. The continuous arcs show the intersection of the symmetry planes with a sphere of arbitrary radius with center at the point of intersection of the axes

Let us now pass over to possible combinations of symmetry operations and their interaction, i.e., to groups of symmetry operations.

2.3 Fundamentals of Group Theory

2.3.1 Interaction of Operations

Let us consider the point symmetry of a quartz crystal, whose perfect shape is depicted in Fig. 1.10. The figure is brought into self-coincidence under the following symmetry operations:

$$g_0 = e, \quad g_1 = 3, \quad g_2 = 3^2, \quad g_3 = 2_x, \quad g_4 = 2_y, \quad g_5 = 2_u, \tag{2.21}$$

where g_1 is a rotation through an angle $2\pi/3$ in a counterclockwise direction about the axis denoted by 3 in Fig. 1.10; g_2 is a rotation through $2 \times 2\pi/3$ in a counterclockwise direction about axis 3 (or, what is the same, through $2\pi/3$ in a clockwise direction); g_3, g_4, g_5 are rotations through π about the axes denoted by 2_x, 2_y, and 2_u in Fig. 1.10, perpendicular to axis 3 and positioned at an angle of $2\pi/3$ to each other.

Successive performance of two (or more) symmetry operations is also a symmetry operation, since in virtue of conditions (2.1) and (2.2) the object remains unchanged after the first (and each) operation. Thus, in our example, the twice-performed operation g_1 is equivalent to operation g_2, which is recorded as $g_1 g_1 = g_1^2 = g_2$. Similarly, $g_1 g_4 = g_3$, etc. (It is implied that at action $g_i g_j$ operation g_j comes first.) Operations g_1 and g_2 are reverse to one another: $g_1 = g_2^{-1}$; operations g_3, g_4, g_5 are self-inverse: $g_3 = g_3^{-1}$.

The symmetry operation also include the *identity*, or *unit* operation $g_o = e = 1$, which transforms nothing. Geometrically, it corresponds to a state of rest or to a rotation through 2π about any axis and is inherent in any object, including an asymmetric one. Despite the apparent uselessness of the operation e it plays an important part in the formalism of symmetry theory. It is easy to see that the performance of any operation followed by the inverse one is equivalent to a unit operation: $gg^{-1} = e$. The result of several operations may also be reduced to a unit operation. In our example, $g_1 g_2 = e$, $g_1^3 = e$, $g_4^2 = e$, etc. This, as well as the above-discussed general properties of symmetry, show, as we shall see immediately, that from the mathematical point of view a set of symmetry operations is in line with the group concept.

2.3.2 Group Axioms

In mathematical theory of sets, compositions of their elements are considered only from the point of view of their mutual relationships. If in a set of elements

$\{g_1, g_2, \ldots\}$ four definite rules (group axioms) are fulfilled, it is called a group G. The group axioms are formulated thus:

1) in G, the "group operation" – "multiplication" is defined, so that the product of any pair of elements $g_i \in G$ and $g_j \in G$ is an element g_k, which is also contained in G,

$$g_i g_j = g_k \in G; \tag{2.22}$$

2) for any elements of a group the multiplication is associative,

$$g_i(g_j g_l) = (g_i g_j) g_l; \tag{2.23}$$

3) there is a unit element $e \in G$ such that for any $g_i \in G$

$$e g_i = g_i; \tag{2.24}$$

4) for any $g_i \in G$ there is an inverse element g_i^{-1}, so that

$$g_i g_i^{-1} = e. \tag{2.25}$$

From the set of axioms it follows that the unit element is unique and $eg_i = g_i e$, and also that the inverse element is unique, and $g_i^{-1} g_i = g_i g_i^{-1}$.

From the above-discussed properties of symmetry transformations (2.1), (2.2) and the examples it follows that their set satisfies the group axioms, i.e., a set of symmetry operations forms a group.[5] A product of the elements of group $g_i g_j$ is always an element of a group, but the result, generally speaking, depends on the sequence of the elements,

$$g_i g_j \neq g_j g_i. \tag{2.26}$$

When applied to symmetry operations, it means that if their order is changed (firstly either g_i or g_j is performed), the resultant operation may prove to be different. In so-called commutative (or Abelian) groups the result is independent on the sequence of the operations

$$g_i g_j = g_j g_i. \tag{2.27}$$

Thus, the theory of symmetry is actually that of symmetry groups; it makes extensive use of the mathematical techniques of abstract group theory, but assigns a geometric or physical interpretation to each element of the group.

The crystallographic groups have definite designations, which will be discussed in more detail further on. Thus the symmetry group of the shape of quartz (Fig. 1.10) is denoted by 32 (which is read "three-two") or D_3 (D-three).

---

[5] According to the traditional nomenclature symmetry operations g_i are "elements of a group", mathematically speaking. At the same time crystallographers make wide use of the "symmetry element" – axes, planes, etc. – invariant geometric forms associated with the relevant operations. One should take care to make distinction between these terms and to use them correctly.

2.3.3 Principal Properties of Groups

Apart from the symmetry groups there are various other groups with a different concrete meaning of the elements and operations (for instance, a set of real numbers with group action – addition, sets of permutations, etc.). If the geometric, arithmetic, physical, etc. meaning of the group elements is not indicated, then the group G is called abstract.

A group may contain one, several, or an infinite number of elements. The order n of a group is the number of its elements. A group is called finite if n is finite. Thus, group $D_3 = \{g_o = e, g_1, g_2, g_3, g_4, g_5\}$ has order $n = 6$.

An extremely important concept in group theory is *isomorphism*. If mutually unique (one-to-one) correspondence can be established between the elements of two groups so that to the product of any two elements of one of the groups there corresponds the product of the respective elements of the other, these groups are called isomorphous. Thus, groups $G = \{g_1, g_2, \ldots, g_n\}$ and $H = \{h_1, h_2, \ldots, h_n\}$ are isomorphous,

$$G \leftrightarrow H, \quad \text{if } g_i \leftrightarrow h_i, \quad g_j \leftrightarrow h_j, \quad g_i g_j \leftrightarrow h_i h_j. \tag{2.28}$$

If two groups are isomorphous, their orders are the same. For instance, the groups of rotations of space through angles $2\pi/N$ are all isomorphous to a group of n complex numbers $\exp(2\pi i n/N)$, $(0 \leqslant n \leqslant N)$ in which the group operation is complex multiplication.

Isomorphous groups are, from the standpoint of group theory, realizations of one and the same abstract group. Therefore regularities established in abstract groups hold good for all concrete groups isomorphous to them, and this is precisely where the generalizing value of group theory lies.

Since all the regularities reduce to the law of multiplication of elements, the properties of the abstract group G are completely determined by its multiplication table, which is also called Cayley's square. For finite group, this table has the form

	g_1	g_2	$\cdots$	g_n
g_1	g_1^2	$g_1 g_2$	$\cdots$	$g_1 g_n$
g_2	$g_2 g_1$	g_2^2	$\cdots$	$g_2 g_n$
$\vdots$	$\vdots$	$\vdots$		$\vdots$
g_n	$g_n g_1$	$g_n g_2$		g_n^2.

(2.29)

Since $g_i g_j = g_l$, table (2.29) will be assigned if it is indicated to which of the elements $g_1, \ldots, g_n$ each of the n^2 elements $g_i g_j$ is equal. For instance, for the above-discussed group 32 (2.21) the multiplication table is (the operation given in the column is performed first, then the operation in the row)

	e	3	3^2	2_x	2_y	2_y
e	e	3	3^2	2_x	2_y	2_u
3	3	3^2	e	2_y	2_u	2_x
3^2	3^2	e	3	2_u	2_x	2_y
2_x	2_x	2_u	2_y	e	3^2	3
2_y	2_y	2_x	2_u	3	e	3^2
2_u	2_u	2_y	2_x	3^2	3	e.

(2.30)

In symmetry groups their elements – operations – have a concrete geometric meaning. As we shall see below, some distinct symmetry groups, i.e., those differing geometrically (for instance in one of them g_1 is a reflection, while in another, a rotation through π), may have the same multiplication table, i.e., be isomorphous.

Two groups G and H may be in unidirectional correspondence, which is called *homomorphism* and which is not so complete as isomorphism (2.28)

$$G \to H, \quad \begin{matrix} g_{i_1} \searrow \\ g_{i_2} \to h_i, \\ g_{i_k} \nearrow \end{matrix} \quad \begin{matrix} g_{j_1} \searrow \\ g_{j_2} \to h_j, \\ g_{j_k} \nearrow \end{matrix} \quad g_{i_s} g_{j_t} \to h_i h_j \quad (s, t = 1, \ldots, k). \tag{2.31}$$

Group G is of a higher order than H. Several elements $g_{i_1}, g_{i_2} \ldots, g_{i_k} \in G$ are mapped onto one element $h_i \in H$, but the group operation is preserved. For instance, the following mapping of group 32 (2.21) onto the group of numbers $\{1, -1\}$: $g_0, g_1, g_2 \to 1$, $g_3, g_4, g_5 \to -1$ is homomorphous with the group operation, which is the multiplication of these numbers.

Let us briefly consider some other concepts of group theory.

2.3.4 Cyclic Groups, Generators

If a group G contains an element g such that its powers g^l exhaust all the elements of the group, i.e.,

$$G = \{g, g^2, \ldots, g^l, \ldots, g^n = e\}, \tag{2.32}$$

such a group is called cyclic, and its order is equal to n. Such are all the symmetry groups of rotation through $2\pi/n$, which are denoted by C_n. Such an element g_i, whose powers are the other elements of the group, is called a generating element, or a generator. If the group is not cyclic, one can select several elements in it, whose powers and products yield all the n elements of group G.

The definition of a group by a multiplication table (2.29) is pictorial, but redundant. Using generating elements and assigning the defining relationships between them, we also obtain a complete description of the group. Thus, for

group 32 (2.21) the generators may be g_1 and any one of g_3, g_4, g_5; the defining relationships are as follows, cf (2.30):

$$g_1^3 = g_3^2 = (g_1 g_3)^2 = e. \tag{2.33}$$

2.3.5 Subgroup

If it is possible to choose, from the elements g_i ($i = 1, \ldots, n$) of group G, some subset of elements g_k ($k = 1, \ldots, n_k$, $n_k \leqslant n$), which itself forms a group G', i.e., which satisfies all the group axioms (2.22–25); such a subset is called a subgroup of group G, which is recorded as $G' \subset G$.

For instance, group $32 = D_3$ (2.21), (2.30) has subgroup 3 consisting of three elements: g_0, g_1, and g_2, which is a group of rotations though $2\pi/3$ about the vertical axis. The group contains still another subgroup, namely subgroup 2 of rotations through π about the horizontal axis: g_0, g_3 (or g_4, or g_5).

Some groups have no subgroups, except trivial ones: group $e \subset G$ (of order 1) and the group itself: $G \subset G$.

The order of subgroup n_k is the divisor of the order of the finite group n

$$n{:}n_k = p; \tag{2.34}$$

p is called the subgroup index.

One can say that group $G \supset G'$ is a supergroup of G' or that G is an extension of group G'.

2.3.6 Cosets, Conjugates, Classes, Expansion with Respect to a Subgroup

Let G' be a subgroup of G, $G' \subset G$. If element $g_i \in G$ is not contained in the subgroup G', we can form coset $g_i G'$(left), or $G' g_i$ (right) which consists of all the products $g_i g'_j$ (or $g'_j g_i$), where g'_j runs through the elements of G. For instance, in group 32 (2.21) one can take $G' = \{g_0, g_1, g_2\}$, and then the left coset $g_3 G'$ will consist, according to the multiplication table (2.30), of elements $\{g_3, g_4, g_5\}$, and group G can be expanded with respect to the subgroup G' by representing G in the form of the union (symbol $\cup$) of the cosets of G'

$$G = g_0 G' \cup g_1 G' \cup \ldots \cup g_p G' \tag{2.35}$$

This formula can also be regarded as an extension of the group G' to G. Note that, with given G and G', the systems of cosets $\{g_0, g_1, \ldots, g_p\}$ can be chosen in different ways.

An element of group g is said to be conjugate to element g_k if G contains an element g_j such that

$$g_k = g_j^{-1} g_i g_j. \tag{3.36}$$

Thus, in group 32 elements g_3 and g_4 are conjugate: $g_2^{-1} g_3 g_2 = g_4$. If we fix g_i and take all $g_j \in G$ in (2.36), then a collection of (distinct) g_k forms a class of conjugate elements. Group 32 has three such classes: $\{g_0\}$, $\{g_1, g_2\}$, $\{g_3, g_4, g_5\}$.

Subgroup H of group G is called an invariant subgroup or a normal divisor if element $h_k = g_i^{-1} h_j g_i \in H$ for any $g_i \in G$ and $h_j, h_k \in H$, i.e., if H forms a class of conjugate elements in G,

$$H = g_i^{-1} H g_i. \tag{2.37}$$

In group 32, subgroup $\{e, g_1, g_2\}$ is normal, while $\{e, g_3\}$ is not.

The normal divisor H of group G is used to introduce the factor-group concept. We form cosets $g_i H (= H g_i)$ by virtue of (2.37). A factor group is denoted by

$$G/H \tag{2.38}$$

and is a group whose elements are the cosets themselves together with $H = g_0 H$. The multiplication table for a factor group, with due regard for the rule of class multiplication,

$$(g_i H)(g_j H) = g_i g_j H, \tag{2.39}$$

has the form

	$g_0 H$	...	$g_p H$
$g_0 H$	$g_0^2 H$	...	$g_0 g_p H$
$\vdots$			
$g_p H$	$g_p g_0 H$	...	$g_p^2 H.$

(2.40)

The order of a factor group is equal to the index of H in G. The factor-group concept is used in analyzing the relationship between space and point symmetry groups and in a number of other cases.

2.3.7 Group Products

Two groups H and K, of which all elements, except the unit element $h_0 = e = k_0$, are distinct, can be arranged into new groups G.

Group $G = H \otimes K$ is called the *external direct product* of H and K if each element $g \in G$ can be written as the product $g = hk$. The multiplication law is

$$h_i g_j \otimes h_k g_l = h_i h_k g_j g_l. \tag{2.41}$$

Both initial groups are invariant subgroups, i.e., normal divisors of the newly formed group G.

Group $G = H \circledS K$ is called the *semidirect* product of groups H and K if all g can be expressed as $g = hk$, $kH = Hk$.

The multiplication law is

$$h_i g_j \circledS h_k g_l = h_i (g_j h_k g_j^{-1}) g_j g_l. \tag{2.42}$$

In this case the invariant subgroup – the normal divisor of G – is only subgroup H (it stands first in the semidirect product).

New symmetry groups can be obtained by using direct or semidirect products and also by considering the subgroups of these products. Let us discuss the following example. We take a group of one-dimensional translations T_1 on a plane. This group is infinite but can be assigned a *basis* $\{0, t\}$, where t is a translation whose repetition assigns the other elements of the group: $2t$, $3t, \ldots$ (Fig. 2.11a). Let us form its semidirect product with the point group of reflection $M = \{e, m\}$, so that the line of reflection is parallel to the translation axis (Fig. 2.11b). The product is

$$G = T_1 M = \{0, t, 2t, \ldots\} \circledS \{e, m\} = \{0e, te, 2te, \ldots, 0m, tm, 2tm, \ldots\}. \tag{2.43}$$

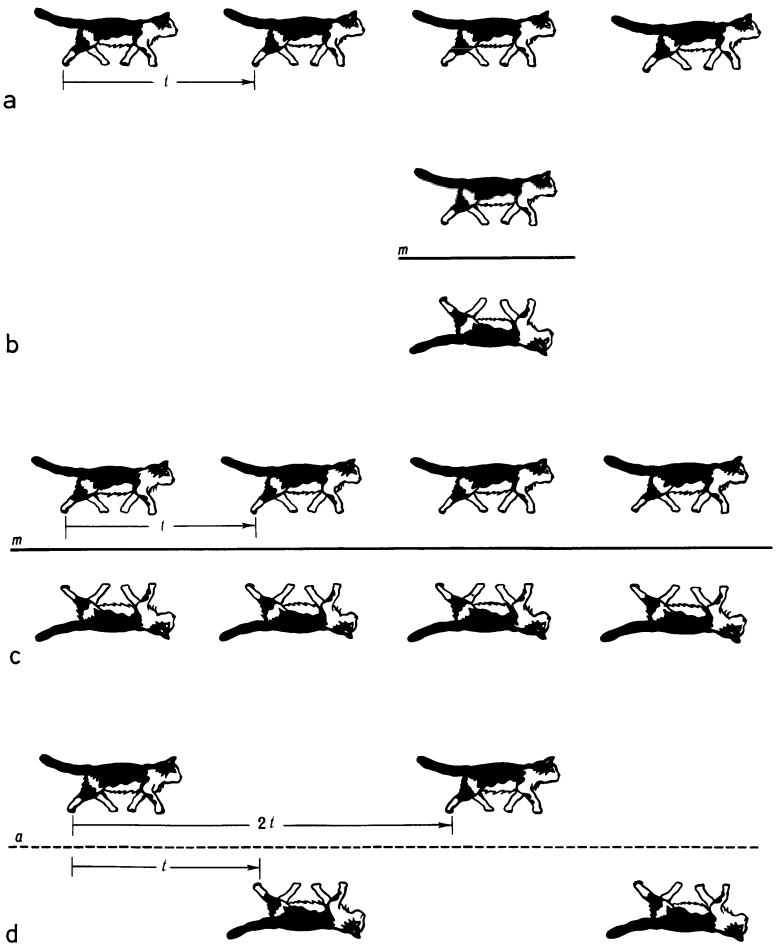

Fig. 2.11a–d. Formation of a product of groups and singling out of a nontrivial subgroup from it. (**a**) Translation group of an arbitrary figure; (**b**) reflection group; (**c**) their product (symmorphous group); (**d**) nontrivial subgroup of the product: the glide-reflection group (non-symmorphous)

Each of the initial groups T_1 and M can be called a trivial subgroup (divisor) of the new group. The new group T_1 Ⓢ M (Fig. 2.11c) contains a new element $tm = a$, a glide – reflection operation. It turns out that in this group we can now isolate a subgroup which does not coincide with its trivial subgroups T_1 and M. This subgroup is: $A = \{0e, 2te, \ldots, 0a, 2ta, \ldots\}$ (Fig. 2.11d). Thus, new symmetry operations of the type $a = tm$, obtained by composing different geometrical operations – elements of both initial groups T and M – can exist independently within the framework of the new group, the nontrivial subgroup $A \subset T_1$ Ⓢ M of the product of the two groups. In crystallography, groups of the type T_1 Ⓢ M, obtained as group products, are called symmorphous, and their nontrivial subgroups of the type A, nonsymmorphous groups.

2.3.8 Group Representations

Each group G is characterized by the multiplication table of its elements g_i. If the elements are represented by some numbers, symbols, functions, etc., which have an identical multiplication table, this is an exact, or faithful, i.e., isomorphous, representation of group G. In a homomorphous mapping, $G \to H$, the order of the group of representation H is less than that of G and is its divisor. In group theory in general, and in the theory of symmetry groups in particular, the main role is played by representations Γ of groups G by square matrices $M(G)$,

$$M(G) = \begin{bmatrix} a_{11} & a_{12} & \ldots & a_{1n} \\ a_{21} & a_{22} & \ldots & a_{2n} \\ \vdots & \vdots & & \vdots \\ a_{n1} & a_{n2} & \ldots & a_{nn} \end{bmatrix} = (a_{ij}), \tag{2.44}$$

where the a_{ij} are real or complex numbers. To the multiplication of elements G there corresponds multiplication of matrices, which is performed according to the matrix multiplication rule

$$\sum_j a_{ij} a_{jk} = c_{ik}. \tag{2.45}$$

Matrix multiplication is governed by group axioms. The unit element is represented by a unit matrix, for which $a_{ij} = 0$, $a_{ii} = 1$. A trivial representation of any group is the representation of all its elements by unity, i.e., by a matrix of order one, $M = a_{11} = 1$. Homomorphous representations $G \to H$ are possible where the order of group H, represented by Γ, is less than that of group G. An exact-isomorphous representation is possible, where $G \leftrightarrow H$.

Thus, a point group can be represented by a set of three-dimensional matrices $D_k = (a_{ij})_k$ (2.6) of transformations of coordinates on the basis (X_1, X_2, X_3); each of the matrices D_k corresponds to a definite operation g_k of this group (so-called vector representation, of dimension three)

$$g_k \leftrightarrow (a_{ij})_k, \quad G = \{g_1, g_2, \ldots\} \leftrightarrow \{D_1, D_2, \ldots\} = D. \tag{2.46}$$

According to the matrix multiplication rules the multiplication table of these matrices corresponds to that of elements g_k. Different representations of the same group G can be obtained by choosing a certain matrix S and forming products SDS^{-1} with the initial representation. If it is found that for two representations $\Gamma_a(D_1, D_2, \ldots)$ and $\Gamma_b(D_1, D_2, \ldots)$ the condition

$$SD_kS^{-1} = D_k' \tag{2.47}$$

is fulfilled, these two representations are called equivalent, while S in this case defines the linear transformation of the basis.

Any square matrix can be represented thus:

$$\begin{array}{c|c} A_1 & B_2 \\ \hline B_1 & A_2 \end{array}, \tag{2.48}$$

where A_1 and A_2 are square matrices. A transformation by S may result in such matrices in which $B_1, B_2 = 0$, and the block-diagonal matrices A_1 and A_2 have a smaller dimensionality. This kind of representation is called reducible.

If this cannot be achieved by any transformation S, i.e., $B_1 \neq 0$ or $B_2 \neq 0$, the representation is called irreducible.

If three-dimensional matrices can be reduced in this way to matrices composed of two- or one-dimensional irreducible blocks A, the group will be represented more economically. For instance, there is the following exact two-dimensional irreducible unitary representation for group 32 (2.21, 30):

$$\begin{matrix} g_0 & g_1 & g_2 & g_3 \end{matrix}$$
$$\begin{bmatrix} 1 & 0 \\ 0 & 1 \end{bmatrix} \begin{bmatrix} 0 & 1 \\ -1 & -1 \end{bmatrix} \begin{bmatrix} -1 & -1 \\ 1 & 0 \end{bmatrix} \begin{bmatrix} 1 & 0 \\ -1 & -1 \end{bmatrix} \tag{2.49}$$
$$\begin{matrix} g_4 & g_5 \end{matrix}$$
$$\begin{bmatrix} -1 & -1 \\ 0 & 1 \end{bmatrix} \begin{bmatrix} 0 & 1 \\ 1 & 0 \end{bmatrix},$$

and a one-dimensional representation, but no longer exact (homomorphous mapping of the group):

$$\begin{matrix} g_0 & g_1 & g_2 & g_3 & g_4 & g_5 \\ 1 & 1 & 1 & -1 & -1 & -1. \end{matrix} \tag{2.50}$$

The sum of the diagonal elements – the trace of the representation matrix

$$\sum a_{ii} = \chi(g) \tag{2.51}$$

– is called the character of the representation of the group element. It is easy to see that $\chi(g_0)$ determines the dimensionality of the representation. The characters of all the equivalent representations are the same. One and the same group may have several irreducible representations; for finite groups their number is equal to the number of classes of the conjugate elements in the group.

An analysis of symmetry group representations suggests a number of conclusions concerning their relationships. At the same time it enables one to reveal

the deeper meaning and regularities in the symmetry concept itself. Thus, the group of transformations (2.1), which is governed by the group axioms (2.22–25), was introduced in relation to the symmetry condition (2.2) for self-coincidence of a function upon transformation. It is, however, possible to perform group transformations on any asymmetric objects or functions and see which symmetric properties they contain (we shall return to this in Sect. 2.9).

Since group representations contain concise information about all their properties, they serve as an important tool for investigating the properties of symmetric physical systems: atoms, molecules, crystals, and the spaces of physical values both in classical and quantum-mechanical problems. It is possible, not only to analyze the "static" symmetry of these systems or spaces, but also to investigate their possible changes in dynamics or under external effects. The representations of symmetry point groups will be discussed in Sect. 2.6.

2.4 Types of Symmetry Groups and Their Properties

2.4.1 Homogeneity, Inhomogeneity, and Discreteness of Space

Groups of space symmetry can be divided into types which are defined by the homogeneity or inhomogeneity of space and its subspaces of smaller dimensionality, i.e., planes or straight lines in three-dimensional space.

The concept of space homogeneity can be formulated for two cases – infinite continuous space and infinite discrete space. Examples of the former are an empty Euclidean space and an anisotropic crystalline substance considered as a continuum from the macroscopic point of view. An example of the latter is a crystalline substance considered at the microscopic level; its atomicity is actually expressed by the geometric condition of discreteness.

In both cases the space consists of an infinite number of symmetrically equal points. But a continuous space is a continuum of only such points: all its points are symmetrically equal. In a discrete space, not all the points are symmetrically equal.

The geometric postulate of microhomogeneity ("discrete homogeneity") can be formulated as follows:

a) there exists a sphere of a radius R, which may be chosen at any place in space; there will be within it a point $\boldsymbol{x}'$ symmetrically equal to any preassigned point $\boldsymbol{x}$ of space (homogeneity);
b) there exist in space such points (at least one point $\boldsymbol{x}$) that around them, within a sphere of radius r, there is not a single point symmetrically equal to them (discreteness).

The requirement *a*) means that there is an operation $g[\boldsymbol{x}] = \boldsymbol{x}'$ satisfying the symmetry condition $F(\boldsymbol{x}) = F(\boldsymbol{x}')$ (2.1, 2), and

$$|\boldsymbol{\tau} - (\boldsymbol{x}' - \boldsymbol{x})| < R, \tag{2.52}$$

where τ is an arbitary vector (Fig. 2.12a): it may be equal to zero or be infinitely small, or indefinitely large, and arbitrarily directed. Since there is an indefinitely large number of symmetrically equal points, there is also an indefinitely large number of operations g, and therefore $G \ni g$ is a group of infinite order. According to the general definition of symmetry (2.1, 2), each operation g transforming a given point x to x' also transforms any other point of space to one symmetric to it, i.e., it transforms the entire space into itself.

The requirement *b*) is written

$$|x - x''| < r, \tag{2.53}$$

where x is a certain point, and x'' is not derivable from x by any operation $g \in G$ (Fig. 2.12b).

Both these requirements, taken together, can be reformulated as a requirement for the finiteness of the fundamental (independent) region, or *stereon.* Such a region is a part of space consisting of symmetrically unequal points[6] (see Sect. 2.5). Then its finiteness – it is not infinitely small – ensures the fulfillment of condition *b*). On the other hand it is not infinitely large and hence there are points outside it which are symmetrically equal to the points within the region [(condition *a*)].

Since within a sphere r with center at point x there are no points symmetrically equal to it, then always

$$R > r/2. \tag{2.54}$$

If we take any point, then, within a sphere R, contacting it, there is a point equal to it, and therefore the distance d between the closest equal points

$$d < 2R. \tag{2.55}$$

This means that any equal points can be joined by a broken line with vertices at the equal points, whose links are less than $2R$.

We have considered the (r, R) conditions (2.52, 53) and their corollaries (2.54, 55) in a space with symmetrically equal points which thus can be described by some group G of infinite order.

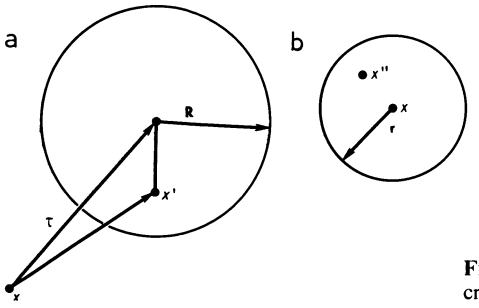

Fig. 2.12a,b. Homogeneity sphere (**a**) and discreteness sphere (**b**)

[6] Terms "fundamental cell", or " asymmetric unit" are also used – see Sect. 2.5.5.

It is worth noting that there may exist point systems satisfying the (r, R) conditions, but not describable by any group. Let us consider, for instance, a system of points – centers of molecules in a liquid. This is a discretely homogeneous (r, R) system which, incidentally, has approximately the same values of r and R as a crystal. A gas is also a homogeneous system, but with R larger than in a liquid. However, a symmetry group cannot be assigned in these systems and, knowing the position of one point, we cannot find those of the others.

For (r, R) systems described by a group we defined the concept of symmetric equality of their points. In (r, R) systems which cannot be described by a symmetry group, it is also necessary to indicate in what sense the points are equal. One can speak only of geometric points, as in the example with the centers of molecules in a liquid. In the case of a liquid crystal one can already speak of "oriented" points satisfying the (r, R) condition, since the elongated molecules are here approximately parallel to each other.

2.4.2 Types of Symmetry Groups and Their Periodicity

A homogeneous discrete symmetric space is described by the (r, R) condition (2.52, 53) and by a group G. We have not yet established, however, which particular operations $g_i \in G$ are possible here, and which of them are obligatory.

The existence of translations is clearly consistent with the (r, R) condition. It would suffice if the largest translation a_i were smaller than $2R$ (2.55). But, as we shall see below, the inverse statement is also true: group G with the (r, R) condition always contains a translation subgroup T

$$G_{(r,R)} \supset T. \tag{2.56}$$

This is Schönflies' theorem.

In a continuous homogeneous space conditions (2.52, 53) become

$$R \to 0, r \to 0. \tag{2.57}$$

This means that the fundamental region shrinks to a point. The subgroup of discrete parallel translations (2.56) turns into a continuous group of infinitesimal translations $T_\tau (\tau \to 0)$, i.e., all the points of a continuous homogeneous space are translationally equal. As in the case of a discrete space, group $G \supset T_\tau$ may also contain other symmetry operations, including infinitely small rotations in a space of $m \geqslant 2$ dimensions.

A homogeneous space has discrete or infinitesimal translations in all of its m dimensions. Cases are possible where the space is inhomogeneous, but in a subspace of $n (< m)$ of its dimensions the homogeneity condition is fulfilled [at $n = 2$ or 1 the spheres mentioned in the microhomogeneity postulate (2.52, 53) are replaced by circles and segments, respectively]. If a space has no homogeneous subspaces ($n = 0$), it is fully inhomogeneous.

The types of symmetry groups corresponding to these cases will be denoted by G_n^m, $m \geqslant n$, which implies, unless otherwise stipulated, discrete groups, i.e.,

groups periodic in n dimensions. Thus, in three-dimensional space, G_3^3 are space groups; G_2^3, layer groups; G_1^3, rod groups; and G_0^3, point groups. Finite (in all dimensions) figures in three-dimensional space, i.e., figures occupying only part of the space, are therefore inconsistent with the homogeneity condition and hence are described by groups G_0^3. Groups G_1^3 are used for describing figures infinitely extended in one direction and finite in two directions, and G_2^3, for figures infinitely extended in two directions and finite in one direction. Groups G_3^3 describe crystals[7] as infinite objects – structures periodic in three dimensions. As we shall see below, in groups G_2^3 at least one plane remains invariant, i.e. it transforms into itself in all symmetry operations; in G_1^3 one straight line, and in G_0^3 one point. Such planes, lines, and points are called singular. In two-dimensional space, groups G_2^2, G_1^2, and G_0^2 are possible, and in one-dimensional space, G_1^1 and G_0^1.

If a group possesses operations of the second kind, it is called a group of the second kind G^{II}; if a group has only operations of the first kind, it is called a group of the first kind G^{I}.

The following is true: each group G necessarily contains a subgroup of all of its motions; in particular, G^{II} contains subgroup G^{I}

$$G^{I} \supset G^{I},\ G^{II} \supset G^{I},\ G \supset G^{I}. \tag{2.58}$$

Indeed, G^{I} consists only of motions. Any group G^{II} also contains operations of the first kind g^{I} (at least $e = g^{I}$, but there may be other g^{I} as well). Then, by compiling a multiplication table for $G^{II} = \{ \ldots g_i^{I} \ldots, \ldots g_k^{II} \ldots \}$, due account being taken of (2.17, 19, 20), we obtain

	g_i^{I}	g_k^{II}
g_i^{I}	g_j^{I}	g_l^{II}
g_k^{II}	g_f^{II}	g_h^{I}

(2.59)

We can see that all the g_i^{I} form group G^{I}; the upper left-hand square retains only the results of their interaction $\{\ldots g_j^{I} \ldots\}$. The elements g_k^{II} do not form a group, since their products $g_k^{II}\, g_{k'}^{II} = \{\ldots g_h^{I} \ldots\} \in G^{I}$.

G^{I} is a subgroup of G^{II} of index 2, since to each operation $g_j^{I} \in G$ there corresponds an operation $g_l^{II} = g_j^{I} g_k^{II}$.

Thus, from (2.58) it follows that in order to establish whether some group or other has a translation subgroup, it will suffice to ascertain that its motion subgroup contains a translation subgroup

$$G \supset G^{I} \supset T_n\{t_1, \ldots, t_n\}. \tag{2.60}$$

Another point is as follows. Operations g_i of groups G describing a homogeneous space may either themselves be rotations of both kinds, i.e., simple or inversion ones, or contain rotational components of both kinds (screw axes,

[7] Naturally, when considering the atomic structure of crystals we abstract ourselves from the boundedness of a piece of crystalline substance in space and assume it infinitely extended.

glide reflections), but they may not contain these components (translations). With products of operations $g_i g_k$, which have rotations or rotational components, these components act exclusively on one another. In this case, if translational components are present as well, they also act, but yielding only parallel displacements of points of space. Thus, rotations (rotational components) of both kinds of groups G of a homogeneous space themselves form a group

$$G_{\text{rot}} = K. \tag{2.61}$$

We shall see later that it is a crystallographic point group.

Let us now consider space groups of different dimensionalities.

2.4.3 One-Dimensional Groups G^1

If a one-dimensional space, which is a straight line, is inhomogeneous, it has a special point and the corresponding groups are G_0^1. Here, the only symmetry operation, with the exception of identity $g_0 = e$, is inversion $\bar{1}$ (which is a reflection m in a point). So, only two groups of type G_0^1 exist: 1 and $\bar{1}$.

In a one-dimensional homogeneous space, for any point A in an adjacent segment of length $2R$ there is, by (2.52), a point A' symmetrically equal to it with respect to group G^1 (2.54) (Fig. 2.13a). But this implies parallelism, i.e., translational equality of A' and A and the existence of an operation of translation t along a straight line. A repetition of this operation will thus give an infinite row of regularly spaced points (Fig. 2.13b). The corresponding group is infinite, cyclic,

$$T_1 = \{\ldots t^{-i}, \ldots, t^{-1}, t^0, t^1, \ldots, t^i, \ldots\}, \quad i = 0, 1, \ldots, \infty.$$

Besides group $T_1 = G^1$, in one-dimensional homogeneous space there exists one group G^{II}: in addition to t it contains elements $\bar{1}$.

Group T_1, which is regarded as an abstract group, is unique. But from the standpoint of metric properties of space, taking into account the magnitude of period $t = a$, it has an infinite number of realizations, and each of them can be obtained from any other by a homogeneous affine deformation – extension or contraction of a straight line. Besides, each group $T_1 \ni t$ contains a subgroup with translation pt, p being an arbitrary integer: $T_t \supset T_{pt}$. Abstractly, they are isomorphous: $T_t \leftrightarrow T_{pt}$. If we neglect the discreteness requirements (2.53), the straight line is a continuum; it also admits of infinitely small translations $\tau \to 0$, to which a continuous limiting group T_τ corresponds. Metrically, its subgroup is any group $T_\tau \supset T_t \supset T_{pt}$.

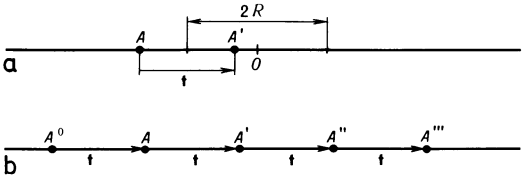

Fig. 2.13a,b One-dimensional space. (**a**) point A' symmetrically equal to A; (**b**) origin of a translation group

One-dimensional space is either inhomogeneous or homogeneous, and hence it has no other groups except G_0^1 and G_1^1.

2.4.4 Two-Dimensional Groups G^2

These groups are groups of transformations of two-dimensional space, which is a plane, into itself. If this space is inhomogeneous, it contains a singular point, and the groups are G_0^2 point groups.

Let us choose in this space some direction and assign along it an operation (and hence a group) of one-dimensional translation t (Fig. 2.14a). Thus, there exist groups of type G_1^2. There is no periodicity along any other direction. Along the singular direction t microhomogeneity conditions (one-dimensional) (2.52, 53) hold true. An example of such a space is given in Fig. 2.14b.

We shall now assign, in a space $m = 2$, two noncollinear vectors of translations t_1 and t_2. In this way we obtain group T_2 if type G_2^2, which will transform any point into a twice-periodic array of points – a plane net or a two-dimensional lattice (Fig. 2.15a). This space is homogeneous and discrete.

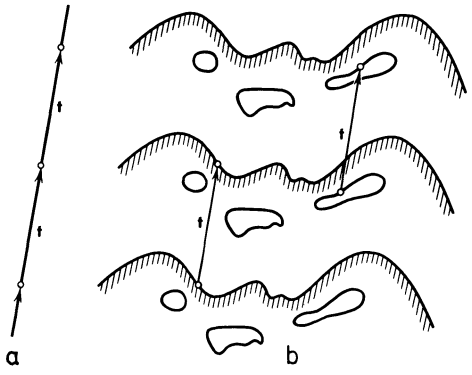

Fig. 2.14a,b. Two-dimensional space. (**a**) group of one-dimensional translation in it; (**b**) example of such a space with one-dimensional periodicity

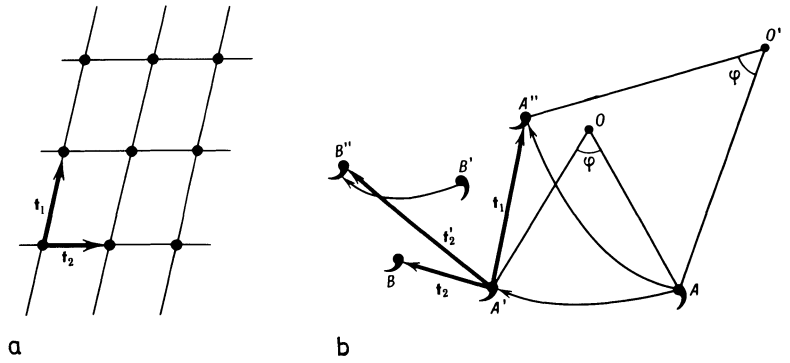

Fig. 2.15a,b. Twice-periodic two-dimensional space. (**a**) translation net; (**b**) proof of existence of two noncollinear translations in a homogeneous plane

Let us consider the question whether, besides $G_2^2 \supset T_2$, there may be some other symmetry groups G^2 containing no T_2 and transforming a homogeneous plane into itself. We shall prove that this is not so. According to (2.58) it is sufficient to convince oneself that there are no such groups among the motion groups G^1. By Chasles' theorem (Fig. 2.3) there could be (if they exist) groups containing only rotations.

We start with two arbitrary symmetrically equal points A and A' of two-dimensional space "rotated" through some angle and find their Chasles center O (Fig. 2.15b). Let us take some other Chasles center O' symmetrically equal to O and perform a rotation through the same angle φ about it. Then A will transform into point A''. Points A' and A'' are turned by the same angle φ relative to A; hence they are parallel, and there is a translation $\boldsymbol{t}_1$ between them; so there exists an infinite row of such points. Now take some point symmetrically equal to A' away from the row A', A'', ... If it is parallel to A', as, for instance, B, then there is a translation $\boldsymbol{t}_2$ noncollinear with $\boldsymbol{t}_1$, which proves the theorem. On the other hand, if a chosen point, for instance B', is turned relative to A', then there always will be a Chasles center upon rotation about which point B' will be transferred to point B'' parallel to A'. Thus, in this case, too, there is a translation $\boldsymbol{t}'_2$, i.e., it exists in all cases.

As we shall see in Sect. 2.7.2, T_2 contains an infinite number of translations, which are generated by two basic ones: $\boldsymbol{t}_1$ and $\boldsymbol{t}_2$.

Consequently, groups of transformation of homogeneous two-dimensional space into itself are groups $G_2^2 \supset T_2$, i.e., they always contain a two-dimensional subgroup of translations T_2 with a basis $\{\boldsymbol{t}_1, \boldsymbol{t}_2\}$. This is Schönflies' theorem for two-dimensional space, according to which any (r, R) system whose points are equivalent with repsect to some group possesses a subgroup of translations.

This can also be proved by another method, which will be useful in considering three-dimensional space.

From the (r, R) condition (2.52, 53) it follows that rotation angles are finite. Indeed, taking on a plane an axis (point) N (Fig. 2.16), we find by (2.52), in a circle of radius R contacting it a point N' symmetrically equal to N. Another point N'', which is obtained from N' by rotation about N, must, by (2.53), lie outside the circle r around N'. This gives the following condition for the rotation

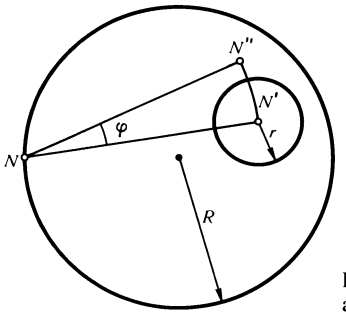

Fig. 2.16. The proof of the finiteness of the angle of rotation about a point of the (r, R) system

angle:

$$\varphi > r/2R \tag{2.62}$$

and the order of the axis

$$N < 4\pi R/r. \tag{2.63}$$

Thus, by the action of axis N it is possible to obtain from any point A a finite set of rotated points symmetrically equal to it, and by the action of an identical axis lying in a different place another set of points rotated through the same angles. Consequently, the points of these sets are pairwise parallel, and hence there exists a translation.

We shall now consider homogeneous nondiscrete (continuous) groups G^2. Here, infinitesimal translations in one or two directions are possible, i.e., semicontinuous groups $T_{\tau_1\tau_2}$ and continuous groups $T_{\tau_1\tau_2}$. A two-dimensional space with a group $G_2^2 \supset T_{\tau_1\tau_2}$ may have points (axes) of rotation of infinite order, i.e., a group $T_{\tau_1\tau_2}\infty$ is possible. If it is supplemented by reflections, we obtain a limiting group $T_{\tau_1\tau_2}\infty m$, which describes an "empty" two-dimensional space; its subgroups are any groups G^2.

Thus, any group of transformations of a homogeneous plane $G^2 \supset T_2$ and the two-dimensional groups belong to types G_0^2, G_1^2, G_2^2.

2.4.5 Crystallographic Groups

The rotation angles φ (2.62) in two-dimensional discrete space are finite, and the order of the axes is $N < 4\pi R/r$ (2.63).

But the presence of a net structure in such a space, which is associated with the translation group $T_2 \subset G_2^2$, leads to a stronger restriction, one of the most important in crystallography. It states that in crystal only operations of rotation symmetry (simple, screw, or mirror rotations) of the 1st, 2nd, 3rd, 4th, and 6th order exist. Let us prove this.

Consider a plane net and the possible rotations of the plane which bring the net into self-coincidence. The rotational points (axes),[8] if they are present, themselves are points of this plane. The translation operations t_1 and t_2 bring all the translationally equal points, including the rotational points (axes), into coincidence; therefore, the points form a net. We choose in the net a number of such points for which the distance between them is the shortest. Let us consider the action of some rotation point N from this row on the two points N' and N'' (Fig. 2.17). If $N = 2$, then N will transfer N' into N'', and vice versa, i.e., the existence of axis 2 is possible. If $N = 3$ (or 6), its action from N' and N'' will produce points 3; the shortest distance between the closest points in this whole set is the same and equal to a. Thus, the existence of axes 3 and 6 is also possible.

[8] A rotation point in two-dimensional space about which a plane is rotated (it is also called "rotacenter") is an analog of rotation axes in three-dimensional space.

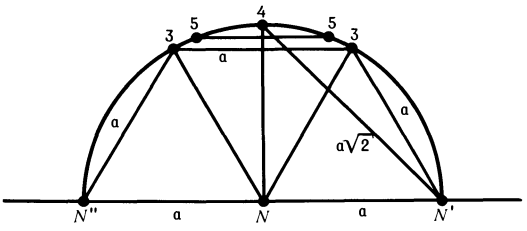

Fig. 2.17. Proof that in a two-dimensional net there can exist only crystallographic rotations of order 1, 2, 3, 4, or 6

If $N = 4$, there arises a point 4 with a diagonal distance from N' and N'' of $a\sqrt{2}$, which is greater than a. It means that the existence of axis 4 does not contradict the convention adopted. But if $N = 5$, the distance between the points 5–5 produced from N' and N'' is less than a. This contradicts the initial assumption that a is the shortest distance in the net. Consequently, axis 5 is not possible. The same will occur for any $N \geqslant 7$. Thus, groups $G_2^2 \supset T$ may contain translation operations exclusively of the 1st, 2nd, 3rd, 4th, and 6th order.

This proof has been carried out for two-dimensional groups, but it is also true for the three-dimensional case. The point is that the discrete groups $G_3^3 \equiv \Phi$, which describe a three-dimensional crystal space, always contain a three-dimensional subgroup of translations T_3, and since $T_3 \supset T_2$, then $\Phi \supset T_3 \supset T_2$. The three-dimensional group T_3 derives a space lattice from any point, and the lattice contains two-dimensional nets described by group T_2. If the lattice contains rotation axes N, they are necessarily positioned perpendicularly to some plane net of the lattice. The rotation about the axis brings the net into self-coincidence; if there were no such coincidence the axis would not be an axis of symmetry. But these axes can be, as we have seen, only of the 1st, 2nd, 3rd, 4th, and 6th order.

The same is true for the axes $\bar{N}$ and N_α. Being projected onto the net, any axis yields rotational points, and hence they can be of the orders indicated above. So, only one-, two-, three-, four-, and sixfold axes are possible in crystals. Among the symmetry groups the term "crystallographic" is attached to groups containing only some of the axes of these orders: simple, screw, or inversion, and the axes themselves are called crystallographic. Note that discrete groups G_2^2, $G_3^3 \equiv \Phi$, as well as G_2^3 are crystallographic in their intrinsic properties, since they contain a subgroup T_2, i.e., they do not include noncrystallographic groups. Other types of groups, however, may contain both cyrstallographic and noncrystallographic groups. Thus, the number of point groups G_0^3 is infinite, but there are 32 crystallographic groups K among them. They coincide with the rotation groups or rotational components (of both kinds) of a homogeneous discrete three-dimensional space G_{rot} (2.61).

2.4.6 Three-Dimensional Groups G^3

By analogy with the above discussion it is easy to infer that apart from groups G_0^3 (point groups) there exist, in inhomogeneous three-dimensional space,

groups G_1^3 with a singular direction – one-dimensionally-periodic groups – and groups G_2^3 with a singular plane – twice periodic. Indeed, by adding a third dimension to groups G_2^2 without making this dimension periodic, we obtain groups G_2^3. If, along some direction noncoplanar to the singular plane, we assign a translation, groups $G_3^3 \equiv \Phi$ will be obtained. These are Fedorov space groups. Parallel to the singular direction in G_1^3 the condition of one-dimensional homogeneity is fulfilled, and parallel to the singular plane in G_3^2, the condition of two-dimensional homogeneity.

The question arises, again, whether the groups G_3^3, which contain a translational subgroup exhaust all the groups of symmetric transformation of a homogeneous discrete three-dimensional space into itself. This is proved in Schönflies' theorem. We shall not give the proof in full, but shall indicate its main stages.

It is required to establish whether there exist, under the (r, R) condition (2.52, 53), groups of motions $G_3^{3(I)}$ without translations, i.e, consisting only of simple and/or screw rotations.

For simple rotations, we can arrive at condition (2.62) $\varphi > r/2R$ precisely as was discussed for the two-dimensional case (Fig. 2.16), this time not with a circle, but with a sphere $2R$ contacting the rotation axis.

The case of screw rotation is more complicated, because this motion has a translational component displacing any point A along the axis of screw rotation. This prevents direct utilization of the r condition (2.53), as in (2.62). Therefore a combination of screw motions is considered.

If the screw axes are parallel, then by (2.55) the distance d between the closest of them is less than $2R$. Let us consider screw motion $\tilde{u}$ along one, and reverse motion $\tilde{u}^{-1}$ along the other. This will bring any point back into the plane perpendicular to these axes. If the angular components $\varphi_{\tilde{u}}$ and $\varphi_{\tilde{u}^{-1}}$ are added together, this will yield a simple rotation through $2\varphi_u$, and then, according to (2.62),

$$\varphi_u > r/4R. \tag{2.64}$$

If they compensate one another, this will already give a parallel translation in the plane indicated.

The most complicated case is when the axes of screw motions are nonparallel. This case is analyzed by Schönflies and other authors [2.2–6] by considering the displacements of some point A under the action of some complex operation ("commutator") $w = uv'u'^{-1}v''^{-1}$ composed of screw rotations. It is found that in this case, too, condition (2.62) is fulfilled. So, in all cases of simple or screw rotations $\varphi > r/4R$ (2.63, 64). It follows that a rotation group (a group of rotational components G_{rot} of the group G^3) of three-dimensional discrete homogeneous space is finite. Then, obtaining from point A a set of points symmetrically equal to it with a finite number of different orientations, we shall have an identical set, with the same orientations, at a different place as well. But this will imply parallelism of the points of these sets, i.e., the existence of translations.

Reasoning similar to that we used for the two-dimensional case suggests that there are three noncoplanar translations. This proves Schönflies' three-dimensional theorem.

$$G_3^3 \equiv \Phi \supset T_3\{t_1, t_2, t_3\}. \tag{2.65}$$

Thus, symmetry groups of three-dimensional homogeneous discrete space – Fedorov groups – are thrice periodic. Group T_3 transforms any point into a three-dimensionally periodic infinite system of points – a space lattice.

The concrete metric values of three basic vectors of translations t_1, t_2, and t_3 (repetition periods) are denoted as a, b, c or a_1, a_2, a_3. A parallelepiped constructed on a, b, c as edges is called a repeat parallelepiped, or a unit cell. Three basic translations generate an infinite number of other translations of the space lattice (see Sect. 2.8.1).

With infinitely small translations τ in one or two directions we obtain three-dimensional discrete-continuous groups $T_3 : T_{t_1 t_2 \tau_3}$, $T_{t_1 \tau_2 \tau_3}$, and, with translations τ in all the three directions, a continuous group $T_{\tau_1 \tau_2 \tau_3}$. Groups $G_3^3 \supset T_{t_1 \tau_2 \tau_3}$ may contain axes ∞ perpendicular to $\tau_2 \tau_3$. If $G_3^3 \supset T_{\tau_1 \tau_2 \tau_3}$, then axes ∞ may be of any orientation, i.e., the group is $T_{\tau_1 \tau_2 \tau_3}\ \infty\infty$. If we also add any operation of the second kind (for instance, m) into it, we obtain a group of the highest symmetry of a three-dimensional continuous isotropic medium (and, in particular, an empty Euclidean space) $T_{\tau_1 \tau_2 \tau_3}\ \infty\infty m$. Its subgroups are all the groups G^3, and hence, G^2 and G^1.

The conclusions from our consideration of symmetry groups in one-, two-, and three-dimensional space are summarized in Table 2.1; Table 2.2 gives the numbers of crystallographical groups.

Table 2.1. Types of symmetry groups

	Space			
m	Inhomogeneous	Inhomogeneous with homogeneous subspace	Homogeneous	Limiting group
1	G_0^1	—	$G_1^1 \supset T_1$	$\bar{1}T_{\tau_1}$
2	G_0^2	$G_1^2 \supset T_1$	$G_2^2 \supset T_2$	$T_{\tau_1 \tau_2} \infty m$
3	G_0^3	$G_1^3 \supset T_1$, $G_2^3 \supset T_2$	$G_3^3 \supset T_3$	$T_{\tau_1 \tau_2 \tau_3}\ \infty\infty m$

Table 2.2. Number of crystallographic groups G_n^m

	n			
m	3	2	1	0
3	230	80	75	32
2	—	17	7	10
1	—	—	2	2

It should be mentioned that with decreasing dimensionality $m' < m$ of space and with the same $n(< m)$ the corresponding groups are subgroups of space of a higher dimensionality.

$$G_n^{m'} \subset G_n^m \ (m' < m). \tag{2.66}$$

Below we shall consider each G_n^m type of groups separately. We also dwell on other possibilities of group classification, for instance by the presence or absence of operations of the second kind or generally some operations or other.

2.5 Geometric Properties of Symmetry Groups

2.5.1 Symmetry Elements

Symmetry operations may be associated with the presence in space of certain *points*, *straight lines*, or *planes* with respect to which these operations are performed.

Each of the symmetry operations $g_i \in G$ (except the identity) accomplishes a transformation $g_i[\boldsymbol{x}] = \boldsymbol{x}_i$; it can be said that it transfers point $\boldsymbol{x}$ to point $\boldsymbol{x}_i$. Points of space, generally speaking, then change their positions, but some of them do not. The condition

$$g_i[\boldsymbol{x}] \equiv \boldsymbol{x}_i = \boldsymbol{x} \tag{2.67}$$

defines the locus of such points. Points, lines, or planes which remain unmoved in a symmetry operation, i.e., which satisfy condition (2.67), are symmetry elements corresponding to this operation.

For a symmetry group $G \ni g_i$ of order n one can write n equations (2.67). If the group is cyclic, all of them define one and the same symmetry element. This also refers to each cyclic subgroup of a given group – each of them defines one symmetry element.

For rotation operations, the symmetry element is a straight line – the axis about which this rotation is performed (Fig. 2.18). This follows from the very definition, but can be derived formally from (2.67) with due regard for the rotation matrix (2.14). For a reflection operation (2.15), the symmetry element is a mirror plane (Fig. 2.6a). For an inversion, the symmetry element is a point, the center of symmetry (Fig. 2.6c).

For mirror (inversion) rotations, the solution of (2.67) is a single point; for screw rotations and glide reflections, (2.67) has no solutions. However, in these symmetry operations there are such lines or planes (we call them invariant) which are brought into self-coincidence as a whole after the transformation, i.e., their points $\boldsymbol{x}$, although changing their position when transferred to $\boldsymbol{x}_i$, remain on the invariant line or plane. Thus, a symmetry element corresponding to a given symmetry operation is a plane, a straight line, or a point which remains unmoved in a given operation, and, lacking these, it is an invariant line or plane which is brought into self-coincidence in a given operation.

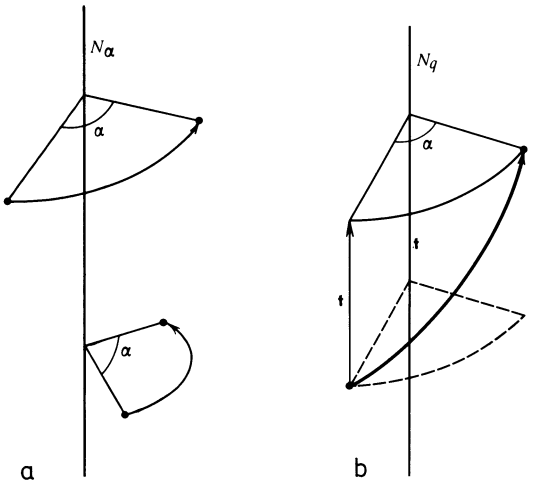

Fig. 2.18a,b. Rotation (**a**) and screw (**b**) symmetry axes

Thus, for operations of mirror (inversion) rotations (Fig. 2.5), any point (with the exception of $x = 0$) changes its position. But the axis of such a rotation, as a whole, has been brought into self-coincidence, reversing its "ends" after this symmetric transformation – each of its points has been transferred to a point of the same line. Mirror-rotation axes of even order also contain a simple rotation axis – an unmoved symmetry element. For a mirror rotation, the plane perpendicular to the axis and passing through the origin is also brought into self-coincidence, but to describe this operation it will suffice to indicate only the axis as the symmetry element.

The symmetry elements for a translation-containing rotation are also invariant; these elements are displaced along themselves. Thus, to screw rotations there correspond straight lines – screw axes of symmetry; they shift in themselves, according to the translational component of this operation (Fig. 2.18b). To glide reflections there correspond glide-reflection planes, which also shift in themselves in the direction of action of the translation component (Fig. 2.6b). A symmetry group may contain one or several cyclic subgroups, and then one or several identically or differently named symmetry elements correpond to it.

The set of symmetry elements of a given group characterizes it consistently and unambiguously. All points of space x obey operations $g_i \in G$ of a given group, while the symmetry elements themselves are invariant sets of points. Then any symmetry operation which brings the symmetry element corresponding to it into self-coincidence simultaneously brings the other symmetry elements of identical type into coincidence with each other. In short, it can be said that the symmetry elements of a given group are symmetric with respect to each other and to themselves.

We have considered symmetry elements for all operations of three-dimensional space, except translations. The geometric image of these operations, as we know, may serve as an infinite lattice of points derived from a given point by

translations t_1, t_2, t_3. Being displaced parallel to itself by any translation, a lattice carves translationally equal points out of the space (see Fig. 1.15).

2.5.2 Summary and Nomenclature of Symmetry Elements

In this book we shall mainly use the international nomenclature adopted in the "International Tables for X-ray Crystallography" proposed by C. Hermann and C. Mauguin with some adjustments. *Shubnikov's* nomenclature [2.7, 8] is close to it. Sometimes we shall also use the widespread symbols of A. Schönflies.

We shall consider successively all the symmetry elements corresponding to the various operations in three-dimensional space. We shall denote the symmetry elements by the same symbols as are used for the corresponding generating symmetry operations, for instance, m, n, 6, and $\bar{3}$. The symbol of one or several generating operations also implies the corresponding group. Other nongenerating operations of the group (if they exist) will be denoted by the powers of the generating operations, for instance 3^2 and 4^3. We shall consider all the crystallographic symmetry elements.

Rotation axes. In rotation through an angle $\alpha = 2\pi/N$ the symbol N indicates the order of the axis. So these axes are denoted by the figure corresponding to their order. The crystallographic axes are: 1, 2, 3, 4, and 6 (Fig. 2.19a). The general designation of the axis is N, which also denotes the corresponding group containing the entire set of operations of rotations about such an axis. Operation 1 corresponds to a "rotation" through 2π, i.e., it is the identity operation e. The rotation axes are called: a rotation axis (or simply an axis) of the first order, of the second order, etc., or, for short, a twofold axis, a threefold axis, a fourfold axis, and a sixfold axis. According to International Tables, rotation axes are supposed to have the following short names: —monad, 2—diad, 3—triad, 4—tetrad, and 6—hexad.

A mirror-reflection plane, or simply a symmetry plane or a mirror plane (Figs. 2.6a, 19b), and the corresponding operation are denoted by the letter m or by the symbol $\bar{2}$, since this operation is simultaneously an inversion rotation of the second order.

Inversion-rotation axes[9] are at the same time mirror-rotation axes (see Fig. 2.5), but with the unit rotation angle differing by π. Inversion-rotation axes with a rotational component $\alpha = 2\pi/N$ (and the corresponding operations and groups) are denoted by a barred figure corresponding to the rotation order: $\bar{1}$, $\bar{2}$, $\bar{3}$, $\bar{4}$, and $\bar{6}$ (Fig. 2.19b).[10] These axes are called inversion axes of corresponding order: for instance, the inversion axis of the fourth order, or the fourfold inversion axis. The most important particular case is the *center of symmetry* $\bar{1}$,

---

[9] The term "rotatory-inversion" axis is also used.

[10] Previously, in the Russian literature $\bar{N}$ signified a mirror-rotation axis, while inversion axes were not used at all.

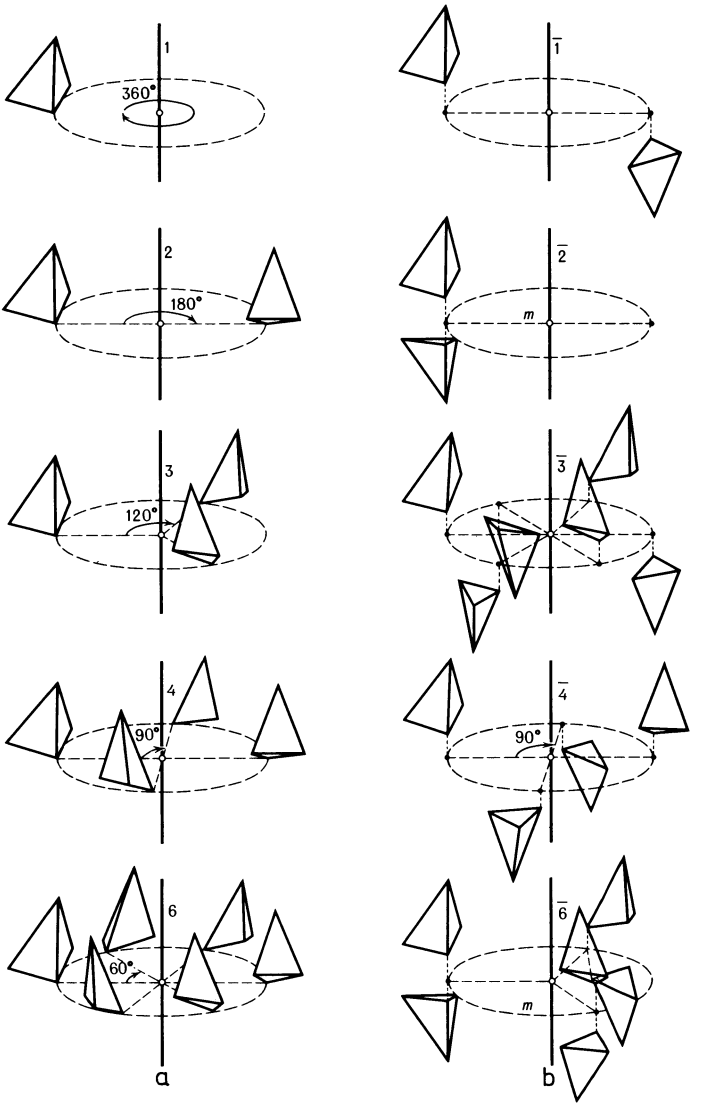

Fig. 2.19a,b. Crystallographic rotation (**a**) and inversion-rotation (**b**) symmetry axes and their action on an asymmetric figure – a tetrahedron

which is also called the inversion center (Fig. 2.6c, $\bar{1}$ in Fig. 2.19b). Mirror-rotation axes are called just this; they (and their respective operations and groups) are denoted by the figure corresponding to the order with a tilde ($\tilde{}$) over them: $\tilde{1}$, $\tilde{2}$, $\tilde{3}$, $\tilde{4}$ and $\tilde{6}$.

Inversion and mirror rotations are related as follows: $\bar{N}_\alpha = \tilde{N}_{\alpha-\pi}$ (Fig. 2.5). Hence for the axes $\bar{1} = \tilde{2}$, $\bar{2} = \tilde{1} = m$, $\bar{3} = \tilde{6}$, $\bar{4} = \tilde{4}$, $\bar{6} = \tilde{3}$ (Fig. 2.19b) and for operations $\bar{3} = \tilde{6}^{-1}$, $\bar{4} = \tilde{4}^{-1}$, $\bar{6} = \tilde{6}^{-1}$.

Mirror rotations of even order $2\tilde{N}'$ contain simple rotations N'; therefore, the symmetry element – axis $\tilde{4} = \bar{4}$ is simultaneously rotation axis 2, and $\tilde{6} = \bar{3}$, axis 3.

All the enumerated symmetry elements are inherent both in point and space groups. The latter also have symmetry elements with a translational component. Let us consider them.

Screw axes, or, more precisely, axes of screw rotations, have an angular α_s and a translational t_s component

$$\alpha_s = 2\pi/N, \quad N = 2, 3, 4, 6, \tag{2.68}$$

$$t_s = \frac{q}{N} t, \quad q = 1, 2, 3, 4, 6. \tag{2.69}$$

This relationship is due to the fact that $N^N = 1$ and $t_s^{N/q} = (N/q)t_s = t$, i.e., there is a translation operation t along the screw axis in the lattice. Expression (2.69) shows that the quotient of division of the index of the screw rotation q by the order of axis N determines the value of t_s. The general symbol of screw axes is N_q. They are depicted in Fig. 2.20.

At $q < N/2$ the screw axes are right-handed, and at $q > N/2$, left-handed; at $q = N/2$ $\alpha_s = \pi$, clockwise and counter clockwise rotations are equivalent; and these axes are simultaneously right- and left-handed or, what is the same, non-right- and non-left-handed. The simplest screw axis is 2_1. In a right-handed screw motion along the axis normal to the drawing (from it to the observer and with an counter clockwise rotation) we have axes 3_1, 4_1, and 6_1 ($q = 1$). A screw motion can also be performed by following a left-handed screw. For the left-handed axis 3_1^l the left-handed rotation $\alpha_s = -2\pi/3$ can be replaced by a right-handed rotation $\alpha_s = 2 \times 2\pi/3$, and the left-handed axis 3_1^l is denoted as the right-handed 3_2. Similarly, the left-handed axes 4_1^l are denoted as the right-handed 4_3, and the left-handed 6_1^l, as the right-handed 6_5. Axis 6_2-right-handed, contains axes 3_2 and 2; axis $6_2^l = 6_4$ – left-handed, contains 3_1 and 2. Axes 4_3 and 4_1 contain axis 2_1; axis 6_1, contains 3_1, and axis 6_5 contains 3_2. Axis 4_2 contains axis 2; and axis 6_3 contains axes 3 and 2_1. Axes 2_1, 4_2, and 6_3, as was indicated, are neutral in the sense of right- or left-handedness.

Glide-reflection planes. When a glide-reflection operation is repeated (cf. Fig. 2.11d), its translational component $\boldsymbol{t}'$ is doubled, and the resulting translation $2\boldsymbol{t}'$ must coincide with one of the lattice periods. Such operations (and planes) are denoted by a, b, or c in accordance with the designation of the unit cell along which the glide occurs (Fig. 2.21). Thus, for operation a the translational component α_1 is equal to $a/2$, where a is the lattice period. Glide-reflection operations with a component $\boldsymbol{t}'$ along the diagonals of the unit cell faces are also possible: $\boldsymbol{t}' = (\boldsymbol{a} + \boldsymbol{b})/2$, or $(\boldsymbol{a} + \boldsymbol{c})/2$, or $(\boldsymbol{b} + \boldsymbol{c})/2$. The corresponding symmetry elements are diagonal glide-reflection planes denoted by n. Finally, in tetragonal and cubic lattices the glide-reflection operations with $\boldsymbol{t}'$ along the space diagonals are possible

$$\boldsymbol{t}' = (\boldsymbol{a} \pm \boldsymbol{b})/4, \quad \boldsymbol{t}' = (\boldsymbol{b} \pm \boldsymbol{c})/4, \quad \boldsymbol{t}' = (\boldsymbol{c} \pm \boldsymbol{a})/4, \quad \boldsymbol{t}' = (\boldsymbol{a} \pm \boldsymbol{b} \pm \boldsymbol{c})/4.$$

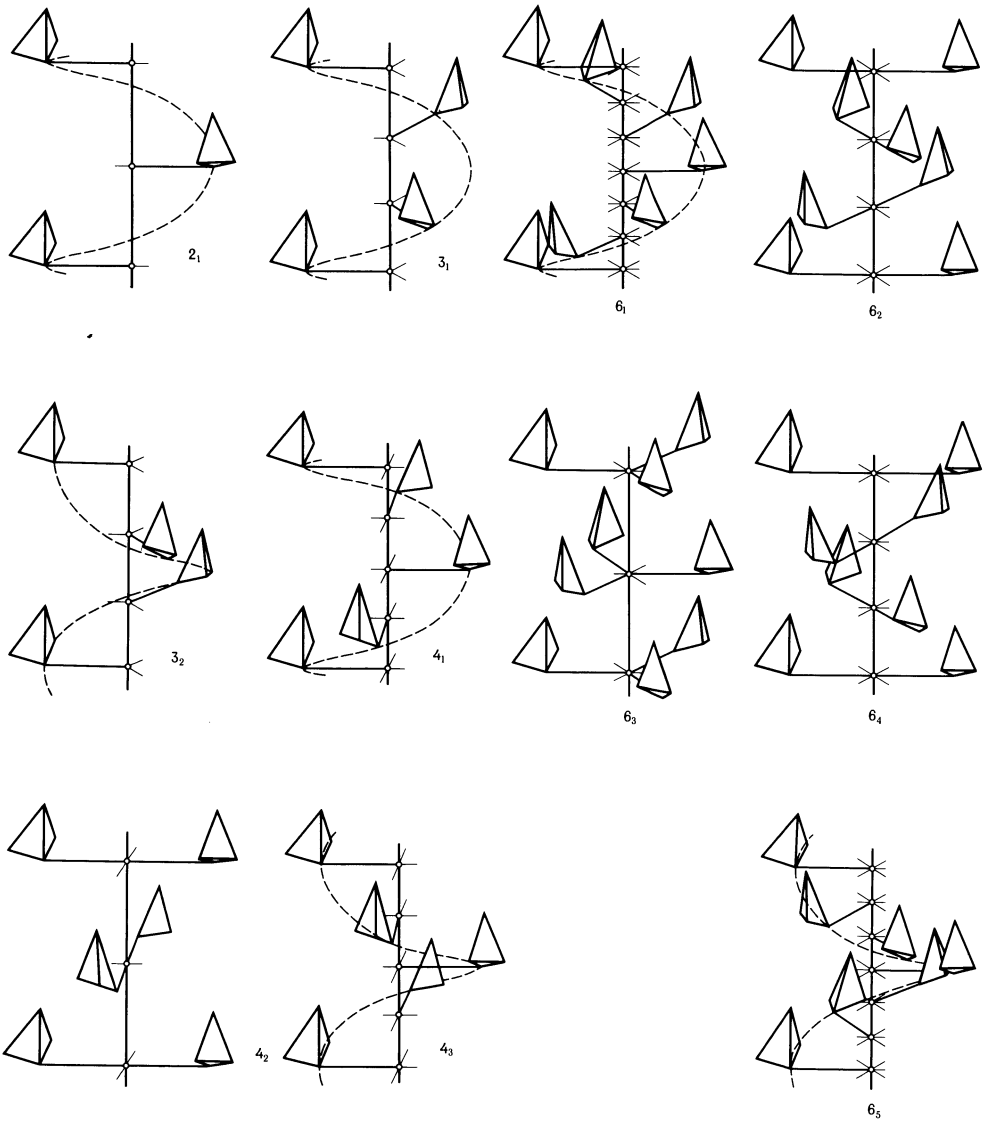

Fig. 2.20. Crystallogaphic screw axes and their action on an asymmetric tetrahedron

The corresponding symmetry elements are diamond glide-planes *d*. The graphical notation of all the symmetry elements is given in Fig. 2.22.

We know how the operations corresponding to each symmetry element transform space. Here we shall note thay any plane perpendicular to the rotation axis is brought to self-coincidence by rotation; a plane perpendicular to a mirror or screw axis is transferred into a position parallel to itself by rotation. Any straight line perpendicular to the reflection plane turns over and is brought

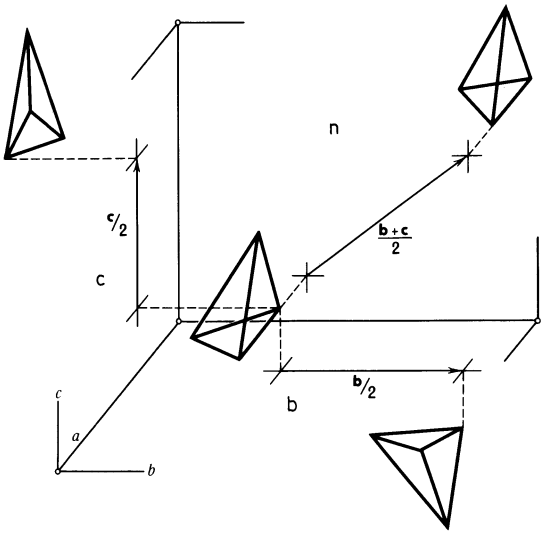

Fig. 2.21. Glide-reflection operations *c*, *b*, and *n*

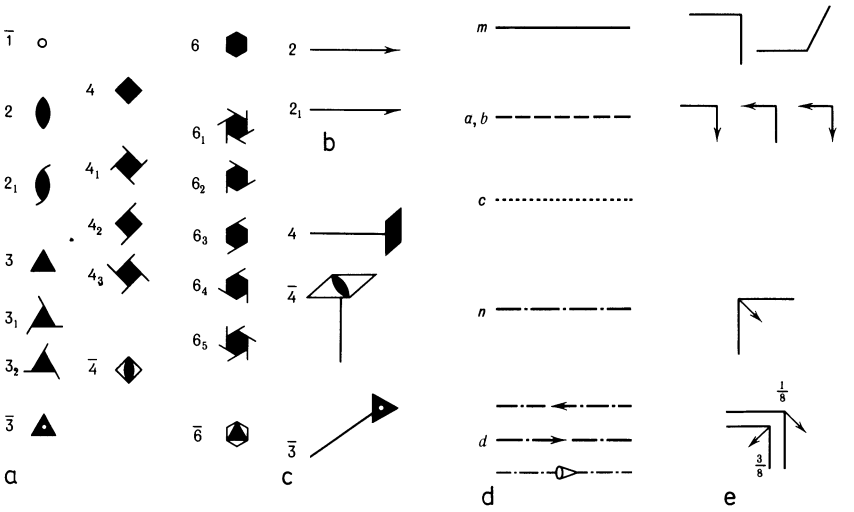

Fig. 2.22a–e. Graphical notation for symmetry elements.
(a) symmetry axes perpendicular to the plane of the drawing; **(b)** axes 2 and 2_1 parallel to the plane of the drawing; **(c)** symmetry axes parallel or oblique to the plane of the drawing (the straight line is mounted by a symbol distorted in perspective); **(d)** symmetry planes perpendicular to the plane of the drawing; **(e)** symmetry planes parallel to the plane of the drawing

into self-coincidence upon reflection. In glide reflection such a straight line is transferred to a position parallel to itself by turning over. In two-dimensional space the symmetry elements are the rotation points N and the lines of reflection: m stands for mirror reflection, and a, b, and n for glide reflection, which are denoted graphically in the same way as in the three-dimensional case.

2.5.3 Polarity

This concept is one of the important characteristics of directions in crystals. It is possible to go in opposite directions along any straight line. If the two directions are equivalent, the line is nonpolar and is transformed into itself by some operation which reverses (brings into coincidence) its opposite "ends". Thus, in three-dimensional space the action is performed by axis $2_\perp$ or plane $m_\perp$, perpendicular to this line, or by the inversion center $\bar{1}$ lying on it.

If the indicated operations are not present, the sequence of the points of the line in opposite directions is different, generally speaking, and the straight line (and the vector lying in it) is called polar. The "ends" of such a line, for instance the points of its emergence from different sides of a crystalline polyhedron, are different. But a polar line may be symmetric "along itself" when it is, for instance, a symmetry axis (noninversional) or when it lies in the symmetry plane. If we take into account the space symmetry, a polar line may also be equal to itself translationally. Since symmetry axes are straight lines, they may be either polar or nonpolar. Thus, inversion axes are always nonpolar, while rotation axes may be polar, provided they do not intersect with symmetry elements $\bar{1}$, m, or 2. The polarity of the physical properties of crystals corresponds to that of directions in crystals.

2.5.4 Regular Point Systems

Consider some group G. Each of the symmetry operations $g_i \in G$ performs a transformation $g_i[\boldsymbol{x}] = \boldsymbol{x}_i$. We choose any point $\boldsymbol{x}(x, y, z)$ and apply all the operations g_i to it. Each of these operations will give one new point $\boldsymbol{x}_i$, and as a result we obtain, in the general case, n points (Fig. 2.23).

The set of points derived from any starting point $\boldsymbol{x}$ by all the operations g_i of group G,

$$\boldsymbol{x}, \boldsymbol{x}_1, \boldsymbol{x}_2, \ldots, \boldsymbol{x}_{n-1}, \tag{2.70}$$

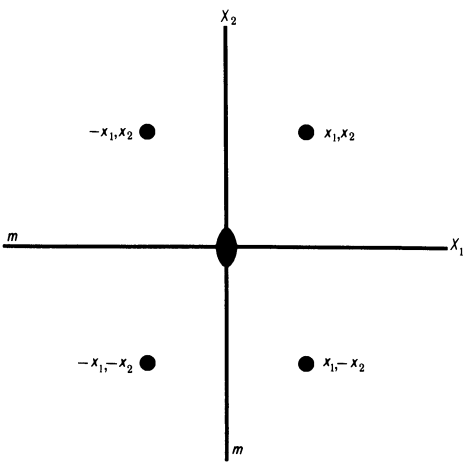

Fig. 2.23. Regular point system of group *mm*

is called a *regular point system* (RPS).[11] These points are symmetrically equal. RPS is written as the set of coordinates of each of the points, and the coordinates of the multiplied points, x_i, y_i, z_i are expressed in terms of the coordinates of the starting point xyz (see Fig. 2.81). In the general case, when a point is not located on a symmetry element, it is called a point of general position. The starting point $\boldsymbol{x}$ can be chosen anywhere. As a result of multiplication it yields n points (2.70), which together make RPS of general position.

Joining adjacent points of general positions derived by the point group with straight lines we obain a convex polyhedron with equal vertices called an isogon.

As we have already noted, a crystallographic "point" is asymmetric, and hence each point of RPS of general position is also asymmetric. The situation is different when a point lies on a symmetry element satisfying condition (2.67), i.e., on a rotational symmetry axis, a symmetry plane, or an invariant point of an inversion axis. As a set of RPS of general positions approaches such a symmetry element, these points draw closer together until they merge completely on it at the value $\boldsymbol{x} = \boldsymbol{x}'$ (Fig. 2.24). If the symmetry element was generated by a cyclic subgroup of order n_k, then n_k points will merge on it, and the point will become n_k-tuple. Such points are called points of special position. One can speak of the symmetry of such a point (the result of merging of n_k symmetric points) and naturally assign to it the symmetry of the symmetry element on which it is located – the symmetry of position. Thus all points lying on plane m have this symmetry; they are mirror-equal to themselves; and this symmetry element consists of such points. Points lying on axis N and making it up are "rotationally" equal to themselves.

Thus, apart from RPS of general position, symmetry groups may include RPS of special positions containing n/n_k points. If a group has essentially different subgroups, then there are as many essentially different regular point systems with a multiplicity n_k and a number of points n/n_k. At the intersection (if any) of symmetry elements, points arising as a result of the action of cyclic subgroups merge together; the symmetry of such points is the common symmetry of the intersecting elements.

At a singular point of point groups, all the symmetry elements intersect; this point has the symmetry of the given point group. In this case RPS consists of one point; its multiplicity is equal to the order of group n.

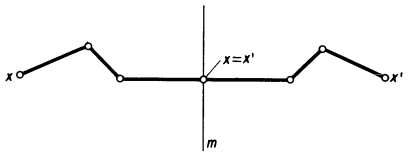

Fig. 2.24. Merging of asymmetric points of general positions x and x' into a symmetric point of special position

[11] The term "orbit" of group G is also widely used.

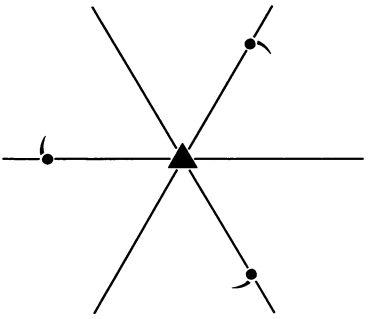

Fig. 2.25. Set of three points transformed into each other by the operation 3. If the points are symmetric, the set seems to have symmetry $3m$, but if they are asymmetric (with tails), no symmetry planes arise

All groups containing translation operations are of infinite order. Points of RPS, however, are reproduced in such groups not only by translation operations, but also by other operations of this group. In this case, there is a finite set of symmetry operations and a finite number n of points of general position within the unit cell. Translation operations reproduce each of them into an infinite number of unit cells. Therefore, when one speaks of the order of symmetry groups with translations and of their RPS, one implies the number of points n and their arrangement within one unit cell. In each regular system of points we indicate: a) their point symmetry, b) the order of this symmetry, c) the multiplicity, and d) their coordinates (Fig. 2.81).

Any RPS uniquely characterizes group G if the points of RPS are crystallographically "labelled", i.e, if they are assigned the symmetry of the positions they occupy (points of general position are asymmetric, points of special positions have certain symmetry). Thus, a crystallographically labelled RPS determines group G, and conversely, knowing G, we can derive all its RPS.

If, however, the points of some RPS are assigned a higher symmetry than that of the positions they occupy, an apparent overstatement of the symmetry of RPS derived by group G may occur (Fig. 2.25). Thus, a geometric point denoted only by its coordinates x, y, z has (in distinction to the crystallographical point with symmetry 1) the highest spherical symmetry. Therefore, in depicting symmetry groups the point of general position is given some features of asymmetry (the asymmetry of its environmental space). We have used asymmetric labels – tetrahedra; "commas", dots with plus or minus signs, etc., are also used (see Fig. 2.81).

The concept of regular point systems corresponding to a given symmetry group finds the most extensive application in space-group theory and in the description of crystal structure, but it can also be used in studying other groups of symmetry. The concept of regular systems of figures derived from a given one by operations $g_i \in G$ is quite similar to the concept of regular point systems.

2.5.5 Independent Region

This concept defines important geometric properties of a symmetric space. Let us take a point of general position x in space with symmetry G_0^2 (Fig. 2.26) and

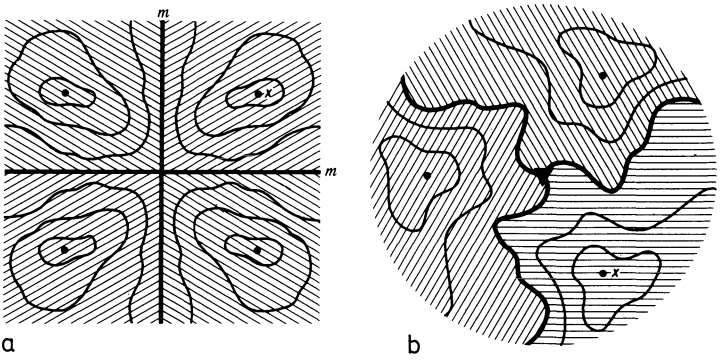

Fig. 2.26a,b. Formation of asymmetric independent regions as exemplified by two-dimensional groups *mm* (**a**) and 3 (**b**)

begin to "blow up" its environmental space region in an absolutely arbitrary manner. Let us do the same with the regions surrounding the other points of this RPS, applying the same "blowing-up" law to them. We continue "blowing-up" until the regions touch each other and fill the entire space. It is clear that the loci of such contacts are determined by condition (2.67), but no other limitations on the shape of the regions thus obtained arise. This means that the rotation axes of symmetry in three-dimensional space lie on the surface of an asymmetric region and are common lines of contact of these regions, while on the plane the common points are the points of rotation (see Fig. 2.26b). The center of symmetry $\bar{1}$ also lies on the boundary of such a region. Mirror planes in three-dimensional space (lines of symmetry in two-dimensional space) will always be the boundaries of such regions (see Fig. 2.26a), otherwise their boundaries are absolutely arbitrary. Let us call such regions in the three-dimensional case *stereons*. It is easy to see that stereons are equal in shape to each other, because any point of any one of them (including the boundary one) will be in one-to-one correspondence (by virtue of operations $g_i \in G$) with the symmetrically equal points in each of the other stereons. The number of stereons is equal to the number of points in RPS of general positions, i.e., to the order of group n. Hence, a symmetric object (function, figure) which is subordinate to a symmetry group of order n consists of n equal parts – stereons, the volume of each part being equal to V/n, where V is the volume of the entire object. Thus, from the concept of invariance (2.2) in symmetry transformation (2.1) follows the obligatory presence of equal parts in the object.

A stereon is an independent (fundamental) region of a given group. In such a region it is possible to assign an arbitary function f of variables $x_1, \ldots, x_m$. Then symmetry operations $g_i \in G$ will automatically construct from it a function F defined throughout the space.

Note that an independent region taken separately is asymmetric, i.e., it possesses no symmetry, since, by definition, the points within it are not transformed into each other by symmetry operations of group G describing the space.

But it is possible, by drawing the boundaries of independent regions arbitrarily, to impart some symmetry to the external shape of an independent region artificially (Fig. 2.27a, b), provided we regard it as a "box" for an empty space. But when using the right to assign any function in this region, we see immediately that the points of the independent region are not equal symmetrically, i.e., that it is asymmetric in its essence.

Here we must dwell on the so-called local symmetry inherent in the crystalline structures of certain molecular compounds and proteins. The asymmetric region of the space group of such a structure may contain several (usually two) identical molecules, and they are related, only to one another, by a symmetry operation, for instance, by axis 2. This operation is local, it does not belong to space group G_3^3. Local axis 2 or some other local symmetry element may be positioned in an absolutely arbitrary manner in the unit cell (two-dimensional example in Fig. 2.27c). Therefore such a local point symmetry inside the asymmetric region is called noncrystallographic. At the same time, the local symmetry elements lying inside the stereon are multiplied together with it by all the operations of group G_3^3. The local symmetry of position of some structural units does not contradict the fact that the independent region as a part of space remains asymmetric, since the surrounding of these parts by other identical parts no longer obeys the action of local symmetry operations, because they do not transform the entire space into itself.

Added together, stereons fill the space completely. For point groups stereons are infinite, but when converging to the singular point they become more and more narrow. Their shape can be described by the intersections of the boundaries with the surface of the sphere. For periodically discrete groups, stereons are finite.

Intuition suggests, and this is indeed the case, that each symmetry group – point, space, or any other – can be assigned with the aid of the shape of the figure of an asymmetric stereon specific to it. The shape of the stereon surface is such that it determines its unique joining with the corresponding parts of the surface of other identical stereons. Such parts may be called complementary. As we have mentioned earlier, the choice of the shape of a given stereon, apart from the

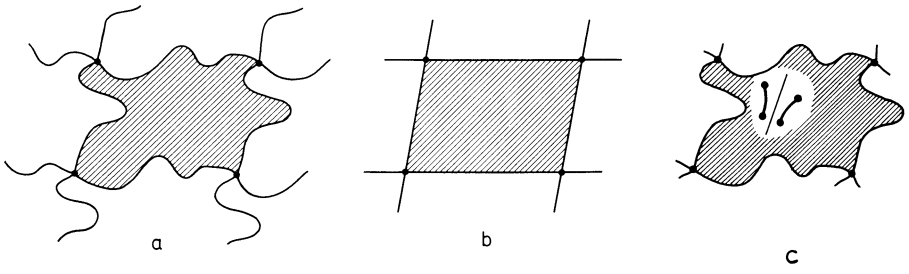

Fig. 2.27a–c. An asymmetric (**a**) and an artificially symmetricized (**b**) independent region in a two-dimensional translation group G_2^2; (**c**) local point symmetry of two "molecules" in the independent region

condition of its being framed by rotation axes, symmetry planes, and inversion centers, is arbitrary. But being chosen, the shape determines the connection of stereons, and hence a given group, uniquely. If stereons have plane faces, one must indicate the mode of connection of such plane regions of adjacent stereons. The mutual arrangement of such figures filling the space will define the symmetry group. This will be a regular system of figures of general positions.

The concept of an asymmetric independent region is widely used in interpreting and describing the structure of crystals, since assignment of the arrangement of atoms or molecules in it within the framework of a given space group defines the whole space structure.

In the case of a homogeneous space independent regions are finite. We shall now illustrate some of their properties as exemplified by two-dimensional groups G_2^2. Two-dimensional independent regions will be called *planions*. Planions of different groups may have either curvilinear or straight boundaries (Fig. 2.28; see also Fig. 2.57).

Figures with straight boundaries – polygons filling the plane – are called *planigons* (Fig. 2.29). A planigon may be a planion (i.e., an asymmetric unit) or a

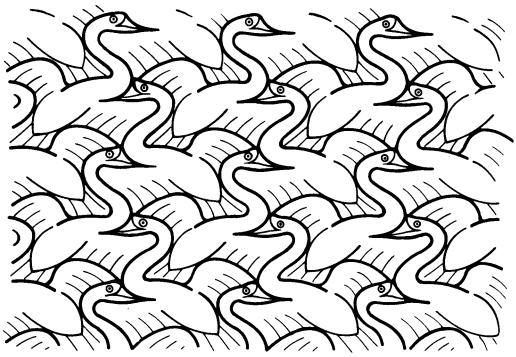

Fig. 2.28. Filling of a plane with two-dimensional asymmetric figures (Escher's drawing). Plane group *pg* [2.9]

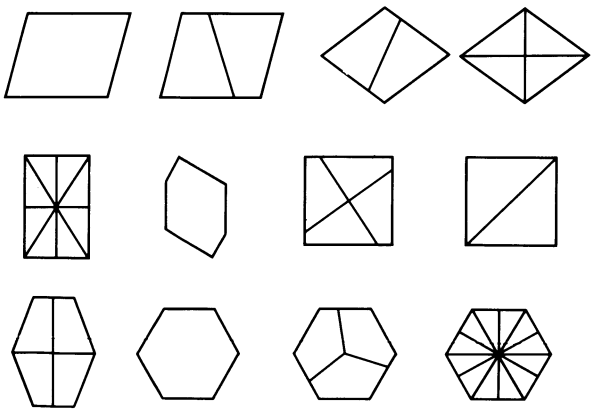

Fig. 2.29. Examples of planigons and parallelogons

symmetric collection of several such regions. In all, 46 types of division of a plane into planigons are known. If the edges of a planigon are mutually parallel and if the planigons themselves are parallel, they are called *parallelogons.*

Another type of polygons filling the plane completely are plane isogons. In distinction of planigons, which contain points of a regular system within them, isogons are obtained by joining points of a regular system with straight lines.

A similar problem of filling a three-dimensional space with stereons and various types of polyhedra will be considered below (Sect. 2.8).

2.5.6 Description of a Symmetric Object by Groups of Permutations

We have already said that in constructing a symmetry theory it is possible to proceed from the conditions of invariance (2.2) in transformation (2.1), but it is also possible to define a symmetry by postulating the condition of the presence of equal parts in an object. In Sect. 2.1.1 we obtained such parts, which are none other than independent asymmetric units, from conditions (2.1) and (2.2). Let us show now that one can proceed in the opposite way.

Suppose an object consists of n equal parts, each of which is positioned equally with respect to all the others (and hence with respect to the nearest parts) and these n parts exhaust the entire contents of the object: it contains nothing else. Observing such a symmetric object from outside, we can mark these equal parts in some way or other, for instance number them (Fig. 2.30a). Equal parts can be interchanged, and such replacements can be described in the form of permutation of the respective numbers:

$$s = \begin{pmatrix} 1, 2, \ldots, & i, \ldots, n \\ b_1, b_2, \ldots, & b_i, \ldots, b_n \end{pmatrix}. \tag{2.71}$$

In expression (2.71) the upper row denotes the numbering of places i; the numbers b_i in the lower row indicate to what site that part was transferred after permutation. Thus, in our example of Fig. 2.30b,c the permutations

$$s_1 = \begin{pmatrix} 1 & 2 & 3 & 4 & 5 \\ 4 & 2 & 3 & 1 & 5 \end{pmatrix}, \quad s_2 = \begin{pmatrix} 1 & 2 & 3 & 4 & 5 \\ 2 & 5 & 3 & 4 & 1 \end{pmatrix}. \tag{2.72}$$

mean that in the first case part 1 took the place of 4, and 4 took the place of 1 – they have changed places, while the other parts remained in place; in the second case three parts have changed places $1 \rightarrow 2$, $2 \rightarrow 5$, and $5 \rightarrow 1$. In the general case, all the n parts can change places (Fig. 2.30d). One can thus perform two or more permutations consecutively and express the final result as a single permutation. Such operations are called multiplication of permutations.

Let us now consider permutations under which *all* the parts change places (or all remain in place – a "unity" permutation); we select only those under which the mutual arrangement (neighboring) of the object parts remains also

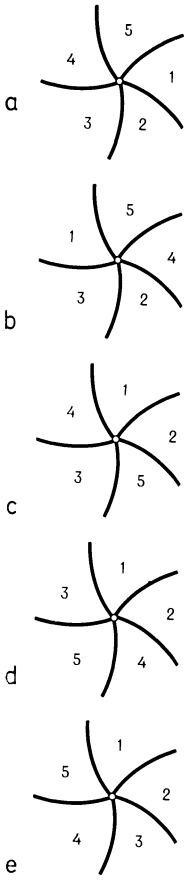

Fig. 2.30a–e. Symmetric figure consisting of five equal parts, and some permutations of these parts

unchanged as a whole. For instance, of the two permutations of Figs. 2.30d and e

$$s_3 = \begin{pmatrix} 1 & 2 & 3 & 4 & 5 \\ 2 & 4 & 5 & 3 & 1 \end{pmatrix}, \tag{2.73}$$

$$s_4 = \begin{pmatrix} 1 & 2 & 3 & 4 & 5 \\ 2 & 3 & 4 & 5 & 1 \end{pmatrix}, \tag{2.74}$$

this condition is satisfied by the second: the replacement of parts in it occurs by the cyclic law.

It is easy to see that such permutations of n parts form a group and are isomorphous to some group of symmetry (in our example, to the group of rotations $2\pi/5$). Further, we can introduce a coordinate system and pass on to geometric consideration of the properties of these groups. Thus, in constructing a symmetry theory we can also proceed from the definition of symmetry on the basis of the equality and equal positioning of the parts.

But still, from the geometric standpoint, the construction of the theory of symmetry from conditions (2.2) of invariance of objects under transformations (2.1) is more general than on the basis of the equality of the parts of the object. The point is that in this approach the resulting equal parts (stereons) can be chosen, as we have seen, in absolutely different ways, and the condition of their symmetric arrangement is obtained automatically. If, however, we proceed from equal parts, we assign beforehand their definite "form" and demand beforehand that they occupy identical positions with respect to one another.

At the same time it is interesting that from the standpoint of permutation theory the concept of symmetry expands in some sense. Symmetry operations (with the exception of the unity one) transform the entire space as a whole, and each independent region into another. When considering equal and identically mutually arranged parts in an object we can perform permutation operations in it which interchange ("mix") only certain parts (2.72) or which interchange all the parts, but without preserving their mutual arrangement (2.73), while the object as a whole remains unaltered. It can be shown that a set of any permutations of n parts of the type (2.73) is a group (the number of permutations is equal to $n!$ – 120 in our example), and their subgroup is a group of the permutations of the type (2.74) isomorphous to the group of symmetry operations.

2.5.7 Enantiomorphism

We have established that any symmetric object can be represented as a collection of equal asymmetric parts (stereons). Let this object be described by a point, space, or any other symmetry group G^{I} containing only operations of the first kind – motions – and, hence, containing no reflections or inversions. In this case all these parts are congruently equal to each other, and there are no parts mirror-equal to them in the object. (A particular case of such an object is an asymmetric object described by point group 1). Let us construct an object which is mirror-equal to the one described, reflecting it in a plane m lying anywhere (Fig. 2.31a, b). The object will consist of the same number of congruently equal asymmetric parts, and these parts will be mirror-equal to those of the first object.

Two objects described by a symmetry group containing operations of the first kind only and mirror-equal to each other are called enantiomorphous. One of such objects, no matter which, is customarily called right, and the other, left (by analogy with the right and left arm). Their parts (independent regions), which are mirror-equal to each other, are also called right and left (see Fig. 2.31c,d). To indicate that objects belong to the right or left enantiomorphous variety, one can also use the term "chirality" (from the Greek $\chi\varepsilon\iota\rho$, arm). Enantiomorphous forms of molecules and crystals are widespread (Fig. 2.32).

Let us now consider any arbitrary object which is described by groups of the second kind G^{II}. These groups contain simultaneously operations of the first and second kind $G^{\mathrm{II}} \ni g_i^{\mathrm{I}}, g_k^{\mathrm{II}}$. Then the set of operations $g_i^{\mathrm{I}} \in G$ forms a subgroup of

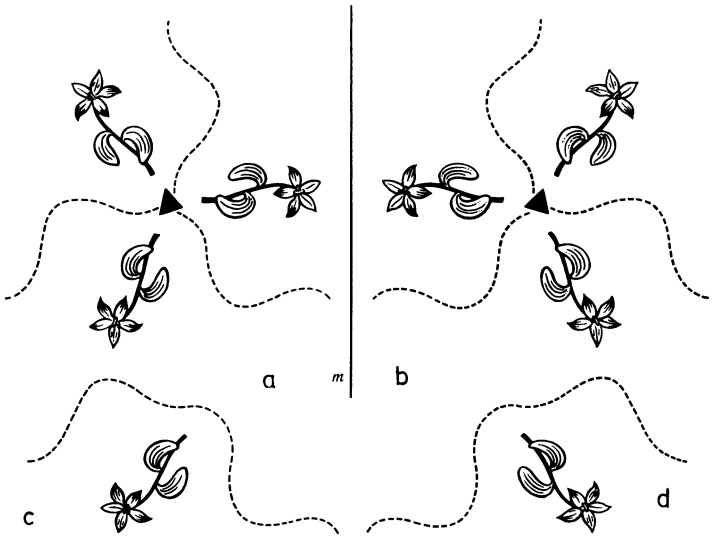

Fig. 2.31a–d. Enantiomorphous figures.
(**a**) symmetric object, whose parts are transformed into each other by first-kind operations; (**b**) an object enantiomorphous (mirror-equal) to it; (**c, d**) enantiomorphous independent regions of these two objects

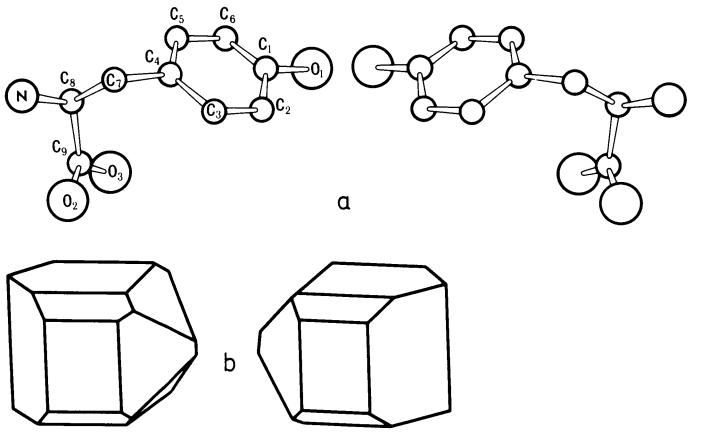

Fig. 2.32a, b. Examples of enantiomorphous objects.
(**a**) molecules of amino acids of *L*- and *D*- tyrosine; (**b**) crystals of right-handed and left handed tartaric acid

index 2 of motions of the initial group of the second kind $G^{II} \supset G^{I} \ni g_i^I$; therefore, groups G^{II} are always groups of even order. Herefrom follow some consequences.

Among equal asymmetric regions of such an object there are regions of two types: right and left, which are mirror-equal; their number is the same, being

equal to the order n of subgroup G^{I}, while their total number is equal to the order $2n$ of group G^{II}. Any operation of the second kind transforms only parts of different chirality into each other (right into left), and any operation of the first kind G^{I}, only of the same chirality (right into right, left into left).

Objects described by groups G^{II} can be called self-enantiomorphous, and from them one can isolate sets of "right" and "left" parts (Fig. 2.33); these sets, when regarded as separate objects, are enantiomorphous (Fig. 2.31c,d).

Each of these two enantiomorphous sets is transformed into itself by group G^{I}, which is the same for both. Note that a point group $G_0^{3,\mathrm{I}}$ of enantiomorphous objects is always the same. This is also true for most of the space groups Φ[12].

The problem of enantiomorphism is one of the most interesting problems in crystallography and physics. It plays a particularly important part in biology. Since any right and left constructions from atoms are absolutely equivalent energetically because they are symmetrically equal, they must be found in approximately equal numbers, which is actually almost always observed in inorganic nature. A remarkable exception is the molecular organization of living systems, which are built up, as a rule, of only one ("left") variety of biological

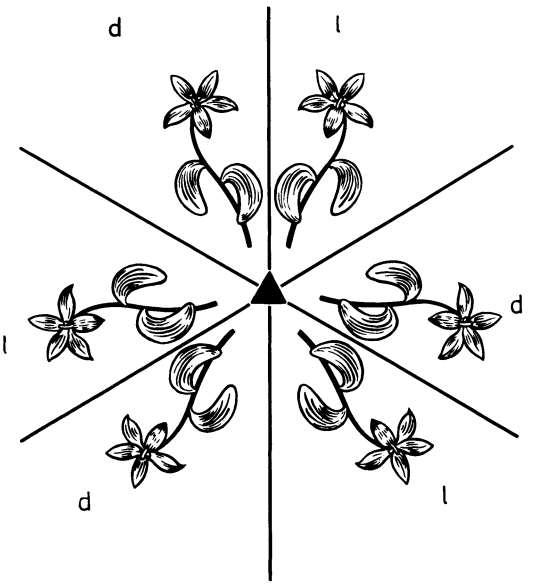

Fig. 2.33. An object described by a second-kind symmetry group. One can isolate a set of right (d) and left (l) parts. Each set is described by the first-kind group 3

[12] Some three-dimensionally periodic enantiomorphous objects are described, not by one, but by two enantiomorphous space groups. The point is that there are screw axes N_q of different chirality, for instance 3_1 and 3_2 (see Fig. 2.20), and, correspondingly, pairs of space groups containing only one sort of such axes (see Sect. 2.8.8). The crystalline structures described by such pairs of groups are enantiomorphous. An example is the structure of right and left quartz, whose point group is the same, 32. The chirally different pairs of space groups are abstractly isomorphous.

molecules. But this peculiarity is not revealed at the macroscopic level of organization of living organisms. Their symmetry is extremely diversified. So, very many organisms, among them most of the animals and man himself, in the outward shape of their bodies are mirror-symmetric. But there exist animals and plants with a high axial symmetry of the second kind, and also some organisms having point symmetry of the first kind, including asymmetric and enantiomorphous forms.

Problems of enantiomorphism, symmetry, and asymmetry are fundamental in analysis of the foundations of matter – in considering the structure of elementary particles and their interactions and play an important part in cosmological theories.

We have established the general geometric properties of symmetry groups. Let us now proceed to the particular types of groups.

2.6 Point Symmetry Groups

2.6.1 Description and Representation of Point Groups

Symmetry operations of point groups leave at least one singular point of space unmoved. We shall derive all the possible point groups G_0^3 and give special attention to the 32 crystallographic point groups. We denote them by K; they are also called classes. These groups describe the symmetry of the external shape and minimum symmetry of the macroscopic properties of crystals. The 32 crystallographic point groups K were first found by *Hessel* [2.10] and, independently, by *Gadolin* [2.11].

Point groups can be represented with the aid of an axonometric drawing of the symmetry elements and the corresponding regular point systems or regular systems of figures. Stereographic projection is then widely used.

Let us consider one of the features of RPS of general position in groups G_0^3. These points are symmetrically equal, and hence the vectors drawn to them from the special, fixed point are also equal. This means that the points of general position of any point group are situated on the surface of a sphere. Therefore any point symmetry transformations can be regarded as rotations (proper and improper) of a sphere, which transform its points to points symmetrically equal to them. In other words, groups G_0^3 are isomorphous to the groups of rotation (of both kinds) of a sphere. The axes and planes of symmetry pass through the center of the sphere, their intersections with the surface – points and arcs of great circles – represent the spherical projection of these symmetry elements (Fig. 2.34).

A spherical projection is very pictorial, but is difficult to represent, and therefore we must switch from it to a plane drawing, done by using a stereographic projection (Fig. 2.35a). This is the same projection which is used to represent the globe surface on a geographical map by two plane "hemispheres"

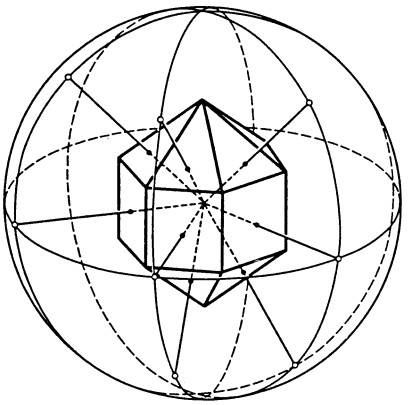

Fig. 2.34. Spherical projection of a crystal

with a network of parallels and meridians. The equator of a stereographic projection corresponds to the equatorial section of a spherical projection, and the poles, to the emergences of the normal to this section. All the central sections of the sphere, and hence the planes of symmetry of the point groups, are represented on a stereographic projection as arcs of great circles (in a particular case, as straight lines) passing through diametrically opposite points (Fig. 2.35b).

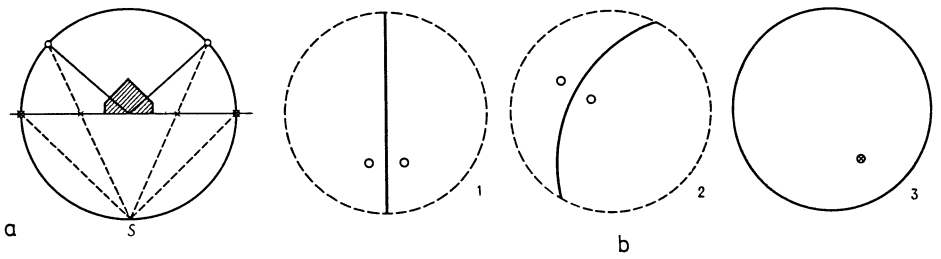

Fig. 2.35a,b. Stereographic projection.
(**a**) the principle of construction of a stereographic projection; (**b**) symmetry plane perpendicular (1), inclined (2), and parallel (3) to the plane of the drawing. Mirror-equal points are denoted by circles (if they are on the upper hemisphere) or by crosses (if they are on the lower)

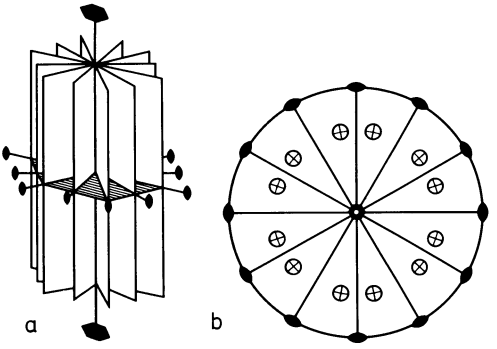

Fig. 2.36a,b. Set of symmetry elements of the point group $\bar{6}/mmm$ on an isometric (**a**) and a stereographic (**b**) projection. The latter also shows symmetrically equal points

Incidentally, it is usually sufficient to depict the emergences of the symmetry elements on one ("upper") hemisphere of this projection. If we must distinguish the points of the "upper" and "lower" hemispheres, they can be depicted as open circles and crosses, respectively (Fig. 2.35b). Figure 2.36 shows a perspective representation of the set of symmetry elements of one of the point groups and the corresponding stereographic projection.

2.6.2 On Derivation of Three-Dimensional Point Groups G_0^3

There are different methods for deriving symmetry groups. Almost all these methods are based on examination of all the permissible combinations of generators (generating elements) of groups, group theory or geometric analysis of these combinations, and proofs that this examination is exhaustive. There are algorithms for derivation of symmetry groups based on the isomorphism of their operations with other algebraic classes of elements, for instance substitutions. We shall use the method of examination on the basis of geometric considerations, because it gives the spatial idea of symmetry, which is most important to crystallography.

As we know, symmetry operations of point groups are simple N and mirror $\tilde{N}$ (or inversion $\bar{N}$) rotations. Cyclic groups are characterized by the presence of one symmetry element. But several distinct and differently oriented symmetry elements may pass through the singular point. Each of them, as we know, transforms itself into itself by the action of "its own" operation $g_i \in G_0^3$ and transforms all the other elements into equivalent ones. The task of deriving groups G_0^3 actually consists in finding closed sets of operations g_i and the corresponding geometric combinations of symmetry elements.

Indeed, axis N will reproduce any axis inclined to it into N axes and any plane nonperpendicular to it into N planes. Any plane will double the number of planes or axes intersecting it, unless they coincide with it or are perpendicular to it. Therefore "oblique" symmetry elements will give new ones, and these will generate the next ones, etc. A finite point group can clearly be obtained if the elements combined are so positioned that their mutually reproducing action brings, immediately or after a finite number of operations, the elements being generated into coincidence with the existing ones.

To consider interaction of operations we shall use theorems I and III of Sect. 2.2.4, which states that the action of any rotation axis can be replaced by that of two mirror planes passing through it (see Fig. 2.9a), and the action of two intersecting rotation axes is equivalent to that (i.e., causes the appearance) of a third axis (see Fig. 2.10).

One rotation axis N is always possible. If there are two axes N_1 and N_2, then there is a third axis N_3. Let us join, on a spherical projection, their emergences by arcs of a great circle, which will yield a spherical triangle, and the entire sphere will be divided into such triangles (Fig. 2.37). The angles at the vertices of these triangles a_i are half the elementary rotation angle of the corresponding

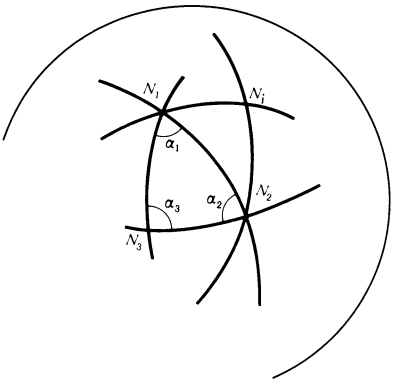

Fig. 2.37. Emergence of symmetry axes at the sphere surface.

axis. The sum of the angles of a spherical triangle exceeds π; therefore,

$$\frac{2\pi}{2N_1}+\frac{2\pi}{2N_2}+\frac{2\pi}{2N_3}>\pi, \quad \text{i.e.} \quad \frac{1}{N_1}+\frac{1}{N_2}+\frac{1}{N_3}>1. \tag{2.75}$$

The following possibilities arise. The first case is that of a single principal axis N_3 of any order, and $N_1 = 2$, and $N_2 = 2{:}N22$. Although at first sight there are numerous combinations of axes of any order, according to (2.75) only the following are possible (we write the names of the axes directly): 332, 432, 532. These are the so-called rotation groups. This consideration of the division of a spherical surface into spherical triangles, which limits the combination of axes, resembles to some extent the consideration of a plane with a group T_2 (see Fig. 2.17), which limits the order of corresponding crystallographic axes $N = 1, 2, 3, 4, 6$. If the point group is of the second kind, then $G_0^{3,\mathrm{II}} \supset G_0^{3,\mathrm{I}}$ by (2.58), i.e., it contains a subgroup of all its rotations, and thus only the same combinations of axes are possible in it.

The number of point groups is infinitely large. Therefore, following *Shubnikov* [2.7, 8], we divide them into families. A family is characterized by definite group generators and the relationships between them, and also by its continuous limiting group , so that all the groups of a given family are its subgroups. Each given family also contains crystallographic groups K. We shall give the family symbol in international and Schönflies notation. Each family will be represented by a scheme in which its symbol will be indicated at the top, then followed by the generator of the group and, finally, by the limiting group of the family. We shall indicate the mutual orientation of the symmetry elements, if required. For groups containing only one principal axis, N or $\tilde{N}$ we shall write out, in separate rows, the axes of odd and even orders. Groups K are always the first two in the upper row and the first three in the lower.

The difference between the odd and even rows is substantial because the corresponding groups have some peculiarities. For instance, one of these peculiarities is the presence or absence of polar directions. For crystallographic

groups of each family we shall give the picture of arrangement of their symmetry elements.

2.6.3 Point Group Families

To begin with, we shall consider families consisting of groups of the first kind.

I. Groups $N - C_n$ (Fig. 2.38; see also Fig. 2.19a):

$$\begin{array}{lll} & 1\ 3\ 5\ 7\ \ldots & \\ N & & \infty. \\ & 2\ 4\ 6\ 8\ \ldots & \end{array}$$

These groups are cyclic of order $n = N$, $g_i^n = g_0 = e$; they have a single element of symmetry, axis N of rotation. Any point of this axis is singular. If $n = n_1 \cdot n_2$, then axes $N_1, N_2, \ldots$ coincide with axis N, i.e., group N contains subgroups $N_1, N_2, \ldots$ In odd groups ($N = 2n + 1$) all the directions are polar, and in even ones ($N = 2n$) the directions perpendicular to N are nonpolar. The principal axis N in groups of this family is always polar.

II. Groups $N2 - D_n$ (Fig. 2.39):

$$\begin{array}{lllllll} & (12 = 2) & & 32 & & 52 & & 72 \ldots & \\ N,\ 2(2 \perp N) & & & & & & & & \infty\ 2. \\ & & 22 = 222 & & 42 = 422 & & 62 = 622 & \ldots & \end{array}$$

In these groups there is a single principal axis N and axis 2 perpendicular to it. Condition $2 \perp N$ is obligatory, since otherwise the action of axis 2 would give another axis N. Because N and 2 are perpendicular, axis 2 only "reverses" axis N and brings it into self-coincidence. The parentheses contain the group 2, already derived in family I, in a different orientation.

All these groups contain the principal axis N and n axes 2 as symmetry elements. The presence of n axes 2 in odd groups is understandable: the principal axis N reproduces n times the axis 2 perpendicular to it. In even groups the action of N on axis 2 yields $n/2$ equivalent axes, because the even powers of this operation will bring each such axis 2 into self-coincidence (although with opposite ends). Here, however, another set arises of $n/2$ axes 2 corresponding to the products of operations $N \cdot 2$. As an example let us consider the simplest case where axis 2 is the principal one (see Fig. 2.39). Axis 2 perpendicular to it is already itself symmetric with respect to the first (and vice versa), and it would

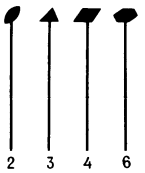

Fig. 2.38. A set of symmetry elements of crystallographic groups of rotations N–C_n

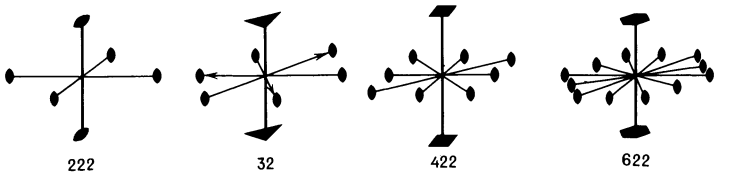

Fig. 2.39. Set of symmetry elements of crystallographic groups of family $N2 - D_n$

seem that this group must contain only two axes 2 (one besides the principal). But according to Euler's theorem (see Fig. 2.10) a third axis, 2, arises perpendicular to both. Since this third axis is not derived by symmetry operations from the second, it is customary to write the symbol of this group as 222, rather than 22, although the latter is sufficient, because it contains the generating operations. The situation with the other even groups of this family is similar.

The principal axis N of family II is nonpolar. The order of the groups of this family is $2n$; they contain groups N and 2 as subgroups.

We shall now pass on to groups with a single principal axis, which contain operations of the second kind.

IIIa. Groups of inversion rotations $\bar{N} - S$ (Fig. 2.40; see also Fig. 2.19b):

$$\begin{array}{lllllllll}
 & \bar{1} & & \bar{3} & \bar{5} & & \bar{7} & \bar{9} & \ldots \\
\bar{N} & & & & & & & & \\
 & \bar{2} = m & & \bar{4} & \bar{6} = 3/m & & \bar{8} & \overline{10} = 5/m & \ldots \\
 & & & & & & & & \infty/m. \\
 & & \tilde{1} & & & \tilde{3} & & & \tilde{5} \ldots \\
\tilde{N} & & & & & & & & \\
 & \tilde{2} & & \tilde{6} & \tilde{4} & \widetilde{10} & & \widetilde{14} \; \tilde{8} \; \widetilde{18} &
\end{array}$$

These are inversion-rotation groups; all of them are cyclic. The order of the groups is $\bar{N}_{\text{even}} - n$, $\bar{N}_{\text{odd}} - 2n$. Each of the groups of inversion rotations $\bar{N}$ is equivalent to one of the groups of mirror rotations $\tilde{N}$. Rules of correspondence of groups $\bar{N}$ and $\tilde{N}$ are as follows: odd groups (axes) of one name are even groups (axes) of the other name, i.e., $\bar{N}_{\text{odd}} = 2\tilde{N}$, $\tilde{N}_{\text{odd}} = \overline{2N}$. Twice-even (multiples of four) groups (axes) are equivalent. Groups $\bar{2}$, $\bar{6}$, $\overline{10}$ are actually groups N_{odd}/m of the IIIb family (Fig. 2.40).

Let us now consider groups containing planes m in addition to the principal axis N. The requirement for uniqueness of the principal axis N makes it possible to arrange the plane in two ways: with m perpendicular to N, which is denoted as $\frac{N}{m}$ (or N/m), or with axis N lying in this plane, which is designated as Nm. If we assume that the principal axis is vertical, then, according to Schönflies, the first

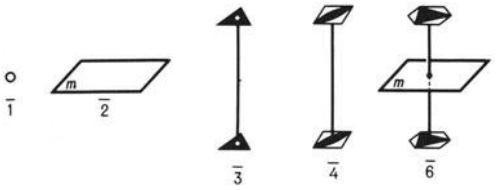

Fig. 2.40. Set of symmetry elements of crystallographic groups of inversion rotations $\bar{N} - S$

groups have the notation C_{nh}(h being the horizontal plane), and the second, C_{nv} (v being the vertical plane).

III. Groups $N/m - C_{nh}$ (Fig. 2.41):

$$(1/m = m) \qquad (3/m = \bar{6}) \qquad (5/m = \overline{10}) \ldots$$

N, $m(m \perp N)$ ∞/m.

$$2/m \qquad 4/m \qquad 6/m \ldots$$

The order of the groups is $2n$. Groups with odd N (enclosed in parentheses) were already contained in family IIIa. Groups of IIIa and IIIb have the limiting group in common and therefore can be regarded as two subfamilies of one and the same family.

IV. Groups $Nm - C_{nv}$ (Fig. 2.42):

$$(1m = m) \qquad 3m \qquad 5m \qquad \ldots$$

N, $m(N \in m)$ ∞mm.

$$2m = mm2 \qquad 4m = 4mm \qquad 6m = 6mm \ldots$$

These groups, with the exception of the principal axis N, have other n planes passing through the principal axis as symmetry elements. The appearance of

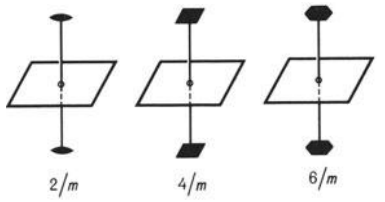

Fig. 2.41. Set of symmetry elements of crystallographic groups of rotations with reflections in planes perpendicular to the principal axis, $N/m - C_{nh}$

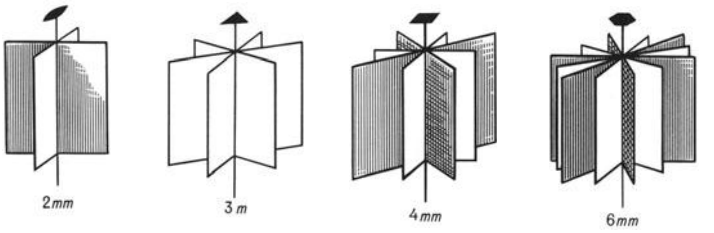

Fig. 2.42. Set of symmetry elements of crystallographic groups with reflections in planes coinciding with the principal axis, $Nm - C_{nv}$

n planes, in accordance with the order of the axis, is understandable for odd groups, and for even groups it is explained in the same way as for axes 2 in groups $N2$. Therefore their formulae (second row) have the form Nmm. The order of groups Nm is equal to $2n$.

Let us consider the combination of symmetry planes with inversion (or mirror) axes. If these elements are perpendicular, we do not obtain new groups, since the groups of inversion (or mirror) rotations are themselves subgroups of groups N/m. When the planes coincide with the axes, new groups arise.

Va. Groups $\bar{N}m - D_{nd}$ (Fig. 2.43):

$$(\bar{1}m = 2/m) \qquad \bar{3}m \qquad \bar{5}m \quad \ldots$$

$$\bar{N},\ m(\bar{N} \in m) \qquad\qquad \infty/mm.$$

$$(\bar{2}m = mm2) \quad \bar{4}m = \bar{4}2m \quad (\bar{6}m = \bar{6}m2) \quad \ldots$$

In these groups, in addition to the generating elements, axes 2 arise perpendicular to $\bar{N}$; in odd and twice-even groups they bisect the angles between the planes of symmetry. Group $\bar{2}m = mm2$ is already familiar to us.

Since $\bar{6} \equiv 3/m$, $\overline{10} \equiv 5/m$, groups $\bar{6}m2$, etc., in the second row above, could also be considered in the next subfamily Vb. In them, axes 2, perpendicular to the principal, arise; they lie at the intersection of the horizontal and vertical planes.

Let us consider groups containing both horizontal and vertical planes m.

Vb. Groups $\dfrac{N}{m}m - D_{nh}$ (Fig. 2.44):

$$N,\ m_{\perp}, m_{\parallel}(N \in m_{\parallel})$$

$$\left(\frac{1}{m}m = mm2\right) \quad \left(\frac{3}{m}m = \bar{6}m2\right) \quad \left(\frac{5}{m}m = \overline{10}m2\right) \ldots$$

$$\infty/mm.$$

$$\frac{2}{m}m = mmm \qquad \frac{4}{m}m = 4/mmm \qquad \frac{6}{m}m = 6/mmm \ldots$$

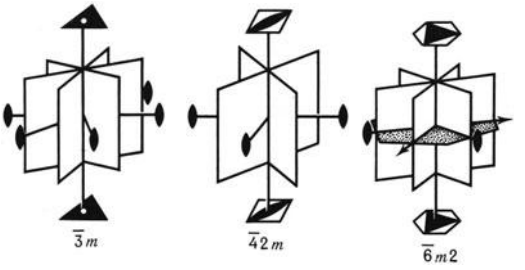

Fig. 2.43. Set of symmetry elements of crystallographic groups of inversion rotations with reflections in planes coinciding with the inversion-rotation axis, $\bar{N}m - D_{nd}$

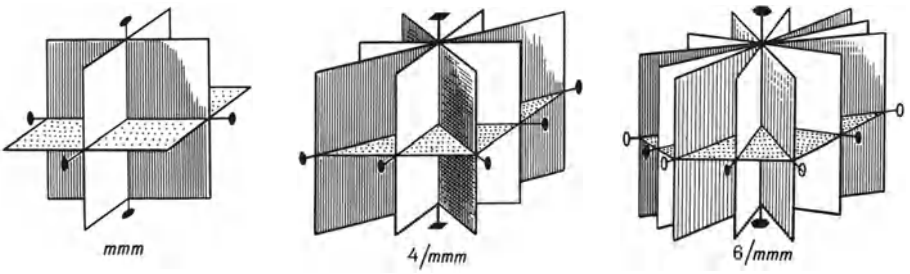

Fig. 2.44. Set of symmetry elements of crystallographic groups of rotations with reflections in symmetry planes coinciding with the principal symmetry axis and perpendicular to it, $\left(\frac{N}{m}m - D_{nh}\right)$

The intersection of the horizontal and vertical planes m generates axes 2. Therefore the full symbols of the even groups are

$$\frac{2}{m}\frac{2}{m}\frac{2}{m};\quad \frac{4}{m}\frac{2}{m}\frac{2}{m};\quad \frac{6}{m}\frac{2}{m}\frac{2}{m}.$$

The order of all the groups of this family is $4n$.

The limiting group ∞/mm contains, as subgroups, all the groups of the above-listed families I–V, including their limiting groups.

We have exhausted all the possibilities of constructing point groups with a single principal axis. Let us now pass on to groups with oblique axes, which are very few in number, as we have seen before.

VI. Groups N_1N_2 (Fig. 2.45)

3; 2, 4, 5 $\quad 23 - T,\quad 432 - O,\quad 532 - Y;\quad \infty\,\infty$

These are groups of rotations with an "oblique" arrangement of the axes. According to (2.75) the number of such groups is only three.

The orders of these three groups are 12, 24, and 60, respectively. Among them, the first two are crystallographic groups K. Like families I and II, these

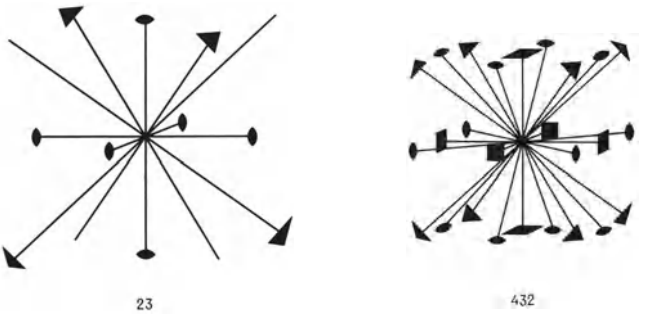

Fig. 2.45. Set of symmetry elements of cubic crystallographic rotation groups

groups are of the first kind, and all of them taken together exhaust the groups of the type $G_0^{3,1}$.

Adding planes m (or center $\bar{1}$), we obtain groups of the second kind.

VII. Groups $\bar{N}_1 N_2$ (Fig. 2.46)

3; $\bar{1}$, m; 2, 4, 5 $m\bar{3}$—T_h, $\bar{4}3m$—T_d $m\bar{3}m$—O_h, $m\bar{5}m$—Y_h; $\infty\,\infty\, m$.

These are groups of proper and improper rotations with an "oblique" arrangement of the axes and mirror planes. Addition of planes m passing through axes 2 (or inversion $\bar{1}$ as well) to group 23 gives group $m\bar{3}$; this group can be denoted also by $\tilde{6}/2$ or $\bar{3}/2$. Addition of planes m passing through axes 3 to 23 gives group $\bar{4}3m$, in which axes 2 turn into $\bar{4}$. This group does not contain $\bar{1}$. Addition of m (or $\bar{1}$) to 432 gives $m\bar{3}m$, in which the symmetry planes pass through axes 4, 3, 2. Axes 3 in it become axes $\tilde{6} = \bar{3}$. Another arrangement of the planes would have produced additional symmetry axes, which is impossible for finite groups. Similar addition of m to 532 gives the group $m\bar{5}m$.

The orders of groups VII are 24, 24, 48, 120. The first three of them are groups K.

Groups of families VI and VII are groups of transformation of regular polyhedra into themselves – only of their rotations or also reflections (Fig. 2.47). All the crystallographic groups in them are subgroups of group O_h of transformations of a cube and an octahedron into themselves (Fig. 2.47a,b), and therefore these groups are called cubic. Groups T and T_d transform a tetrahedron into itself (Fig. 2.47c). The interaxial angles in cubic groups are shown in Fig. 2.48. The value of the tetrahedral angle between the axes running from the tetrahedron center to its vertices (i.e., between axes 3) is equal to 109°28′16″.

Groups Y and Y_h are groups of transformation of an icosahedron or pentagondodecahedron into itself (Fig. 2.47e,f); they are called icosahedral. These noncrystallographic groups are of great interest, because they describe the structure of closed pseudospherical objects, in particular, various artificial shells (Fig. 2.50a). Icosahedral packings of atoms are observed in a number of structures (Fig. 2.50b) though, naturally, it is only local symmetry because, as we

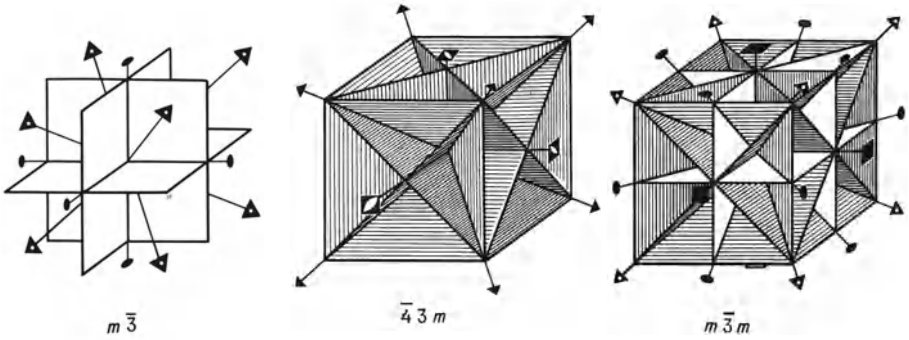

Fig. 2.46. Set of symmetry elements of cubic crystallographic groups with reflections

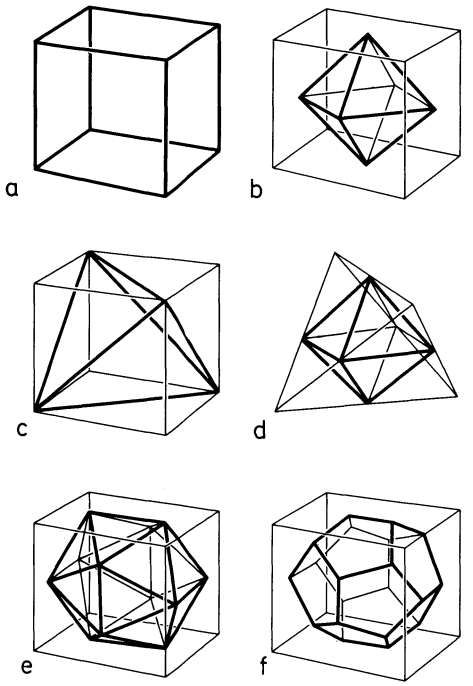

Fig. 2.47a–f. Regular polyhedra and their relation.
(**a**) cube; (**b,c**) octahedron and tetrahedron inscribed in a cube; (**d**) relation between an octahedron and a tetrahedron; (**e,f**) icosahedron and dodecahedron inscribed in a cube

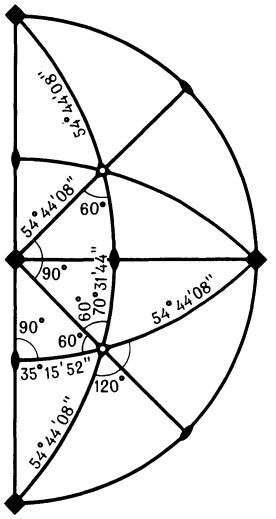

Fig. 2.48. Angles between axes in cubic groups

know, 5-fold axes are prohibited in crystals. Icosahedral point symmetry is exhibited by the so-called spherical viruses [Ref. 2.13, Fig. 2.29].

Thus, we have derived all the point groups G_0^3, whose number is infinite; the number of families is 7 (9 with subfamilies), of which 2 are finite. The number of crystallographic groups K is 32. The stereographic projections of all the 32

crystallographic and 2 icosahedral point groups according to the families and subfamilies are given in Fig. 2.49. In the same figure the symbols of continuous limiting groups and figures illustrating them are given.

The limiting group of proper and imporper rotations $\infty\,\infty\,m$ contains, as subgroups, all the point groups and, in particular, all the limiting groups of families I–V. The limiting group of rotations $\infty\,\infty$ contains all the groups of the first kind (I, II, VI) as subgroups.

We did not concern ourselves with two-dimensional point groups. They are very easy to find. If there is a singular point, a plane can be brought to self-coincidence either exclusively by rotations N about this point or also by

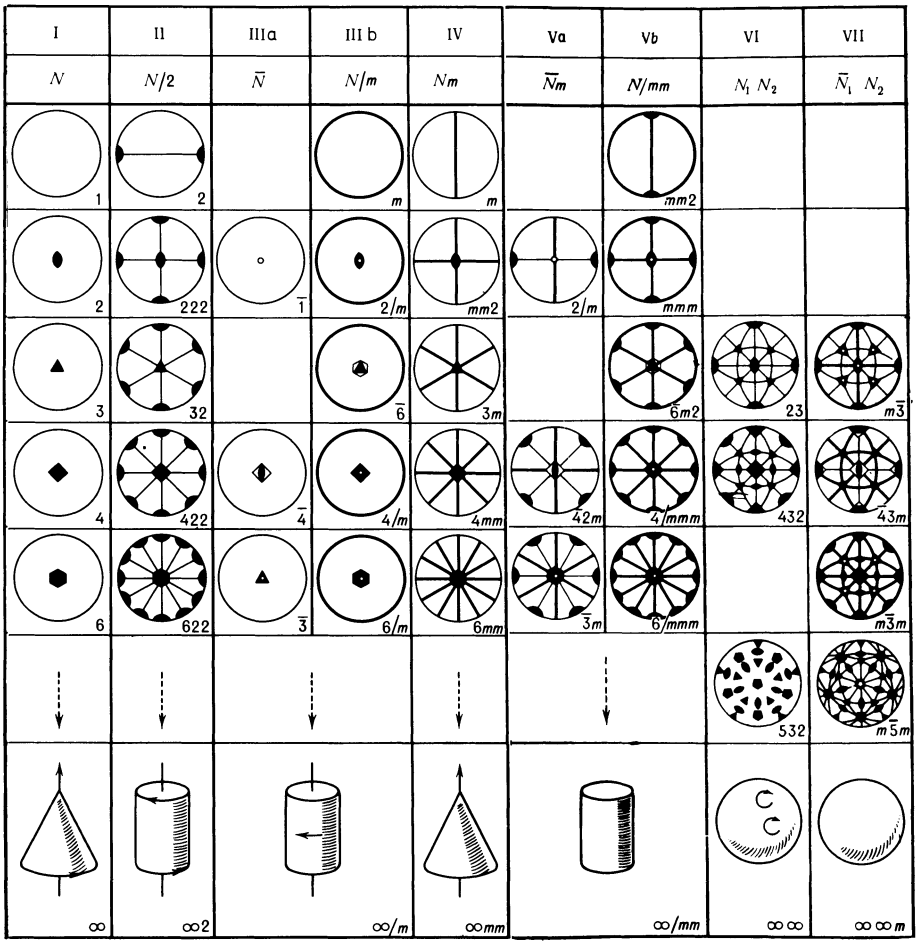

Fig. 2.49. Stereographic projections of 32 crystallographic and 2 icosahedral groups with indication of the limiting group and with the figure illustrating it. The symmetry planes are denoted by solid lines. The circular arrows in the lower-row figures indicate the rotation of the figure as a whole or of the points of its surface; the straight arrows show the polar directions

reflections in the line of symmetry m passing through it. Therefore, as is easy to see, all the groups G_0^2 are groups N or Nm, i.e., they are isomorphous to families I and IV of the three-dimensional groups. There are 10 crystallographic two-dimensional point groups (see the representations of groups of families I and IV in Fig. 2.49).

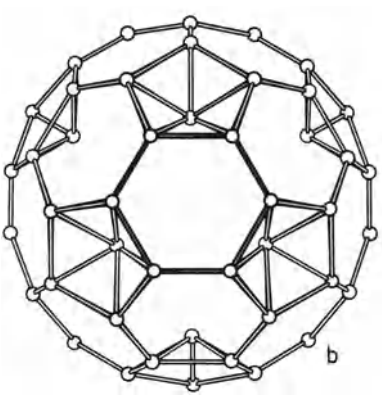

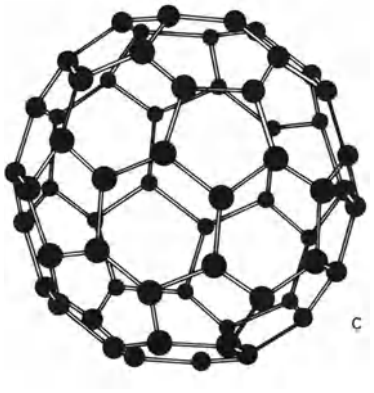

Fig. 2.50a–c. Examples of objects exhibiting an icosahedral symmetry $Y_h - m\bar{5}m$.
(**a**) pseudospherical architectural construction made up of triangular elements according to icosahedral symmetry. Five triangles group together at 12 points of the pseudosphere; (**b**) upper outer half of a complicated group of 84 atoms in one of the boron modifications. The group shows icosahedral symmetry. Inside (not shown) is a regular icosahedron made up of boron atoms and bound with the "depressed" atoms of the outer shell [2.12]; (**c**) the molecule of an allotropic carbon modification consisting of sixty carbon atoms – fullerene C_{60}

2.6.4 Classification of Point Groups

Figure 2.49 and Tables 2.3–5 show all the crystallographic point groups and some of their characteristics. In addition to the international and Schönflies' designations Table 2.3 includes the convenient notation of *Shubnikov* [2.7, 8], in which the point (·) between the symmetry elements denotes their parallelism; and two points (:) their perpendicularity; and the stroke, the oblique disposition

Table 2.3. Symbols and names of the 32 point groups of symmetry

Syngony	Symbol			Symmetry formula	Name of the class
	International	After Shubnikov	After Schönflies		
Triclinic	1	1	C_1	L_1	Monohedral
	$\bar{1}$	$\tilde{2}$	$C_i = S_2$	C	Pinacoidal
Monoclinic	2	2	C_2	L^2	Dihedral axial
	m	m	$C_{1h} = C_s$	P	Dihedral axisless
	$2/m$	$2{:}m$	C_{2h}	L^2PC	Prismatic
Orthorhombic	222	2:2	$D_2 = V$	$3L^2$	Rhombotetrahedral
	$mm2$	$2{\cdot}m$	C_{2v}	L^22P	Rhombopyramidal
	mmm	$m{\cdot}2{:}m$	$D_{2h} = V_h$	$3L^23PC$	Rhombodipyramidal
Tetragonal	4	4	C_4	L^4	Tetragonal-pyramidal
	422	4:2	D_4	L^44L^2	Tetragonal-trapezohedral
	$4/m$	$4{:}m$	C_{4h}	L^4PC	Tetragonal-dipyramidal
	$4mm$	$4{\cdot}m$	C_{4v}	L^44P	Ditetragonal-pyramidal
	$4/mmm$	$m{\cdot}4{:}m$	D_{4h}	L^44L^25PC	Ditetragonal-dipyramidal
	$\bar{4}$	$\bar{4}$	S_4	L_4^2	Tetragonal-tetrahedral
	$\bar{4}2m$	$\bar{4}{\cdot}m$	$D_{2d} = V_d$	$L_4^22L^22P$	Tetragonal-scalenohedral
Trigonal	3	3	C_3	L^3	Trigonal-pyramidal
	32	3:2	D_3	L^33L^2	Trigonal-trapezohedral
	$3m$	$3{\cdot}m$	C_{3v}	L^33P	Ditrigonal-pyramidal
	$\bar{3}$	$\tilde{6}$	$C_{3i} = S_6$	L_6^3C	Rhombohedral
	$\bar{3}m$	$\tilde{6}{\cdot}m$	D_{3d}	$L_6^33L^23PC$	Ditrigonal-scalenohedral
Hexagonal	$\tilde{6}$	$3{:}m$	C_{3h}	L^3P	Trigonal-dipyramidal
	$\tilde{6}m2$	$m{\cdot}3{:}m$	D_{3h}	L^33L^24P	Ditrigonal-dipyramidal
	6	6	C_6	L^6	Hexagonal-pyramidal
	622	6:2	D_6	L^66L^2	Hexagonal-trapezohedral
	$6/m$	$6{:}m$	C_{6h}	L^6PC	Hexagonal-dipyramidal
	$6mm$	$6{\cdot}m$	C_{6v}	L^66P	Dihexagonal-pyramidal
	$6/mmm$	$m{\cdot}6{:}m$	D_{6h}	L^66L^27PC	Dihexagonal-dipyramidal
Cubic	23	3/2	T	$3L^24L^3$	Tritetrahedral
	$m\bar{3}$	$\tilde{6}/2$	T_h	$3L^24L_6^33PC$	Didodecahedral
	$\bar{4}3m$	$3/\bar{4}$	T_d	$3L_4^24L^36P$	Hexatetrahedral
	432	3/4	O	$3L^44L^36L^2$	Trioctahedral
	$m\bar{3}m$	$\tilde{6}/4$	O_h	$3L^44L_6^36L^29PC$	Hexoctahedral

Note. In the "symmetry formula" we have the following symbols used sometimes in textbooks: (L) axes, (C) center, and (P) plane of symmetry; each symbol is preceded by the number of the relevant elements.

of these elements. Also included is the "symmetry formula" (indicating the number of each symmetry element of a given group) and the name of the class.

Table 2.5 gives the matrices of the generating operations. These matrices depend on the choice of the reference axes. This choice is made in conformity with the crystal symmetry using definite rules, which are called the crystal setting. (This will be discussed in Sect. 3.2.1; see Table 3.5.)

The point groups are classified according to a number of features. Our derivation was based on the classification by the limiting symmetry group which, as we shall see further on, also plays an important part in analyzing the physical properties of crystals. However, analysis of these properties makes it possible to classify groups K according to other features as well. If we divide the families according to the symmetry operations, then families I, II, and VI are of the first kind, their elements are only rotation axes, and enantiomorphism is possible in them. All the other families are of the second kind.

The above derivation of point groups according to the families actually consisted in consideration of the possible direct and semidirect products (2.41, 42) of some simplest initial groups – axial N, inversion $\bar{1}$, and reflection m, with their geometrically permissible mutual orientations. A summary of 32 crystallographic groups recorded in this manner is given in Table 2.4. Inversion groups may also contain planes; mirror groups contain no inversion center. Group $\bar{4}$, which has neither m, nor $\bar{1}$, is placed among the latter conventionally; it is a nontrivial subgroup of group $4/m = 4 \otimes \bar{1} \supset \bar{4}$.

We can see that among the 32 groups K there are 11 groups of the first kind, K^{I}, and 21 of the second kind K^{II}. Among the latter, 11 groups have an inversion center. In classifying the groups according to the presence of a single principal axis we obtain families I–V, and according to the presence of several axes of order 3 and higher, families VI–VII – cubic groups. The scheme of subordina-

Table 2.4. Rotation, inversion, and mirror groups K

Rotation groups K^{I}	Groups K^{II}	
	Inversion	Mirror
1	$\bar{1}\ (= 1 \otimes \bar{1})$	$m (= 1 \otimes m)$
2	$2/m = 2 \otimes \bar{1}$	$mm2 = 2 \otimes m$
3	$\bar{3} = 3 \otimes \bar{1}$	$\bar{6} = 3 \otimes m$; $3m = 3 \circledS m$
4	$4/m = 4 \otimes \bar{1}$	$4mm = 4 \circledS m$; $\bar{4}$
$6 = 3 \otimes 2$	$6/m = 6 \otimes \bar{1}$	$6mm = 6 \circledS m$
$222 = 2 \otimes 2$	$mmm = 222 \otimes \bar{1}$	$\bar{4}2m = 222 \circledS m$
$32 = 3 \circledS 2$	$3m = 32 \otimes \bar{1}$	$\bar{6}m2 = 32 \otimes m$
$422 = 4 \circledS 2$	$4/mmm = 422 \otimes \bar{1}$	—
$622 = 6 \circledS 2$	$6/mmm = 622 \otimes \bar{1}$	—
$23 = 222 \circledS 3$	$m\bar{3} = 23 \otimes \bar{1}$	$\bar{4}3m = 23 \circledS m$
$432 = 23 \circledS 2$	$m\bar{3}m = 432 \otimes \bar{1}$	—

tion of the limiting groups of the families is as follows:

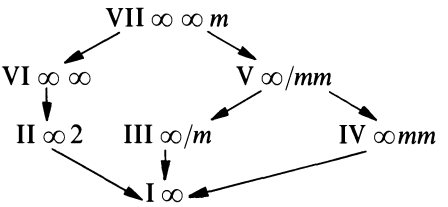

Each lower-lying group is a subgroup of the senior group joined to it by an arrow. Analogous subordination schemes can be written for each point group. Similarly, for each of the point groups one can find those groups ("supergroups") whose subgroup it is. Note that all the 32 crystallographic groups K are the subgroups of two groups: cubic $m\bar{3}m$ and hexagonal $6/mmm$.

An important division of the crystallographic groups K is the division into seven syngonies (or systems). This division is based on the point symmetry of the space lattice of the crystal, which manifests itself in the symmetry of the unit parallelelpiped and is expressed in definite relationships between its periods and angles. The division of groups K according to this principle is due to the fact that the symmetry in question is crystallographic and determined by the presence of a space lattice in crystals. In Sect. 2.8., we shall treat the lattice symmetry and the division into syngonies in detail; at this junction we shall only characterize them.

The characteristics of the syngonies and the distribution of the groups K among them are given in Tables 2.3 and 2.5. In the general case of triclinic syngony all the periods are unequal to each other: $a \neq b \neq c$, and the interaxial angles also differ from each other $\alpha \neq \beta \neq \gamma$ and from 90°; in the highest, cubic syngony $a = b = c$ and $\alpha = \beta = \gamma = 90°$. The remaining cases – the hexagonal, trigonal (it is also called rhombohedral), tetragonal, orthorhombic, and monoclinic syngonies – are intermediate and are characterized by the values of all or some of the angles of 90° (or 60°) and the equality of all or some periods.

Groups K are groups of symmetry of the shape (habit) of crystals. They, and hence the syngony of crystals, can be found by goniometrical measuring of the external form of the crystal[13]; this can also be done by x-ray diffraction, of course. All the groups K belonging to a given syngony are a subgroup of a higher group characterizing the syngony. Such a group is called holohedral. This name originates from the consideration of the crystal habit (see Sect. 3.2.4) and means "completely-faced".

Point groups of symmetry describe not only the external shape (habit) of crystals, but also their properties. With respect to the point group K of a crystal, point groups G_{P_i} describing its intrinsic properties are supergroups of K. The highest group of certain properties may also be the limiting point group

[13] When measuring the external form by goniometry (see Chap. 3), a complex of possible faces turns out to be the same both for hexagonal and trigonal crystals. Therefore some authors unite them into one system. At such approach, there are 6 (and not 7) systems.

Table 2.5. Matrices of point group generators

Syngony and metric relation	International symbols	Generator matrices in the orthogonal system of coordinates		
Triclinic, $a \neq b \neq c$, $\alpha \neq \beta \neq \gamma$,	1	$\begin{bmatrix} 1 & 0 & 0 \\ 0 & 1 & 0 \\ 0 & 0 & 1 \end{bmatrix}$		
	$\bar{1}$	$\begin{bmatrix} -1 & 0 & 0 \\ 1 & -1 & 0 \\ 0 & 0 & -1 \end{bmatrix}$		
Monoclinic, $a \neq b \neq c$, $\gamma \neq \alpha = \beta = 90°$	2	$\begin{bmatrix} -1 & 0 & 0 \\ 0 & -1 & 0 \\ 0 & 0 & 1 \end{bmatrix}$		
	m	$\begin{bmatrix} 1 & 0 & 0 \\ 0 & 1 & 0 \\ 0 & 0 & -1 \end{bmatrix}$		
	$2/m$	$\begin{bmatrix} -1 & 0 & 0 \\ 0 & -1 & 0 \\ 0 & 0 & 1 \end{bmatrix}$	$\begin{bmatrix} 1 & 0 & 0 \\ 0 & 1 & 0 \\ 0 & 0 & -1 \end{bmatrix}$	
Orthorhombic $a \neq b \neq c$, $\alpha = \beta = \gamma = 90°$	222	$\begin{bmatrix} 1 & 0 & 0 \\ 0 & -1 & 0 \\ 0 & 0 & -1 \end{bmatrix}$	$\begin{bmatrix} -1 & 0 & 0 \\ 0 & -1 & 0 \\ 0 & 0 & 1 \end{bmatrix}$	
	$mm2$	$\begin{bmatrix} -1 & 0 & 0 \\ 0 & 1 & 0 \\ 0 & 0 & 1 \end{bmatrix}$	$\begin{bmatrix} -1 & 0 & 0 \\ 0 & -1 & 0 \\ 0 & 0 & 1 \end{bmatrix}$	
	mmm	$\begin{bmatrix} -1 & 0 & 0 \\ 0 & 1 & 0 \\ 0 & 0 & 1 \end{bmatrix}$	$\begin{bmatrix} 1 & 0 & 0 \\ 0 & -1 & 0 \\ 0 & 0 & 1 \end{bmatrix}$	$\begin{bmatrix} 1 & 0 & 0 \\ 0 & 1 & 0 \\ 0 & 0 & -1 \end{bmatrix}$
Tetragonal, $a = b \neq c$, $\alpha = \beta = \gamma = 90°$	4	$\begin{bmatrix} 0 & 1 & 0 \\ -1 & 0 & 0 \\ 0 & 0 & 1 \end{bmatrix}$		
	$\bar{4}$	$\begin{bmatrix} 0 & -1 & 0 \\ 1 & 0 & 0 \\ 0 & 0 & -1 \end{bmatrix}$		
	422	$\begin{bmatrix} 0 & 1 & 0 \\ -1 & 0 & 0 \\ 0 & 0 & 1 \end{bmatrix}$	$\begin{bmatrix} 1 & 0 & 0 \\ 0 & -1 & 0 \\ 0 & 0 & -1 \end{bmatrix}$	
	$4/m$	$\begin{bmatrix} 0 & 1 & 0 \\ -1 & 0 & 0 \\ 0 & 0 & 1 \end{bmatrix}$	$\begin{bmatrix} 1 & 0 & 0 \\ 0 & 1 & 0 \\ 0 & 0 & -1 \end{bmatrix}$	
	$4mm$	$\begin{bmatrix} 0 & 1 & 0 \\ -1 & 0 & 0 \\ 0 & 0 & 1 \end{bmatrix}$	$\begin{bmatrix} -1 & 0 & 0 \\ 0 & 1 & 0 \\ 0 & 0 & 1 \end{bmatrix}$	
	$\bar{4}2m$	$\begin{bmatrix} 0 & -1 & 0 \\ 1 & 0 & 0 \\ 0 & 0 & -1 \end{bmatrix}$	$\begin{bmatrix} 1 & 0 & 0 \\ 0 & -1 & 0 \\ 0 & 0 & -1 \end{bmatrix}$	
	$4/mmm$	$\begin{bmatrix} 0 & 1 & 0 \\ -1 & 0 & 0 \\ 0 & 0 & 1 \end{bmatrix}$	$\begin{bmatrix} 1 & 0 & 0 \\ 0 & 1 & 0 \\ 0 & 0 & -1 \end{bmatrix}$	$\begin{bmatrix} -1 & 0 & 0 \\ 0 & 1 & 0 \\ 0 & 0 & 1 \end{bmatrix}$
Trigonal, in rhombohedral axes $a = b = c$, $\alpha = \beta = \gamma \neq 90°$ (description in hexagonal axes is also possible)	3	$\begin{bmatrix} -1/2 & \sqrt{3/2} & 0 \\ -\sqrt{3/2} & -1/2 & 0 \\ 0 & 0 & 1 \end{bmatrix}$		

Table 2.5 (*continued*)

Syngony and metric relation	International symbols	Generator matrices in the orthogonal system of coordinates
Trigonal (*continued*)	$\bar{3}$	$\begin{bmatrix} 1/2 & -\sqrt{3/2} & 0 \\ \sqrt{3/2} & 1/2 & 0 \\ 0 & 0 & -1 \end{bmatrix}$
	32	$\begin{bmatrix} -1/2 & \sqrt{3/2} & 0 \\ -\sqrt{3/2} & -1/2 & 0 \\ 0 & 0 & 1 \end{bmatrix}$ $\begin{bmatrix} 1 & 0 & 0 \\ 0 & -1 & 0 \\ 0 & 0 & -1 \end{bmatrix}$
	3*m*	$\begin{bmatrix} -1/2 & \sqrt{3/2} & 0 \\ -\sqrt{3/2} & -1/2 & 0 \\ 0 & 0 & 1 \end{bmatrix}$ $\begin{bmatrix} -1 & 0 & 0 \\ 0 & 1 & 0 \\ 0 & 0 & 1 \end{bmatrix}$
	$\bar{3}m$	$\begin{bmatrix} 1/2 & -\sqrt{3/2} & 0 \\ \sqrt{3/2} & 1/2 & 0 \\ 0 & 0 & -1 \end{bmatrix}$ $\begin{bmatrix} -1 & 0 & 0 \\ 0 & 1 & 0 \\ 0 & 0 & 1 \end{bmatrix}$
Hexagonal, $a = b \neq c$, $\alpha = \beta = 90°$, $\gamma = 120°$	6	$\begin{bmatrix} 1/2 & \sqrt{3/2} & 0 \\ -\sqrt{3/2} & 1/2 & 0 \\ 0 & 0 & 1 \end{bmatrix}$
	$\bar{6}$	$\begin{bmatrix} -1/2 & -\sqrt{3/2} & 0 \\ \sqrt{3/2} & -1/2 & 0 \\ 0 & 0 & -1 \end{bmatrix}$
	$\bar{6}m2$	$\begin{bmatrix} -1/2 & -\sqrt{3/2} & 0 \\ \sqrt{3/2} & -1/2 & 0 \\ 0 & 0 & -1 \end{bmatrix}$ $\begin{bmatrix} -1 & 0 & 0 \\ 0 & 1 & 0 \\ 0 & 0 & 1 \end{bmatrix}$
	622	$\begin{bmatrix} 1/2 & \sqrt{3/2} & 0 \\ -\sqrt{3/2} & 1/2 & 0 \\ 0 & 0 & 1 \end{bmatrix}$ $\begin{bmatrix} 1 & 0 & 0 \\ 0 & -1 & 0 \\ 0 & 0 & -1 \end{bmatrix}$
	6/*m*	$\begin{bmatrix} 1/2 & \sqrt{3/2} & 0 \\ -\sqrt{3/2} & 1/2 & 0 \\ 0 & 0 & 1 \end{bmatrix}$ $\begin{bmatrix} 1 & 0 & 0 \\ 0 & 1 & 0 \\ 0 & 0 & -1 \end{bmatrix}$
	6*mm*	$\begin{bmatrix} 1/2 & \sqrt{3/2} & 0 \\ -\sqrt{3/2} & 1/2 & 0 \\ 0 & 0 & 1 \end{bmatrix}$ $\begin{bmatrix} -1 & 0 & 0 \\ 0 & 1 & 0 \\ 0 & 0 & 1 \end{bmatrix}$
	6/*mmm*	$\begin{bmatrix} 1/2 & \sqrt{3/2} & 0 \\ -\sqrt{3/2} & 1/2 & 0 \\ 0 & 0 & 1 \end{bmatrix}$ $\begin{bmatrix} 1 & 0 & 0 \\ 0 & 1 & 0 \\ 0 & 0 & -1 \end{bmatrix}$ $\begin{bmatrix} -1 & 0 & 0 \\ 0 & 1 & 0 \\ 0 & 0 & 1 \end{bmatrix}$
Cubic, $a = b = c$, $\alpha = \beta = \gamma = 90°$	23	$\begin{bmatrix} -1 & 0 & 0 \\ 0 & -1 & 0 \\ 0 & 0 & 1 \end{bmatrix}$ $\begin{bmatrix} 0 & 1 & 0 \\ 0 & 0 & 1 \\ 1 & 0 & 0 \end{bmatrix}$
	432	$\begin{bmatrix} 0 & 1 & 0 \\ -1 & 0 & 0 \\ 0 & 0 & 1 \end{bmatrix}$ $\begin{bmatrix} 0 & 1 & 0 \\ 0 & 0 & 1 \\ 1 & 0 & 0 \end{bmatrix}$
	$m\bar{3}$	$\begin{bmatrix} 1 & 0 & 0 \\ 0 & 1 & 0 \\ 0 & 0 & -1 \end{bmatrix}$ $\begin{bmatrix} 0 & -1 & 0 \\ 0 & 0 & -1 \\ -1 & 0 & 0 \end{bmatrix}$
	$\bar{4}3m$	$\begin{bmatrix} 0 & -1 & 0 \\ 1 & 0 & 0 \\ 0 & 0 & -1 \end{bmatrix}$ $\begin{bmatrix} 0 & 1 & 0 \\ 0 & 0 & 1 \\ 1 & 0 & 0 \end{bmatrix}$
	$m\bar{3}m$	$\begin{bmatrix} 0 & 1 & 0 \\ -1 & 0 & 0 \\ 0 & 0 & 1 \end{bmatrix}$ $\begin{bmatrix} 0 & -1 & 0 \\ 0 & 0 & -1 \\ -1 & 0 & 0 \end{bmatrix}$ $\begin{bmatrix} 0 & 1 & 0 \\ 1 & 0 & 0 \\ 0 & 0 & -1 \end{bmatrix}$

Note. The above matrices (a_{ij}) correspond to the transformation of the coordinates of points (2.4,6). The elements of matrix a_{ij} are determined as cosines $a_{ij} = \cos(X_i' X_j)$ between the transformed X_i' and the original X_j axis (Sect. 2.2.3).

G_{lim} corresponding to a given property, while group K is the lowest in this set: $G_{\text{lim}} \ni G_{p_i} \ni K$. Such a manifestation of a different, but subordinated point symmetry of a crystal in its various properties is called the maximum and minimum symmetry principle.

If a crystal is subjected to an external effect whose point symmetry is G', this effect may desymmetrize the phenomenon, and the symmetry of the observed properties is described by relation $G_{\text{pi}} \ni K \cap G'$, where $\cap$ is the symbol of intersection of the groups (an intersection is a group containing elements common to the two groups included in it). Thus, in the case of external effects the symmetry of the properties is a supergroup of the indicated intersection; this is the Curie principle [2.14].

It should be noted that groups K also find application in describing regular concretions of crystals (twins, triplets, etc.) [Ref. 2.13, Chap. 5].

2.6.5 Isomorphism of Groups *K*

In terms of the abstract theory of groups some point groups are isomorphous, i.e., they make up one and the same abstract group. This is because the operations of the abstract group, $q_i \in G$ with their multiplication rules in accordance with Cayley's square, may have a different geometric meaning in three-dimensional space.

Let us consider, for instance, three groups of the fourth order: 222, $2/m$, and $mm2$. These groups are isomorphous, which follows from the multiplication Table 2.6, although the geometric meaning of the operations, q_2, q_3, and q_4 is different for each of them.

All the cyclic groups of the same order are clearly isomorphous as well because they represent the degrees of some operation irrespective of its geometric meaning. Therefore, for instance, families N and $\tilde{N}$, and also families $N/2$ and N/m, are isomorphous. Table 2.7 lists 18 abstractly different groups **K** and the corresponding 32 crystallographic groups K. Each abstract group can be assigned by its generating elements and the defining relations between them. These are indicated in Table 2.7.

Table 2.6. Isomorphism of groups 222, $2/m$, and $mm2$

Group[a]	Operation				Multiplication table[b]				
	g_1	g_2	g_3	g_4	n	1	2	3	4
$2_x2_y2_z$	1	2_x	2_y	2_z	1	1	2	3	4
$2/m$	1	2	m	$\bar{1}$	2	2	1	4	3
$m_xm_y2_z$	1	m_x	m_y	2_z	3	3	4	1	2
					4	4	3	2	1

[a] Indices x,y,z in operation 2 indicate the direction of the axis, and in m they show to which axis this mirror plane is perpendicular.

[b] Only the operation numbers are given.

Table 2.7. Abstract groups **K**

Group order	Defining relations	Groups K
1	$A = e$	1
2	$A^2 = e$	$\bar{1}$,2,m
3	$A^3 = e$	3
4	$A^4 = e$	4,$\bar{4}$
4	$A^2 = B^2 = (AB)^2 = e$	2/m, mm2, 222
6	$A^6 = e$	6, $\bar{6}$, $\bar{3}$
6	$A^3 = B^2 = (AB)^2 = e$	32, 3m
8	$A^2 = B^2 = C^2 = (AB)^2 = (AC)^2 = (BC)^2 = e$	mmm
8	$A^4 = B^2 = ABA^3B = e$	4/m
8	$A^4 = B^2 = (AB)^2 = e$	4mm, 422, $\bar{4}$2m
12	$A^6 = B^2 = ABA^5B = e$	6/m
12	$A^6 = B^2 = (AB)^2 = e$	$\bar{3}m$, $\bar{6}m$2, 6mm, 622
12	$A^3 = B^2 = (AB)^3 = e$	23
16	$A^2 = B^2 = C^2 = (AB)^2 = (AC)^2 = (BC)^4 = e$	4/mmm
24	$A^4 = B^2 = (AB)^3 = e$	432, $\bar{4}$3m
24	$A^3 = B^2 = (A^2BAB)^2 = e$	$m\bar{3}$
24	$A^2 = B^2 = C^2 = (AB)^2 = (AC)^2 = (BC)^6 = e$	6/mmm
48	$A^4 = B^6 = (AB)^2 = e$	$m\bar{3}m$

2.6.6 Representations of Point Groups K

In Sect. 2.3 we established that group G can be represented by an isomorphous (2.28) or homomorphous (2.31) group H, whose elements may be numbers, matrices, etc.

An exact (isomorphous) representation of groups K is given by matrices $D(g)$ (2.6) of transformation of coordinates corresponding to the given operation $g \in K$. A set of such matrices forms an exact vector representation (of dimensionality 3) of the corresponding group; according to the matrix multiplication rules (2.45) the multiplication table of these matrices corresponds that of elements g_i. (The matrices of the generating operations are given in Table 2.5).

For instance, for group $K = 2/m$ the vector representation of D with a special choice of axes X_1, X_2, X_3 (Table 2.5) has the form:

$$2/m = \{\quad 1, \qquad 2, \qquad \bar{1}, \qquad m\ \}, \tag{2.76}$$

$$\updownarrow$$

$$D(2/m) = \left\{ \begin{bmatrix} 1 & 0 & 0 \\ 0 & 1 & 0 \\ 0 & 0 & 1 \end{bmatrix}, \begin{bmatrix} -1 & 0 & 0 \\ 0 & -1 & 0 \\ 0 & 0 & 1 \end{bmatrix}, \begin{bmatrix} -1 & 0 & 0 \\ 0 & -1 & 0 \\ 0 & 0 & -1 \end{bmatrix}, \begin{bmatrix} 1 & 0 & 0 \\ 0 & 1 & 0 \\ 0 & 0 & -1 \end{bmatrix} \right\}. \tag{2.77}$$

It is easy to see that, for instance, that the multiplication $2.\bar{1} = m$ corresponds to the multiplication of the relevant matrices from (2.77).

Proceeding from this kind of vector representation of group K it is possible, by switching to other orthogonal axes X_1^*, X_2^*, X_3^* with the aid of a nonspecial transformation S, to obtain other, equivalent, representations of the same group $D^*(g) = SD(g)S^{-1}$. But for all the equivalent representations the trace of the matrix – the character of the representation $\chi(g)$ (2.51) – is preserved.

Thus, the characters of elements $\chi(g)$ of group $2/m$ in all vector orthogonal-equivalent representations $D(G)$ are equal to

$$\chi(g) = \{\chi(1) = 3, \chi(2) = -1, \chi(\bar{1}) = -3, \chi(m) = 1\}. \tag{2.78}$$

By following definite rules it is possible to obtain, from vector representations of groups K, tensor representations of degree $3^2, \ldots, 3^s$, which is important in analyzing the physical properties of crystals described by tensors of different ranks. The corresponding matrices $D^2, \ldots, D^s$ are multiplied using the tensor multiplication rules.

On the other hand, vector representations can be reduced into irreducible components – diagonal square blocks of the type A (2.48). Thus, each of the matrices of the vector representation $D(2/m)$ can be represented as a direct sum of three matrices, for instance,

$$D(2) = \begin{bmatrix} -1 & 0 & 0 \\ 0 & -1 & 0 \\ 0 & 0 & 1 \end{bmatrix} = \begin{bmatrix} -1 & 0 & 0 \\ 0 & 0 & 0 \\ 0 & 0 & 0 \end{bmatrix} \oplus \begin{bmatrix} 0 & 0 & 0 \\ 0 & -1 & 0 \\ 0 & 0 & 0 \end{bmatrix} \oplus \begin{bmatrix} 0 & 0 & 0 \\ 0 & 0 & 0 \\ 0 & 0 & 1 \end{bmatrix}. \tag{2.79}$$

Taking these degenerate 3×3 matrices with one significant matrix element D_{ii} for a one-dimensional square block, let us construct two one-dimensional (antisymmetric) representations $D_{ii}(G)$ of group $2/m$,

$$\begin{aligned} 2/m &= \{1, \quad 2, \quad \bar{1}, \quad m\}, \\ &\updownarrow \\ D_{11}(2/m) &= \{1, -1, -1, \quad 1\} = D_{22}(2/m), \end{aligned} \tag{2.80}$$

$$\begin{aligned} &\updownarrow \\ D_{33}(2/m) &= \{1, \quad 1, -1, -1\} \end{aligned} \tag{2.81}$$

(subscripts ii mark the position of the matrix element $D_{ii}(g)$ in split 3×3 matrices). Correlating numbers ± 1 with elements $g \in K$, it is possible to construct, in addition to these two, two more one-dimensional representations: a trivial unity (fully symmetric) representation,

$$\{1, 1, 1, 1\} \tag{2.82}$$

and a sign-alternating (antisymmetric) one,

$$\{1, -1, 1, -1\}. \tag{2.83}$$

The latter forms a representation of group $2/m$, since $2.\bar{1} \leftrightarrow (-1)(1) = (-1) \leftrightarrow m$, etc. Thus, group $2/m$ has only four one-dimensional representations. Noting that for one-dimensional matrices, the matrix $D(g)$ itself coincides with

the character $\chi(g)$ of the representation, we write the result in the form of the character table

Γ_i	1	2	$\bar{1}$	m
Γ_1	1	1	1	1
Γ_2	1	1	−1	−1
Γ_3	1	−1	1	−1
Γ_4	1	−1	−1	1

(2.84)

Here, the first row contains the group elements, and the first column, one-dimensional representations symbolized by Γ_i; in each row Γ_i are quantities $\chi(g) = D(g)$, corresponding to elements $g \in K$.

The number of nonequivalent irreducible representations is equal to the number of classes of conjugate elements (2.36). Therefore, the first row in the character table of irreducible representations of groups K usually lists elements grouped into classes of conjugate elements $\{xgx^{-1}\}$. Isomorphous groups $K_1 \leftrightarrow K_2 \leftrightarrow \mathbf{K}$ split up into an equal number of classes $\{xgx^{-1}\}$ and therefore they have identical irreducible representations Γ_i and a common character table. Thus, by virtue of isomorphism of groups $2/m \leftrightarrow 222 \leftrightarrow mm2$ (Tables 2.6 and 2.7) all of them have one and the same table of characters (2.84). The other important properties of irreducible representations of groups K are as follows:

1) dimensions n_i of the matrices of irreducible representations Γ_i are divisors of the order of groups G;
2) the sum of the squares of dimensions $\sum_i n_i^2$ is equal to the order of G;
3) among representations Γ_i there is always a unity Γ_1.

The characters of the unit (identity) representation χ_i in any Γ_i are equal to the dimension n_i of representation Γ_i. The possible values of characters χ of one-dimensional representations Γ_j of groups K follow from the determining relations of Table 2.7 of the type $A^n = e, n = 1, 2, 3, 4, 6$ for cyclic groups (sub-groups), provided $e \leftrightarrow 1$. This gives $\chi^n = 1$, whence $\chi = \exp(-2\pi i/n)$. To summarize, the following characters are possible: ± 1, $\pm i$, $\varepsilon = \exp(-2\pi i/3)$, $\omega = \exp(-2\pi i/6)$. The real $\chi = \pm 1$ describe operations m, 2, $\bar{1}$, and the complex ones, rotations: ε corresponds to rotation axis 3, i to 4, and ω to 6. In Table 2.8 characters $\chi(g)$ of irreducible representations are given for 11 groups K^{I} (of the second kind). The same characters are inherent in isomorphous groups K^{II} (of the second kind) (see Table 2.7), i.e., another 14 groups or 25 in all. The tables of characters of the remaining seven groups are defined by the fact that these groups are direct products of groups K^{I} and group $\bar{1}$ (see Table 2.5): $mmm = 222 \otimes \bar{1}$, $4/m = 4 \otimes \bar{1}$, $6/m = 6 \otimes \bar{1}$, $m\bar{3} = 23 \otimes \bar{1}$, $4/mmm = 422 \otimes \bar{1}$, $6/mmm = 622 \otimes \bar{1}$, $m\bar{3}m = 432 \otimes \bar{1}$. If group $G = G_1 \otimes G_2$, then, as can be shown, its tables of characters are calculated by the equation

$$\chi_\rho^{\Gamma_i \Gamma_j} = \chi_{\rho_1}^{\Gamma_i} \chi_{\rho_2}^{\Gamma_j} \tag{2.85}$$

where ρ, ρ_1, and ρ_2 are classes of conjugate elements in $G = G_1 \otimes G_2$, G_1, and G_2; $\Gamma_{\rho_k}^{i}$ is the character of element $g \in \rho_k$ in the Γ_i-th representation of group $G_k (K = 1, 2)$.

As to the table of characters of group $\bar{1}$, it is the same as that of group 2 (see Table 2.8). Thus, the number of irreducible representations of all the remaining groups of the type $K^1 \otimes \bar{1}$ is twice that of groups K^1 (or ones isomorphous to them) listed in Table 2.8.

More comprehensive tables of representations also indicate the representations of some group or other by which the coordinates of the functions of the corresponding symmetry are transformed.

Table 2.8. Characters of irreducible representations of crystallographic point groups*

$C_1 - 1$	e
$\Gamma_1 - A$	1

$C_2 - 2$ $C_i - \bar{1}$ $C_s - m$	e e e	C_2 C_i σ_h
$\Gamma_1 - A, A_g, A'$	1	1
$\Gamma_2 - B, A_u, A''$	1	-1

$D_2 - 222$ $C_{2h} - 2/m$ $C_{2v} - mm2$	e e e	C_2^z C_2 C_2	C_2^y σ_h σ_v^y	C_2^x C_i σ_v^x
$\Gamma_1 - A_1, A_g, A_1$	1	1	1	1
$\Gamma_2 - A_2, A_u, A_2$	1	1	-1	-1
$\Gamma_3 - B_2, B_u, B_2$	1	-1	1	-1
$\Gamma_4 - B_1, B_g, B_1$	1	-1	-1	1

$C_4 - 4$ $C_4 - \bar{4}$	e e	C_4 S_4	C_4^2 S_4^2	C_4^3 S_4^3
$\Gamma_1 - A, A,$	1	1	1	1
$\Gamma_2 - B, B$	1	-1	1	-1
Γ_3	1	i	-1	$-i$
Γ_4 E, E	1	$-i$	-1	i

$C_3 - 3$	e	C_3	C_3^2
$\Gamma_1 - A$	1	1	1
Γ_2 E	1	ε	ε^2
Γ_3	1	ε^2	ε

$D_3 - 32$ $C_{3v} - 3m$	e e	$2C_3$ $2C_3$	$3C_2$ $3\sigma_v$
$\Gamma_1 - A_1, A'$	1	1	1
$\Gamma_2 - A_2, A''$	1	1	-1
$\Gamma_3 - E, E$	2	-1	0

$D_4 - 422$ $C_{4v} - 4mm$ $D_{2d} - \bar{4}2m$	e e e	C_4^2 C_4^2 C_2	$2C_4$ $2C_4$ $2S_4$	$2C_2$ $2\sigma_v$ $2C_2$	$2C_2'$ $2\sigma_v'$ $2\sigma_v'$
$\Gamma_1 - A_1, A_1, A_1$	1	1	1	1	1
$\Gamma_2 - A_2, A_2, A_2$	1	1	1	-1	-1
$\Gamma_3 - B_1, B_1, B_1$	1	1	-1	1	-1
$\Gamma_4 - B_2, B_2, B_2$	1	1	-1	-1	1
$\Gamma_5 - E, E, E$	2	-2	0	0	0

$C_6 - 6$ $C_{3i} - \bar{3}$ $C_{3h} - \bar{6}$	e e e	C_6 S_6 S_3	C_6^2 S_6^2 S_3^2	C_6^3 S_6^3 S_3^4	C_6^4 S_6^4 S_3^5	C_6^5 S_6^5 S_3^6
$\Gamma_1 - A, A, A$	1	1	1	1	1	1
$\Gamma_2 - B, B, B$	1	-1	1	-1	1	-1
Γ_3	1	ω^2	$-\omega$	1	ω^2	$-\omega$
Γ_4 E_1, E_1, E_1	1	$-\omega$	ω^2	1	$-\omega$	ω^2
Γ_5	1	ω	ω^2	-1	$-\omega$	$-\omega^2$
Γ_6 E_2, E_2, E_2	1	$-\omega^2$	$-\omega$	-1	ω^2	ω

$D_6 - 622$ $C_{6v} - 6mm$ $D_{3h} - \bar{6}m2$ $D_{3d} - \bar{3}m$	e e e e	C_6^3 C_6^3 σ_h C_i	$2C_6^2$ $2C_6^2$ $2S_3^2$ $2S_6^2$	$2C_6$ $2C_6$ $2S_3$ $2S_6$	$3C_2$ $3\sigma_v$ $3C_2$ $3C_2$	$3C_2'$ $3\sigma_v'$ $3\sigma_v$ 3σ
$\Gamma_1 - A_1$, A_1, A_1', A_{1g}	1	1	1	1	1	1
$\Gamma_2 - A_2$, A_2, A_2', A_{2g}	1	1	1	1	−1	−1
$\Gamma_3 - B_1$, B_2, A_1'', E_g	1	−1	1	−1	1	−1
$\Gamma_4 - B_2$, B_1, A_2'', A_{1u}	1	−1	1	−1	−1	1
$\Gamma_5 - E_1$, E_2, E', A_{2u}	2	2	−1	−1	0	0
$\Gamma_6 - E_2$, E_1, E'', E_u	2	−2	−1	1	0	0

$T - 23$	e	$3C_2$	$4C_3$	$4C_3^2$
$\Gamma_1 - A$	1	1	1	1
Γ_2 } E	1	1	ε	ε^2
Γ_3 }	1	1	ε^2	ε
$\Gamma_4 - F$	3	−1	0	0

$O - 432$ $T_d - \bar{4}3m$	e e	$8C_3$ $8C_3$	$3C_4^2$ $3S_4^2$	$6C_2$ $6\sigma_d$	$6C_4$ $6S_4$
$\Gamma_1 - A_1$, A_1	1	1	1	1	1
$\Gamma_2 - A_2$, A_2	1	1	1	−1	−1
$\Gamma_3 - E$, E	2	−1	2	0	0
$\Gamma_4 - F_1$, F_1	3	0	−1	−1	1
$\Gamma_5 - F_2$, F_2	3	0	−1	1	−1

* Key to the table

I	II
Notation of groups K (Schönflies and international)	Notation of classes of conjugate elements
III	**IV**
Notation of representations	Characters of representations

Note. Symmetry operations (group elements) are symbolized after Schönflies: C_n are rotations ($n = 1,2,3,4,6$); C_i is inversion $\bar{1}$; e is unit operation 1; σ is reflection in planes m; σ_v, σ_h are planes parallel and perpendicular to axes of symmetry; σ_d are diagonal planes in group $\bar{4}3m$; $S_4 - \bar{4}$, $S_3 - \bar{6}$, $S_6 - \bar{3}$ are inversion rotations.

Each class is defined by a characteristic operation (which is a class representative) and by the number of elements included in the class (the corresponding number stands in front of the representative). Irreducible representations are denoted by symbols Γ_i and also by spectroscopic symbols: F (or T) are three-dimensional representations and E, two-dimensional. One-dimensional representations are denoted as follows: A is symmetric, B is antisymmetric with respect to rotations (for groups C_n), A' is symmetric, A'' is antisymmetric with respect to σ (for groups C_s, C_{nh}, D_{nh} with an odd number of mirror planes σ), A_g is symmetric (gerade), and A_u is antisymmetric (ungerade) with respect to inversion (for groups containing inversion C_i). Letters A, B are provided with a subscript 1 if the representation is symmetric with respect to $C_2 \perp C_n$ or σ_v, σ_d, $\| C_n$, and with a subscript 2 if it is antisymmetric.

In the tables of groups D_2, D_{2h}, C_{2v}, axis C_2^z is adopted as the principal; eveness or oddness of the representation is marked by a suffix with respect to C_2^z and σ_v^x. Group D_{3d} is isomorphous with group D_6 by the inverted multiplication law, but its characters are the same.

Representations Γ of groups K are called unitary; some representations are real, as seen from Table 2.8, while others are complex and mutually conjugate. In all, there are 73 one-dimensional nontrivial real representations for groups K, of which 58 are sign-alternating, and 18 complex conjugate pairs.

Representations of point groups are widely used in crystal physics for analyzing physical properties of crystals. They are used in quantum-mechanical consideration of free atoms or atoms in a crystal, especially in spectroscopy and

in the theory of structure and properties of molecules. For instance, irreducible representations of point symmetry groups of molecules are used for transformation of their vibration coordinates; they are also used to describe molecular orbitals responsible for the chemical bond, and so on [Ref. 2.13, Chap. 1].

Irreducible one-dimensional representations are also related to groups of generalized point symmetry (see Sect. 2.9).

2.6.7 Group Representations and Proper Functions

Let us consider, by way of example, the description of the states of a physical system in quantum mechanics. They are characterized by eigen functions, which are solutions of the Schrödinger equation. If a physical system possesses symmetry properties, the relevant Schrödinger equation will be invariant to symmetry transformations $g_i \in G$ of a group of this system. Therefore, at these g_i the wave function corresponding to a definite value of energy will transform to some other function for the same energy level. Using all the elements of the group, we find some number of linearly independent functions $\psi_1, \ldots, \psi_f$, which are linearly related by symmetry transformations. Each element $g \in G$ can therefore be regarded as an operator $\hat{g}$ transforming function ψ_k into a linear combination of functions $\psi_i, \ldots, \psi_f$,

$$\hat{g}\psi_k = \sum_{l=1}^{f} a_{lk}\psi_l. \tag{2.86}$$

Wave functions can always be assumed normalized and orthogonal, and then matrix (a_{lk}) coincides with the quantum-mechanical concept of the matrix of the operator

$$g_{lk} = \int \psi_l^* \hat{g} \psi_k dq. \tag{2.87}$$

It is easy to see now that to the product of two elements of group $\hat{g}\hat{h}$ there corresponds a matrix obtained from matrices (g_{il}), (h_{lk}) according to the conventional matrix multiplication rules. Thus, these matrices form the group representation. Functions $\psi_1, \ldots, \psi_f$, which construct the matrices of the linear representation, are called basis functions, their number coinciding with the dimensionality of the representation. For orthonormalized basis functions the linear representation will be unitary.

If we subject orthonormalized basis functions to the unitary transformation S, we obtain a new system of functions, which are also orthonormalized and define a new representation of the same group. The matrices of the operators of the symmetry group are then equivalent to $\hat{g}' = S\hat{g}S^{-1}$.

A representation of a symmetry group given by basis functions is irreducible (unless this is prevented for special reasons). This representation assigns all the properties of the symmetry of the state with respect to different symmetry transformations. Group theory therefore enables one to obtain important results for a physical system without a complete solution of the Schrödinger equation. For instance, for a system placed in the external field of a definite symmetry, it is possible, by considering representations, to find the splitting of the energy levels [2.14].

2.7 Symmetry Groups G_1^2, G_2^2, G_1^3, G_2^3

The structure of a crystalline substance is described by Fedorov groups $\Phi \equiv G_3^3$. The groups under consideration, G_1^2, G_2^2, G_1^3, G_2^3, containing translations, are also of interest to crystallography, since they include subgroups of Fedorov groups Φ. These groups are also very important in their own right, outside the scope of crystallography proper.

2.7.1 Symmetry Groups G_1^2 of Borders

These two-dimensional groups $G_1^2 \supset T_1 \ni t$ contain a translation t in one, singular direction of two-dimensional space. The objects described by them are any two-dimensional, periodic in one dimension functions or images of the border type on a plane (Fig. 2.51; see also Figs. 2.11c, d; 2.16). They may contain planes (lines of symmetry) m parallel or perpendicular to translations, a glide-reflection plane a, and rotation points (axes) 2. All these groups are crystallographic; there are seven of them (Fig. 2.52).

Fig. 2.51. Example of borders with symmetry $t:m$ [2.15]

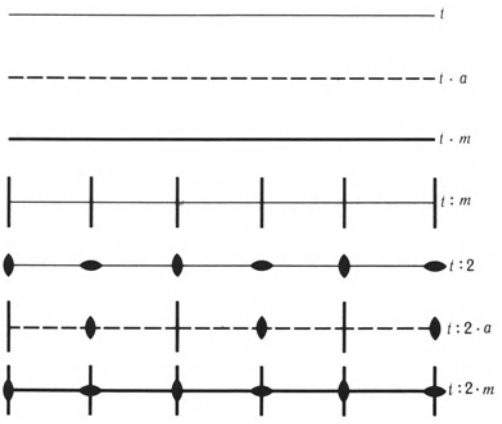

Fig. 2.52. Seven border symmetry groups G_1^2, represented by a set of their symmetry elements

2.7.2 Plane Twice-Periodic Groups G_2^2

These groups play an important part in crystallography, since they are two-dimensional analogs of space groups G_3^3. They describe projections of crystalline structures, their plane two-dimensional sections (in particular, those of electron density distribution), and some other functions used in crystallography. These groups are of great importance in applied art because they reflect the symmetry of patterns on textiles, wall paper, ornaments, etc. (Fig. 1.15).

We know that any such group contains a subgroup of two-dimensional translations $G_2^2 \supset T_2 \ni t_1, t_2$, which are finite provided the discreteness condition is fulfilled (2.53).

Let us consider an arbitrary plane net (Fig. 2.53). A parallelogram constructed on two noncollinear vectors issuing from one point is a unit cell. From Fig. 2.53a it is clear that such a parallelogram can be chosen in an infinite number of ways, in which it will not contain a single point translationally equal to the vertices, i.e., not a single additional point. (The lattice points are also called nodes). The areas of all such primitive parallelograms are equal. Hence, group T_2 may be characterized by a basis – any pair of vectors forming the sides of the primitive, unit parallelogram. Group T_2 consists of an infinite set of translations

$$\boldsymbol{t} = p_1\boldsymbol{a}_1 + p_2\boldsymbol{a}_2, \quad p_1, p_2 = 0, \pm 1, \pm 2, \pm \ldots, \tag{2.88}$$

where $\boldsymbol{a}_1$, $\boldsymbol{a}_2$ are periods, and the group operation is that of vector addition, which correlates a third vector

$$\boldsymbol{t}_1 + \boldsymbol{t}_2 = \boldsymbol{t}_3 \in T_2 \tag{2.89}$$

with any pair $\boldsymbol{t}_1, \boldsymbol{t}_2 \in T_2$.

Introducing the translation operator t, we find that any point $\boldsymbol{x}$ of the plane is transformed by any translation $\boldsymbol{t}$ into a translationally equal point $\boldsymbol{x}'$

$$t[\boldsymbol{x}] = \boldsymbol{x} + \boldsymbol{t} = \boldsymbol{x}', \tag{2.90}$$

and the set of all the points derived from any point by all operations t (2.90) is actually an infinite net.

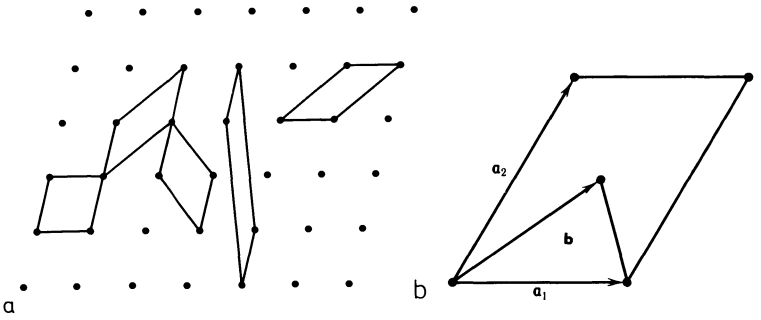

Fig. 2.53a,b. Two-dimensionally periodic net of points. (**a**) different ways for choosing a primitive parallelogram; (**b**) proof of the absence of points inside the unit primitive parallelogram

If, in any choice of a primitive parallelogram, the periods $\boldsymbol{a}_1 \neq \boldsymbol{a}_2$ and the angle between them $\gamma \neq 90°$, the net is called oblique. It is customary to choose as periods the smallest translations $\boldsymbol{a}_1$ and $\boldsymbol{a}_2$. By definition we have chosen such a cell to be empty: it contains no lattice points inside. If we assume, however, that there is such a point inside (Fig. 2.53b), the new translation $\boldsymbol{b}$ will be shorter than the initial ones, which contradicts the condition of the "theorem of emptiness" of a unit parallelogram.

It is, however, possible to choose in an infinite number of ways nonprimitive parallelograms containing one, two, or any number of nodes inside them or on each of the parallel sides. All the translation groups arising will be subgroups of group T_2 (Fig. 2.54). The area of a parallelogram containing q points is q times as large as that of the unit parallelogram. A primitive parallelogram is denoted by P, and a parallelogram containing one lattice point is called centered, since this single point is always at the center, and labelled C.

Groups $G_2^2 \supset T_2$ naturally may contain not only translations, but other operations as well. As we know (see Sect. 2.4), all these groups are crystallographic, i.e., they can only have rotations 1, 2, 3, 4, 6. A complete group of transformations of two-dimensional nets into themselves is called a Bravais two-dimensional group. Taking into consideration the possible point transformations of a net into itself leads to conditions of equality or inequality of $\boldsymbol{a}_1$ and $\boldsymbol{a}_2$ and to definite values of the angles between them. This gives rise to five different two-dimensional groups T_2, which are called Bravais two-dimensional groups, and five respective plane nets (Fig. 2.55). A Bravais orthorhombic group with $a_1' = a_2'$ and $\gamma \neq 90°$ is usually described as a centered rectangular group with $a_1 \neq a_2$ and $\gamma = 90°$. The point symmetry (syngony) of the nodes and nets here is as follows: 2 for oblique nets, *mm*2 for two orthorhombic nets, 4*mm* for a tetragonal (square) net, and 6*mm* for a hexagonal net.

Let us form a semidirect product of a Bravais group and a two-dimensional point group of the corresponding symmetry $T_2 \textcircled{S} G_0^2$. This is associated geometrically with placing a set of symmetry elements of a point group at nodes of two-dimensional nets. The groups G_2^2 thus obtained are symmorphous; there are 5 of them. It should be noted that, when forming symmorphous group G_2^2, interaction of translations $t \in T_2$ with mirror reflection $m \in G_2^2$ will produce new operation – glide reflection g, which was not contained in both G_0^2 and T_2, and a corresponding symmetry element – glide plane. According to the procedure

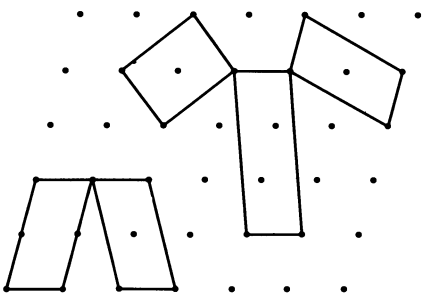

Fig. 2.54. Different nonprimitive parallelograms in a two-dimensional net

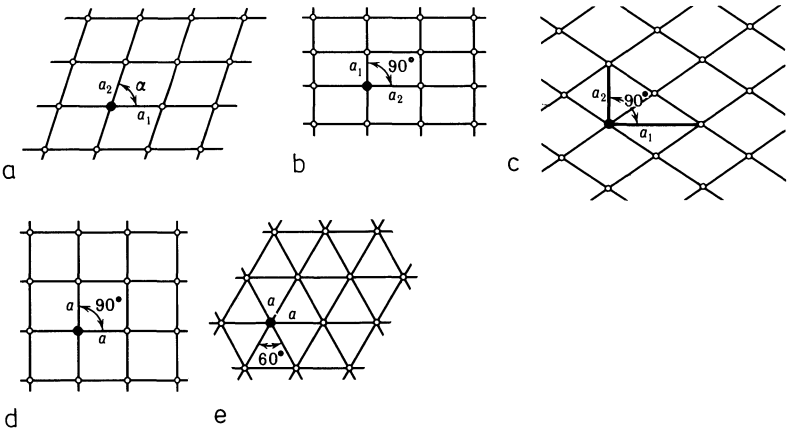

Fig. 2.55a–e. Five types of plane net illustrating two-dimensional Bravais groups. (**a**) oblique, (**b**) orthorhombic primitive, (**c**) orthorhombic centered, (**d**) square, (**e**) hexagonal

illustrated in Fig. 2.11 one can use symmorphous groups to find their nontrivial, nonsymmorphous subgroups, which are also of the type G_2^2. There are 12 such groups. In all, there are 17 groups G_2^2.

All these plane groups are depicted in Fig. 2.56a, which also gives their notation. The corresponding regular systems of points of general positions are shown in Fig. 2.56b. Among groups G_2^2 there are 2 oblique (monoclinic), 7 rectangular (orthorhombic), 3 square (tetragonal), and 5 hexagonal groups. Of these 17 groups, 4 are groups of the first kind and 13 of the second.

Plane figures corresponding to the independent asymmetric region – planion (see Sect. 2.5.5) – for each plane group are presented in Fig. 2.57. By joining these planions we can fill the plane completely. Symmetry transformations of such a division of plane into planions form the corresponding group G_2^2.

2.7.3 Cylindrical (Helical) Groups G_1^3

These groups $G_1^3 \supset T_1 \ni t_1$, which are also called rod groups, describe three-dimensional space and objects in it which are periodic in one direction. This direction X_3 is called singular; in two other dimensions, X_1X_2, the space described by these groups is inhomogeneous and hence nonperiodic. These groups are suitable for describing such objects as rods, chains, ribbons, or screws; their importance lies in the possibility of describing synthetic and natural chain molecules such as polymers.

Operations of the first kind, translating the space along the singular axis, are (with the exception of pure translations) screw rotations, and operations of the second kind, glide reflections c. The axis of the singular direction is unique, and any symmetry operations inherent in groups G_1^3 must leave it unique. It is therefore easy to understand that they may also contain axes N or $\bar{N}$ of any orders coinciding with the singular (principal) axis, planes m passing through or

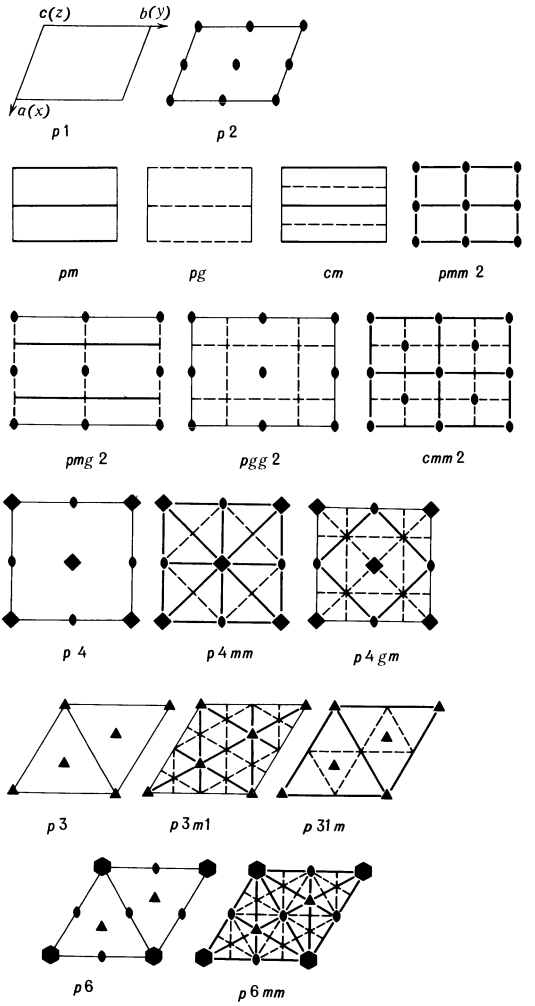

Fig. 2.56. (a) Graphical representation of 17 plane groups G_2^2 [2.16]

perpendicular to it, and the axes 2 perpendicular to it. Any other and differently positioned symmetry elements would generate a new singular axis, which is not allowed.

Cylindrical groups can be derived in several ways. Thus, similarly to what we did for groups G_2^2, it is possible to form a semidirect product of a one-dimensional translation group and point groups (with a single principal axis of any order), $T_1 \textcircled{S} G_0^3$. These (symmorphous) groups, together with their non-trivial (non-symmorphous) subgroups – divisors – form all the groups G_1^3. Nontrivial subgroups can be obtained by increasing the translation $t \ni T_1$ M times and selecting some of the operations.

A characteristic operation for these groups is a screw displacement s_M. It consists of a unit rotation through an angle $\alpha = 2\pi/M$ about the principal axis

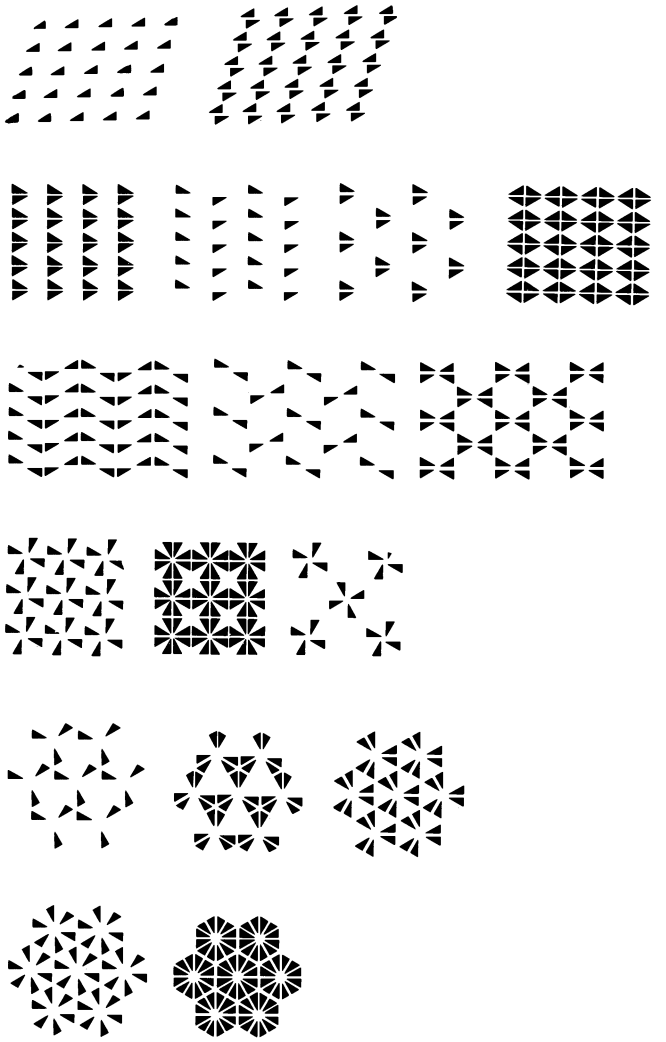

Fig. 2.56. (b) Regular systems of points characterizing 17 plane groups (see notations on Fig. 2.56a, p. 111) [2.16]

with a simultaneous displacement t_s along the axis. The quantity M may be any integer $M = N$, which corresponds to the "integer" screw axis N_q. But any fractional numbers $M = p/q$ are also possible (p and q integers); then $\alpha = 2\pi q/p$ is one-pth part of q rotations (Fig. 2.58a). The period $t = Nt_s$ or pt_s. This means that in a rational screw displacement there is always a translation t. We can also conceive of a case where M is irrational, and then there is no true translation t and the corresponding period, and a case where $\alpha \to 0$, which corresponds to axis ∞_s.

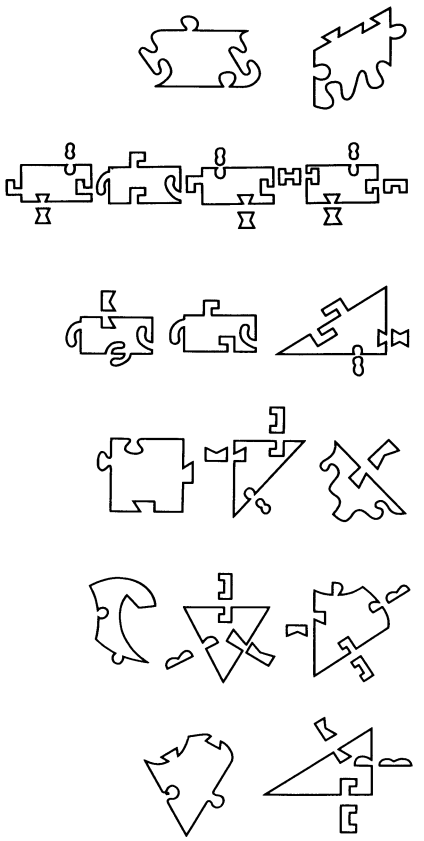

Fig. 2.57. Asymmetric plane figures (planions) characterizing each plane group [2.17]. The arrangement of the figures corresponds to that of the representations of the groups in Fig. 2.56a. Packing of the figures gives the filling of the plane by the corresponding plane group. The "links" fix the figures when joining them along the planes (lines) of symmetry

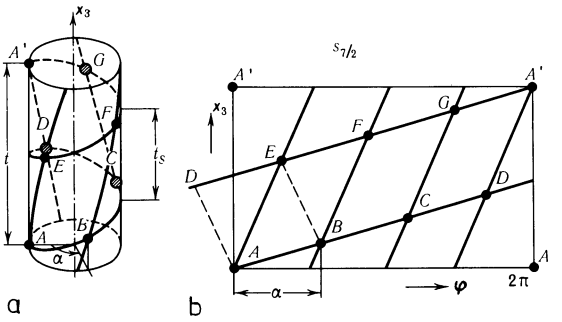

Fig. 2.58a,b. Model of a structure with a helical symmetry. (**a**) screw rotation s_M, $M = p/q = 7/2$; (**b**) radial projection of a structure with symmetry 7/2. The straight lines on the plane net (b) correspond to the helices in (a), *ABFE* is the unit cell of the radial projection. It can be chosen differently, for instance *ABED*

The families of groups G_1^3 are represented in Table 2.9. The upper row contains the generating family of point groups and the left-hand column the generating operation with the translational component.

Groups G_1^3 are conveniently representable with the use of radial projection. Let us write all their operations in the cylindrical system of coordinates r, φ, x_3.

Table 2.9. Families of groups G_1^3

Operation with translation	Point group						
	N	N_2	$\bar{N}$	N/m	Nm	$\bar{N}m$	$\frac{N}{m}m$
$t = s_1$	tN	$tN/2$	$t\bar{N}$	tN/m	tNm	$t\bar{N}m$	tN/mmm
s_M	s_MN	$s_MN/2$					
s_{2N}			$s_{2N}N/m$				
					cNm		$c\frac{N}{m}m$
c	cN	$c\bar{N}$		cN/m			

Now we "wrap" an object (for instance, the one shown in Fig. 2.58a) in a cylindrical surface, whose axis is the principal one, and project its points onto this surface along the rays φ, $x_3 = \text{const}$ perpendicular to the principal axis and radiating from it. The two-dimensional coordinates of the radial projection are φ and x_3 and can be drawn in a plane (Fig. 2.58b). If group G_1^3 contains a subgroup N, then it will be periodic along coordinate φ with a period $\alpha = 2\pi/N$. Such a projection can clearly belong only to one of the groups $G_2^2 \supset T_2$, and the periods t_1, t_2 of the arising net are equal to $t_1 = \alpha r + t_s$, $t_2 = t$. Herefrom we can see still another way for deriving groups G_1^3: it is taken into consideration that in the projection along the principal axis they yield groups G_0^2, and in the radial projection, G_2^2. Since X_3 is the singular direction, among groups G_2^2 only oblique and rectangular groups – the first 9 out of the 17 (Fig. 2.56a) – can be used. In other groups, axes 3, 4 and 6 would be perpendicular to the principal axis which is impossible in this case. The radial projections of all the families G_1^3 are given in Fig. 2.59 in coordinates α, t [2.18]. One unit cell with parameters $2\pi/N$ and t is depicted. There are various possible ways for closing a two-dimensional net characterized by group G_1^3 onto a cylindrical surface depicted by group G_2^2 (Fig. 2.60). The points of the cylindrical net may proceed either along a one-start helix, or along helices with two or more starts.

The relationship of groups G_1^3 and G_2^2, which is described in a radial projection, is not just a geometric abstraction. It finds its physical embodiment in the existence of so-called tubular crystals, which are formed by certain globular proteins (Fig. 2.61). The molecules of these proteins are packed into a monomolecular layer during crystallization; this layer is not plane, however, but closed into a cylindrical surface. It should be remarked that some proteins form plane monomolecular layers, too, which are described by groups G_2^3; these will be treated below.

The formation of tubular crystals indicates that, generally speaking, the requirement for three-dimensional homogeneity (2.52, 53) is not always obligatory for the formation of systems from an infinite number of particles. But in this case a one-dimensional condition similar to (2.52, 53) is feasible.

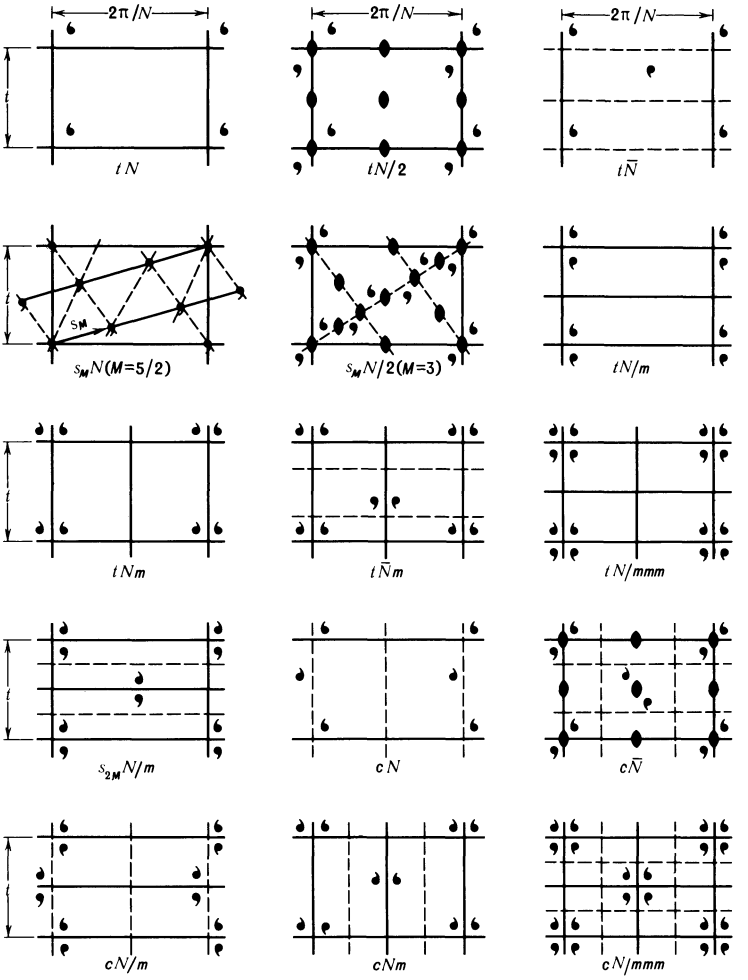

Fig. 2.59. Radial projections of 15 families of groups of the type G_1^3

Regular point systems (RPS) of general positions in groups G_1^3 lie, in the general case, on the surface of a cylinder with an axis N. Thus, these groups are isomorphous to groups of transformation of a circular cylindrical surface into itself (just as groups G_0^3 are isomorphous to the group of transformations of a sphere into itself).

The RPS of groups with $N \geqslant 2$, which contain s_{2N}, c, m, lie on circles, and such groups can be called proper cylindrical, or circular. For groups containing s_M, $M = N/q$, RPS lie on helices; these are proper helical groups.

The groups framed by the dashed line in Table 2.7 are of the first kind; the objects realized in them are enantiomorphous. Such groups describe the molecules of biopolymers – fibrillar proteins, DNA. All the other groups are of the

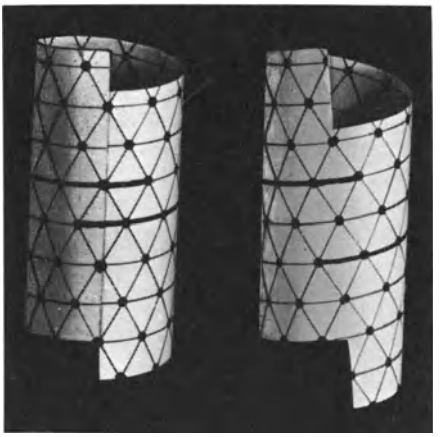

Fig. 2.60. Variants of the closing of a plane net into a cylindrical one which illustrate the possibility of formation of helices with a different number of starts

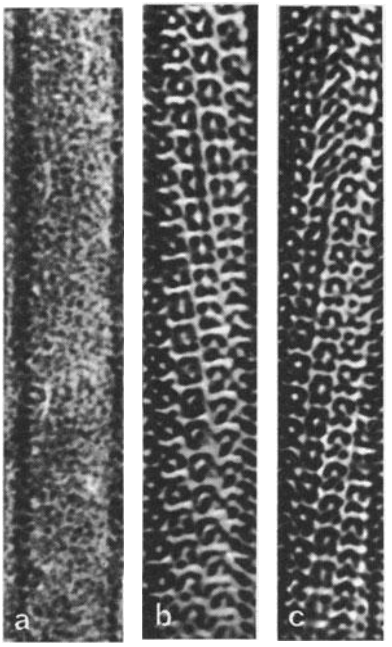

Fig. 2.61a–c. Tubular crystal of the protein of phosphorylase B. (**a**) electron micrograph ($\times 3.5 \cdot 10^5$); (**b, c**) result of optical filtration of the micrograph, which reveals separately the "front" and the "back" wall of the tube and the helical cylindrical packing of the molecules in them [2.19]

second kind. There are 75 crystallographic groups G_1^3. A particular case of groups G_1^3 are symmetry groups of a two-sided plane with one special direction, so-called ribbon symmetry groups. There are 31 of them.

2.7.4 Layer Groups G_2^3

These are symmetry groups of three-dimensional twice-periodic objects [2.20, 21]. They describe, for instance, the structure of walls, nets, panels, honeycombs, and at the atomic-molecular level, separate layers, which can be singled

out in the structure of a number of crystals: layer silicates (Fig. 2.62), graphite [Ref. 2.13, Fig. 2.5c], in β-proteins [Ref. 2.13, Fig. 2.119], various monomolecular layers and films, biological membranes, in smectic liquid crystals, etc.

Groups $G_2^3 \supset T_2$ contain two translations. In the discrete group $T_2 \ni t_1, t_2$ the translations with periods a_1, a_2 lie in the singular plane X_1, X_2; hence, in G_2^3 there is no periodicity along direction X_3 perpendicular to X_1, X_2.

It is clear that subgroups of groups G_2^3 are groups G_2^2, onto which the former are projected along axis X_3. Therefore all the groups G_2^3 are crystallographic and can be subdivided into the same syngonies as groups G_2^2.

All the groups G_2^3 can be derived, using the familiar method, by forming semi-direct products $T_2 \circledS K$ and orienting the symmetry elements of K so that rotations 3, 4 and 6 are performed only about the axes perpendicular to the singular plane (otherwise they would derive from it more identical planes, which is impossible). These (symmorphous) groups, together with all their nontrivial

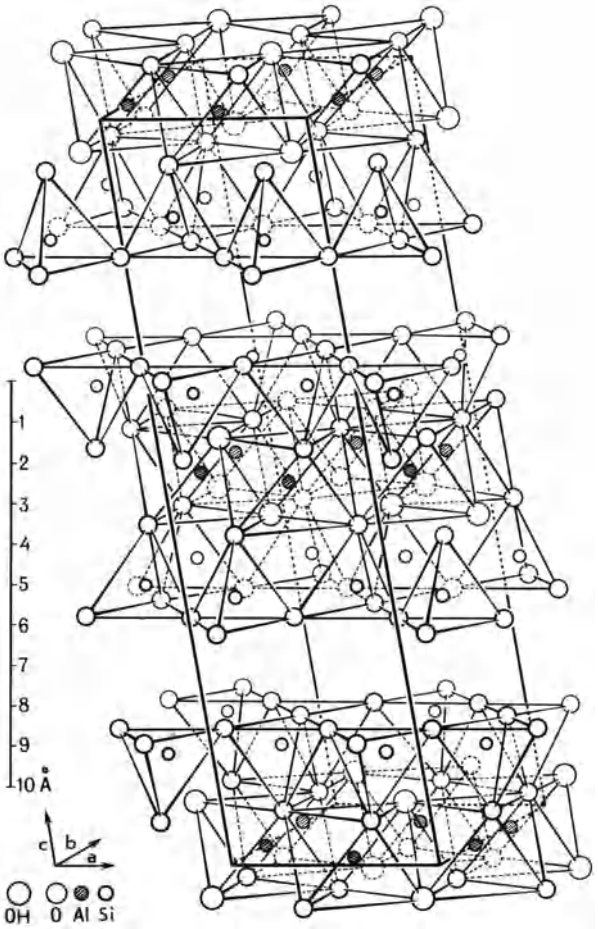

Fig. 2.62. Structure of pyrophyllite built up of three-story layers. Silicon-oxygen tetrahedra adjoin the central octahedral layer from two sides

p 1
1
p 11 m
2
p $\bar{1}$
3
p 11 b
4
p 112
5
p 11 2/m
6
p 11 2/b
7
p 1 m 1
8
p 2 mm
9
p 1 a 1
10
p 2$_1$ am
11
c 1 m 1
12
c 2 mm
13
p 121
14
p 12$_1$ 1
15
c 121
16
p 1 2/m 1
17
p 1 2$_1$/m 1
18
c 1 2/m 1
19
p 1 2/a 1
20
p 1 2$_1$/a 1
21
p mm 2
22
p mmm
23
pbm 2
24
pba 2
26
pbmm
25
pbam
27
cmmm
29
cmm 2
28
p 2$_1$ ma
30
p 2 mb
32
p 2 aa
31
p 2$_1$ ab
33
p 2$_1$ mn
35
p 2 an
34
c 2 mb
36
p 2$_1$ 22
38
p 222
37
p 2$_1$ 2$_1$ 2
39
p maa
41
c 222
40
pban
42
pbmn
44
pmma
43
pbaa
45
pmmn
47
pmab
46
cmma
48

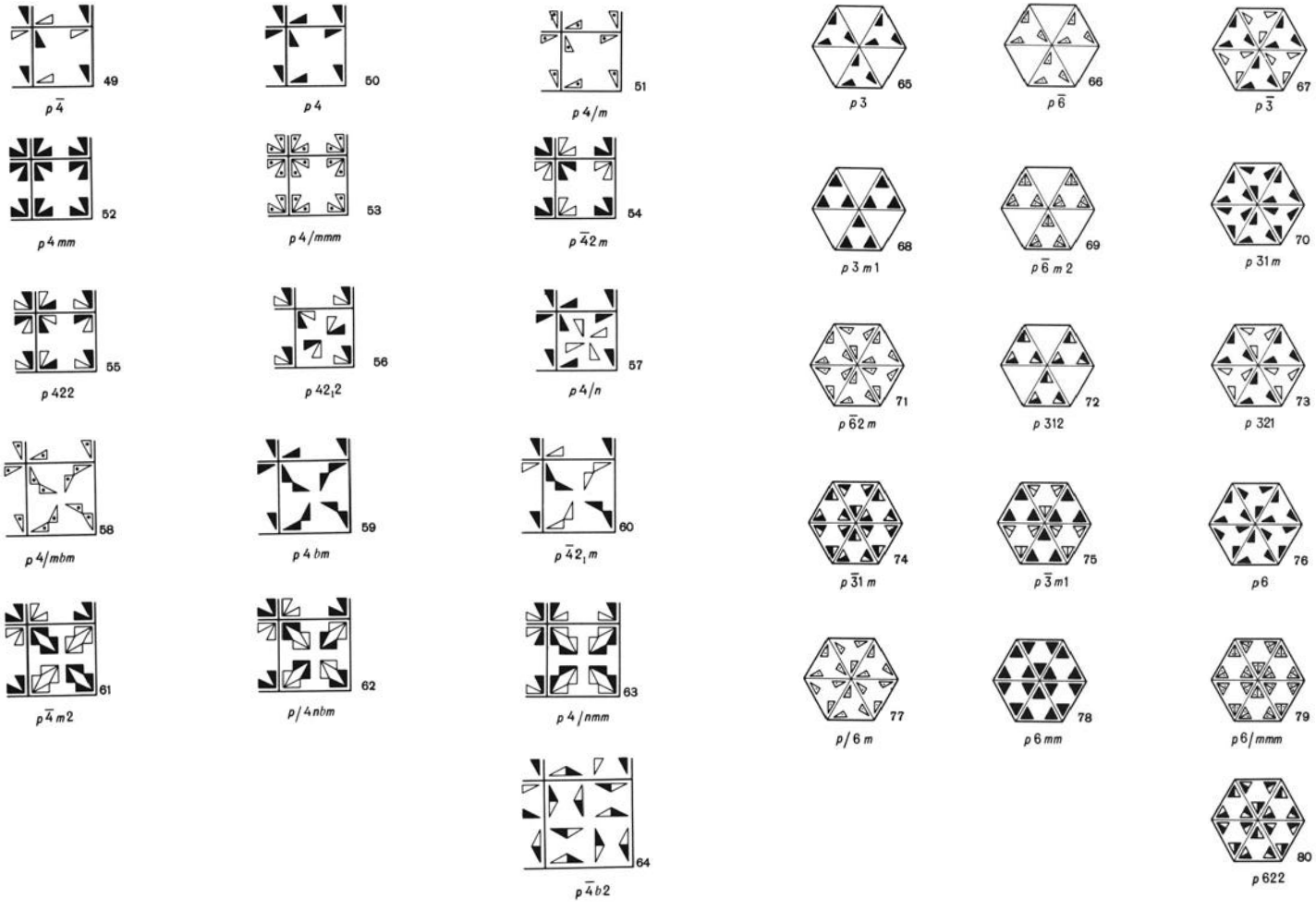

Fig. 2.63. Eighty symmetry groups of layers illustrated by the drawings of their unit cells containing asymmetric figures in general positions arranged in regular systems [2.22]

(nonsymmorphous) subgroups, actually constitute all the groups of the type G_2^3. In them, operations arise which transform points lying on one side of the singular plane X_1, X_2 into symmetrically equal points lying on the other side of, and at the same distance from, it; in this case the two half-spaces ($X_3 \geqslant 0$ and $X_3 \leqslant 0$) are symmetrically equal to one another. The corresponding symmetry elements, which always lie in the special plane, may be axes 2 and 2_1, the glide planes *a*, *b*, and *n*. The other operations are the same as in groups G_2^2; they do not change coordinate x_3.

All the 80 layer groups are depicted in Fig. 2.63 with the aid of a small asymmetric figure – a triangle; their international notation is also given. To distinguish the upper and lower sides of the triangle, one of them (let it be the lower) is colored black, and the other (upper), white. In such operations, which change the third coordinate, triangles lying at any arbitrary height x_3 are flipped, the black sides appear instead of white, and vice versa, x_3 transforms into $-x_3$. If plane X_1, X_2 is a mirror-reflection plane, the triangles are positioned one over another and coincide upon projection. Then they are symbolized as triangles with a dot. Among these groups there are those which have no operations transforming the upper and lower half-spaces into one another, and then the space is asymmetric along axis X_3 perpendicular to X_1, X_2, and all the triangles are white (or black). The unit cell of the layers is an infinite "column" perpendicular to X_1, X_2, with a cross section in the form of a parallelogram of sides a_1 and a_2.

2.8 Space Groups of Symmetry

2.8.1 Three-Dimensional Lattice

The present-day conceptions of the symmetry of the space structure of crystals go back to the work of the French crystallographer A. Bravais, who established, in 1848, 14 types of three-dimensionally-periodic lattices, which are named after him. In 1879, L. Sohncke [2.23], proceeding from the results of C. Jordan (1869), described the groups of motions, i.e., the space groups of the first kind. A full derivation of space groups was carried out by the Russian crystallographer E. S. Fedorov and completed by him in 1890, and a little later, independently, by the German mathematician A. Schönflies. In their correspondence Fedorov and Schönflies put finishing touches to the description of all the 230 space groups.

The Fedorov groups $\Phi \equiv G_3^3$ are groups of transformation of three-dimensional homogeneous discrete space into itself; they describe the atomic structure of crystals. It is the condition of homogeneity and discreteness which determines that all of them are three-dimensionally periodic $\Phi \supset T_3$, and hence crystallographic, with axes only of the 1st, 2nd, 3rd, 4th, and 6th order. (From now on we shall write simply T instead of T_3).

The translation subgroup T of Fedorov group Φ is defined by three noncoplanar (and pairwise noncollinear) basis vectors, $\boldsymbol{a}_1$, $\boldsymbol{a}_2$, and $\boldsymbol{a}_3$,

$$\boldsymbol{t} = p_1\boldsymbol{a}_1 + p_2\boldsymbol{a}_2 + p_3\boldsymbol{a}_3, \quad p_1, p_2, p_3 = 0, \pm 1, \pm 2. \ldots \tag{2.91}$$

The group action in T is vector addition of any $\boldsymbol{t}: \boldsymbol{t}_1 + \boldsymbol{t}_2 = \boldsymbol{t}_3 \in T$. The vector corresponding to a unity operation of a group is denoted by $\mathbf{0}$, and the operation inverse to each operation $\boldsymbol{t}$, by $-\boldsymbol{t}$. A translation group is infinite, Abelian; it is metrically characterized by (2.91). The three vectors, $\boldsymbol{a}_1$, $\boldsymbol{a}_2$, and $\boldsymbol{a}_3$, are the basis if they can represent any lattice translation $\boldsymbol{t}$ according to (2.91). In particular, the three shortest mutually noncoplanar vectors can be taken as a basis. An infinite discrete array of points $\boldsymbol{x}'$ derivable from a given point $\dot{\boldsymbol{x}}$ by the operation $\boldsymbol{x}' = \boldsymbol{x} + \boldsymbol{t}$ forms a geometric invariant of group T – a space lattice. A parallelepiped constructed on $\boldsymbol{a}_1$, $\boldsymbol{a}_2$, $\boldsymbol{a}_3$ is called a unit, or primitive parallelepiped (Fig. 2.64).

This parallelepiped does not contain lattice points, i.e., nodes within it and is said to be empty (cf. Fig. 2.53). As in the two-dimensional case (Fig. 2.53) the three basis vectors, and hence a primitive parallelepiped, can be chosen in an infinite number of ways (Fig. 2.64). The volumes of all the primitive parallelepipeds are the same. Despite the fact that we can choose three basic vectors in a given lattice in different ways, all of them describe metrically one and the same translation group.

At the same time, a lattice has an infinitely large number of nonprimitive parallelepipeds, which contain their edges and/or faces, and/or in the volume, points belonging to the primitive lattice (Fig. 2.54, the two-dimensional example). Their edges are three arbitrary noncoplanar translations $\boldsymbol{t}_1$, $\boldsymbol{t}_2$, $\boldsymbol{t}_3$ out of the whole set (2.91). The volumes of such parallelepipeds are multiples of that of the primitive one. It is obvious that all the groups $T' = \{\boldsymbol{t}_1, \boldsymbol{t}_2, \boldsymbol{t}_3\}$ are sub-groups of $T = \{\boldsymbol{a}_1, \boldsymbol{a}_2, \boldsymbol{a}_3\}$, because the lattice derived by group T' does not cover all the points of the lattice of group T. Abstractly, all the T' are isomorphous, and also isomorphous with T, i.e., group T in the abstract sense is unique.

The possibility of choosing a primitive or nonprimitive unit cell for a given lattice in an infinite number of ways does not mean that it is impossible to indicate an unambiguous method for choosing a unique standard basis. For such a choice the nontranslational symmetry of the lattice is taken into account.

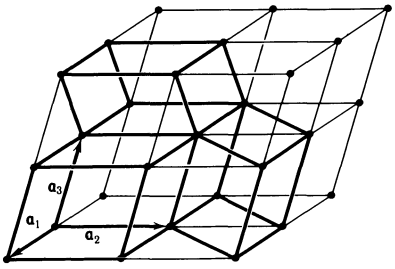

Fig. 2.64. Possibility of different choice of a primitive unit cell in a space lattice

There exist also algorithms for reduction of any unit cell to standard settings, which will be discussed further on (see Sect. 3.52).

2.8.2 Syngonies

Group T derives a lattice from any one point of space. Let us consider a possible point symmetry of a lattice point (they are all identical) and of the lattice as a whole with respect to this point, i.e., let us find the maximum group K retaining a fixed point unmoved and bringing the lattice into self-coincidence.

A set of six vectors, $\boldsymbol{a}_1, \boldsymbol{a}_2, \boldsymbol{a}_3, -\boldsymbol{a}_1, -\boldsymbol{a}_2$ and $-\boldsymbol{a}_3$ comes out of each point of the lattice; they can be used to construct eight unit parallelepipeds; taken together, they make up one large parallelepiped with double-sized edges and the chosen point at its center (Fig. 2.65). It is easy to see that the symmetry K of the point and lattice as a whole with respect to the point coincides with the symmetry of these six vectors and of the large parallelepiped, or with the symmetry of the unit parallelepiped, provided that we take the most symmetric one of all such possible parallelepipeds (and $\boldsymbol{a}_1, \boldsymbol{a}_2, \boldsymbol{a}_3$ corresponding to them) (Fig. 2.66). In this way the point symmetry of the lattice defines the choice of a standard basis. It should be noted that in one case, i.e, in the hexagonal syngony (Fig. 2.66f), the symmetry of the lattice point corresponds to that of the six unit parallelepipeds adjacent to it which, taken together, make up a hexagonal prism. The division of lattices according to the point symmetry K of their points is called the division into *syngonies* (or *systems*). (See footnote 13 on p. 97).

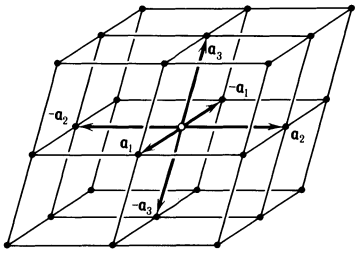

Fig. 2.65. Six vectors $\pm \mathbf{a}_i$ issuing from a lattice point

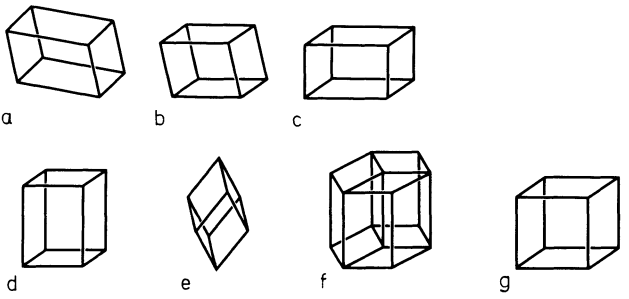

Fig. 2.66a–g. Unit parallelepipeds characterizing seven syngonies.
(a) triclinic, **(b)** monoclinic, **(c)** orthorhombic, **(d)** tetragonal, **(e)** trigonal, **(f)** hexagonal, and **(g)** cubic

There are seven syngonies all in all. They can readily be derived by considering the possible symmetry of parallelepipeds, gradually raising the symmetry of the least symmetric one with edges $a_1 \neq a_2 \neq a_3$ and angles $\alpha \neq \beta \neq \gamma$, or by deforming the most symmetric one, a cube, and reducing its symmetry (Fig. 2.66). The syngonies have the following names: cubic (symmetry of parallelepiped $O_h - m\bar{3}m$), the highest; hexagonal ($D_{6h} - 6/mmm$), tetragonal ($D_{4h} - 4/mmm$), and trigonal ($D_{3d} - \bar{3}m$), intermediate, with one principle axis; and orthorhombic ($D_{2h} - mmm$), monoclinic ($C_{2h} - 2/m$), and triclinic ($C_i - \bar{1}$), the lowest. The holohedral groups of symmetry K (see Sect. 3.2.4), which characterize the syngonies, are subgoups of each other.

The subordination scheme is as follows:

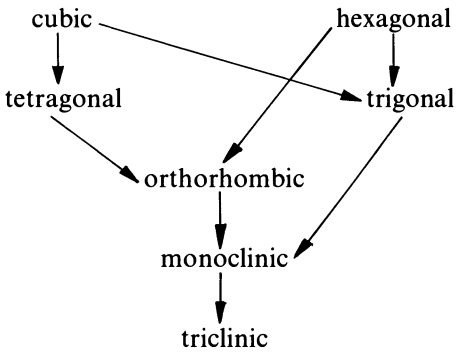

The characteristics of the syngonies were given in Tables 2.3 and 2.4. We have already considered them in the classification of point groups.

2.8.3 Bravais Groups

The lattice point has a point symmetry K (holohedral), which depends on the allocation of the lattice to one of the seven syngonies. The lattice is also transformed into itself by a group of translations T. A full group of motions (of both kinds) that bring the lattice into self-coincidence, i.e., which contains both point symmetry operations and translations, is called a *Bravais group*, and an infinite lattice derived from one point by a Bravais group, a *Bravais lattice*.

The seven parallelepipeds (Fig. 2.66), characterizing the syngonies described by definite metric and angular relationships between the vectors of the basis translations, correspond to the seven Bravais lattices. These parallelepipeds are primitive; therefore, the corresponding Bravais groups and lattices are called primitive and are denoted by letter P.

To find the other Bravais lattices we consider a two-dimensional example of a net with symmetry mm. The point lying on m and the whole lattice, have this symmetry in two cases: the first, if the two shortest translations are oriented one in m and the other perpendicular to it, then $a_1 \neq a_2$, angle $\gamma = 90°$; and the net is

rectangular (Fig. 2.67a); and the second, if a'_1 is directed arbitrarily, angle $\gamma \neq 90°$, but then $a'_2 = a'_1$ because of the presence of m, and the net is orthorhombic (Fig. 2.67b). The second net can also be described as rectangular with translations $\boldsymbol{a}_1 = \boldsymbol{a}'_1 + \boldsymbol{a}'_2$ and $\boldsymbol{a}'_2 = \boldsymbol{a}'_2 - \boldsymbol{a}'_1$, $\gamma = 90°$, but centered: it has a point located at the center of the rectangle, whose vector is $\boldsymbol{a}'_2 = (\boldsymbol{a}_1 + \boldsymbol{a}_2)/2$. In both cases the net and its points have symmetry *mm*, but metric and angular relationships between the minimum basis translations are different, i.e., there are two two-dimensional Bravais lattices and two groups here. The second lattice arises because of the possibility of centering the rectangular primitive lattice. Note that the centering of an oblique net (Fig. 2.67c) with $a_1 \neq a_2$, $\gamma \neq 90°$ will not produce a new Bravais group, since $\boldsymbol{a}'_1 = (\boldsymbol{a}_1 + \boldsymbol{a}_2)/2$, $\boldsymbol{a}'_2 = (\boldsymbol{a}_2 - \boldsymbol{a}_1)/2$ and the relationships for the new values are the same as for the initial: $a'_1 \neq a'_2$, $\gamma \neq 90°$.

In the three-dimensional case, too, non-primitive Bravais lattices and groups are possible; they contain points at the center of one or all the rectangular faces or at the center of the (rectangular) parallelepiped itself. Symmetry K of these parallelepipeds and of each point is the same as that of the primitive, but the set of vectors issuing from each point towards the neighboring ones has become different: it is supplemented by vectors running to the centering points. This means that the syngony remains the same, but the Bravais group (it is characterized precisely by a set of minimum translations) is different.

The requirement for the rectangularity of the centered face leaves only the primitive Bravais group $P\bar{1}$ for the triclinic lattices.

Groups and, hence, lattices centered on one face are called base- or side-centered and denoted by A (centered face a_2a_3), B (a_1a_3), or C (a_1a_2). In this way a nonprimitive Bravais group arises in the monoclinic (Fig. 2.68a) and ortho-

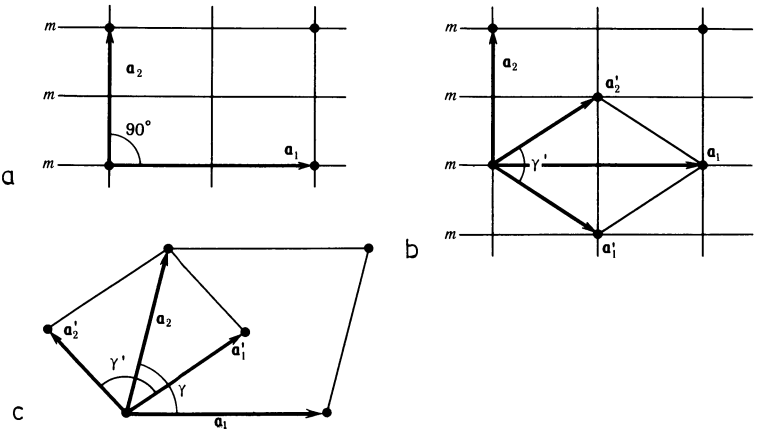

Fig. 2.67a–c. Two-dimensional nets with symmetry *mm*: primitive (**a**) and centered (**b**); centering of an oblique net (**c**) does not produce a new Bravais group

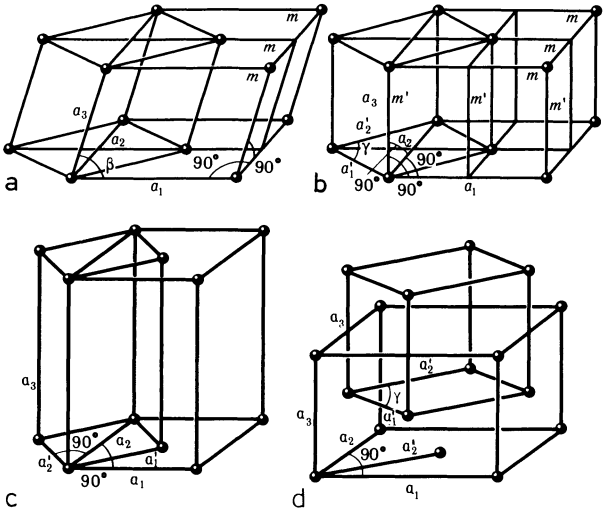

Fig. 2.68a–d. Different possibilities for lattice centering. Appearance of a base-centered Bravais group in a monoclinic (**a**) and orthorhombic (**b**) lattice. Centering of a tetragonal lattice with respect to the basis (**c**) brings us back to the case of a primitive tetragonal lattice. Centering of a orthorhombic lattice with respect to two faces (**d**) will also lead to the centering of the third basal face

rhombic (Fig. 2.68b) syngonies[14]. In the tetragonal syngony (Fig. 2.68c), when $a_1 = a_2$, $\gamma = 90°$, centering of the base gives the same relationships as in the principal lattice: $a'_1 = a'_2$, $\gamma = 90°$, and therefore no new Bravais group arises.

Centering on two faces in the case of orthorhombic (Fig. 2.68d) and other lattices is impossible, since the arising translation a'_1 must also center the basal face.

Centering on all the three faces, which is denoted by F, gives a set of 12 vectors (equal in length) of the form $\boldsymbol{a}_j = \pm (\boldsymbol{a}_i \pm \boldsymbol{a}_k)/2$, where $i, k = 1, 2, 3$ (Fig. 2.69a). A polyhedron drawn over the ends of these vectors is an orthorhombically deformed cubooctahedron (Fig. 2.69b). Bravais face-centered groups arise in this way in the orthorhombic and cubic syngonies, while in the tetragonal syngony they are reduced to the case of P.

Centering of the volume, which is denoted by I, gives a set of eight vectors (equal in length) of the kind $\boldsymbol{a}'_j = (\pm \boldsymbol{a}_1 \pm \boldsymbol{a}_2 \pm \boldsymbol{a}_3)/2$ (Fig. 2.70). A polyhedron drawn over the ends of these vectors coincides in shape with the initial unit cell. This gives new Bravais groups in the orthorhombic, tetragonal, and cubic syngonies.

The primitive parallelepipeds in cubic F and I cells are rhombohedra (Fig. 2.71). Similar primitive unit cells can be singled out in tetragonal and orthorhombic I and F lattices; their faces are parallelograms and rhombs.

As we have already noted, the true symmetry of the lattice point of the hexagonal cell and of a set of unit vectors (there are eight of them) is revealed if we add together three unit parallelepipeds (see Fig. 2.66), which consititute a

[14] In the monoclinic syngony the three-dimensional lattice is characterized by symmetry $2/m$, although the plane nets perpendicular to m have a two-dimensional symmetry mm, as in Fig. 2.67.

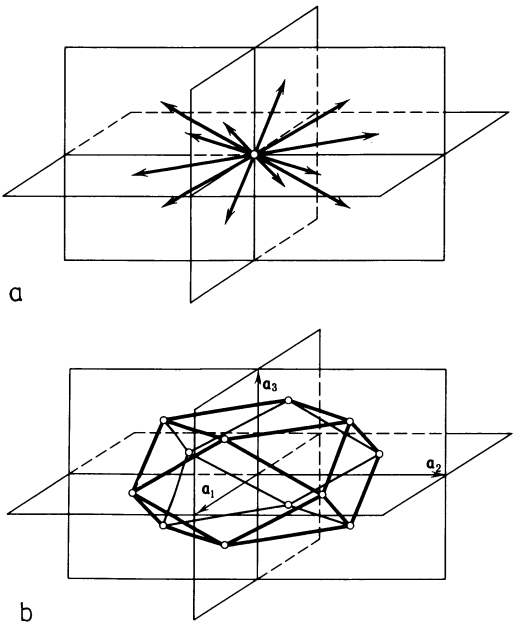

Fig. 2.69a,b. Description of a face-centered lattice. (**a**) a set of 12 vectors directed towards the centers of the faces adjoining the given point (*F*-centering, possible in rectangular cells); (**b**) polyhedron (dodecagon) drawn over these vectors

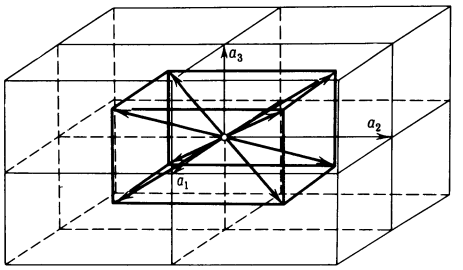

Fig. 2.70. Set of eight vectors directed towards the centers of cells adjoining the given point: *I*-centering, possible in rectangular cells. A polyhedron drawn over their ends coincides in shape with the cell itself

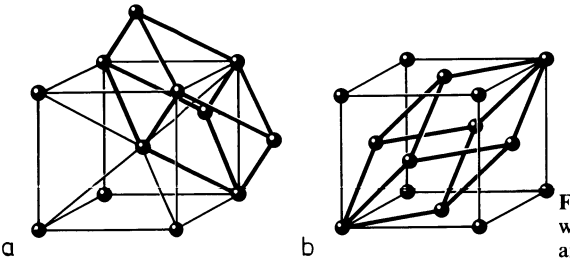

Fig. 2.71a,b. Primitive rhombohedra which can be singled out in cubic *I* (**a**) and *F* (**b**) lattices

hexagonal prism. Here, consideration of the possibilities of centering proves that there are no new Bravais groups.

Only one rhombohedral Bravais lattice – primitive – is possible; it has a trigonal symmetry. But it can be described in the hexagonal setting with additional points and, conversely, a hexagonal cell can be described in the rhombohedral setting (Fig. 2.72).

Thus, we finally obtain 14 Bravais groups and hence, 14 Bravais lattices (Fig. 2.73 and Table 2.10).

Taking into account the possible centering, the operations of translations of the Bravais groups have a form similar to (2.91), but with an additional term $\boldsymbol{t}_c$,

$$\boldsymbol{t} = p_1\boldsymbol{a}_1 + p_2\boldsymbol{a}_2 + p_3\boldsymbol{a}_3 + \boldsymbol{t}_c, \quad p_1, p_2, p_3 = 0, \pm 1, \pm 2, \ldots, \pm\infty \ . \tag{2.92}$$

For instance, when centering on the base $\boldsymbol{t}_c = (\boldsymbol{a}_1 + \boldsymbol{a}_2)/2$, etc. (see Fig. 2. 68b). It is also possible to write $\boldsymbol{t}$ directly through primitive translations, say for a base-centered lattice

$$\boldsymbol{t} = p_1\left(\frac{\boldsymbol{a}_1 + \boldsymbol{a}_2}{2}\right) + p_2\left(\frac{\boldsymbol{a}_1 - \boldsymbol{a}_2}{2}\right) + p_3\boldsymbol{a}_3. \tag{2.93}$$

Operations of the translation group T, being applied to any point $\boldsymbol{x}$ of the crystal space (T is mobile), will derive a lattice of parallel points $\boldsymbol{x}' = \boldsymbol{x} + \boldsymbol{t}$ from it (see Fig. 1.15); this group is *free*. On the other hand, the point symmetry of the lattice and the Bravais group is revealed if one "stopped" lattice is considered.

Points $\boldsymbol{x}$ of space, however, may be interrelated not only by operations of the Bravais groups, but also by other symmetry operations. All the possible groups of such operations are in fact space groups Φ, which will be considered next.

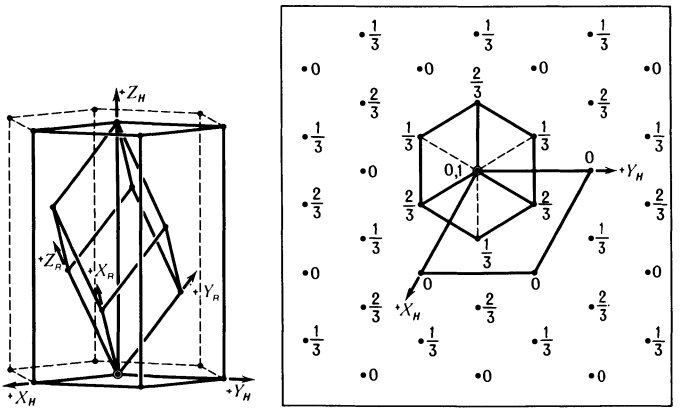

Fig. 2.72a,b. Relation between a hexagonal and a rhombohedral cell. (**a**) axonometric representation; (**b**) projection onto the basal plane; the figures denote the z coordinates of the points

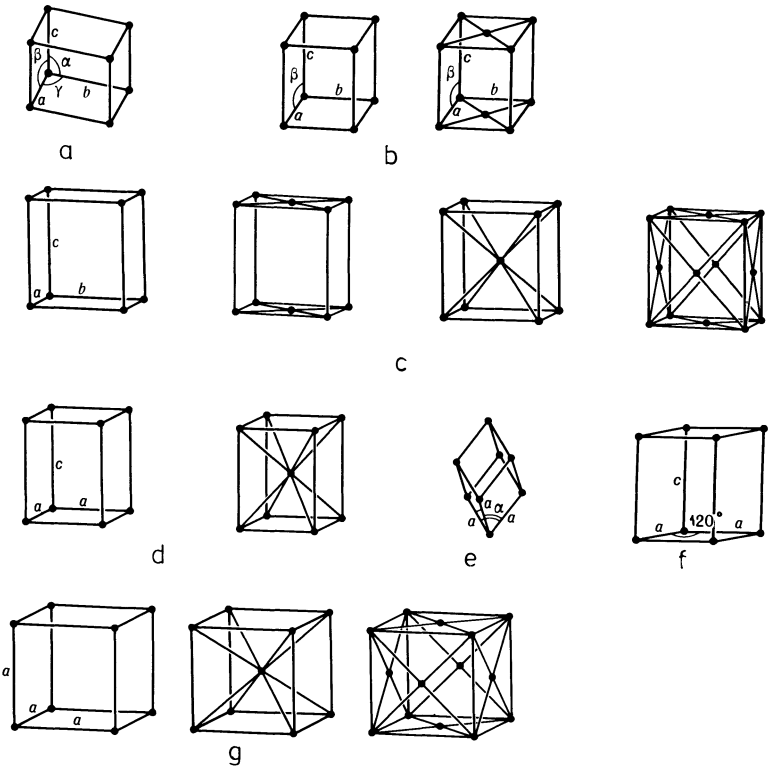

Fig. 2.73a–g. Fourteen Bravais lattices.
(**a**) triclinic; (**b**) monoclinic; (**c**) orthorhombic; (**d**) tetragonal; (**e**) trigonal; (**f**) hexagonal; (**g**) cubic (see Table 2.10)

Table 2.10. 14 Bravais groups (lattices)

Syngony	Centering	Translation group (Schönflies notation)	International symbol
Triclinic	P	Γ_i	$P\bar{1}$
Monoclinic	P	Γ_m	$P2/m$
	$B(C)$	Γ_m^b	$B(C)2/m$
Orthorhombic	P	Γ_0	$Pmmm$
	$C(B,A)$	Γ_0^b	$C(B,A)mmm$
	I	Γ_0^v	$Immm$
	F	Γ_0^f	$Fmmm$
Tetragonal	P	Γ_q	$P4/mmm$
	I	Γ_q^v	$I4/mmm$
Trigonal	R	Γ_{rh}	$R\bar{3}m$
Hexagonal	P	Γ_h	$P6/mmm$
Cubic	P	Γ_c	$Pm\bar{3}m$
	I	Γ_c^v	$Im\bar{3}m$
	F	Γ_c^f	$Fm\bar{3}m$

2.8.4 Homomorphism of Space and Point Groups

We take any asymmetric point A in space together with its asymmetric label – a tetrahedron – and perform all the operations of the given space group over it, being interested only in the components of rotations (proper and improper) of these operations, and disregarding translations and translational components of any operations (if they exist). All the rotations of the obtained points A, A', A'', . . . will be preserved if we transfer these points parallel to themselves to one common point O; all the translations will naturally be lost. For instance, if we had an operation of screw rotation with an axis N_q giving displaced and rotated points, they would now only be rotated about axis N, which corresponds to N_q in its order. To the symmetry operations (and elements) a, b, c, n, d there will correspond m in a parallel orientation. The operations N, $\bar{N}$, and m of groups Φ remain unaltered. The symmetry elements of groups Φ may all intersect at a single point (Fedorov named such a point the "centre of symmetry" attaching to it a different meaning than we do now), but they may not intersect, either. The procedure under consideration transforms all the spatially distributed symmetry elements Φ into point symmetry elements intersecting at a singular point.

All the rotations (of both kinds) of group Φ themselves make up a group, because in performing operations Φ these operation components act only on each other, while the translational component is insignificant. At the same time, these rotations in group Φ are only such that they bring the lattice produced by group $T \subset \Phi$ into self-coincidence. It follows that the group of these rotations is one of the 32 crystallographic point groups K, which is homomorphous with group Φ.

Since each Bravais lattice of a given syngony is described by a holohedral point group K (the most symmetric of all the point groups of this syngony), it is clear that the orientation of the symmetry elements of the space group of this syngony can only be that of the respective elements of the point symmetry of the unit parallelepiped.

The entire set of parallel motions of group Φ consists only of its group of translations $T \subset \Phi$ and translational components α of rotation operations of both kinds, if they exist. Therefore we can write the following symbolic relation:

$$\Phi : (T + \alpha) \leftrightarrow K, \tag{2.94}$$

which means that exclusion of all parallel motions from Φ results in a group K such that the lattice derived by T is described either by K itself, if it is holohedral, or by its supergroup holohedral with respect to K.

As we shall see below, strict group-theoretical relations (2.98, 101) correspond to this geometric reasoning.

A homomorphous mapping of the sets of groups Φ onto definite groups K is not only an abstract notion, but reflects the physical fact of interrelation of the microscopic and macroscopic structure of crystals and has actually originated from it.

Space groups describe the microstructure of a crystal, while point groups its habit. Let us take some crystal which has, say, a screw rotation axis. Let a lattice

net be inclined to this axis. Macroscopically, this net is expressed as a crystal face. The microscopic action of the screw axis consists in rotating this net and displacing it by atomic-scale distances. From the macroscopic point of view it is tangible and measurable only as a rotation, and in the crystal habit we shall see only a simple rotation axis. The same refers to the macroscopic manifestation of other symmetry elements with a translational component: they lose it in macromanifestation. In other words, groups Φ and their symmetry elements are macroscopically "visible" as the respective groups K and their point symmetry elements.

2.8.5 Geometric Rules for Performing Operations and for Mutual Orientation of Symmetry Elements in Groups Φ

The existence of translational symmetry operations $t \in T_3 \subset \Phi$ predetermines the geometric features of their products (successive performances) with other operations $g_i \in \Phi$, which may include point symmetry operations $g_i \in K \subset \Phi$.

Translations will generate, from any line or plane, an infinitely large number of lines or planes parallel to the initial. By definition of a symmetry element (see Sect. 5) its points or the element as a whole are transformed into themselves by all the degrees of the operation generating it, and it is transformed completely into similar elements by other operations. Hence it follows that a lattice always has translations (rows of points) parallel to the axes of symmetry (Fig. 2.74) and translation nets parallel to the planes of symmetry (Fig. 2.75), since such translations displace the indicated elements parallel to themselves. It can be seen from the figures that there are always nets of points perpendicular to axes of any type (Fig. 2.74), and there are always one-dimensional rows of points, i.e., there are translations perpendicular to any plane of symmetry (Fig. 2.75).

Plane m, perpendicular to translation t, is reproduced by it into identical planes spaced at t from each other, but by theorem II of Sect. 2.2.4 and as evident from Fig. 2.9b, one more plane m', parallel to m and spaced at $t/2$, always arises in this case. The same is true for glide-planes perpendicular to t. By analogy, it is easy to understand that if there exist translationally equal axes of symmetry of

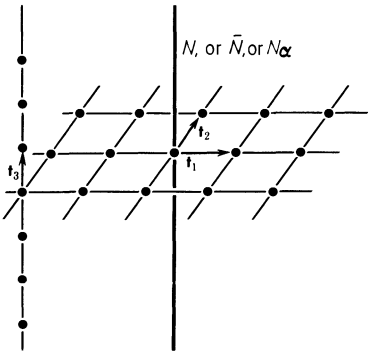

Fig. 2.74. Translation t_3 parallel to the symmetry axis, and a net of translations $t_1 t_2$ perpendicular to it

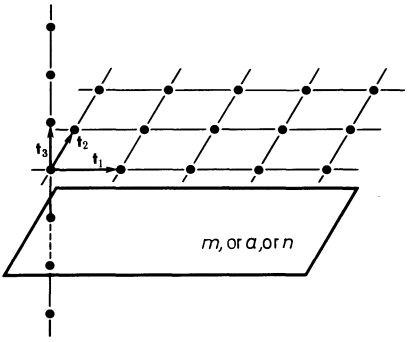

Fig. 2.75. Net of translations $t_1 t_2$ parallel to the symmetry plane, and translation t_3 perpendicular to it

even order, there exist parallel axes of the second order halfway between them. There are also derivative inversion centers at midpoint between translationally equal inversion centers. Thus groups Φ have infinite systems of parallel symmetry elements derivable from some initial ones, both translationally equal and derived, lying halfway between them.

2.8.6 Principles of Derivation of Space Groups. Symmorphous Groups Φ_s

In deriving groups Φ use is made of geometric, arithmetical, combinatorial, group-theoretical, and other methods. We shall proceed from geometric concepts and group theory.

From consideration of translation group T and the Bravais groups, and also from the deduction of homomorphism (with appropriate orientations) of groups Φ and K (2.94). A simple method for deriving symmorphous space groups follows: it is possible to combine operations t_i of group T in its realization as one of the Bravais lattices with operations k of point groups K of appropriate syngony, i.e., to form a semidirect product (2.42) of such groups

$$\Phi_s \equiv T \circledS K. \tag{2.95}$$

Geometrically – in the language of symmetry elements – this is equivalent to placing the symmetry elements of group K at the points of the Bravais lattice of the same symmetry (here, as we know, new, derivative symmetry elements may also arise). Group K in (2.95) may be either a higher, holohedral group of a given syngony, or one of the lower subgroups of the holohedral group (the latter does not contradict the above-formulated requirements). The groups thus obtained were named *symmorphous* by Fedorov.

Let us consider two examples. In the first case the Bravais lattice is monoclinic primitive P, and the point group is $2/m$. A group $\Phi_s = C_{2h}^1 - P2/m$ arises (Fig. 2.76). In accordance with the above rules, additional derivative elements have also arisen within the unit parallelepiped apart from the initial symmetry elements of group K. In the second case the Bravais lattice is tetragonal, body-centered I, and the point group is $\bar{4}2m$. A group $\Phi_s = D_{2d}^9 - I\bar{4}m2$ arises (2.77a–c). Elements with a translational component (inherent in any centered

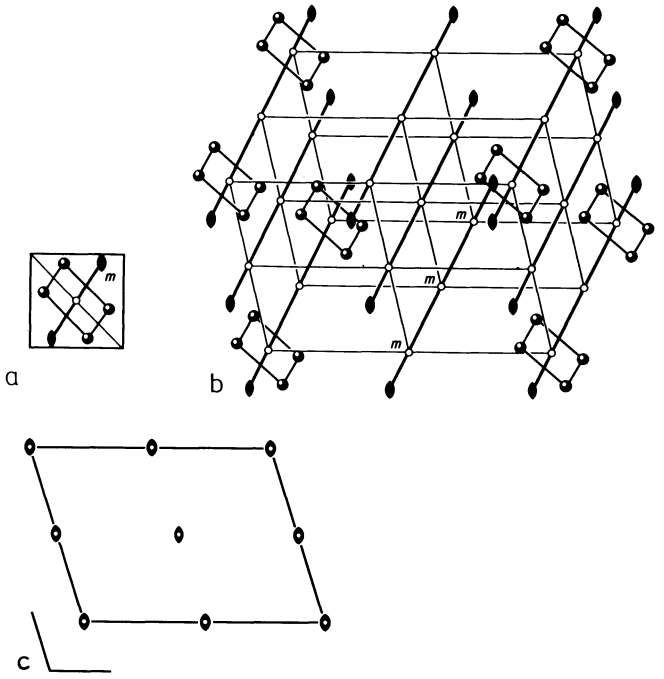

Fig. 2.76a–c. Derivation of a symmorphous space group as a product of a point group and a translation Bravais group.
(**a**) point group $2/m$ and a regular point system in it (for visual clarity, the points are joined by straight lines; they form a rectangle); (**b**) symmetry elements "planted" at the points of a primitive oblique Bravais lattice and regular point systems of group $2/m$ (this produces space group $P2/m$; apart from the initial symmetry elements of group $2/m$, additional elements 2, m, $\bar{1}$ arise in it at half-distances); (**c**) conventional representation of space group $P2/m$ in projection onto an oblique face

Bravais lattice) appear in addition to the derivative elements of point symmetry. With another coincidence of the symmetry elements (rotation of $\bar{4}2m$ through 45°) a group $\Phi_s = D_{2d}^{11} - I\bar{4}2m$ appears (Fig. 2.77d).

In the semidirect product (2.95) the factor T is an invariant (normal) divisor, so that $T = KTK^{-1}$, while K is not. Geometrically, the idea is that the invariant subgroup $T \subset \Phi$ in space can be singled out anywhere (this is a free vector group), while the point subgroup $K \subset \Phi_s$ can be isolated only with respect to certain points of space, namely those at which all the symmetry elements of group $K \ni k_i$ intersect. Here, (2.95) reflects the fact that the operations k_i of group K transform the lattice into itself.

The semidirect product (2.95) can be rewritten

$$\Phi_s \equiv \{t_1, t_2, t_3, \ldots\}\ \{k_1, k_2, \ldots, k_n\} = T_{k_1} \cup T_{k_2} \cup \ldots \cup T_{k_n}, \tag{2.96}$$

where the symbol $\cup$ means joining the cosets $T_{k_j} = \{t_1 k_j, t_2 k_j, t_3 k_j \ldots\}$. The

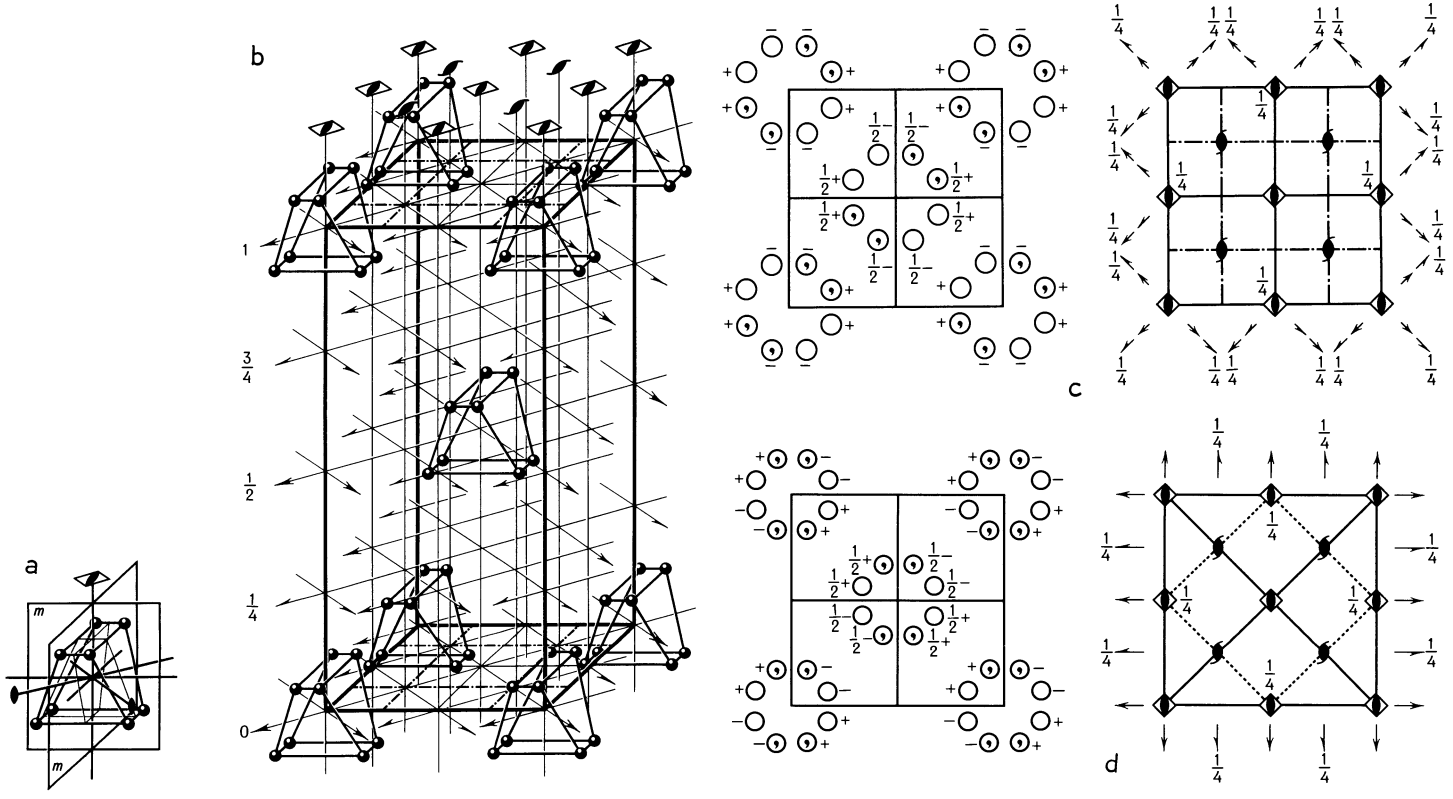

Fig. 2.77a–d. Formation of space groups $I\bar{4}m2$ and $I\bar{4}2m$ as a product of point group $\bar{4}2m$ and tetragonal body-centered Bravais group I.
(**a**) point group $\bar{4}2m$ and a regular point system in it (the points are joined by straight lines forming an isogon, which in this case is a tetrahedron truncated by planes perpendicular to axis $\bar{4}$); (**b**) this polyhedron is repeated at the vertices and at the center of tetragonal cell I (with appearance of vertical axes 2, horizontal diagonal axes 2 and 2_1 alternating at intervals 1/4, and planes n). Here, the point group is brought into coincidence with lattice I so that symmetry planes m coincide with the lateral faces of the cell, which gives space group $I\bar{4}m2$; (**c**) conventional representation of this group together with a regular system of points of general positions; (**d**) conventional representation and a regular system of points of general positions of space group $I\bar{4}2m$ formed on a different coincidence: planes m coincide with the diagonal planes of the cell

cosets themselves are elements of a new group Φ/T, a factor group (2.38). The multiplication law in it

$$T_{k_j}T_{k_i} = T_{k_ik_j} = T_{k_i} \leftrightarrow k_ik_j = k_j \tag{2.97}$$

coincides with the law of multiplication of elements in group K. Thus, in place of the symbolic relation (2.94) we can write exactly

$$\Phi_s \rightarrow \Phi_s/T \leftrightarrow K. \tag{2.98}$$

This means that the symmorphous group Φ_s is homomorphously mapped onto the factor group Φ_s/T with respect to the translation subgroup, and this factor group is isomorphous with the point group K. The unit of the factor group is the translation group $T = eT$ itself; its action is equivalent to the operation $e \in K$, while the other cosets $g_iT = Tg_i \leftrightarrow g_i$, i.e., they correspond to one of the operations $k_i \in K(t_1k_i \rightarrow k_i, t_2k_i \rightarrow k_i, \ldots)$.

The operations of any symmorphous group Φ_s thus consist of operations of the point group, which are characterized by matrices $(a_{ij}) = D$ (2.6), and translation operations of the Bravais group (2.92), i.e, are linear transformations (2.4,5)

$$g_i \in \Phi_s, \quad x' = Dx + t. \tag{2.99}$$

In constructing Φ_s as semidirect products of T and K in accordance with (2.95) it should be borne in mind that one and the same group K may be encountered in different Bravais groups of the given syngony (Table 2.11).

In Table 2.11 the first factor shows the number of groups K, and the second, the number of Bravais groups in each syngony. In the tetragonal, hexagonal, and orthorhombic syngonies, if group K is not the highest, sometimes more than one consistent setting of symmetry elements of K and those of the Bravais group is possible, which gives additional 7 groups (the plus signs in Table 2.11). An example of this kind is given in Fig. 2.77. In all, there are 73 symmorphous groups Φ_s.

If in forming symmorphous groups by (2.95) we take K^{I} of the first kind ($T = T^{\mathrm{I}}$ are themselves of the first kind), we obtain Φ_s^{I} of the first kind, of which there are 24. Accordingly, taking K^{II}, we have Φ_s^{II} of the second kind, of which there are 49.

It is worth noting that the Bravais lattice of spherically symmetric points, taken separately, is described by the most symmetric of the symmorphous

Table 2.11. Distribution of the 73 symmorphous groups Φ_s among the syngonies

Syngony	Number of groups	Syngony	Number of groups
Cubic	$5 \cdot 3 = 15$	Orthorhombic	$3 \cdot 4 + 1 = 13$
Tetragonal	$7 \cdot 2 + 2 = 16$	Monoclinic	$3 \cdot 2 = 6$
Trigonal	$5 \cdot 1 = 5$	Triclinic	$2 \cdot 1 = 2$
Hexagonal	$12 \cdot 1 + 4 = 16$		

Fedorov groups of the corresponding centering of a given syngony. These groups are indicated in Table 2.10.

2.8.7 Nonsymmorphous Groups Φ_n

To obtain the other, nonsymmorphous Fedorov groups, we recall that in the formation of the group product it is possible to isolate nontrivial subgroups in the resultant group. This is illustrated in Fig. 2.11, where the product of the operation of point group m with one-dimensional translation $t \| m$ is considered. From the group G_1^2 formed, a new subgroup with a basis $\{e, a\}$, containing a glide reflection a (Fig. 2.11d), can be singled out.

It should be emphasized that although the translation period in the new group $t' = 2t$ (twice as large as the starting one), this is of no importance now, and it can be taken as the unit period, and the translational component of the glide reflection a will be $t'/2$, as usual. The group obtained is a subgroup of the symmorphous group G_1^2, but it is not identical to any other symmorphous group of this type.

Precisely the same approach holds for groups G_3^3 [2.24]. The unit cells of groups Φ_s enlarged by the same factor in one, two, or all the three directions, contain not only the symmetry elements of the generating point group and the corresponding operations, but also operations with the translational component – glide reflections and screw rotations – if the multiple period is adopted as a basis. Let us take, for instance, six cells, arranged on top of each other, of group Φ_s containing axis 6 (Fig. 2.78). They have operations 6^n ($n = 0, \ldots, 5$), and also $6^n \cdot t', \ldots, 6^n \cdot 5t'$. Out of these we select only $6^n \cdot nt'$. They constitute a screw rotation, and a nontrivial subgroup $\Phi_n \subset \Phi_s$ arises with a period $t = 6t'$, which contains a screw rotation 6_1.

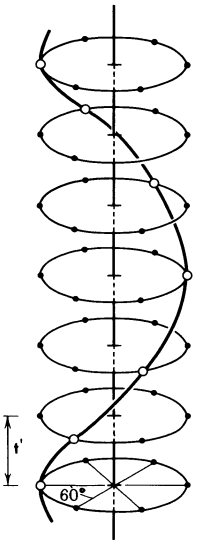

Fig. 2.78. Formation of the nonsymmorphous groups Φ_n. Selection of operation 6_1 in six unit cells (arranged one above another) of a group containing axis 6

Thus we obtain *nonsymmorphous* groups Φ_n, which are nontrivial subgroups of groups Φ_s, $\Phi_s \supset \Phi_n$. Symmorphous and nonsymmorphous groups, taken together, constitute all the Fedorov groups. Accordingly, all the operations–elements $g_i \in \Phi_n$ – are a part (subgroup) of the set of elements $\{ \ldots g_i \ldots \} = \Phi_s$, which are included in a symmorphous group (with multiple translations). Groups $\Phi_n \supset \Phi_s$ are homomorphous to the same point groups K to which Φ_s are homomorphous.

Fedorov divided the nonsymmorphous groups into two types, hemisymmorphous and asymmorphous. Let us take some symmorphous group of the second kind Φ_s^{II}. On doubling its period we can discard those operations of the second kind whose elements intersect at the same point where their axes do. This yields hemisymmorphous groups Φ_h^{II}; all of them are of the second kind; there are 54 of them.

Among symmorphous groups Φ_s, on multiple increase of their periods, it is possible to select such subgroups Φ_n which have no points of intersection of axes of all directions; they are asymmorphous groups Φ_a. A characteristic example of asymmorphous groups are groups with screw axes (cf. Fig. 2.78). Thus, a symmorphous group Φ_s has, by definition (2.95), positions of points whose symmetry is precisely that of the respective point group K. A set of equivalent points of general position, surrounding the point of highest symmetry, and an isogon – polyhedron, formed by them has the same symmetry K – see, for instance, Fig. 2.77a. In a hemisymmorphous group Φ_h^{II} the highest symmetry of the positions of the points is described by one of the subgroups of the first kind K^I of index 2 of group K^{II}, which is homomorphous with Φ_h^{II}, i.e., the position of points in K^{II} splits up into two enantiomorphous positions in K^I. For instance, group *Pmmm* is symmorphous, there are points (and isogons) in it with symmetry *mmm* (Fig. 2.79a); the group *Pnnn* is hemisymmorphous, the highest symmetry of points (and isogons) being 222 (Fig. 2.79b). Similarly, group $Pm\bar{3}m$ is symmorphous with the highest symmetry of position $m\bar{3}m$, group $Pn\bar{3}m$ is

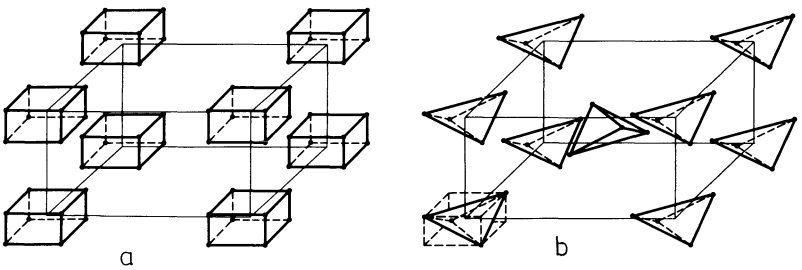

Fig. 2.79a,b. The concept of hemisymmorphous group Φ_h. In the symmorphous group *Pmmm* (**a**) a regular system of eight points has symmetry *mmm*. The same symmetry is exhibited by an isogon (a polyhedron whose vertices are points of a regular point system); in this particular case it is a parallelepiped. In the hemisymmorphous group *Pnnn* (**b**) four points with symmetry 222 are selected from this regular system (222 is a first-kind subgroup of index 2 of group *mmm*), the corresponding isogon is a tetrahedron; another four points, which are enantiomorphous to the first, are located at the center of a unit cell

hemisymmorphous with the highest symmetry of position 432, while group $Pm\bar{3}n$ is asymmorphous; it has no positions with symmetry $m\bar{3}m$ and 432.

The number of groups Φ_a is 103, of which there are 41 Φ_a^I and 62 Φ_a^{II}.

Let us consider the recording of operations of nonsymmorphous groups Φ_n

$$\Phi_n \ni g_i: \quad x' = Dx + \alpha(D) + t, \tag{2.100}$$

where Dx determines, by (2.4) and (2.5), all point symmetry transformations (if they exist) of the given group, $\alpha(D)$ are the components of a screw translation or glide reflection associated with proper or improper rotation, and t is the translation operation of the Bravais group (2.92).

The analytical expression of operations of space groups depends on the choice of the origin. Therefore, in particular, operations of symmorphous groups have the form (2.99) only when the origin is chosen at the point of intersection of all their symmetry elements; if a different point is chosen, operations are written in the most general form (2.100).

We shall now consider briefly the matrix-vector method for the derivation of groups Φ. Any transformation $g_i \in \Phi$ can be written as (D, a_D), where D is the matrix of a proper or improper rotation of group K, and a_D is the displacement vector (2.5). The symmetry transformations of groups K written in the form of primitive vector triads yield 73 integer-nonequivalent finite groups of whole-number matrices corresponding to symmorphous groups. These are called arithmetical classes. To derive all the Fedorov groups it is sufficient to indicate, for each arithmetical class, all the different displacement vectors corresponding to its matrices. A necessary and sufficient condition, which must be satisfied by the displacement vectors under two consecutive transformations D_1 and D_2, is Frobenius' comparison, $Da_{D_1} + a_{D_2} \equiv a \pmod{T}$ [(mod T) means the fulfillment of this relation with an accuracy to a translation group.] There is a method for solving such comparisons, which is standard for all the arithmetical classes [2.22] and which gives all the Φ. The geometric aspect of such a derivation consists in finding all the possible ways for dividing an isogon of the symmorphous group corresponding to a given arithmetical class and the vectors carrying the parts of the isogon over the primitive parallelepiped.

Let us turn once again to the considerations concerning the relationship of any Fedorov groups with point groups. In view of the presence of the term $\alpha(D)$ in expression (2.100) the factor group of the nonsymmorphous group Φ_n with respect to the translation subgroup does not coincide with point group K, as was the case for symmorphous groups according to (2.98). Here, however, some group K' appears, which also includes operations with translational components. It is agreed then that the degree of operations yielding a translation (for instance, $3_1^3 = t$, see Fig. 2.80) is equivalent to a unity operation e, and such a group is called a modulo group, in this case modulo 3_1^3. With this convention group K' turns out to be isomorphous to the respective ordinary point group K, and the factor group is mapped onto the first one of them,

$$\Phi_n/T \leftrightarrow K' \leftrightarrow K. \tag{2.101}$$

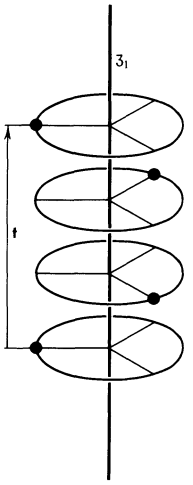

Fig. 2.80. The concept of a modulo group.
In a modulo group, the degree of operations with a translational component, which is equivalent to a translation, is taken to be equivalent to a unity operation, for instance, $3_1^3 = t = e$

This means that (2.98) is valid not only for symmorphous groups Φ_s, but for non-symmorphous Φ_n as well. In other words, the factor group of any Fedorov group with respect to the translation group T is always isomorphous to the crystallographic group K.

2.8.8 Number of Fedorov Groups

The finiteness of the number of Fedorov groups follows from the method of their derivation. Indeed, the number of symmorphous groups Φ_s is finite, since they are a product of a finite number of Bravais groups and a finite number of groups K with a finite number of possible combinations of groups K with Bravais groups. As for the number of groups Φ_n, it is finite, because there are subgroups of the former with a finite (multiple) increase of the periods by 2, 3, 4, 6 (but not more) times. If we take larger multiple periods, no new operations with translational components will be obtained: they will all coincide with the degrees of the existing ones; thus, no new groups can be constructed, either.

Consequently, symmorphous Φ_s, hemisymmorphous Φ_h, and asymmorphous Φ_a constitute all the groups Φ, and their number is therefore $73 + 54 + 103 = 230$. Of these, there are 65 groups Φ^I and 165 Φ^{II}.

Among the groups Φ some have operations performed by screw rotations and the corresponding axes of different chirality $3_1, 3_2, 4_1, 4_3, 6_1, 6_5, 6_2$, and 6_4. If such a group is of the second kind, these axes are always pairwise; if it is of the first kind, they all are of only one chirality (all right-handed or all left-handed). There are 11 pairs of groups of the latter type. Each of them can be obtained by a mirror reflection of its enantiomorphous analog. Abstractly, these 11 pairs of groups Φ are equal.

All the other Fedorov groups are abstractly different, i.e., nonisomorphous. If we regard the indicated pair of groups as one group, the number of groups Φ_a^I will be 30, and the total number of Fedorov groups, 219.

2.8.9 Nomenclature of Fedorov Groups

Table 2.12 lists all the Fedorov groups with their division into symmorphous groups and their subgroups: hemi- and asymmorphous.

Schönflies' notation of space groups is simply the notation of a homomorphous point group with serial number as superscript, for instance D_{3d}^1, D_{3d}^2, ... $D_{3d}^6 \rightarrow D_{3d}$.

Figure 2.81 illustrates the standard representation of one of the space groups, namely D_{2h}^{16} in accordance with the International Tables [Ref. 2.27, Vol. 1]; the representations of all symmetry elements are given in Fig. 2.22. Because of some difficulties in showing oblique symmetry elements that edition gives, for cubic groups, only an analytical description without a graphical. The schemes of these groups can be found in a number of books [2.24, 28, 29].[15]

Table 2.12. Fedorov groups Φ
(symmorphous Φ_s, hemisymmorphous Φ_h, and asymmorphous Φ_a)

Φ_s	Φ_h	Φ_a
$C_1^1 - P1$		
$C_i^1 - P\bar{1}$		
$C_2^1 - P2$		$C_2^2 - P2_1$ (2)
$C_2^3 - B2$		
$C_s^1 - Pm$	$C_s^2 - Pb$ (2)	
$C_s^3 - Bm$	$C_s^4 - Bb$ (2)	
$C_{2h}^1 - P2/m$	$C_{2h}^4 - P2/b$(2)	$C_{2h}^2 - P2_1/m$ (2), $C_{2h}^5 - P2_1/b$ (4)
$C_{2h}^3 - B2/m$	$C_{2h}^6 - B2/b$ (2)	
$D_2^1 - P222$		$D_2^2 - P222_1$ (2), $D_2^3 - P2_12_12$ (4), $D_2^4 - P2_12_12_1$ (8)
$D_2^6 - C222$		$D_2^5 - C222_1$ (2)
$D_2^7 - F222$		
$D_2^8 - I222$		$D_2^9 - I2_12_12_1$ (8)
$C_{2v}^1 - Pmm2$	$C_{2v}^3 - Pcc2$ (2), $C_{2v}^4 - Pma2$ (2), $C_{2v}^6 - Pnc2$ (4), $C_{2v}^8 - Pba2$ (4), $C_{2v}^{10} - Pnn2$ (8)	$C_{2v}^2 - Pmc2_1$ (2), $C_{2v}^5 - Pca2_1$ (4), $C_{2v}^7 - Pmn2_1$ (4), $C_{2v}^9 - Pna2_1$ (8)
$C_{2v}^{11} - Cmm2$	$C_{2v}^{13} - Ccc2$ (2)	$C_{2v}^{12} - Cmc2_1$ (2)
$C_{2v}^{14} - Amm2$	$C_{2v}^{15} - Abm2$ (4), $C_{2v}^{16} - Ama2$ (2), $C_{2v}^{17} - Aba2$ (4)	
$C_{2v}^{18} - Fmm2$	$C_{2v}^{19} - Fdd2$ (8)	
$C_{2v}^{20} - Imm2$	$C_{2v}^{21} - Iba2$ (8), $C_{2v}^{22} - Ima2$ (8)	
$D_{2h}^1 - Pmmm$	$D_{2h}^2 - Pnnn$ (8), $D_{2h}^3 - Pccm$ (2), $D_{2h}^4 - Pban$ (8)	$D_{2h}^5 - Pmma$ (2), $D_{2h}^6 - Pnna$ (8), $D_{2h}^7 - Pmna$ (4), $D_{2h}^8 - Pcca$ (4), $D_{2h}^9 - Pbam$ (4), $D_{2h}^{10} - Pccn$ (8), $D_{2h}^{11} - Pbcm$ (4), $D_{2h}^{12} - Pnnm$ (8), $D_{2h}^{13} - Pmmn$ (4), $D_{2h}^{14} - Pbcn$ (8), $D_{2h}^{15} - Pbca$ (8), $D_{2h}^{16} - Pmna$ (8)

[15] The latest edition of International Tables was published by the International Union Crystallography in 1992 [2.29].

Table 2.12. (continued)

Φ_s	Φ_h	Φ_a
D_{2h}^{19} — *Cmmm*	D_{2h}^{20} — *Cccm* (2), D_{2h}^{21} — *Cmma* (4), D_{2h}^{22} — *Ccca* (8)	D_{2h}^{17} — *Cmcm* (2), D_{2h}^{18} — *Cmca* (8)
D_{2h}^{23} — *Fmmm*	D_{2h}^{24} — *Fddd* (8)	
D_{2h}^{25} — *Immm*	D_{2h}^{26} — *Ibam* (8)	D_{2h}^{27} — *Ibca* (8), D_{2h}^{28} — *Imma* (8)
C_4^1 — *P*4		C_4^2 — $P4_1$ (4), C_4^3 — $P4_2$ (2), C_4^4 — $P4_3$ (4)
C_4^5 — *I*4		C_4^6 — $I4_1 = I4_3$ (4)
S_4^1 — $P\bar{4}$		
S_4^2 — $I\bar{4}$		
C_{4h}^1 — *P*4/*m*	C_{4h}^3 — *P*4/*n* (2)	C_{4h}^2 — $P4_2/m$ (2), C_{4h}^4 — $P4_2/n$ (8)
C_{4h}^5 — *I*4/*m*		C_{4h}^6 — $I4_1/c$ (16)
D_4^1 — *P*422		D_4^2 — $P42_12$ (2), D_4^3 — $P4_122$ (4), D_4^4 — $P4_12_12$ (16), D_4^5 — $P4_222$ (2), D_4^6 — $P4_22_12$ (8), D_4^7 — $P4_322$ (4), D_4^8 — $P4_32_12$ (16)
D_4^9 — *I*422		D_4^{10} — $I4_122$ (16)
C_{4v}^1 — *P*4*mm*	C_{4v}^2 — *P*4*bm* (2), C_{4v}^5 — *P*4*cc* (8), C_{4v}^6 — *P*4*nc* (8)	C_{4v}^3 — $P4_2cm$ (2), C_{4v}^4 — $P4_2nm$ (8), C_{4v}^7 — $P4_2mc$ (2), C_{4v}^8 — $P4_2bc$ (8)
C_{4v}^9 — *I*4*mm*	C_{4v}^{10} — *I*4*cm* (8)	C_{4v}^{11} — $I4_1md$ (16), C_{4v}^{12} — $I4_1cd$ (16)
D_{2d}^1 — $P\bar{4}2m$	D_{2d}^2 — $P\bar{4}2c$ (2)	D_{2d}^3 — $P\bar{4}2_1m$ (4), D_{2d}^4 — $P\bar{4}2_1c$ (8)
D_{2d}^5 — $P\bar{4}m2$	D_{2d}^6 — $P\bar{4}c2$ (2), D_{2d}^7 — $P\bar{4}b2$ (4), D_{2d}^8 — $P\bar{4}n2$ (8)	
D_{2d}^9 — $I\bar{4}m2$	D_{2d}^{10} — $I\bar{4}c2$ (8)	
D_{2d}^{11} — $I\bar{4}2m$		D_{2d}^{12} — $I\bar{4}2d$ (16)
D_{4h}^1 — *P*4/*mmm*	D_{4h}^2 — *P*4/*mcc* (2)	D_{4h}^5 — *P*4/*mbm* (2), D_{4h}^6 — *P*4/*mnc* (8),
	D_{4h}^3 — *P*4/*nbm* (2), D_{4h}^4 — *P*4/*nnc* (8)	D_{4h}^7 — *P*4/*nmm* (2), D_{4h}^8 — *P*4/*ncc* (8), D_{4h}^9 — $P4_2/mmc$ (2), D_{4h}^{10} — $P4_2/mcm$ (2), D_{4h}^{11} — $P4_2/nbc$ (8), D_{4h}^{12} — $P4_2/nnm$ (8), D_{4h}^{13} — $P4_2/mbc$ (8), D_{4h}^{14} — $P4_2/mnm$ (8), D_{4h}^{15} — $P4_2/nmc$ (8) D_{4h}^{16} — $P4_2/ncm$ (8)
D_{4h}^{17} — *I*4/*mmm*	D_{4h}^{18} — *I*4/*mcm* (8)	D_{4h}^{19} — $I4_1/amd$ (16), D_{4h}^{20} — $I4_1/acd$ (16)
C_3^1 — *P*3		C_3^2 — $P3_1$ (3), C_3^3 — $P3_2$ (3)
C_3^4 — *R*3		
C_{3i}^1 — $P\bar{3}$		
C_{3i}^2 — $R\bar{3}$		
D_3^1 — *P*312		D_3^3 — $P3_112$ (3), D_3^5 — $P3_212$ (3)
D_3^2 — *P*321		D_3^4 — $P3_121$ (3), D_3^6 — $P3_221$ (3)
D_3^7 — *R*32		
C_{3v}^1 — *P*3*m*1	C_{3v}^3 — *P*3*c*1 (2)	
C_{3v}^2 — *P*31*m*	C_{3v}^4 — *P*31*c* (2)	
C_{3v}^5 — *R*3*m*	C_{3v}^6 — *R*3*c* (2)	

Table 2.12 (continued)

Φ_s	Φ_h	Φ_a
$D_{3d}^1 - P\bar{3}1m$	$D_{3d}^2 - P\bar{3}1c$ (2)	
$D_{3d}^3 - P\bar{3}m1$	$D_{3d}^4 - P\bar{3}c1$ (2)	
$D_{3d}^5 - R\bar{3}m$	$D_{3d}^6 - R\bar{3}c$ (2)	
$C_6^1 - P6$		$C_6^2 - P6_1$ (6), $C_6^3 - P6_5$ (6)
		$C_6^4 - P6_2$ (3), $C_6^5 - P6_4$ (3),
		$C_6^6 - P6_3$ (2)
$C_{3h}^1 - P\bar{6}$		
$C_{6h}^1 - P6/m$		$C_{6h}^2 - P6_3/m$ (2)
$D_6^1 - P622$		$D_6^2 - P6_122$ (6), $D_6^3 - P6_522$ (6),
		$D_6^4 - P6_222$ (3), $D_6^5 - P6_422$ (3),
		$D_6^6 - P6_322$ (2)
$C_{6v}^1 - P6mm$	$C_{6v}^2 - P6cc$ (2)	$C_{6v}^3 - P6_3cm$ (2), $C_{6v}^4 - P6_3mc$ (2)
$D_{3h}^1 - P\bar{6}m2$	$D_{3h}^2 - P\bar{6}c2$ (2)	
$D_{3h}^2 - P\bar{6}2m$	$D_{3h}^4 - P\bar{6}2c$ (2)	
$D_{6h}^1 - P6/mmm$	$D_{6h}^2 - P6/mcc$ (2)	$D_{6h}^3 - P6_3/mcm$ (2), $D_{6h}^4 - P6_3/mmc$ (2)
$T^1 - P23$		$T^4 - P2_13$ (8)
$T^2 - F23$		
$T^3 - I23$		$T^5 - I2_13$ (8)
$T_h^1 - Pm\bar{3}$	$T_h^2 - Pn\bar{3}$ (8)	$T_h^6 - Pa\bar{3}$ (8)
$T_h^3 - Pm\bar{3}$	$T_h^4 - Pd\bar{3}$ (16)	
$T_h^5 - Im\bar{3}$		$T_h^7 - Ia\bar{3}$ (8)
$O^1 - P432$		$O^2 - P4_232$ (8), $O^6 - P4_332$ (16),
		$O^7 - P4_132$ (16)
$O^3 - F432$		$O^4 - F4_132$ (16)
$O^5 - I432$		$O^8 - I4_132$ (16)
$T_d^1 - P\bar{4}3m$	$T_d^4 - P\bar{4}3n$ (8)	
$T_d^2 - P\bar{4}3m$	$T_d^5 - P\bar{4}3c$ (8)	
$T_d^3 - I\bar{4}3m$		$T_d^6 - I\bar{4}3d$ (8)
$O_h^1 - Pm\bar{3}m$	$O_h^2 - Pn\bar{3}n$ (8)	$O_h^3 - Pm\bar{3}n$ (8), $O_h^4 - Pn\bar{3}m$ (8)
$O_h^5 - Fm\bar{3}m$	$O_h^6 - Fm\bar{3}c$ (8)	$O_h^7 - Fd\bar{3}m$ (8), $O_h^8 - Fd\bar{3}c$ (8)
$O_h^9 - Im\bar{3}m$		$O_h^{10} - Ia\bar{3}d$ (8)

Note. The figures in the parentheses for Φ_h and Φ_a indicate the factor by which the volume of unit cell Φ_s must be multiplied to obtain the particular subgroup [2.21].

Such a scheme represents all or part of the stereographic projection of the symmetry elements intersecting at the characteristic points of cubic groups (Fig. 2.82).

The international notation includes the symbol of the Bravais lattice and indicates (sometimes excessively) the generating symmetry operations (they also denote the elements), which are given in a definite three-position order in accordance with the symbol of the homomorphous point group and the choice of the crystallographic axes X_1, X_2, and X_3. Since the notation contains the symbol of the Bravais lattice and generating operations, it permits full description of the group.

Orthorhombic *mmm* $P2_1/n2_1/m2_1/a$ No. 62 *Pnma* D_{2h}^{16}

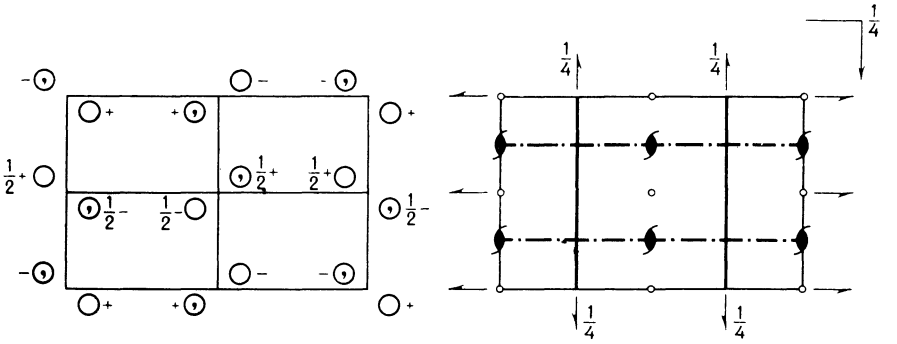

Origin at $\bar{1}$

Number of positions, Wyckoff notation and point symmetry			Co-ordinates of equivalent positions	Conditions limiting possible reflections
				General:
8	*d*	1	x, y, z; $\frac{1}{2}+x, \frac{1}{2}-y, \frac{1}{2}-z$;	*hkl*: No conditions
			$\bar{x}, \frac{1}{2}+y, \bar{z}$; $\frac{1}{2}-x, \bar{y}, \frac{1}{2}+z$;	*0kl*: $k+l=2n$
			$\bar{x}, \bar{y}, \bar{z}$; $\frac{1}{2}-x, \frac{1}{2}+y, \frac{1}{2}+z$;	*h0l*: No conditions
			$x, \frac{1}{2}-y, z$; $\frac{1}{2}+x, y, \frac{1}{2}-z$	*hk0*: $h=2n$
				h00: $(h=2n)$
				0k0: $(k=2n)$
				00l: $(l=2n)$
4	*c*	*m*	$x, \frac{1}{4}, z$; $\bar{x}, \frac{3}{4}, \bar{z}$; $\frac{1}{2}-x, \frac{3}{4}, \frac{1}{2}+z$;	Special: as above, plus no extra conditions
			$\frac{1}{2}+x, \frac{1}{4}, \frac{1}{2}-z$	
4	*b*	$\bar{1}$	$0, 0, \frac{1}{2}$; $0, \frac{1}{2}, \frac{1}{2}$; $\frac{1}{2}, 0, 0$; $\frac{1}{2}, \frac{1}{2}, 0$	*hkl*: $h+l=2n$; $k=2n$
4	*a*	$\bar{1}$	$0, 0, 0$; $0, \frac{1}{2}, 0$; $\frac{1}{2}, 0, \frac{1}{2}$; $\frac{1}{2}, \frac{1}{2}, \frac{1}{2}$	

Symmetry of special projections

(001)*pgm*; $a' = a/2$, $b' = b$ (100)*cmm*; $b' = b$, $c' = c$ (010)*pgg*; $c' = c$, $a' = a$

Fig. 2.81. Presentation of group *Pnma* $- D_{2h}^{16}$ in the International Tables.
Top line: point group, full symbol, number, and abbreviated symbol. Drawing on the left – points of general position, on the right–set of symmetry elements (axis $X = X_1$ is directed downwards, $Y = X_2$ to the right, and $Z = X_3$ towards the reader). Below the drawings on the left–the multiplicity and symmetry of positions, then coordinates of points in general and special positions, and on the right – conditions limiting possible reflections on diffraction patterns. Bottom line: symmetry of projections of the group [Ref. 2.27, Vol. 1]. A more detailed description of all space groups was given in [2.29]

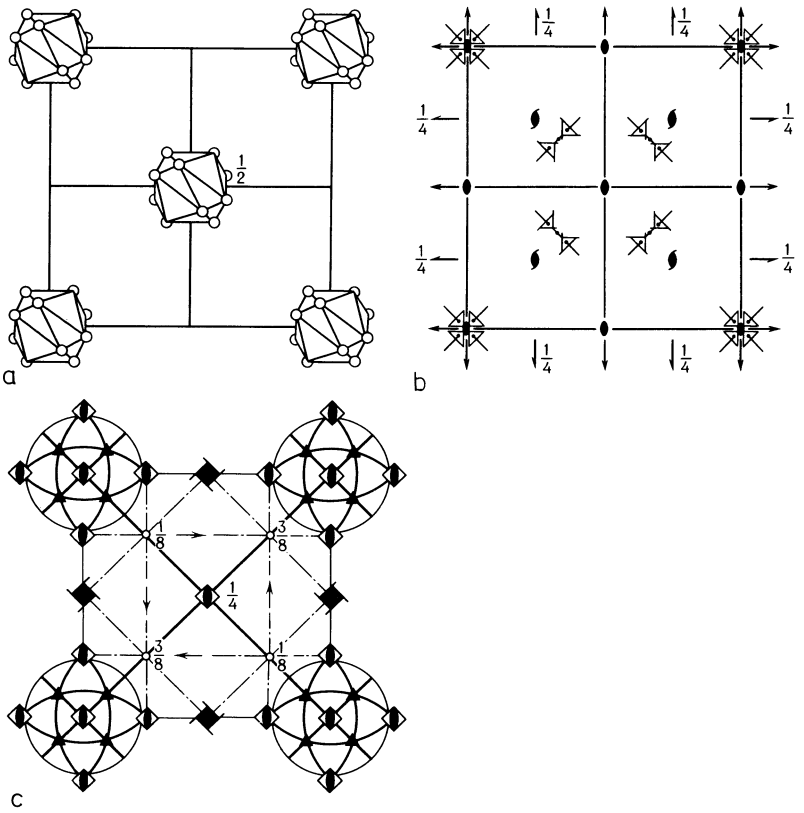

Fig. 2.82a-c. Presentation of the cubic space groups.
(**a**) regular system of points of groups $T^3 - I23$; (**b**) its symmetry elements [2.28]; (**c**) another method for representing symmetry elements: projection of 1/8 of the cell group $O_h^7 - Fd\bar{3}m$ (1/4 of its projection) [2.15]. See also [2.29]

For monoclinic groups, the notation indicates the symmetry axis and the plane of symmetry perpendicular to it (if they exist), for instance *P*2, *Pb*, *C*2/*m*. For orthorhombic groups, the first place is occupied by the designation of the axis parallel to axis X_1, or the plane perpendicular to it, and then the designations are given for axes X_2 and X_3, e.g., *Pmma*, *Iba*2, and *C*222.

In tetragonal and hexagonal groups, first comes the symbol of the principal axis (it passes along X_3) and then the symbol of a plane perpendicular to it after a stroke (if there is such a plane). Further, the planes perpendicular to the sides of the cell base are indicated, if they exist; and if they do not, the axes parallel to these sides, after which, in accordance with the same principle , follow elements parallel to the base diagonal, for instance $P4/n$, $P4_2/mcm$, $I4_1$, $P3_121$, and $P\bar{6}c2$.

In cubic groups, the coordinate axis elements are written first, then the symbol of axis 3 (body diagonal), and finally the elements of the base diagonal,

for instance $Pn\bar{3}$, $F4_132$, $Ia\bar{3}d$. Full symbols give the name of the principal axis in the numerator, and name of the plane perpendicular to it in the denominator, for instance D_{2h}^{17}–$C2/m2/c2_1/m$.

Attention should be drawn to a peculiarity of the international notation of monoclinic and especially orthorhombic groups. By taking a rectangular parallelepiped cell of any orthorhombic group, it is possible to direct axes X_1, X_2, X_3 from any of its vertices along three edges adjacent to it. Since the sequence of recording of the elements and also the name of the side-centered face and glide-planes *a*, *b*, *c* depend on it, the symbol of one and the same group may look different, and thus it determines the choice of the axes as well . For instance, the monoclinic group C_{2h}^6 can be written as *B*2*b* or *C*2*c*; orthorhombic C_{2v}^3 as *Pcc*2, *P*2*aa*, or *Pb*2*b*; and D_{2h}^{16} as *Pnma*, *Pbnm*, *Pmcn*, *Pnam*, *Pmnb*, or *Pcmn*. In tetragonal groups it is sometimes convenient to switch from a primitive lattice *P* to a base-centered *C*, from a body-centered *I* to a face-centered *F*. This will also change the notation, for instance, *I*4*cm* changes to F4*mc*, etc.

International notation indicates the possible Fedorov groups proceeding from their homomorphism with the point groups (combinatorial "class" method by Belov [2.30]). Beginning with orthorhombic class *mm* it is possible, by combining different planes of symmetry (*m*, *n*, *a*, etc.), to write directly the space groups *Pmm*, *Pmn*, *Pmc*, *Pnn*, *Pna*, *Pcc*, *Pca*, and *Pba*. Taking into account the possibility of obtaining identical groups, but in different orientations, yields 16 groups of class *mmm*: *Pmmm*, *Pnnn*, *Pmmn*, *Pnnm*, *Pmna*, etc. If a center or axes of symmetry are present in some class or other as derived elements, they will also remain in the space group, but they may shift relative to the point of intersection of the planes by a quarter or half of the translation in accordance with definite rules. In a similar way axial groups, for instance nine groups Φ from class 222, can be obtained: $P222$, $P222_1$, $P2_12_12$, $P2_12_12_1$, $C222$, $C222_1$, $F222$, $I222$, and $I2_12_12_1$. If we proceed from orthorhombic groups "down" the symmetry, we can form monoclinic and then triclinic groups, and if we go "up", groups of the tetragonal and cubic syngonies. Hexagonal groups are derived similarly.

2.8.10 Subgroups of Fedorov Groups

Group Φ may have, as subgroups, point groups K (i.e., groups without translation) and subgroups which are themselves groups Φ. The former means that the space contains points (and RPS) characterized by a crystallographic group K. We know that the point subgroups of symmorphous groups Φ_s, are, according to (2.95), groups K generating them, and hence all the subgroups K_1 of K, i.e., $\Phi_s \supset K \supset K_1$. Nonsymmorphous groups Φ_n may also contain point subgroups K_1 (see Fig. 2.79b), for each Φ; they can be found in the International Tables and correspond to symmetry K_1 of points of special positions of the given group (see Fig. 2.81). For instance, for group $P4/ncc$, subgroups K will be 4, $\bar{4}$, 222. Of the 230 groups Φ, 217 have subgroups K, 13 do not have them (with the exception of 1) i.e., they do not contain any point symmetry element, but only elements with a translational component (for instance, $P2_12_12_1$, $Pca2_1$, $P6_1$, etc.)

Subgroups of groups Φ, which themselves are groups Φ, can be classified according to different features. Owing to the decrease in the symmetry of the generating point group K (within the same syngony), when the translational group is preserved, translation-equivalent subgroups Φ are formed. And, conversely, with the preservation of K, but with a change in the scale of T or a transfer to centered Bravais groups T, we obtain class-equivalent subgroups Φ. Interestingly, symmorphous Φ_s, belonging to one and the same class K, but with a Bravais group of different centering, are subgroups of each other. Examples are groups $Pm\bar{3}m$, $Fm\bar{3}m$, $Im\bar{3}m$. Besides, as we already know, all $\Phi_n \subset \Phi_s$ owing to the possibility of multiple increase of periods.

A change (decrease) in the generating point group K can be achieved by affine transformations of space. Such transformations include homogeneous extensions (or contractions) and shears. Straight lines then remain straight lines, and planes remain planes, but the angles between them change, generally speaking. Under those affine transformations, where the symmetry K of the unit parallelepiped, i.e., of the syngony, is preserved (Fig. 2.66), group Φ is preserved ("centroaffine equivalence"). For instance, orthorhombic groups Φ remain unchanged upon extension of the space along any one of the reference axes. Cubic groups Φ remain cubic ones upon similarity transformation: uniform expansion (contraction) of the space in all directions, etc.

However, if we perform affine deformation which changes the syngony, i.e., K as well, we obtain a subgroup of the initial group Φ such that some or all angles between its symmetry elements are not preserved. For instance, on extension of cubic groups along the diagonals of a cube we obtain trigonal groups, on their extension along one of the sides of the cube, tetragonal, on extension of groups of medium syngonies along one of the directions perpendicular to the principal axis, orthorhombic or monoclinic, etc. (see scheme on p. 123). Thus, subgroups of Φ in the affine transformation may be groups Φ of any lower syngony. For instance, group T_d^6 has the following subgroups: T^5, C_{3v}^6, C_3^4, D_{2d}^{12}, S_4^2, D^9, C_2^{19}, C_{2v}^3, C_3^4, C_1^1.

If we take into account all the possible ways of formation of subgroups, we shall find that any group Φ is a subgroup either of group $Pm\bar{3}m$, or $P6/mmm$, or both.

2.8.11 Regular Point Systems of Space Groups

Equations of the type (2.99, 100) enable one, with the knowledge of all the operations of group Φ, to obtain from any point x all the other points symmetrically equal to it, i.e., RPS of this group. In practice, however, it is easier to use for this purpose the coordinates of regular point systems of general and special positions given for each space group in the International Tables (see Fig. 2.81). Recall that a point of general position is asymmetric, the number of points in the RPS of general position per unit cell is usually called the order of Φ (although Φ are groups of infinite order). Points of special positions – on point symmetry elements – themselves have their symmetry, and their number is

correspondingly smaller. If Φ contains some point group K as a subgroup: $\Phi \supset K$ (i.e., if Φ has elements of point symmetry), then the RPS of the space group, which is united by this K, possesses such a point symmetry.

As we know, the points of a regular system of group Φ equivalent with respect to K are the vertices of a polyhedron called an isogon. These isogons are arranged regularly in space in accordance with group Φ. In symmorphous groups Φ_s the isogons are given simply by the RPS of point group K contained in (2.95), while their centers are arranged over a lattice derived by the corresponding group T (Figs. 2.76, 77, 79a). For instance, for group *Pmmm* (Fig. 2.79a), we obtain a system of parallel-positioned rectangular parallelepipeds.

On transition to nonsymmorphous groups $\Phi_n \subset \Phi_s$ of the same group K, the RPS of the symmorphous group decomposes into parts, each of them is a RPS of the corresponding subgroup $K_1 \subset K$, $K_1 \subset \Phi_n$, and the isogon of the symmorphous group transforms into another, less symmetric, isogon (Fig. 2.79b).

As we have already mentioned, there are 13 groups Φ which contain no point subgroups, except the trivial 1. They naturally have no isogons.

In describing crystalline structures, each belonging to a definite group Φ, it is indicated for each sort of atoms of the structure what RPS – general or special positions – they occupy, and their coordinates x, y, z are given for only one, "basic", atom of each sort, while the other coordinates are obtained by the formulae of equivalent positions in the International Tables. Different basic atoms A, B, C, ... of the structure may occupy different or identical positions with respect to the RPS symmetry; in the lattter case, of course, their original coordinates x, y, z will be different.

It should be noted that one can often come across the following phrases in the literature: "the structures consist of lattices of atoms A and B, inserted into each other". This means that the indicated atoms occupy positions differing in basal coordinates of RPS of the given group Φ. The same is implied when a "sublattice" of some sorts of atoms is singled out in some "lattice" (i.e., crystalline structure).

2.8.12 Relationship Between the Chemical Formula of a Crystal and Its Space Symmetry

The simplest condition following from translational symmetry is the presence in a unit cell of a total number of atoms equal to, or multiple of, the number of atoms in the chemical formula or, as is customary to say, of an integral number of formula units. Indeed, a unit cell cannot contain fractions of atoms of the formula unit, since then it would not be a geometric repetition unit.[16] The usual numbers of formula units in a unit cell are 1, 2, 4, ... , and in trigonal and hexagonal structures, also 3, 6, ...

[16] We do not have in mind the case of nonstoichiometric structures, when some atoms may occupy their positions statistically.

The formula of a substance and its structure are also linked by another kind of relationship, which is determined by the possible multiplicities of regular point systems. The multiplicities in groups Φ are as follows: 1, 2, 3, 4, 6, 8, 12, 16, 18, 24, etc., upto 192, and in certain groups, only some of these. The atoms of a given element in a structure may be arranged within one RPS, and then the number of these atoms in a unit cell corresponds to the multiplicity of this RPS. The formula of the compound will contain atoms in "crystallographic" ratios given by the multiplicities of this group. But chemically identical atoms may also be arranged within different RPS, of the same or different symmetry. Owing to this latter possibility, compounds with any "noncrystallographic" number of atoms in the chemical formula, for instance 5, 7, etc., can crystallize, i.e., these compounds "select" such groups Φ in which the sum of the multiplicities of RPS is equal to, or a multiple of, the number of atoms of this element in the chemical formula.

The asymmetric (independent) region contains (n'/n)-th part of the atoms of the formula unit, where n' is the number of formula units per unit cell, and n is the order of the group, i.e., the multiplicity of RPS in general position. Thus, the asymmetric region may contain an integral number of formula units, one formula unit, or a fractional part. The latter means that certain atoms, namely those arranged on symmetry elements, are shared by several asymmetric regions.

As the chemical formula becomes more complicated, the space group symmetry of crystals usually is reduced [Ref. 2.13, Chap. 2].

2.8.13 Local Condition of Space Symmetry

Each group, including Φ, derives a regular system of points from one point. The RPS of the Fedorov group $\Phi \equiv G_3^3$ is infinite. If we "look" from any point of such a system at the other points, we shall see the same picture: congruent for groups of the first kind Φ^{I} and congruent or mirror-reflected for groups of the second kind Φ^{II}. This can also be formulated as follows: the sets of vectors going from each point of this system to the others – a 'hedgehogs' ε_∞ covered with an infinite number of spikes – are identical. And, conversely, the congruent or reflection equality of all the "infinite hedgehogs" implies the regularity of an infinite point system.

One may ask whether it is necessary to require the identity of "infinite hedgehogs" ε_∞ to assign the regularity of an infinite point system, i.e., space symmetry, or would it suffice to assign certain "finite hedgehogs" [2.31].

The statement of the problem here is as follows: we assign a discrete homogeneous point system satisfying conditions (2.52), i.e., the presence of a homogeneity sphere R, and (2.53), i.e., the presence of a discreteness sphere r. This means that we assign an (r, R) system. The condition of equality of the points with respect to the symmetry group is not assigned. Instead the condition of congruent or reflection equality of certain finite "hedgehogs" is assigned.

Let us see whether we can derive a space symmetry from "finite hedgehogs" and what is their size.

Take any point A_0 of our system and points nearest to it (Fig. 2.83). Let us define the term "nearest". First, we take the very nearest point A_1; by (2.55) it lies not farther than at a distance of $2R$. At the midpoint segment A_0A_1 we draw a plane m_1 perpendicular to it. Now we take two next nearest noncoplanar points A_2 and A_3 and construct planes m_2 and m_3 in the same way . We do likewise further on until the planes $m_1, \ldots, m_k$ cutting each other form a closed polygon about A_0. The hedgehog $A_0 - A_1, \ldots, A_0 - A_i, \ldots, A_0 - A_k$ will be called the (least) finite "hedgehog" $\varepsilon_k = \varepsilon$. This is Dirichlet's method of constructing polygons. One of the peculiarities of Dirichlet's construction is that all the points of the polygon thus obtained are closer to its starting point A_0 than to any other point $A_1, \ldots$, etc. (The same is true for any other similar polygon with respect to its starting point).

By the condition of congruence of the "hedgehogs", the closed polyhedra formed about each point are equal and contact by equal faces. Owing to the conditions of convexity and equality of the polyhedra themselves and also to their contacting along equal faces, the space is filled completely, which is illustrated for the two-dimensional case in Fig. 2.83. This filling of space with equal figures is the same as the filling of space with fundamental regions – stereons consisting of unequal points (for a plane, planions), which can be constructed about regular system points assigned by a group, as discussed above (Sect. 2.5.5). Indeed, it is really so: the assignment of a local "hedgehog" defines a polyhedral stereon – stereohedron, and this is equivalent to assigning a group, i.e., a regular point system.

Note that all the "hedgehogs" ε_k and stereons S_k of a given system have, in the general case, point symmetry 1 [cases where points, their "hedgehogs", and the corresponding polyhedrons are symmetric (all with the same point

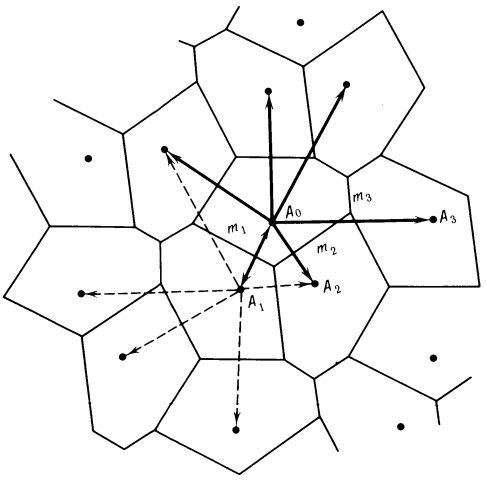

Fig. 2.83. Two-dimensional regular system of points satisfying the (r, R) conditions, construction of "hedgehogs", and Dirichlet's polyhedra for it

symmetry), are also possible.] We join to stereons S_0 (of point A_0), stereon S_1 (of point A_1) along their common equal face and, similarly, all the k stereons along all the other faces of stereon S_0. We call the motions g_i transforming stereon S_0 into stereons $S_1, \ldots, S_k$ basis motions; g_0 is a unity motion.

Stereons $S_1, \ldots, S_k$ surrounding S_0, and their points $A_1, \ldots, A_k$ can clearly be transformed into each other through points A_0 by motions of the type $g_i^{-1} g_k$, and any other stereons, by products of some number of basis motions. Hence, the entire set of points – centers of "finite hedgehogs" – is a regular system and is described by a group.[17]

In Sect. 2.5.5 it was inferred that assignment of a group in a homogeneous space defines an independent region, a stereon, in it. The converse is also true: the local conditions of equality of "hedgehogs" also defines the equality of stereons and the unique way of their joining, which results in complete filling of the space, i.e., defines a group (Fig. 2.83).

To put it differently, the regularity of an infinitely extended discrete homogeneous space is ensured by the identity of the regularity of its limited parts, provided that any such limited part is identically surrounded (in a finite volume) by the others.

2.8.14 Division of Space

The stereons of each group fill the space completely, i.e, they form the division of space. Their number in a unit cell is equal to the number of points of general position in the RPS. Planes m and axes N fringe such regions, i.e., are their boundaries.

Apart from the indicated properties to limit the surface of stereons by symmetry elements and to possess mutual complementarity, no other special limitations are imposed on the shape of stereons. Plane-face stereons, i.e., stereohedra, can be constructed by Dirichlet's method. The shape of a stereohedron depends on the metric characteristics, the specific choice in it of the position of a point, a unit cell (translations, angles), and on the regular system for which the Dirichlet region is constructed.

Therefore, for each space group, there is a great number of combinatorically (i.e., with respect to the number of faces and their shape) different stereohedra. E. S. Fedorov and other mathematicians and crystallographers concerned themselves with stereohedra. B. N. Delone supplied the algorithm for the derivation of stereohedra for any group and proved that the number of different divisions of space into identical convex polyhedra is finite. Thus, for the triclinic group $P\bar{1}$ this number is equal to 180.

Figure 2.84 gives examples of stereohedra: *a* are symmetric stereohedra for group $Fd\bar{3}m$ assigning the shape of the Dirichlet region around the C atom in

[17] Strictly speaking, this reasoning is applicable only to an asymmetric stereon with asymmetric faces. But the final result formulated in this section is valid in any case.

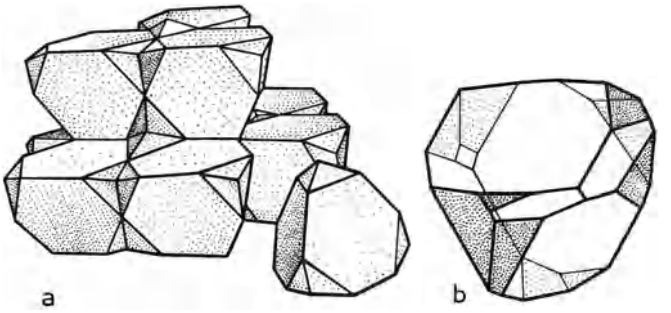

Fig. 2.84a,b. Examples of stereohedra. (**a**) symmetric stereohedra in the diamond structure, which surround one C atom, their packing, and an individual stereohedron; (**b**) 18-face stereohedron in group $P\bar{1}$ [2.5]

the diamond structure; *b* is one of the 180 asymmetric stereohedra of group $P\bar{1}$. Figure 2.83 for the plane group $p3$ can be regarded as a cross section of stereohedra in the form of prisms, for the space group $P3 - C_3^1$. The stereons may have either curved (Fig. 2.85) or plane faces, being stereohedra.

The shape of stereons for each group Φ characterizes the group uniquely. Piling up of stereons by joining their complementary surfaces or equal faces defines the symmetry operations of a given group.

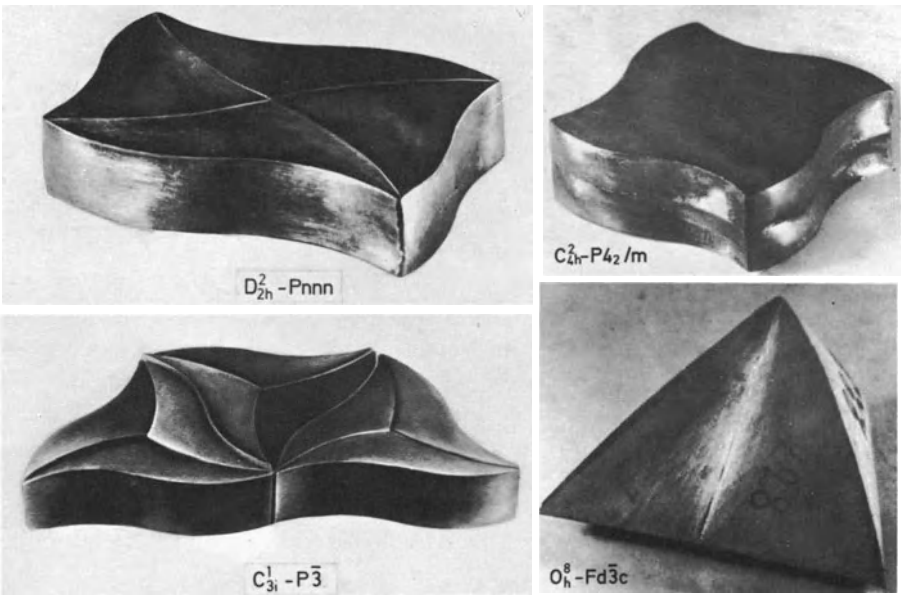

Fig. 2.85. Examples of three-dimensioal figures – stereons – asymmetric independent regions unambiguously characterizing a given group Φ and filling space completely [2.32]

An asymmetric region surrounds the point of general positions of a regular system. It is, however, also possible to construct regions surrounding points of particular positions, which have definite point symmetry. These regions also fill the space completely. Such a region will naturally have the symmetry K of the point which it surrounds. This region can also be constructed as a plane-face one, and then it will be some symmetric polyhedron. It is obvious that such regions can be divided into asymmetric stereons. Taking, in a given group Φ, the regular point systems with an ever-increasing symmetry, we shall obtain more and more symmetric polyhedra filling the space completely.

If we take the RPS with the highest symmetry K in a given group Φ_s, its points will form a Bravais lattice. We are thus approaching a special and important case of polyhedra filling the space completely, such that are derived from each other by operations of translation group T. This is an analog of the two-dimensional problem on parallelogons (see Fig. 2.29). There is one node of the Bravais lattice for each of the polyhedra.

Such polyhedra, adjoining each other with their equal and parallel (in a separate polyhedron and in their entire set) faces, were named parallelohedra by Fedorov. A particular case of parallelohedra for primitive lattices are unit parallelepipeds themselves, which characterize the syngony (Fig. 2.66).

Figure 2.86 portrays five most symmetric Fedorov parallelohedra – a cube, a rhombododecahedron, a cubooctahedron, an elongated rhombododecahedron, and a hexagonal prism, corresponding to the cubic lattices, P, F, and I, the tetragonal lattice F, and the hexagonal lattice H. Figure 2.87 shows how some of them fill out the space. These five parallelohedra are different in their combinatory structure, i.e., in the number of faces and edges bounding them. The five basic parallelohedra can be subjected to affine deformations, but remain parallelohedra which fill the space without gaps and overlappings.

The set of all these parallelohedra interested Fedorov because he associated the derivation of space groups with them. The crystal space described by symmorphous groups Φ_s can be filled with such parallelohedra. If the group is hemisymmorphous Φ_h, however, this will already be some composite parallelohedron and, in asymmorphous groups Φ_a, a stereohedron of definite shape.

Important particular types of parallelohedra can be obtained by Dirichlet's construction, joining a point of the Bravais lattice with all the nearest points by straight lines and drawing, at the midpoints of the segments obtained and perpendicular to them, planes which, on intersecting, will close the desired figure (Fig. 2.88, example of two-dimensional construction). Such a region in

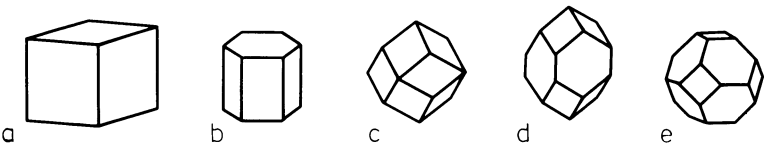

Fig. 2.86a–e. Five most symmetric parallelohedra, (**a**) cube, (**b**) hexagonal prism, (**c**) rhombododecahedron, (**d**) elongated rhombododecahedron, and (**e**) cubooctahedron

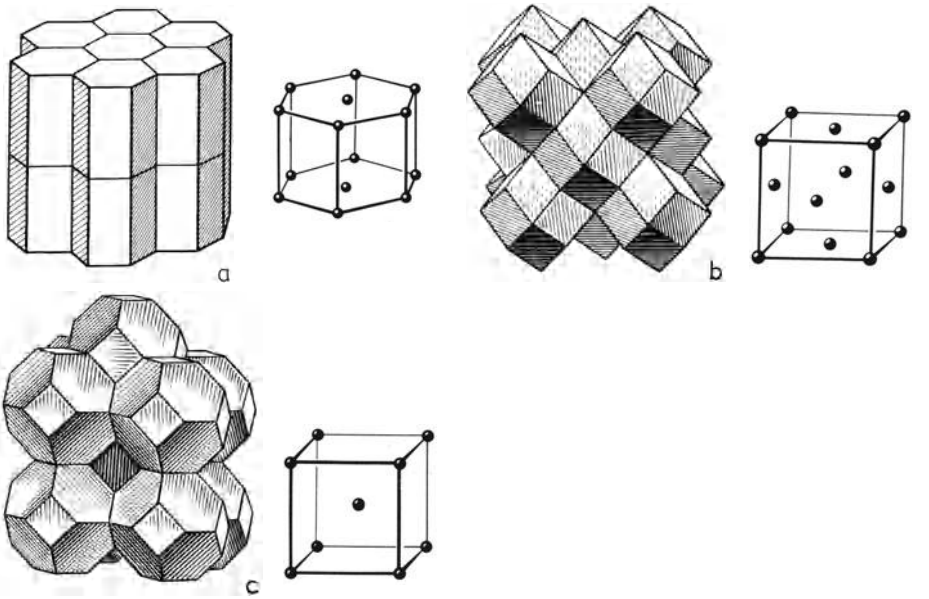

Fig. 2.87a–c. Filling of space by hexagonal prisms (**a**), rhombododecahedra (**b**), and cubooctahedra (**c**), and the corresponding lattices

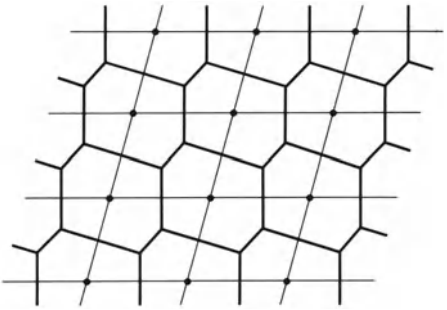

Fig. 2.88. Construction of Dirichlet's two-dimensional region

a real space is called the Dirichlet region, or the Wigner–Seitz cell. Such polyhedra in the reciprocal space are used for describing energy zones (Brillouin zones) in crystals and for some other purposes [Ref. 2.13, Chap. III]. The Dirichlet region is always centrosymmetric, and so are its faces. It is clear that if the Bravais group is rectangular and primitive, the Dirichlet region coincides in shape with the unit parallelepiped. In other cases this is not so.

Five Dirichlet regions coincide with the five respective Fedorov parallelohedra (Fig. 2.86). For less symmetric lattices, variations of these forms are obtained; different forms arise for some Bravais lattices depending on the different ratios between the edges and angles of the unit cell. There are 24

variations named after Delone (including the above five) [2.33, 34]. They are shown in Fig. 2.89.

Let us now see whether or not the theory of filling the space with parallelohedra, stereohedra, or stereons of arbitrary shape can be related to the physical causes for the formation of the crystalline structure. Assignment of a unique way for joining stereons defines, as we have established, the entire three-dimensional structure with a certain group G_3^3, i.e., it dictates periodicity according to Schönflies' theorem. The same is true for symmetric stereons. Doesn't this geometric condition enable us to explain the existence of the lattice?

In the case of molecular structures this approach is indeed close to the truth, since molecules are ready-made building blocks of a crystal which are packed owing to the molecular interaction energy. This is why we can take a molecule and some space around it for a stereon, because the condition of equality of the surrounding of a given molecule by its nearest neighbors is fulfilled, since only such equality leads to the minimum of energy of the whole system (see Sect. 1.2.3). The same reasoning can be used in respect to structures built up of atoms of a single sort, i.e., atoms of elements, provided the atoms occupy a single regular point system. For instance, for cubic face-centered structures of metals a parallelohedron is represented by a rhombododecahedron (Fig. 2.87b). True enough, the question remains, why this parallelohedron has this particular shape, and not a different one.

With more complicated structures, however, the geometric approach contributes little to the understanding of the causes for the formation of the three-dimensionally periodic structure. This is already evident in such molecular structures where the molecule centers occupy two, rather than one, regular point systems, which does happen, though rarely. Then the interaction forces inside the geometric region which define the structure are the same as between the regions. This also refers to inorganic structures which contain atoms of different sorts in the unit cell.

As an example let us consider a two-dimensional structure of the type NaCl (Fig. 2.90a). Its "atoms" occupy high-symmetry positions, and its two-dimensional stereon (shaded) contains 1/8 Na "atom" and 1/8 Cl "atom". For the three-dimensional case the stereon of the structure of NaCl looks as shown in Fig. 2.90b, its volume is 1/192 unit cell, and it contains 1/48 Na "atom" and 1/48 Cl "atom". The stereons are all identical and identically packed relative to each other, as they should be, but such a division of the crystal space does not have any evident physical meaning.

Still greater difficulties and ambiguities arise in consideration of complicated structures of inorganic compounds which contain in the unit cell, and hence in its asymmetric region, a great number of atoms occupying several different regular point systems.

Assume that we already know the structure. Even if we have chosen in it, in some way, a geometric stereon containing the "chemical formula unit" (and we know that its choice is often ambiguous) then, as in the case of molecular structures with two molecules in the asymmetric region, the interaction energy

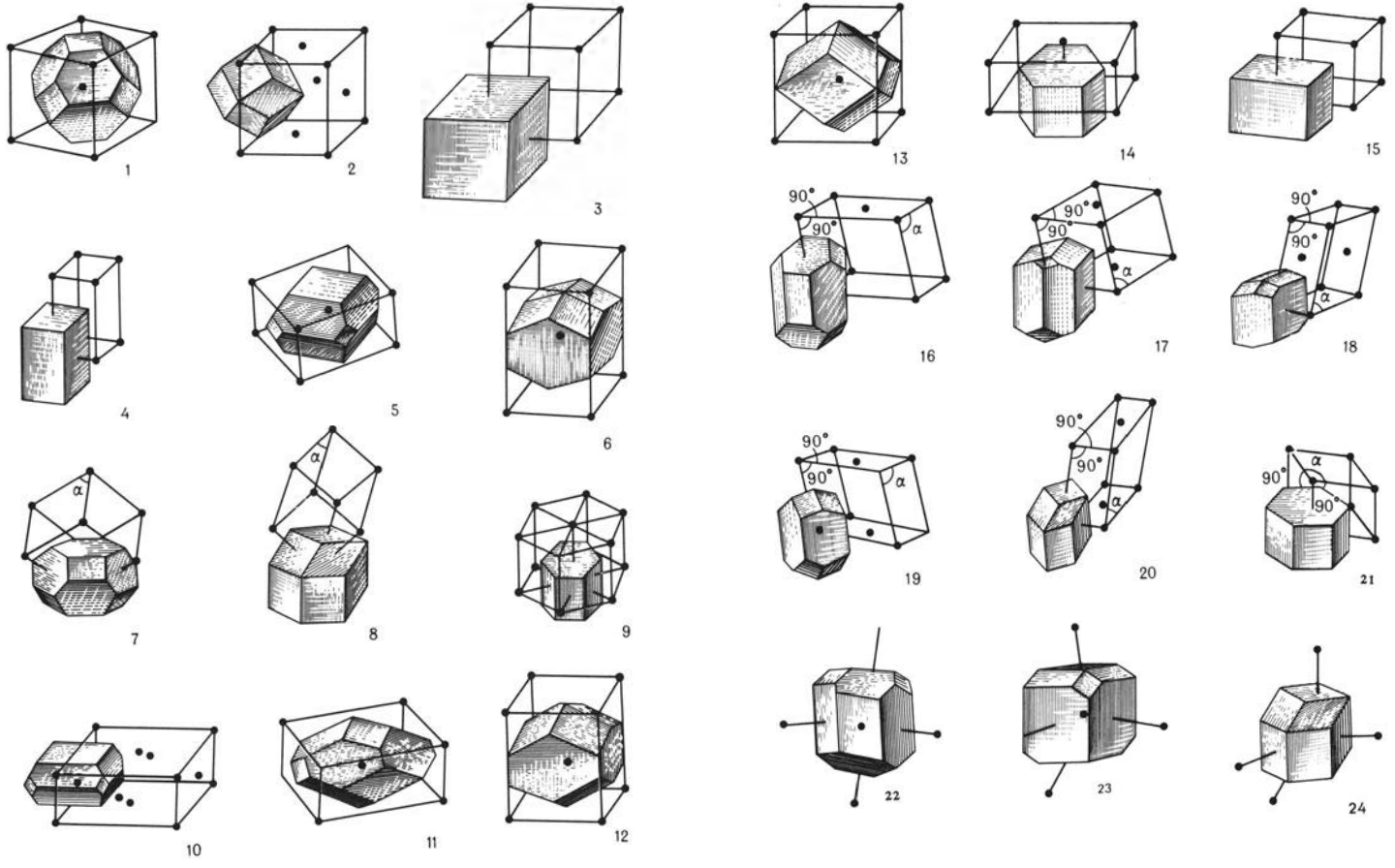

Fig. 2.89. Twenty-four sorts of parallelohedra filling space completely, and the corresponding lattices. (*1–3*) cubic; (*4–6*) tetragonal; (*7,8*) rhombohedral;(*9*) hexagonal; (*10–15*)orthorhombic; (*16–21*) monoclinic; (*22–24*) triclinic [2.33]

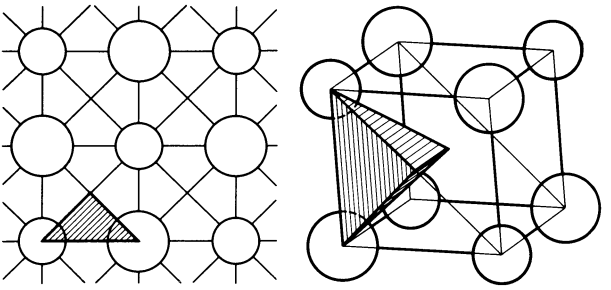

Fig. 2.90a, b. Two-dimensional structure of the NaCl type (**a**), and arrangement of a stereon of the three-dimensional structure of NaCl in 1/8 of the unit cell (**b**)

of atoms inside the stereon is the same as for the atoms of the neighboring stereons. Equilibrium in the structure is established, not owing to the interaction between "ready-made blocks" – they simply do not exist – but due to the interaction of the assembly of atoms as a whole, as we discussed in Chap. 1.

2.8.15 Irreducible Representations of Groups Φ

Fedorov groups contain information on the geometry of the crystalline structure. The possibilities of their utilization are extended with the aid of the theory of irreducible representations. This enables one to solve problems relating to the dynamics of the lattice, its electron and magnetic structures, phase transitions, physical properties, etc. We shall consider this briefly.

The crystal structure can be described by periodic functions (with lattice periods $\boldsymbol{a}_j$), so that any vector $\boldsymbol{r}$, when translated, is transformed into a vector of the type $\boldsymbol{r} + \boldsymbol{a}_j$ or, in the general case, $\boldsymbol{r} + \boldsymbol{t}$ (2.91). Therefore an irreducible representation of group Φ is given by the functions of the type

$$\psi_j(\boldsymbol{r}) = u_{jH}(\boldsymbol{r}) \exp(\boldsymbol{Hr}), \tag{2.102}$$

where $\boldsymbol{H}$ is the so-called reciprocal-lattice vector (see Sect. 3.4.3). To rotational (of both kinds) operations of group Φ in a physical space there correspond rotations of vectors $\boldsymbol{H}$ in $\boldsymbol{H}'$, $\boldsymbol{H}''$, etc., in the reciprocal space, and in the general form for symmorphous groups Φ_s expression (2.102) transforms into the corresponding linear combination ψ, as in (2.86). In this way the irreducible representations of groups Φ_s are related to those for groups K. For nonsymmorphous groups Φ_n it is necessary to take into account not only translations $\boldsymbol{a}_j$, but also the translational components $\boldsymbol{a}_j/p$ of screw rotations and glide reflections.

As an example of the possibilities afforded by the use of representations of groups Φ we refer to the theory of second-order phase transitions. In distinction from the first-order phase transitions, when a considerable rearrangement of the atoms and a jumpwise change in some properties takes place, and the symmetry of the new phase may not be related to that of the initial, phase transitions of the second order are attended by a slight displacement of atoms (for instance, in barium titanate), or cessation of "rotation" of some atomic groups, for instance NH_4 in ammonium chloride, while the crystal state changes continuously. But

the symmetry cannot change "gradually"; it changes jumpwise at the point of second-order phase transition. Φ_1 of the less symmetric (low-temperature) phase is a subgroup of group Φ of the more symmetric phase $\Phi \ni \Phi_1$, i.e., it "loses" some of its elements in phase transition. The functions ρ describing the structure of both phases differ by some $\Delta\rho$,

$$\rho(\boldsymbol{r}) = \rho_0(\boldsymbol{r}) + \Delta\rho(\boldsymbol{r}). \tag{2.103}$$

Function $\Delta\rho$ can be expanded in basis functions of the type (2.102),

$$\Delta\rho = \sum_{i,n} c_i^n \psi(\boldsymbol{r}). \tag{2.104}$$

The phase transition of the second order, however, is associated with only one of n irreducible representations of group Φ of the high-symmetry phase; hence

$$\Delta\rho = \sum_i c_i \psi_i(\boldsymbol{r}). \tag{2.105}$$

Thus, consideration just on the basis of symmetry and representation theory defines the physics of such transformations to a great extent, and by using this technique it is also possible to calculate a number of specific physical and thermodynamic characteristics.

Another way to extend the possibilities inherent in space groups consists in their generalization with the aid of the concepts of antisymmetry and color symmetry (see Sect. 2.9, also [Ref. 2.13, Chap. IV]).

In concluding our discussion of the properties of space symmetry groups of crystals, we wish to point out that these groups describe the time-average structure of the crystal lattice and find most extensive application in the structure analysis of crystals and in solid-state physics. The additional potentialities of the space group theory are realized with the aid of the theory of representations and by extension of groups through introducing nongeometric characteristics. All these techniques are widely used in various problems of the physics of the crystalline state.

2.9 Generalized Symmetry[18]

2.9.1 On the Extension of the Symmetry Concept

Symmetry is defined as the invariance of an object F, i.e., its equality to itself, under transformations g_i of group G (2.1) and (2.2)

$$g_i[\boldsymbol{x}] = \boldsymbol{x}', \quad F(\boldsymbol{x}') = F(\boldsymbol{x}).$$

[18] This section was written in cooperation with V. A. Koptsik.

In defining symmetry in this way, we also said that the property of objects to show some symmetry is relative. This relativity may be taken into consideration when defining the symmetry operation (2.1) or defining the very concept of the equality of an object (and hence the equality of its parts) to itself (2.2); these two aspects may be interrelated.

We have considered the symmetry group of one-, two-, and three-dimensional space, mainly three-dimensional groups, and isometric transformations g satisfying the requirement (2.9) for the preservation of lengths and angles. This requirement can be changed both within and outside the framework of Euclidean space, and then a different symmetry arises. On the other hand, geometric equality alone may prove an insufficient characteristic for describing the properties of physical objects in three-dimensional space, and one can introduce additional (4th, 5th, etc.) nongeometric variables which may be continuous or discrete and may take a finite or an infinite number of values. Formally, this can be considered as passing on to a space of more than three dimensions.

Thus, the generalization of three-dimensional isometric symmetry is passing on to a four-dimensional space, for instance to a four-dimensional Euclidean space, in which all four variables are equivalent. In the transition to four-dimensional space, no pictorial geometric constructions are possible. But since n-periodic groups G_n^m of an m-dimensional space are characterized by their $(m-1)$-dimensional projections, and all the groups G_n^3 are known, they can be used for constructing symmetry groups G_n^4. Thus, there are 227 crystallographic point groups G_0^4 and 4895 "Fedorov" groups, of which 112 are enantiomorphous.

The concept of classical symmetry can also be modified by approximate fulfillment of either condition (2.1) or condition (2.2), or both. This is how various "statistical" symmetries arise; they are used in describing distortions in the crystal structures and in analyzing systems less ordered than crystals.

2.9.2 Antisymmetry and Color Symmetry

Groups in which three variables remain geometric coordinates of space, while the fourth has a different physical meaning, are of importance in crystallography and physics. Such a variable may be time or physical values associated with it, a phase of a wave function or, in the reciprocal space, a phase of a complex function [2.35, 36]. The discrete fourth variable may be a spin, a charge sign, etc. Such generalizations of symmetry are called antisymmetry and color symmetry; they were proposed and developed by *Shubnikov* [2.7], *Shubnikov* and *Belov* [2.8] and others [2.30, 37–44].

To elucidate the essence of antisymmetry we shall consider, as an example, the projection of the layer groups G_2^3 (see Fig. 2.63) onto a plane X_1, X_2 along axis X_3, which yields, as we know, 17 plane groups G_2^2 (asee Fig. 2.56). Note that those of the groups G_2^3 which transform the third coordinate (together with transformation of x_1, x_2 or without it), change the values x_3 to $-x_3$ and in no other way. Figure 2.91a,b gives examples of such groups.

We can now regard such groups as two-dimensional $G_2^{2,1}$ (two variables have the meaning of two geometric coordinates, as before), but each geometric point x_1, x_2 has an additional characteristic, a "load" x_3, which takes only two discrete opposite values. It is most convenient to assume that these values $x_3 = +1$, $x_3' = -1$ are "anti-equal". Visually, this characteristic can be interpreted as the "color" of the point x_1x_2: "white" (+ 1) or "black" (− 1). By means of transformations bringing x_3 into coincidence with x_3' at equal x_1, x_2 we obtain "grey" points (Fig. 2.91c).

As a result, in projecting those of the 80 groups G_2^3 in which the transformation of x_3 with a simultaneous change in x_1 and x_2 took place we obtain 46 plane-antisymmetry groups $G_2^{2,1}$ (see Fig. 2.63). If we also take into consideration "grey" or neutral plane groups (x_3 are projected into x_3' while x_1, x_2 do not change), of which there are 17, and single-color groups (the transformations of x_3 into x_3' is absent), of which there are also 17, the number of plane groups $G_2^{2,1}$ and groups G_2^3 coincides, making up 80. Figure 2.92 is the "Horse-man", a picture by *Escher* [2.45], which is described by the antisymmetry group of Fig. 2.91a.

The nongeometric characteristic of a point may take more than two discrete values. Let us project onto a two-dimensional plane those space groups G_3^3 in

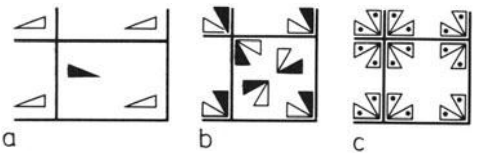

Fig. 2.91a–c. Examples of two-dimensional antisymmetry groups
(a,b) groups of the type G_2^3 interpreted as two-dimensional antisymmetry groups $G_2^{2,1}$ (triangles disposed in the same plane change their color (sign) on certain operations $g' \in G_2^{2,1}$); **(c)** "grey group", which brings to coincidence opposite signs (colors) in a figure

Fig. 2.92. Figure described by antisymmetry group pg' [2.9]

which the coordinate x_3 takes 3, 4, or 6 discrete values, respectively, because of the presence of screw axes 3_1, 4_1, or 6_1, and interpret these values as the "load" of the appropriate point x_1, x_2. Thus we obtain, not a two-valued (black-white), but a multivalued, 3, 4, 6 "color" symmetry. Examples of such color groups $G_2^{2,(p)}$ (there are 15 of them) are given in Plate I.

A theory of antisymmetry and color symmetry groups may be constructed in several different ways. One of them we have seen: if the high-dimensional groups G_n^m are known, we can consider their projections G_n^{m-1} along a variable which takes a finite number of values.

Another method consists, on the contrary, in increasing the order of the geometric group G_n^m by introducing new operations of group P, which acts in the space of physical variables, and in forming the direct product

$$\begin{aligned} P \otimes G &= \{p_1, \ldots, p_k\}\{g_1, \ldots, g_n\} = \{p_1 g_1, \ldots, p_1 g_n, \ldots, p_k g_1, \ldots, p_k g_n\} \\ &= G^{(p)}. \end{aligned} \tag{2.106}$$

This group is a set (finite or infinite) of binary elements in which the group operation $p_i g_j \cdot p_k g_l = p_i p_k g_j g_l$ is introduced and all the group axioms are fulfilled. This method for obtaining new generalized groups on the basis of the representation theory is also associated with this construction. The general way of forming of new groups consists in making wreath products of P and G groups

$$P \wr G = \overset{n}{\otimes} P \circledS G = G^{(w)}, \tag{2.107}$$

where $\overset{n}{\otimes}$ denotes a multiple product of P by itself, n being the order of G.

Antisymmetry groups in a space of m dimensions will be denoted as groups $G_n^{m,1}$; the unity in the superscript indicates that there is one antisymmetric variable additional to m, and the color groups will be designated as $G_n^{m,(p)}$ or $G_n^{m,(w)}$. Crystallographic antisymmetry point groups will be denoted by K' (the prime indicates antisymmetry of the group of operation); color groups are denoted by K.

Groups with more than one antisymmetric variable, namely with l such variables, are possible; they will be symbolized $G_n^{m,l}$ (l-multiple antisymmetry).[19]

2.9.3 Antisymmetry Point Groups

Let us introduce a fourth "antisymmetric" variable $x_4 = \pm 1$ in three-dimensional space. The operation $g[x_4] = x_4'$ changing this variable alone is called the anti-identity operation and is denoted by $1'$; $(1')^2 = 1$. In antisymmetry, there are four types of equality between geometrically equal objects: identity, mirror equality, anti-identity, and mirror anti-equality. These types of equality are illustrated in Fig. 2.93. The ordinary operation of reflection m changes the

[19] Antisymmetry groups are also designated $G_n'^m$. They and color groups are often written as $G_{m,n}^g$, where the suffix m (the dimensionality of a space) is shifted below, and the superscript characterizes some generalized symmetry.

Plate I.a

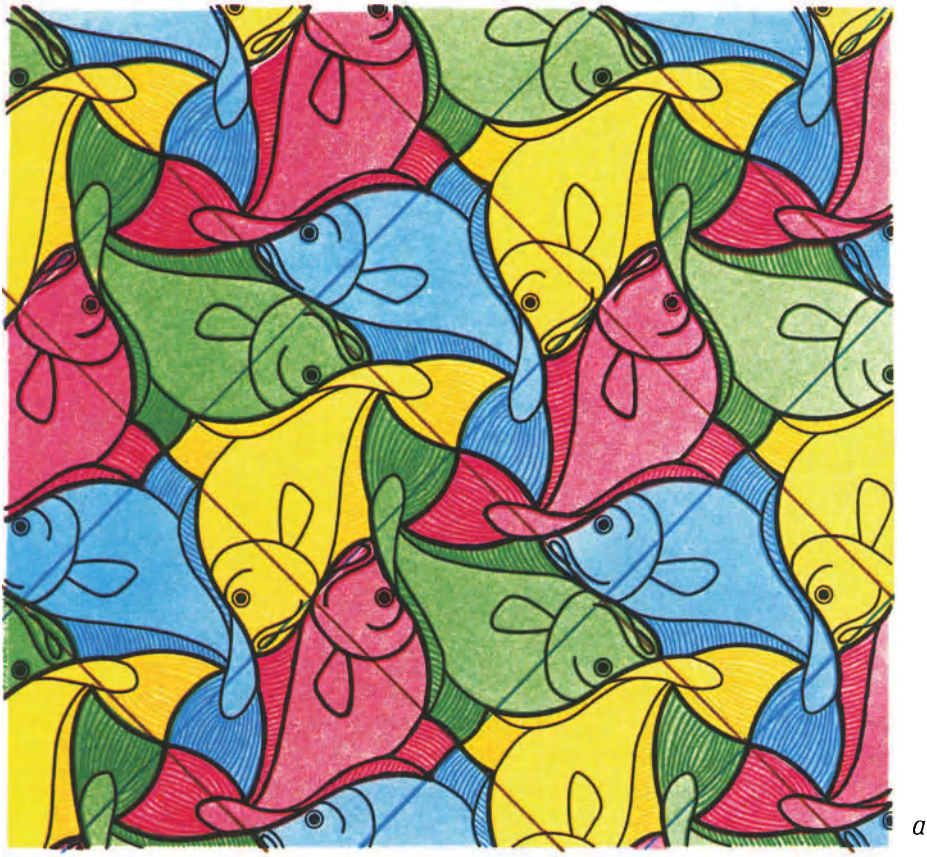

a

Plate Ia–d. Colored two-dimensional groups.
(**a**) figure illustrating group $P4_1$ [2.9]; (**b, c, d**) mosaics illustrating different groups [2.46, 47]

Plate I.b

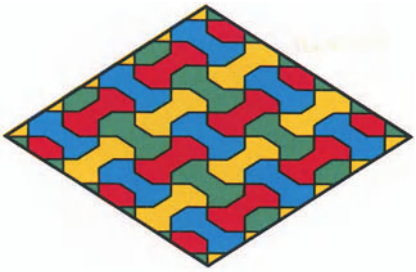

Fdd

*P*6

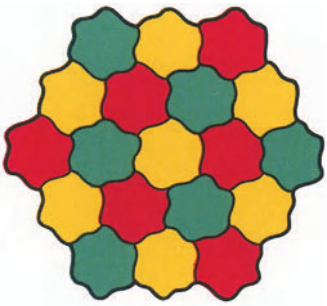

*R*3

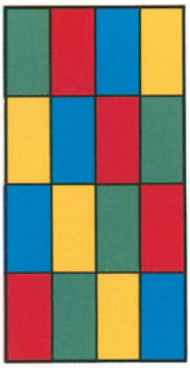

Fdd

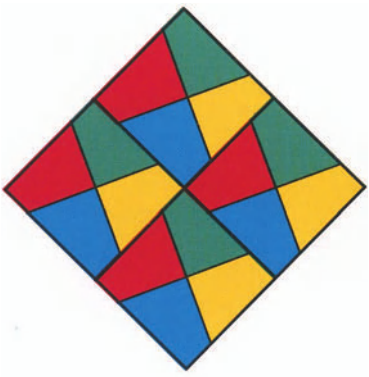

$P4_1$

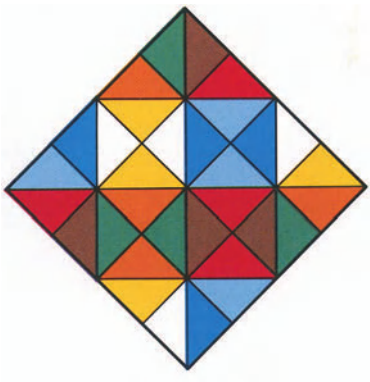

$I4_1md = F4_1dm$

Plate I.c

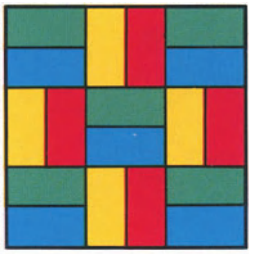

$P4_1$

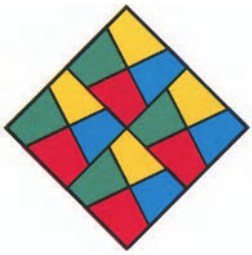

$P4_3$

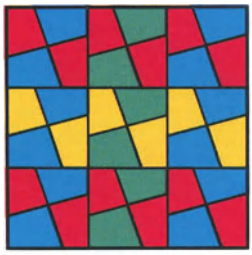

$I4_1$

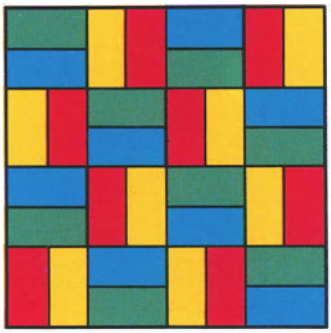

$I4_1$

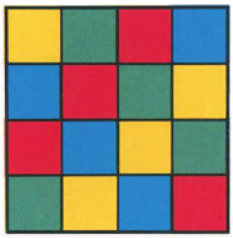

$I4_1md = F4_1dm$

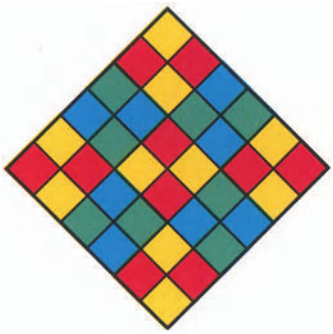

$I4_1cd = F4_1dc$

$F\,dd$

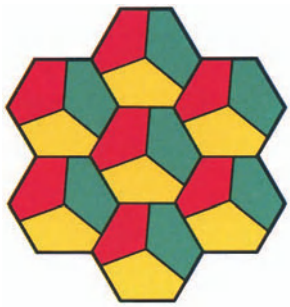

$P3_1$

Plate I.d

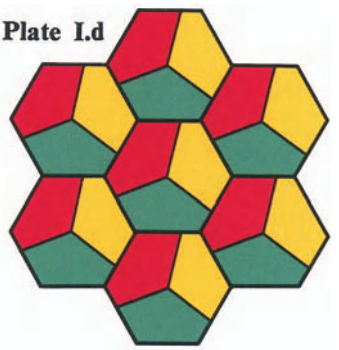

$P\,3_2$

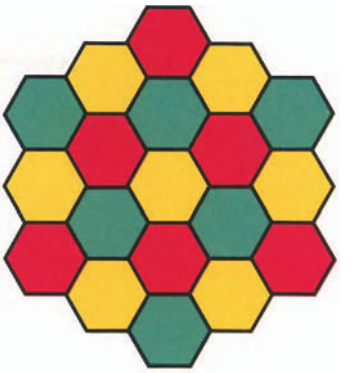

$R\,3m$

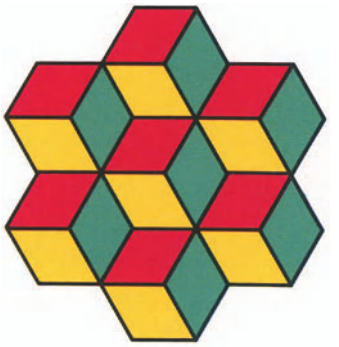

$P\,6_2$

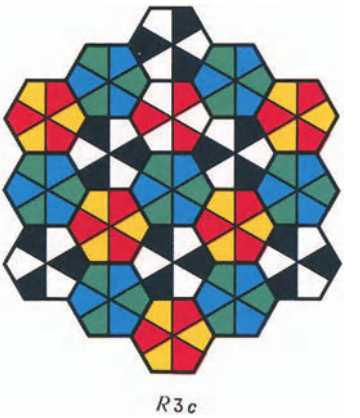

$R\,3c$

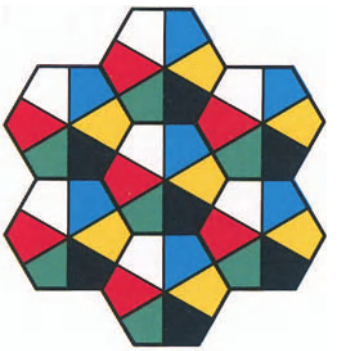

$P\,6_5$

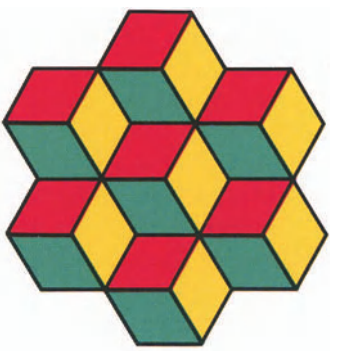

$P\,6_4$

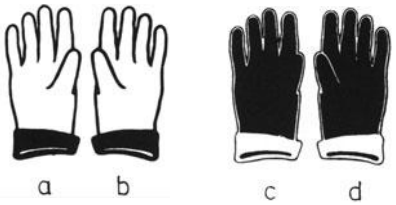

Fig. 2.93. Four gloves illustrating four types of equality in the case of antisymmetry: $a = a$, $b = b$, . . . identity; $a - b$, $c - d$ mirror equality; $a - c$, $b - d$ anti-identity; $a - d$, $b - c$ mirror anti-equality

chirality of the glove; it transforms the right glove into the left; to the anti-identity $1'$ there corresponds a change of color, while a reflection with a change of color $m1' = m'$ changes both the chirality and the color of the glove simultaneously. From any symmetry operation g_i in three-dimensional space it is thus possible to construct an "anti-operation" $g_i' = g_i^{1'}$. Antisymmetry operations in three-dimensional space act on the coordinates of point $\boldsymbol{x}(x_1 x_2 x_3 x_4)$ as follows:

$$g_i'[x_1 x_2 x_3 x_4] = [g_i(x_1 x_2 x_3), 1'(x_4)]; \quad (x_4) = \pm 1; \quad 1'(x_4) = -x_4. \quad (2.108)$$

The matrix of antisymmetry point transformations – proper and improper rotations and antirotations – has the form

$$\begin{bmatrix} a_{11} & a_{12} & a_{13} & 0 \\ a_{21} & a_{22} & a_{23} & 0 \\ a_{31} & a_{32} & a_{33} & 0 \\ 0 & 0 & 0 & a_{44} \end{bmatrix}, \quad |a_{ij}| = \pm 1, \quad a_{44} = \begin{cases} +1 \text{ for operations } g, \\ -1 \text{ for operations } g'. \end{cases}$$

(2.109)

The function F in the four-dimensional space of variables (2.107) is invariant (2.2) to generalized symmetry transformations, but, viewed in three-dimensional space, it changes the signs of its parts after these transformations, i.e., it is antisymmetric.

We can see that the requirement for the equality $F(\boldsymbol{x}) = F(\boldsymbol{x}')$ in a space of m dimensions may [on transition to the $(m-1)$th dimension] generate new requirements for the relationship between $F(\boldsymbol{x}_{(m-1)})$ and $F(\boldsymbol{x}'_{(m-1)})$, which do not reduce to equality after transformation, but lead to "anti-equality" or "color" equality. This broadens the very concept of "symmetric" equality.

By analogy with the ordinary symmetry elements it is possible to introduce elements of antisymmetry. Each of them simultaneously with the geometric action inherent in it, changes the sign of the fourth variable. Antisymmetry groups are composed of both operations – ordinary symmetry and antisymmetry – in other words, they possess the symmetry elements of both types. The operations and elements of antisymmetry are denoted in the same way as the ordinary ones, but with a prime: m', N', $\bar{N}'$. It is convenient to depict these elements using another color (Plate II).

Senior point groups K' can be obtained by using (2.106), forming a direct product of group $K = \{k_1 \ldots k_i \ldots\}$ by group $1' = \{1, 1'\}$:

$$K \otimes 1' = \{k_1, \ldots, k_n, k_1', \ldots, k_n'\}. \quad (2.110)$$

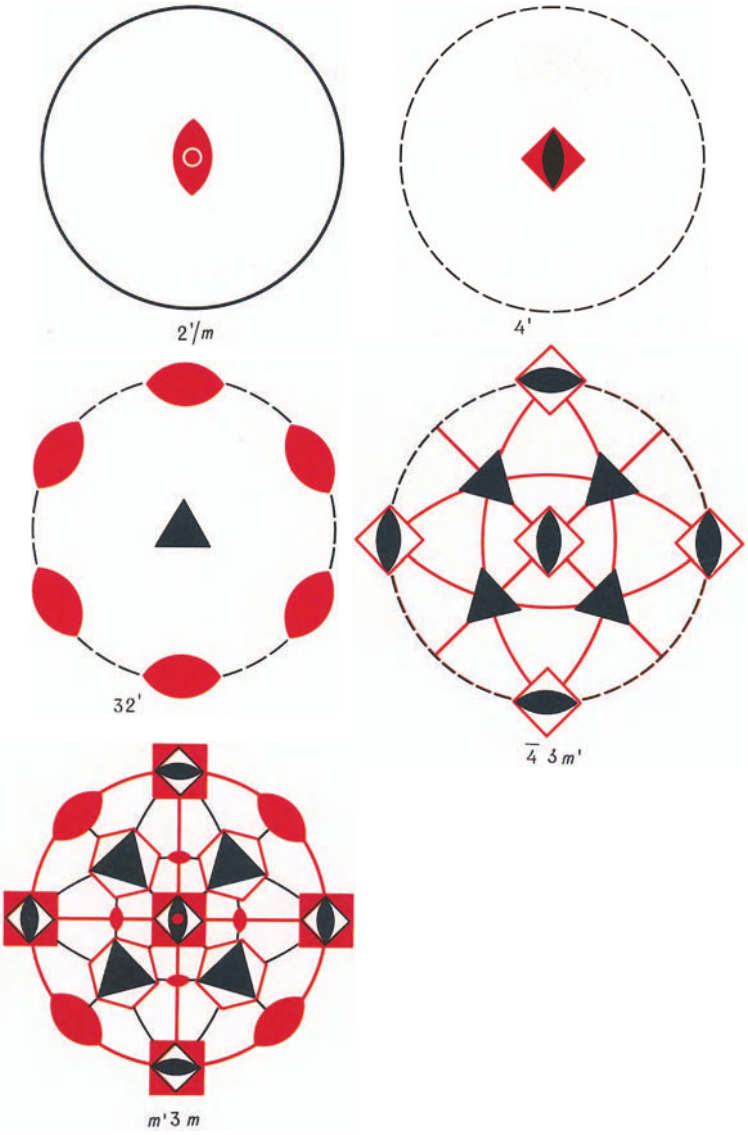

Plate II. Stereographic projections of some point antisymmetry groups (the antisymmetry elements are colored red) [2.24]

Selecting nontrivial subgroups $K' \subset K \otimes 1'$, which contain no anti-identity operation $1'$, we obtain 58 black-and-white antisymmetry point groups. The number of groups containing $1'$, i.e., grey (neutral) groups, will be the same as that of groups K, i.e., 32. The number of single-color groups containing no k_i' will be the same; they naturally coincide with K. There are 122 groups altogether. Plate II shows stereographic projections, and Fig. 2.94 figures and polyhedra, which illustrate some antisymmetry point groups K'.

Antisymmetry and color-symmetry groups are contained, in a sense, within the groups of ordinary symmetry. This can be shown with the aid of irreducible representations. We shall consider, as an example, the point group $K\,mm2 = C_{2v}$. Let us take an asymmetric figure (function) f_1 and, acting on it by operations of group $K = \{1, 2, m_x, m_y\}$, construct the parts f_2, f_3, and f_4, symmetrically equal to f_1 (Fig. 2.95). The sum $F_1 = f_1 + f_2 + f_3 + f_4$ will be a function with the symmetry $mm2$ satisfying condition (2). The table of irreducible representations of the group is as follows (see Table 2.8):

Γ_j	1	2	m_x	m_y
Γ_1	1	1	1	1
Γ_2	1	1	−1	−1
Γ_3	1	−1	1	−1
Γ_4	1	−1	−1	1

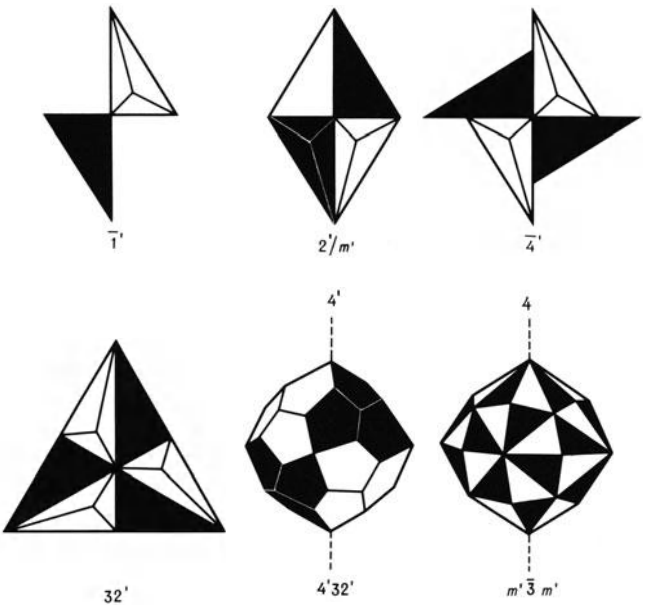

Fig. 2.94. Examples of antisymmetric figures and polyhedra [2.48]

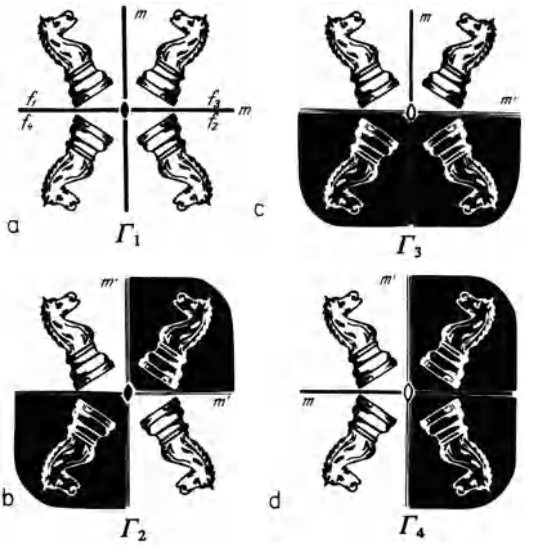

Fig. 2.95a–d. Derivation and relationship of the groups $mm2$ (**a**), $m'm'2$ (**b**), $mm'2'$ (**c**, **d**) using irreducible representations of the group $mm2$

We can see that the symmetric function F_1 is transformed into itself by the first unit representation, with positive signs of its parts f_i corresponding to this transformation (Fig. 2.95a). But other representations offer different possibilities: multiplying f_i by ± 1 in the sequence they are written in Γ_2, Γ_3, and Γ_4, we obtain antisymmetric functions $F_2 = f_1 + f_2 - f_3 - f_4$, $F_3 = f_1 - f_2 + f_3 - f_4$, $F_4 = f_1 - f_2 - f_3 + f_4$ shown in Fig. 2.95b–d. Function F_2, which is transformed by Γ_2, determines the group $K' = m'm'2$. In the sense of antisymmetry groups, functions F_3 and F_4 coincide and determine group $K' = mm'2'$. In the general case, too, for any group K one can find such functions F, which, being transformed by $k_i \in K$, are multiplied by characters $\chi_{(k_1)}$ of one-dimensional representations. Thus, one-dimensional real representations Γ_k of groups K generate antisymmetry groups K' and directly indicate their structure [2.50]. Hence, 58 nonequivalent one-dimensional real representations of groups K (out of 73, with an accuracy to selection of axes) actually correspond to 58 black-and-white groups K. From this consideration it is also clear that groups K' are abstractly indistinguishable from the respective K, since K' have the same representations as K: both reduce to 18 abstract groups K (Table 2.7). Table 2.13 lists 90 antisymmetry point groups K'.

Symmetry K' is exhibited, for instance, by the wave functions of atoms and molecules, which are transformed according to the proper representations [Ref. 2.13, Figs. 1.3, 1.23]; groups K' are point groups of magnetic symmetry of those crystals in which the magnetization vector can take two values [2.51]. Groups K' also describe the point symmetry of the reciprocal space with due regard for the phases of structure amplitudes, see Eqs. (4.45, 46).

Table 2.13. Ninety antisymmetry groups K'

Triclinic	$m'm'2$	$42'2'$	Trigonal	$6/m1'$	$6'/m'm'm$
$1'$	$mm'2'$	$4mm1'$	$31' = 3'$	$6/m'$	$6/m'm'm'$
$\bar{1}1'$	$mmm1'$	$4m'm'$	$\bar{3}1'$	$6'/m'$	$6/m'mm$
$\bar{1}'$	$m'm'm'$	$4'mm'$	$\bar{3}'$	$6'/m$	$6/mm'm'$
Monoclinic	mmm'	$\bar{4}2m1'$	$321'$	$6221'$	Cubic
$21'$	$m'm'm$	$\bar{4}2'm'$	$32'$	$62'2'$	$231'$
$2'$	Tetragonal	$\bar{4}'2m'$	$3m1'$	$6'2'2$	$m\bar{3}1'$
$m1'$	$41'$	$\bar{4}'2'm$	$3m'$	$6mm1'$	$m'\bar{3}'$
m'	$4'$	$4/mmm1'$	$\bar{3}m1'$	$6m'm'$	$4321'$
$2/m1'$	$\bar{4}1'$	$4/m'm'm'$	$\bar{3}m'$	$\bar{6}'mm'$	$4'32'$
$2/m'$	$\bar{4}'$	$4/m'mm$	$\bar{3}'m'$	$\bar{6}m21'$	$\bar{4}3m1'$
$2'/m$	$4/m1'$	$4'/mmm'$	$\bar{3}'m$	$\bar{6}m'2'$	$\bar{4}'3m'$
$2'/m'$	$4/m'$	$4'/m'm'm$	Hexagonal	$\bar{6}'m2'$	$m'\bar{3}m1'$
Orthorhombic	$4'/m'$	$4/mm'm'$	$61'$	$\bar{6}'m'2$	$m'\bar{3}'m'$
$2221'$	$4'/m$		$6'$	$6/mmm1'$	$m'\bar{3}'m$
$2'2'2$	$4221'$		$\bar{6}1'$	$6'/mmm'$	$m\bar{3}m'$
$mm21'$	$4'22'$		$\bar{6}'$		

2.9.4 Point Groups of Color Symmetry

A discrete nongeometric variable x_4 in three-dimensional space can be assigned, not two (as in the case of antisymmetry) but several values. This gives rise to color (multicolor) symmetry proposed by N. V. Belov. In constructing composite color groups (2.106) one should bear in mind the correspondence of the orders of geometric transformations of group G and the color permutations of group P. Point groups $K^{(p)}$ can also be found by proceeding from representation of groups K, namely by considering those which have complex characters $\chi = \pm i$, $\varepsilon = \exp(-2\pi i/3)$, $\omega = \exp(-2\pi i/6)$. Thus, as in the above considerations, we obtain 18 cyclic groups $K^{(p)}$, which correspond to 18 complex conjugate representations of point groups K (see Table 2.8). In these, the "color" variable takes 3, 4, or 6 values, and each of them can be assigned a "color" of its own, indicating the sequence of values $x_4^1, \ldots x_4^{(p)}$. "Color" polyhedra, corresponding to some groups $K^{(p)}$, are shown in Plate III. Point groups $K^{(p)}$ can be used, for instance, for describing the magnetic, real face and sectorial structures of single crystals.

On the basis of the group-extension method, by including both antisymmetry and color symmetry into the generalization of point symmetry and with the aid of substitution groups it is possible to obtain color groups with crystallographic values of the color variable up to 48. These groups $K^{(p)}$ are constructed by the algorithm $K^{(p)} \to P \leftrightarrow K/H$, where $H \subset K$ is the invariant classical subgroup of group K of index p. The number of such groups is 81 or 134 (in the latter case, with the inclusion of color enantiomorphism). They are isomorphous to the corresponding groups K.

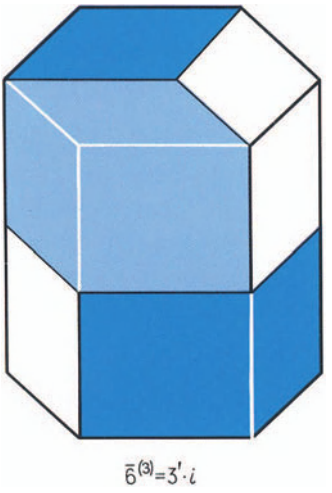

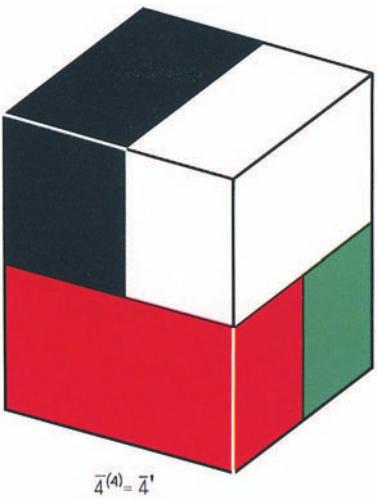

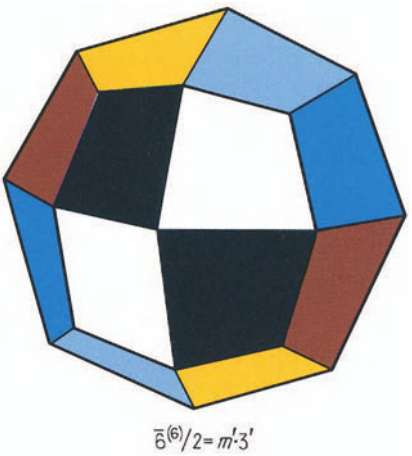

Plate III. Color polyhedra illustrating some color symmetry groups [2.52]

In addition to the above described groups there are color point groups of *Van der Waerden* and *Burckhardt* [2.44] $K^{(p)}_{WB}$ and groups of Wittke and Garrido [2.53, 54] $K^{(w)}_{WG}$ isomorphous to them and derived by the law of direct (2.106) or wreath product (2.107).

In an object described by the color subgroup $K^{(p)}_{WB}$ it is possible to select a set of points of the same color (domains), with p domains of different color. Groups $K^{(p)}_{WB}$ have a noninvariant subgroup $H_i^{(p)} \subset K^{(p)}_{WB}$, which preserves a fixed i-th color, i.e, describes the domain, and an invariant (classical) subgroup H, which is the intersection of all the conjugate $H_i^{(p)}$. Groups $K^{(w)}_{WG}$ are obtained by replacement of certain color elements by classical ones in such a way that one of the $H_i^{(p)}$ transforms into isomorphous H_i [2.49].

There exist also noncrystallographic color point groups of the indicated types, including icosahedral ones, where the number of colors may be a multiple of 5.

The distribution of antisymmetry and of color groups of all types with respect to the number of colors p is given in Table 2.14.

A color group of P symmetry can be denoted by the symbol $K^{(p)}(H_i/H)$. With the aid of such symbols it is possible to analyze the chirality of these groups. If H is chiral, then the corresponding color group is also chiral. If $K^{(p)}$ is chiral, but H is not, then "color chirality" arises, i.e., reflection in a "color mirror" with pairwise change of colors.

Noncrystallographic $G_0^3 \neq K$ and continuous (limiting) three-dimensional point groups also permit "antisymmetric" and "color" generalization. In limiting groups (see Fig. 2.50), only generators m' and $2'$, but not axes ∞, can be antisymmetric. There are seven such groups; ∞/m', $\infty 2'2'$, $\infty m'm'$, $\infty/m'mm$, $\infty/mm'm'$, $\infty/m'm'm'$, and $\infty \infty m'$. There exist an infinite number of limiting color groups, and axis ∞ can itself be a color axis $\infty^{(p)}$ with an infinite number of colors.

Table 2.14. The number of crystallographic point groups of generalized symmetry

p	$K^{(p)}$	$K^{(p)}_{WB}, K^{(w)}_{WG}$
2	58	—
3	7	10
4	30	11
6	17	23
8	9	8
12	11	16
16	1	1
24	5	4
48	1	—
Total	58 + 81	73

2.9.5 Space and Other Groups of Antisymmetry and Color Symmetry

By analogy with point groups K' and $K^{(p)}$ it is possible to construct groups of antisymmetry, multiple antisymmetry, and color symmetry corresponding to the different types of G_n^m groups – layer, rod, etc. We began our exposition of ideas of generalized symmetry with the description of two-dimensional $G_2^{2,1}$ and $G_2^{2,(p)}$ groups. The diagram of subordination of groups of symmetry and multiple antisymmetry $G_n^{m,l}$ is given in Fig. 2.96. It can be seen that as l increases, the number of groups increases very rapidly. The same refers to classical groups. For a space of $m = 2, 3, 4$ dimensions there exist 10, 32, and 227 point groups, 5, 14, and 64 Bravais groups [2.6, 56]; and 17, 230, and 4895 Fedorov groups, respectively.

Let us consider space antisymmetry groups $G_3^{3,1} \equiv \Phi' \equiv$ III – "Shubnikov" groups [2.57, 58].

Since they include the anti-identity operation $1'$, the antitranslation operation $t = t1'$ also arises. In addition to the 14 ordinary translation Bravais groups there are another 14 antitranslation groups and 22 combined translation and antitranslation groups (altogether 50); the combined groups are denoted as ordinary groups, but with an anticentering index, for instance P_C, C_A, etc. Examples are presented in Fig. 2.97. Groups III are symbolized as ordinary space groups, but with a prime, if the corresponding element is an antielement, for instance $Pm'n2_1'$, P_14_2nm, etc. Their drawings can be conveniently made in two colors (Plate IV): black for the elements of symmetry, and red for the elements of antisymmetry; antiequal points have different colors.

There are altogether 1651 groups III: 1191 are black-and-white, 674 without and 517 with antitranslations, and there are 230 grey and 230 single-colored groups. From the isomorphism of point $K' \leftrightarrow K$ and translation $T' \leftrightarrow T$ groups the isomorphism of III $= \Phi' \leftrightarrow \Phi$ also follows, i.e., the number of abstract groups corresponding to III is 219. Similarly to isomorphism of $G_2^{2,1} \leftrightarrow G_2^3$, the groups

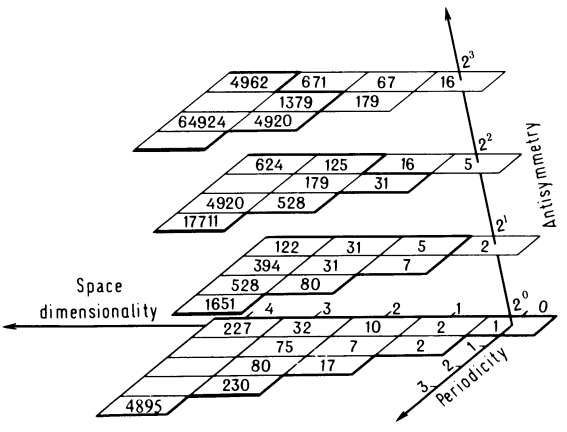

Fig. 2.96 Number of symmetry and multiple-antisymmetry groups and their subordination [2.55]. (2^0) classical groups, (2^1) antisymmetry groups, (2^2) group of two-fold and (2^3) of three-fold antisymmetry

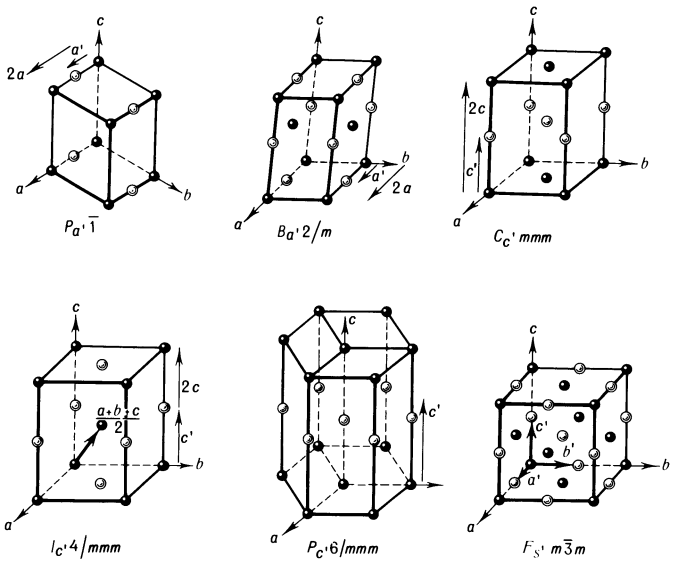

Fig. 2.97. Some antisymmetric Bravais groups

of four-dimensional three-dimensionally periodic layers are isomorphous to the Shubnikov groups

$$\text{III} \equiv G_3^{3,1} \leftrightarrow G_3^4.$$

A physical function described by Shubnikov groups is, for example, the stationary spatial arrangement of the atomic spins in crystals with magnetic properties. The time-average distribution of electrons and nuclei in a crystal of any compound obeys the ordinary symmetry Φ, but within this symmetry there is no variable describing the orientation of the magnetic moments. If the magnetic moment can take only two values (parallel and antiparallel spins) in a system, the magnetic structure is characterized by one of the groups III (Fig. 2.98). Antisymmetry can also be used for describing ferroelectric structures (positive and negative charges of ions) and structures with "vacant" or "filled" coordination polyhedra.

By analogy with space groups of antisymmetry Φ' one can form space groups of color symmetry $\Phi^{(p)}$. There may be color groups $\Phi^{(p)}$ both with and without color translation subgroups. Thus, we have 817 cyclic and 2125 noncyclic, with respect to color, permutation groups, altogether 2942 groups. Of these, 111 are three-color, 2170 four-color, and 661 six-color. The groups $\Phi^{(p)}$ with higher color multiplicities are not derived. Groups $\Phi^{(p)}$ and also so-called position groups $G_3^{3(w)}$, constructed according to the principle of wreath product (2.107) of P and Φ, can be used for describing ordered magnetic structures, in which the magnetic moments of the atoms are arranged not in two, but in several substructures with their own symmetry (Fig. 2.99). In groups $\Phi^{(p)}$ the loads affect only the function

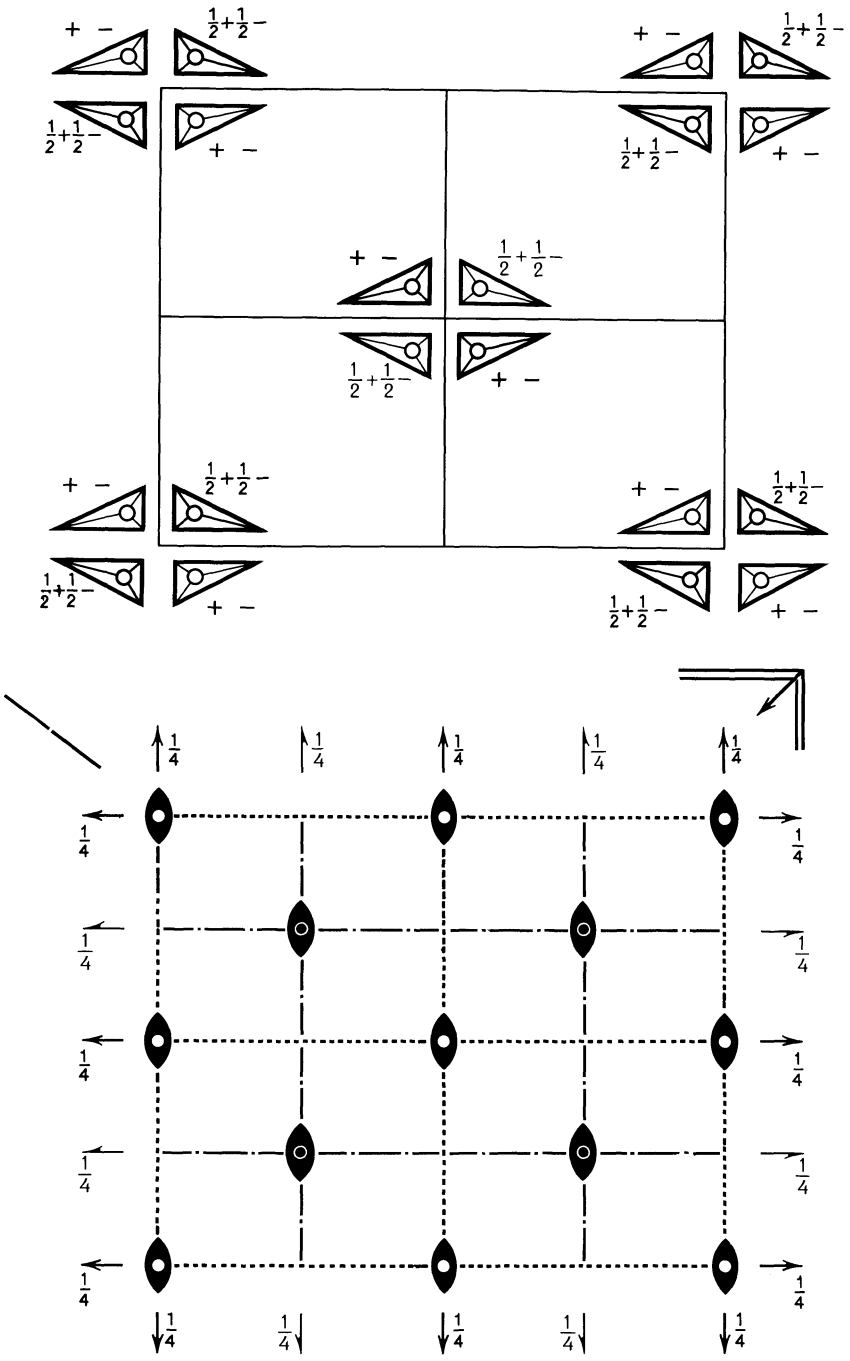

$Ш^{403}_{58} - P_cnnm$

Plate IVa, b. Examples of space antisymmetry (Shubnikov) groups [2.24]. (**a**)$Ш^{403}_{58} - P_cnnm$; (**b**) $Ш^{93}_{165} - P\bar{3}'c1$ (see p. 174)

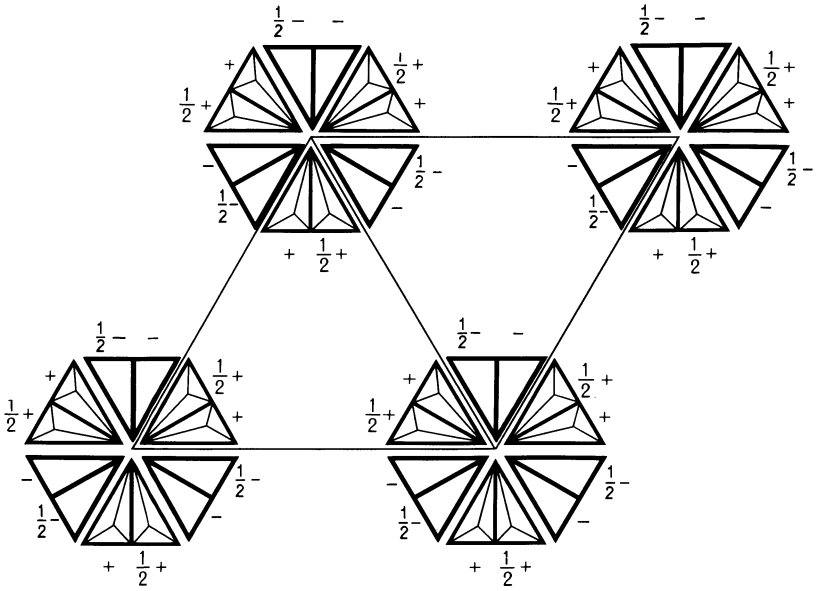

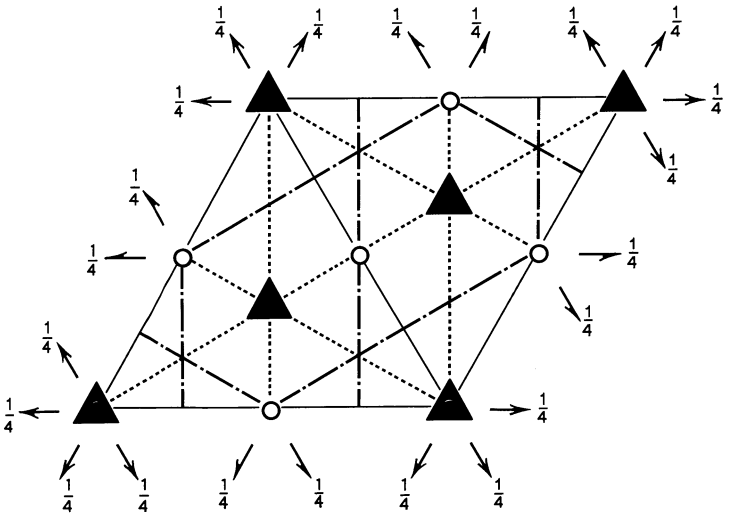

$W_{165}^{93} - P\bar{3}'c1$

Plate IVb.

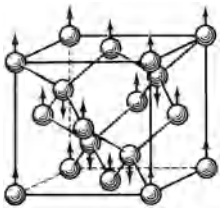

Fig. 2.98. Structure described by an antisymmetry group. Position of cobalt atoms (A positions) in the structure of $CoAl_2O_4$ (of the spinel type, space group $O_h^7 - Fd\bar{3}m$). Orientations of magnetic moments (conventionally indicated by arrows) of Co atoms are opposite, which is described by antisymmetry group $\text{III}_{227}^{132} - Fd'\bar{3}m'$

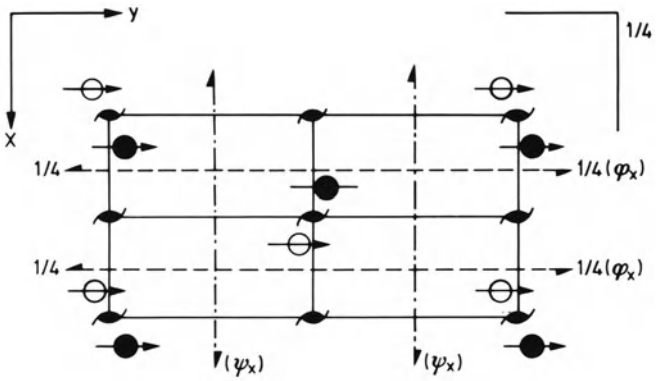

Fig. 2.99. Structure of MnP described by a color symmetry group ($T < 50$ K).
Black and white circles: Mn ions at a height $z = 1/4$ and 3/4, respectively; the arrows are the projections of the magnetic moments forming a helix about X. Space group $P2_1/b\ 2_1/n\ 2_1/m$, with due consideration for the magnetic structure of the symmetry operation, acquire color loads, and the group is recorded as

$$\Phi^{(p)} = 1^{2'_x} \otimes Pa^{(\psi_x^2)} \frac{2^{(\psi_x)}}{b^{(\psi_x)}} \frac{2^{(\psi_x)}}{n^{(\psi_x)}} \frac{2_1}{m};$$

$a^{(\psi_x^2)}$ means that a translation by vector a is accomplished by a rotation $\psi_x^2 = 2\psi$ of the magnetic moment about the X axis, and glide-plane $b^{\psi x}$ performs, besides the corresponding translation, an additional local rotation ψ_x (due to load ψ_x). This structure can also be described with the aid of group $\Phi^{(q)}$

of spin density at the points of its determination. Magnetic structures can also be described by position groups $\Phi^{(q)}$, in which the loads affect geometric and spin variables simultaneously. Position color groups can also be used in describing the distribution of defects in real crystals, or in describing space modulated structures [Ref. 2.13, Chap. I, Sect. 6.5].

2.9.6 Symmetry of Similarity

If, in symmetry transformation (2.1) we do not require the fulfillment of isometry condition (2.9), i.e., preservation of lengths, angles, areas, and volumes, we proceed to the generalized concept of equality (2.2).

In the symmetry of similarity two figures are considered equal if they are similar. As we recede from the singular point of the singular axis of the figure, the

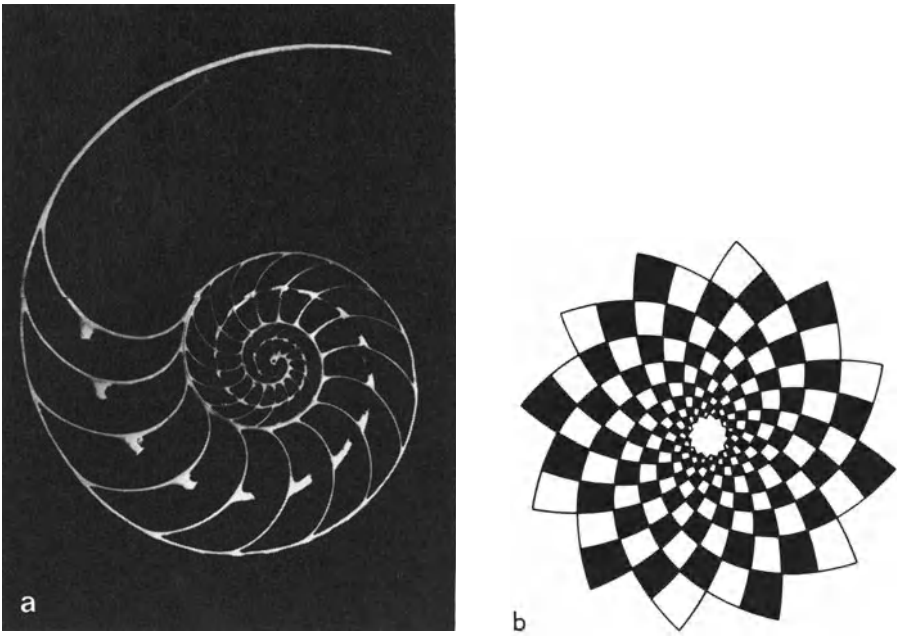

Fig. 2.100a, b. Figures with similarity symmetry. (**a**) thin section of the shell of a Nautilus mollusk; (**b**) 24-start spiral. This figure can also be regarded as possessing elements of antisymmetry [2.7]

distances in the "equal" parts of the figures increase proportionally (Fig. 2.100) which is automatically taken into account by symmetry operations. The corresponding groups are isomorphous to groups G_1^3.

Another possibility of nonisometric symmetry is "oblique" symmetry, described by so-called homology groups, in which, for instance, plane m reflects points not necessarily along a line perpendicular to it. Proceeding further on this path, we can advance to "curvilinear" symmetry, etc.

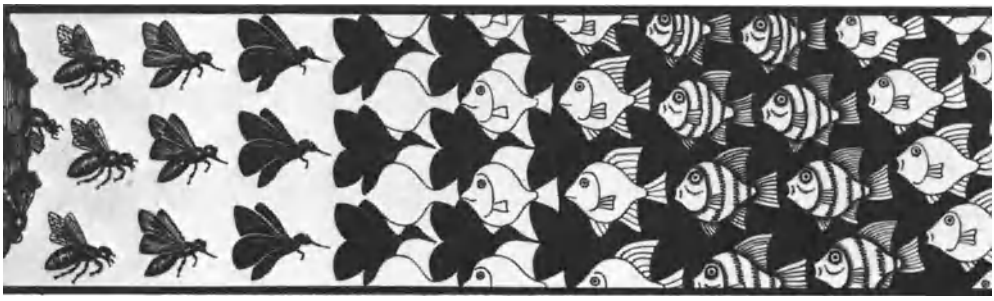

Fig. 2.101. Escher's drawing (fragment) illustrating the idea of gradual change in the 'approximate' equality of figures in translation symmetry [2.45]

2.9.7 Partial Symmetry

Symmetry can be regarded with respect not to all, but to some of variables $m' < m$ describing an object F. Then the object will be symmetric relative to these m' variables and asymmetric, or disymmetric, as they say, relative to the other $(m - m')$ variables. These m' variables may be discrete; for instance they may describe the presence or absence of some characteristic or its many-valuedness. Such an approach can be used in describing the structure of certain objects, and in particular, objects of nature – plants and animals.

2.9.8 Statistical Symmetry. Groupoids

After symmetry transformation $g[x] = x'(1)$ the object F may prove to be not precisely (2.2), but only approximately (statistically), similar to itself

$$F(x') \approx F(x), \tag{2.111}$$

and the measure of this similarity can be determined quantitatively. For instance, in a disordered crystalline structure, in solid solutions, some of the translationally equal atoms (or whole unit cells) are replaced by other atoms, "approximately" equal to the basic ones. It is possible to indicate the filling coefficient or other characteristics of such approximate equality.

The idea of gradual variation in F under translation symmetry is illustrated in Fig. 2.101.

The symmetric transformation (2.1) $g[x] = x'$ may itself be performed inaccurately (statistically). Thus, many polymers and liquid crystals consist of strictly equal molecules, i.e., $F(x) = F(x'')$; however, the values of x'' do not exactly coincide with x', but are statistically distributed around this most probable value in accordance with some function indicating the translational and angular components of the probable deviation of x'' from x'. This is another aspect of statistical symmetry.

There exist objects, where both the group transformation (2.1) and the condition of self-equality of $F(2)$ are fulfilled.

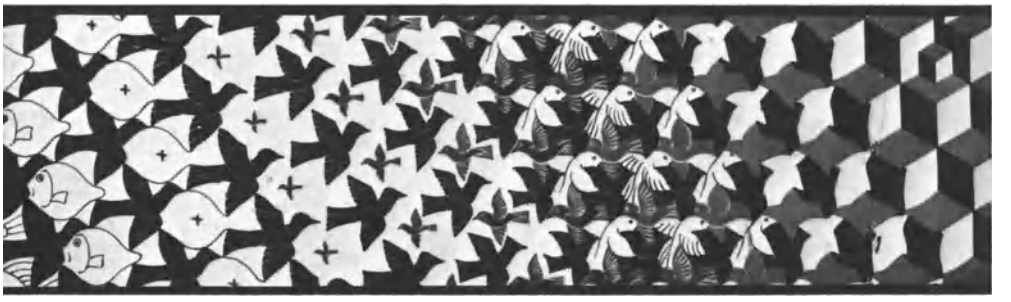

Another generalization of symmetry is the theory of groupoids which is used by *Dornberger-Schiff* [2.59] (see also [2.60]) for describing ordered-disordered (OD) structures. Groupoids are the most general algebraic sets satisfying only one of the group axioms: to every two of its elements there corresponds the third element of this set. If the first element is transformed into the second, and the second into the third, a transformation of the first element into the third exists. But here the object, as a whole, is not transformed into itself, as is the case in a group-symmetrical transformation (1), (2). Using the theory of groupoids, one can describe, for example, different variants of stacking of layers in structures of silicates. The groupoids describing layered OD-structures break down into 400 families.

The development of the theory of symmetry has been advancing vigorously in recent years. An important question which we have not mentioned in this chapter concerns interaction of the symmetry of objects and the environment. This will be treated in [2.14].

3. Geometry of the Crystalline Polyhedron and Lattice

Crystallography as an exact science originated from the study of the outward shape of crystals. Observations of the habit – plane faces, angles between them – and investigations into the regularities revealed led to an unambiguous conclusion about the regularity of the internal structure, namely the existence of three-dimensional periodicity, i.e., a crystal lattice. Later on, the crystal lattice was revealed directly by means of x-ray diffraction.

Observation and measurement of crystal faces and establishment of the laws of their arrangement are the subject of so-called geometric crystallography of the crystalline polyhedron, the chief method of which is goniometry (measurement of angles between crystal faces). The geometric crystallography of the lattice studies its absolute metric characteristics – repetition periods and angles of the unit cell. Simultaneously, the point symmetry of the crystal is established. At present, the principal technique of geometric crystallography is the x-ray method, while goniometry, which had played the leading part before x-ray diffraction was discovered, is used only for describing the outward shape of crystals.

3.1 Basic Laws of Geometric Crystallography[1]

3.1.1 Law of Constancy of Angles

Natural or synthetic crystals grown under definite conditions exhibit well-developed flat faces and edges between them. The existence of faces and edges and the laws of their mutual arrangement are macroscopic manifestations of the existence of the crystal lattice.

The crystal habit is characterized primarily by the presence of flat faces. For many crystals the flat faces are maintained very strictly. At the same time there are various types of disturbances of the flat faces of actual crystal forms associated with defects in the structure and the conditions of formation of the crystals.

---

[1] Sections 3.1.1–3 were written in cooperation with M. O. Kliya.

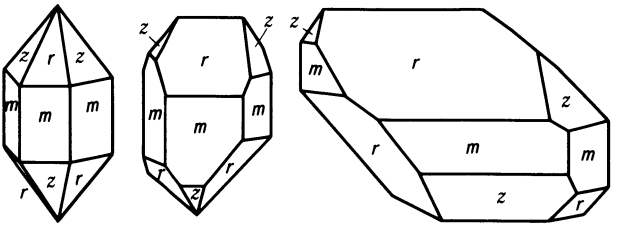

Fig. 3.1. Three quartz crystals with corresponding faces developed differently

Note that crystalline polyhedra have a relatively small number of faces. Crystals of a definite substance may have a different habit, but as a rule one can single out faces encountered often and those encountered more rarely.

The small number of faces and the almost constant presence of some of them on the crystals served as a ground for establishing the first basic law of geometric crystallography – *the law of constancy of interfacial angles.* If we take several crystals of a given substance, it is possible to arrange them in space so that certain faces are parallel (Fig. 3.1). They are called *corresponding* faces. The law of constancy of angle (Stenon's law) states: "Interfacial angles between the corresponding faces are constant".

The constancy of angle is preserved under given thermodynamic conditions and in the absence of external effects. For many crystals it holds with a high degree of accuracy – up to fractions of minutes. Deviations from stoichiometry, the presence of impurities, etc., and also external effects alter the angles but slightly.

3.1.2 Law of Rational Parameters. Lattice

The second basic law of geometric crystallography is Haüy's *law of rational parameters.* It establishes that the arrangement of all the faces observed on a set of crystals of a given substance can be characterized by certain rationally related integers.

The law of rational parameters is as follows: if we select the direction of three noncoplanar edges of a crystal as its reference axes, then the intercepts p_1, p_2, p_3, and p'_1, p'_2, p'_3 made on them by any pair of faces and called parameters[2] relate as integers (Fig. 3.2)

$$\frac{p'_1}{p_1} : \frac{p'_2}{p_2} : \frac{p'_3}{p_3} = h_1 : h_2 : h_3 = h : k : l. \tag{3.1}$$

[2] In the crystallographic literature, axes and parameters are denoted both by identical letters with suffixes ($a_1a_2a_3$; $a_1^*a_2^*a_3^*$; $p_1p_2p_3$; $h_1h_2h_3$) and by special letters (a, b, c; h, k, l). We shall use them interchangeably as dictated by convenience.

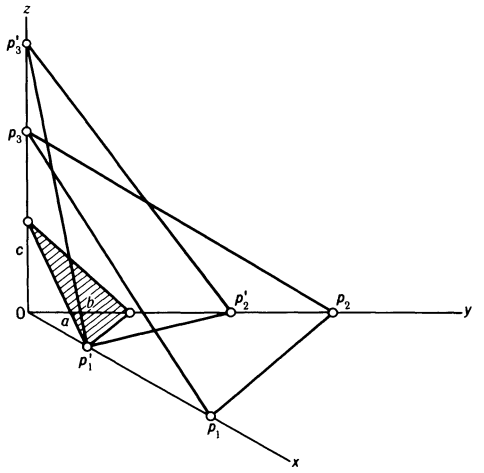

Fig. 3.2. The law of rational parameters

Therefore the law just mentioned is also called the law of rational intercepts. The parameters of one of the faces cutting all the axes may be taken as units of measurement along each axis and called unitary parameters a, b, c. Such a face may be called a *unit* face. Then the angle of inclination of the other observed faces of crystals may be expressed as p_1a, p_2b, p_3c, where the factors p_1, p_2, p_3, which were proposed by Ch. S. Weiss in 1818, are positive or negative integers. Only the ratio of the lengths of unit parameters can be determined by inspecting the habit, but not their absolute values. The three integers $p_1p_2p_3$ characterizing each face can then be found. If the face is parallel to one or two axes, the relevant Weiss indices are infinite.

From the law of rational parameters (Fig. 3.2) the existence of a lattice with unit cell edges a, b, and c follows unambiguously.

Any vector of such a lattice can be described by Weiss indices

$$\boldsymbol{t}_{p_1p_2p_3} = p_1\boldsymbol{a}_1 + p_2\boldsymbol{a}_2 + p_3\boldsymbol{a}_3. \tag{3.2}$$

It is clear that the directions of the possible edges of crystals are defined by the vector $\boldsymbol{t}_{p_1p_2p_3}$ and have the corresponding indices, and that the same indices can be employed to describe crystal faces by using (3.1). As we have already emphasized, the law of rational parameters (3.1) was established first, from which follows the existence of the lattice (3.2). Proceeding from the lattice (3.2) one can obviously obtain the law of rational parameters (3.1) (Sect. 1.1.5, Fig. 1.13).

The notation proposed by Miller in 1839 proved to be more convenient for describing crystal faces. Miller's indices h, k, l are the least integers inversely proportional to the numbers p_1, p_2, and p_3 in (3.1), when p'_1, p'_2, p'_3 are taken to be equal to unity, i.e., when the face making these intercepts is unit one.

At the same time Weiss's indices p_1, p_2, p_3 remain convenient for denoting the directions of edges and other straight lines in a crystal lattice.

3.2 Crystalline Polyhedron

3.2.1 Ideal Shape. Bundle of Normals and Edges

The crystal habit is governed by two basic laws, those of constancy of angles and of rational parameters. But it also obeys the crystallographic point symmetry K. The fact that there are only 32 crystallographic point groups, which were derived in studying the crystal habit, as well as the two indicated laws, follows from the existence of the crystal lattice. An (individual) crystalline polyhedron is a single crystal grown under equilibrium conditions, on which a definite combination of edges and faces is observed.

The habit of a crystal that exhibits an ideal (or perfect) shape strictly obeys the group K describing the crystal (Fig. 3.3). As has already been noted, the shape of an actual single crystal depends on the conditions of formation of the crystal. Because of the possible nonuniformity of actual conditions of growth (temperature gradients, concentration, etc.), the actual shape may differ drastically from the ideal [Ref. 3.1, Chap. 1]. Nevertheless, if the faces and edges of a crystal of a given substance are defined clearly enough, one can make a geometric description independent of its particular habit.

According to the law of constancy of angles, during the growth of crystals each face and each edge shifts parallel to itself. This also applies to the orientation of the corresponding faces and edges of different crystals of one and the same compound. The orientation of each face can be assigned by a normal to it. A set of such normals drawn from a common origin will thus completely describe the mutual angular orientation of the faces of a given crystal. The lines of intersection of the faces, the edges, can also be drawn from this origin. This kind of construction is called a face-and-edge bundle. With its aid, any crystal of a given substance with an identical set of faces receives a unified description irrespective of its individual features. The spherical projection of a normal-and-edge bundle (Fig. 3.4), or the corresponding stereographic projection gives a quantitative description of the interfacial angles and other geometric regularities of the habit.

Crystal edges are denoted by three indices in square brackets, and faces, by three indices in parentheses. The edges $[p_1p_2p_3]$ in such a set correspond to the

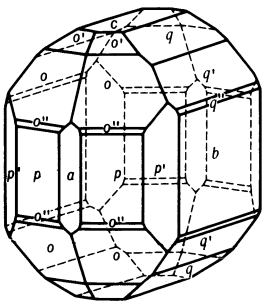

Fig. 3.3. Ideal shape of K_2SO_4 crystals. Faces belonging to the same simple form are labelled identically

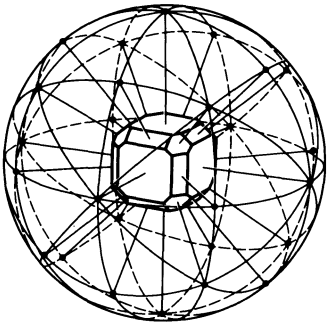

Fig. 3.4. Spherical projection of faces (*dots*) and zones (*great circles*)

lattice vectors $\boldsymbol{t}_{p_1p_2p_3} = p_1\boldsymbol{a}_1 + p_2\boldsymbol{a}_2 + p_3\boldsymbol{a}_3$, where p_i are Weiss indices, $\boldsymbol{a}_i$ are the unit cell vectors, and the crystal faces (hkl) have normal vectors $\boldsymbol{H}_{hkl}$ with Miller indices h, k, l, see (3.27).

It should be stressed that the indices of the faces (as well as the edges) must not have common factors. The face and edge indices may be either positive or negative. If we change all the signs in the symbol (hkl) for $(\bar{h}\bar{k}\bar{l})$, it will mean description of two opposite, but parallel, faces with a common normal $\boldsymbol{H}_{hkl}$. Thus it is senseless to change the signs of all the indices (hkl) (similarly, symbols $[p_1p_2p_3]$ and $[\bar{p}_1\bar{p}_2\bar{p}_3]$ imply one and the same edge).

From the formal consideration of the lattice one might conclude that any net of a lattice with arbitrary indices hkl can be a face of a crystal. In fact, however, this is not the case. During the growth of crystals, only faces with small values of the indices hkl, usually up to 3–5, are generally formed, and in exceptional cases up to 10 [Ref. 3.1, Chap. 1]. Faces with the least indices have the largest number of net points per unit surface area, i.e., the highest reticular density. This was noted by A. Bravais, who formulated a rule according to which habit faces (i.e., those most often present in a crystal) are the faces with the highest reticular density.

3.2.2 Simple Forms

The entire set of faces of an ideal crystalline polyhedron can be divided into sets of symmetrically equal faces, i.e., faces transformable into each other by point symmetry operations of a group K.

A set of faces obtained from one assigned crystallographic plane by application of all the symmetry operations of group K to it and cutting each other along the intersection lines – edges – is called a simple form. These faces are symmetrically equal in their geometry and also to their physical and chemical properties.

If a set of planes of a simple form does not close the space (see, for instance, Fig. 3.7a–e, g), it is called *open*. Open forms are characteristic of crystals of lower syngonies and are possible in all the syngonies, with the exception of cubic. If the space is closed (Figs. 3.7f, h; 10–15), a convex polyhedron is formed, which is a *closed* form. Such a polyhedron is an isohedron, i.e., an "equifacial polyhedron".

Since to each simple form there corresponds a bundle of symmetrically equal normals, it can also be obtained by drawing planes tangent to points of emergence of these normals onto the sphere (Fig. 3.5). In other words, a sphere can be inscribed in a simple form.

From the foregoing it follows that to each regular point system (RPS) of group K there corresponds a simple form, and hence the number of faces in this simple form corresponds to the multiplicity of such a regular point system. We can see that from the standpoint of the theory of symmetry, the concept of the simple form may be associated with the concept of a regular point system of a crystallographic group K. But in considering simple forms one also takes into consideration the mutual intersection of the symmetrically equal planes forming them, i.e., the edges. Therefore, in certain groups, several simple forms may correspond to one regular point system, because the possibilities of different intersections depend on the orientation of the initial plane relative to the symmetry elements. We shall explain this with reference to group 3 (Fig. 3.6). If the initial plane is perpendicular to axis 3, its normal coincides with this axis. By the action of this axis the plane is transformed into itself, and its symmetry, as well as that of the corresponding point of particular positions, is 3 (Fig. 3.6a). The point of general positions has a multiplicity of 3, two simple forms correspond to this regular point system: a general one – a trigonal pyramid (Fig. 3.6c), when the plane is inclined to axis 3, and a particular one – a trigonal prism (Fig. 3.6d), when the plane is parallel to axis 3. The face symmetry in the latter two cases is 1.

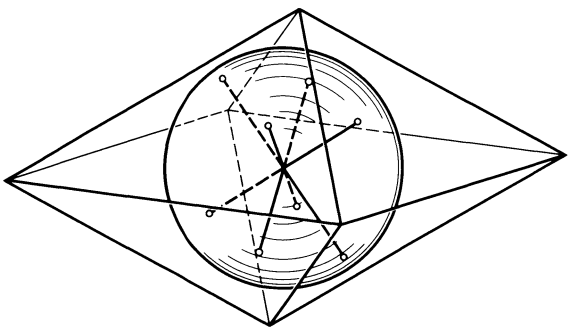

Fig. 3.5. Sphere inscribed in a simple form

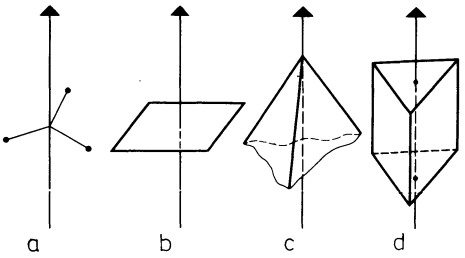

Fig. 3.6a–d. Simple forms of group 3. (**a**) points of general positions in group 3; (**b**) monohedron, (**c**) trigonal pyramid, (**d**) trigonal prism

To avoid this ambiguity, which takes place for all the axial groups N, one usually fixes, on the axis of symmetry the point corresponding to the center of the stereographic projection. Then, in the above example, to RPS lying on the equator there corresponds a prism, to those lying outside the equator, a pyramid, and to the polar point, a monohedron.

A simple form is called general if all its faces are not parallel and not perpendicular to one and the same symmetry element and do not cut the equivalent symmetry elements at equal angles, and it is called special if this condition is not met. The symmetry of faces of a general form is 1. The number of faces of a simple form of general positions is equal to the order of group K.

The derivation of simple forms precisely consists in successive examination of forms of general and different special positions for each group K. It is done conveniently with the aid of a set of normals of a stereographic projection.

The names of the simple forms which we list below derive from the Greek numbers (mono – one, di – two, etc.) and from the words "hedron" – face and "gon" – angle.

In the lower syngonies[3] open forms are possible – a monohedron (pedion) in group 1 (Fig. 3.7a), a pinacoid in group $\bar{1}$ (Fig. 3.7b), and dihedra (doma) in groups m and 2 (Fig. 3.7c, d). In m and 2, monohedra and dihedra are also possible. In orthorhombic groups, a rhombic prism, tetrahedron, pyramid, and bipyramid are added (Fig. 3.7e–h). Intermediate syngonies are characterized, apart from monohedra and pinacoids, by prisms (Fig. 3.8), pyramids (Fig. 3.9), bipyramids (Fig. 3.10), tetrahedra (Fig. 3.11), rhombohedra (Fig. 3.12), scalenohedra (Fig. 3.13), and trapezohedra (Fig. 3.14). The latter are possible in groups of the first kind K^1 and are characterized by the absence of symmetry

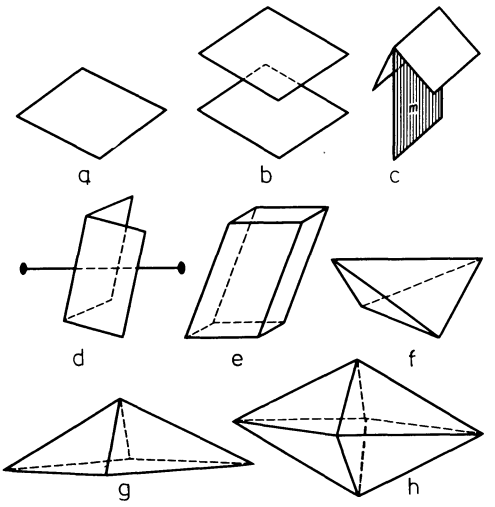

Fig. 3.7a–h. Simple forms of lower syngonies.
(**a**) monohedron, (**b**) pinacoid, (**c**) dihedron with a plane, (**d**) dihedron with an axis, (**e**) rhombic prism, (**f**) rhombic tetrahedron, (**g**) rhombic pyramid, (**h**) rhombic dipyramid

[3] As it was mentioned, another, equivalent term for "syngony" is "system".

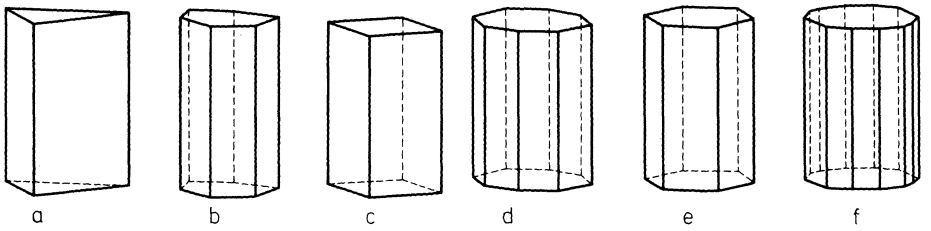

Fig. 3.8a–f. Prisms of intermediate syngonies.
(**a**) trigonal, (**b**) ditrigonal, (**c**) tetragonal, (**d**) ditetragonal, (**e**) hexagonal, (**f**) dihexagonal

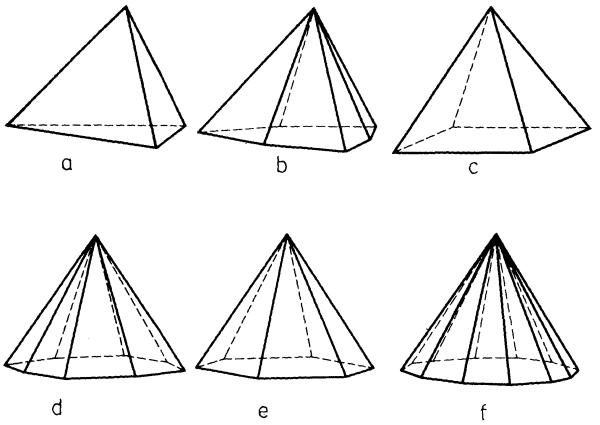

Fig. 3.9a–f. Pyramids of intermediate syngonies.
(**a**) trigonal, (**b**) ditrigonal, (**c**) tetragonal, (**d**) ditetragonal, (**e**) hexagonal, (**f**) dihexagonal

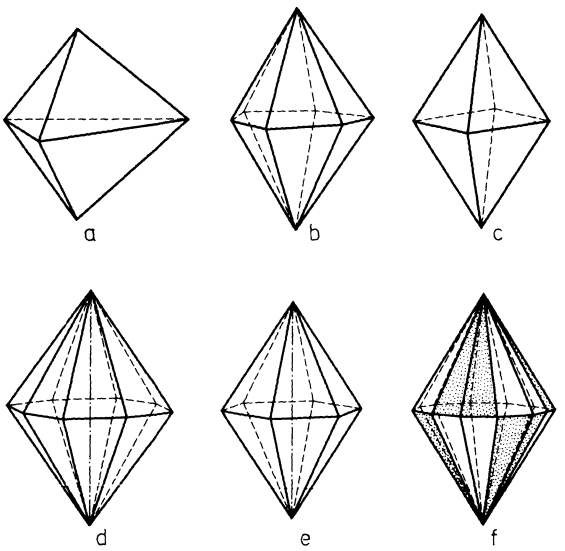

Fig. 3.10a–f. Bipyramids of intermediate syngonies. (**a**) trigonal, (**b**) ditrigonal, (**c**) tetragonal, (**d**) ditetragonal, (**e**) hexagonal, (**f**) dihexagonal

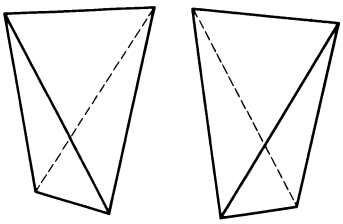

Fig. 3.11. Positive and negative tetragonal tetrahedra

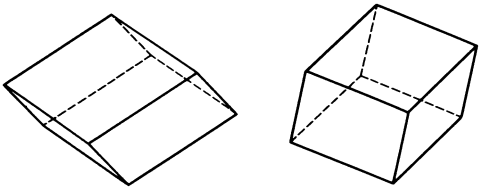

Fig. 3.12. Positive and negative rhombohedra

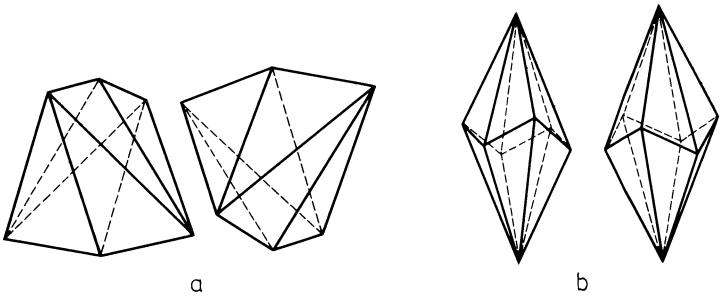

Fig. 3.13a, b. Positive and negative scalenohedra. (a) tetragonal, (b) ditrigonal

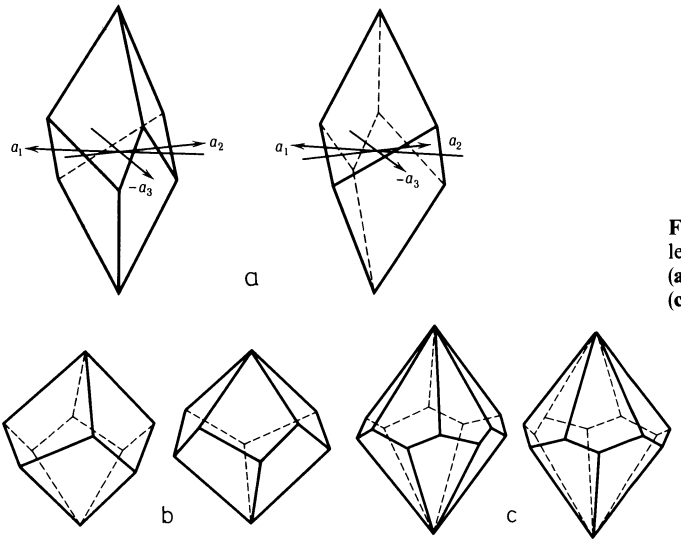

Fig. 3.14a–c. Right- and left-handed trapezohedra. (a) trigonal, (b) tetragonal, (c) hexagonal

planes and inversion axes. The upper pyramid of the trapezohedron is turned with respect to the lower by a certain angle not equal to half of the unit angle of rotation about the principal axis. Trapezohedra in this group K^1 may be right-handed or left-handed, i.e., they are enantiomorphous. In cubic groups all the simple forms are closed (Fig. 3.15). They are derived from the shapes of the tetrahedron (see the tetrahedron series in Fig. 3.15a–f), the octahedron (see the

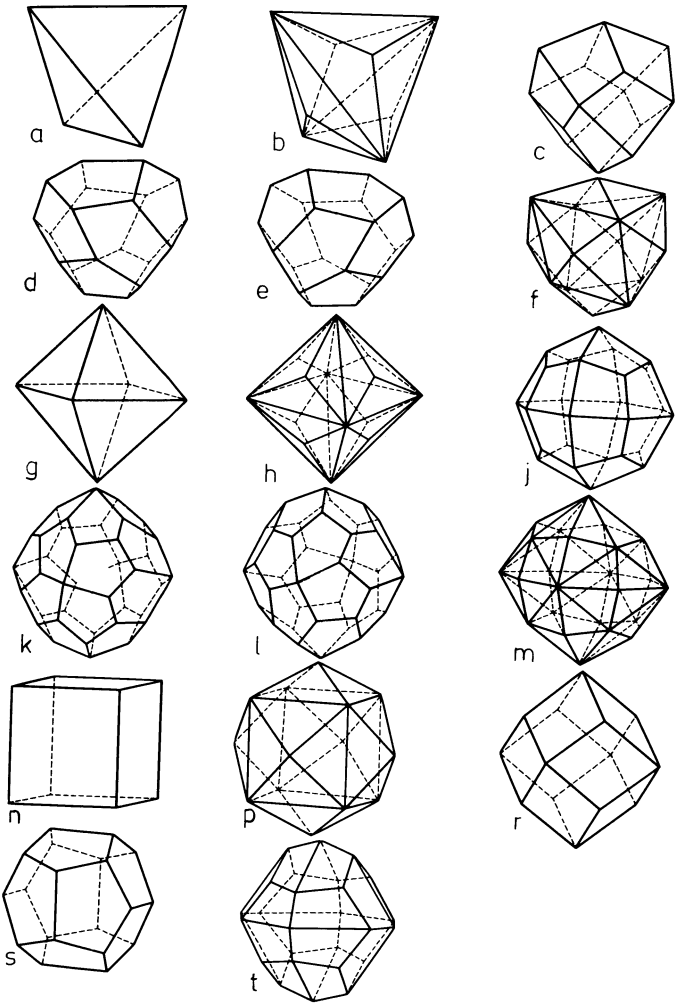

Fig. 3.15a–t. Simple forms of the cubic syngony. (**a**) tetrahedron, (**b**) trigontritetrahedron, (**c**) tetragontritetrahedron, (**d, e**) right-handed and left-handed pentagontritetrahedron, (**f**) hexatetrahedron, (**g**) octahedron, (**h**) trigontrioctahedron, (**j**) tetragontrioctahedron, (**k, i**) right-handed and left-handed pentagontrioctahedron, (**m**) hexaoctahedron, (**n**) cube (hexahedron), (**p**) pyramidal cube (tetrahexahedron), (**r**) rhombododecahedron, (**s**) pentagondodecahedron, (**t**) didodecahedron

octahedron series in Fig. 3.15g–m), and the cube (see the cube series in Fig. 3.15n–r). Cubic groups of the first kind also have enantiomorphous forms.

In all, there are 47 geometrically different simple forms (Figs. 3.7–15).

3.2.3 Distribution of Simple Forms Among Classes

This distribution is given in Tables 3.1–4. We can see that in addition to triclinic classes which have one simple form, each class (point group) K allows of three or five, or seven simple forms.[4] A given class K is, as a rule, characterized by *the general form.* Therefore the names of the classes correspond to the name of the simple form of general positions in the given class, for instance rhomboprismatic ($2/m$), trigonally pyramidal (3), etc. The same simple form may be encountered in different crystal classes (a general form of one class may be realized as a special form in another class). But the symmetry of faces of a geometrically identical simple form may differ from one class to another. For instance, an axial dihedron and a dihedron with a plane are distinguished (Fig. 3.7c, d). A monohedron is possible in ten different classes (which corresponds to the ten plane classes). In real crystals this difference reveals itself in studying the physical properties of face surfaces, primarily of their growth, solution, and etch figures; and other peculiarities of the face sculpture. For instance, cubes of different classes of the cubic syngony have different hatching of the faces in accordance with the symmetry (Fig. 3.16).

Table 3.1. Simple forms of lower syngonies

Simple form	Triclinic		Monoclinic			Rhombic		
	Class							
	1	$\bar{1}$	2	m	$2/m$	222	$mm2$	mmm
Monohedron (1)	+		+	+			+	
Pinacoid (2)		+	+	+	++	+	+	+
Dihedron (2)			+	+			+	
Rhombic pyramid (4)							+	
Rhombic prism (4)					+	+	+	+
Rhombic tetrahedron (4)						+		
Rhombic bipyramid (8)								+

Note: The figure standing next to the name of the simple form indicates the number of its faces, the plus sign, the presence of a simple form in this class, and two pluses, the presence of two symmetrically different faces of simple forms.

[4] It is taken into consideration here that class $2/m$ includes two pinacoids differently positioned relative to the symmetry elements of the class, and classes $\bar{4}2m$ and $\bar{3}m$ each include two prisms with different arrangements (Table 3.1–3).

Table 3.2. Simple forms of tetragonal syngony

Simple form	Class						
	4	$\bar{4}$	4/*m*	422	4*mm*	$\bar{4}$2*m*	4/*mmm*
Monohedron (1)	+				+		
Pinacoid (2)		+	+	+		+	+
Tetragonal pyramid (4)	+				+		
Tetragonal prism (4)	+	+	+	+	+	++	+
Tetragonal tetrahedron (4)		+				+	
Ditetragonal pyramid (8)					+		
Tetragonal bipyramid (8)			+	+		+	+
Ditetragonal prism (8)				+	+	+	+
Tetragonal scalenohedron (8)						+	
Tetragonal trapezohedron (8)				+			
Ditetragonal bipyramid (16)							+

Table 3.3. Simple forms of trigonal and hexagonal syngonies

Simple form	Class											
	3	$\bar{3}$	32	3*m*	$\bar{3}$*m*	6	$\bar{6}$	6/*m*	622	6*mm*	$\bar{6}$*m*2	6/*mmm*
Monohedron (1)	+			+		+				+		
Pinacoid (2)		+	+		+		+	+	+		+	+
Trigonal pyramid (3)	+			+								
Trigonal prism (3)	+		+	+			+				+	
Ditrigonal pyramid (6)				+								
Trigonal bipyramid (6)			+				+				+	
Ditrigonal prism (6)			+	+							+	
Hexagonal pyramid (6)				+		+				+		
Hexagonal prism (6)		+	+	+	++	+		+	+	+	+	+
Rhombohedron (6)		+	+		+							
Trigonal trapezohedron (6)			+									
Ditrigonal bipyramid (12)											+	
Ditrigonal scalenohedron (12)					+							
Hexagonal trapezohedron (12)									+			
Hexagonal bipyramid (12)					+			+	+		+	+
Dihexagonal pyramid (12)										+		
Dihexagonal prism (12)					+				+	+		+
Dihexagonal bipyramid (24)												+

The total number of simple forms which differ geometrically is 146 and, if we also include enantiomorphous pairs, 193. In classes with polar directions the faces hkl and $\bar{h}\bar{k}\bar{l}$ which are parallel to each other, may not be derived from each other by symmetry operations of group K. The simple forms corresponding to them are geometrically identical, but they differ in the physical properties of the

Table 3.4. Simple forms of cubic syngony

Simple form	Class				
	23	$m3$	432	$\bar{4}3m$	$m\bar{3}m$
Tetrahedron (4)	+			+	
Hexahedron (6)	+	+	+	+	+
Octahedron (8)		+	+		+
Rhombododecahedron (12)	+	+	+	+	+
Pentagondodecahedron (12)	+	+			
Trigontritetrahedron (12)	+			+	
Tetragontritetrahedron (12)	+			+	
Pentagontritetrahedron (12)	+				
Hexatetrahedron (24)				+	
Trigontrioctahedron (24)		+	+		+
Tetragontrioctahedron (24)		+	+		+
Pentagontrioctahedron (24)			+		
Tetrahexahedron (24)			+	+	+
Didodecahedron (24)		+			
Hexoctahedron (48)					+

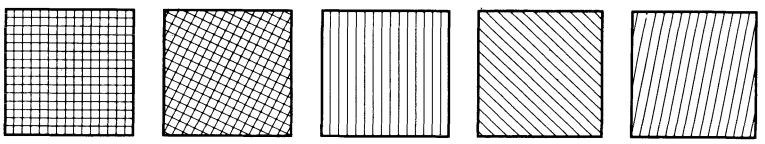

Fig. 3.16. Proper symmetry of the faces of five cube varieties belong to different classes of the cubic syngony

faces. The forms of such a pair are called positive and negative; for instance, there are a positive and a negative tetrahedron in group 23. The number of simple forms, with an allowance for such differences, is 318. If we take into account the differences in the space symmetry of the crystals, the number of distinct simple forms will be equal to 1403.

The faces of a simple form are symmetrically equal, so the indices in their symbols (hkl) are transformed in accordance with the transformations of the corresponding group K (see Sect. 3.4). The indices (hkl) of the faces of a given simple form may differ only in the signs or in their permutations with or without a change of sign. The indices of a generally situated face (hkl) are all nonzero. For instance, in the intermediate syngonies the symbols (hkl) of the faces of a general simple form are obtained by changing the signs of the three indices and permutations of indices h and k taken for some fixed face. In faces of special positions, either one or two indices are equal to zero, or some indices are equal to each other (in the intermediate syngonies these indices are h and k).

We shall see below in (3.7) that in the trigonal and hexagonal syngonies the first two indices h and k are replaced by a symmetric triad of indices hki $[i = -(h + k)]$, and the fourth, l, remains unchanged. If the symbol of all the faces belonging to the given simple form, i.e., the symbol of the simple form as a whole, is to be indicated, its indices (positive) are placed in braces: $\{hkl\}$.

3.2.4 Holohedry and Hemihedry

The analysis of the habit of crystals and simple forms is associated with the classical crystallographic division of the crystal classes within each syngony into holohedral (i.e., "full-faced"), hemihedral (having half the full number of faces in the holohedral class), and sometimes tetartohedral (having 1/4 of the faces). The holohedral class is the highest in a given syngony, and any other class of it is its subgroup. Take, for instance, the holohedral tetragonal class $4/mmm$ and its general simple form – the ditetragonal bipyramid (Fig. 3.17). We can select, in several ways, half the faces from it ("hemihedry") and, extending them, close them up with each other, so that we obtain the general simple forms of the subgroups of index 2 of this group, namely groups $4mm$, $4/m$, 422, $\bar{4}2m$. For instance, selection of the faces of the upper bipyramid alone will lead to class $4mm$, the selection shown in Fig. 3.17b will give a tetragonal trapezohedron, etc. We can similarly pass on to tetartohedry.

3.2.5 Combinations of Simple Forms

As a rule, crystals exhibit faces belonging to several simple forms, and in this case one speaks of their *combinations*. Open simple forms can obviously exist on crystals only in combinations with other, open or closed forms, and closed forms can be present both in combinations or separately.

The principle of formation of combinations is shown in Fig. 3.18: the simple forms "cut" each other, producing a convex polyhedron. The particular dimensions of the resulting faces depend obviously on the number of simple forms combined and on the linear dimensions of each of them. Simple forms of the same name, but with different indices $\{hkl\}$, may also be combined. Physically, the appearance of some or other faces is associated with their growth rate

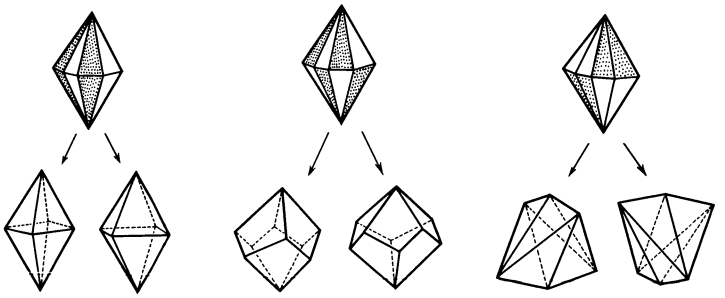

Fig. 3.17. Derivation of general forms for hemihedral classes of the tetragonal syngony

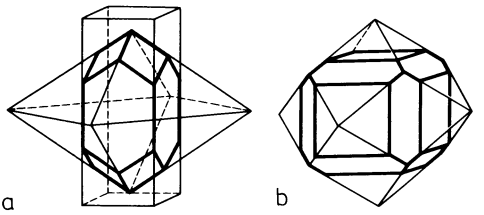

Fig. 3.18a, b. Formation of combinations of simple forms.
(a) tetragonal prism and tetragonal bipyramid, **(b)** rhombododecahedron and cube

[Ref. 3.1, Chap. 1]: faces with the least growth rates are the ones usually revealed. Therefore crystals of one and the same substance grown in different conditions may have different habits.

The ideal form of a crystal can be constructed by taking each simple form on a set of normals whose lengths are proportional to the growth rate of the faces of this form. The actually observed number of simple forms on crystals is usually small, not more than 3–5.

Each of the simple forms of a given class K has its symmetry. Hence, when various crystal forms appear in combination, the crystal faces of each of them, due to their intersection, are symmetrically equal, i.e., they are equal polygons. The surface of a perfect crystalline form, indeed, consists of several sorts of such equal polygons, i.e., of combinations of simple forms. If only one simple form is present, only one sort of polygon forms the habit. Different crystalline polyhedra will be presented below (Fig. 3.18).

Group K of a given crystalline polyhedron naturally also describes all the other elements of the habit, namely its edges and vertices. The number of these elements is related by Euler's equation for convex polyhedra

$$F + V - E = 2, \tag{3.3}$$

where F is the number of faces, V of vertices, and E of edges.

3.2.6 The Zone Law

Since edges are intersections of faces, their arrangement is interrelated. The condition for edge $[p_1p_2p_3]$ to belong to face (hkl) or, what is the same, for face (hkl) to intersect some other face along edge $[p_1p_2p_3]$ has the form

$$p_1h + p_2k + p_3l = 0. \tag{3.4}$$

This relation follows immediately from condition (3.2) for the existence of a crystal lattice, whose plane nets correspond to the macroscopic faces, and the rows of points to the edges (see Sect. 3.4.2). By (3.4), several distinct faces (hkl) may be parallel to a certain direction – edge $[p_1p_2p_3]$. A set of such faces is called a zone. The edge (direction) $[p_1p_2p_3]$ is called the zone axis. From the two equations of the type (3.4) it is possible to find the zone axis if the two planes $(h_1k_1l_1)$ and $(h_2k_2l_2)$ intersecting along this axis are known. Putting these indices into (3.4)

$$h_1p_1 + k_1p_2 + l_1p_3 = 0, \quad h_2p_1 + k_2p_2 + l_2p_3 = 0$$

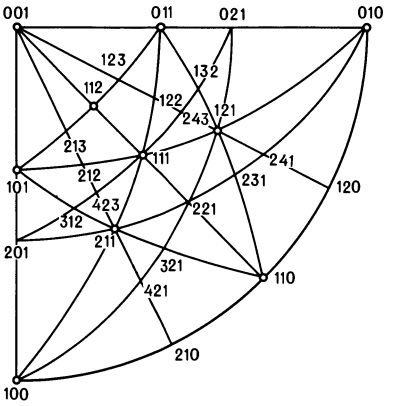

Fig. 3.19. Development of a face complex

and solving these equations, we obtain

$$p_1 = k_1 l_2 - l_1 k_2, \quad p_2 = l_1 h_2 - h_1 l_2, \quad p_3 = h_1 k_2 - k_1 h_2. \tag{3.5}$$

The simplest examples of zones are coordinate zones. For instance, all the faces $(0kl)$ are parallel to the coordinate edge $[p_1 00]$. In a face-and-edge bundle the normals of the faces $\boldsymbol{H}_{hkl}$ are perpendicular to the zone axis $\boldsymbol{t}_{p_1 p_2 p_3}$ and their emergences onto the spherical or stereographic projection lie on the same great circle whose plane is perpendicular to the zone axis $[p_1 p_2 p_3]$.

Each face has at least two nonparallel edges $[p_1 p_2 p_3]$ and $[p'_1 p'_2 p'_3]$ and therefore belongs to at least two zones. Knowing the indices of the two edges, we can find the indices of the face by (3.4),

$$h = p_2 p'_3 - p_3 p'_2, \quad k = p_3 p'_1 - p_1 p'_3, \quad l = p_2 p'_1 - p_1 p'_2. \tag{3.6}$$

Edges – the sides of the faces, which are polygons, – obey the general relation (3.4). This is Weiss' *zone law*: each plane parallel to two actual or possible edges of a crystal is an actual or possible face of the crystal, and (reciprocally) each direction parallel to the line of intersection of two actual or possible crystal faces is its actual or possible edge. The zone law enables one to find new, potential faces and edges from the observed ones. This procedure is called the development of complexes of edges and faces (Fig. 3.19).

3.3 Goniometry

3.3.1 Crystal Setting

Goniometry is concerned with measuring angles between crystal faces. In connection with the development of x-ray analysis this method has ceased to be the most important technique in geometric crystallography, but it still retains its

importance in morphology and the theory of crystal growth, the practice of crystal physics and crystal technology, mineralogy, and a number of other fields.

Goniometric measurements of crystals and microcrystals are used, in conjunction with data on chemical composition, for phase analysis of synthetic and natural substances.

By measuring interfacial angles one can determine the class K of a crystal and hence its syngony[5], the axial ratio $a:b:c$, and angles α, β, and γ of the unit cell, and can also index all the faces and edges. Since in goniometry only the axial ratio is found and one of the parameters is taken to be unity, the number of values characterizing the cell is five, in the general case. The cubic cell has no relative metric characteristics, while its angles are equal to 90°, and thus it is not characterized in any way in goniometry.

We know that each crystal has a space lattice with definite metric parameters, but the unit cell axes may be chosen in different ways. To be able to compare the results of investigations of different crystals of the same substance or to identify an unknown crystal by using data available in the literature, one must have a rule for choosing the coordinate axes a, b, and c of crystals. The choice of these axes is called crystal setting. The origin of this term is associated with the technique of goniometric measurements, i.e., with the most convenient and correct setting of a crystal for measurements on a goniometer head.

The choice of coordinate axes is dictated, in the first place, by the symmetry, i.e., the allocation of the crystal to a syngony with a characteristic axial ratio $a:b:c$ and angles α, β, and γ of the unit cell. The axes are chosen along the axes of symmetry of the crystal or along the normals to the symmetry planes m. The rules for choosing the axes are indicated in Table 3.5.

It is necessary to distinguish between positive and negative directions of axes X, Y, Z: the positive are chosen so that when viewed from the positive end of axis Z the rotation from X to Y is counterclockwise. In intermediate syngonies, axis Z is always chosen to be the principal, i.e., axis 3, 4, or 6 is taken for Z. A technique characteristic of setting crystals is the choice of unit face (111) which cuts off axial units a, b, c on the coordinate axes (see Table 3.5).

In rectangular syngonies – cubic, tetragonal, and orthorhombic – axes X, Y, Z are chosen along symmetry axes orthogonal to each other. In the tetragonal syngony, the shortest (in the basal plane) period should be chosen as $a = b$. In the hexagonal syngony, axes X and Y to which $a = b$ correspond are arranged at an angle of 120° to each other, but there is a third axis U, symmetrically equal to them, which also makes angles of 120° with X and Y. Using these three equivalent axes in the basal plane, we obtain three indices h, k, and i as the symbols of planes, too, instead of the pair h and k, while index l, which corresponds to axis Z, is determined in the usual way. The trace of the section of plane XYU by any plane $(hkil)$ is the straight line L (Fig. 3.20), which makes intercepts x, y, and $-u$ on the axes. From the figure it follows that $x:(x+u) = y:(-u)$,

[5] See footnote on p. 97.

Table 3.5. Crystal setting

Syngony	Crystallographic axes	Unit face
Triclinic	Axes X, Y, Z are parallel to actual or possible crystal edges Axis Z, which is parallel to the axis of the most developed zone, is placed vertically 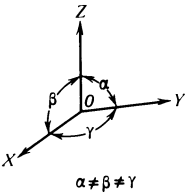 $\alpha \neq \beta \neq \gamma$	The unit face makes unequal intercepts on the crystallographic axes 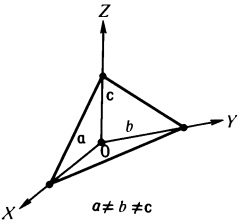 $a \neq b \neq c$
Monoclinic	Axis Y is brought into coincidence with axis 2 or with the perpendicular to m and is placed horizontally. The axes X and Y are chosen in the plane perpendicular to Y, parallel to the actual or possible edges of the crystal. Axis Z is vertical 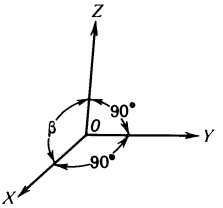 $\alpha = \gamma = 90° \neq \beta$	The unit face makes unequal intercepts on the crystallographic axes 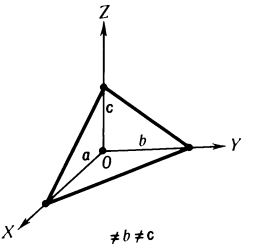 $\neq b \neq c$
Orthorhombic	Axes X, Y, Z are brought into coincidence with three axes 2 or with one axis 2 (vertical), and with the perpendiculars to the two planes m 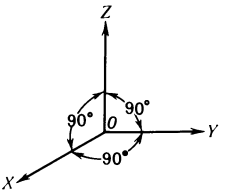 $\alpha = \beta = \gamma = 90°$	The unit face makes unequal intercepts on the crystallographic axes 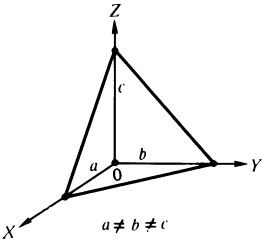 $a \neq b \neq c$

Table 3.5. (*continued*)

Syngony	Crystallographic axes	Unit face
Tetragonal	The vertical axis Z is brought into coincidence with axis 4 or $\bar{4}$. Axes X and Y are chosen in the plane perpendicular to Z or along axes 2, or along perpendiculars to planes m, or along the directions parallel to the actual or possible edges of the crystal 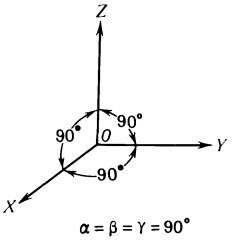 $\alpha = \beta = \gamma = 90°$	The unit face makes equal intercepts on the horizontal axes X and Y and an intercept unequal to them along axes Z 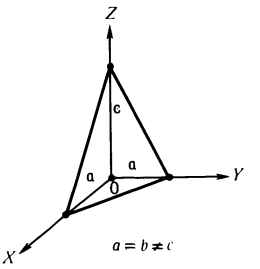 $a = b \neq c$
Trigonal and hexagonal	Hexagonal setting. Vertical axis Z is brought into coincidence with axis 6 or $\bar{6}$, or 3 or $\bar{3}$. Axes X, Y, U are chosen in the plane perpendicular to Z, or along axes 2, or along perpendiculars to the planes m, or along the directions parallel to the actual or possible edges of the crystal 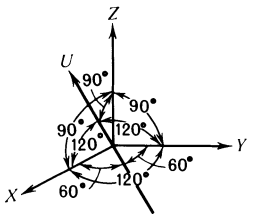	The unit face makes equal intercepts on the two horizontal axes and an intercept unequal to them along Z. The unit face is either parallel to one horizontal axis (a) or makes an intercept on it which is half the length of those on the other two horizontal crystallographic axes (b) 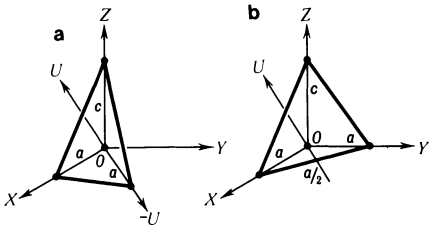
Cubic	The axes are brought into coincidence with the three axes 4 or with $\bar{4}$, or (in the absence of fourfold axes) with 2 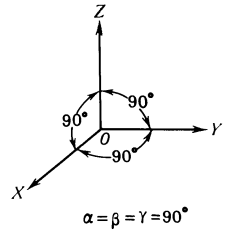 $\alpha = \beta = \gamma = 90°$	The unit face makes equal intercepts on the crystallographic axes 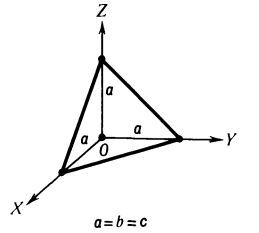 $a = b = c$

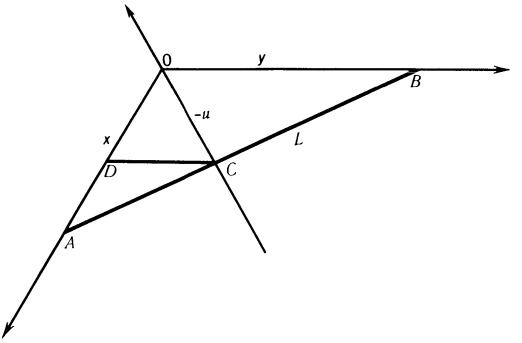

Fig. 3.20. Relationship between the indices in the hexagonal system

whence $x^{-1} + y^{-1} + u^{-1} = 0$. But the inverse values of the intercepts are indices, i.e.,

$$h + k + i = 0, \quad i = -(h + k). \tag{3.7}$$

Thus, in the hexagonal syngony the symbols of the planes have four indices, for instance $(11\bar{2}0)$, $(3\bar{1}24)$, $(20\bar{2}1)$, etc., but only three of them are independent. The same refers to the description of rhombohedral crystals in the hexagonal system of coordinates.

In the monoclinic and triclinic syngonies consideration of only crystal symmetry does not permit an unambiguous choice of axes. In monoclinic crystals the symmetry fixes only one axis – axis 2 or the normal to m; this axis is usually chosen as axis Y. For X and Z it is customary to choose the shortest periods in the plane perpendicular to axis Y so that angle β is obtuse. This setting is called crystallographic. In the x-ray (and crystallophysic) setting of monoclinic crystals, axis 2 or the normal to m is sometimes taken as axis Z.

When only the goniometric method was available, the problem of correct crystal setting sometimes involved great difficulties. Ambiguities arose not only in the setting of triclinic and monoclinic crystals, but also tetragonal (the basis axes can be turned through 45°), hexagonal, and trigonal (the basis axes can be turned through 30°). At present such problems are easily solved by using the x-ray method.

There is a general algorithm for the reduction of any, arbitrarily chosen, unit cell of any symmetry to the standard cell, which corresponds to the only correct setting (see Sect. 3.5.2).

3.3.2 Experimental Technique of Goniometry

As already indicated, goniometry is used for studying the habit of crystals, orienting them in crystallophysical or other investigations, and sometimes also at the preliminary stage of x-ray analysis.

Goniometers of different types are used depending on the size of the crystal, the number of its faces, and the quality of their surface. The most common types

of them are contact and reflecting goniometers. Both may be one-circle (i.e., with a single circle divided into degrees) or two-circle.

The contact-type one-circle goniometer (Fig. 3.21) consists of a protractor and an arm pivoted on it. When measuring a dihedral angle the goniometer is applied to the crystal so that the edge between the faces is parallel to the rotation axis of the arm. Such goniometers ensure an accuracy up to 30′ and are used where the large size of the crystal or the imperfection of its face surfaces prevents more accurate measurement.

Optical goniometers are based on the principle of successive reflections of light beams from different faces of the crystal (Fig. 3.22a). With the use of plasticine or wax a crystal K is mounted to a crystal holder connected to a stage, which rotates together with the circle. The edge between the faces being measured (the zone axis) must be set parallel to the rotation axis. A light beam from a source falls on the crystal through a collimator. An observer sees in a telescope the image of the light source, the so-called signal, only when one of the crystal faces (a_1) takes a position normal to the bisector of the angle made by the optic axes of the collimator and the telescope.

Having read the angle in accordance with the indicated position and turning the crystal together with the circle so that face a_2 replaces a_1 (or is located parallel to it), the value of angle β between the normals to these faces is found from the difference between the readings. Angle $\beta = 180° - \alpha$, where α is the interfacial angle. A complete revolution of the crystal makes it possible to measure all the axes of one zone of the crystal. With this crystal setting only one zone can be measured, which is a disadvantage of a one-circle goniometer. To measure all the zones it is necessary to change the orientation of the crystal several times by positioning it differently on the crystal holder.

The reflecting two-circle or theodolite goniometer (Fig. 3.22b) enables one to make a complete goniometric determination at one setting of a crystal. This instrument was introduced into practice by E. S. Fedorov and V. Goldschmidt in 1893. It enables one to determine the position of the normals to each of the faces by measuring both angular coordinates simultaneously – the polar angle ρ, which varies from 0 to 180°, and the longitude φ, which varies from 0 to 360°; these

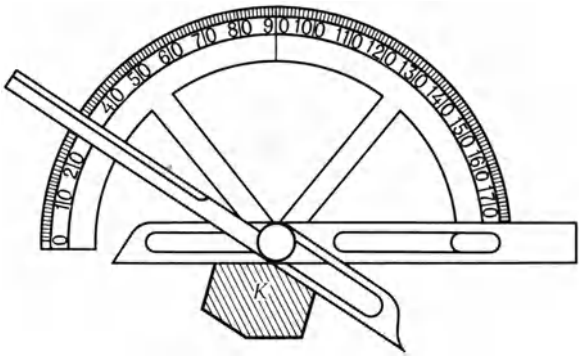

Fig. 3.21. General view of the contact goniometer

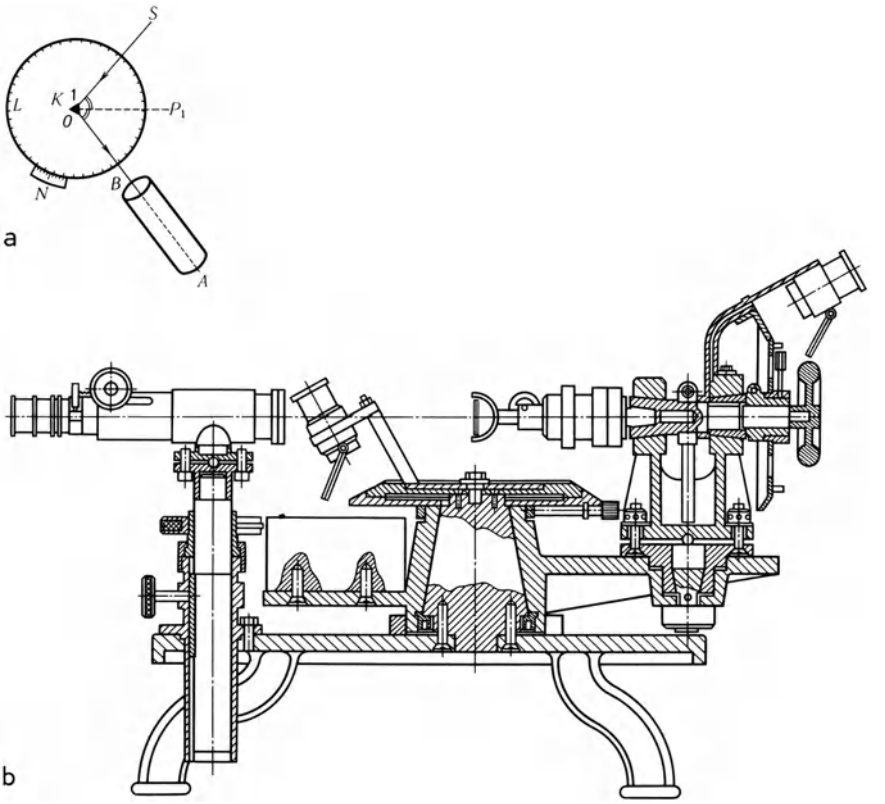

Fig. 3.22. (**a**) Scheme of single-circle reflection goniometer (*K*: crystal, *SO*: incident beam, *OA*: reflected beam, *BA*: telescope); (**b**) two-circle Goldschmidt goniometer

angles are read on the horizontal and vertical circle, respectively. A new technique – photogoniometry – is gaining wide acceptance. In it, light reflections from a part of the crystal surface are simultaneously registered on a photographic film; the mean coverage of the projection sphere is 2.0 sterad. By using intermediate reflections from the internal surface of a paraboloid of revolution (into whose focus the crystal is placed) one can obtain a gnomonic projection of the crystal faces directly on the film [3.2] (Fig. 3.23a, b).

3.3.3 Goniometric Calculations

The indices of crystal faces can be calculated using angle measurements. Faces can be indexed either trigonometrically or graphically. The former method produces an accurate result, but is laborious, especially for low-symmetry crystals. The formulae for the angles between the normals H_{hkl} to the faces, between the normals H_{hkl} and edges $t_{p_1p_2p_3}$, and between different edges will be given below (Sect. 3.5.3).

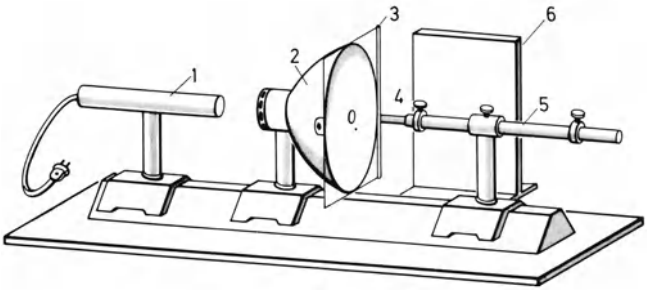

Fig. 3.23. (**a**) Diagram of the photogoniometer: *1*: illuminating laser; *2*: parabolic mirror; *3*: film cassette; *4*: crystal; *5*: crystal holder; *6*: auxiliary screen

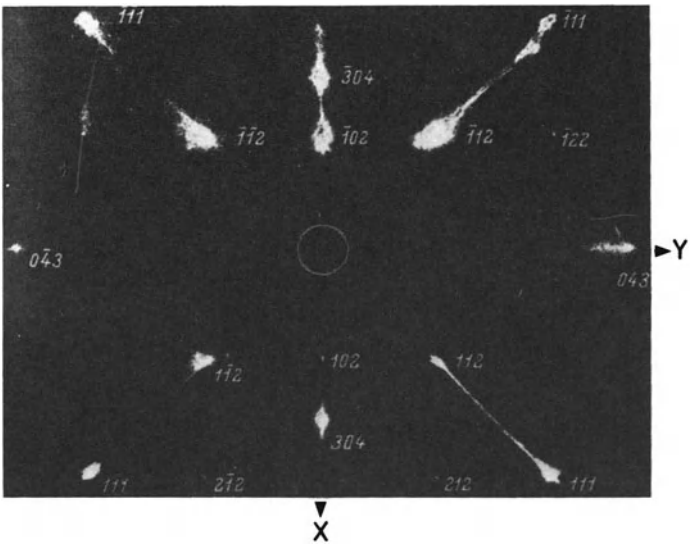

Fig. 3.23. (**b**) Photognomonic projection of a pyrite crystal [3.2]

The graphical method provides a lower, but practically quite sufficient accuracy and is very pictorial. It is best realized with the aid of a stereographic projection, on which the central sections of the spherical projection are mapped into arcs (or straight lines) passing through diametrically opposite points (great circle arcs). For this purpose use is made of Wulff's stereographic net of meridians and parallels, 20 cm in diameter, with divisions of 2° (Fig. 3.24). A set of meridians (great circles) on it gives the description of a zone if it is rotated about the central point in the plane of the drawing. An important property of the stereographic projection is the fact that the angles between the two great circles on the sphere of the spherical projection are equal to the angles between their mapping on the stereographic projection.

From given ρ and φ for all the faces, the emergences of normals H_{hkl} are marked on the Wulff's net, giving the stereographic projection of the crystal.

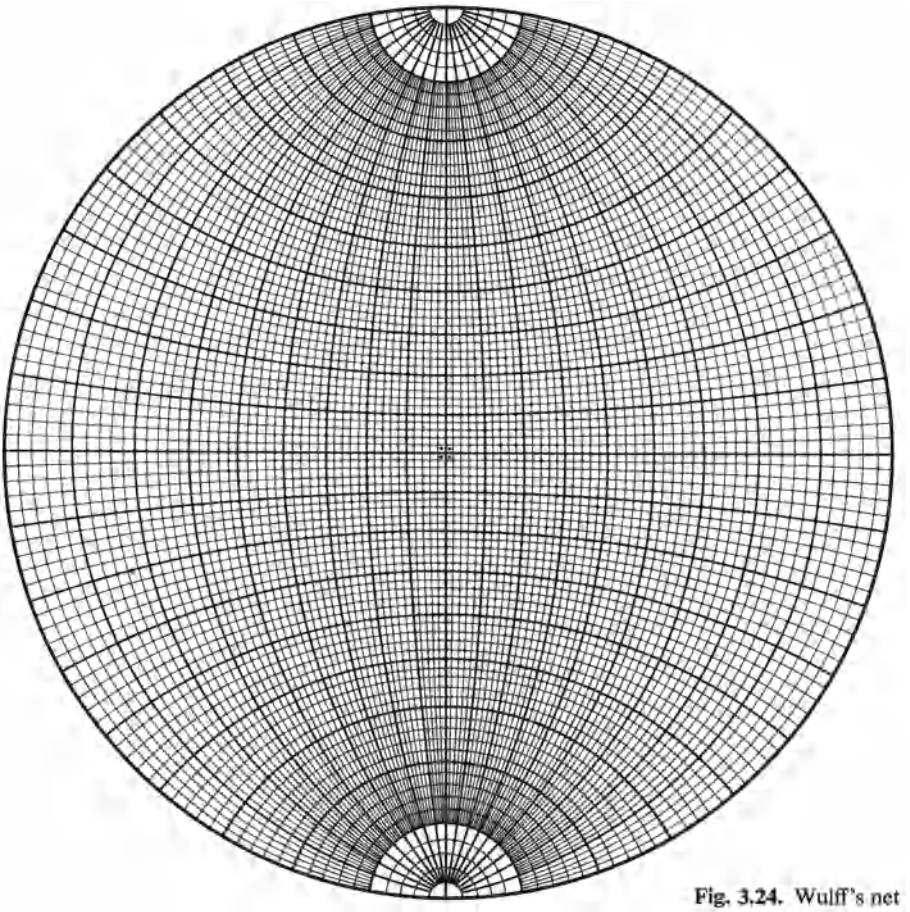

Fig. 3.24. Wulff's net

Fig. 3.24. Wulff's net

The zones are then marked (they correspond to the great circles), and the zone axes (edges) are found. The taken set of angles between the faces is seen directly from the drawing, and thus the syngony can be determined. When choosing the reference axes of the crystal, one should follow the rules of crystal setting (see Table 3.5).

To determine the $a:b:c$ ratio and the face indices, use is made of the following relation, which will be proved in Sect. 3.5.3:

$$\cos \varphi_{a_i(H)} = h_i/a_i H. \tag{3.8}$$

Here, φ is the angle between the normal to the face and the corresponding reference axis measured directly on the stereographic projection.

Taking a unit face (111) (all h_i are equal to unity), we obtain from (3.8)

$$a:b:c = \frac{1}{\cos \varphi_x} : \frac{1}{\cos \varphi_y} : \frac{1}{\cos \varphi_z}, \tag{3.9}$$

where φ_x, φ_y, φ_z, are the angles between the normal to the unitary face and axes X, Y, Z. If no unit face is observed, a pair of faces of the types (110) and (011) may serve as an alternative. On the other hand, the indices of any face (hkl) are determined from (3.8) and (3.9) by the relation

$$h:k:l = \frac{\cos\psi_x}{\cos\varphi_x}:\frac{\cos\psi_y}{\cos\varphi_y}:\frac{\cos\psi_z}{\cos\varphi_z}, \tag{3.10}$$

where ψ_x, ψ_y, ψ_z are the angles between the normal to the face and axes X, Y, Z.

There is also a purely graphical method of indexing based on the zone law (3.4). Indeed, two faces determine, by (3.5), the zone, i.e., the great circle, corresponding to edge $[p_1p_2p_3]$. On the other hand, the intersection of two zones determines, by (3.6), the indices of the possible face. The new face, in turn, can be used for constructing one more zone, etc. This procedure is called zone development. Coincidence of the possible faces with the measured defines their indices.

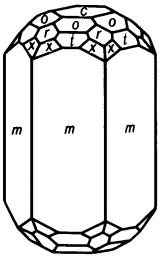

Fig. 3.25. Beryl $Be_3Al_2(SiO_3)_6$; $a:c = 1:0.4989$.
Combination of a pinacoid $c\{0001\}$ with a hexagonal prism $m\{10\bar{1}0\}$, three hexagonal bipyramids: $o\{10\bar{1}1\}$, $t\{20\bar{2}1\}$, and $r\{11\bar{2}1\}$ and a dihexagonal dipyramid $x\{\bar{3}211\}$

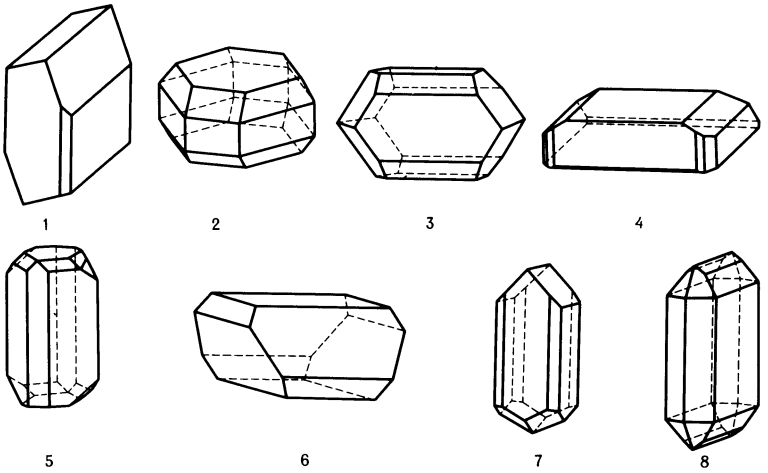

Fig. 3.26. Examples of crystal habit representing all the 32 crystallographic classes.
1 – 1 (calcium sulphate hexahydrate $CaSO_4 \cdot 6H_2O$); 2 – $\bar{1}$ [boric acid $B(OH_3)$]; 3 – 2 [dextra tartaric ammonium $(NH_4)_2C_4H_4O_6$]; 4 – m (paratoluidoisobutyric ester $CH_3 \cdot C_6H_4 \cdot NH \cdot C(CH_3)_2 \cdot CO_2 \cdot C_2H_5$); 5 – $2/m$ (β-sulphur); 6 – 222 (silver nitrate $AgNO_3$); 7 – $mm2$ [triphenylmethane $CH(C_6H_5)_3$; 8 – mmm (potassium nitrate KNO_3);

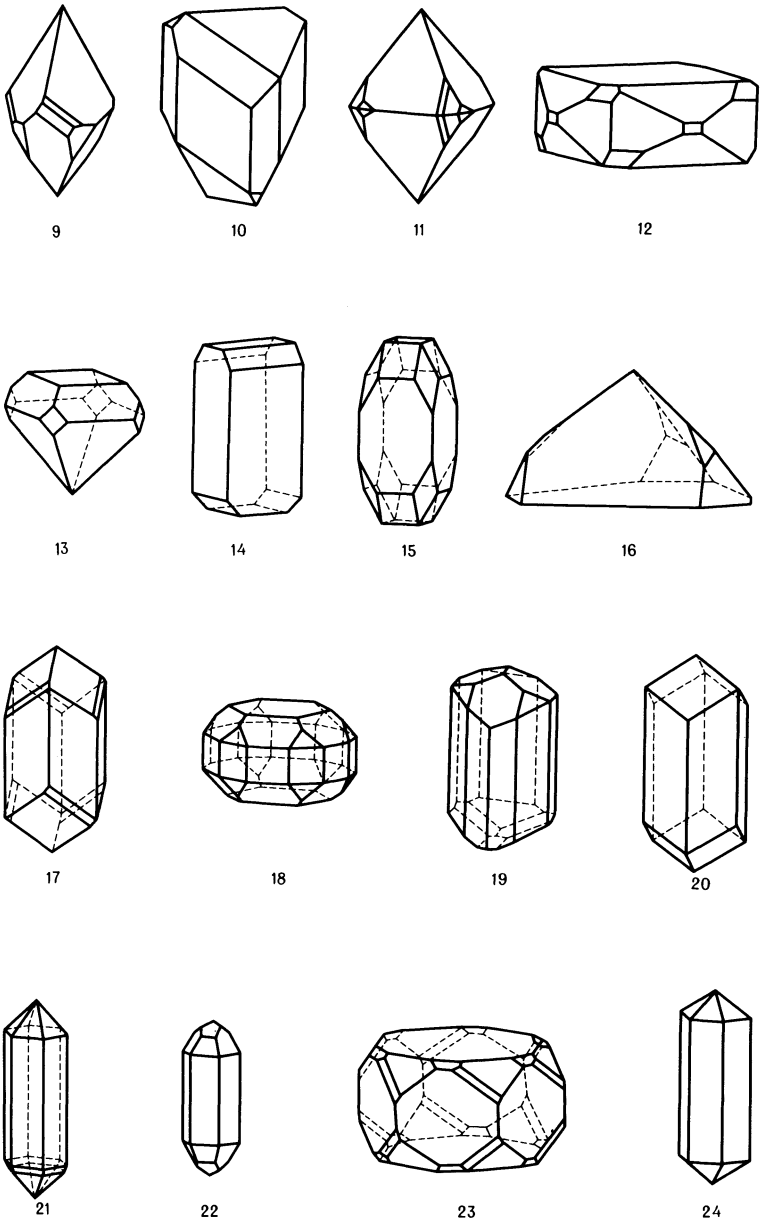

Fig. 3.26 (continued). 9 – 4(wulfenite $PbMoO_4$); 10 – $\bar{4}$ (kaneite $Co_4\,B_2As_2O_{12}\cdot 4H_2O$); 11 – 4/*m* (scheelite $CaWO_4$); 12 – 422 (potassium trichloroacetate $K[Cl_3\,CCO_2]$); 13 – 4*mm* (pentaeritrite $C_5H_{12}O_4$); 14 – $\bar{4}2m$ (urea CH_4N_2O); 15 – 4/*mmm* (calomel Hg_2Cl_2); 16 – 3 (sodium periodate $Na_2I_2O_8\cdot 6H_2O$); 17 – $\bar{3}$ (dioptase CuH_2SiO_4); 18 – 32 (potassium dithionate $K_2S_2O_6$); 19 – 3*m* (tourmaline $NaMg_3Al_6\,[(OH_4)(BO_3)_3Si_6O_{18}]$); 20 – $\bar{3}m$ (hydroquinone $C_6H_6O_2$); 21 – 6 [right-handed strontium antimonyl tartrate $Sr(SbO)_2\,(C_4H_4O_6)_2$]; 22 – $\bar{6}$ (silver biphosphate $(Ag_2\cdot HPO_4)$; 23 – 6/*m* (apatite $Ca_5\,[(OH,Cl\cdot F)/(PO_4)_3]$); 24 – 622 (potassium silicomolybdate $K_4MoO_{12}SiO_{40}$);

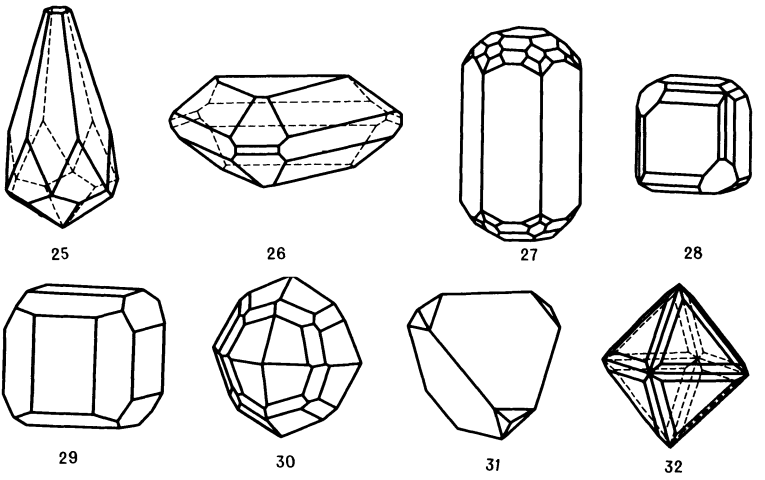

Fig. 3.26 (continued). 25 – $6mm$ (silver iodide AgI); 26 – $\bar{6}m2$ (benitoite BaTi $[Si_3O_9]$);27 – $6/mmm$ [beryl $Be_3Al_2(Si_6O_{18})$]; 28 – 23 (right-handed sodium chlorate $NaClO_3$); 29 – $m\bar{3}$ (pyrite FeS_2); 30 – 432 (ammonium chloride NH_4Cl); 31 – $\bar{4}3m$ [grey ore $(SbAs)_2$ $(Cu_2FeZn)_4S_7$]; 32 – $m\bar{3}m$ (lead glance PbS)

A detailed description of the method and calculations in goniometry can be founded in many manuals on crystallography. As an example, Fig. 3.25 shows the perfect form of a beryl, $Be_3Al_2(SiO_3)_6$, and describes its simple forms.

Examples of the habit of crystals representing each of the 32 crystallographic classes K are given in Fig. 3.26.

3.4 Lattice Geometry

3.4.1 Straight Lines and Planes of the Lattice

A space lattice is a system of points situated at the ends of vectors $\boldsymbol{t}$(3.2),

$$\boldsymbol{t}_{p_1p_2p_3} = p_1\boldsymbol{a}_1 + p_2\boldsymbol{a}_2 + p_3\boldsymbol{a}_3,$$

constructed from three coordinate noncoplanar vectors $\boldsymbol{a}_1, \boldsymbol{a}_2, \boldsymbol{a}_3$, which determine the primitive cell. This expression is basic to geometric crystallography; from it follows, in particular, the law of rational parameters.

Thus, an infinite lattice $T(\boldsymbol{x})$ can be described as

$$T(\boldsymbol{x}) = \sum_{p_1} \sum_{\substack{p_2 \\ -\infty}}^{+\infty} \sum_{p_3} \delta(x - p_1a_1,\, y - p_2a_2,\, z - p_3a_3)$$

$$= \sum_{\substack{p_1p_2p_3 \\ -\infty}}^{+\infty} \delta(\boldsymbol{r} - \boldsymbol{t}_{p_1p_2p_3}), \tag{3.11}$$

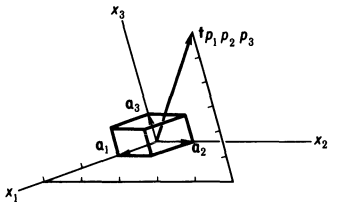

Fig. 3.27. Vector $t_{p_1p_2p_3}$ determining the line $[p_1p_2p_3]$ ($p_1 = 3, p_2 = 5, p_3 = 6$) assigned in a coordinate system with unit vectors $\boldsymbol{a}_1, \boldsymbol{a}_2, \boldsymbol{a}_3$

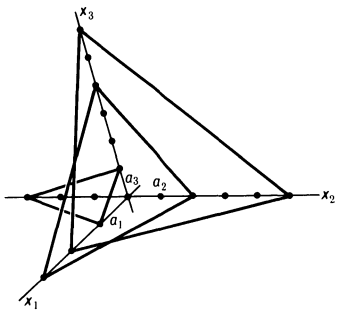

Fig. 3.28. Planes with the Weiss indices p_1, p_2, p_3 (256), (324), ($1\bar{3}1$)

where the δ-function is equal to unity at the points $\boldsymbol{r} = \boldsymbol{t}_{p_1}\, \boldsymbol{t}_{p_2}\, \boldsymbol{t}_{p_3}$ and to zero at all the other points.

Hence each point is characterized by a triplet of integers p_1, p_2, p_3. One can draw straight lines through points, which are called rows; and planes, which are called lattice nets. The position of a row can conveniently be defined by a pair of neighboring points through which it passes. In particular, if one of them is taken as initial (Fig. 3.27), then the other, p_1, p_2, p_3 defines such a line, and its symbol $[p_1, p_2, p_3]$ is a triad of indices in square brackets.

The position of a plane is defined by three noncollinear points. If three such points lie on reference axes, the plane makes the following intercepts on them: p_1a_2 on the first, p_2a_2 on the second, and p_3a_3 on the third, and the triad of numbers p_1, p_2, p_3 are in this case the Weiss indices of the plane (Fig. 3.28).

Because of the periodicity of the lattice (3.2) the rows and nets contain an infinite number of points. It is clear that any pair of intersecting or parallel rows defines the net whereas any pair of intersecting nets defines the row. Indices $p_1p_2p_3$, or any values derived from them, are sufficient for describing the lattice unless one is interested in the metric characteristics of the crystal. If one wishes to calculate the distances, angles, etc., the absolute values of unit translations a_i should be known, according to (3.2).

3.4.2 Properties of Planes

Suppose there is a plane with Weiss indices p_1, p_2, p_3 (Fig. 3.28). Its equation has the form

$$\frac{x_1}{p_1a_1} + \frac{x_2}{p_2a_2} + \frac{x_3}{p_3a_3} = 1, \tag{3.12}$$

and if we express the coordinates in axial units $x'_i = x_i/a_i$, then

$$\frac{x'_1}{p_1} + \frac{x'_2}{p_2} + \frac{x'_3}{p_3} = 1.$$

This can be rewritten

$$hx'_1 + kx'_2 + lx'_3 = p, \tag{3.13}$$

where

$$h = h_1 = p_2p_3, \quad k = h_2 = p_1p_3, \quad l = h_3 = p_1p_2, \quad p = p_1p_2p_3. \tag{3.14}$$

The triplets of integers h, k, l or h_1, h_2, h_3 are Miller indices or, as is customary to say, simply the indices of planes or faces. Indices h_i (as well as indices p_i) may be either positive or negative. The symbol of the lattice planes is the same as that of the faces: (hkl), a triad of indices enclosed in parentheses. But, distinct from faces, when the common divisor of the indices (if it exists) is cancelled, in analysis of planes in atomic structures of crystals this is not the case; for instance, one may write (422) for a plane; face (211) corresponds to this plane.

Through each lattice point it is possible to draw a plane with indices $(h_1h_2h_3)$; it will be parallel to the plane given by (3.13). The two-dimensional case ($p_1 = 2$, $p_2 = 3$, $h_1 = 3$, $h_2 = 2$) is depicted in Fig. 3.29 and the three-dimensional plane (324) – in Fig. 3.30. For plane $(h_1h_2h_3)$ passing through the origin

$$h_1x'_1 + h_2x'_2 + h_3x'_3 = 0\,, \tag{3.15}$$

which is precisely the equation of the face.

Let us see how many planes $(h_1h_2h_3)$ are between the zero (3.15) and the pth (3.13) planes. The translation a_1 repeats the zero plane (3.15) p_1 times, i.e., through the points lying on axis X it is possible to draw p_1 planes ($p_1 = 2$ in Fig. 3.29), and this set will be repeated p_2 times by translation a_2($p_2 = 3$ in Fig. 3.29), and their total number in the two-dimensional case is equal to p_1p_2, while in the three-dimensional it is $p_1p_2p_3$ due to the repetition p_3 times by translation a_3. Each of the planes contains translationally equal (i.e., parallel

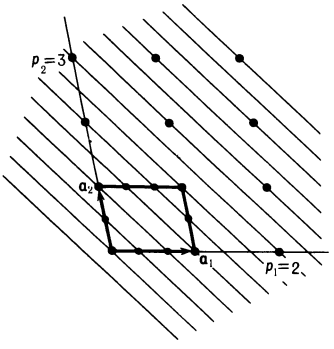

Fig. 3.29. Relationship between the Weiss (p_1, p_2) and Miller (h_1, h_2) indices in the two-dimensional case ($p_1 = 2$, $p_2 = 3$, $h_1 = 3$, $h_2 = 2$)

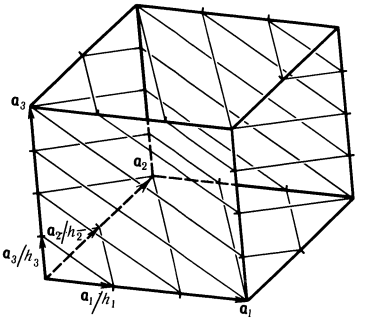

Fig. 3.30. Family of lattice planes with Miller indices: $h_1 = 3$, $h_2 = 2$, $h_3 = 4$

and equally spaced) nets consisting of an infinite number of points. Thus, any integers $p = 0, \pm 1, \pm 2, \ldots$ are possible in (3.13). When in (3.15) $x_i' = p_i$, i.e., when x_i' are integers (p_1 are the indices of vectors $\boldsymbol{t}_{p_1p_2p_3}$, and thus of the possible edges), we obtain the condition for $\boldsymbol{t}_{p_1p_2p_3}$, to lie in the plane – face $(h_1h_2h_3)$,

$$h_1p_1 + h_2p_2 + h_3p_3 = 0,$$

i.e., the zone law (3.4).

Depending on the particular values of h_1, h_2, h_3, in the general case several planes of this family pass within a unit cell (see Figs. 3.29, 30), thus dividing the edges of the primitive cell and its diagonals into certain equal segments according to the rules: edges $\boldsymbol{a}_1, \boldsymbol{a}_2, \boldsymbol{a}_3$ are cut into h_1, h_2, h_3 parts, respectively; the face diagonals, into $h_2 + h_3$, $h_3 + h_1$, $h_1 + h_2$ parts; and the body diagonal, into $h_1 + h_2 + h_3$ parts.

Indeed, for the plane $(h_1h_2h_3)$ nearest to the origin, in (3.13) $p = 1$, and the intercepts made by this plane on the axes are equal to $x_i' = 1/h_i$ (or $x_i = a_i/h_i$, Figs. 3.29, 30). The rules for the diagonals can be obtained in the same way.

3.4.3 Reciprocal Lattice

The distance between a pair of neighboring planes of the (hkl) family is called an interplanar spacing and is denoted by d_{hkl}. It is measured along the normal to plane (hkl) and depends on the metric parameters $\boldsymbol{a}_1, \boldsymbol{a}_2, \boldsymbol{a}_3$ of the unit cell.

Let us construct a normal vector $\boldsymbol{H}_{hkl}$ to each plane (hkl) and define its length as the reciprocal of the interplanar distance d_{hkl}:

$$|\boldsymbol{H}_{hkl}| = d_{hkl}^{-1}. \tag{3.16}$$

In the general case of the oblique unit cell (Fig. 3.31) the normal to the coordinate plane is given by a vector product of the type $[\boldsymbol{a}_i\boldsymbol{a}_j]$ – a vector whose modulus is equal to the area of face a_ia_j of the cell, and the distances between the coordinate planes are the quotients of division of the cell volume by the area of this face. The cell volume is defined by the mixed product.

$$\Omega = \boldsymbol{a}_1[\boldsymbol{a}_2\boldsymbol{a}_3] = \boldsymbol{a}_2[\boldsymbol{a}_3\boldsymbol{a}_1] = \boldsymbol{a}_3[\boldsymbol{a}_1\boldsymbol{a}_2]. \tag{3.17}$$

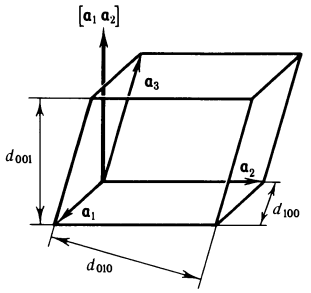

Fig. 3.31. Interplanar distances d_{100}, d_{010}, d_{001}, and normal $[\boldsymbol{a}_1\boldsymbol{a}_2]$ to (001) plane in the general case of an oblique cell

Thus,

$$d_{100} = \frac{\Omega}{|[\boldsymbol{a}_2\boldsymbol{a}_3]|}, \quad d_{010} = \frac{\Omega}{|[\boldsymbol{a}_3\boldsymbol{a}_1]|}, \quad d_{001} = \frac{\Omega}{|[\boldsymbol{a}_1\boldsymbol{a}_2]|}. \tag{3.18}$$

This defines, by (3.16), the three vectors $\boldsymbol{H}_{100} = \boldsymbol{a}_1^*$, $\boldsymbol{H}_{010} = \boldsymbol{a}_2^*$, $\boldsymbol{H}_{001} = \boldsymbol{a}_3^*$:

$$\boldsymbol{a}_1^* = \frac{[\boldsymbol{a}_2\boldsymbol{a}_3]}{\Omega}, \quad \boldsymbol{a}_2^* = \frac{[\boldsymbol{a}_3\boldsymbol{a}_1]}{\Omega}, \quad \boldsymbol{a}_3^* = \frac{[\boldsymbol{a}_1\boldsymbol{a}_2]}{\Omega}, \tag{3.19}$$

normal to the coordinate planes. Hence,

$$d_{100} = a_1^{*-1}, \quad d_{010} = a_2^{*-1}, \quad d_{001} = a_3^{*-1} \tag{3.20}$$

(Fig. 3.31). In the particular case of orthogonal lattices (Fig. 3.32)

$$a_1^* = a_1^{-1} = d_{100}^{-1}, \quad a_2^* = a_2^{-1} = d_{010}^{-1}, \quad a_3^* = a_3^{-1} = d_{001}^{-1}. \tag{3.21}$$

From (3.19) it follows that

$$\boldsymbol{a}_i\boldsymbol{a}_j^* = \begin{cases} 1, & i = j, \quad (3.22a) \\ 0, & i \neq j. \quad (3.22b) \end{cases}$$

Let us now find $\boldsymbol{H}$ for an arbitrary plane with Miller indices $(h_1h_2h_3)$ (Fig. 3.33), repeating the same procedure as for the coordinate planes, but with an additional construction. In place of the unit cell we consider a small cell with basis vectors

$$\boldsymbol{a}_1' = \frac{\boldsymbol{a}_1}{h_1} - \frac{\boldsymbol{a}_3}{h_3}, \quad \boldsymbol{a}_2' = \frac{\boldsymbol{a}_2}{h_2} - \frac{\boldsymbol{a}_3}{h_3}, \quad \boldsymbol{a}_3' = \frac{\boldsymbol{a}_3}{h_3}. \tag{3.23}$$

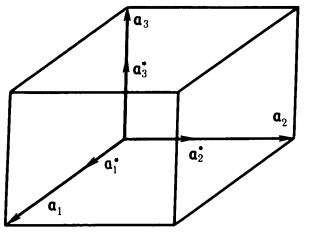

Fig. 3.32. Coincidence in the directions of the basis vectors $\boldsymbol{a}_1$, $\boldsymbol{a}_2$, and $\boldsymbol{a}_3$ of direct and $\boldsymbol{a}_1^*$, $\boldsymbol{a}_2^*$, and $\boldsymbol{a}_3^*$ of reciprocal lattice in an orthogonal cell

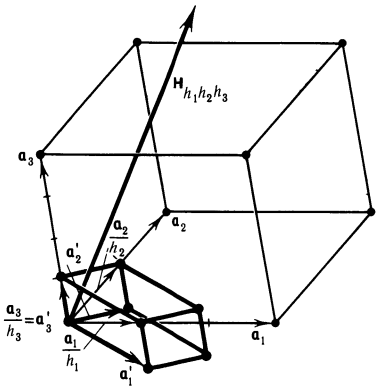

Fig. 3.33. General case of construction of vector $\boldsymbol{H}_{h_1h_2h_3}$ which is normal to plane $(h_1h_2h_3)$ ($h_1 = 3$, $h_2 = 2$, $h_3 = 4$)

Vectors $\boldsymbol{a}_1'$ and $\boldsymbol{a}_2'$ lie in plane $(h_1h_2h_3)$, and the vector product $[\boldsymbol{a}_1'\boldsymbol{a}_2']$ defines the direction of $\boldsymbol{H}_{h_1h_2h_3}$ and the area of small face, while $\Omega = \boldsymbol{a}_3'[\boldsymbol{a}_1'\boldsymbol{a}_2']$, i.e.,

$$d_{h_1h_2h_3} = \frac{\Omega'}{|[\boldsymbol{a}_1'\boldsymbol{a}_2']|}, \quad \boldsymbol{H}_{h_1h_2h_3} = \frac{[\boldsymbol{a}_1'\boldsymbol{a}_2']}{\Omega'}. \tag{3.24}$$

Using (3.22) and (3.23), we find that $[\boldsymbol{a}_1'\boldsymbol{a}_2'] = (h_1\boldsymbol{a}_1^* + h_2\boldsymbol{a}_2^* + h_3\boldsymbol{a}_3^*)\,\Omega'$, $\Omega' = \Omega/hkl$, i.e., that

$$\boldsymbol{H}_{hkl} = h_1\boldsymbol{a}_1^* + h_2\boldsymbol{a}_2^* + h_3\boldsymbol{a}_3^*. \tag{3.25}$$

We obtain a remarkable result: the set of vectors $\boldsymbol{H}_{hkl}$ (3.25) is expressed in terms of basis vectors $\boldsymbol{a}_1^*$, $\boldsymbol{a}_2^*$, $\boldsymbol{a}_3^*$ with integral coordinates hkl, which are precisely the Miller indices of planes (hkl). In other words, the ends of vectors $\boldsymbol{H}_{hkl}$ form the lattice $T^*(S)$ constructed on the vectors $\boldsymbol{a}_1^*$, $\boldsymbol{a}_2^*$, $\boldsymbol{a}_3^*$ (Fig. 3.34) exactly as the

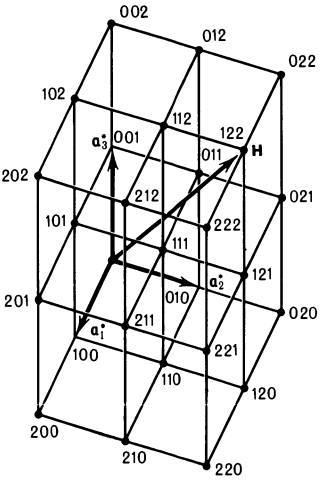

Fig. 3.34. Reciprocal lattice as a set of points with basis $\boldsymbol{a}_1^*$, $\boldsymbol{a}_2^*$, $\boldsymbol{a}_3^*$ and one of the vectors $\boldsymbol{H}$ in it ($\boldsymbol{H}_{122}$)

vector of space lattice $\boldsymbol{t}_{p_1p_2p_3}$ (2) forms the lattice $T(\boldsymbol{x})$ constructed on the vectors $\boldsymbol{a}_1$, $\boldsymbol{a}_2$, $\boldsymbol{a}_3$ (Fig. 3.27),

$$T^*(\boldsymbol{S}) = \sum_{\substack{hkl \\ -\infty}}^{+\infty} \delta(\boldsymbol{S} - \boldsymbol{H}_{hkl}), \tag{3.26}$$

where δ is the delta function.

A lattice having a vector $\boldsymbol{H}_{hkl}$ with basic vectors $\boldsymbol{a}_1^*$, $\boldsymbol{a}_2^*$, $\boldsymbol{a}_3^*$ is called the *reciprocal lattice*, vectors $\boldsymbol{a}_1^*$, $\boldsymbol{a}_2^*$, $\boldsymbol{a}_3^*$ (which are also labelled $\boldsymbol{a}^*$, $\boldsymbol{b}^*$, $\boldsymbol{c}^*$) are called the coordinate vectors of the reciprocal lattice; they are the edges of the unit cell of the reciprocal lattice. From (3.22) and (3.25) follows

$$\boldsymbol{H}_{hkl}\boldsymbol{a}_1/h_1 = 1, \quad \boldsymbol{H}_{hkl}\boldsymbol{a}_2/h_2 = 1, \quad \boldsymbol{H}_{hkl}\boldsymbol{a}_3/h_3 = 1. \tag{3.27}$$

The reciprocal lattice is defined in three-dimensional reciprocal space having dimensionality of "reciprocal-lengths". If one has to distinguish the initial lattice of the crystal, defined in real space, from the reciprocal lattice, the former is called an "atomic" or "direct" lattice.

From (3.22) it follows that the atomic lattice is the reciprocal to the reciprocal lattice, i.e. they are reciprocals, and it is possible to replace the asterisked symbols in (3.19) by those without asterisks, and vice versa, for instance Ω is replaced Ω^*, which is calculated using (3.17) when $\boldsymbol{a}_i$ is replaced by $\boldsymbol{a}_i^*$. Expression (3.22a) shows the mutual reciprocity of equally denoted coordinate vectors of the two lattices, and (3.22b), the perpendicularity of any pair of differently denoted coordinate vectors of these lattices.

The relationship of the atomic and reciprocal lattices can also be formulated as follows: straight lines – rows in one lattice are perpendicular to the planes with the same indices in the other, the distances between the points in one are reciprocal to the interplanar spacings in the other.

It follows, for instance, that a bundle of normals to the nets of an atomic lattice – faces – is a bundle of straight lines of points in the reciprocal lattice, and vice versa; that the rows of points of the atomic lattice are perpendicular to the nets of the reciprocal lattice, etc. All this enables one to write down straightforwardly, using vector $\boldsymbol{H}_{hkl}$(3.16, 25), many relations characterizing the atomic lattice. Thus, the equations of the plane (3.13) and (3.15) are rewritten simply as a scalar product of vector $\boldsymbol{r}$, whose end is on this plane, and vector $\boldsymbol{H}$,

$$\boldsymbol{r}\boldsymbol{H} = P, \quad \boldsymbol{r}\boldsymbol{H} = 0,$$

and the zone law (3.4), as

$$\boldsymbol{t}_{p_1p_2p_3}(\boldsymbol{H}_{hkl}/H_{hkl}) = 0. \tag{3.28}$$

We have derived the reciprocal lattice proceeding from the assignment of vector $\boldsymbol{H}_{hkl}$ normal to plane (hkl) of the atomic lattice and equal in length to d_{hkl}^{-1} (3.16), and have obtained its properties (3.19, 22, 25). Conversely, the reciprocal lattice can be derived from (3.19) or from (3.22) and acquires the properties of (3.16) and (3.27). One more derivation of the reciprocal lattice arises automatically in consideration of diffraction phenomena (Chap. 4).

The reciprocal lattice is an important mathematical image which finds numerous applications in geometric crystallography, in diffraction theory and structure analysis of crystals, and in solid-state physics.

3.5 Lattice Transformations

3.5.1 Transformation of Coordinates and Indices in the Atomic and Reciprocal Lattices

The unit cell in the lattice can be chosen in an infinite number of ways, and any such cell can be transformed into any other (Fig. 3.35). In practice it is important to pass from an arbitrary unit cell to the one assigned by the rules of symmetry for a given syngony (Table 3.5) or by the reduction algorithm (see Sect. 3.5.2). It may also be necessary sometimes to change from one unit cell of a given crystal to another, for instance from centered to primitive, or from a rhombohedral description to hexagonal, etc. In x-ray investigation of crystals it is necessary to establish the relationship between the intrinsic crystallographic coordinate system of a crystal and the orthogonal coordinate system of an instrument. In such transformations from one coordinate system to another, the point coordinates and the indices of lines and planes also change. Let us see how their new values are expressed in terms of the old.

Denoting the new axes by $\boldsymbol{A}_i$ [they are vectors of lattice (3.2)] and the old by $\boldsymbol{a}_i$, we get

$$\begin{aligned} \boldsymbol{A}_1 &= \alpha_{11}\boldsymbol{a}_1 + \alpha_{12}\boldsymbol{a}_2 + \alpha_{13}\boldsymbol{a}_3, \\ \boldsymbol{A}_2 &= \alpha_{21}\boldsymbol{a}_1 + \alpha_{22}\boldsymbol{a}_2 + \alpha_{23}\boldsymbol{a}_3, \\ \boldsymbol{A}_3 &= \alpha_{31}\boldsymbol{a}_1 + \alpha_{32}\boldsymbol{a}_2 + \alpha_{33}\boldsymbol{a}_3, \end{aligned} \tag{3.29}$$

i.e. $\boldsymbol{A}_i = (\alpha_{ik})\,\boldsymbol{a}_k$,

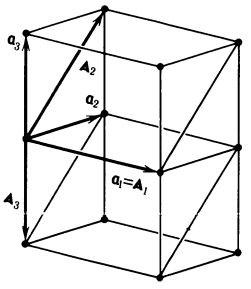

Fig. 3.35. Example of selection of a new cell with basis vectors $\boldsymbol{A}_1$, $\boldsymbol{A}_2$, $\boldsymbol{A}_3$ in a lattice assigned previously by vectors $\boldsymbol{a}_1$, $\boldsymbol{a}_2$, $\boldsymbol{a}_3$

where (α_{ik}) is the transformation matrix. In turn,

$$\begin{aligned} \boldsymbol{a}_1 &= \beta_{11}\boldsymbol{A}_1 + \beta_{12}\boldsymbol{A}_2 + \beta_{13}\boldsymbol{A}_3, \\ \boldsymbol{a}_2 &= \beta_{21}\boldsymbol{A}_1 + \beta_{22}\boldsymbol{A}_2 + \beta_{23}\boldsymbol{A}_3, \\ \boldsymbol{a}_3 &= \beta_{31}\boldsymbol{A}_1 + \beta_{32}\boldsymbol{A}_2 + \beta_{33}\boldsymbol{A}_3, \end{aligned} \tag{3.30}$$

i.e. $\boldsymbol{a}_i = (\beta_{ik})\,\boldsymbol{A}_k$,

where (β_{ik}) is a transformation matrix reciprocal to (α_{ik}).

The coefficients of the direct and reciprocal matrices satisfy the relations

$$\left.\begin{aligned} &\alpha_{1i}\beta_{k1} + \alpha_{2i}\beta_{k2} + \alpha_{3i}\beta_{k3} \\ &\alpha_{i1}\beta_{1k} + \alpha_{i2}\beta_{2k} + \alpha_{i3}\beta_{3k} \end{aligned}\right\} = 1(i = k) \text{ or } 0(i \neq k). \tag{3.31}$$

This is easy to check by substituting into (3.30), in place of $\boldsymbol{A}_k$, their expressions in terms of $\boldsymbol{a}_i$ in accordance with (3.29).

The radius vector of point X_1, X_2, X_3 (which was x_1, x_2, x_3 in the old system) is invariant to a change in the reference system

$$\begin{aligned} \boldsymbol{r} &= x_1\boldsymbol{a}_1 + x_2\boldsymbol{a}_2 + x_3\boldsymbol{a}_3, \\ \boldsymbol{R} &= X_1\boldsymbol{A}_1 + X_2\boldsymbol{A}_2 + X_3\boldsymbol{A}_3. \end{aligned} \tag{3.32}$$

Whence, at $\boldsymbol{r} = \boldsymbol{R}$, we find by (3.30):

$$\begin{aligned} X_1 &= \beta_{11}x_1 + \beta_{21}x_2 + \beta_{31}x_3, \\ X_2 &= \beta_{12}x_1 + \beta_{22}x_2 + \beta_{32}x_3, \\ X_3 &= \beta_{13}x_1 + \beta_{23}x_2 + \beta_{33}x_3, \end{aligned} \tag{3.33}$$

i.e. $\mathbf{X}_i = (\beta_{ki})\,x_k$.

Rows β in (3.30) have become columns in (3.33); matrix (β_{ik}) has been reflected through its diagonal and become a transposed matrix (β_{ki}). Such a transformation is called *countervariant* in contrast to the *covariant* transformation (3.29, 30). Similarly, from (3.29, 32) we obtain

$$x_i = (\alpha_{ki})\,X_k. \tag{3.34}$$

In a particular case, if $\boldsymbol{r} = \boldsymbol{R}$, and in (3.32) the vector of lattice (3.2) $\boldsymbol{t} = \boldsymbol{T}$, then x_i are the indices of p_i straight lines in the old system, and also X_i are the indices of P_i straight lines in the new. Therefore, relations (3.33) and (3.34) also hold for the transformation of the indices of the straight lines,

$$P_i = (\beta_{ki})\,p_k, \tag{3.35}$$

$$p_i = (\alpha_{ki})\,P_k. \tag{3.36}$$

Let us now consider the transformation of the indices of planes $h_1h_2h_3$ (old ones) into the new $H_1H_2H_3$. To do this, we substitute (3.34) into (3.15) for the

nodal plane and collect the terms with X_1, X_2, X_3:

$$(\alpha_{11}h_1 + \alpha_{12}h_2 + \alpha_{13}h_3)\,X_1 + (\alpha_{21}h_1 + \alpha_{22}h_2 + \alpha_{23}h_3)\,X_2 + (\alpha_{31}h_1 + \alpha_{32}h_2 + \alpha_{33}h_3)\,X_3 = 0. \tag{3.37}$$

Thus,

$$H_i = (\alpha_{ik})\,h_k, \quad h_i = (\beta_{ik})\,H_k. \tag{3.38}$$

We have at once the reciprocal relation, which is obtained similarly to (3.37). These transformations are the same as (3.29, 30); they are covariant.

Let us now find the rules for transforming the vectors of the reciprocal lattice, using the relation (3.22) and set up the expression

$$\sum_{i=1}^{3} \boldsymbol{a}_i \boldsymbol{a}_i^* = 3 = \sum_{i=1}^{3} \boldsymbol{A}_i \boldsymbol{A}_i^*. \tag{3.39}$$

Denoting $\boldsymbol{a}_i$ by $\boldsymbol{A}_k$ on the left by (3.29) or $\boldsymbol{A}_i$ by $\boldsymbol{a}_k$ on the right by (3.30), we find

$$\boldsymbol{a}_i^* = (\alpha_{ki})\,\boldsymbol{A}_k^*, \quad \boldsymbol{A}_i^* = (\beta_{ki})\,\boldsymbol{a}_k^*. \tag{3.40}$$

These transformations are countervariant, and they all have the same coefficients α and β. Finally, for coordinates x_i^* and X_i^* in the reciprocal space, as well as for indices h_i and H_i (3.38), which are also the indices of the straight lines in the reciprocal lattice

$$X_i^* = (\alpha_{ik})\,x_k^*, \quad x_i^* = (\beta_{ik})\,X_k^*, \tag{3.41}$$

i.e., the transformations are covariant.

When setting a crystal in x-ray crystallography, one expresses the coordinates of nodes $h_1h_2h_3$ in the reciprocal space in the Cartesian system X_i^* ($X_1^* = X^*$, $X_2^* = Y^*$, $X_3^* = Z^*$). By analogy with (3.41)

$$X_i^* = (\alpha_{ik})\,h_k, \quad h_i = (\beta_{ik})\,X_k^*, \text{ where} \tag{3.42}$$

$$(\beta_{ik}) = \begin{Vmatrix} a_x & a_y & a_z \\ b_x & b_y & b_z \\ c_x & c_y & c_z \end{Vmatrix}. \tag{3.43}$$

The elements of this matrix are the projections of the edges of the reciprocal unit cell onto orthogonal axes.

We can see that all the transformations in the reciprocal lattice are opposite in variance (covariant vs countervariant) to similar transformations in an atomic lattice. Within each of these lattices, the transformations of the axes and of the indices of the planes, on the one hand, and of the coordinates or the indices of the lines, on the other, are opposite in variance. The rules of mutual reciprocity

of the two lattices are fulfilled automatically here: the indices of the lines in one are the indices of the planes in the other.

These transformations can be written in a unified symbolic form

$$\begin{array}{l} \\ H_1A_1 = \\ H_2A_2 = \\ H_3A_3 = \\ \\ \\ \end{array} \begin{array}{c} \longrightarrow h_1 \quad h_2 \quad h_3 \\ \longrightarrow \boldsymbol{a}_1 \quad \boldsymbol{a}_2 \quad \boldsymbol{a}_3 \\ \left\| \begin{array}{ccc} \alpha_{11} & \alpha_{12} & \alpha_{13} \\ \alpha_{21} & \alpha_{22} & \alpha_{23} \\ \alpha_{31} & \alpha_{32} & \alpha_{33} \end{array} \right\| \\ \| \quad \| \quad \| \\ \boldsymbol{a}_1^* \quad \boldsymbol{a}_2^* \quad \boldsymbol{a}_3^* \\ x_1 \quad x_2 \quad x_3 \end{array} \begin{array}{l} \\ A_1^* X_1 \\ A_2^* X_2 \\ A_3^* X_3 \\ \\ \\ \end{array} , \tag{3.44}$$

$$\begin{array}{l} \\ h_1a_1 = \\ h_2a_2 = \\ h_3a_3 = \\ \\ \\ \end{array} \begin{array}{c} \longrightarrow H_1 \quad H_2 \quad H_3 \\ \longrightarrow \boldsymbol{A}_1 \quad \boldsymbol{A}_2 \quad \boldsymbol{A}_3 \\ \left\| \begin{array}{ccc} \beta_{11} & \beta_{12} & \beta_{13} \\ \beta_{21} & \beta_{22} & \beta_{23} \\ \beta_{31} & \beta_{32} & \beta_{33} \end{array} \right\| \\ \| \quad \| \quad \| \\ \boldsymbol{A}_1^* \quad \boldsymbol{A}_2^* \quad \boldsymbol{A}_3^* \\ X_1 \quad X_2 \quad X_3 \end{array} \begin{array}{l} \\ a_1^* x_1 \\ a_2^* x_2 \\ a_3^* x_3 \\ \\ \\ \end{array} , \tag{3.45}$$

It will be noted that X_i^* and x_i^* (3.41) are transformed into one another in the same way as H_i and h_i, while P_i and p_i (3.35, 36), are transformed as X_i and x_i. The symbol $\longrightarrow$ corresponds to covariant transformations, and the symbol $\longrightarrow$, to countervariant.

The volumes of unit cells assigned by vectors $\boldsymbol{A}$ and $\boldsymbol{a}$ and those of the respective reciprocal cells relate as

$$\Omega_A : \Omega_a = |\alpha_{ik}| : 1 = 1 : |\beta_{ik}| = n = \Omega_{a*} : \Omega_{A*}, \tag{3.46}$$

i.e., this ratio is defined by the moduli of the determinants of the transformation matrices and is equal to n – the ratio of the number of points in the respective cells. If a is a primitive cell, then n is the number of points in a large, nonprimitive cell A.

Let us consider examples of some transformations. For instance, if $\boldsymbol{A}_1 = \boldsymbol{a}_1$, $\boldsymbol{A}_2 = \boldsymbol{a}_2 + \boldsymbol{a}_3$, $\boldsymbol{A}_3 = -\boldsymbol{a}_3$ (Fig. 3.35), the matrix takes the form

$$\left\| \begin{array}{ccc} 1 & 0 & 0 \\ 0 & 1 & 1 \\ 0 & 0 & \bar{1} \end{array} \right\| \tag{3.47}$$

The matrices of some transformations between primitive P, body-centered I, and face-centered F cells are as follows:

$$P \to I \qquad I \to P \qquad P \to F \qquad F \to P$$

$$\left\| \begin{matrix} -\frac{1}{2} & \frac{1}{2} & \frac{1}{2} \\ \frac{1}{2} & -\frac{1}{2} & \frac{1}{2} \\ \frac{1}{2} & \frac{1}{2} & -\frac{1}{2} \end{matrix} \right\|, \quad \left\| \begin{matrix} 0 & 1 & 1 \\ 1 & 0 & 1 \\ 1 & 1 & 0 \end{matrix} \right\|, \quad \left\| \begin{matrix} 0 & \frac{1}{2} & \frac{1}{2} \\ \frac{1}{2} & 0 & \frac{1}{2} \\ \frac{1}{2} & \frac{1}{2} & 0 \end{matrix} \right\|, \quad \left\| \begin{matrix} \bar{1} & 1 & 1 \\ 1 & \bar{1} & 1 \\ 1 & 1 & \bar{1} \end{matrix} \right\|. \tag{3.48}$$

Another example is transition from a rhombohedral cell R to a hexagonal H of thrice its volume (Fig. 2.72)

$$H \to R \qquad R \to H$$

$$\left\| \begin{matrix} \frac{2}{3} & \frac{1}{3} & \frac{1}{3} \\ -\frac{1}{3} & \frac{1}{3} & \frac{1}{3} \\ -\frac{1}{3} & -\frac{2}{3} & \frac{1}{3} \end{matrix} \right\|, \quad \left\| \begin{matrix} 1 & \bar{1} & 0 \\ 0 & 1 & \bar{1} \\ 1 & 1 & 1 \end{matrix} \right\|. \tag{3.49}$$

3.5.2 Reduction Algorithm

Each lattice is uniquely defined by its unit cell. But in one and the same lattice it is possible to choose the unit cell in an infinite number of ways. As a result, the same crystal may receive geometrically different descriptions in experimental x-ray or goniometric investigations. Therefore, it is necessary to have criteria leading to an unambiguous description of the lattice by a certain unique cell, and an algorithm which permits transition from any cell of a given lattice to this unique, or "reduced", cell. This algorithm was given by *Delone* et al. [3.3].

In all crystals, with the exception of triclinic and monoclinic, the choice of such a cell can be made on the basis of symmetry, and the reduced cell is the Bravais parallelepiped. In a monoclinic cell the symmetry unambiguously defines one axis b, which coincides with 2 or is a normal to m. But in symmetric lattices, too, the initial choice of the cell may accidentally contradict the symmetry.

Let us consider *the reduction algorithm* (without proof). The metric and angular parameters of a unit cell are different in nature. Any cell is completely defined by its unit cell vectors and by the inversed body-diagonal vector $\boldsymbol{d}_0$

(Fig. 3.36), so that their sum is equal to zero

$$\boldsymbol{a}_0 + \boldsymbol{b}_0 + \boldsymbol{c}_0 + \boldsymbol{d}_0 = 0. \tag{3.50}$$

We shall describe the initial arbitrary cell by six homogeneous parameters given by the pairwise scalar products of the vectors appearing in (3.50):

$$\begin{aligned} P_0 &= b_0 c_0 \cos\alpha_0, \quad S_0 = a_0 d_0 \cos\psi_{0a}, \\ Q_0 &= c_0 a_0 \cos\beta_0, \quad T_0 = b_0 d_0 \cos\psi_{0b}, \\ R_0 &= a_0 b_0 \cos\gamma_0, \quad U_0 = c_0 d_0 \cos\psi_{0c}, \end{aligned} \tag{3.51}$$

where ψ are the angles between the edges and diagonal. Here,

$$\begin{aligned} a_0^2 &= -S_0 - Q_0 - R_0, \quad b_0^2 = -T_0 - R_0 - P_0, \\ c_0^2 &= -U_0 - P_0 - Q_0, \quad d_0^2 = -S_0 - T_0 - U_0. \end{aligned} \tag{3.52}$$

A reduced unit cell is a cell for which all the angles

$$\alpha, \beta, \gamma, \psi_a, \psi_b, \psi_c \geqq 90°. \tag{3.53}$$

Hence, in accordance with (3.51), for it, all the

$$P, Q, R, S, T, U \leqq 0. \tag{3.54}$$

On the other hand in the initial cell, from which we have to pass to a reduced cell, some angles may be acute, and some $P_0, \ldots, U_0$ (3.51) positive, respectively.

The reduction algorithm consists of the following. We place the identical parameters of the initial cell on the symbol

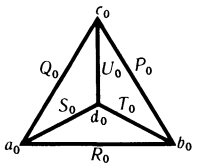

(3.55)

which can conveniently be thought of as the image of a tetrahedron whose vertices are vectors (3.50) and whose edges, joining the vertices, are the corresponding scalar products (3.51). We take, among the initial parameters, any positive one, say, Q_0 [if none is available, then the cell is already reduced in

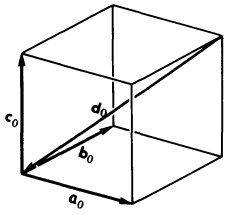

Fig. 3.36. Unit cell and inverse body diagonal $\boldsymbol{d}_0$

accordance with (3.54)], and switch to the new symbol according to the following scheme:

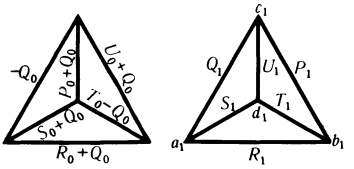

(3.56)

i.e., we have $Q_1 = -Q_0$, $U_1 = P_0 + Q_0$, etc. In the new hexad of parameters Q_1 is already negative. The rules for transition from (3.55) to (3.56) are as follows:

1) we subtract the chosen positive parameter from the parameter standing on the opposite edge ($T_0 - Q_0$);
2) we add it to all the other parameters ($S_0 + Q_0, \ldots$);
3) we interchange any two of the last four parameters and such as stand on edges converging at one of the vertices adjacent to the initial edge Q_0 (i.e., we interchange $P_0 + Q_0$ and $U_0 + Q_0$) in (3.56); and
4) we change the sign of the parameter under consideration.

This transition will produce new a_1, b_1, c_1, d_1, and angles; there is a certain corresponding transition matrix (3.29). In our example (3.56) $a_1 = a_0$, $b_1 = b_0 + c_0$, $c_1 = -c_0$, $d_1 = d_0 + c_0$, and the transition matrix is (3.47). Transformation (3.55, 56) must be repeated until we obtain a symbol with all nonpositive $P_n, \ldots, U_n \leqslant 0$ (3.54). The possible equality of some of them to zero means that the corresponding angles (3.51) are right angles.

The form of the terminal symbol – equality of certain $P, Q, \ldots, U$ to zero or to each other and their mutual arrangement – allocates the lattice to one of the 24 Delone varieties [3.3] (Fig. 2.89), and thus to one of the 14 Bravais groups. For instance, some of these symbols have the form

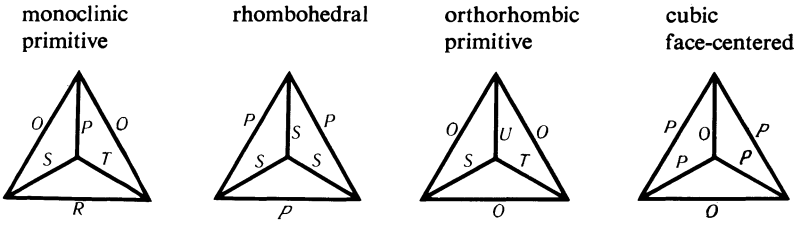

(3.57)

In addition to the tabulated symbols we can get another five symbols, which can be reduced to the tabulated by one reduction step through zero. According to definite rules the values of the reduced $\boldsymbol{a}, \boldsymbol{b}, \boldsymbol{c}, \boldsymbol{d}$ assign the basis vector $\boldsymbol{a}_{(B)}, \boldsymbol{b}_{(B)}, \boldsymbol{c}_{(B)}$ of the corresponding Bravais parallelepiped. This reduction does not necessarily yield the three shortest unit cell vectors [3.4–6], which define the so-called Buerger cell, but they are among the seven vectors, the reduced four vectors $\boldsymbol{a}, \boldsymbol{b}, \boldsymbol{c}, \boldsymbol{d}$, and $\boldsymbol{a} + \boldsymbol{b}, \boldsymbol{a} + \boldsymbol{c}, \boldsymbol{b} + \boldsymbol{c}$. For triclinic lattices we must select from among

them, as periods, the three shortest noncoplanar vectors. In primitive monoclinic lattices the reduced vectors include the vector running along axes 2, which gives one period, while the other two are chosen from among the shortest vectors of the plane net perpendicular to axes 2, which form an obtuse angle. If the monoclinic lattice is centered (on one of the rectangular faces), one chooses for the second period the least possible edge of the plane net perpendicular to axis 2, from which a centered side face is obtained, and for the third period, the shortest of the vectors of this plane net which makes an obtuse angle with the second period.

It should be noted that in some cases it is most expedient to choose a monoclinic or triclinic cell not only by following formally the geometric rules given by the reduction algorithm, but also by proceeding from the crystallochemical features of the structure. The directions of the axes will correspond to clearly revealed directions, for instance to those of the layers of polyhedra in layer silicates, some chains in crystals with a chain structure, etc.

In contrast to the unit cell of a crystal (in direct space) the angles of a reduced reciprocal cell are not obtuse: $\alpha^*, \beta^*, \gamma^* \leqslant 90°$. A reduced reciprocal cell can be found from a reduced direct cell.

3.5.3 Computation of Angles and Distances in Crystals

By using the vector formulae (3.2, 22, 25) and expanding the corresponding scalar products it is possible to obtain equations for determining angles in an atomic and reciprocal lattice, which are used, in particular, in geometric crystallography – see (3.6, 8). Thus from (3.27) it follows that the angle between the normal to the plane (face) (hkl) and the axial vector [relation (3.8)] is equal to

$$\cos \varphi_{H,a_i} = h_i/a_i H_{hkl}.$$

The angles between point rows, between the normals to the planes, and between the planes and the rows are defined by the equations

$$\cos \varphi_{tt'} = \frac{(tt')}{tt'}, \quad \cos \varphi_{HH'} = \frac{(HH')}{HH'}, \quad \cos \varphi_{tH} = \frac{(tH)}{tH}. \tag{3.58}$$

In the general case the products (3.58) are rather complicated; the last equation is simpler, since its numerator is equal to $(p_1h_1 + p_2h_2 + p_3h_3)$. In practical computations one must switch from these and other above-derived equations assigned in vector form to equations containing the lengths of periods a, b, c and the angles between them α, β, γ. The computations are made in crystallographic coordinates, i.e., the unit cell is assigned according to the syngony (Table 3.5). Whenever necessary, the unit cell is reduced, or transition to a more convenient setting is performed by (3.44, 45).

For each syngony we write down the equations expressing the periods and angles of the reciprocal cell via the same quantities of the atomic lattice. These equations also hold for the reverse transition; then each asterisked quantity must be replaced by one without an asterisk, and vice versa.

We shall also give equations for interplanar distances d_{hkl}, which define the length of vector $H = d^{-1}$, and for the distances r_{ik} between the points in the unit cell (interatomic distances); the coordinates x_i, y_i, z_i, x_k, y_k, z_k are expressed in fractions of the corresponding period (i.e., $x_i = x_{abs}/a_i$, etc.). If in the equations for r we put $x_i - x_k = p$, etc., we obtain equations for the lengths of vectors $\boldsymbol{t}$ of the lattice.

1) General case – triclinic lattice: a, b, c are arbitrary; angles α, β, $\gamma \neq 90$ or $60°$.

$$\Omega = abc\sqrt{1 - \cos^2\alpha - \cos^2\beta - \cos^2\gamma + 2\cos\alpha\cos\beta\cos\gamma},$$

$$a^* = \frac{bc\sin\alpha}{\Omega}, \quad b^* = \frac{ac\sin\beta}{\Omega}, \quad c^* = \frac{ab\sin\gamma}{\Omega},$$

$$\cos\alpha^* = \frac{\cos\beta\cos\gamma - \cos\alpha}{\sin\beta\sin\gamma}, \quad \cos\beta^* = \frac{\cos\gamma\cos\alpha - \cos\beta}{\sin\alpha\sin\gamma},$$

$$\cos\gamma^* = \frac{\cos\alpha\cos\beta - \cos\gamma}{\sin\alpha\sin\beta};$$

$$H_{hkl}^2 = \frac{1}{d_{hkl}^2} = h^2a^{*2} + k^2b^{*2} + l^2c^{*2} + 2hka^*b^*\cos\gamma^* + 2klb^*c^*\cos\alpha^*$$
$$+ 2lhc^*a^*\cos\beta^* = (1 - \cos^2\alpha - \cos^2\beta$$
$$- \cos^2\gamma + 2\cos\alpha\cos\beta\cos\gamma)^{-1}\left[\frac{h^2}{a^2}\sin^2\alpha + \frac{k^2}{b^2}\sin^2\beta\right.$$
$$+ \frac{l^2}{c^2}\sin^2\gamma + \frac{2kl}{bc}(\cos\beta\cos\gamma - \cos\alpha) + \frac{2lh}{ca}(\cos\gamma\cos\alpha - \cos\beta)$$
$$\left. + \frac{2hk}{ab}(\cos\alpha\cos\beta - \cos\gamma)\right];$$

$$r_{ik}^2 = (x_i - x_k)^2a^2 + (y_i - y_k)^2b^2 + (z_i - z_k)^2c^2 + 2(y_i - y_k)(z_i - z_k)bc\cos\alpha$$
$$+ 2(x_i - x_k)(z_i - z_k)ac\cos\beta + 2(x_i - x_k)(y_i - y_k)ab\cos\gamma.$$

2) Monoclinic lattice: a, b, c are arbitrary, $\alpha = \gamma = 90°$; $\beta < 90°$.

$$\Omega = abc\sin\beta,$$

$$a^* = \frac{1}{a\sin\beta}, \quad b^* = \frac{1}{b}, \quad c^* = \frac{1}{c\sin\beta},$$

$$\alpha^* = 90°, \quad \beta^* = 180° - \beta, \quad \gamma^* = 90°;$$

$$H_{hkl}^2 = \frac{1}{d_{hkl}^2} = \frac{h^2}{a^2\sin^2\beta} + \frac{k^2}{b^2} + \frac{l^2}{c^2\sin^2\beta} - \frac{2hl\cos\beta}{ca\sin^2\beta},$$

$$r_{ik}^2 = (x_i - x_k)^2a^2 + (y_i - y_k)^2b^2 + (z_i - z_k)^2c^2$$
$$+ 2(x_i - x_k)(z_i - z_k)ac\cos\beta.$$

3) Orthorhombic lattice: $a \neq b \neq c$, $\alpha = \beta = \gamma = 90°$.

$$\Omega = abc, \quad a^* = \frac{1}{a}, \quad b^* = \frac{1}{b}, \quad c^* = \frac{1}{c}, \quad \alpha^* = \beta^* = \gamma^* = 90°;$$

$$H_{hkl}^2 = \frac{1}{d_{hkl}^2} = \frac{h^2}{a^2} + \frac{k^2}{b^2} + \frac{l^2}{c^2},$$

$$r_{ik}^2 = (x_i - x_k)^2 a^2 + (y_i - y_k)^2 b^2 + (z_i - z_k)^2 c^2.$$

4) Tetragonal lattice: $a = b$, c is arbitrary, $\alpha = \beta = \gamma = 90°$.

$$\Omega = a^2 c, \quad a^* = b^* = \frac{1}{a}, \quad c^* = \frac{1}{c},$$

$$\alpha^* = \beta^* = \gamma^* = 90°;$$

$$H_{hkl}^2 = \frac{1}{d_{hkl}^2} = \frac{h^2 + k^2}{a^2} + \frac{l^2}{c^2},$$

$$r_{ik}^2 = [(x_i - x_k)^2 + (y_i - y_k)^2]\, a^2 + (z_i - z_k)^2 c^2.$$

5) Hexagonal lattice: $a = b$, c is arbitrary, $\alpha = \beta = 90°$, $\gamma = 120°$.

$$\Omega = a^2 c \frac{\sqrt{3}}{2}, \quad a^* = b^* = \frac{2}{a\sqrt{3}}, \quad c^* = \frac{1}{c},$$

$$\alpha^* = \beta^* = 90°, \quad \gamma^* = 60°;$$

$$H_{hkl}^2 = \frac{1}{d_{hkl}^2} = \frac{4}{3a^2}(h^2 + k^2 + hk) + \frac{l^2}{c^2},$$

$$r_{ik}^2 = a^2[(x_i - x_k)^2 + (y_i - y_k)^2 - (x_i - x_k)(y_i - y_k)] + c^2 (z_i - z_k)^2.$$

The computation procedure requires only indices h and k, but there are also equations using the three basis vectors and three indices h, k, and $i = -(h + k)$. Note that the three basis vectors in the reciprocal lattice are arranged at angles of 60°.

Rhombohedral lattice: $a = b = c$, $\alpha = \beta = \gamma \neq 90°$, it can be reduced to the hexagonal description of a', c': $a' = 2a \sin \alpha/2$, $c' = a\sqrt{3}\sqrt{1 + 2\cos\alpha}$, with the transformation matrix (3.49).

6) Cubic lattice: $a = b = c$, $\alpha = \beta = \gamma = 90°$.

$$\Omega = a^3, \quad a^* = a^{-1}, \quad a^* = 90°; \quad H_{hkl}^2 = \frac{1}{d_{hkl}^2} = \frac{h^2 + k^2 + l^2}{a^2},$$

$$r_{ik}^2 = [(x_i - x_k)^2 + (y_i - y_k)^2 + (z_i - z_k)^2]\, a^2.$$

It should be mentioned that in computer calculations of oblique lattices it is sometimes more convenient to use Cartesian, rather than crystallographic, coordinates. The relationship between them is defined by the general equations (3.43, 44), though the coefficients α_{ik} and β_{jl} in this case are not integers or rational fractions, but may have any values.

4. Structure Analysis of Crystals

In 1912 x-ray diffraction in crystals was discovered, and soon afterwards the structures of rock salt and diamond were determined. This laid the foundation of x-ray structure analysis introducing the physicists to the world of atomic structures of crystals. Later on, two more similar methods – electron and neutron diffraction – came into being.

From the mathematical standpoint, the diffraction of short-wave coherent radiation by systems of atoms is the problem of finding the wavefront and intensity in the process of scattering. The determination of the structure of an object from the experimentally observed diffraction field is the reverse problem. It reduces to the solution of complicated sets of equations or integral equations and often has no unambiguous solutions. Both diffraction theory and structure analysis are applied not only to single crystals, but also to less ordered systems, e.g. polycrystals, liquid crystals, solutions of molecules and macromolecules, to liquids and amorphous solids, and finally, to gases.

Structure analysis uses various experimental methods. These depend essentially on the ordering of the substance studied and on the type of radiation used. These methods will be the subject of the present chapter.

4.1 Fundamentals of Diffraction Theory

4.1.1 Wave Interference

The study of the atomic structure of a substance is based on the diffraction phenomena caused by its interaction with x-rays, electrons, or neutrons. The theory of diffraction, i.e., the relationship between the diffraction pattern and the spatial arrangement of the atoms, is the same for all three types of radiation. We shall present in a general form, mostly with respect to the x-ray method but with due reference to electron and neutron diffraction where required.

If we allow an x-ray beam to go through an assembly of atoms, the electron shells of atoms will interact with the incident wave, scattering it. The direction of wave propagation is defined by wave vector $\boldsymbol{k}$, whose modulus is equal to

$$|\boldsymbol{k}| = 2\pi/\lambda, \tag{4.1}$$

where λ is the wavelength.

The general expression for a plane monochromatic wave is

$$A \exp[i(\boldsymbol{k} \cdot \boldsymbol{r} + \alpha)], \tag{4.2}$$

where A is the amplitude, $\boldsymbol{r}$ is the radius vector of the points of space, and α is the initial phase.

This expression does not contain time as a parameter because we are interested not in the process of wave propagation in time, but in the diffraction pattern at any given moment. This is sufficient for establishing the relative phase difference arising in interference of scattered waves, since this difference depends exclusively on the spatial arrangement of the atoms and is constant in time.

Thus, if two waves propagating in the same direction are in phase, they enchance one another and produce a wave with a doubled amplitude, (Fig. 4.1a) which is constructive intereference; if they are out of phase ($\alpha = \pi$), they extinguish one another, which is destructive interference (Fig. 4.16); intermediate phase difference changes both the amplitude and phase (Fig. 4.1c).

When radiation is scattered by an object both elastic (without any loss of energy or change in wavelength λ) and inelastic scattering arise. The most important scattering is elastic, and it is this scattering that determines the diffraction pattern, whose analysis then allows one to determine the arrangement of atoms in the object.

Diffraction by crystals can be interpreted as "reflection" of x-rays by the planes of the crystal lattice (Fig. 4.2).

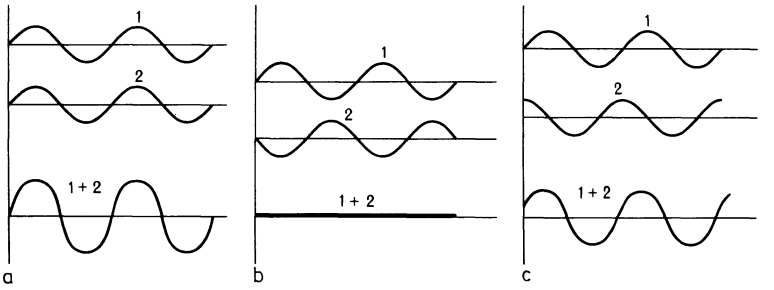

Fig. 4.1a–c. Interaction of two waves (1) and (2) with the same amplitude. (**a**) doubling of the amplitude when the waves are in phase, (**b**) mutual annihilation of the waves in counterphase, (**c**) change of amplitude and phase in the general case of a phase shift

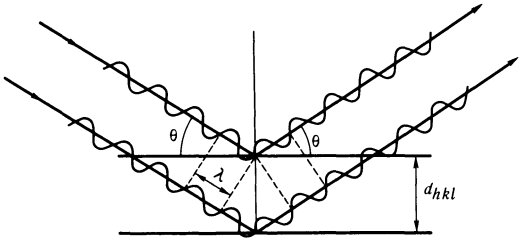

Fig. 4.2. The derivation of the Bragg–Wulff formula

"Reflection" takes place only when the waves scattered by parallel planes are in phase and enhance one another, i.e., when the path difference for waves scattered by neighboring planes is equal to an integral number n of wavelengths λ,

$$n\lambda = 2d_{hkl}\sin\theta. \tag{4.3}$$

This is the Bragg–Wulff law [4.1, 2], which relates the directions of the propagation of scattered beams (θ angles) to the interplanar distances d_{hkl} [see (3.24)] in the lattice; n is the reflection order. If this condition fails, then, owing to the presence in the crystal of a very large number of planes, the difference in phase arising at reflection from different planes leads to the complete disappearance of the scattered beams for any angles different from those given by condition (4.3). Although the geometric derivation of (4.3) yields a correct result, the physical essence of the interference phenomenon as an interaction of secondary waves resulting from the action of the initial wave throughout the object is not evident. The Bragg–Wulff equation, as well as the Laue conditions considered below (4.29), indicates that diffracted beams can be obtained for a given d_{hkl} in monochromatic radiation (i.e. at constant λ), owing to the change in crystal orientation (i.e. in θ angles); and for a fixed crystal in polychromatic radiation reflection arises at the appropriate λ.

4.1.2 Scattering Amplitude

In a general approach, secondary waves coming from all the points of the object are considered. Suppose we have two scattering centers O and O' (Fig. 4.3). We choose the origin ($r = 0$) at one of them; and the position of the other is given by vector $\boldsymbol{r}$. The incident plane wave excites these centers, and each of them becomes the source of a secondary spherical wave. In general the initial wave arrives at both centers with a different phase; therefore, the scattered waves will also have different initial phases. Interfering, the waves will enhance or weaken one another in some directions depending on whether they are in or out of phase (Fig. 4.1). Note that if λ greatly exceeds $\boldsymbol{r}$, the distance between the scattering centers, there will be no phase difference on scattering in any direction, and the intensity then will not depend on the angle.

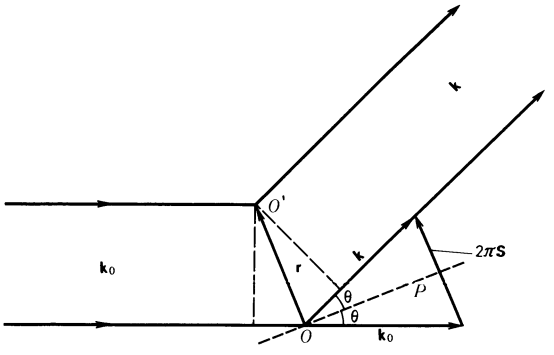

Fig. 4.3. Scattering by two point centers

Interatomic distances lie within the range of 1–4 Å. Therefore no diffraction by assemblies of atoms can be observed, for instance, with visible-light waves, which have a wavelength of several thousand angstroms. Thus follows the impossibility of obtaining in the optical wavelength range a magnified image of the atomic structure of a substance, because the production of an image ultimately involves interference.

X-rays, neutrons, and electrons, on the contrary, have suitable wavelengths (about 1 Å) and so they give interference effects on scattering by assemblies of atoms. Thus, these radiations are suitable, in principle, for obtaining the image of atomic structures.

Let us now find the path difference between a plane wave scattered in the direction $\boldsymbol{k}$ by a point in position $\boldsymbol{r}$ and a wave scattered by point $\boldsymbol{r} = 0$ in the same direction. This difference (Fig. 4.3) is equal to $\boldsymbol{k}\cdot\boldsymbol{r} - \boldsymbol{k}_0\cdot\boldsymbol{r} = (\boldsymbol{k} - \boldsymbol{k}_0)\cdot\boldsymbol{r}$. Thus, if the initial wave is of unit amplitude ($A = 1$), the scattering center in position $\boldsymbol{r}$ gives a wave

$$f\exp[\mathrm{i}(\boldsymbol{k} - \boldsymbol{k}_0)\cdot\boldsymbol{r}] = f\exp[2\pi\mathrm{i}(\boldsymbol{S}\cdot\boldsymbol{r})]. \tag{4.4}$$

Coefficient f indicates the scattering power of this center, which may, generally speaking, be of any value. Equation (4.4) contains vector $\boldsymbol{S}$

$$\boldsymbol{S} = \frac{\boldsymbol{k} - \boldsymbol{k}_0}{2\pi}, \quad |\boldsymbol{S}| = \frac{2\sin\theta}{\lambda}, \tag{4.5}$$

perpendicular to plane P in Fig. 4.3, with respect to which one can measure the scattering angle 2θ.

If the object placed in the path of the initial wave consists of n scattering centers with a scattering powers f_j, located at points $\boldsymbol{r}_j$, the amplitude of the scattered wave will be, according to (4.4),

$$\sum_{j=1}^{n} f_j \exp[2\pi\mathrm{i}(\boldsymbol{S}\cdot\boldsymbol{r}_j)] = F(\boldsymbol{S}). \tag{4.6}$$

The quantity $F(\boldsymbol{S})$ is called *the scattering amplitude* of a given object. For a "point" scattering center, the quantity f_j is constant and independent of $\boldsymbol{S}$. Expression (4.6) for the scattering amplitude is of universal application as, by generalizing the concept of scattering power f of a given center, one can take for it any physical scattering unit – an electron, an atom, a molecule, a group of molecules, etc.

The physical "points", which interact with x-rays (electromagnetic waves) in an object and scatter them, are electrons.[1] Each of them becomes the source of a secondary scattered wave of the same frequency and wavelength as the incident one. The amplitude of scattering by an electron is proportional to that

[1] Positively charged atomic nuclei also oscillate in the electric field of the primary beam and emit secondary waves. But due to the presence of m in the denominator of (4.7) the scattering on them will be $m_Z/m_e \approx 10^4$ times less and can be neglected.

of the initial wave and is given by

$$f_{e.x} = \frac{1}{R}\frac{e^3}{mc^2}\sin\varphi, \tag{4.7}$$

where R is the distance to the point of observation, e and m are the charge and the mass of the electron, respectively, and c is the light velocity; $\sin\varphi$ accounts for the polarization of the incident wave (for more details see Sect. 4.5.2).

If we assume the amplitude of scattering by one electron to be equal to unity, then scattering of x-rays by any object in these "electron" units will be described by the following expression according to (4.6):

$$F(\boldsymbol{S})(\text{el. units}) = \sum_{j=1}^{n} f_j(\text{el. units})\exp[2\pi i(\boldsymbol{S}\cdot\boldsymbol{r})]. \tag{4.8}$$

To express the scattering amplitude in absolute units, F must be multiplied by $f_{e.x}$.

$$F_{abs}(\boldsymbol{S}) = F(\boldsymbol{S})f_{e.x}. \tag{4.9}$$

From now on we shall use (4.8) as the scattering amplitude of x-rays without a special indication that it is expressed in electron units. When calculating the absolute values of intensity (see Sect. 4.5), the value of $f_{e.x}$ must also be taken into consideration.

4.1.3 Electron Density Distribution. Fourier Integral

Instead of a discrete set of n points at positions $\boldsymbol{r}_j$ one can consider the continuously distributed scattering power of the object. Since (as we have just noted) x-rays are scattered by electrons, "the scattering matter" for them is the time-average electron density of the object $\rho(\boldsymbol{r})$. This function is equal to the average number of electrons $n_e(\boldsymbol{r})$ in a volume element Δv_r near point $\boldsymbol{r}$ divided by this volume element,

$$\rho(\boldsymbol{r}) = n_e(\boldsymbol{r})/\Delta v_r. \tag{4.10}$$

This description also corresponds to the quantum-mechanical approach: the time-average electron density is given by the square of the wave function of a given object

$$\rho(\boldsymbol{r}) = |\Psi(\boldsymbol{r})|^2. \tag{4.11}$$

With this approach, the sum of the discrete scattering centers in (4.8), must be replaced by an integral over the continuously changing function $\rho(\boldsymbol{r})$:

$$\begin{aligned} F(\boldsymbol{S}) &= \int\rho(\boldsymbol{r})\exp[2\pi i(\boldsymbol{S}\cdot\boldsymbol{r})]\,dv_r \\ &= \iiint_{x,y,z=-\infty}^{+\infty} \rho(xyz)\exp[2\pi i\,(xX + yY + zZ)]\,dx\,dy\,dz = \mathscr{F}[\rho], \end{aligned} \tag{4.12}$$

where dv_r is an element of the scattering volume; X, Y, Z are the three

coordinates of vector $\boldsymbol{S}$; and $\mathcal{F}$ is the Fourier operator. This expression assigns the amplitude as a function of vector $\boldsymbol{S}$, i.e., it defines scattering in any direction $\boldsymbol{k} = \boldsymbol{k}_0 + 2\pi\boldsymbol{S}$.

In its mathematical form this integral, which describes diffraction, is a Fourier integral. The function $F(\boldsymbol{S})$, which describes scattering, is given in the space of vector $\boldsymbol{S}$, so-called reciprocal space. $F(\boldsymbol{S})$ is an "image" in the reciprocal space of function $\rho(\boldsymbol{r})$, which describes the structure of the object in direct space, and is in one-to-one correspondence with it. With the aid of (4.12) it is possible to consider a variety of problems: scattering from atoms, molecules, crystals, and continuous objects of different shape and with different distribution of scattering power within them.

The distribution of the electron density $\rho(\boldsymbol{r})$ in an object depends on the distribution $\rho_i(\boldsymbol{r})$ of electrons in the constituent atoms and the mutual arrangement of these atoms. The maximum values (peaks) of function $\rho(\boldsymbol{r})$ correspond to the centers of the atoms, and the smaller values are due to the distribution of the outer electrons involved in chemical bonding. If the centers of the atoms are located at points $\boldsymbol{r}$, the electron density of such an assembly of n atoms is expressed by the continuous function

$$\rho(\boldsymbol{r}) = \sum_{j=1}^{n} \rho_j(\boldsymbol{r} - \boldsymbol{r}_j). \tag{4.13}$$

In this description of the electron density $\rho(\boldsymbol{r})$ in a crystal or a molecule as a superposition of the electron densities of separate atoms $\rho_i(\boldsymbol{r})$ we neglect the fine effects of redistribution of ρ_i in the outer valency shells of the atoms during the formation of the chemical bond. The electron density $\rho(\boldsymbol{r})$ is positive (non-negative) everywhere.

The Fourier integral (4.12) is suitable for describing phenomena of diffraction of any radiation from objects in which the inhomogeneities are commensurate with the corresponding wavelength. Therefore it is used both in the theory of all diffraction methods and in the optical diffraction theory applied to simulation of x-ray and electron diffraction (Fig. 4.11).

4.1.4 Atomic Amplitude

The atomic amplitude defines scattering by an isolated atom; it is also often called the atomic factor. Inserting the electron density of the atom, $\rho_a(\boldsymbol{r})$ into (4.12) we obtain the atomic amplitude

$$f(\boldsymbol{S}) = \int \rho_a(\boldsymbol{r}) \exp[2\pi i(\boldsymbol{S}\cdot\boldsymbol{r})]\, dv_r. \tag{4.14}$$

To a sufficiently good approximation, the electron shells of atoms are spherically symmetric $\rho_a(\boldsymbol{r}) = \rho_a(r)$ and therefore it is possible to write the Fourier integral (4.12) in spherical coordinates

$$f(s) = \int_0^\infty 4\pi r^2 \rho_a(r) \frac{\sin sr}{sr} dr. \tag{4.15}$$

Here, $s = 2\pi|\boldsymbol{S}| = 4\pi(\sin\theta)/\lambda$. Thus, f depends exclusively on the value of modulus s and is a spherically symmetric function in reciprocal space. To calculate $f_x(s)$ for x-rays it is necessary to know the electron densities of atoms $\rho_a(\boldsymbol{r})$. They have been calculated with a high accuracy by methods of quantum mechanics for all atoms [Ref. 4.3, Chap. 1, Sect. 1]. The values of $f_x(s)$ have been calculated and tabulated as well [Ref. 4.4, Vol. 4]. The deviations from spherical symmetry, for instance because of covalent bonding, are small, and whenever necessary can be taken into account as a correction to the spherically symmetric function $f(s)$ (4.15) [4.5]. But for the vast majority of problems of structure analysis, the spherically symmetric approximation (4.15) is sufficient.

For $s \to 0$, $(\sin sr)/sr \to 1$ and

$$f_x(0) = \int \rho_a(\boldsymbol{r})\, dv_r = Z. \tag{4.16}$$

Thus, with a zero scattering angle the atomic amplitude is simply an integral of the electron density over the volume of the atom, which is equal to the number of electrons in it. As the scattering angle increases, the function f_x decreases. Such functions for certain atoms, the so-called f_x curves, are presented in Fig. 4.4a [4.6]. Separate scattering from different electronic shells of atoms may be calculated. Figure 4.4b shows partial amplitudes of atomic scattering by K and L electron shells of carbon. It is seen that the outer L electrons do not scatter x-rays significantly in the "distant" region of reciprocal space (at $\sin\theta/\lambda > 0.6$ Å^{-1}) [4.7]. Taking into account scattering by different electron shells it is essential in x-ray investigations of the chemical bond in atoms using difference Fourier series (see Sect. 4.7.10, and also [Ref. 4.3, Chap. 1, Sect. 2.7]).

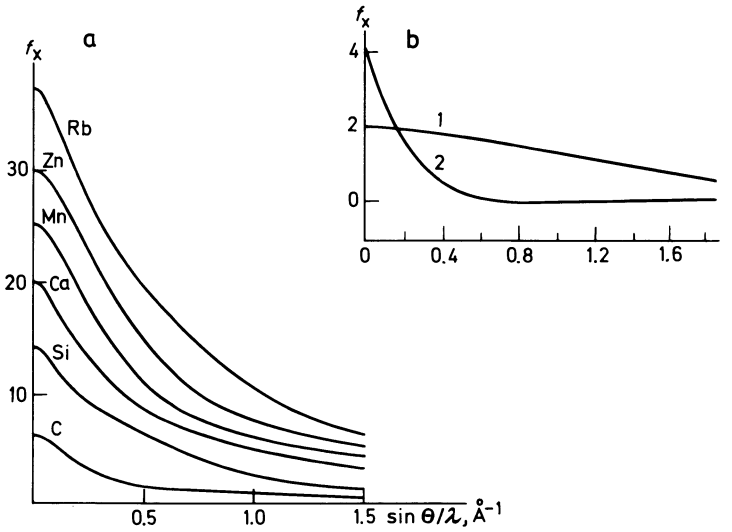

Fig. 4.4a,b. Curves of the atomic amplitudes of x-ray scattering f_x for some elements (**a**); curves of amplitudes of x-ray scattering by K-shell (1) and L-shell (2) of carbon (**b**)

In the special case of what is called anomalous x-ray scattering the atomic factor f_x has a small additional complex component – see (4.146).

Since the physical nature of scattering of a given radiation by a substance depends on atomic scattering, the specific features of the other two methods – electron and neutron diffraction – are clearly seen from comparison of the atomic amplitudes for these radiations, f_e and f_n, with the amplitudes for x-rays, f_x.

The scattering of electrons is due to their interaction with the electrostatic potential of atoms $\varphi(\boldsymbol{r})$, which depends on the potential of the positively charged nucleus, and that of the negatively charged electron shells, which screen it. If we insert the potential of the atom $\varphi_a(\boldsymbol{r})$ into (4.14) and (4.15) instead of the function of the electron density $\rho_a(\boldsymbol{r})$, we obtain the atomic amplitudes f_e of electron scattering. In this way $f_e(s)$ for all atoms have been calculated; some of them are given in Fig. 4.5 [4.6]. Since the potential is defined by the charge distribution, the amplitudes f_e and f_x are also related

$$f_e(s) = \frac{8\pi^2 me^2}{h^2} \frac{Z - f_x(s)}{s^2}. \tag{4.17}$$

Here, h is Planck's constant.

The curves $f_e(s)$ are less dependent on the atomic number Z. On the average $f_e(0) \sim Z^{1/3}$, whereas $f_x(0) \sim Z$ (4.16). Therefore the relative contribution from light atoms to scattering in the presence of heavy atoms is larger in electron diffraction than in x-ray diffraction. It means that the "detectability" of light atoms in the presence of heavy ones is better in electron than in x-ray analysis.

Neutron scattering occurs on atomic nuclei due to the nuclear-interaction forces, which have a very short range, about 10^{-13} cm. Therefore, to neutron waves with $\lambda \approx 10^{-8}$ cm a nucleus is a "point"; it scatters neutrons equally in all directions, i.e., the neutron scattering amplitudes are independent of the scattering angle $f_n(\sin\theta/\lambda) = f_n(0)$.

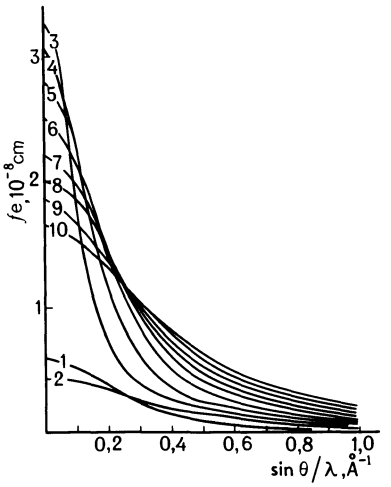

Fig. 4.5. Curves of atomic amplitudes of electron scattering f_e for some elements. The curve number corresponds to that of the element

Here, the general principle of the theory of scattering is valid, which finds expression in the properties of the Fourier integral (4.12): the smaller the object, i.e., the more compact the function $\rho(\boldsymbol{r})$ in direct space, the larger the region of reciprocal space (the higher values of $|\boldsymbol{S}|$) in which amplitude $F(\boldsymbol{S})$ is distributed. Conversely, the larger the object in direct space, the smaller its image is in reciprocal space. Thus, the potential of atoms $\rho(\boldsymbol{r})$ is more "smeared out" than its electron density $\rho(\boldsymbol{r})$, while the curves $f_e(s)$ are more "contracted" towards the low values of S than the $f_n(s)$ curves, So, for neutrons, when the scattering object – the nucleus – converges to a point, the f_n curves do not fall off. (Figs. 4.6, 7).

The neutron scattering amplitudes f_n only slightly depend on the atomic number Z, and f_n of some nuclei are negative, as distinct from the atomic amplitudes for x-rays and electrons, which are always positive. This promotes efficient neutron diffraction investigation of structures consisting of atoms with significantly differing Z. The dependencies of f_x, f_e, and f_n on the atomic number Z, averaged over the scattering angles, for the first few elements of the Periodic Table are presented in Fig. 4.8.

The neutron has a magnetic moment. Therefore, besides interaction with nuclei, an additional "magnetic" scattering of neutrons arises from electron shells of atoms possessing a magnetic moment. These include, among others, the

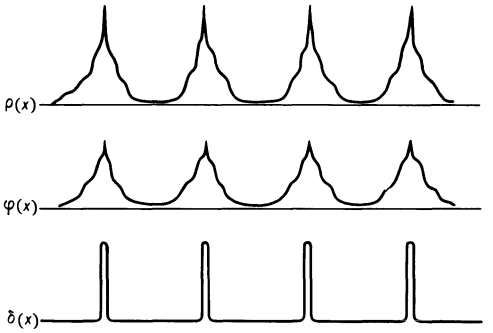

Fig. 4.6. One-dimensional scheme of distribution of electron density $\rho(x)$, electrostatic potential $\varphi(x)$, and nuclear scattering power $\delta(x)$ in a crystal with atoms at rest

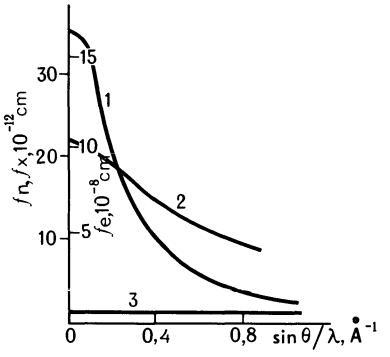

Fig. 4.7. Comparison of the dependence of the absolute values of atomic scattering amplitudes for electrons (*1*), x-rays (*2*), and neutrons (*3*) on sin θ/λ (for Pb)

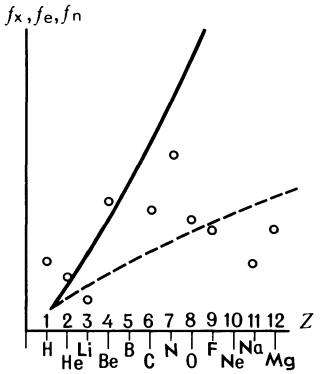

Fig. 4.8. Relative dependencies of the atomic scattering amplitudes for x-rays (—), electrons (----), and neutrons (○ ○ ○) averaged over $\sin\theta/\lambda$ for the atomic numbers Z from 1 to 12

d-shells of transition metals. The corresponding amplitude $f_{n,m}$ is defined by the space distribution of electrons with an uncompensated moment and can be computed by the general equation (4.12).

The interaction of each of these radiations with a substance is characterized by the absolute value of the amplitudes: $f_x \sim (10^{-12} - 10^{-11})$ cm for x-rays, $f_e \sim 10^{-8}$ cm for electrons, and $f_n \sim 10^{-12}$ cm for neutrons. Hence, electrons interact with a substance most vigorously, several orders of magnitude more strongly than x-rays or neutrons. Electron and neutron scattering is treated in more detail in Sects. 4.8 and 4.9.

4.1.5 The Temperature Factor

Atoms in crystals are in the state of thermal motion. The function of electron density $\rho(\boldsymbol{r})$, which defines scattering, is the time-average electron density; the duration of a diffraction experiment greatly exceeds the periods of the thermal vibrations of atoms. To take into account the thermal motion, one must know functions $w(\boldsymbol{r})$, which give the time-average distribution of centers of atoms about their equilibrium position. This function will "smear out" the electron density (and also the potential and the nuclear density) of an atom at rest $\rho(\boldsymbol{r})$, which defines the atomic amplitudes (4.14).

Let us find the electron density distribution in such a moving atom. To do this, we multiply the electron density upon displacement of an atom to point $\boldsymbol{r}'$, i.e., $\rho(\boldsymbol{r} - \boldsymbol{r}')$, by the probability $w(\boldsymbol{r}')$ of its being at this point, and take an integral throughout the volume

$$\rho_{aT}(\boldsymbol{r}) = \int \rho(\boldsymbol{r} - \boldsymbol{r}')\, w(\boldsymbol{r}')\, dv_{r'}. \tag{4.18}$$

This is a particular case of the problem of finding the scattering amplitude for complex systems when the amplitude for some scattering unit is known and the law of mutual arrangement of these units is assigned.

If in general case a function $f_1(\boldsymbol{r})$ is distributed according to a law assigned by another function $f_2(\boldsymbol{r})$, the joint distribution will be expressed by the integral

$$\int f_1(\boldsymbol{r} - \boldsymbol{r}')\, f_2(\boldsymbol{r}')\, dv_{r'} = f_1(\boldsymbol{r}) * f_2(\boldsymbol{r}). \tag{4.19}$$

Such an integral is called the convolution integral, or simply the convolution of functions f_1 and f_2. It possesses very important property: if the Fourier integrals (4.12) of some functions are known, the Fourier integral of the convolution is the product of the Fourier integrals of each function

$$\mathcal{F}[f_1(\boldsymbol{r})] = F_1(\boldsymbol{S}), \quad \mathcal{F}[f_2(\boldsymbol{r})] = F_2(\boldsymbol{S}), \quad \mathcal{F}[f_1(\boldsymbol{r}) * f_2(\boldsymbol{r})] = F_1(\boldsymbol{S})F_2(\boldsymbol{S}). \tag{4.20}$$

These relations are known as the convolution theorem.

Thus (4.18) is nothing else but the convolution

$$\rho_{aT}(\boldsymbol{r}) = \rho_a(\boldsymbol{r}) * w(\boldsymbol{r}). \tag{4.21}$$

The Fourier integral (4.12) of function $w(\boldsymbol{r})$ describing the thermal motion is precisely the temperature factor

$$f_T(\boldsymbol{S}) = \int w(\boldsymbol{r}) \exp[2\pi i(\boldsymbol{r} \cdot \boldsymbol{S})]\, dv_r. \tag{4.22}$$

According to (4.21) and to the convolution theorem (4.20) the function of scattering by an atom in thermal motion, which is called the atomic-temperature factor, is

$$f_{aT}(\boldsymbol{S}) = f_a(\boldsymbol{S}) f_T(\boldsymbol{S}). \tag{4.23}$$

The "smearing-out" of function $w(\boldsymbol{r})$, i.e., of the amplitude of the thermal vibrations of atoms, depends on many factors. It is approximately inversely proportional to the forces of chemical bonding of atoms in molecules and crystals, inversely proportional to the atomic mass, and directly proportional to the temperature. In most cases function $w(\boldsymbol{r})$ is anisotropic. But in the first approximation one can assume isotropy, i.e., the spherical symmetry of the thermal vibrations of atoms.

Spherically symmetric vibrations are described by the Gaussian distribution with a root mean square (r.m.s.) displacement of the atom from the equilibrium position $\sqrt{\overline{u^2}}$

$$w(\boldsymbol{r}) = w(r) = \frac{1}{(2\pi\overline{u^2})^{3/2}} \exp(-r^2/2\overline{u^2}), \tag{4.24}$$

and the corresponding temperature factor is

$$f_T(S) = \exp(-2\pi\overline{u^2}S^2) = \exp\left[-B\left(\frac{\sin\theta}{\lambda}\right)^2\right], \quad B = 8\pi^2\overline{u^2}. \tag{4.25}$$

Expression (4.25) is obtained from (4.24) with an allowance for (4.15). For different crystals the displacement $\sqrt{\overline{u^2}}$ is about 0.05–0.10 Å (for inorganic crystals) and may reach 0.5 Å (for organic crystals).

In the general case of anisotropic vibrations of atoms the r.m.s. displacement varies in direction. The corresponding function $w(\boldsymbol{r})$ for harmonic vibrations has the form

$$w(\boldsymbol{r}) = \frac{1}{(2\pi)^{3/2}\sqrt{\overline{u_1^2}\,\overline{u_2^2}\,\overline{u_3^2}}} \exp\left[-\frac{1}{2}\left(\frac{x_1^2}{\overline{u_1^2}} + \frac{x_2^2}{\overline{u_2^2}} + \frac{x_3^2}{\overline{u_3^2}}\right)\right], \tag{4.26}$$

where x_1, x_2, x_3 are the coordinates of the displacement vector $\boldsymbol{r}$ along the axes of an ellipsoid characterizing the thermal vibrations, and $\sqrt{\overline{u_i^2}}$ are the r.m.s. displacements along these axes. The axes of these ellipsoids do not generally coincide with those of the crystal (Fig. 4.9a). Function $f_T(\boldsymbol{S})$ has the form

$$f_T(\boldsymbol{S}) = \exp[-2\pi^2(\overline{u_1^2}S_{x_1}^2 + \overline{u_2^2}S_{x_2}^2 + \overline{u_3^2}S_{x_3}^2)], \tag{4.27}$$

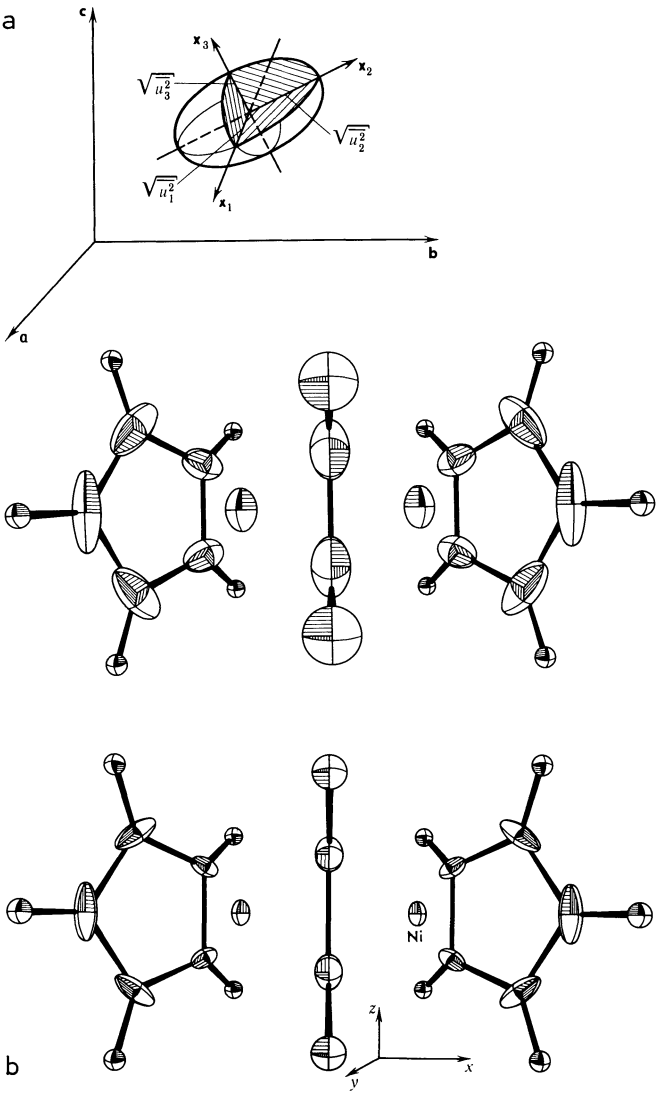

Fig. 4.9a,b. Ellipsoids of thermal vibrations of atoms in a lattice. (**a**) general case of arbitrary orientation, (**b**) anisotropy of atomic vibrations in the structure of nickel μ-acetylene-bis-cyclopentadiene at 300 K (top) and 77 K (bottom). Molecules of acetylene are at the center, those of cyclopentadiene on the sides [4.8]

where S_{x_i} is the projection of vector $\boldsymbol{S}$ onto the axes in a reciprocal space, which are parallel to the principal axes x_i of the ellipsoid of thermal vibrations.

Thus, the harmonic vibrations of each atom in the crystalline structure are, in the general case, described by three semiaxes $\sqrt{\overline{u_i^2}}$ of the vibration ellipsoid and by the three angles specifying the orientation of this ellipsoid, i.e., by six parameters. Naturally, the lower the temperature, the smaller are the thermal vibrations of the atoms – the fact which is recognized in x-ray structure analysis (Fig. 4.9b).

Spherical averaging of (4.27) will give us again (4.25). Thermal vibrations of an atom asymmetrically surrounded by other atoms can deviate from a harmonic law. In this case the surface describing thermal vibrations is not a centrosymmetric ellipsoid like the one shown in Fig. 4.9a. Anharmonic corrections are usually very small and can be neglected for most structures. Still, for some structures and for the explanation of their physical properties, accounting for the anharmonicity becomes important. To do this, additional multipliers which contain coefficients of 3, 4 and higher-order tensors describing the anharmonicity of the atom's displacement from the equilibrium positions are introduced into $w(\boldsymbol{r})$, (4.26), and $f_T(\boldsymbol{S})$, (4.27), respectively. These coefficients can be determined in a precision x-ray experiment [4.9, 10].

4.2 Diffraction from Crystals

4.2.1 Laue Conditions. Reciprocal Lattice

The structure of crystals is three-dimensionally periodic. The simplest image of a periodic structure is a one-dimensional point lattice with a period a (Fig. 4.10). Let us consider the diffraction of an incident monochromatic wave impinging on it at an angle α_0. The secondary waves will maximally enhance each other when scattered at angles α such that the path difference BC–DB is an integral number h of wavelengths λ

$$a(\cos\alpha - \cos\alpha_0) = h\lambda. \tag{4.28}$$

Here, the diffraction is independent on the angle ψ, which describes the "rotation" of the scattered beam about the axis of the point row under consider-

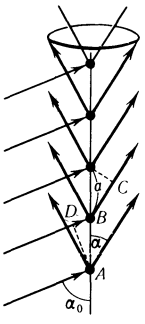

Fig. 4.10. Diffraction from a row of points

ation – the scattering is cylindrically symmetric, and the scattered beams form cones whose axis is the axis of this row.

Let us now consider diffraction by a three-dimensionally periodic lattice. The set of its points is described by (3.2, 11), with a lattice vector $\boldsymbol{t} = p_1\boldsymbol{a}_1 + p_2\boldsymbol{a}_2 + p_3\boldsymbol{a}_3$, and expression (4.28) for $i = 1, 2, 3$ are the conditions of diffraction from a lattice; these are the three so-called Laue conditions. For each of the rows, directions of the scattered beams along cones are possible (Fig. 4.10). But in a three-dimensional lattice Laue conditions (4.28) must be fulfilled for three directions simultaneously. This means that only those reflections are possible which correspond to the lines of intersection of all three cones having axes $\boldsymbol{a}_1$, $\boldsymbol{a}_2$, and $\mathbf{a}_3$. Keeping in mind (4.1), we rewrite Laue's conditions in vector form

$$\begin{aligned} &\boldsymbol{a}_1 \cdot (\boldsymbol{k} - \boldsymbol{k}_0) = 2\pi h, \quad \boldsymbol{a}_1 \cdot \boldsymbol{S} = h, \\ &\boldsymbol{a}_2 \cdot (\boldsymbol{k} - \boldsymbol{k}_0) = 2\pi k, \quad \boldsymbol{a}_2 \cdot \boldsymbol{S} = k, \\ &\boldsymbol{a}_3 \cdot (\boldsymbol{k} - \boldsymbol{k}_0) = 2\pi l, \quad \boldsymbol{a}_3 \cdot \boldsymbol{S} = l, \end{aligned} \tag{4.29}$$

which will give the possible values of vector $\boldsymbol{S}$ at scattering by a three-dimensional lattice. These conditions, however, are nothing else but conditions (3.25, 27) for determining the vector of the reciprocal lattice $\boldsymbol{H}_{hkl}$ from the main vectors of the crystal lattice $\boldsymbol{a}_i$. Thus, in diffraction from a crystal, the directions of the scattered beams are defined by

$$\boldsymbol{S} = \boldsymbol{H}_{hkl} = h\boldsymbol{a}^* + k\boldsymbol{b}^* + l\boldsymbol{c}^*, \quad \boldsymbol{k} = \boldsymbol{k}_0 + 2\pi\boldsymbol{H}_{hkl}. \tag{4.30}$$

We have considered the three-dimensionally periodic lattice of scattering points as the simplest image of a crystal. A complete description of the crystalline structure will be obtained by assigning its electron density function $\rho(\boldsymbol{r})$.

An infinite point lattice is described by (3.11)

$$T(\boldsymbol{r}) = \sum_{\substack{p_1 p_2 p_3 \\ -\infty}}^{+\infty} \delta(\boldsymbol{r} - \boldsymbol{t}_{p_1 p_2 p_3}).$$

An infinite crystal, each unit cell of which is "filled" with an electron density $\rho_{\text{cell}}(\boldsymbol{r})$, will be written as a convolution $T * \rho_{\text{cell}}$

$$\rho_\infty(\boldsymbol{r}) = \rho_{\text{cell}}(\boldsymbol{r}) * \left[\sum_{\substack{p_1 p_2 p_3 \\ -\infty}}^{+\infty} \delta(\boldsymbol{r} - \boldsymbol{t}_{p_1 p_2 p_3}) \right]. \tag{4.31}$$

We have seen that if function $\rho(\boldsymbol{r})$ is arbitrary, $F(\boldsymbol{S})$ exists at any values of $\boldsymbol{S}$, and integral (4.12) is taken from $-\infty$ to $+\infty$ in infinite limits. If the function is periodic, however, the Fourier integral is taken within the period and is nonzero only at discrete values of $\boldsymbol{S}$, becoming Fourier coefficients (terms). The corresponding expressions in the one-dimensional case are as follows:

$$\int_{-\infty}^{+\infty} \rho(x) \exp(2\pi i x X)\, dx = F(X), \tag{4.32}$$

$$\frac{1}{a} \int_0^a \rho(x) \exp(2\pi i h/a)\, dx = F_h. \tag{4.33}$$

Thus, the scattering amplitudes $F(X) = F(h/a)$ are nonzero only at $X = h/a$. Similarly, for the three-dimensional case the Fourier coefficients take the form

$$F_{hkl} = \int_0^a \int_0^b \int_0^c \rho(xyz) \exp\left[2\pi i\left(\frac{hx}{a} + \frac{ky}{b} + \frac{lz}{c}\right)\right] dx\, dy\, dz$$
$$= \int \rho(\boldsymbol{r}) \exp[2\pi i(\boldsymbol{r} \cdot \boldsymbol{H}_{hkl})]\, dv_r, \tag{4.34}$$

where h, k, l are integers. We have again arrived at conditions (4.29, 30), because the index in exponent (4.34) contains the scalar product of vector $\boldsymbol{r}$ and vector $\boldsymbol{H}_{hkl}$ of the reciprocal lattice, i.e., the permissible values of vector $\boldsymbol{S} = \boldsymbol{H}_{hkl}$ (4.29, 30). The Fourier integral (4.34) not only determines these permissible values, but also enables one to calculate the scattering amplitude $\boldsymbol{F}_{hkl}$.

Similarly to (4.33), in (4.34) we should have written the factor $1/\boldsymbol{a}[\boldsymbol{bc}] = \Omega^{-1}$ before the integral, where $\boldsymbol{a}$, $\boldsymbol{b}$, and $\boldsymbol{c}$ are the unit cell vectors, and Ω its volume. However, this factor is usually omitted so that the expression for structure amplitude F (4.34) can have the same dimensionality as f (4.14) and the Fourier integral (4.12). It must be introduced into the final expression for the amplitude of scattering from the crystal.

Taking into account (3.26), which describes the set of nodes of the reciprocal lattice, we find that the expression of the complete Fourier transform of an infinite crystal has the form

$$F_\infty(\boldsymbol{S}) = \frac{F_{hkl}}{\Omega} T^*(\boldsymbol{S}) = \sum_{hkl} \frac{F_{hkl}}{\Omega} \delta(\boldsymbol{S} - \boldsymbol{H}_{hkl}). \tag{4.35}$$

This is a three-dimensionally periodic set of nodes, each described by a delta function and placed at the ends of vectors $\boldsymbol{H}_{hkl}$. The weights of these nodes are different and defined by complex values F_{hkl} which are called structure amplitudes.

The reciprocal lattice has been introduced formally as a set of points at the ends of the vectors of normals $\boldsymbol{H}_{hkl}$ to the crystal planes with indices (hkl), and the length of the normals is inverse to the interplanar distance d_{hkl}, see (3.19),

$$|\boldsymbol{H}_{hkl}| = d_{hkl}^{-1}.$$

We can now see that in considering diffraction phenomena and the Fourier integral the concept of the reciprocal lattice arises automatically. Indeed, this could be expected, bearing in mind that the result of the interaction of a periodic wave with the periodic structure of the crystal must itself have a periodic character. The geometric meaning of the reciprocal space and the reciprocal lattice is naturally independent of the way they are introduced. But now this concept acquires a real physical meaning – vectors $\boldsymbol{H}_{hkl}$ define the directions of beams scattered by the crystal. Further on we shall see some other physical realizations of the reciprocal lattice concept.

Thus, on scattering from a nonperiodic object (atom, molecule, etc.) the distribution of amplitude $F(\boldsymbol{S})$ in reciprocal space is continuous, i.e., scattering with some intensity can occur in any direction. On scattering from crystals only

a definite, discrete, set of directions of the diffracted beams is possible [determined by conditions (4.29, 30)]. These beams can also be interpreted as "reflections" from crystal planes (hkl) with spacings d_{hkl}, since from (4.5), (4.30) and (3.19) it follows that $2 \sin\theta/\lambda = |\boldsymbol{H}_{hkl}|$, which is the Bragg–Wulff equation (4.3).

4.2.2 Size of Reciprocal Lattice Nodes

The Fourier integral (4.34) leads to the concept of "point" nodes $\delta(\boldsymbol{S} - \boldsymbol{H}_{hkl})$ of the reciprocal lattice described by the discrete indices h, k, l, since the periodic function $\rho(\boldsymbol{r})$ in it is infinitely extended, and integration is taken over its periods. But actually a scattering crystal has finite dimensions and a definite shape and volume V; it contains a finite number of unit cells. Therefore, the nodes of the reciprocal lattice in an actual diffraction experiment are not points $\delta(\boldsymbol{S} - \boldsymbol{H}_{hkl})$, but have a finite size and a definite shape depending on those of the crystal.

To take into account the finiteness of the crystal dimensions and describe its shape, one can introduce the shape function

$$\Phi(\boldsymbol{r}) = \begin{cases} 1 & \text{inside the crystal} \\ 0 & \text{outside the crystal,} \end{cases} \tag{4.36}$$

and then the function $\rho_\infty(\boldsymbol{r})$ (4.31) of an infinite crystal will be transformed, by multiplying by $\Phi(\boldsymbol{r})$ (4.36), into the function $\rho_{cr}(\boldsymbol{r})$ of a crystal (Fig. 4.11) with the shape $\Phi(\boldsymbol{r})$

$$\rho_{cr} = \rho_\infty(\boldsymbol{r})\,\Phi(\boldsymbol{r}) = \left\{ \rho_{cell}(\boldsymbol{r}) * \left[\sum_{\substack{p_1 p_2 p_3 \\ -\infty}}^{+\infty} \delta(\boldsymbol{r} - \boldsymbol{t}_{p_1 p_2 p_3}) \right] \right\} \Phi(\boldsymbol{r}). \tag{4.37}$$

The scattering amplitude of an infinite crystal is given by (4.35). The Fourier transform (amplitude) of the crystal shape is defined by

$$\mathscr{F}[\Phi] = D(\boldsymbol{S}) = \int_V \Phi(\boldsymbol{r}) \exp[2\pi i (\boldsymbol{S}\boldsymbol{r})]\, dV_r = \int_\Phi \exp[2\pi i (\boldsymbol{S}\boldsymbol{r})]\, dV_r. \tag{4.38}$$

According to the convolution theorem $\rho_\infty(\boldsymbol{r})\Phi(\boldsymbol{r})$ in (4.37) will be replaced in the Fourier transformation by the convolution of each of the transforms, which are known; they are (4.35) and (4.38). Thus, for a finite crystal

$$\mathscr{F}_{cr}(\boldsymbol{S}) = \left[\sum_{hkl} \frac{F_{hkl}}{\Omega} \delta(\boldsymbol{S} - \boldsymbol{H}_{hkl}) \right] * D(\boldsymbol{S}). \tag{4.39}$$

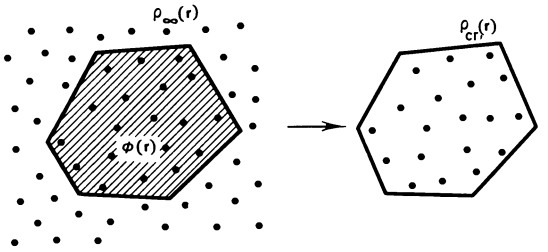

Fig. 4.11. Action of a shape function $\Phi(\boldsymbol{r})$ (two-dimensional scheme)

The convolution of each of the functions $\delta(\boldsymbol{S} - \boldsymbol{H}_{hkl})$ of the point nodes of the reciprocal lattice with $D(\boldsymbol{S})$ means that each of these nodes will now take the form D, i.e.,

$$\delta(\boldsymbol{S} - \boldsymbol{H}_{hkl}) * D(\boldsymbol{S}) = D(\boldsymbol{S} - \boldsymbol{H}_{hkl}).$$

Hence, a node of the reciprocal lattice of an actual finite crystal has a density distribution $D(\boldsymbol{S})$ depending on the crystal shape; this distribution is the same for all the nodes, including that at the origin 000. The amplitude of scattering by a finite crystal of the shape $\Phi(\boldsymbol{r})$ is described by the expression

$$F_{cr}(\boldsymbol{S}) = \frac{1}{\Omega} \sum_{hkl} F_{hkl} D(\boldsymbol{S} - \boldsymbol{H}_{hkl}) \tau. \tag{4.40}$$

To investigate the effect of the dimensions and shape of the crystal $\Phi(\boldsymbol{r})$ on the diffraction peaks we consider a simple example – a crystal in the shape of a parallelepiped with edges $A_1 A_2 A_3$. Then

$$\begin{aligned} D(\boldsymbol{S}) &= \int_{-A_1/2}^{A_1/2} \int_{-A_2/2}^{A_2/2} \int_{-A_3/2}^{A_3/2} \exp[2\pi i(xX + yY + zZ)]\, dx\, dy\, dz \\ &= \frac{\sin \pi A_1 X}{\pi X} \frac{\sin \pi A_2 Y}{\pi Y} \frac{\sin \pi A_3 Z}{\pi Z}. \end{aligned} \tag{4.41}$$

The functions of one of the cofactors of (4.41) and its square are depicted in Fig. 4.12. The halfwidth of function $D(\boldsymbol{S})$ is inversely proportional to the dimension A_i of the crystal in the corresponding direction. Thus, the reciprocal lattice nodes in an actual diffraction experiment are some small finite regions, whose linear dimensions in reciprocal space are equal to A_i^{-1}. This means that the diffracted beams have a finite angular halfwidth $\Delta\theta \sim A_i^{-1}$; the larger the crystal, the narrower the beams. The value of each cofactor of (4.41) at its

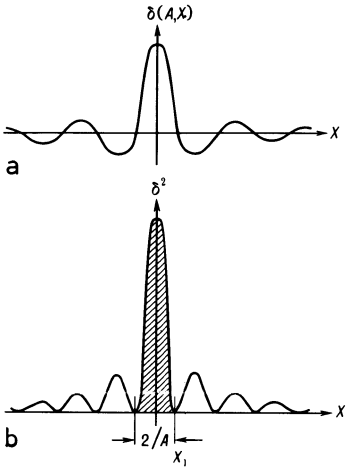

Fig. 4.12a,b. Function $\delta(A,x) = \sin \pi Ax/\pi x$ (**a**) and its square (**b**)

maximum is equal to A_i and, hence, $D(\boldsymbol{S})$ at the maximum has a value $A_1 A_2 A_3 = V$ – the volume of the crystal.

Note that the area under the peaks formed by the square of each of the cofactors of (4.41) is

$$\int_{-\infty}^{+\infty} \frac{\sin^2 \pi A_i X}{(\pi X)^2} dX = A_i, \tag{4.42}$$

i.e., an integral over the values of $|D|^2$

$$\int |D(\boldsymbol{S})|^2 \, dv_s = A_1 A_2 A_3 = V \tag{4.43}$$

is equal to the volume of the crystal.

4.2.3 Reflection Sphere

We shall now revert to the analysis of the diffraction conditions (4.29, 30). In diffraction of monochromatic radiation, i.e., at a constant, λ, these conditions are realized by an elegant geometric construction, which is known as the Ewald reflection sphere in reciprocal space (Fig. 4.13). If $\boldsymbol{k}_0$ and $\boldsymbol{k}$ are the directions of the incident and scattered wave, the set of the ends of vectors $\boldsymbol{S}$ lies on the Ewald sphere, described by vector $\boldsymbol{k}$ and having a radius λ^{-1}. The condition $\boldsymbol{k} = \boldsymbol{k}_0$ corresponds to the value of $\boldsymbol{S} = 0 = \boldsymbol{H}_{000}$, i.e., to the zero node of reciprocal space. Let us now construct a reciprocal lattice starting with vectors $\boldsymbol{a}_1^*$, $\boldsymbol{a}_2^*$,

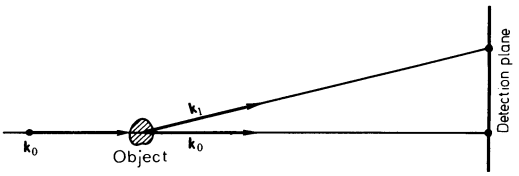

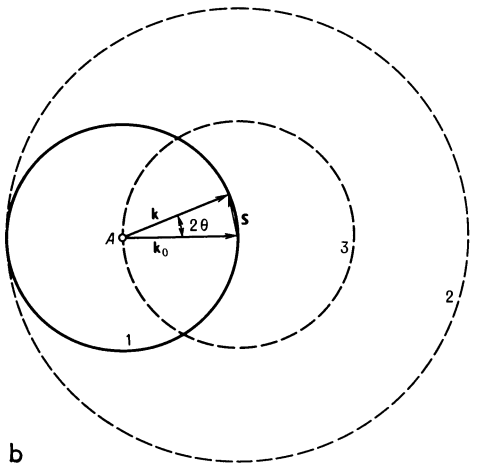

b

Fig. 4.13a,b. Formation of diffraction pattern (**a**) and the corresponding Ewald construction (**b**). (*1*) reflection sphere, (*2*) limitation sphere, (*3*) locus of the centers of the reflection spheres

$\boldsymbol{a}_3^*$ from the zero node (Fig. 4.14 shows the corresponding two-dimensional construction). Its orientation will be defined by that of the crystal with respect to $\boldsymbol{k}_0$. The condition for the formation of a diffraction beam with indices *hkl* consists in intersection by the reflection sphere of the node *hkl* of the reciprocal lattice; this is precisely the condition $\boldsymbol{S} = \boldsymbol{H}_{hkl}$ (4.31). Thus, the formation of diffraction beams depends on the crystal orientation and the sphere radius λ^{-1}. In x-ray and neutron diffraction $\lambda \sim 1 - 2$Å, which is comparable with the periods of unit cells ($\sim$ 10Å), and the sphere has an appreciable curvature with respect to the planes of the reciprocal lattice. The intersection of node 000 by the sphere means that scattering always occurs in the direction $\boldsymbol{k} = \boldsymbol{k}_0$, i.e., in the direction of the initial beam. A diffracted beam – "*hkl*-reflection" – will appear when the sphere intersects some *hkl* node depending on the crystal orientation and the direction $\boldsymbol{k}_0$. The sphere may also intersect two or, sometimes, several nodes, then a number of reflections will appear simultaneously. It may also intersect no nodes (with the exception of 000); thus no reflections arise at all.

So, if we have a monochromatic beam of x-rays or neutrons and the crystal is fixed, then to obtain the assigned reflection *hkl* it is necessary to orient the crystal appropriately. Various x-ray diffraction methods (see Sect. 4.5) make it possible to record the entire set of nodes of the reciprocal lattice by setting the crystal successively into different reflecting positions (Fig. 4.15).

In electron diffraction $\lambda \sim 0.05$ Å, the curvature of the Ewald sphere is small, its segment is nearly flat (Fig. 4.14), and one can record simultaneously the set of reflections belonging to the zero plane of the reciprocal lattice, i.e., the plane passing through node 000.

If the reflection sphere radius is λ^{-1}, we can, by changing the directions of beam $\boldsymbol{k}_0$ (or the object orientation relative to it), obtain information on the values of $F(\boldsymbol{S})$ within the "limitation sphere" of a radius $S_{\max} = 2\lambda^{-1}$ (Fig. 4.13b). Thus, as already noted, the wavelength used determines, in principle, the amount of information which can be obtained from a diffraction experiment. The wavelength must be sufficiently small so that the entire function $F(\boldsymbol{S})$ (i.e.,

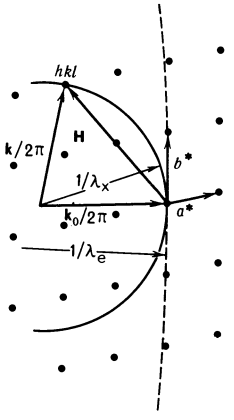

Fig. 4.14. Ewald's sphere in the reciprocal lattice of a crystal: for x-ray diffraction (——) and for electron diffraction (-----)

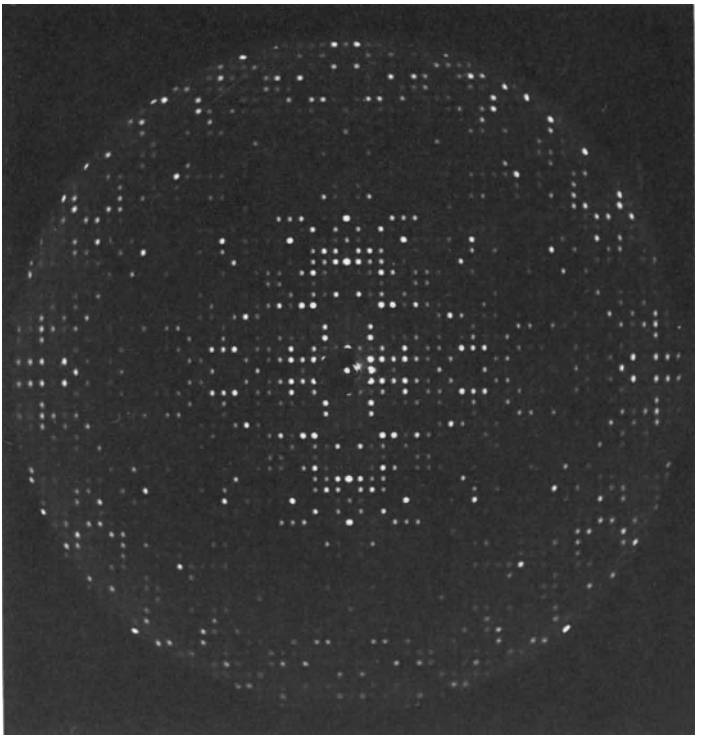

Fig. 4.15. Precession x-ray photograph of *hk*0-zone of a crystal of protein aspartate-transaminase (courtesy of N. I. Sosfenov).
Precession angle 9°, CuKα radiation, Ni-filter, rotating-anode apparatus, $V = 35$ kV, $i = 30$ mA

the range where it differs from zero) is within the limitation sphere. In practice, such a variation of $F(\boldsymbol{S})$ actually takes place with the wavelengths λ usually used in diffraction methods, because of the drop in atomic amplitudes with increasing $\boldsymbol{S}$ and the action of the temperature factor.

On the other hand, if $\lambda > 2_i a$, where a_i is the largest lattice period, the radius of the Ewald sphere will be so small compared with $\boldsymbol{a}_i^*$ that the sphere will not intersect a single node, and in this case no reflections from the crystal will be observed.

4.2.4 Structure Amplitude

We have established that the directions of possible scattered beams depend on the geometry of the reciprocal lattice, which is periodic in a reciprocal space with a unit cell $\boldsymbol{a}^*$, $\boldsymbol{b}^*$, $\boldsymbol{c}^*$. In a diffraction experiment, however, its periodicity is expressed only in the arrangement of nodes *hkl*, while their "weights" are different and assigned by the values of F_{hkl} (4.34). These values depend on the

distribution $\rho(\boldsymbol{r})$ of the electron density in the unit cell of the crystal (4.34), being its Fourier terms, and hence they depend on the arrangement of the atoms in the cell.

Let us now express ρ of the cell as a sum of electron densities $\rho_{(aT)_j} = \rho_j$ of each of its atoms j with the coordinates $\boldsymbol{r}_j$ (4.13): $\rho = \Sigma \rho_j(\boldsymbol{r} - \boldsymbol{r}_j)$ and insert this expression into Fourier integral (4.34). For each ρ_j we obtain, according to (4.22, 23) the atomic temperature factor f_{jT}, but with an additional, so-called phase factor $\exp 2\pi i(\boldsymbol{r}_j \cdot \boldsymbol{H})$, which takes into account the position of the atom in the cell. Therefore

$$F_{hkl} = \sum_{j=1}^{n} f_{jT}(\sin\theta/\lambda) \exp[2\pi i(\boldsymbol{r}_j \cdot \boldsymbol{H}_{hkl})] = \sum_{j=1}^{n} f_{jT} \exp[2\pi i(hx_j + ky_j + lz_j)]. \tag{4.44}$$

Here, the coordinates are expressed in fractions of the period $x_i = x_{iabs}/a_i$. This formula is precisely the scattering amplitude of one unit cell of the crystal, the so called structure amplitude (or structure factor).

It should be noted that if we take into consideration the anisotropic temperature factor (4.26), the computation of F_{hkl} (4.44) will be more complicated, since then the values f_{jT} themselves depend on $\boldsymbol{H}_{hkl}$ because of the "oblique" orientation of the ellipsoid of thermal vibrations with respect to the coordinate axes.

The conditions for the appearance of a strong reflection from the crystal, i.e., for a high value of F_{hkl}, are a high "population density" of the atoms of a given system of crystallographic planes hkl, to which vector $\boldsymbol{H}_{hkl}$ is perpendicular (Figs. 3.30, 34), and a small number of atoms between them. If the atoms are distributed uniformly both in and between planes, then the phases of waves scattered by them in the direction hkl are different, and waves weaken each other, which reduces the reflection amplitude or "extinguishes" it altogether.

The scattering amplitude F_{hkl} is a complex value

$$\begin{aligned} F &= A + iB, \\ A &= \Sigma f_j \cos 2\pi(hx_j + ky_j + lz_j), \\ B &= \Sigma f_j \sin 2\pi(hx_j + ky_j + lz_j). \end{aligned} \tag{4.45}$$

One can also write F in terms of modulus $|F|$ and phase α

$$\begin{aligned} &\tan\alpha = B/A, \quad |F| = \sqrt{A^2 + B^2}, \\ &A = |F| \cos\alpha, \quad B = |F| \sin\alpha, \\ &F = |F| \exp i\alpha. \end{aligned} \tag{4.46}$$

4.2.5 Intensity of Reflections

So far we have been speaking of amplitudes of scattering in a direction defined by vector $\boldsymbol{S}$ in the general case, or by the vector $\boldsymbol{H}$ of the reciprocal lattice for

crystals. In an experiment the time-average scattering intensity, which is proportional to the square of the amplitude modulus, is recorded

$$I_{hkl} \sim |F_{hkl}|^2 = F_H F_H^* = A^2 + B^2. \tag{4.47}$$

Attention must be given to the following important circumstance. As follows from (4.47), in a diffraction experiment only the measurement of the scattering amplitude moduli can be realized physically, while their phases are lost. This, as we shall see below (in Sect. 4.7), seriously complicates the determination of the structure of crystals from the diffraction data.

The expressions (4.45) and (4.46) for the structure amplitude, and hence for the intensity (4.47), contain the atomic temperature factors of all the atoms $f_{i\mathrm{T}}$ (4.23) of the structure, as well as the trigonometric factor for each of them. This factor may take different values – from -1 to $+1$, which results in different values of F_{hkl}. At the same time $f_{j\mathrm{T}}$ decreases gradually with increasing $\sin\theta/\lambda$, i.e., towards the periphery of the reciprocal lattice. The average value of $[\exp 2\pi i(\boldsymbol{r}\cdot\boldsymbol{H})]^2 = 1$, and therefore from (4.44, 47) it follows that the drop in intensities with increasing $\sin\theta/\lambda$ is determined by the equation

$$\bar{I}_{hkl}(\sin\theta/\lambda) = \overline{|F_{hkl}|^2} = \sum_{j=1}^{N} f_{j\mathrm{T}}^2(\sin\theta/\lambda). \tag{4.48}$$

Thus, although the intensities I_{hkl} are different, they decrease, on the average, with an increase in $\sin\theta/\lambda$. The "limit" of their observation usually lies near $|\boldsymbol{H}_{\max}| = d_{\min}^{-1} = 1 - 2\ \text{Å}^{-1}$ and mainly depends on the decrease of the average temperature factor (4.25). Since the curves of the atomic factors f_{aj} are known and $f_{a\mathrm{T}} = f_a f_{\mathrm{T}}$ (4.23), it is possible, by using (4.48), to find the value of the average temperature factor from the average I and the theoretical value of f_a.

There exists one more expression relating the intensities and $f_{a\mathrm{T}}^2$, which is called the law of conservation of intensity. From Fourier's series theory it is known that the sum of the squares of the moduli $|F_H|^2$ of all the Fourier coefficients is constant; it is determined by the rms value of the initial function $\rho(\boldsymbol{r})^2$

$$\sum_H |F_H|^2 = \frac{1}{\Omega}\int \rho^2(\boldsymbol{r})\, dv_r. \tag{4.49}$$

On the other hand, ρ can be expressed via (4.13) in terms of the electron densities of separate atoms ρ_i, and the latter, by inverting the Fourier integral of the type (4.15), again through atomic temperature factors. Finally, this will yield, with due regard for (4.47),

$$\sum_H I_H = \frac{1}{\Omega}\sum_j \int f_{j\mathrm{T}}^2(S) 4\pi S^2 dS. \tag{4.50}$$

We can see that the sum of the intensities taken over all the nodes $\boldsymbol{H}_{hkl}$ of the reciprocal lattice is constant, and can be computed beforehand for a crystal in accordance with (4.50) on the basis of the curves of the atomic temperature factor.

4.2.6 Thermal Diffusion Scattering

So far we have referred to scattering due to the three-dimensional periodicity of the crystalline structure, which can be recorded as the intensities of the diffraction pattern I_{hkl} concentrated at the nodes of the reciprocal lattice. The lattice, however, shows one more type of periodicity. We have spoken of the thermal motion of atoms, which is accounted for by the temperature factor (4.22). But that expression did not include all components of thermal motion. The vibrations of atoms in the lattice are interrelated. They are treated as a system of acoustic waves, phonons, which is characterized by the phonon spectrum of the crystal [Ref. 4.3, Chap. 4]. The phonon wavelengths Λ are multiples of periods a_1, a_2, and a_3. The Fourier transform (4.12) of the function describing a set of such waves leads to the following. The scattering maxima I_T of these waves are situated around the nodes $\boldsymbol{H}_{hkl}$ of the reciprocal lattice and are smeared-out regions. The intensity I_T is several orders weaker than the intensities I_{hkl} because of the crystal structure. Nevertheless, thermal diffusion scattering is detected by using special techniques (Fig. 4.16). Naturally, I_T is temperature dependent. The shape of the maxima and their length in different directions depend on the anisotropy of the amplitudes of the acoustic waves in the crystal.

4.2.7 Symmetry of the Diffraction Pattern and Its Relation to the Point Symmetry of the Crystal

The reciprocal lattice (4.35) is periodic, provided we disregard the "weight" of its nodes F (or I); if we do include the weights, however, it becomes aperiodic, and the symmetry can be described by one of the crystallographic point groups K. From (4.45, 46) it is seen that the structure amplitudes of reflections hkl and $\bar{h}\bar{k}\bar{l}$, i.e., of nodes $\boldsymbol{H}$ and $\bar{\boldsymbol{H}}$, which are centrosymmetric in the reciprocal lattice with

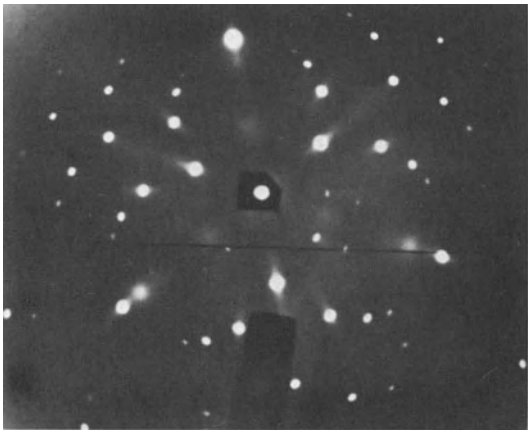

Fig. 4.16. X-ray pattern of a pentaerythrite with thermal diffusion maxima (courtesy of E. V. Kolontsova)

respect to node 000, are complex conjugate quantities

$$F_H = F_{hkl} = F^*_{\bar{h}\bar{k}\bar{l}} = F^*_{\bar{H}}, \tag{4.51}$$

and hence their moduli $|F|$ and observed intensities I (4.47) are identical

$$I_H = I_{\bar{H}}. \tag{4.52}$$

This relation is known as Friedel's law: the reciprocal lattice is centrosymmetric; its nodes $\boldsymbol{H}$ and $\bar{\boldsymbol{H}}$ have the same weight. Consequently, the symmetry group of intensity distribution in the reciprocal lattice is one of the eleven centrosymmetric (inversion) point groups K (see Table 2.4), which are called Laue classes, when referred to diffraction phenomena. The presence of the center of symmetry in the diffraction pattern is independent of whether the structure itself belongs to a centrosymmetric or noncentrosymmetric point group K and to the corresponding space group Φ. In other words, it is impossible to establish from the symmetry of the reciprocal lattice whether or not a given crystal has a center of symmetry; the diffraction pattern unavoidably "adds" a center of symmetry to a point group K. Thus, to the observed Laue class K of the diffraction pattern there may correspond a crystal of either the same centrosymmetric group K, or of some one of its noncentrosymmetric subgroups K (Table 2.3).

Note that since a syngony is defined by its highest centrosymmetric group, a diffraction experiment which gives the Laue class of the crystal also makes it possible to directly find its syngony.

It should be borne in mind that if we take into consideration the complex nature of F_{hkl}, then in describing the distribution of these values in the reciprocal lattice we can use point groups of antisymmetry K' and of color symmetry $K^{(p)}$. For instance, for noncentrosymmetric groups F_{hkl} and $F_{\bar{h}\bar{k}\bar{l}} = F^*_{hkl}$ will be antiequal. But for the description of the experimentally observed distribution of intensities I_{hkl}, only eleven Laue centrosymmetric classes can be used. The determination of the Laue class from the diffraction pattern does not exhaust the possibilities of obtaining other information about crystal symmetry from it: indeed, so far we have only tried to find out what can be deduced from the symmetry of this pattern.

Friedel's law may be violated under special conditions. One of such cases is the so-called anomalous x-ray scattering, when the atomic amplitude f (4.20), which is real, acquires an imaginary component (see Sect. 4.7). Then (4.52) ceases to hold, and $I_H \neq I_{\bar{H}}$. Other violations of Friedel's law are associated with taking into account the peculiarities of scattering from single crystals as a whole and are described by dynamic theory of scattering (Sect. 4.3).

4.2.8 Manifestation of Space-Symmetry of a Crystal in a Diffraction Pattern. Extinctions

The expression for the structure factor (4.44) includes the coordinates of atoms $\boldsymbol{r}_i$ in the unit cell. If the space group of a crystal is asymmetric, $P1$, expression

(4.44) is final. All the other groups have symmetric relationships between the coordinates of the points, i.e., they have regular point systems (RPS) (Sect. 2.5). The atoms in the cell can occupy one or several such RPS. Figure 2.81 gives an example of RPS for one of the space groups, D_{2h}^{16}. The coordinates xyz of all the n atoms of a given RPS can be expressed in terms of the coordinates xyz of one atom in the independent region of the cell. Using this fact, it is convenient to transform, with the aid of the corresponding trigonometric relations, the general expression for structure factor (4.44), so that each RPS of n atoms (where n is the multiplicity of the position) is represented by one expression. Then the structure factor will break down into k terms, each of them representing a set of atoms occupying one regular point system with a multiplicity of n, so that the sum $k_1n_1 + k_2n_2 + \ldots + k_in_i = N$ is the total number of atoms in the unit cell.

The simplest example of the effect of symmetry is the action of a center of symmetry $\bar{1}$. If an origin is chosen in it then, together with the atom in position xyz, there is an atom in centrosymmetric position $\bar{x}\bar{y}\bar{z}$. Then exp in (4.44) is replaced by cos, and F becomes a real value with a plus or minus sign, $B = 0$, $\alpha = 0$ or π:

$$F_{hkl} = 2\sum_{j=1}^{N/2} f_j \cos 2\pi(hx + ky + lz). \tag{4.53}$$

Summation is done only over symmetrically independent atoms. Other symmetry operations (taking into account the position of the corresponding symmetry elements in the cell, which, as mentioned above, is directly expressed in the set of coordinates of RPS) will lead to other simplifications in the equations for F (4.44, 45). Thus, the presence of simple or glide planes of symmetry manifests itself so that (4.44) and (4.45) are transformed into factors of the type

$$\begin{matrix}\cos & \cos & \cos \\ 2\pi hx & 2\pi ky & 2\pi lz. \\ \sin & \sin & \sin\end{matrix} \tag{4.54}$$

Figure 4.17 reproduces the general and special forms of the structure factor for the group D_{2h}^{16} according to the International Tables. Such formulae exist for all space groups. It is worth noting that in computer calculations it is sometimes easier to use the main formula (4.45) or, in the presence of a center of symmetry, (4.53) and the coordinates of all the points.

If the space group Φ of the crystal is such that it contains symmetry elements with a translational component – screw axes, or glide-reflection planes – or if the translation subgroup T of group Φ is centered, it is directly manifested in the structure of the reciprocal lattice and results in the appearance of the so-called extinctions, i.e., systematic absences of reflections hkl, for which $F_{hkl} = 0$.

Let us consider, for instance, the action of screw axis 2_1 coincident with axis z. Here, along with the atom in position xyz, the cell will contain an atom in position $\bar{x}$, $\bar{y}$, $z + 1/2$. We substitute these coordinates into the expression for structure factor (4.44) for reflections $00l$ along the axis c^* of the reciprocal lattice.

Pnma No. 62

D_{2h}^{16}

Origin at $\bar{1}$. $\pm\left|x,y,z;\ \frac{1}{2}+x,\frac{1}{2}-y,\frac{1}{2}-z;\ \bar{x},\frac{1}{2}+y,\bar{z};\ \frac{1}{2}-x,\bar{y},\frac{1}{2}+z\right|$

$$A = 8\cos 2\pi\left(hx - \frac{h+k+l}{4}\right)\cos 2\pi\left(ky + \frac{k}{4}\right)\cos 2\pi\left(lz + \frac{h+l}{4}\right);\ B = 0$$

$\begin{cases} h+l=2n \\ k=2n \end{cases}$	$A = 8\cos 2\pi hx \cos 2\pi ky \cos 2\pi lz$ $F(hkl) = F(\bar{h}\bar{k}\bar{l}) = F(\bar{h}kl) = F(h\bar{k}l) = F(hk\bar{l})$
$\begin{cases} h+l=2n \\ k=2n+1 \end{cases}$	$A = -8\sin 2\pi hx \sin 2\pi ky \cos 2\pi lz$; $A = B = 0$ if $h = 0$ $F(hkl) = F(\bar{h}\bar{k}\bar{l}) = -F(\bar{h}kl) = -F(h\bar{k}l) = F(hk\bar{l})$
$\begin{cases} h+l=2n+1 \\ k=2n \end{cases}$	$A = -8\sin 2\pi hx \cos 2\pi ky \sin 2\pi lz$; $A = B = 0$ if $h = 0$ or $l = 0$ $F(hkl) = F(\bar{h}\bar{k}\bar{l}) = -F(\bar{h}kl) = F(h\bar{k}l) = -F(hk\bar{l})$
$\begin{cases} h+l=2n+1 \\ k=2n+1 \end{cases}$	$A = -8\cos 2\pi hx \sin 2\pi ky \sin 2\pi lz$; $A = B = 0$ if $l = 0$ $F(hkl) = F(\bar{h}\bar{k}\bar{l}) = F(\bar{h}kl) = -F(h\bar{k}l) = -F(hk\bar{l})$

$$\rho(XYZ) = \frac{8}{V_c}\Bigg\{\sum_0^\infty\sum_0^\infty\sum_0^\infty{}^{h+l=2n,\ k=2n} F(hkl)\cos 2\pi hX\cos 2\pi kY\cos 2\pi lZ$$
$$- \sum_0^\infty\sum_0^\infty\sum_0^\infty{}^{h+l=2n,\ k=2n+1} F(hkl)\sin 2\pi hX\sin 2\pi kY\cos 2\pi lZ$$
$$- \sum_0^\infty\sum_0^\infty\sum_0^\infty{}^{h+l=2n+1,\ k=2n} F(hkl)\sin 2\pi hX\cos 2\pi kY\sin 2\pi lZ$$
$$- \sum_0^\infty\sum_0^\infty\sum_0^\infty{}^{h+l=2n+1,\ k=2n+1} F(hkl)\cos 2\pi hX\sin 2\pi kY\sin 2\pi lZ\Bigg\}$$

Fig. 4.17. General and special expressions for the structure factor and the electron-density function for the space group *Pnma*-D_{2h}^{16} ([Ref. 4.4, Vol. 1], see also [4.11])

Since $h = k = 0$, these reflections are insensitive to the coordinates x, y of the atoms, and

$$F_{00l} = \sum f_j \left\{\exp(2\pi ilz) + \exp\left[2\pi il\left(z+\frac{1}{2}\right)\right]\right\}. \tag{4.55}$$

For odd l this expression goes to zero, and for even ones it is nonzero. In other words, the presence of a screw axis manifests itself in the reciprocal lattice by extinctions of reflections on the corresponding reference axis of the reciprocal lattice. If the screw axis were axis 3_1, then reflections $00l$ only with $l = 3n$ would be present, while reflections with $l \neq 3n$ would be absent, etc.

Assume now that we have a glide-reflection plane a perpendicular to axis b which produced a point with coordinate $x + 1/2, \bar{y}, z$ from any point xyz. Setting up a sum for these two points similarly to (4.55), we find that in the zero plane ($k = 0$) of the reciprocal lattice (parallel to the glide plane in the atomic lattice) possessing reflections $h0l$, those of them with $h \neq 2n$ are absent. On the other hand, reflections $h0l$ with even $h = 2n$ are not extinguished.

The explanation of the effect of symmetry elements with a translational component on the diffraction pattern, which we derived formally for the expression for the structure factor (4.44), is very simple. For an x-ray "reflection" from

a crystal plane, only the atomic coordinates along vector $\boldsymbol{H}_{hkl}$ are essential for the value of the structure factor, i.e. those in projection onto this vector, which is normal to the given plane, while the atomic coordinates in the plane are not essential. But in projection, for instance, onto screw axis 2_1 the structure actually has a halved period because of the presence of the translational component (Fig. 4.18), and this means that the period in the reciprocal lattice for this direction is doubled, i.e., is equal to $2c^*$ and not c^*, and there are no nodes with odd l. The effect of glide planes is explained similarly: the structure in projection onto such a plane has a halved period along the glide component, and the period in the reciprocal lattice on the corresponding coordinates plane is doubled accordingly, i.e., odd reflections are extinguished. It is significant that extinctions due to screw axes or glide planes arise only on coordinate axes or on planes of the reciprocal lattice, respectively, because no multiple reduction in period is obtained for projections along other directions (Fig. 4.18c).

Extinctions due to the centering of atomic lattices A, B, C, I, F refer to the entire set of reflections hkl of the reciprocal lattice, and not only to its coordinate axes or planes. Let us assume that the lattice is a C-lattice, i.e., it is centered on face ab, and to each point x, y, z there is a corresponding point $x + 1/2$, $y + 1/2$, z. Similarly to (4.55) we find that for any hkl, only those F_{hkl} do not vanish for which $h + k = 2n$, and if $h + k \neq 2n$, then $F_{hkl} = 0$, i.e., the corresponding reflections are extinguished. The absence of these reflections simply follows from the existence of a primitive cell with $\boldsymbol{a}' = (\boldsymbol{a} - \boldsymbol{b})/2$, $\boldsymbol{b}' = (\boldsymbol{a} + \boldsymbol{b})/2$, where $\boldsymbol{a}$ and $\boldsymbol{b}$ are the periods of the centered cell (Fig. 4.19a). The primitive reciprocal vectors in this case are equal to $\boldsymbol{a}'^* = (\boldsymbol{a}^* - \boldsymbol{b}^*)$, $\boldsymbol{b}'^* = (\boldsymbol{a}^* + \boldsymbol{b}^*)$ (Fig. 4.19b); all the reflections in the reciprocal lattice with a primitive reciprocal cell are observed, but if we switch to its nonprimitive indexing, we shall obtain the above-mentioned condition $h + k = 2n$. If the lattice is centered on all the three faces, then only those reflections will be observed for whose indices the conditions $h + k = 2n$, $h + l = 2n$ and $k + l = 2n$ are fulfilled simultaneously. When the lattice is body-centered, only those reflections are observed for which $h + k + l = 2n$. The last two cases account for the fact that the reciprocal lattice has nodes hkl: in the first

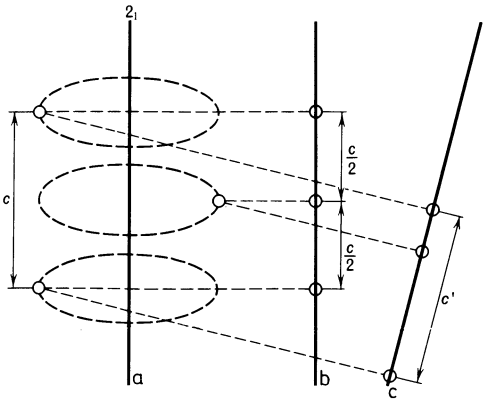

Fig. 4.18. A structure with axis 2_1 (**a**) projected onto this axis (**b**) and onto an arbitrary direction (**c**)

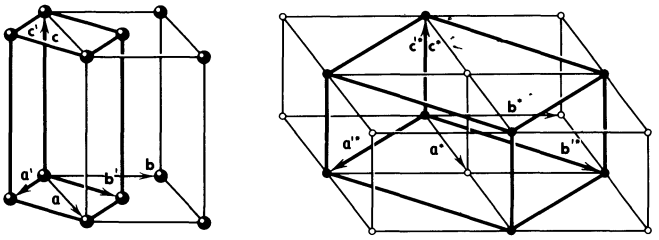

a b

Fig. 4.19a,b. Base-centered cell ***a, b, c*** in the direct space (**a**) and the corresponding cell ***a*, b*, c**** in reciprocal space (**b**). Solid lines denote primitive cell ***a'***, ***b'***, ***c'*** and the corresponding cell ***a'**, *b'**, *c'****

case only at the vertices and at the center of the reciprocal lattice with doubled periods, and in the second, at the vertices and at the centers of the faces (Fig. 4.20). Therefore it is sometimes said that the reciprocal lattice of a base-centered atomic lattice is base-centered (Fig. 4.20b), that of a body-centered one, face-centered (Fig. 4.20c), and that of a face-centered one, body-centered (Fig. 4.20d).

Thus, if a point group of a crystal K is expressed in the symmetry of a reciprocal lattice as one of the Laue classes, then the Bravais group and the symmetry elements of group Φ with a translational component manifest themselves in the diffraction pattern through extinctions (but the point symmetry elements of groups Φ do not manifest themselves). Hence, each group Φ is described in the reciprocal lattice by conditions limiting possible reflections, i.e., by a certain definite set of extinctions or by their absence. For instance, for D_{2h}^{16}–*Pnam* (full designation $P2_1/n\ 2_1/a\ 2_1/m$) the translation group is primitive, and therefore there are no extinctions for reflections of the general form *hkl*; plane n causes extinctions of reflections $0kl$ with $k + l \neq 2n$; and plane a, of reflections $h0l$ with $h \neq 2n$. But the same extinctions are characteristic of another group C_{2v}^{9}–$Pna2_1$, because in the first case m does not affect extinctions, and axis 2_1 was present in the first group. Thus, the same set of extinctions characterizes, in the general case, not one, but several groups (although some Φ are determined by them unambiguously). In all, 120 "x-ray groups" are known, which differ in the Laue class and the set of extinctions; they comprise 230 space groups. Consequently, a diffraction experiment enables one to allocate a crystal to one of several groups Φ, and sometimes to determine it unambiguously. In addition, in some groups Φ extra extinctions arise if atoms occupy not general, but special positions. The extinction tables for groups Φ corresponding to them are given in the International Tables [4.4, 11] (Fig. 2.81) and many other publications.

Diffraction data, however, contain one more kind of information on crystal symmetry which is built into the total set of values of the structure factors. As we know, the coordinates of the atoms in the cell are symmetrically related, and they enter into the trigonometric factor (4.44, 45). But these equations also contain the atomic temperature factors f_{iT} (23) which systematically reduce

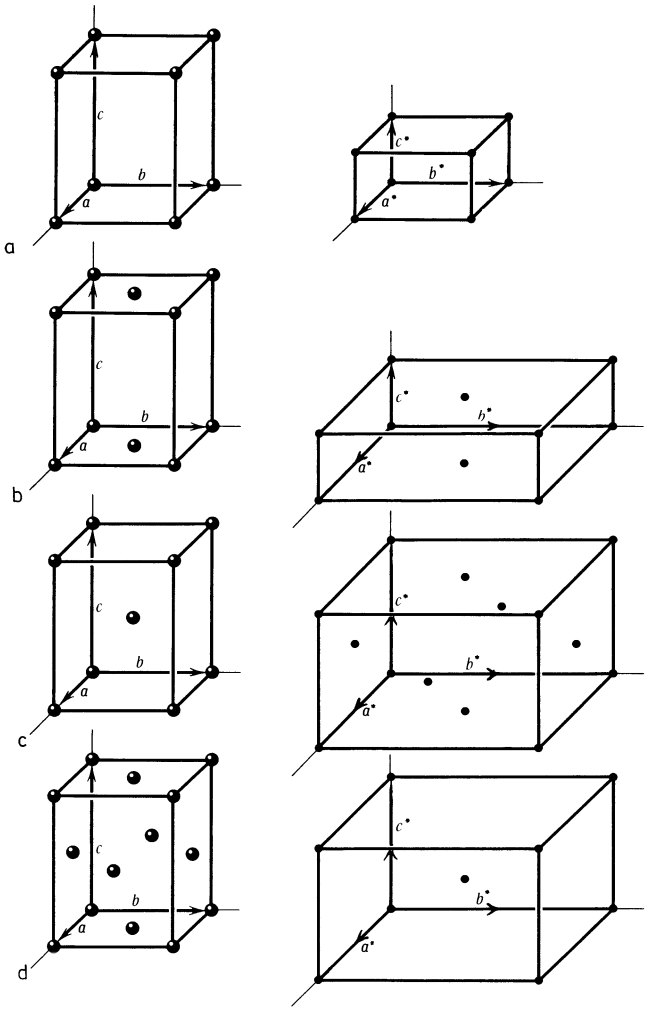

Fig. 4.20a–d. Atomic and corresponding reciprocal lattices: (**a**) primitive–primitive, (**b**) base-centered–base-centered, (**c**) body-centered–face-centered, (**d**) face-centered–body-centered

F with increasing $\sin\theta/\lambda$. To obtain values depending only on the disposition of the atoms, it is customary to introduce the so-called unitary structure factors $\hat{F}_{hkl}$

$$\hat{F}_{hkl} = \frac{F_{hkl}}{\sum_{j=1}^{N} f_{j\mathrm{T}}} = \sum_{j=1}^{N} n_j \exp[2\pi\mathrm{i}(hx + ky + lz)],$$

$$n_j = \frac{f_{j\mathrm{T}}}{\sum_{j=1}^{N} f_{j\mathrm{T}}}. \tag{4.56}$$

Here, n_j are constant numbers if all the atoms in the cell are the same, and are almost constant numbers if they are different, since to a satisfactory approximation $f_{j\mathrm{T}}$ curves for different atoms are similar.

Let us consider the total set of $|\hat{F}|$ irrespective of their indices hkl, making the natural assumption that the argument of the trigonometric factor takes all values from 0 to 2π with equal probability. All the $|\hat{F}_H|$ are within the limits of $0 \leqslant \hat{F}_H \leqslant 1$, and according to (4.56) the average value of the square $|\hat{F}|^2 = \Sigma n_j^2$. The symmetry will affect the nature of the function describing the statistical distribution of $|\hat{F}_H|$ among these values. Indeed, if the cell shows no symmetry then, by (4.45), F_{hkl} are distributed over the complex plane within a circle. If there is a center of symmetry $\bar{1}$ in structure (4.52), they are already distributed over the real axis along the straight line $(-1, +1)$. This difference affects the form of the integral cumulative distribution function $N(\zeta)$, where $\zeta = |\hat{F}|^2/|\overline{\hat{F}}|^2$, which shows the fraction of reflections for which the intensities are less than or equal to ζ, and also influences the value $x = |\hat{F}^2|/|\overline{\hat{F}}|^2$, namely

$$
\begin{aligned}
&{}_1N = 1 - \mathrm{e}^{-\zeta}, \quad {}_1x = \pi/4 = 0.785, \\
&{}_{\bar{1}}N = \operatorname{erf}\sqrt{\frac{\zeta}{2}}, \quad {}_{\bar{1}}x = 2/\pi = 0.637.
\end{aligned}
\tag{4.57}
$$

The center of symmetry can be located most efficiently by constructing curves $N(\zeta)$ from $|\hat{F}^2_{\mathrm{obs}}|$ and comparing them with the theoretical (Fig. 4.21). In the same way it is possible to establish (unless it follows from other data) the presence of axis 2 (or 2_1), whose action in projection is similar to that of the center of symmetry, from a reflection zone of the type $h0l$. One more manifestation of symmetry in values $|F|^2$ will be considered in Sect. 4.7; it is associated with the construction of the so-called interatomic-distance function.

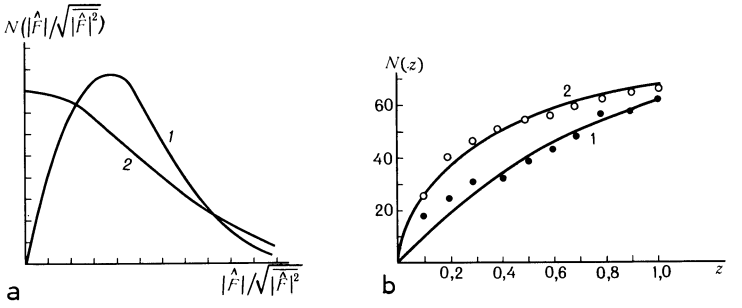

Fig. 4.21a,b. Functions of intensity distribution for crystals with and without a center of symmetry. **(a)** curves of the distribution of structure amplitudes for a noncentrosymmetric (*1*) and a centrosymmetric (*2*) crystal, **(b)** comparison of calculated (——) and experimental distribution $N(\zeta)$ for a centrosymmetric (*2*) and a noncentrosymmetric (*1*) crystal: (· · ·) horse methemoglobin with a resolution > 6 Å [4.12], (∘ ∘ ∘) β-naphthol, projection [100] [4.13]

4.3 Intensity of Scattering by a Single Crystal. Kinematic and Dynamic Theories[2]

4.3.1 Kinematic Theory

In the preceding section we considered scattering of short waves in a crystal and focused our attention on those peculiarities of scattering which follow from the periodic structure of the crystal lattice. Our calculation essentially consisted in the summing of elementary waves arising throughout the volume of the crystal under the effect of the initial, incident wave. The theory of scattering based on this approach is called the kinematic theory. It explains the fundamental property of diffraction from crystals – the discreteness of the directions of scattered beams – and allows us to calculate the intensity of these beams, but only to a certain approximation, which is valid under definite conditions.

The kinematic theory ignores the following circumstances. When an incident wave is propagating in a crystal, its amplitude must diminish gradually, because energy is lost on excitation of secondary scattered waves, and thus the initial wave is weak when it reaches the "farthest" crystal cells. It is also weakened by absorption. The factor of greatest importance, which is not described by the kinematic theory, is that the secondary, diffracted waves themselves interfere both with the initial wave and among themselves and experience, in turn, scattering and absorption.

The theory which takes into account the entire set of these phenomena is called dynamic theory. Kinematic theory is an approximation to this more general theory.

But since dynamic effects develop gradually as the initial wave penetrates into the crystal, the kinematic approach yields fairly accurate results for sufficiently small thicknesses. Indeed, at small thicknesses the primary wave does not weaken considerably, the secondary waves have not yet gained enough intensity, and the absorption effects are not considerable, either.

In other words, kinematic theory is valid when the absolute intensity of the scattered beams is weak compared with that of the incident beam. Estimates (we shall give them below) show that the kinematic approximation can be used for calculating the intensity of x-ray reflections at less-than-critical crystal thicknesses

$$A^K < 10^{-4} - 10^{-3}\,\text{cm}. \tag{4.58}$$

When the thickness of the scattering crystal exceeds A^K, the dynamic theory should be employed.

Crystals used in x-ray structure investigations have linear dimensions of several tenths of a millimeter, which greatly exceeds A^K (4.58), and nevertheless the intensities observed are well described by the equations of kinematic theory,

---

[2] This section was written in cooperation with Z. G. Pinsker.

as has been confirmed experimentally. This is due to the real structure of crystals. Such a crystal represents a mosaic of crystal blocks about 10^{-5} cm in size, which are more or less misoriented with respect to each other by angles of the order of fractions of a minute [Ref. 4.3, Chap. 5]. Such a crystal is called perfectly (ideally) mosaic. The coherent interaction of the scattered waves in such a crystal, i.e., interference, occurs within a single block; thus, the condition of applicability of kinematic theory is fulfilled. As for scattering by a mosaic crystal as a whole, it is defined by the sum of intensities of scattering by each block. The mosaic structure is taken into consideration by introducing some corrections.

If a crystal has a perfect, nonmosaic structure, then at thicknesses of $A > A^K$ the scattering is described by dynamic theory equations.

4.3.2 Integrated Intensity of Reflection in Kinematic Scattering

Let us consider the intensity of reflection by a single crystal in kinematic scattering. Suppose the crystal is in the reflecting position at the Bragg angle and gives a reflection *hkl*, which is recorded on an x-ray photograph (Fig. 4.22). The Ewald sphere then intersects the node *hkl*, as shown in Fig. 4.14. The amplitude of scattering by a crystal of shape Φ is determined by (4.40), and the intensity of the reflection *hkl*, by one of its terms $\Omega^{-2}|F_{hkl}|^2|D(xyz)|^2$, where D is the shape amplitude.

The intensity distribution in the diffraction spot is determined by the distribution of values of this function in its section by the Ewald sphere and by projection of each point of the section onto the plane of the x-ray photograph. This depends, naturally, on the angle of rotation of the crystal. Let us find the integrated intensity of the reflection from the fixed crystal, i.e., the total intensity over all the points of the reflection or, what is the same, the intensity scattered within the three-dimensional angular region encompassing the reflection.

Integration over the coordinates x, y of the x-ray photograph in direct space can be replaced (assuming the portion of Ewald's sphere to be a plane) by integration over the cross section of the node *hkl* in a reciprocal space with coordinates X', Y. As can be seen from Fig. 4.22, the factor of proportionality between these coordinates is $R/\lambda^{-1} = R\lambda$, where R is the distance from the crystal to the film (detector), and $L(\theta)$ is an angular factor depending on the mutual angular orientation of the crystal and detector. The scattered wave is spherically symmetric, i.e., its intensity drops off $\sim R^{-2}$. Thus, with due regard for (4.7),

$$I(\theta_Z) = \frac{I_0}{R^2}\left(\frac{e^2}{mc^2}\right)\frac{|F_{hkl}|^2}{\Omega^2} L(\theta)|D(XYZ)|^2 (R\lambda)^2\, dX\, dY. \tag{4.59}$$

Here, I_0 is the intensity of the incident beam.

For a crystal in the form of a parallelepiped, integration with respect to X and Y will yield values A_1 and A_2. The third factor $|D|^2$ depends on the angle

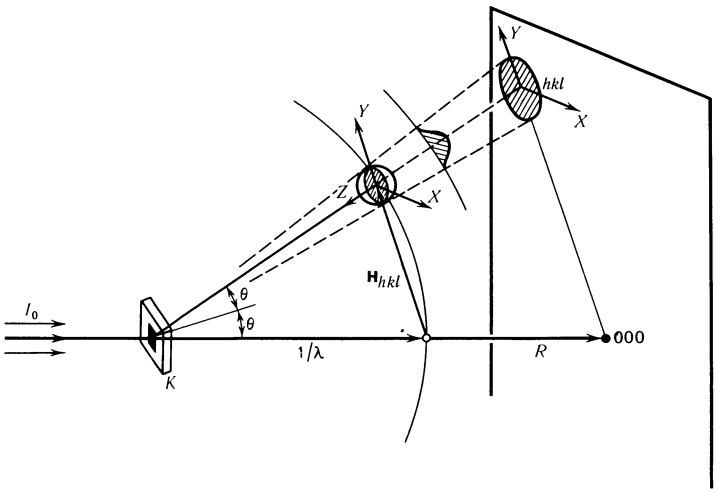

Fig. 4.22. Section of *hkl*-node by the Ewald sphere in the reciprocal space along plane XY and the formation of the corresponding *hkl*-reflection on the x-ray pattern. The point and reflection are scaled up. Crystal (K) with surface $S = A_1A_2$ is irradiated with a primary beam of intensity I_0

of rotation of the crystal θ and the corresponding value of $(\sin \pi A_3 Z/\pi Z)^2$, as follows from (4.41). When the center of the node ($Z = 0$) is intersected by the sphere this factor is equal to A_3^2. Then, in place of (4.59), we get the equation

$$I_{hkl} = I_0\left(\frac{e^2}{mc^2}\right)^2 L(\theta)\lambda^2\left|\frac{F_{hkl}}{\Omega}\right|^2 VA, \tag{4.60}$$

where $V = A_1A_2A_3$ is the crystal volume, and $A_3 = A$ is its thickness.

Introducing the value $A_1A_2 = S$ (the area of the irradiated surface of the crystal) we find that the ratio of the scattered intensity to the intensity I_0S received by the crystal from the initial beam, i.e., the coefficient of the integrated reflection from a crystal fixed at the Bragg angle, is

$$\frac{I_{hkl}}{I_0S} = L(\theta)\left(\frac{e^2}{mc^2}\right)^2 \lambda^2\left|\frac{F_{hkl}}{\Omega}\right|^2 A^2. \tag{4.61}$$

This expression, which was derived in the kinematic approximation, shows that the coefficient of the integrated reflection is proportional to the square of the crystal thickness A. Naturally, this can be true only up to certain thickness A^K, otherwise the scattered intensity would exceed the initial. Therefore the following relation may be adopted as the criterion of applicability of the kinematic approximation:

$$\lambda\left|\frac{F_{abs}}{\Omega}\right| A^K \lesssim 1, \tag{4.62}$$

where $F_{abs} = F_{hkl}e^2/mc^2$. [See [4.14]. The factor $L(\theta)$ is of the order of unity].

Assuming for simplicity that all the atoms in the cell scatter in phase, i.e., that $F_{abs} = \Sigma f_{e.x.}$ and the value of $f_{e.x.} \approx 10^{-11} - 10^{-12}$ cm, the volume per atom $\sim 10^{-23}$ cm^3, and $\lambda \approx 10^{-8}$ cm, we find from (4.62) that $A^K \lesssim 10^{-4}$. This is actually the thickness limit at which the kinematic theory ceases to be valid. For real crystals, A^K has different values, of course, because the magnitude of the structure amplitudes depends on the arrangement of the atoms in the cell and also (through $f_{e.x}$) on the atomic number.

Equation (4.60) gives the integrated intensity of the reflection *hkl* from a fixed crystal in the reflecting position which corresponds to the exact intersection of the center of the node *hkl* by the Ewald sphere. In determining the intensities in structure analysis it is, however, practically impossible to bring the crystal into an exact reflecting position for measuring each reflection. In actual practice all the methods for detection and measurement of intensities are based on the fact that the crystal is rotated in the beam. Then, as the Ewald sphere intersects the nodes of the reciprocal lattice, various reflections, recorded in turn on the x-ray photograph, will appear and disappear. As the sphere "traverses" the node *hkl* in the third direction (Fig. 4.22), the intensity of each separate reflection increases in accordance with the function $[\sin^2 \pi A_3 Z/(\pi Z)^2]$ (Fig. 4.12b), reaches a maximum, and then falls off. Thus the intensity is integrated in the third direction, i.e., over the whole volume of the node of the reciprocal lattice. The x-ray photograph or the detector records precisely this integrated intensity I^{int}_{hkl}. It is noteworthy that integration over the angles automatically takes into account the disorientation of the mosaic blocks with respect to each other; hence they "reflect" at closely similar angles, so that all these reflections find themselves in the common region of the reciprocal lattice and produce a single reflection *hkl* on the x-ray photograph.

Integration in the third direction excludes (within the framework of the kinematic theory) the dependence on the crystal thicknesses A, and therefore only the dependence on the total volume of the mosaic crystal V remains. The integrated intensity equations naturally depend on the specific geometry of the x-ray photography method, this being accounted for by the angular factor L (Lorentz factor) [4.15], and also on the angular velocity of crystal rotation $\dot{\omega}$. In the final analysis the following expression for integrated intensity is obtained:

$$I^{int}_{hkl} = I_0 \left(\frac{e^2}{mc^2} \right) pL \frac{\lambda^3 V}{\dot{\omega} \Omega^2} |F_{hkl}|^2 B \mathscr{E} G . \tag{4.63}$$

Here, p is the polarization factor, B is the transmission factor (depending on the absorption coefficient μ), G is the correction for anomalous scattering, and $\mathscr{E}$ is the extinction coefficient. This coefficient depends on the mosaic structure of the crystal and has two components. One of them accounts for the slight drop in intensity due to dynamic effects in each separate block. This is the so-called primary extinction. At the same time, the mosaic blocks standing first in the path of the wave and from which the reflection occurs deprive the following blocks of part of the energy of the incident wave, and this causes the so-called

secondary extinction. The summary action of both these effects (the second plays a more important part) is given by the coefficient $\mathscr{E}$, which is determined experimentally.

Real single crystals studied by x-rays have, in addition to mosaic structure, many other structural distortions inside each block, such as point defects and dislocations. The number of such defects is usually not very large (less than $10^{10}\,\mathrm{cm}^{-3}$) and, as indicated by theoretical estimates and experimental data, this does not affect (4.63) significantly.

Thus, for integrated intensity, the relation $I_{hkl}^{\mathrm{int}} \sim |F_{hkl}|^2$ is valid in kinematic theory. This fact is the experimental basis of x-ray and other diffraction methods of investigating the crystal structure.

If a crystal abounds in various defects, such as those occurring in solid interstitial and substitutional solutions or in stressed crystals, where lattice distortions and displacements of atoms from equilibrium positions take place, x-ray scattering becomes sensitive to such distortions. Static displacements of atoms act statistically just as their thermal motion does, which leads to an additional drop in intensity of far reflections in accordance with (4.22) for the temperature factor. Lattice distortions cause variations in the unit cell dimensions and thereby affect the shape of the nodes of the reciprocal lattice (see Sect. 4.6). The study of the distortions to crystal structure comprises a special branch of x-ray structure analysis [Ref. 4.3, Chap. 5].

4.3.3 Principles of Dynamic Theory

The dynamic theory describes scattering of short waves in perfect ("ideal") and near perfect crystals. Dynamic consideration is based on taking into account the interactions with energy exchange of all waves in the crystal, both the initial and the diffracted waves [4.16].

Since its appearance in the 1920s, the theory of dynamic scattering of x-rays has been developing in two forms. One of them – Ewald–Laue theory – considers the general problem of propagation of electromagnetic waves in a periodic medium. The other theory goes back to the ideas of Darwin, who proceeded from the kinematic approximation and took into account multiple scattering, interaction and absorption of waves scattered by crystal planes. In principle, for perfect crystals the two theories are equivalent, but their use depends on each particular problem.

In studying x-ray diffraction from ideal crystals, two basic cases (Fig. 4.23) are considered: the Laue case – interference of beams passing through a crystal plate, and the Bragg case – interference of beams emerging on the same side of the crystal as the incident beam.

In dynamic consideration, relationships are established between the rocking curves from crystals and the width of the wave front, the shape and orientation of the crystal, and the degree of its perfection. Other important problems here are the interpretation of the image of the internal defects of crystals obtained in diffracted beams, and also x-ray interferometry. In classical structure analysis,

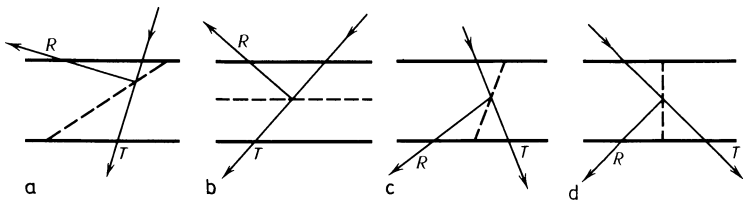

Fig. 4.23a–d. Arrangement of the crystal surface and the reflected beam: (R) reflected beam, (T) transmitted beam. **Bragg case:** (**a**) asymmetric, (**b**) symmetric. **Laue case:** (**c**) asymmetric, (**d**) symmetric. The dashed line denotes the orientation of the reflecting plane

i.e., determination of atomic coordinates in the unit cell of the crystal, dynamic theory is not used. At the same time, the theory is promising for determining symmetry and also for precise determination of the moduli of structure amplitudes $|F_H|$ for simple structures directly from the geometry of the diffraction pattern.

4.3.4 Darwin's Treatment

Darwin constructed a theory of dynamic scattering for the Bragg case, taking advantage of the fact that the kinematic approach is valid for separate thin "reflecting planes" of a crystal [4.17]. These planes fill the crystal half-space and are parallel to its plane surface (Fig. 4.24). The incident wave is reflected from these planes in conformity with the Bragg–Wulff condition (4.3). The ratio of the amplitude of the reflected wave A_r to that of the initial A_0 is defined by the structure factor and is equal to some coefficient $iq(\theta)$. On the other hand, the transmitted wave, "scattered" in the direction of the initial, has weakened slightly, and the corresponding amplitude ratio is equal to $iq(0)$ (the quantity i covers the phase difference). The same can be said about any wave entering the rth plane inside the crystal. But due to repeated Bragg reflections and transmissions, the amplitude of the wave from the $(r-1)$th plane, impinging on plane r, is not the same as the initial. By using the recurrence relations for the coefficients of reflection R and transmission T through planes $(r-1)$, r, and $(r+1)$ it is possible to obtain the expression for the intensity of the beam reflected by a thick plate. If the crystal is rotated slowly near the Bragg angle, the curve for the coefficient of reflection R for such a perfect crystal (without absorption) has

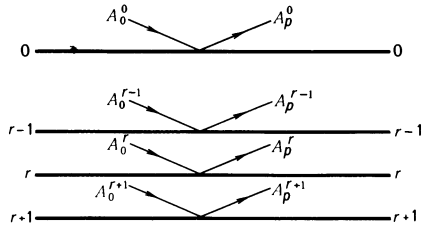

Fig. 4.24. The formation of diffracted beams by successive reflections from planes parallel to the crystal surface

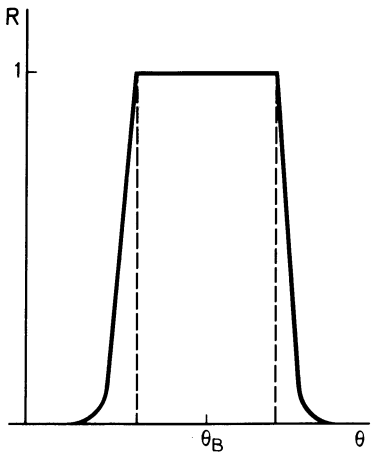

Fig. 4.25. Reflection curve for the perfect crystal without absorption

the shape shown in Fig. 4.25. Coefficient R in the region of the maximum is equal to unity, but the angular width of this region is small, of the order of 10–40″.

For a crystal plate of thickness $A = Nd$, where d is the interplanar spacing and N is the number of planes, and for a nonpolarized initial wave the coefficient of integrated reflection is expressed as

$$R^{\text{int}} = \frac{8}{3\pi} \frac{e^2}{mc^2} \frac{1 + |\cos 2\theta|}{2 \sin 2\theta} \mathrm{N}\lambda^2 \, |F_H| . \tag{4.64}$$

We can see that the intensity is here proportional to the first power of $|F_H|$ in distinction from kinematic theory for a mosaic crystal, where it is proportional to $|F_H|^2$ (4.63).

Because of the dynamic interaction of the primary and reflected waves, the wave propagated in the initial direction is weakened. This phenomenon – primary extinction – is particularly significant for strong reflections, but it can practically be neglected for sufficiently small crystals, i.e., for the mosaic blocks of a perfectly mosaic crystal.

4.3.5 Laue–Ewald Treatment

This theory analyzes interaction of an electromagnetic wave with a crystalline medium with a periodic electron density $\rho(\boldsymbol{r})$, a dielectric constant ε, and a polarization $\chi = \varepsilon - 1$. Diffraction phenomena in such a case are described by a solution of Maxwell's equation for the induction vector $\boldsymbol{D}$

$$\frac{\partial^2 \boldsymbol{D}}{\partial t^2} = - c^2 \, \mathrm{curl} \, \mathrm{curl} \, \boldsymbol{D}/\varepsilon. \tag{4.65}$$

As a result of the interference of the initial and all the excited secondary waves, an electromagnetic field is set up in the crystal. Its amplitude varies with the

periodicity of the lattice itself, and hence the solution can be represented as a sum of a series of plane waves

$$\boldsymbol{D} = \sum_m \boldsymbol{D}_m \exp\{2\pi i[vt - (\boldsymbol{k}_0 \cdot \boldsymbol{r} + \boldsymbol{H}_m \cdot \boldsymbol{r})]\}, \tag{4.66}$$

where $\boldsymbol{k}_0$ is the wave vector of the initial (refracted) wave that entered the crystal, $\boldsymbol{r}$ is the radius vector in the lattice, and $\boldsymbol{H}_m$ is the vector of the reciprocal lattice.

The polarization χ can be expanded in a Fourier series, which finally gives the relation

$$\frac{k_m^2 - K^2}{k_m^2} \boldsymbol{D}_m = \sum_n \chi_{m-n} \boldsymbol{D}_{n[m]} . \tag{4.67}$$

Here, $\boldsymbol{K}$ is the wave vector of the incident wave in a vacuum; $\boldsymbol{k}_m = \boldsymbol{k}_0 + \boldsymbol{H}_m$ are the wave vectors in the crystal; $\boldsymbol{D}_n[m]$ is the component $\boldsymbol{D}_n$ perpendicular to vector $\boldsymbol{k}_m$; and χ_{m-n} is the Fourier component of polarization χ for reflection $\boldsymbol{H}_{m-n}$

$$\chi_H = -\frac{e^2}{mc^2} \frac{\lambda^2}{\pi} \frac{F_H}{\Omega} . \tag{4.68}$$

The system (4.67) formally contains an infinite number of equations, but their number is practically limited because of the drastic reduction in $\boldsymbol{D}_m$ with increasing difference $k_m^2 - K^2$.

Of greatest importance is the case when, along with initial (refracted, more precisely) wave, one more strong diffracted (reflected) wave arises in the crystal, which interacts with the initial. This is the so-called two-wave solution. As in kinematic theory, dynamic reflection can also be interpreted with the aid of the Ewald sphere in the reciprocal lattice (Fig. 4.26), but here the sphere does not necessarily intersect point $\boldsymbol{H}$, which may be at a certain distance from the

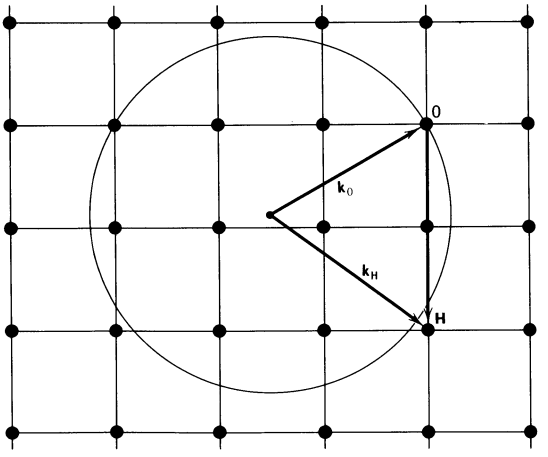

Fig. 4.26. Appearance of an x-ray diffraction maximum according to dynamic theory in the case of nonexact intersection of point H by Ewald's sphere

sphere. This is due to the fact that as a result of refraction of the wave at the vacuum – crystal interface vector $\boldsymbol{K}$ does not exactly coincide with $\boldsymbol{k}_0$. In the two-wave solution, in place of vectors D_0 and D_H, one considers their scalar σ and π components $D_{0\perp}$, $D_{0\parallel}$, $D_{h\perp}$, and $D_{h\parallel}$, with a polarization perpendicular and parallel to the plane of incidence.

The equations for the amplitudes have the following form (the symbols $\perp$ and $\parallel$ are omitted):

$$\frac{k_0^2 - K^2}{k_0^2} D_0 = \chi_0 D_0 + \chi_h D_h, \quad \frac{k_h^2 - K^2}{k_h^2} D_h = \chi_h D_0 + \chi_0 D_h . \tag{4.69}$$

The solution of this system gives four waves for each polarization state. Two distinct interference effects arise as a result of interaction of these four waves.

The first is due to the fact that in a transparent crystal (without absorption) refracted and diffracted waves interact. In the simplest case of a centrosymmetric crystal and symmetric reflection from a system of planes perpendicular to the entrance face, the rocking curve has a finite width and is symmetric with respect to the Bragg angle.

For a certain fixed point of the maximum the amplitudes of the refracted and diffracted waves within the crystal are periodic functions of the depth z, which is perpendicular to the entrance face. The period of these amplitudes is the extinction length.

$$\tau_y = \tau_0 (1 + y^2)^{-1/2}, \tag{4.70}$$

where τ_0 is the extinction length at the exact Bragg condition, and y is some function of the angular deviation from θ within the maximum.

The value of y is defined by the equation

$$y = \frac{1}{2C\left[\frac{\gamma_h}{\gamma_0}(|\chi_{hr}|^2 - |\chi_{hi}|^2)\right]^{1/2}} \left[2\Delta\theta \sin 2\theta + |\chi_{0r}|\left(1 - \frac{\gamma_h}{\gamma_0}\right)\right]. \tag{4.71}$$

Here, C is the polarization factor, which is equal to unity for σ polarization and to $\cos 2\theta$ for π polarization: $\gamma_{0,h} = \cos(\boldsymbol{k}_{0,h}\, \boldsymbol{n})\, \boldsymbol{n}$ is the inward normal to the surface, and χ_{hr} and χ_{hi} are the real and imaginary part of the Fourier component of the crystal polarization, respectively.

Periods τ_0 are of the order of $10^5 - 10^6$ Å; they increase for weak reflections.

Another interference effect arising in the wave field of a crystal is due to interaction of two refracted waves, as well as of two diffracted waves. Here, the periods of variation of the amplitude along depth are equal to d_h of the reflecting planes.

The values of the coefficients of reflection R and transmission T for the Laue case – transmission through a transparent crystal plate of thickness A – are calculated with an allowance for the boundary conditions on the exit face. For a parallel-sided crystal plate it appears that the quantities R and T are periodic functions of the crystal thickness and the angle of incidence within the angular

interval of the corresponding maximum. This is the so-called Pendellösung (or pendulum solution) (Fig. 4.27)

$$R_h(y) = \frac{\gamma_h}{\gamma_0}\left|\frac{D_h^{(d)}}{D_0^{(a)}}\right| = \frac{\sin^2 \dfrac{\pi d}{\tau_0}\sqrt{1+y^2}}{1+y^2}, \tag{4.72}$$

$$T_h(y) = \left|\frac{D_0^{(d)}}{D_0^{(a)}}\right| = 1 - R_h(y). \tag{4.73}$$

The subsidiary maxima of this solution for R_h at a fixed value of A decrease. With a small increase in thickness A (in the transparent crystal approximation) the oscillations on curves R and T disappear, the respective values being denoted by $\bar{R}$ and $\bar{T}$ (Fig. 4.28).

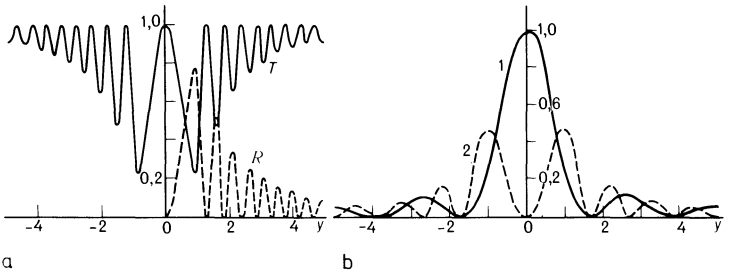

Fig. 4.27a,b. Change in the values of R and T in the region of the maximum for a transparent crystal. (**a**) curves R and T correspond to thickness $A = 2n\tau_0$ [4.14], (**b**) curves at different crystal thicknesses; subsidiary maxima of the pendulum solution (*1*) $A = (2n+1)\tau_0/2$; (*2*) $A = n\tau_0$ are shown [4.18]

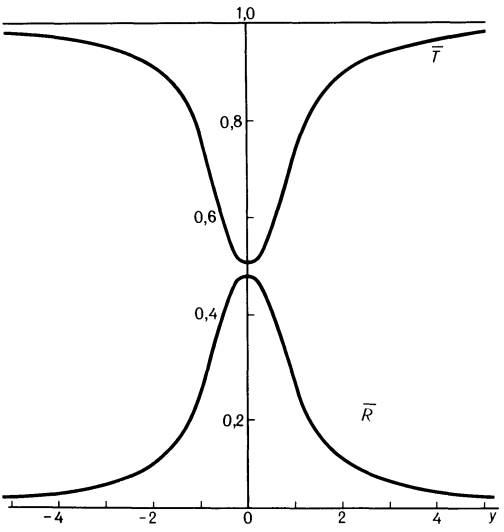

Fig. 4.28. Profile of the maxima of averaged functions $\bar{R}$ and $\bar{T}$ [4.16]

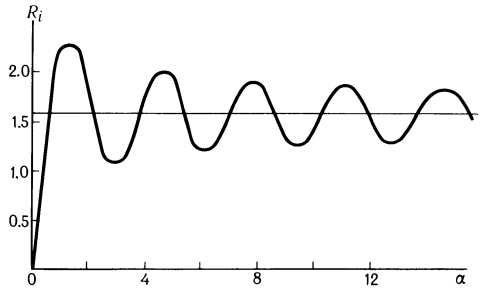

Fig. 4.29. Curve of integrated reflection [4.18]

If a crystal plate is wedge shaped, the values of R and T on the exit face represent a periodic function with a period $\tau' \approx \tau/\sin\mu$, where μ is the wedge angle, and the arising pattern shows lines of equal thickness. This effect can be used for determining structure amplitudes, since according to (4.68, 71–73) the values of $|F_H|$ are related to D via χ_h. Such measurements are highly accurate and are used for precise investigations of the distribution of the electron density in crystals with a simple structure [Ref. 4.3, Chap. 2].

Integration over the entire intensity maximum at reflection from a transparent parallel-side crystal plate in the Laue case gives the value of the integrated intensity

$$R_i = \frac{\pi}{2} \int_0^{2\alpha} J_0(x)\, dx, \quad \alpha = \frac{\pi A C}{\lambda \gamma_0 \gamma_h} |\chi_h|. \tag{4.74}$$

The integral of the Bessel function $J_0(x)$ depends only on the upper limit 2α, and the value of R_i increases linearly with increasing α in the region of small α values, and then oscillates with a decreasing amplitude near the average value $\pi/2$ (Fig. 4.29). The region of linear increase in R_i is nothing else than the range of applicability of kinematic theory. Regarding $\alpha \approx 0.7$ as the limiting value, we find (for a symmetric reflection) for a crystal thickness A^K, for which the kinematic approximation holds, the value

$$A^K = \frac{0,7 \cos\theta}{(e^2/mc^2)\, |F_H/\Omega|\, \lambda}, \tag{4.75}$$

which practically coincides with (4.62). This yields, for instance, $A \approx 1.25 \times 10^{-3}$ cm for the 333 reflection from Si for Mo$K\alpha$ radiation and $A \approx 1.5 \times 10^{-4}$ cm for the 220 reflection from Ge for Cu$K\alpha$ radiation. From (4.75) it follows that for crystals of heavy elements with a simple structure, i.e., for large values of $|F_H|/\Omega$, A^K is small. And conversely, for complicated organic crystals A^K is comparatively large and may reach 10^{-2} cm.

4.3.6 Dynamic Scattering in an Absorbing Crystal. Borrmann Effect

The scattering in thick crystals depends essentially on the diffraction mechanism of x-ray absorption.

The most interesting phenomenon in dynamic scattering in an absorbing crystal is the effect of anomalous transmission, or the Borrmann effect [4.19, 20]. The full value of the absorption coefficient for the quantities R and T is formed, algebraically, from the mean value σ_c and diffraction contribution $(\sigma_h + \sigma'_h)$. Here, an anomalously large absorption occurs for one field, and, contrariwise, an abrupt decrease in absorption – anomalous transmission – for the other.

A pictorial physical model of the Borrmann effect is associated with interference of the refracted and diffracted waves for each of the two fields. As a result of this interference the maxima of the amplitudes of the quasi-standing waves in the first field coincide with the system of atom-filled planes (hkl), which results in strong absorption of this field. The maxima for the second field occur halfway between the indicated planes, which yields anomalous transmission (Fig. 4.30).

For a given linear coefficient of absorption μ the Borrmann effect manifests itself strongly enough already at values $\mu A > 10$, where A is the crystal thickness. Thus, for a germanium crystal for Cu$K\alpha$ radiation this corresponds to $A > 0.28$ mm, for Mo$K\alpha$ radiation, to $A > 0.35$ mm, and for a silicon crystal to $A > 0.7$ and 7.0 mm, respectively. The Borrmann effect results in the disappearance of the secondary maxima and a sharp asymmetry of the transmission curve in the medium-thickness region. The rocking curves remain symmetric about the y axis (Fig. 4.31).

In reflection from a thin crystal plate (the Bragg case) the boundary conditions change substantially, and two effects take place. One part of the wave field is reflected back and, interfering with the initial wave field, gives, upon emergence through the entrance face, secondary maxima at the sides of the overall

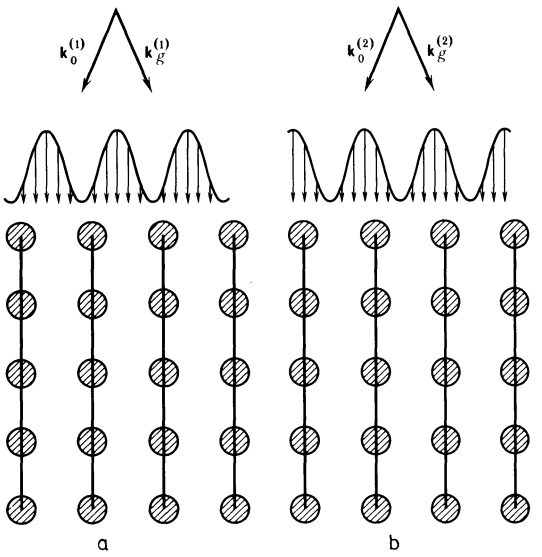

Fig. 4.30a,b. Physical model of the Borrmann effect.
(**a**) anomalous transmission, nodes of quasi-standing waves are on atomic planes, (**b**) anomalous absorption, antinodes are on the atomic planes [4.14]

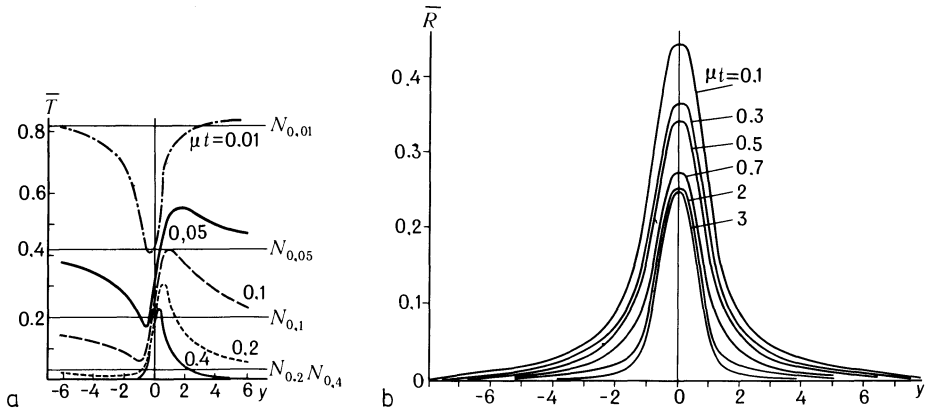

Fig. 4.31a,b. Curves of transmission and reflection for an absorbing crystal in symmetric recording for a series of increasing values of μt(t is the thickness). (**a**) transmission maxima T (reflection 200 NaCl, Cu$K\alpha$ radiation, $\mu = 160\,\mathrm{cm}^{-1}$ [4.21]; (**b**) reflection maxima (reflection of 220 Si, Mo$K\alpha$ radiation, $\mu = 13.4\,\mathrm{cm}^{-1}$). [4.22]. N levels correspond to normal absorption at the appropriate thicknesses

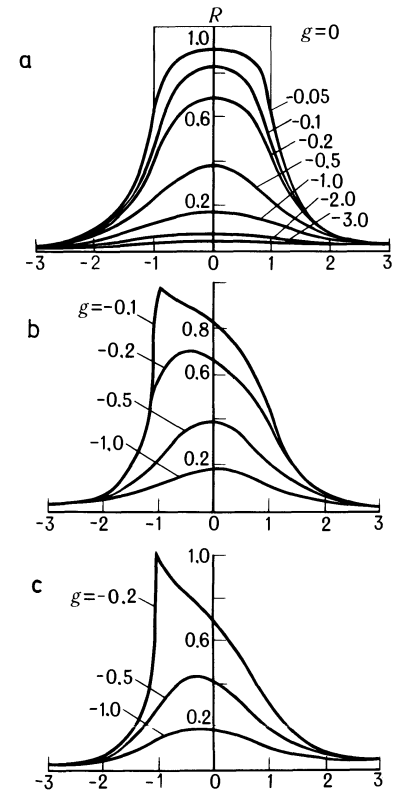

Fig. 4.32a–c. Curves of Bragg reflection from a thick absorbing crystal, corresponding to different values of parameters g and κ.

$$g = -\frac{\chi_{0i}\left[1 + \frac{|\gamma_h|}{\gamma_0}\right]}{2C|\chi_{hr}|\sqrt{\frac{|\gamma_h|}{\gamma_0}}} \qquad \kappa = \frac{|\chi_{hi}|}{|\chi_{hr}|}.$$

(**a**) $-\kappa = 0$; (**b**) $-\kappa = 0.1$; (**c**) $-\kappa = 0.2$

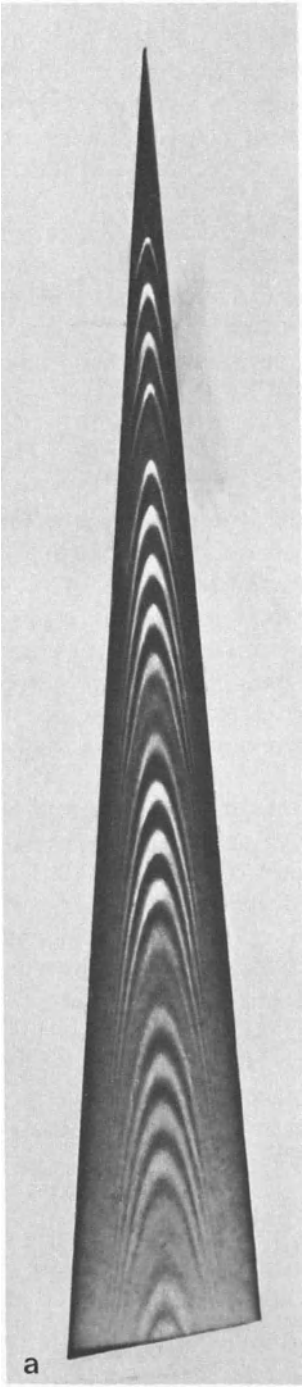

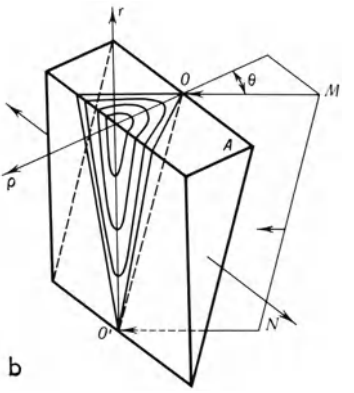

Fig. 4.33a,b. Pendellösung fringes in the form of hyperbolae arising in transmission of a spherical wave through a crystal wedge.
(**a**) interference pattern [4.24]; (**b**) propagation of the wave front in a wedge-shaped crystal and the formation of hyperbolic maxima on the exit face [4.25]

maximum. The other part emerges through the lower boundary of the plate, which leads to the transmission effect for the Bragg case.

The symmetric shape of the maximum (Fig. 4.27) with a flat top in the region of full reflection, which is typical of a transparent (with low absorption) semi-infinite crystal, becomes more and more asymmetric with increasing in absorption, with a sharp maximum at one of the boundaries of the indicated region (Fig. 4.32).

In the problems of classical dynamic theory briefly described here we considered cases of incidence of a plane wave on a crystal in the form of an infinite plate or semispace. At present, the generalized dynamic theory is being developed, in which the incident wave may have any shape for surface of equal phase and any front width, while the crystal may have an arbitrary shape (Fig. 4.33).

4.3.7 Experimental Investigations and Applications of Dynamic Scattering

One of the most important tasks in investigating the dynamic scattering of x-rays in crystals is to establish the exact correlation between the experimentally measured scattering parameters and their theoretical analogs.

In experimental studies of dynamic scattering, x-rays of a definite wavelength fall on the crystal under investigation which is set in the reflecting position. If the crystal is fixed, one can study the space distribution of the intensity of the diffracted rays. X-ray diffraction topography is based on this. If we rotate the crystal near the exact reflecting position, we can study the intensity distribution by the rocking curves method.

The curves are measured in double-and triple-crystal x-ray spectrometers, in which an incident x-ray beam is collimated and monochromatized with the aid of reflection from a monochromator crystal or two such crystals.

The rocking curve, which is measured in the Bragg classical scheme of a double-crystal spectrometer after Bragg (Fig. 4.34) is a convolution of the rocking curves of both crystals and does not coincide with the theoretical value of the diffraction maximum. The increase in the angular width of the experimental curve is due to angular and spectral broadening (i.e., nonparallelism and nonmonochromatism) of the incident beam.

The effect of these factors on the shape and width of the rocking curve can be made small by using a three-crystal x-ray spectrometer (Fig. 4.35). By using

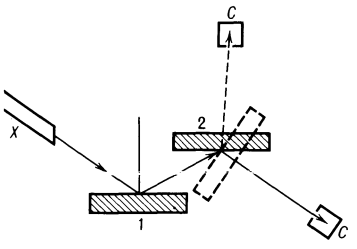

Fig. 4.34. Diagram of the double-crystal spectrometer after Bragg. (*X*) x-ray source; (*C*) detectors; (*1*) monochromator crystal; (*2*) crystal under investigation. The solid and dashed lines denote, respectively, the parallel and the inclined positions of crystals *1* and *2*

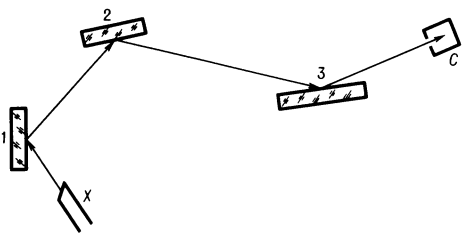

Fig. 4.35. Scheme of the three-crystal spectrometer

different mutual positions of two fixed crystals – monochromators 1 and 2 – and using asymmetric reflection, one can obtain a practically parallel, monochromatic and fully polarized beam falling on the crystal under investigation. In other words, in a three-crystal spectrometer, the above-mentioned approximation of a plane incident wave is realized experimentally.

With the aid of such a beam it is possible to measure the so-called proper curves of diffraction reflection, compare them with the corresponding theoretical values, and study fine diffraction effects, which require a high angular resolution. For instance, the asymmetry of the rocking curve, predicted by the theory for an absorbing crystal, was first discovered experimentally only with the aid of a triple-crystal spectrometer.

Precise investigations of the shape of the rocking curve and its variations supply quantitative information on the structural perfection of the crystal under examination, since all the changes in the parameters of the curve are entirely due to distortions of the ideal structure.

X-ray topography consists in obtaining the image of the whole crystal in a single Bragg reflection. Imagine that there is a parallel x-ray beam of large cross section. (This has recently been realized with the aid of beams of x-ray synchrotron radiation – see Sect. 4.5). If we place a crystal in a reflecting position in this beam, the "reflection" will have the size of the crystal and show its internal structure. In practice, when conventional sources are available, this is realized for thin crystal plates by the Lang method – scanning the plate according to the Laue scheme under a narrow incident x-ray beam with synchronous motion of a photographic plate under the reflected beam (Fig. 4.36a).

In this way the image – topogram of the entire crystal – is obtained (Fig. 4.36b). If to take a topogram in a synchrotron radiation beam (Fig. 4.36c), we can detect rapid changes in the real structure of a crystal on phase transitions, in the course of growth, etc.

If a crystal has some defect, for instance a dislocation, then during the propagation of a wave through it a phase difference arises with respect to the wave which has not transmitted through this defect. Such a phase contrast leads to a change in the image on the corresponding site of the topogram as compared with the other regions of the crystal. The particular manifestation of the defect – brightening or darkening – depends on the crystal thickness and the extinction length. For instance, at $\mu A < 1$ (a "transparent" crystal) dislocations with a Burgers vector parallel to vector $\boldsymbol{H}_h$ of the reflection employed appear as

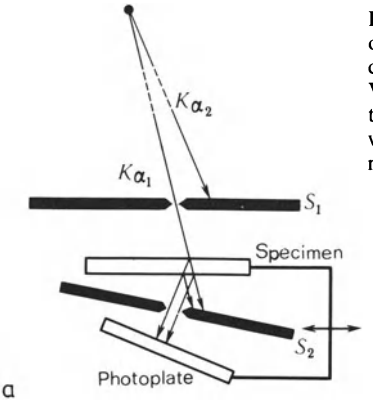

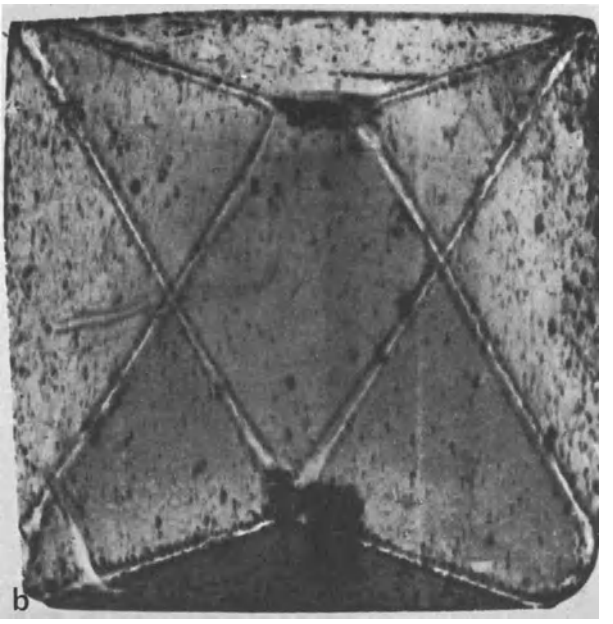

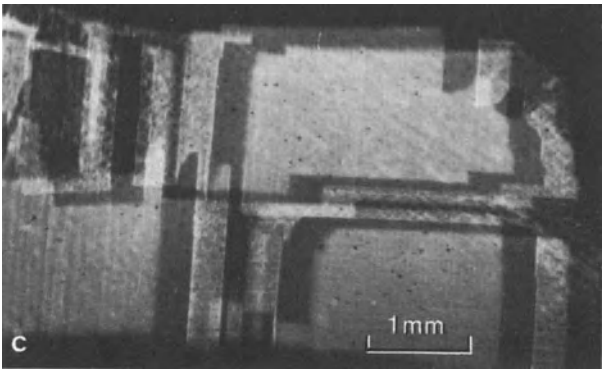

Fig. 4.36a–c. X-ray diffraction topography method. (**a**) geometry after A. R. Lang., (**b**) x-ray topogram of natural diamond obtained by the Lang method, × 15 (courtesy of V. F. Miuskov) (**c**) topogram of a KD_2PO_4 crystal obtained in a synchrotron x-ray beam. The domain structure which arises below the Curie point ($T = 115$ K) has been revealed (courtesy of O. P. Aleshko-Ozhevsky)

dark lines. Photography in the "absorbing"-crystal regime ($\mu A \gg 1$) is also used. The topograms also show the boundaries of large mosaic blocks, slip bands, and the interference effects of the pendulum solution. The study of these phenomena is the subject of the theory of image formation, which has been developing vigorously in recent years, not only for x-ray, but also for electron and neutron diffraction.[3]

The Lang method requires a total exposure of several hours, whereas the use of a beam of synchrotron radiation reduces it to seconds, which makes it possible, in principle, to study changes in real structure during deformation, phase transitions, etc.

Of great interest are the methods of x-ray interferometry and moiré pattern, which have been developing in recent years. Here, one observes the repeat interference of an x-ray beam which has passed through a system of crystal plates with a perfect structure.

A diagram of an x-ray interferometer is given in Fig. 4.37. The whole instrument, which consists of three crystal plates – separator S, mirror M, and analyzer A and their common base – is carved out of a large perfect single crystal. The thicknesses of plates ($\mu A \approx 20$) are chosen in such a way that each plate is anomalously transparent only for the second field in accordance with the classical theory. An incident x-ray beam splits on S in two and on passing this and the other plates is reflected from the same system of plates consecutively forming refracted and diffracted waves. If the analyzer grating A is displaced or turned with respect to the "common" grating of S, M, and A, or if it has defects, the pattern of the emerging beams will reveal a moiré pattern. The instrument can also be used for observing and interpreting moiré patterns at preassigned conditions of displacement or rotation of the analyzer plate. With a parallel

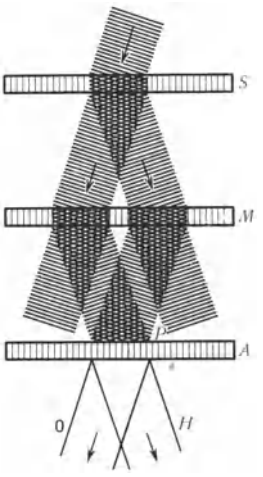

Fig. 4.37. Diagram of an interferometer according to Laue scheme [4.26]

[3] X-ray topography of defects and interferometry are also discussed in [Ref. 4.3, Chap. 5].

arrangement of the reflecting planes in S and M, if they differ in the values of the interplanar distances d_h, a dilatation moiré pattern with a period $\Lambda = d_1 d_2/\Delta d$ will appear. This makes it possible to detect extremely small disturbances in periodicity, of the order of 10^{-8} of a period d_h, i.e., $\Delta d \approx 10^{-16}$ cm. If the periods coincide, but the crystals have a small relative turn about the axis perpendicular to the plates, a rotational moiré pattern appears; its period $\Lambda_R \approx d/\varphi$, where φ is the rotation angle (Fig. 4.38). In this case, too, the sensitivity threshold of the moiré pattern to the variation in φ is extremely high, $\Delta\varphi = 10^{-8}$ rad is detected.

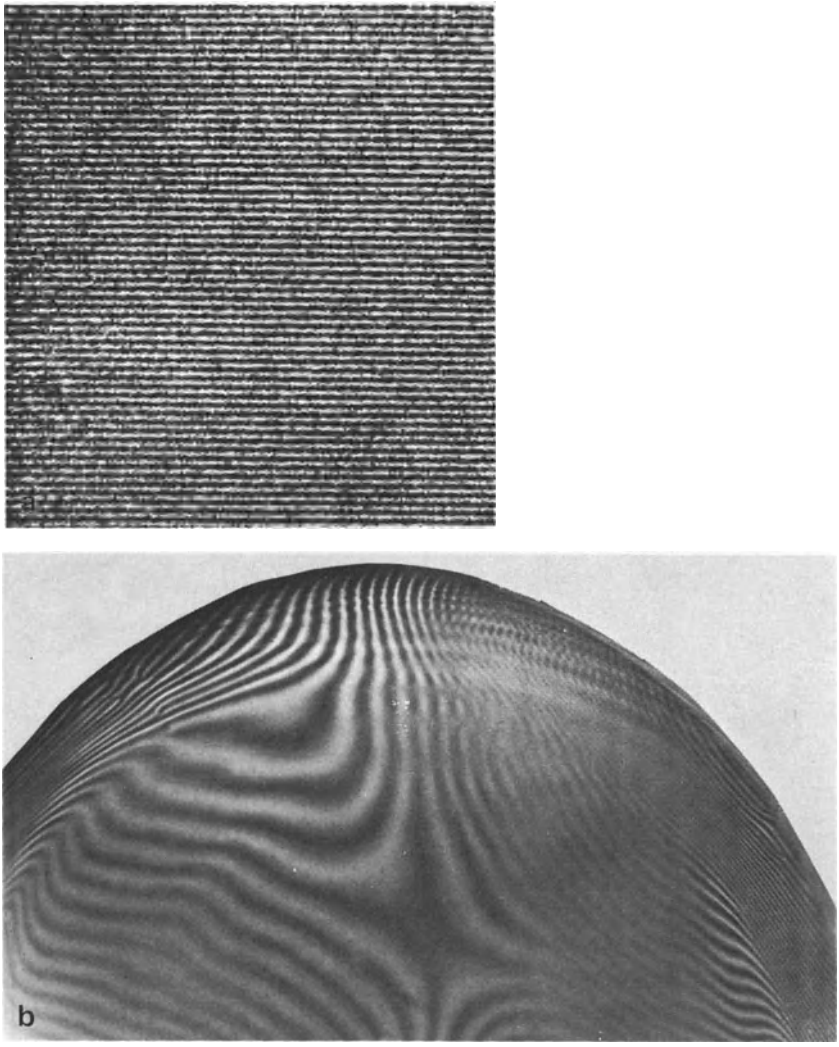

Fig. 4.38a,b. X-ray diffraction moiré of silicon crystals. **(a)** rotation moiré pattern from two Si platelets, rotation angle 2.5″ [4.27]; **(b)** complex moiré pattern: *top left* moiré from dislocations, *bottom right and left* rotation moiré, *top center* dilatation moiré, *center* mixed moiré (courtesy of V. F. Miuskov)

In moiré patterns one can also visualize lattice defects, namely dislocations (Fig. 4.38b).

Thus, dynamic theory, which was first developed for perfect crystals, is also becoming a tool for investigations of imperfections in crystals. It should be emphasized that diffraction from crystals intermediate in size between those to which one can apply either purely kinematic or purely dynamic theories is the most difficult for analysis.

4.4 Scattering by Noncrystalline Substances

4.4.1 General Expression for Intensity of Scattering. Function of Interatomic Distances

X-ray and other diffraction methods supply the most accurate information on the crystal structure, but they can also be used for studying the structure of less ordered systems – polymers, liquid crystals, amorphous solids, liquids, and gases. The closer the order in the system to that in a crystal, the more features inherent in diffraction from a crystal are retained in scattering from such a system.

Since condensed noncrystalline systems have no long-range order, it is impossible in practice to calculate their scattering amplitudes, but direct calculation of the scattering intensity is feasible.

Let us consider such a possibility. The Fourier integral (4.12) or expressions of the type (4.44) following from it with an allowance for (4.25), i.e.

$$F(\boldsymbol{S}) = \sum_{j=1}^{N} f_{j\mathrm{T}} \exp\left[2\pi \mathrm{i}(\boldsymbol{r}_j \cdot \boldsymbol{S})\right] \tag{4.76}$$

are universal; they give the amplitude of scattering from an assembly of any N atoms in positions $\boldsymbol{r}_j$ and having atomic-temperature factors $f_{j\mathrm{T}}$. We know that only strictly discrete directions of scattered beams are possible for a crystal in accordance with the condition $\boldsymbol{S} = \boldsymbol{H}_{hkl}$ (4.30). But for an arbitrary object, $\boldsymbol{S}$ may have any value, i.e., scattering with a noticeable intensity is possible in any direction $\boldsymbol{k} = \boldsymbol{k}_0 + 2\pi\boldsymbol{S}$ (Fig. 4.13). The intensity is defined, by analogy with (4.47), as

$$I(\boldsymbol{S}) = |F(\boldsymbol{S})|^2 = F(\boldsymbol{S})\, F^*(\boldsymbol{S})\,. \tag{4.77}$$

It can naturally be calculated after $F(\boldsymbol{S})$ is obtained from (4.76). But how can we assign all the atomic positions $\boldsymbol{r}_j$, say, in such a system as a liquid? It is possible, however, to obtain a different expression for intensity I if we insert the scattering amplitude taken from (4.76) into (4.77), bearing in mind that for F^* the distance $\boldsymbol{r}_j$ is replaced by $-\boldsymbol{r}_j$. This will yield

$$I(\boldsymbol{S}) = \sum_{j=1}^{N} \sum_{k=1}^{N} f_{j\mathrm{T}} f_{k\mathrm{T}} \exp 2\pi \mathrm{i}\left[(\boldsymbol{r}_j - \boldsymbol{r}_k) \cdot \boldsymbol{S}\right]. \tag{4.78}$$

Equation (4.78) is exactly the same as (4.76), but the atomic-temperature factors appearing in (4.76) are now replaced by their products, and the atomic coordinates $\boldsymbol{r}_j$, by the coordinate differences $\boldsymbol{r}_j - \boldsymbol{r}_k = \boldsymbol{r}_{jk}$, which are nothing else but interatomic distances. Hence the intensity can be calculated from the set of interatomic distances in the object, without knowledge of the atomic coordinates. This is extremely important for most noncrystalline substances, because it is particularly difficult to know the arrangement of constituent atoms, but one can assign functions which describe statistically all the possible interatomic distances.

Quite similar expressions are obtained if we proceed from the description of the scattering density of a substance as a continuous function $\rho(\boldsymbol{r})$, whose scattering amplitude is $F(\boldsymbol{S})$ (4.12). Equation (4.77) contains both the amplitude $F(\boldsymbol{S})$ and $F^*(\boldsymbol{S})$. The former is a Fourier transform of $\rho(\boldsymbol{r})$: $F(\boldsymbol{S}) = \mathscr{F}[\rho(\boldsymbol{r})]$, and the latter, of the inverted function $\rho(-\boldsymbol{r})$: $F^*(\boldsymbol{S}) = \mathscr{F}[\rho(-\boldsymbol{r})]$. By the convolution theorem (4.20) the product of amplitudes is a Fourier transform of the convolution of the corresponding functions

$$\mathscr{F}[\rho(\boldsymbol{r}) * \rho(-\boldsymbol{r})] = F(\boldsymbol{S})\, F^*(\boldsymbol{S}) = I(\boldsymbol{S}), \tag{4.79}$$

and such a convolution [cf (4.19)] has the form

$$Q(\boldsymbol{r}) = \rho(\boldsymbol{r}) * \rho(-\boldsymbol{r}) = \int \rho(\boldsymbol{r}')\, \rho(\boldsymbol{r}' - \boldsymbol{r})\, dv_{\boldsymbol{r}'}\,. \tag{4.80}$$

Function Q is called function of interatomic distances in the object. It has high values when atoms are at points $\boldsymbol{r}'$ and $\boldsymbol{r}' - \boldsymbol{r}$. But this means precisely that in this case $\boldsymbol{r}$ is the interatomic distance. On the other hand, the intensity is a Fourier integral (4.79) of function $Q(\boldsymbol{r})$ (4.80).

4.4.2 Spherically Symmetric Systems: Gas, Liquid, and Amorphous Substances

Let us revert to (4.78). It contains N^2 terms, N of them with $j = k$ being separated into a "zero" term $\Sigma f_{j\mathrm{T}}^2$ with an exponential factor, which turns into unity, because $\boldsymbol{r}_{jj} = \boldsymbol{r}_j - \boldsymbol{r}_j = 0$. This term corresponds to the distances of the atoms to "themselves". Let us use (4.78) to calculate the intensity of scattering of molecules in a gas. The arrangement of the atoms in a molecule is described by a set of $\boldsymbol{r}_j$, and hence of interatomic distances $\boldsymbol{r}_{jk}$. But in a gas the molecules have random orientations and, accordingly, function $I(\boldsymbol{S})$ (4.78) must be spherically averaged. As in (4.15), such averaging gives

$$I(\boldsymbol{S}) = \sum_{j=1}^{N} f_{j\mathrm{T}}^2 + \sum_{j \neq k}^{N,\,N-1} f_{j\mathrm{T}}\, f_{k\mathrm{T}}\, \frac{\sin 2\pi S r_{jk}}{2\pi S r_{jk}}\,. \tag{4.81}$$

The most effective method for studying the structure of free molecules in a gas or vapor is electron diffraction analysis because of the strong interaction (the large absolute value of f) of electrons with atoms (see Sect. 4.8 below). An electron diffraction pattern of molecules in vapors is a set of diffuse rings

(Fig. 4.39d). The measurement of $I(S)$ helps to find the set of interatomic distances r_{jk} in a molecule and, as a result, leads to a model of its structure.

Scattering by condensed noncrystalline systems of atoms depends on the nature of their ordering and symmetry. Let us imagine that the ideal crystalline structure disorders gradually and that periodicity though exists, but only approximately (see Fig. 1.22). In reciprocal space such "paracrystalline" systems will be represented by smeared-out nodes of the reciprocal lattice; their smearing-out increases rapidly with increasing $|\boldsymbol{S}|$, and $F(\boldsymbol{S})$ vanishes at some $|\boldsymbol{S}_{\max}| = R^{-1}$. Here, R is the average radius of ordering, i.e., the distance at which it is still possible to find a correlation in the arrangement of the atoms of the object. The structure and smearing-out of the scattering intensity function $I(\boldsymbol{S})$

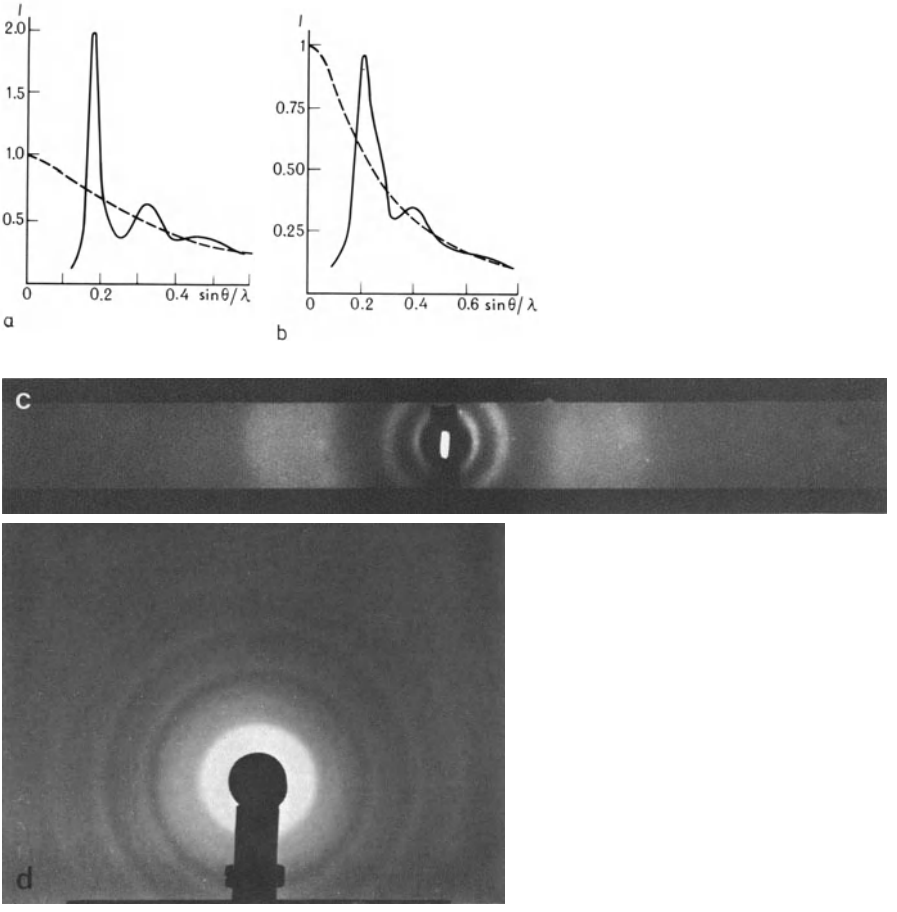

Fig. 4.39a–d. Diffraction from liquids.
(a) x-ray scattering curve $I(S)$ for liquid lead; **(b)** the same for germanium (the dashed line denotes the variation in the intensity of independent coherent scattering); **(c)** x-ray pattern of methyl alcohol (courtesy of A. F. Skryshevsky) **(d)** electron diffraction pattern of gaseous benzene (courtesy of L. V. Vilkov)

will also depend on the anisotropy of ordering: the interference peaks are "sharper" in those directions along which the object is more ordered, and smeared out in those along which it is less ordered. It is possible to calculate the intensity once the function of interatomic distances is given by the set $\boldsymbol{r}_{jk} = \boldsymbol{r}_j - \boldsymbol{r}_k$ according to (4.78) or as a continuous function $Q(\boldsymbol{r})$ (4.80).

Gases, liquids, and amorphous solids are statistically isotropic, and their structure is described by the radial distribution function $Q(r) = W(r)$, which gives a description of the interatomic distances $\boldsymbol{r}$ in terms of probabilities, but with no information about spatial orientation (Fig. 1.22). Then $I(\boldsymbol{S}) = I(S)$, too, is a spherically symmetric function; we know only moduli S (length of vectors $\boldsymbol{S}$), and the exponent in (4.78) is replaced by the known factor $(\sin 2\pi Sr)/2\pi Sr$. An x-ray, neutron, or electron diffraction pattern is in this case similar to a diffraction pattern from molecules in a gas and constitutes a set of smeared-out diffusive rings (Fig. 4.39).

4.4.3 Systems with Cylindrical Symmetry: Polymers and Liquid Crystals

The symmetry of function $I(\boldsymbol{S})$ depends on that of the object, which also defines the symmetry of $Q(\boldsymbol{S})$. A characteristic ordering for polymers, both natural and synthetic, is the packing of their chain molecules parallel to each other, but with a random angular (azimuthal) orientation of these molecules or their groups. Liquid crystals exhibit the same, approximately parallel orientation of molecules. Such objects possess a statistically cylindrical symmetry. Then the same symmetry will have intensity function $I(\boldsymbol{S})$ which consists of more or less diffuse annular regions in the reciprocal space. Vector $\boldsymbol{S}$ is in this case given by only two cylindrical coordinates: $\boldsymbol{S} = \boldsymbol{S}(S_R, Z)$; Z is the axis of cylindrical symmetry in the reciprocal space. The intersection of such annular regions by the reflection sphere actually gives an x-ray diffraction pattern consisting of more or less diffuse arcs arranged along the so-called layer lines (Fig. 4.40). The distance between them, c^*, is inversely proportional to the periodicity of the chain molecules c.

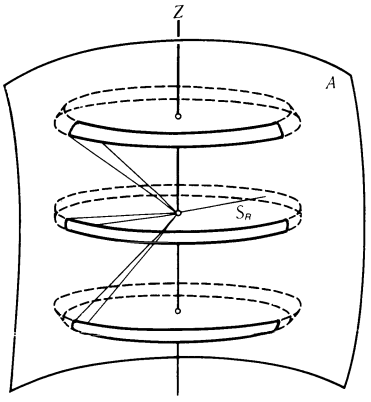

Fig. 4.40. Formation of smeared-out rings from reciprocal-lattice points in the case of a cylindrically symmetric object and their intersection by the Ewald sphere A

The structure amplitude in the case of diffraction by chain molecules results from the transformation of the general expression (4.44) to cylindrical coordinates, which yields

$$F(R,\psi,Z) = \sum_{n=-\infty}^{+\infty} \exp\left[i\pi\left(\Psi + \frac{\pi}{2}\right)\right] \int_0^\infty \int_0^{2\pi} \int_0^c \rho(r,\psi,z) J_n(2\pi rR) \times \exp\left[-i(n\psi) + 2\pi \frac{zl}{c}\right] r\,dr\,d\psi\,dz\,. \tag{4.82}$$

Here, r, ψ, and z are the cylindrical coordinates in real space, R, ψ, $Z = l/c$ are those in reciprocal space; and J_n is the Bessel function.

Of special interest is diffraction by helical molecules. In this case (4.82) includes, and only some of the Bessel functions determined by the selection rule

$$l = mp + (nq/N), \tag{4.83}$$

where l is the number of the layer line, p, q, and N are the spiral parameters of a helix $S_{p/q}$, N (see Sect. 2.7), and n and m are integers. The selection rule leads to a peculiar arrangement of reflections in the form of a "diagonal cross"on x-ray photographs from helical molecules. This is illustrated by the optical diffraction pattern of Fig. 4.41 and by the x-ray photographs of [Ref. 4.3, Fig. 2.156].

The structure analysis of noncrystalline materials is based on the possibility of finding, by the Fourier transformation (4.80) of the observed intensity distribution, function $Q(r)$, which is cylindrically symmetric for polymers, or $W(r)$ function of radial distribution for liquids and amorphous solids, molecules, and gases. In the case of spherical symmetry, by analogy with (4.15),

$$Q(r) = \frac{1}{2\pi^2} \int_0^\infty I(s) r^2 \frac{\sin sr}{sr}\,dr, \tag{4.84}$$

where r and s are spherical coordinates. Upon some normalization of the intensity, $Q(r)$ changes to $W(r)$.

In the case of cylindrical symmetry

$$Q(r,z) = 2 \int_0^\infty \int_0^\infty I(R,Z)\, J_0(2\pi rR) \cos(2\pi zZ)\, 2\pi R\,dR\,dZ\,. \tag{4.85}$$

Here, r, z and R, Z are the cylindrical coordinates in real and reciprocal space,

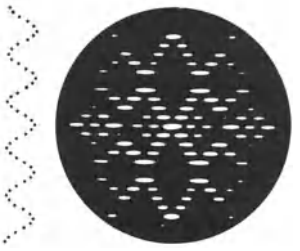

Fig. 4.41. Helical structure (left, symmetry s_{10}) and the optical diffraction pattern from it (right)

and J_0 is the zero-order Bessel function. Of course, interatomic-distance function is not a structure, but it is closely related to the structure and enables one to make many conclusions about it. A similar approach, i.e., the calculation of interatomic-distance functions, is used in studying the crystal structure this problem will be discussed in detail later on.

Thus, the structure and peculiarities of the intensity function $I(\boldsymbol{S})$ in reciprocal space, which is revealed in a diffraction experiment, is directly associated with the structure of the scattering object. The more ordered the object, the more orderly and "sharper" it is expressed in the reciprocal space, and the more detailed is the information which can be obtained about it from a diffraction experiment. The less ordered is the object, the "smoother" is its representation in the reciprocal space and the less information is obtained from a diffraction experiment. This, however, does not mean that the potentialities of such an experiment have dwindled, but it simply reflects its physical adequacy to the order of the structure under investigation. Indeed, while the structure of a crystal with a hundred atoms in the unit cell is described by a total of up to $10^3 - 10^4$ parameters and it gives several thousand I_{hkl} in the reciprocal lattice, the structure of a liquid is described by the statistical function $W(r)$, which has several peaks, and, consequently, the function $I(\boldsymbol{S})$ is also poorly defined.

4.4.4 Small-Angle Scattering

Diffraction methods can be used not only at the level of atomic resolution, but also at a resolution of 10 – 1000 Å. Such a scale permits determination by the diffraction methods of some important characteristics of biological macromolecules, which have molecular weights of the order of 10^6 and more, namely, their shape, volume, mutual arrangement of their subunits, etc. A similar problem is the determination of the shape and size of submicroscopic segregations of a new phase in solid solutions, the particle size in various disperse systems, etc.

Here, the electron density of an object or, more precisely, the difference between it and the density of the surrounding medium, can be assumed constant, $\rho(\boldsymbol{r}) = \Phi(\boldsymbol{r}) = \text{const}$, to a first approximation, while outside the object this difference is equal to zero. The shape function $\Phi(\boldsymbol{r})$ describes the external form and size of the particle (macromolecule). The scattering amplitude for such an object is defined by the familiar expression (4.38)

$$D(S) = \int \Phi(\boldsymbol{r}) \exp[2\pi \mathrm{i}(\boldsymbol{S}\boldsymbol{r})]\, dv_r = \int_{\Phi} \exp[2\pi \mathrm{i}(\boldsymbol{S}\boldsymbol{r})]\, dv_r .$$

$D(\boldsymbol{S})$ can be found analytically or numerically. Since function $\Phi(\boldsymbol{r})$ is nonzero in a large (in the "diffraction" sense) volume, function $D(\boldsymbol{S})$ is, contrariwise, concentrated near $|\boldsymbol{S}| \to 0$, i.e., at small scattering angles, near the initial beam. For particles with a cross section A this area is defined by (4.41) through the value A^{-1}, i.e., for instance, for $A \approx 100$ Å and $\lambda = 1.5$ Å, function $D(\boldsymbol{S})$ is

concentrated in an angular interval of $\sim 1^0$, whereas diffraction due to distances between atoms, for instance in crystals, encompasses "large" angles up to 90°.

An analysis of the shape of a zero peak $I_0(\boldsymbol{S}) = K|D(\boldsymbol{S})|^2$ makes it possible to solve the reverse problem as well, namely finding the shape of the scattering object from the intensity of small-angle x-ray scattering. Then, using (4.41) or similar equations, one can determine the particle dimensions along different directions. The problem of finding the shape of particles is complicated by the fact that they are often randomly oriented, and this considerably smooths out the scattering curve. But a number of geometric parameters of a particle – its radius of gyration $\int \rho(r) r^2 \, dv / \int \rho(r) dv$, volume, and surface – can be determined unambiguously from the small-angle scattering curve. Measurements of small-angle scattering on the absolute scale determine the molecular weights of microparticles and the mass per unit length for chain molecules. The details of the shape of the object can be revealed by constructing hypothetical models and comparing their theoretical scattering curves with the experimental.

At present small and medium-angle diffraction can be interpreted with the use of the Fourier–Bessel transformation in spherical coordinates. It is also possible to solve the inverse problem, i.e., to determine spherical multipole components of electron density proceeding from the experimental scattering curve with allowance for the object symmetry [4.28]. Thus the electron density of the structure can be obtained directly from the experimental data (Fig. 4.42).

In the case of disperse systems of unequal particles – powders, porous bodies, and solid solutions – it is possible to determine both the average particle size and the particle size distribution.

Measurement of scattering in the immediate vicinity of the primary beam is a complicated task; it requires construction of special small-angle cameras to measure scattering beginning with a few angular seconds and minutes.

Along with small-angle scattering of x-rays, small-angle scattering of neutrons and electrons has found ever-increasing applications in recent years.

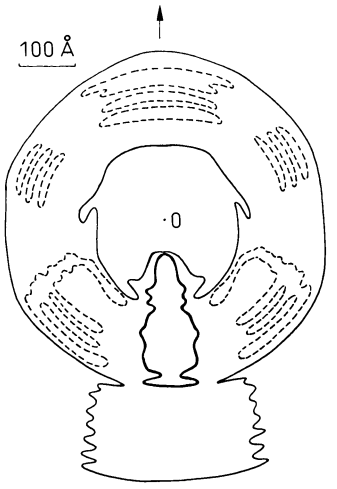

Fig. 4.42. Electron-density map of T7 bacteriophage in a cross section through the cylindrical symmetry axis (indicated by an arrow). The solid line denotes the level 0.38 $e\text{Å}^{-3}$ (hydrated protein), the dashed line designates the level 0.42 $e\text{Å}^{-3}$ (strongly hydrated DNA), and the thick line represents the 0.52 $e\text{Å}^{-3}$ level (slightly hydrated DNA) [4.29]

4.5 Experimental Technique of X-Ray Structure Analysis of Single Crystals[4]

4.5.1 Generation and Properties of X-Rays

X-rays are electromagnetic waves with a wavelength λ from 10^{-2} to 10^{2} Å. In x-ray structure analysis wavelengths of about 1 Å are used.

The refractive index q of x-rays is less than unity, although very close to it:

$$q = 1 - 1,3 \cdot 10^{-6} \rho\lambda^2, \tag{4.86}$$

where ρ is the density of the substance in g/cm^3, and λ is in Å. Since q is close to unity, x-rays cannot be focused with the aid of any lenses. In x-ray optics beams are usually formed with the aid of apertures. It is also possible to use mirrors with complete external reflection and diffraction methods for beam focusing.

The source of x-radiation is an electron x-ray tube (Fig. 4.43). In it, electrons emitted by the heated cathode (a tungsten filament) are accelerated by the electric field and directed to the metallic anode. When the electrons are slowed down abruptly in the anode substance, their energy is transformed into photons of x-radiation

$$h\nu = E_1 - E_2, \tag{4.87}$$

where E_1 and E_2 are the electron energy before and after collision with the anode.

The maximum frequency ν_{max} (the minimum wavelength λ_{min}) corresponds to a full stoppage of the electrons ($E_2 = 0$)

$$h\nu_{max} = \frac{hc}{\lambda_{min}} = E_1 = eU, \tag{4.88}$$

where U is the accelerating voltage. Since E_2 may have any magnitude less than E_1, the continuous spectrum from the long-wave side is limited only by the absorption of soft x-rays in the material of the tube window and in the air.

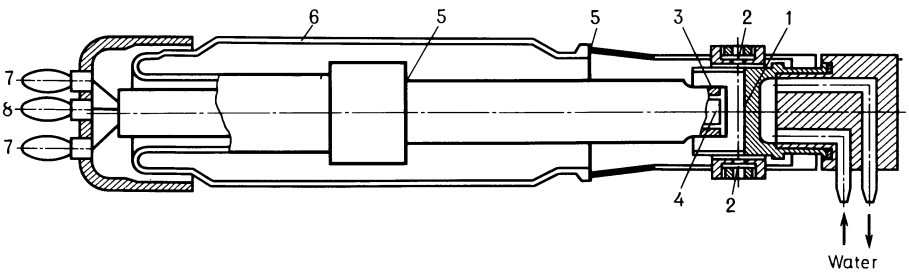

Fig. 4.43. X-ray tube. (*1*) anode; (*2*) windows; (*3*) focusing cup; (*4*) filament; (*5*) metal-glass seal; (*6*) glass body; (*7*) filament terminals; (*8*) focusing electrode terminal

[4] Sections 4.5 and 4.6 were written by D. M. Kheiker. See also Sect. 5.3.

Figure 4.44 shows continuous spectra from a tungsten anode. The radiation intensity is defined by the expression

$$I = piU. \tag{4.89}$$

Here, i is the anode current, $p = 1.1 \times 10^{-9} ZU$ is the portion of the energy of the electron beam transformed into x-radiation, Z is the atomic number of the anode material, and U is the accelerating voltage. The intensity maximum in the continuous spectrum is associated with a wavelength of approximately $3\,\lambda_{min}/2$.

If the energy of the accelerated electrons exceeds that of the excitation threshold, i.e., is sufficient to eject an electron from an inner shell of the atom, lines of characteristic x-radiation appear against the background of the continuous spectrum (Fig. 4.45). The electrons of the atom, passing from the outer shells with a high energy E to a vacancy in an inner shell, emit photons

$$h\nu = E - E_0. \tag{4.90}$$

The value of $h\nu$ depends on the system of energy levels characteristic of each element. The spectral lines are divided into series K, L, M, N, . . . , depending on which shell the electron was removed from. Inside each series there are several lines $\alpha_1, \alpha_2, \ldots, \beta_1, \beta_2, \ldots$ in accordance with the level from which the energy transition occurred.

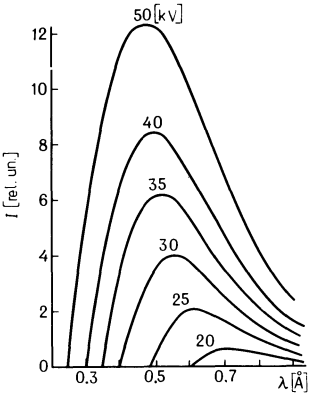

Fig. 4.44. Continuous x-ray spectra at different accelerating voltages (tungsten anode)

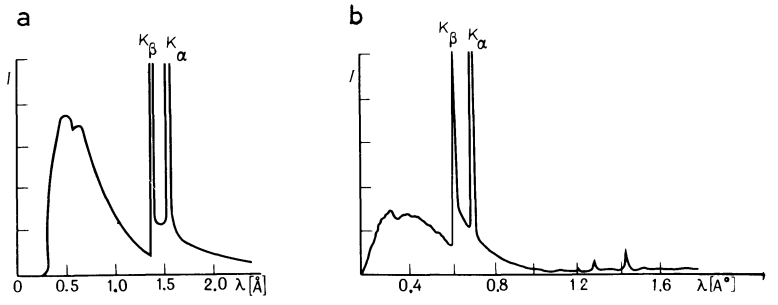

Fig. 4.45a,b. Radiation spectra of x-ray tubes with a copper (**a**) and a molybdenum (**b**) anode

The most intensive lines are $K\alpha_1$ (electron transition $L_{III} - K_I$) and a slightly weaker line $K\alpha_2(L_{II} - K_I)$, which is close to it. The intensity of the line $K\beta_1$ ($M_{III} - K_I$), equals 15–25% of that of $K\alpha_1$. The other lines have still lower intensities. The frequency of a line changes from one element to another in accordance with the Moseley's law

$$\sqrt{\nu} = c(Z - \sigma), \tag{4.91}$$

where c and σ are constants.

$K\alpha_1$ and $K\alpha_2$ lines of metals from chromium ($Z = 24$) to molybdenum ($Z = 42$), with wavelengths in the range from 2.3 to 0.7 Å, are most commonly used as monochromatic radiation in x-ray structure analysis.

At a constant power of the anode current $W = iU$ the intensity of the characteristic radiation I_c increases as $(U - U_k)^{1.5}/U$, where U_k is the excitation threshold, while the intensity of the continuous spectrum I increases as U [see (4.89)]. The maximum of the ratio I_c/I is achieved at $U = 3U_k$.

The predominant part of the electron beam energy is spent on heating the anode, about 1% is transformed into x-radiation, and less than 0.1% into characteristic radiation. The heat released at the anode limits the power of the radiation source, and therefore the tubes have to be cooled. There are x-ray tubes of different design and power, with different sizes of the focal (emitting) spot – from several micrometers (in microfocus tubes) to several millimeters (in normal-focus tubes) depending on their purpose. The tube power ranges from 0.01 to 100 kW and the quantum flux density at a distance of 100 mm from the source varies from 10^9 to 10^{13} $cm^{-2} \cdot s^{-1}$.

The smaller the dimensions of the focus, the better the conditions of heat removal and the higher the power per unit area of the focus, and hence the greater is the brightness of the x-radiation source. But the total power of the tube is then reduced, and so is the quantum flux density. For instance, in a 20 W microfocus tube with a focus diameter of 40 μm the specific load is 15 kW/mm^2, while the quantum flux density at a distance of 125 mm is 0.006×10^2 $cm^{-2} \cdot s^{-1}$; in a 1.5 kW tube with a normal focus of 1×10 mm^2 the specific power output is 0.15 kW/mm^2, while the quantum flux density at the same distance is 0.45×10^{12} $cm^{-2} \cdot s^{-1}$. The total and specific power of the tubes can be increased by a factor of 10–20 by rotating a water-cooled hollow cylindrical anode.

Modern x-ray equipment for structure analysis is designed for a voltage of up to 60 kV and ensures a radiation stability of 0.03–0.3%. The x-ray beam from the tube is then collimated and monochromatized.

The most common collimation system consists of three apertures (or slits). The first aperture cuts the necessary area out of the projection of the focus spot, the second aperture restricts the size of the beam incident on the specimen, and the third cuts off additional radiation which is due to the second diaphragm (Fig. 4.46).

The operation of a crystal monochromator is based on Bragg–Wulff reflection (4.3): with fixed d and θ the crystal isolates from the spectrum a narrow spectral interval of width depending on the mosaic.

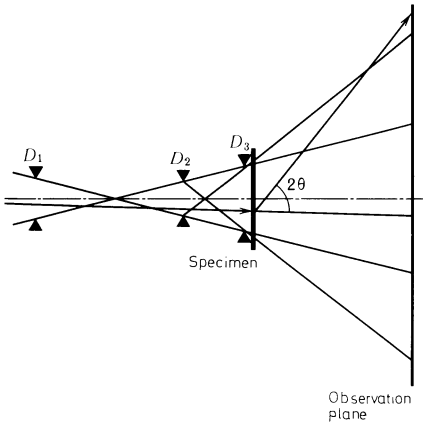

Fig. 4.46. Primary-beam collimator consisting of three apertures D_1, D_2, and D_3

To improve focusing, bent crystal monochromators are used. The ray diagram for monochromators is shown in Fig. 4.47. The bend must be such that the angle of incidence is constant for all the rays of the diverging beam, while the reflected rays converge at a single point. This can be achieved, for instance, by bending the crystal around a circle with a radius equal to the diameter of the focusing circle on which the crystal surface rests (the Johannson method). Monochromators use perfect single crystals of quartz, pyrolytic graphite, etc.

In recent years, synchrotron radiation from annular electron accelerators – synchrotrons and storage rings – have been used as powerful x-ray sources. Moving in a circular orbit, the electrons emit a quasicontinuous electromagnetic spectrum with $\lambda(I_{max})$ Å

$$\lambda(I_{max}) = 2.35R/E^3. \tag{4.92}$$

Here, R is the radius of the electron orbit in meters, and E is the electron energy in GeV. Thus, at $E = 2.2$ GeV and $R = 6.15$ m, $\lambda(I_{max}) = 1.4$ Å; this kind of radiation is suitable for x-ray structure analysis. The radiation is strictly polarized in the plane of the electron orbit and directed tangentially to it. After monochromatization it is possible to obtain a photon flux density of 10^{15} mm^{-2} s^{-1}, which is 3–5 orders higher than the flux from powerful tubes.

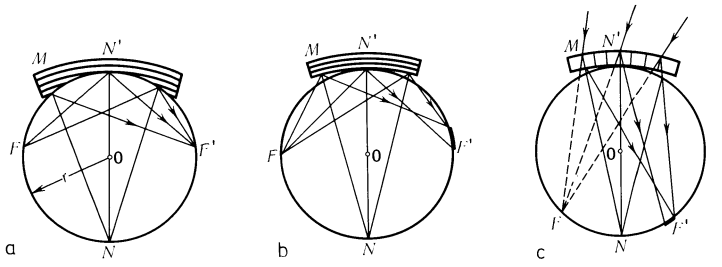

Fig. 4.47a–c. Methods of monochromatization by bent crystals. (**a**) Johannson's; (**b**) Johann's; (**c**) Coshua's. (M) bent monochromator crystal; (F) real (or imaginary) focus; (F') focus image in diffracted rays; (O) center of the focusing circle; (r) radius of this circle, (NN') crystal curvature radius

Isotopic sources are also used in x-ray investigations. The nucleus of such an isotope captures the K electron from the nearest orbit. When electrons from higher orbits pass to such a vacated orbit, a characteristic spectrum arises. Such sources are portable and stable, but their intensity is low. Specific sources producing coherent γ quanta with a wavelength suitable for x-ray analysis are Mössbauer sources, for instance those of ^{125}Te or ^{119}Sn nuclei.

4.5.2 Interaction of X-Rays with a Substance

The propagation of x-rays through a substance is attended by the following basic processess:

I) coherent scattering giving diffracted beams; x-ray photons change direction without any loss of energy;
II) incoherent scattering, in which the photons deflect from their initial direction and part of the photon energy is transferred to the recoil electron (Compton effect), and
III) absorption, when part of the photon energy is spent on ejecting an electron from an atom, while the remaining energy is transferred to this photo-electron (photoeffect). The excited atom, returning to the normal state, emits a photon of a lower energy (secondary fluorescent radiation) or a so-called Auger electron (secondary photoeffect).

As a result of these processes the intensity of the primary beam decreases exponentially in passing through a layer of substance of thickness l

$$I = I_0 \exp(-\mu l), \tag{4.93}$$

where μ is the summary coefficient of attenuation.

The absorption coefficient is approximately proportional to λ^3, and also to Z^3. On this dependence are superimposed absorption jumps (edges) corresponding to the energy of the photons, which may remove an electron from some atomic shell.

By using filters made of an element with a suitable Z and by taking advantage of its selective absorption near the K edge, one can reduce the short-wave component of the background on x-ray photographs and eliminate β lines.

Let us consider the coherent scattering of x-rays by electrons. According to classical electrodynamics a free electron in the alternating electromagnetic field of an incident x-ray wave is set into vibration with a frequency of an electric vector and becomes a dipole with a variable moment, which will, in turn, be the source of scattered radiation with the same frequency. The intensity of radiation of a vibrating electron, see (4.7), at a linear polarization of the primary beam of intensity I_0 is equal to

$$I_e = I_0 \left(\frac{e^2}{mc^2}\right)^2 \frac{1}{R^2} \sin^2 \varphi, \tag{4.94}$$

where φ is the angle between the scattered beam and the dipole axis, and R is the distance from the emitting electron.

If the primary beam is polarized, and $K_{\parallel}$ and $K_{\perp}$ are the coefficients of polarization in the scattering plane and perpendicular to it, the electron emission intensity is equal to

$$I_e = I_0 \left(\frac{e^2}{mc^2}\right)^2 \frac{1}{R^2} (K_{\perp} + K_{\parallel} \cos^2 2\theta), \tag{4.95}$$

where 2θ is the scattering angle ($\varphi_{\parallel} = 90^\circ - 2\theta, \varphi_{\perp} = 90^\circ$).

If the primary beam is not polarized, then $K_{\parallel} = K_{\perp} = 1/2$, and

$$I_e = I_0 \left(\frac{e^2}{mc^2}\right)^2 \frac{1}{R^2} \frac{1 + \cos^2 2\theta}{2}. \tag{4.96}$$

It is usually assumed that the magnetic structure of crystals does not affect the scattering of x-rays and can be investigated only by neutron diffraction (see Sect. 4.9). In actual fact, the interaction of x-rays with the magnetic moment of atoms (i.e., those which have unpaired electrons) takes place, although it is very weak (by a factor of 10^{-6} weaker than charge scattering). Therefore one can observe "magnetic" peaks of scattering from ferro- or antiferromagnetics [4.30, 31].

Considerable scope for further improvements is opened by the use of powerful sources of synchrotron radiation. Of great interest is also the application of magnetic scattering occurring at absorption edges of magnetic f-elements, e.g., holmium [4.32].

4.5.3 Recording of X-Rays

The intensity of x-ray scattering patterns is measured by the photographic method or with the aid of photon counters. In photographic recording the film can, simultaneously or consecutively, record x-ray beams scattered by the specimen at different angles, i.e., it is a two-dimensional detector. The effect of x-rays on a photographic film is the same as that of visible light and consists in photochemical decomposition of silver bromide. The blackening D is defined as the logarithm of the ratio of the intensities of a light beam transmitted through an irradiated area of the film J and a beam transmitted through nonirradiated area of it J_0

$$D = \lg(J/J_0). \tag{4.97}$$

The blackening of the film in the range of 0.3–1.2 is proportional to the number of incident x-ray photons per unit area.

In visual estimation of blackenings, use is made of the method of blackening marks – standard spots with a constant blackening ratio 1: $\sqrt{2}$:2:2 $\sqrt{2}$ . . . or with a smaller interval, with which the observed blackenings of the reflections of the x-ray photographs are compared.

Accurate measurements of blackenings are made by optical microphotometers or microdensitometers, which record either blackening or peak profiles in the form of a curve, and by computer-controlled microdensitometers.

Another basic technique for recording x-rays is the diffractometric method based on the use of various x-ray quantum counters of the ionization, scintillation, semiconductor, etc., type. As a rule, a counter can record a narrow beam of rays in a small angular interval, i.e., it is a point detector.

Gas discharge proportional counters and scintillation counters are the most common; the latter combine a luminescent crystal which lights up under the effect of x-ray quanta, and a photoelectronic multiplier. Ge or Si semiconductor detectors are also used.

The efficiency of a detector is defined by the ratio of the number of recorded photons to that of photons incident on the input window of the detector, and equals 60–98%. We shall discuss diffractometric devices in more detail further on.

4.5.4 Stages of X-Ray Structure Analysis of Single Crystals

Determination of the structure of crystals, i.e., of the atomic coordinates and other parameters of the structure, consists of two stages: a) obtaining and processing diffraction data (including determination of symmetry and unit cell) and b) finding the atomic structure or determining the electron density distribution by mathematical techniques. The first stage is covered by Sect. 4.5, 6 and the second, by Sect. 4.7.

An x-ray experiment, in turn, consists of two stages. The first is a preliminary investigation: the lattice parameters and symmetry are determined, the crystal is oriented, its mosaic structure is established, and the absorption curves are found. The second stage consists in measuring the integrated intensities of the entire set of reflections from the crystal.

It should be noted that the crystal orientation and the precise determination of the cell may constitute a separate problem. The determination of the cell parameters is used for identifying substances existing as small single crystals. Crystal orientation is employed in studying the direction of growth, epitaxy, and topotaxy, and in technical applications of single crystals. Precise measurement of the lattice parameters is used in investigating solid solutions, the thermal expansion tensor, etc. Single-crystal diffraction data also help to investigate thermal diffusion scattering, i.e., the phonon spectrum of crystals.

X-ray investigation is sometimes preceded by the selection of a specimen and its preliminary inspection with the aid of optical goniometry and crystalloptical methods.

The structure of single crystals is examined in a monochromatic or polychromatic (white) radiation. In the former case, we can, in accordance with Ewald's construction (Fig. 4.136), record either only one or several reflections at a time, and therefore it is always necessary to use methods in which the crystal can successively be set into different reflecting positions. In the latter case Ewald's construction is a continuous series of reflection spheres with a radius from $r_{min} = \lambda_{max}^{-1}$ to $r_{max} = \lambda_{min}^{-1}$, so that a large number of reflections appear simultaneously.

4.5.5 Laue Method

This method consists in taking x-ray photographs of a fixed single crystal in a parallel polychromatic beam. In this case the ordinary Ewald construction is modified. We replace a continuous series of reflection spheres, corresponding to different λ, by a single sphere of unit radius, and simultaneously change the scale of vectors $\boldsymbol{H}_{hkl}$. Then the nodes of the reciprocal lattice will be transformed into radial segments of length

$$q_{hkl} = \{\boldsymbol{H}_{hkl}\,\lambda_{\min};\ \boldsymbol{H}_{hkl}\,\lambda_{\max}\}.$$

As follows from Fig. 4.48, at point M the sphere will be intersected by segments corresponding to several orders of reflection; rays with a wavelength $\lambda_1 = OM/H_{hkl}$, $\lambda_2 = OM/H_{2h2k2l}$ etc., will be scattered in the direction of O_1M, i.e., the consecutive orders of reflections hkl are represented by a single spot.

Laue photographs are taken as follows. The white radiation, including the characteristic spectral lines, of a tungsten or molybdenum (sometimes copper) anode is directed towards the specimen through a "point" collimator D_1D_2 (Fig. 4.49). The film is placed behind the specimen, thus recording a Laue transmission photograph (Fig. 4.49a), or in front of the specimen, thus giving a "back" Laue photograph (Fig. 4.49b). In the latter case the specimen may be bulky.

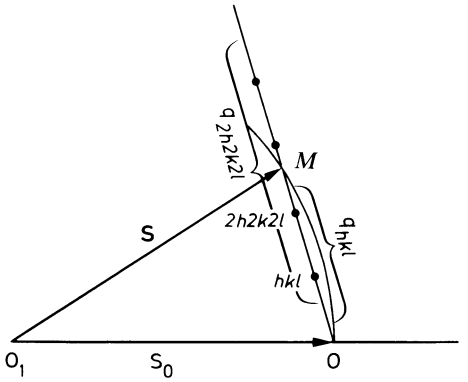

Fig. 4.48. Ewald's construction for Laue case

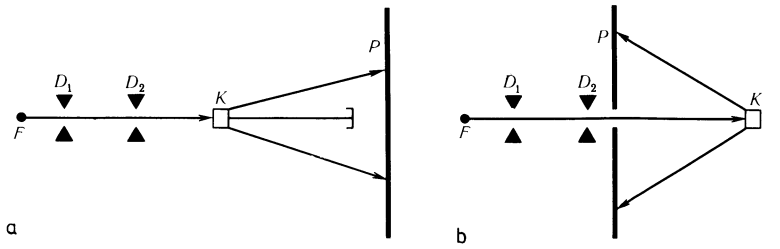

Fig. 4.49a,b. Front (**a**) and back (**b**) Laue photographs

The Laue method is used to determine the symmetry of the crystals and also their orientation, for such purposes as placement in other cameras, machining, etc. At present the Laue technique is widely used in the high-speed acquisition of integral-intensity data obtained with the use of a white synchrotron radiation, especially in protein crystallography (Sect. 5.3).

The construction in Fig. 4.48 points to a simple relationship between the position of the spot on the film and the direction of the normal of the reflecting system of planes. The projection of the bundle of normals onto the plane – the so-called gnomonic projection – is considered. The normal and the reflected beam lie in the same plane, which intersects the gnomonic projection along the central line. The distance of the projection of the normal N_{hkl} from the center of gnomonic projection O_2 for the Laue photograph is equal to

$$O_2N_{hkl} = 2\cot\theta = 2\cot\left(\frac{1}{2}\arctan\frac{OP}{L}\right), \tag{4.98}$$

where OP is the distance of the spot from the trace of the primary beam on the film, and L is the specimen-film distance.

The symmetry of the reciprocal lattice of the crystal is established by analyzing the gnomonic or stereographic projections and obtaining Laue photographs along the main directions. The sets of reflections of one zone are arranged on the Laue photograph on a conical section (ellipse, parabola, or hyperbola), whose axis is that of the zone. On switching to a gnomonic projection the zones will be represented by straight lines.

An important property of Laue photographs (Fig. 4.50) is that if the picture is taken along an axis or symmetry plane of a crystal, the pattern will possess the

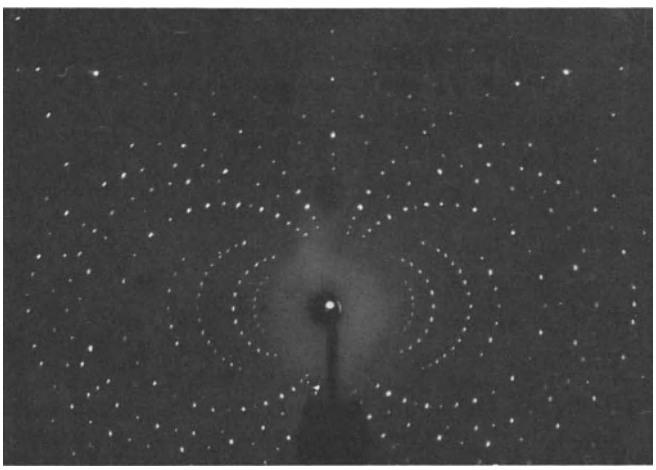

Fig. 4.50. Laue photograph of a crystal of $[C(NH_2)_3]_4\ [UO_2O_2(CO_3)_2].\ 2H_2O$ obtained on an unfiltered molybdenum radiation: the trace of the primary x-ray beam coincides with the line of intersection of two symmetry planes

same symmetry elements. Therefore, after taking a picture of a crystal with arbitrary orientation to find the principal symmetry axes, other Laue photographs taken along these principal axis are used to determine the crystal symmetry.

A Laue photograph is a plane two-dimensional image, and hence its symmetry is described by one of the ten two-dimensional crystallographic groups. By comparing Laue photographs taken along different directions it is possible to allocate the point group K of the crystal to one of the eleven Laue classes, which, regardless of whether K has a center of symmetry, "add" to it the symmetry of the reciprocal lattice (see Sect. 4.2.6).

The most rapid technique for orientation and establishing the symmetry on the basis of the Laue method is the use of an electrooptical convertor, by which the diffraction pattern is amplified many times over, and the researcher can directly observe the diffraction pattern on the display. The storage of the diffraction pattern in a computer, its color display and further processing are possible. The same can be done with the aid of two-dimensional detectors.

4.5.6 Crystal Rotation and Oscillation Methods

These methods are based on the fact that during the rotation of a crystal about an axis which does not coincide with the direction of the primary beam the nodes of its reciprocal lattice will intersect in turn the sphere of reflection. To obtain x-ray photographs by these methods, a parallel monochromatic beam is directed towards a small single crystal (0.2–1.0 mm) and the crystal is rotated in a full ($\omega = 360°$) or limited angular interval ω about an axis perpendicular to the primary beam. The crystal is oriented so that the rotation axis coincides with some axis of the atomic lattice, for instance $\boldsymbol{a}_1$; then the $\boldsymbol{a}_2^*\boldsymbol{a}_3^*$ planes of the reciprocal lattice are perpendicular to the rotation axis. In rotation, these planes, which are called layer planes, intersect the reflection sphere in circles spaced at a_1^{-1} (Fig. 4.51). The diffracted rays are arranged on cones with apexes at the center of the reflection sphere and axes coinciding with the rotation axis. The cone angle is $\pi - 2\nu$. The film may be placed in a flat or a cylindrical cassette whose axis coincides with the rotation axis. Then the cones are recorded on the film as straight layer lines (Fig. 4.52). From the distances between the layer lines it is possible to find the period a_1 along the rotation axis

$$\nu_i = \arctan \frac{l_i}{R}, \quad a_1^{-1} = \frac{\sin \nu_i}{i\lambda}, \tag{4.99}$$

where l_i is the distance of the ith layer line from the zero line on the x-ray photograph, and R is the radius of the film.

For the rotation axis one can choose not only coordinate, but also some other simple axes, for instance [110] and [111].

During the rotation of the crystal, all the nodes of the reciprocal lattice situated in the toroid traced by the reflection sphere will consecutively occupy

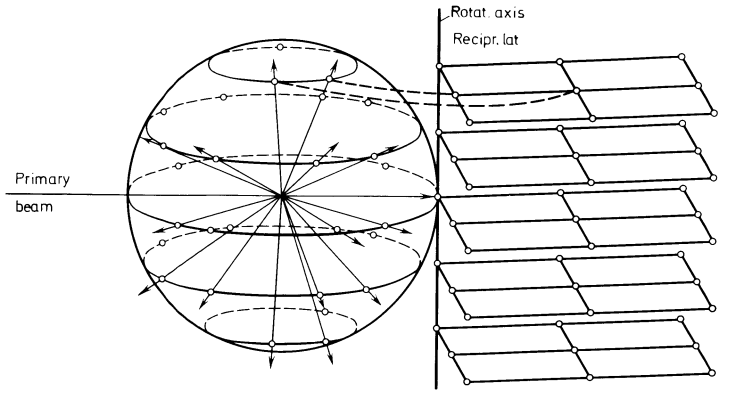

Fig. 4.51. Ewald's construction for x-ray rotation patterns

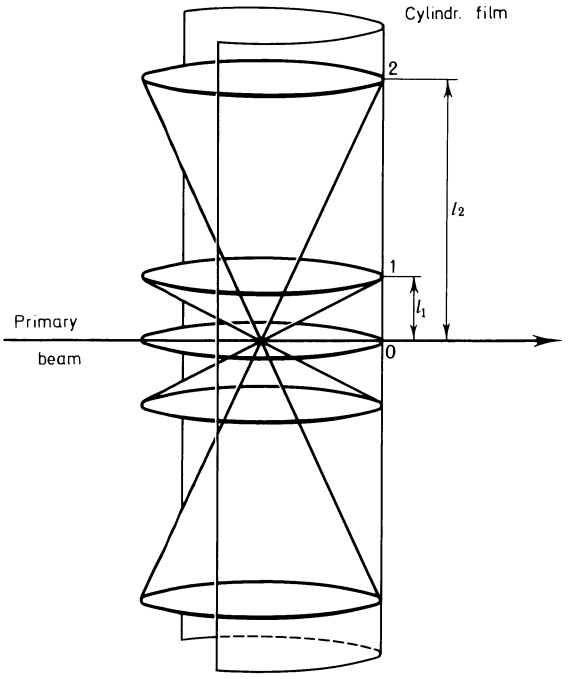

Fig. 4.52. Layer lines which are formed on intersection of interference cones with a cylindrical film, in the rotation method. *0, 1, 2* are layer line numbers

reflection position; in the layer planes these will be rings – toroidal cross sections (Fig. 4.53). Under oscillation within small angular intervals, fewer nodes will appear in the reflecting position; these nodes are situated in crescentlike regions of the layer planes.

The distance of the spot from the middle generatrix is proportional to the angle Υ. Using Ewald' construction, it is possible to determine from angle Υ the

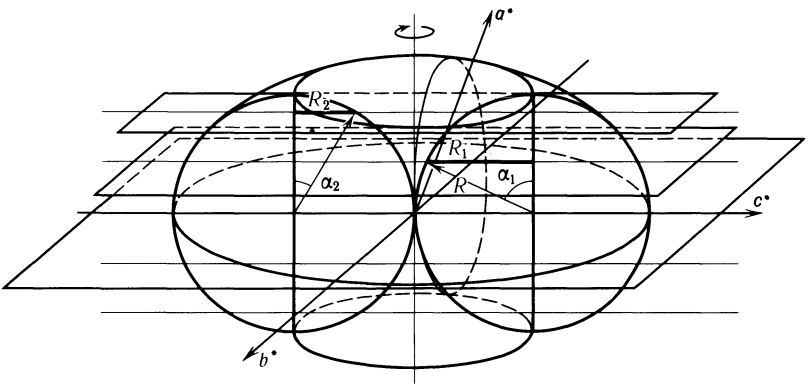

Fig. 4.53. Toroid which contains reciprocal lattice points occurring in the reflecting position when x-ray rotation photographs are taken. R is radius of the reflection sphere; R_1 and R_2 are radii of the sections of a sphere by the first and the second layer plane, respectively; α_1 and α_2 are cone angles

cylindrical coordinate of the node of the reciprocal lattice ξ (the distance to the rotation axis)

$$\cos \Upsilon = \frac{2 - \sin^2 \nu - \lambda^2 \xi^2}{2 \cos \nu}. \tag{4.100}$$

Thus, x-ray rotation photographs help to establish two cylindrical coordinates of the node in reciprocal space: ξ and $\zeta = \sin \nu$. The third cylindrical coordinate φ, associated with the crystal rotation angle ω at which the reflection arises,

$$\varphi = \omega - \arcsin\left(\lambda \frac{\xi^2 + \zeta^2}{2\zeta}\right), \tag{4.101}$$

remains unknown. With a small unit cell this coordinate can be obtained by drawing a circle of radius ξ in the net of the layer plane calculated from parameters a_2^* and a_3^*. The coordinate φ and indices h and k of the nodes on the circle are assigned to the corresponding spot on the x-ray photograph.

An x-ray rotation photograph is shown in Fig. 4.54. An indexed photograph allows one to determine the extinctions and to measure the intensities I_{hkl}. But if the unit cell is large, the reciprocal cell is small, and some spots on the layer lines are superimposed, making unambiguous indexing impossible.

An x-ray oscillation photograph within a narrow range of angles ω precludes superpositions and ambiguity in indexing. From a series of such photographs one can obtain a complete set of intensities for structure investigation. There are special cameras (for instance the Arndt-Wonnacott camera) which are used for taking a series of oscillation pictures from single crystals with large cell parameters. All the layer planes are registered simultaneously in such cameras in a narrow range of rotation angles. The measurements of such photographs can be

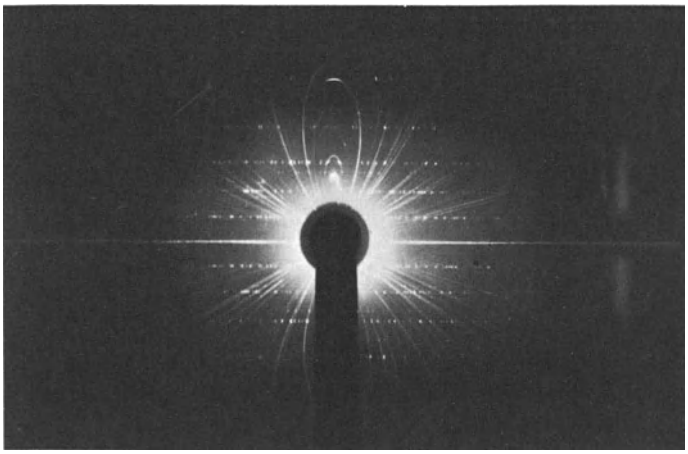

Fig. 4.54. Rotating-crystal x-ray photograph of vinogradovite; MoK_α radiation

done only with the aid of automatic microdensitometers; the densitometer data are processed by a computer. Figure 4.55 is an x-ray photograph taken in an Arndt-Wonnacott camera.

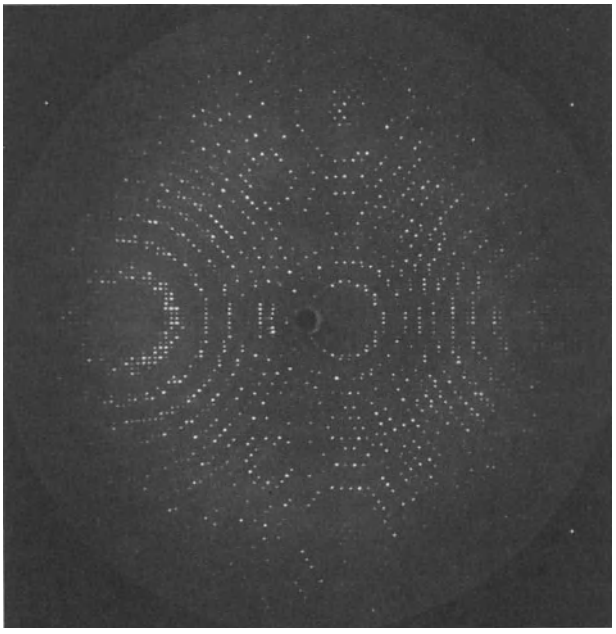

Fig. 4.55. X-ray photograph of a single crystal of the protein catalase Penicillium vitale (a = 144 Å, c = 134 Å) taken in oscillation camera in the angular range of 0.6°, CuK_α radiation, rotation axis c, crystal-film distance 75 mm (courtesy of V. R. Melik-Adamian)

4.5.7 Moving Crystal and Film Techniques

The motion of the film during the rotation of the crystal makes it possible to separate the reflections by their third coordinate and thus to prevent superpositions and ambiguity of indexing of diffraction spots. In the Weissenberg camera, or the x-ray goniometer the geometry is similar to that of the rotation camera, but only one cone of diffracted rays, corresponding to one layer plane, is isolated with the aid of a cylindrical screen (Fig. 4.56).

A cylindrical x-ray film moves along the rotation axis simultaneously with the rotation of the crystal (Fig. 4.56). The coordinate on the film, which is measured along the generator, directly yields the value of the rotation angle ω of the crystal. Thus, the position of the slit in the screen determines angle ν and coordinate ζ, while the two coordinates on the film allow us to calculate the cylindrical coordinates ξ and φ of the node of the reciprocal lattice with the aid of (4.100, 101). The orthogonal coordinates of the node are

$$Z^* = \zeta, \quad X^* = \xi \cos \varphi, \quad Y^* = \xi \sin \varphi. \tag{4.102}$$

The indices of the plane (or the coordinates of the node of the reciprocal lattice in oblique crystallographic axes) are obtained from (3.42, 43).

Since only one layer plane is registered in an x-ray goniometer at a time, the primary beam may be inclined at an angle $\mu = -\nu$ to the rotation axis, the angle being different for each layer plane. In this case the equi-inclination scheme is used (Fig. 4.57). Because of this inclination the ring which limits the effective region on the layer plane turns into a circle, and the toroid in reciprocal space into a limiting sphere of radius $2\lambda^{-1}$. The equi-inclination camera has, in principle, no dead (i.e., unrecorded) zones in reciprocal space. Figure 4.58 is an x-ray photograph obtained in a Weissenberg-type x-ray goniometer.

The recording of the layer plane can also be performed by other methods. One of them – rotation of the film in its own plane about an axis parallel to the

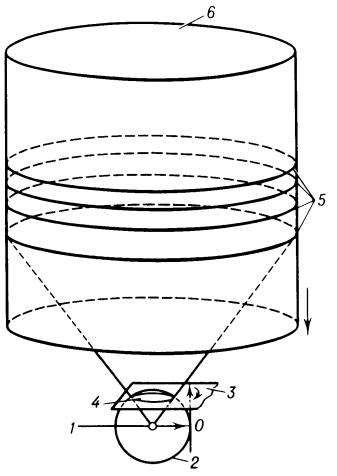

Fig. 4.56. Diagram of the Weissenberg method. (*1*) primary beam; (*2*) reflection sphere; (*3*) *n*th plane of the reciprocal lattice; (*4*) section of the reflection sphere by this plane; (*5*) projection of the sections; (*6*) cylindrical film

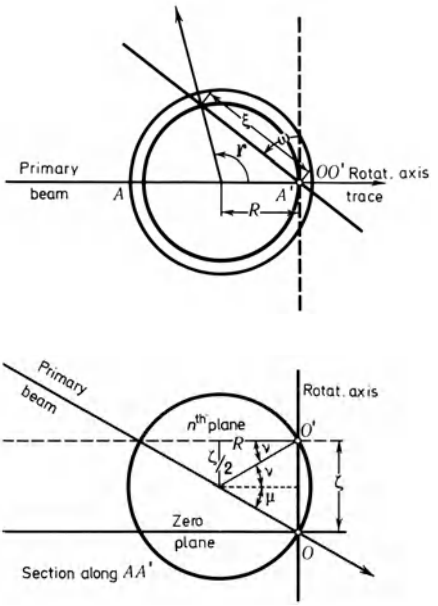

Fig. 4.57. Ewald sphere in Weissenberg's equi-inclination method

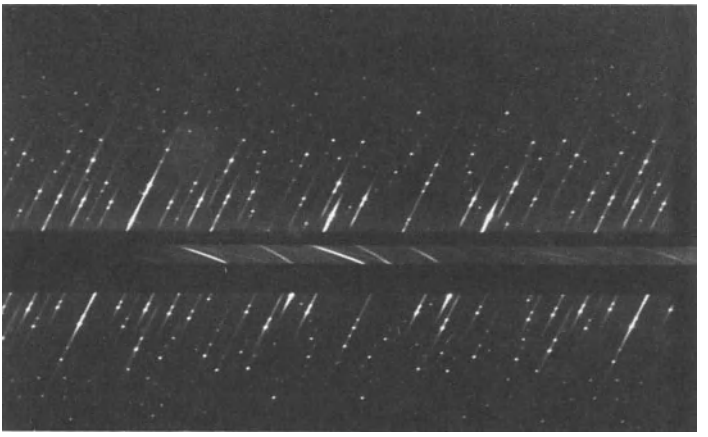

Fig. 4.58. Weissenberg's x-ray photograph of $K_2HSO_4(IO_3)$ (MoK_α radiation)

rotation axis of the crystal (De Jong and Bouman's scheme) – is employed in the camera for photography of the reciprocal lattice (CPRL) (Fig. 4.59). If the distance between the rotation axes of the crystal and film is chosen appropriately, the film shows an undistorted image of the layer plane of the reciprocal lattice (Fig. 4.60). Then the position of the rotation axis of the film relative to the circle of intersection of the diffraction cone with the film must be similar to the position of the rotation axis of the crystal relative to the intersection of the reflection sphere with the layer plane. Owing to the simplicity of indexing, such photographs are especially convenient for determining systematic extinctions.

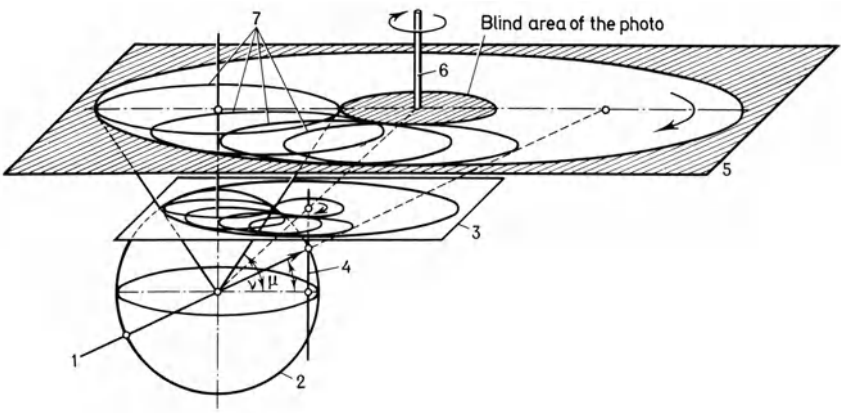

Fig. 4.59. Diagram for obtaining an undistorted image of the reciprocal lattice plane.
(*1*) primary beam; (*2*) reflection sphere; (*3*) *n*th reciprocal lattice plane; (*4*) crystal rotation axis; (*5*) film; (*6*) film rotation axis; (*7*) projections of the sections

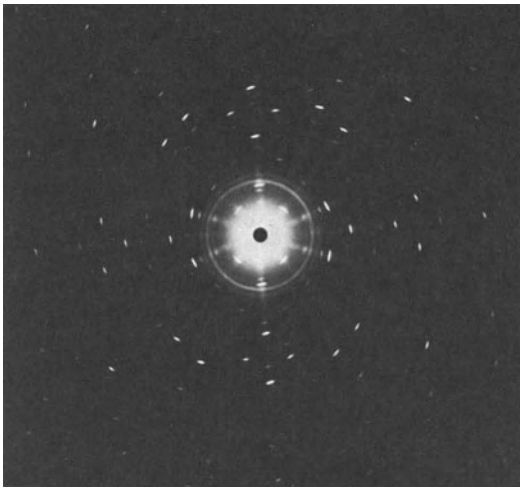

Fig. 4.60. X-ray photograph of $KScGe_2O_6$ single crystal obtained in CPRL camera. Mo-radiation, the reflections on the x-ray photograph correspond to an undistorted image of the reciprocal lattice

Another scheme is employed in Buerger's precession camera, in which the crystal and film are in correlated precession motion (Fig. 4.61); such an x-ray photograph is shown in Fig. 4.15. Here, the reflection circle shifts relative to the layer plane as in a CPRL camera. But in distinction to CPRL, where the reflection circle is fixed, in the precession camera the reflection circle moves over the reflection sphere, and the x-ray pattern is an undistorted image of the planes of the reciprocal lattice parallel to the axis of the goniometer head (Fig. 4.15).

By using Laue and x-ray rotation photographs and also by visualizing the diffraction pattern, one can determine the crystal orientation and the unit cell.

In all these methods the reflection on the x-ray photograph has a definite shape and size, which depends on the crystal (its shape, mosaic structure, etc.),

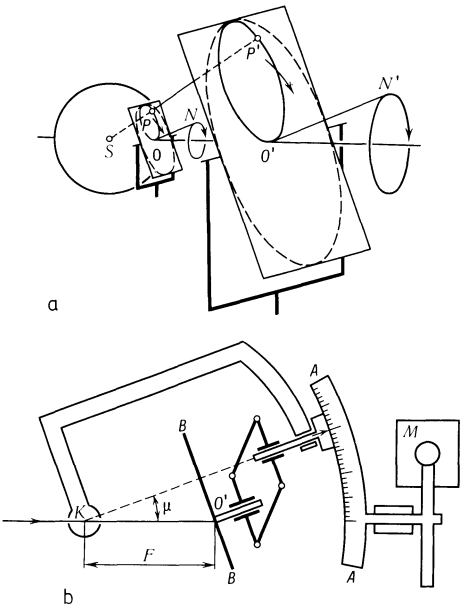

Fig. 4.61a,b. Obtaining an undistorted image of the reciprocal lattice plane in a precession camera.
(**a**) general diagram; (**b**) kinematic scheme (*O*) zero node of the reciprocal lattice; (*S*) center of the reflection sphere; (*P*) reciprocal lattice point; (*P'*) image of this point; (*N*) normal to the recorded plane of the reciprocal lattice; (*N'*) normal to the film plane; (*M*) motor; (*AA*) arc for setting the angle of inclination of the primary beam; (*BB*) film; (*C*) crystal; (*F*) crystal – film distance; (*O*) point on the film corresponding to the zero point of the reciprocal lattice or to its projection onto the *i*th plane

the geometry, and various instrumental functions. After the background is eliminated one can obtain the integrated intensity of the reflection, i.e., the total darkening of the entire area under the reflection spot (the number of quanta it has received), which is proportional to $|F|^2$.

The integrated intensity is defined by (4.63)

$$I_{hkl}^{\text{int}} = I_0\left(\frac{e^2}{mc^2}\right)^2 pL\frac{\lambda^3 V}{\dot{\omega}\,\Omega^2}\,|F_{hkl}|^2\; B\mathscr{E}G. \tag{4.103}$$

The Lorentz factor L takes into account the geometry of the various methods. For instance, for the inclination x-ray goniometer it is equal to

$$(\cos\mu\cos\nu\sin\Upsilon)^{-1}. \tag{4.104}$$

Indexing of reflection and visual estimation of their intensities are superseded by automatic computer-controlled densitometers. In addition to measuring the experimental integral intensities the computer accomplishes their primary processing, i.e., performs the transition from I_{hkl}^{int} to $|F_{hkl}|$ with due regard for the angular factors. In such instruments the x-ray photograph is placed on a rotating drum and is scanned over the entire area. The number of points measured may reach 10^6–10^7.

Computer programs provide for refinement of the matrix α_{ik} (3.43), cell parameters, and crystal orientation by several reflections on the x-ray photograph, the calculation of the spot positions from their indices *hkl*, integration of the intensity in a certain area around the spot, and determination and subtraction of the background.

In automatic microdensitometers of another type measurements are made on the flat x-ray film by turns in the region of each spot; the reflections are brought to the optic axis and scanned at spaces of 50–100 μm, i.e., at approximately 100 points per spot. The minimum densitometer measuring rate is 2–3 s per reflection, i.e., several minutes for the whole x-ray photograph. The number of quanta measured in photographic method is 10^2–10^3 s^{-1} with an accuracy of 3–5%.

4.5.8 X-Ray Diffractometers for Investigating Single Crystals*

In x-ray diffractometers a scintillation or proportional counter serves as a detector. This permits measuring the photon flux intensity in the range of 10^{-1}–10^6 s^{-1} with an accuracy of 0.5–1%.

Diffractometers of an inclination design have a geometry similar to that of Weissenberg's x-ray goniometer (Fig. 4.57). The layer plane is isolated by inclining the counter at angle ν. By rotating the counter through angle Υ about an axis coaxial with the rotation axis of the crystal ω, the input aperture of the counter is brought into coincidence with the diffracted beam (Fig. 4.62a).

In equatorial four-circle diffractometers (Fig. 4.62b) the counter is in the equatorial plane, the axis of the goniometer head can be inclined at an angle χ. The reciprocal lattice node under investigation is brought to the plane bisecting the angle 180°–2θ between the primary and diffracted beams by rotating the goniometer head through angle Φ about its axis. By inclining the axis of the goniometer head at angle χ the reciprocal lattice node is brought to the bisector of the angle 180°–2θ. Then the counter is rotated through an angle of 2θ, which corresponds to the condition $2\sin\theta/\lambda = H_{hkl}$, the bisectorial plane turning automatically through angle $\omega = \theta$. This method of bringing the plane (hkl) of the

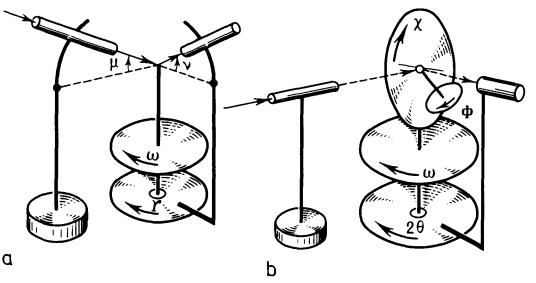

Fig. 4.62a,b. Diffractometer setting angles. (**a**) inclination methods [μ, ν: angles of inclination of the primary beam (tube) and the diffracted beam (counter); ω, Υ: angles of rotation of the crystal and the counter about the principal axis of the goniometer]; (**b**) equatorial methods (Φ: angle of rotation of the crystal about of goniometer-head axis; χ: angle of inclination of Φ axis, ω angle of rotation of the χ circle, 2θ; angle of rotation of the detector)

* See also Sect. 5.3

crystal into the reflecting position, and the counter on the diffracted beam, is called the inclination method. For this method, the setting angles are determined as follows:

$$\Phi = \varphi, \quad \chi = \rho, \quad \omega = \theta,$$
$$2\theta = 2\arcsin \lambda \frac{H_{hkl}}{2}, \tag{4.105}$$

where φ, ρ, and H_{hkl} are the spherical coordinates of the reciprocal lattice node.

When rotating the goniometer head through angle Φ about its axis (horizontal in this method), the reciprocal lattice node is brought into the equatorial plane, and then, by turning through angle ω about the vertical axis, onto the bisector of the angle $180°–2\theta$

$$\Phi = \varphi + 90° \quad \chi = 90°,$$
$$\omega = \theta + 90° - \rho, \quad 2\theta = 2\arcsin \lambda \frac{H_{hkl}}{2}. \tag{4.106}$$

In the general case, it is possible to change all the setting angles Φ, ω, χ, and 2θ. One can also assign the value of the azimuthal angle ψ – the angle of rotation of the reflecting plane about the normal.

Also, κ-goniometers are used in which, instead of an χ ring, there is an additional axis of rotation with an angle of inclination to the ω axis less than 90°.

Angle settings of a crystal and a counter in automatic diffractometers are performed by follow-up systems, which include angle encoders accurate to 0.01–0.02°. The average time of measurement of the integral intensity of one reflection is about 1 min.

In investigating protein crystals, which have very large cell periods and give 10^4–10^5 reflections, it is possible to measure 10–20 reflections arising simultaneously. This is done by multichannel diffractometers with banks of several counters or coordinate diffractometers with mosaic or position-sensitive detectors.

A chain of counters can be used as a one-dimensional detector, and a miniature-counter mosaic as a two-dimensional [4.33]. Other types of detector such as multiwire proportional chambers can detect and measure the intensities at 256×256 points of square net (grid), delay lines are used for determining the coordinates of reflections.

Two-coordinate television-type detectors using a thin scintillator polycrystalline ZnS screen are also employed. The screen is coupled optically with an electrooptical brightness amplifier and a TV tube.

With cell parameters up to 100 Å, a diffractometer with a one-dimensional detector may have an efficiency 10 times higher than that of a single-channel diffractometer, and diffractometers with a two-dimensional detector, 100 times and more.

4.5.9 Diffractometric Determination of the Crystal Orientation, Unit Cell, and Intensities

Rapid and accurate determination of the orientation and cell can be accomplished in a four-circle, a computer-controlled diffractometer.

Several reflections are first sought by systematic investigation of some region in the reciprocal space by means of consecutive changes of the setting angles or by combining photographic operations with the search on the diffractometer. Then the setting angles of the crystal are adjusted in cycles, for instance by determining the mid-points of the peak consecutively for all the angles. First, the cylindrical coordinates are determined $\xi = H_{hkl} \cos\chi$, $\zeta = H_{hkl} \sin\chi$, and then $X^*Y^*Z^*$ according to (4.102) are calculated.

An analysis of the lattice in reciprocal space is carried out as follows. Five to fifteen vectors $\boldsymbol{H}_i (i = 1, \ldots, N)$ are measured; they are supplemented by derivative vectors $\boldsymbol{H}_j = \boldsymbol{H}_i - \boldsymbol{H}_k$, which represent the differences of the initial vectors. The radius vectors $|\boldsymbol{H}_i|$ and $|\boldsymbol{H}_j|$ are aligned in increasing order, and the three smallest noncoplanar ones are chosen from among them and taken as $\boldsymbol{a}^*$, $\boldsymbol{b}^*$, and $\boldsymbol{c}^*$. The vectors $\boldsymbol{a}^*$, $\boldsymbol{b}^*$, and $\boldsymbol{c}^*$ define matrix α_{ik} (3.43). Inversion of α_{ik} by (3.31) gives β_{ik}, which defines the trial cell by the components of the projections of its axes β_{ik} onto the orthogonal axes.

Using the $\boldsymbol{a}$, $\boldsymbol{b}$, and $\boldsymbol{c}$ obtained and running through the nodes in the direct trial lattice in the order of increasing p_1, p_2, and p_3, the computer selects those radius vectors $\boldsymbol{t}_{p_1 p_2 p_3}$ which, being adopted as the edge of the unit cell, will yield a near-integer Miller indices for all the initial X^*, Y^*, and Z^*

$$h_i = \beta_{i1} X^* + \beta_{i2} Y^* + \beta_{i3} Z^*. \tag{4.107}$$

For instance,

$$k = b_x X^* + b_y Y^* + b_z Z^*.$$

The ultimate choice of $\boldsymbol{a}$, $\boldsymbol{b}$, and $\boldsymbol{c}$, and hence also hkl, is made on the basis of analysis of the values of $\boldsymbol{t}_{p_1 p_2 p_3}$ and the angles between the assumed cell edges.

Matrix β, constructed from the $\boldsymbol{a}$, $\boldsymbol{b}$, and $\boldsymbol{c}$ finally chosen, contains information on the six parameters of the cell

$$\begin{aligned} a &= \sqrt{[M]_{11}}, \quad \alpha = \arccos \frac{[M]_{23}}{bc}, \\ b &= \sqrt{[M]_{22}}, \quad \beta = \arccos \frac{[M]_{13}}{ac}, \\ c &= \sqrt{[M]_{33}}, \quad \gamma = \arccos \frac{[M]_{12}}{ab}, \end{aligned} \tag{4.108}$$

where $M = \beta\beta^{tr}$ (β^{tr} is the transposed matrix). The refinement is made by the least-squares method, bringing the experimental and calculated coordinates of the nodes to a better agreement.

In a computer-controlled diffractometer this procedure is carried out automatically, as a result the computer delivers the data on the cell and uses the matrix α found for obtaining the orthogonal coordinates X_i^* (3.42), the spherical coordinates, and the setting angles of the crystal and counter. The diffractometer sets the crystal and counter in the necessary orientation for subsequent measurements.

To measure the integrated intensities, the mosaic structure of the crystal under investigation and its transmission curves are first determined on the diffractometer. Then the following operations are carried out according to computing and controlling programs:

- calculating the setting angles and parameters for measuring the integrated intensity;
- setting the angles of rotation of the crystal and the counter with selection of the optimum combination of the different speeds of the instrument; selecting the attenuation filter;
- estimating the integrated intensity and optimizing the peak and background measurements, excluding the measurement of weak reflections and their theoretical evaluation;
- measuring the integrated intensity;
- various adjustments and checkups; and
- primary processing and optimization of measurements of reflections in relation to their intensity.

The diffraction function obtained from experiment is the convolution of the diffraction function of the crystal itself and of a number of instrumental functions which are associated with the imperfections of the instrument and the measuring conditions. These functions take into account the divergence of the primary beam, the spectrum of the radiation used, the block-mosaic structure of the specimen, and its finite dimensions. As a result, the diffraction intensity is proportional to the integrated density I_{hkl}^{int} (4.103). The inclusion of the instrumental functions helps to determine all the parameters of the experiment and the scanned volume around each node in the reciprocal space.

The most common procedure for taking the background into account is its measurement on the periphery of the diffraction maxima and linear interpolation to the area under the peak. Errors in making allowance for the background are due to its nonlinearity.

Absorption may also be allowed for by preparing specimens of definite geometric shape (spheres, cylinders, parallelepipeds), for which the absorption integral is tabulated. Another way is to calculate the absorption factor on a computer using the data on the shape, dimensions, and absorption of the specimen or using the experimental transmission curves as crystal is rotated about the normal to the reflecting plane.

The correction $\mathscr{E}$ for extinction in (4.103) arises because we compute the integrated intensity of reflection in the kinematic approximation, while the actual values lie between the values obtained in the kinematic and dynamic

approximation (see Sect. 4.3). It depends on the average size of the blocks and their angular spread and can be determined by computing $|F_H|$ and comparing the weak and strong (for which it is substantial) experimentally observed $|F_H|_{obs}$, or by other methods.

Despite the validity of Friedel's law (4.52), it is customary to measure both the hkl and $\bar{h}\bar{k}\bar{l}$ reflection intensities, which improves the measuring accuracy. At the same time, in the presence of anomalously scattering atoms the difference between $|F_H|$ and $|F_{\bar{H}}|$ is often measurable experimentally. This can be used for structure analysis.

Thus, automation of an x-ray experiment on the basis of densitometry or diffractometry considerably speeds it up and increases its accuracy. In a densitometer it is impossible to optimize an experiment with feedback: the experiment is completed in the x-ray camera before the film is developed. A diffractometer, on the contrary, allows one to perform an experiment with feedback. Besides, the accuracy of intensity measurements in a diffractometer is higher. The advantage of the photographic method is that the result of the experiment (x-ray film accessible for reprocessing) is preserved.

Systems of automation in structure analysis reduce the experiment time for investigation of a crystal with a moderately complicated structure (with 80–100 atoms in an asymmetric unit) to one or two weeks. The automatic system controlling the experiment may be coupled by a direct communication channel with a computer, where the structure analysis is performed.

4.6 X-Ray Investigation of Polycrystalline Materials

4.6.1 Potentialities of the Method

A substance to be investigated is not always available in the form of a single crystal. Moreover, in many natural and synthetic technically important materials the crystalline substance is in the form of a polycrystal or powder, and it is essential to be able to study its structure and properties just in this state. A polycrystalline material consists of a multitude of small crystals; it may be an aggregate of tightly bonded crystals, as in the case of metals, alloys, many minerals, and ceramic materials, or a fine powder of a given substance. A polycrystalline substance also may be composed of small crystals of different phases.

X-ray investigation of polycrystalline specimens is used for:

1) determination of the unit cell of an unknown substance;
2) analysis of simple structures;
3) phase analysis: qualitative, i.e., identification of the crystalline phases in minerals, alloys, etc., by comparison of the d_{hkl} and I_{hkl} values, with tabulated data; and quantitative, i.e., determination of the amount of the phases in the mixture of crystals, and also investigation of phase transitions;

4) determination of the average sizes of crystals and grains in a specimen, or their distribution by sizes, which is done by measuring the diffraction line profiles;
5) studying the internal stresses from the profile of the lines and their displacement of lines; and
6) studying the textures, i.e., the establishment and description of preferred orientation in polycrystalline specimens.

If the small crystals of the specimen have all the possible spatial orientations with equal probability, it is equivalent to spherical rotation of one small crystal and, hence, of its reciprocal lattice, in which each node $\boldsymbol{H}_{hkl}$ occupies all the positions on the surface of a sphere of radius H_{hkl}. Thus, the reciprocal lattice of a polycrystalline specimen is represented by a set of such spheres of radius H_{hkl} with a weight proportional to $|F_{hkl}|^2$.

To a parallel monochromatic beam there corresponds a reflection sphere of radius λ^{-1}. It intersects the concentric spheres of the reciprocal lattice in circles. The diffracted rays issuing from the center of the reflection sphere form a family of cones with apex angles of $4\theta = 4 \arcsin(\lambda H_h/2)$. From this construction it is clear that a polycrystalline specimen gives all the diffraction beams hkl simultaneously. An x-ray photograph of a polycrystal is often called a Debye diagram. The interplanar distances are found by the Bragg–Wulff equation $d_{hkl} = \lambda/2 \sin\theta$.

4.6.2 Cameras for Polycrystalline Specimens

In the Debye–Scherrer camera the film is placed in a cylinder whose axis coincides with that of a thin column-like specimen. In this arrangement the film intersects all the cones of the diffracted rays in arcs, which are curves of the fourth order. From the distance between the centrosymmetric lines on a Debye photograph it is easy to determine the angle θ

$$\theta_{hkl} = \frac{l_{hkl}}{4R} \frac{180^\circ}{\pi}, \tag{4.109}$$

where R is the camera radius. Figure 4.63 shows the Debye photograph of α-SiO_2.

In a Debye–Scherrer camera a powder specimen usually has the form of a cylinder which is prepared either by packing a powder in a capillary or by glueing the powder on a filament. The crystals must be as small as possible (not larger than 0.01 mm), otherwise the set of orientations will be insufficient, sphere H_{hkl} will not be filled with nodes completely, and the Debye line will consist of separate points. To increase the set of orientations of the crystals forming the line and make it continuous, the specimen is sometimes rotated about its own axis during the experiment. There are cameras with rotation about two axes (in this case a Debye photograph can be obtained even from one small crystal).

The resolution of an x-ray photograph is the higher and the accuracy of determination of angles θ the better, the thinner is the cylindrical specimen and

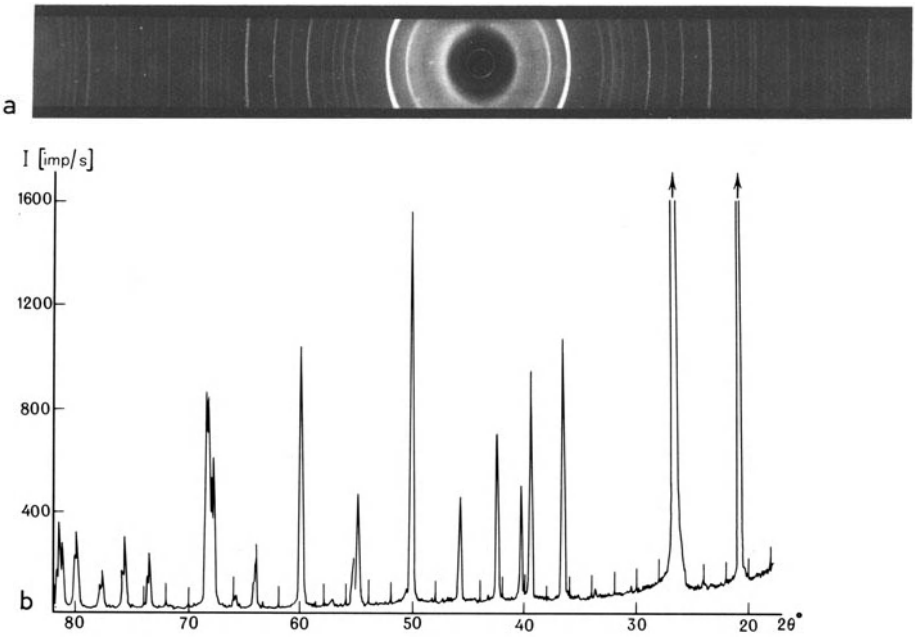

Fig. 4.63a,b. Debye diagram of α-SiO_2 obtained in an x-ray camera (**a**) and in a powder diffractometer (**b**)

the more parallel the primary beam. But at the same time the illumination of the Debye camera decreases with a consequent increase of exposure time. Focusing cameras according to Zeeman–Bolin, Preston, and Guinier have no such shortcomings.

Diagrams of cameras with focusing according to Zeeman–Bolin and Preston are shown in Fig. 4.64. A narrow slit (a radiation source), a bent specimen, and a photographic film are placed on a cylindrical surface. The focusing is based on

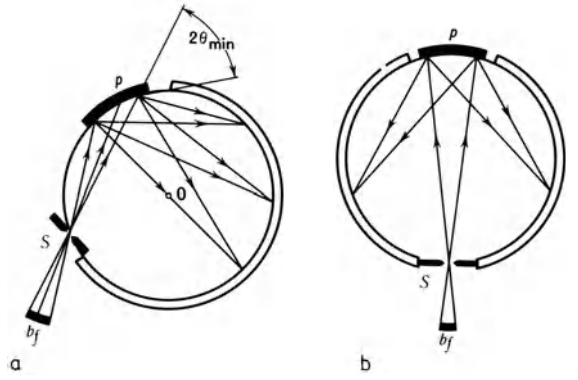

Fig. 4.64a,b. Geometric schemes of focusing cameras.
(**a**) camera with Zeeman–Bolin focusing; (**b**) focusing camera for back photography (Preston camera). (b_f) width of the focus projection, (S) entrance slit, (p) specimen

the theorem on the equality of angles inscribed in a circle and subtended by the same arc. Rays reflected from different points of the specimen merge together to a certain approximation, into a single sharp line. The position of line l_{hkl} is taken from the midpoint of the radiation source, $\theta_{hkl} = l_{hkl}/4R$, where R is the radius of the focusing circle. This type of focusing does not permit recording reflections with angles $\theta < 15$–$20°$.

If the beam divergence does not exceed 1°–2°, the bent specimen may be replaced by a flat one, touching the focusing circle. If the film is arranged on a circle of radius R with its center in the middle of the specimen, focusing will be obtained for only one line, for which radius R is equal to the distance from the middle of the specimen to the focusing point. This kind of focusing is called asymmetric focusing according to Bragg–Brentano. If the radiation source (or the slit) is at the distance R from the middle of the specimen, we obtain symmetric Bragg–Brentano focusing (Fig. 4.65).

In the simplest case, the processing of x-ray photographs consists in measuring the distance between the lines and switching to the values of θ, and then to d_{hkl} according to the Bragg–Wulff equation and the visual estimate of the intensities.

Microphotometry of Debye photographs (along a single straight line perpendicular to the diffraction lines) yields at once the positions of the lines, their intensities, and profiles.

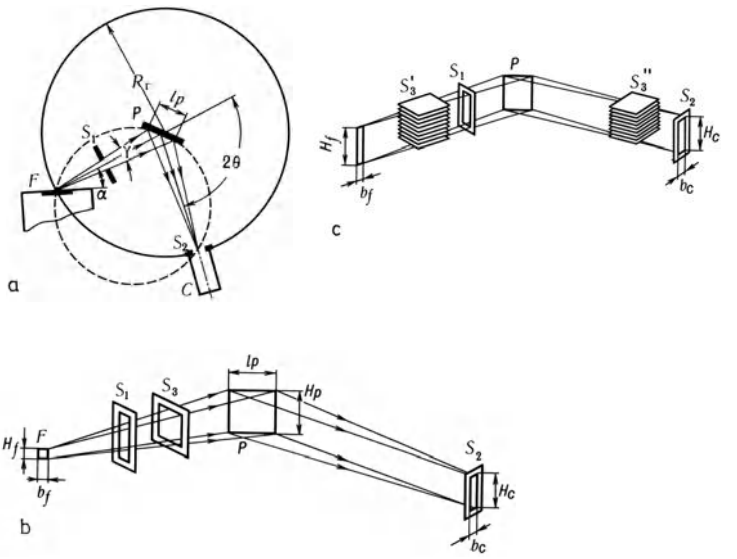

Fig. 4.65a–c. Ray path in a diffractometer with Bragg–Brentano focusing. (**a**) in the equatorial plane; (**b**) in the case of low projection of the focal spot; (**c**) in the case of high projection of the focal spot.
(S_1, S_3) beam forming slits; (S_2) slit in front of the counter C; (α) angle of selection of the primary beam; (γ) divergence angle; (H_f, b_f) dimensions of the projection of focus F; (H_c, b_c) dimensions of the slit in front of the counter; (H_p, b_p) dimensions of the specimen; (R_r) goniometer radius

4.6.3 Indexing of Debye Photographs and Intensity of Their Lines

To determine a unit cell from a Debye photograph it must first be indexed, i.e., each line must be assigned *hkl* indices. In principle, the indexing problem can always be solved. In the general case of a triclinic unit cell d_{hkl} is defined by six parameters: three periods and three angles. Hence, knowing the indices of six lines from six equations of the general type of the quadratic form H_{hkl}^2 (see Sect. 3.5.3), it is possible to determine the cell parameters. But the solution of the problem is impeded by the fact that Debye photographs usually have no reflections with weak F, and many reflections (usually with small d_{hkl}) merge together. These facts hinder indexing or make it ambiguous, especially for large low-symmetry unit cells.

In the case of high-symmetry crystals the task is simplified. For cubic crystals

$$\sin^2 \theta_{hkl} = \frac{\lambda^2}{4a^2}(h^2 + k^2 + l^2). \tag{4.110}$$

Therefore, for them the ratios of the squares of the sines are determined by a series of integers: for a primitive cell $1:2:3:4:5:6:8:9:10:\ldots$, for a face-centered cell $3:4:8:11:12:16:19:\ldots$, for a body-centered cell $2:4:6:8:10:12:14\ldots$. If an x-ray photograph for a cubic cell cannot be indexed, a hexagonal or tetragonal cell is assumed. For these cells indexing is done graphically with the aid of the so-called Hull curves, which give $\log d_{hkl}^2$ for any c/a. In the case of orthogonal crystals, the differences of the squares are used $[(d^{-1})^2 = H^2]$

$$H_{h_i k_i l_i}^2 - H_{h_j k_j l_j}^2 = \frac{1}{d_{h_i k_i l_i}^2} - \frac{1}{d_{h_j k_j l_j}^2}$$
$$= \left(\frac{h_i^2}{a^2} + \frac{k_i^2}{b^2} + \frac{l_i^2}{c^2}\right) - \left(\frac{h_j^2}{a^2} + \frac{k_j^2}{b^2} + \frac{l_j^2}{c^2}\right), \tag{4.111}$$

which are identical for series of lines in accordance with Pythagorean theorem.

The most commonly encountered differences are of the type h^2/a^2, or k^2/b^2, or l^2/c^2, which correspond to the orthogonal basis vectors $\boldsymbol{H}_{h00}$, $\boldsymbol{H}_{0k0}$, and $\boldsymbol{H}_{00l}$, whence the parameters a, b, c are determined.

Similar techniques are used in analyzing monoclinic crystals. A number of mathematical algorithms for determining low-symmetry cells have been proposed. The correctness of indexing is checked by the agreement of the calculated and experimental values of d_{hkl}^2. If necessary, the cell obtained can be transformed to the standard setting by the reduction algorithm (4.51–57).

The use of computers for indexing speeds up the calculation, but does not eliminate the above difficulties.

The integrated intensity of the diffraction line *hkl* of the Debye photograph is equal to the area of a peak whose profile is measured along coordinate θ. In a sphere of radius H_{hkl}, and hence in the given line, all the symmetrically equal nodes of the reciprocal lattice, or, in other words, all the reflections from the crystallographically equal planes, merge together. The number of such planes

depends on the symmetry of the crystal and is called the multiplicity factor p; it is equal to the number of planes in the simple form of the crystal (see Tables 3.1, 4) and therefore depends on the indices of the planes and on the crystal symmetry; the multiplicity factors have values of 48, 24, 16, 12, 8, 6, 4, 3, 2, and 1. If the symmetry is lower, reflections with equal d_{hkl}, but unequal $|F_{hkl}|$, may merge together in one line of the Debye photograph; lines whose d_{hkl} accidentally coincide can also merge in one line.

The intensity of the Debye line is given by

$$I = I_0 \left(\frac{e^2}{mc^2} \right)^2 \frac{1 + \cos^2 \theta}{32\pi r^2 \sin^2 \theta \cos \theta} \frac{\lambda^3 V}{\Omega^2} |F_{hkl}|^2 pB\mathscr{E}G. \tag{4.112}$$

Here, r is the radius of the Debye ring on the flat film. As we have already noted, in the case of simple structures, the set of I_{hkl} obtained from a Debye photograph may be used for a complete structure analysis.

4.6.4 Diffractometry of Polycrystalline Specimens

In single-channel x-ray diffractometers for polycrystals the photographic film is replaced by a detector with a narrow input slit. Scintillation and proportional counters are usually employed as detectors. The diffraction pattern is recorded consecutively as the detector moves, permitting utilization of symmetric Bragg–Brentano focusing. The analytic slit of counter S_2 and radiation source F, the projection of the tube focus, are arranged on the goniometer circle of radius R, through the center of which the surface of the flat specimen p passes (Fig. 4.65). When the counter is turned through an angle of 2θ, the specimen turns simultaneously through θ so that its surface continuously touches the circle of focusing with a variable radius

$$r = R/(2 \sin \theta). \tag{4.113}$$

Goniometers may be provided with attachments for rotating or oscillating coarse-grained specimens, studying the textures, for investigations at small scattering angles and at low and high temperatures. Multichannel diffractometers with Zeeman–Bolin focusing can record a series of diffraction lines at one time by means of several counters, and diffractometers with a coordinate detector can record the entire x-ray diffraction pattern.

A set of reflections hkl of a polycrystalline specimen can be obtained by using a polychromatic radiation. A semiconductor detector with a high amplitude resolution (1.5–3%) is set at a constant scattering angle of $2\theta_{\text{const}}$. By accumulating pulses, corresponding to different wavelengths, in different channels with the aid of a multichannel amplitude analyzer we obtain a diffraction spectrum as a function of λ, from which we find the interplanar distances $d = \lambda (2 \sin \theta_{\text{const}})^{-1}$ by the Bragg–Wulff equation. This is convenient for experiments, for instance, at high pressures or temperatures, since during measurements under these conditions the diffracted rays emerge from the goniometer through a single slit and in a single direction.

The intensity of the diffraction peak in a polycrystalline diffractometer is given by the expression

$$I_{hkl} = I_0 \left(\frac{e^2}{mc^2} \right)^2 pL \frac{\Omega \lambda^3 p_{hkl}}{\dot{\omega}} A \frac{S}{v^2} F_{hkl}^2 \frac{1}{\rho_i}, \tag{4.114}$$

where S is the cross section of the primary beam, p_{hkl} is the multiplicity factor, $A \approx (2\mu)^{-1}$ is the transmission factor for a flat specimen according to Bragg–Brentano, ρ is the density of the substance, L is the Lorentz factor, and $\dot{\omega}$ is the angular velocity of rotation of the specimen.

The introduction of instrumental functions takes into account various factors affecting the position and profile of the diffraction peak and also helps in estimating the measuring errors. Of great importance is the Rietveld analysis of polycrystalline materials (see Sect. 5.5).

4.6.5 Phase Analysis

X-ray phase analysis is used in mineralogy, studies of metals, and materials science and is a versatile and rapid method. It is based on the fact that an x-ray powder diagram of a given phase is characterized by a set of d_{hkl} and I_{hkl}, while an x-ray diagram of a multiphase specimen is a superposition of x-ray pictures of the separate phases.

Phase analysis can be carried out by the photographic or diffractometric method. It requires reference data which are collected in special manuals. The most complete x-ray data are given in the card files of the ASTM. At present, there are several versions of computer-assisted information systems for automatic qualitative phase analysis.

Quantitative x-ray phase analysis is based on the dependence of the intensity of reflection on the contents, x_j, as of the corresponding phase and is carried out using powder diffractometers. The intensity expression (4.114) can be rewritten as

$$I_j(hkl) = I_0 m_j(hkl) \frac{S}{2\mu} \frac{\Omega}{\dot{\omega}} \frac{x_j}{\rho_j}, \tag{4.115}$$

where $m_j(hkl)$ is the reflecting power of the plane hkl of the jth phase. It follows that I_j is proportional to x_j/ρ_i. This helps to determine x_j by measuring certain reference I_{hkl} and introducing the necessary corrections for absorption.

4.6.6 Investigation of Textures

A "true" polycrystalline specimen contains, with equal probability, crystals with all the orientations. Despite the anisotropy of the properties of individual small crystals, such a substance is statistically isotropic. In a number of cases, however, for instance, during the growth of crystals in orienting fields, during plastic deformation of metals (rolling, drawing, etc.), and when the small crystals have a fiberlike or platelike structure, they acquire a preferred orientation, called texture.

A preferred orientation can be characterized by the density distribution of normals $\boldsymbol{H}_{hkl}$ to a given crystallographic plane hkl over a sphere. Such a distribution is called a "pole figure"; its coordinates are ρ and φ. A pole figure is constructed for certain special directions in a specimen, for instance, the coordinate directions [100], [010], and [001], on the basis of photographic or diffractometric data.

Measurement of the intensity of the diffraction pattern in a diffractometer with the counter and specimen fixed gives a value proportional to the density of the normals in the direction of the bisector of the angle of $180°-2\theta$ made by the primary and diffracted ray from the specimen. To investigate the directions making an angle ρ with the normal to the specimen surface, the normal has to be deflected from the indicated bisector. A full pole figure can be investigated by changing the angle ρ consecutively and recording the diffraction pattern each time with a slow rotation of the specimen in its proper plane. The x-ray pattern will show the intensity as a function of angle φ. Automatic texture diffractometers have been developed for investigating the textures. Figure 4.66 illustrates the pole figure of a texture due to rolling.

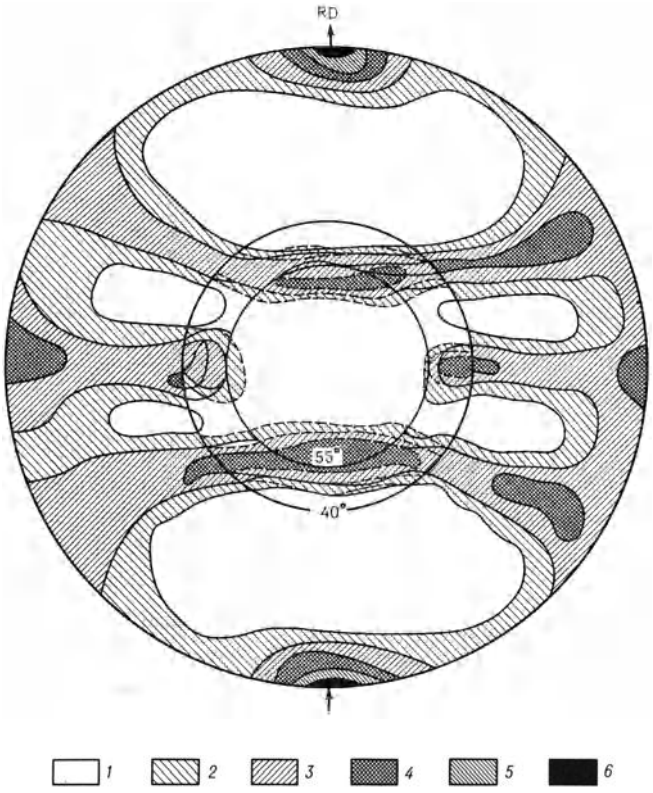

Fig. 4.66. Pole figure [110] of an Fe–Si alloy. Hatching of the regions of the polar figure denotes the different density of the normals in density units of the pole figure of a specimen without a preferred orientation. (*1*) less than 1/2; (*2*) 1/2–1; (*3*) 1–2; (*4*) 2–4; (*5*) 8; (*6*) more than 8. (*RD*) direction of rolling

4.6.7 Determination of the Sizes of Crystals and Internal Stresses

The width and shape of the diffraction line in an x-ray photograph of a polycrystal depend on the size of the small crystals. We know that the size of the nodes of the reciprocal lattice is inversely proportional to that of the small scattering crystal in the corresponding direction (4.41). The size of the small crystal A in the direction of the normal to plane hkl is related to the half width of the broadened diffraction line β by the equation

$$A = nd = \frac{\lambda}{\beta \cos \theta}, \tag{4.116}$$

where n is the number of interplanar spacings d_{hkl}. Equation (4.116) gives the averaged value of A.

The effect of the broadening of the diffraction line on a Debye diagram becomes noticeable if the particle size is less than 1000 Å. Crystals exceeding 10^4 Å in size can be regarded as infinitely large in terms of their effect on the line width. The lower limit of the sizes lies in the range of $\sim$ 10 Å, when the width of the scattering lines becomes close to the one in diffraction from amorphous substances.

Equation (4.116), which gives the average size of the small crystals, does not take into consideration their size distribution. Additionally, the broadening of the diffraction line on the Debye patterns is due to contributions from various distortions in three-dimensional periodicity inherent in a real crystal: microstresses, errors in sequences of the layers, etc., which in fact gives rise to some set of d about the average value d_{hkl}. The line profile depends in a complicated way on the causes of its broadening. In precise measurements this helps in finding the character and quantitative parameters of the defects and the sizes of the small crystals. Thus, the method of Fourier transformation of the line profile helps to find the functions of crystal size distribution and of microdeformations.

4.7 Determination of the Atomic Structure of Crystals

4.7.1 Preliminary Data on the Structure

The experimental data for crystal structure determination, i.e., for finding the arrangement of the atoms in the unit cell and other parameters of the structure, consist of a set of values of $|F_H|$. In the preceding sections we described the experimental technique and procedure for determining the unit cell and the symmetry and finding the values of $|F|^2$ from an x-ray diffraction experiment. In principle, any structure can be determined from these data alone, but the use of other information facilitates structure analysis.

Such information includes, in the first place, the chemical composition of the substance. The chemical formula is almost always known, and the building

block of a crystal – the unit cell – may contain only an integral number n of "formula units". A diffraction experiment yields the unit cell volume Ω and, if the density of the substance ρ has been measured, then

$$n \approx \Omega\rho/Mm_{\mathrm{H}}, \tag{4.117}$$

where M is the molecular weight of the "formula unit" (Dalton), and m_{H} is the mass of the hydrogen atom.

The data on the point symmetry K obtained from Laue patterns can be supplemented by goniometric, crystallooptical, and crystallophysical measurements. These may be helpful in establishing the presence or absence of polar directions, a center of symmetry, the allocation of the crystal to the point group of the first or second kind, etc. (see Chap. 2 and also [4.34]).

The x-ray group, which is determined from the extinctions, together with the statistics of intensities (see Sect. 4.2) and the data on group K, often gives unambiguously the Fedorov group Φ of the crystal or narrows down the choice of Φ to two or three groups.

The number of atoms of each sort which must be placed in the unit cell is known from (4.117) and from the chemical formula; assume n_1 atoms of sort A_1, n_2 of A_2, n_3 of A_3, ... The numbers n_i are compared with the multiplicities n of the special and general positions of the regular point systems in the given group Φ (see Fig. 2.81), and thereby the possible positions are determined. Sometimes, especially in organic structures, when the chemical formula units of the structure are also the physical building units – molecules – the regular system of points which they can occupy in the given group Φ is defined unambiguously.

In structure interpretation it is customary to use crystallochemical data on the atomic radii, the packing of atoms or molecules, the shape of the latter, the coordination, isomorphism, and also analogies with other structures, etc. [Ref. 4.3, Chap. 1, Sect. 4]. Such information is particularly useful in interpreting relatively simple structures and when diffraction experiments supply insufficient data, for instance, when only an x-ray powder photograph can be obtained.

Structure determination in the strict sense begins after establishing all the indicated geometric, symmetry, and crystallochemical data with which the solution must fit in. It has already been noted that x-ray structure analysis can also be carried out without the knowledge of the chemical formula or with just approximate data on it, then it can be used instead of chemical analysis.

4.7.2 Fourier Synthesis. Phase Problem

The integral (4.34), which determines the value of the scattering amplitude $F(\boldsymbol{S})$ for an object with an electron density $\rho(\boldsymbol{r})$, is a Fourier integral. This latter possesses the property of reversibility, which consists in the fact that knowing the function $F(\boldsymbol{S})$ one can compute $\rho(\boldsymbol{r})$ from it with the aid of an inverse Fourier transform. I $\rho(\boldsymbol{r})$ is the electron density of the crystal, i.e., a three-

dimensionally periodic function the inverse Fourier transform is the Fourier series

$$\rho(xyz) = \frac{1}{\Omega} \sum_h \sum_k \sum_l F_{hkl} \exp\left[-2\pi i \left(\frac{hx}{a} + \frac{ky}{b} + \frac{lz}{c} \right) \right], \tag{4.118}$$

whose coefficients are the structure amplitudes F_{hkl} of reflections hkl. Thus, knowing F_{hkl}, i.e., their moduli and phases α_{hkl} (4.46), one can, by summing the series (4.118), construct the electron density distribution $\rho(\boldsymbol{r})$. This is the solution of the structure since the peaks of $\rho(\boldsymbol{r})$ give the arrangement of all the atoms ρ_i according to (4.13).

The Fourier synthesis consists in superposition of individual harmonics, i.e. the terms of the series (4.118),

$$|F_{hkl}| \cos 2\pi \left(\frac{hx}{a} + \frac{ky}{b} + \frac{lz}{c} + \alpha_{hkl} \right), \tag{4.119}$$

each term being a plane wave of spatial density with a wavelength (the distance between the wave maxima) of d_{hkl}, a normal $\boldsymbol{H}_{hkl}$, and an amplitude F_{hkl}. One two-dimensional harmonic is shown in Fig. 4.67a. This is the physical embodiment, so to speak, of a system of parallel reflecting planes (hkl) of the crystal (cf Fig. 3.29); the reflecting power – the atomic population of such a system – is expressed by the absolute value of the amplitude $|F_{hkl}|$. The same harmonic, being perpendicular to $\boldsymbol{H}_{hkl}$, can be displaced to any position along this vector, and its d_{hkl} and $|F_{hkl}|$ remain unaltered. But this displacement is determined exactly by the value of phase α_{hkl}. Superposition of harmonics, each with $|F|$ and α of its own, yields an ever more complicated picture (Fig. 4.67b, c) and, finally, their entire set (4.118) corresponds to the electron density distribution of the crystal (Fig. 4.67d), which is usually denoted by contours of equal density (Fig. 4.68).

Obtaining the image of the object by calculation on the basis of diffraction data can be interpreted as follows. The formation of an image in optics (for instance, in a light or electron microscope) can be divided into two stages. The first consists in the scattering of incident radiation by the object and the formation of diffracted beams with amplitudes $F(\boldsymbol{S})$. This stage is exactly the same as in x-ray scattering and corresponds to the Fourier expansion. At the second stage the scattered beams are focused with the aid of lenses, and the image of the object is formed, which corresponds to the Fourier synthesis. There are no lenses for x-rays, however, and therefore the second stage, i.e., the formation of the image, must be realized by computation. Thus, the Fourier synthesis from the experimental F_H serves as a "mathematical microscope" with atomic-scale resolution.

Owing to the decrease in the atomic temperature factor f_{aT}, the intensities weaken gradually, on the average, with increasing $\sin\theta/\lambda$, see (4.48), and disappear altogether at a certain limiting value of $(\sin\theta/\lambda)_{max} = 1/2d_{min}$. This is the natural limit of the diffraction field. The last (with d_{min}) Fourier harmonics correspond to the finest details of the electron density. Therefore the quantity

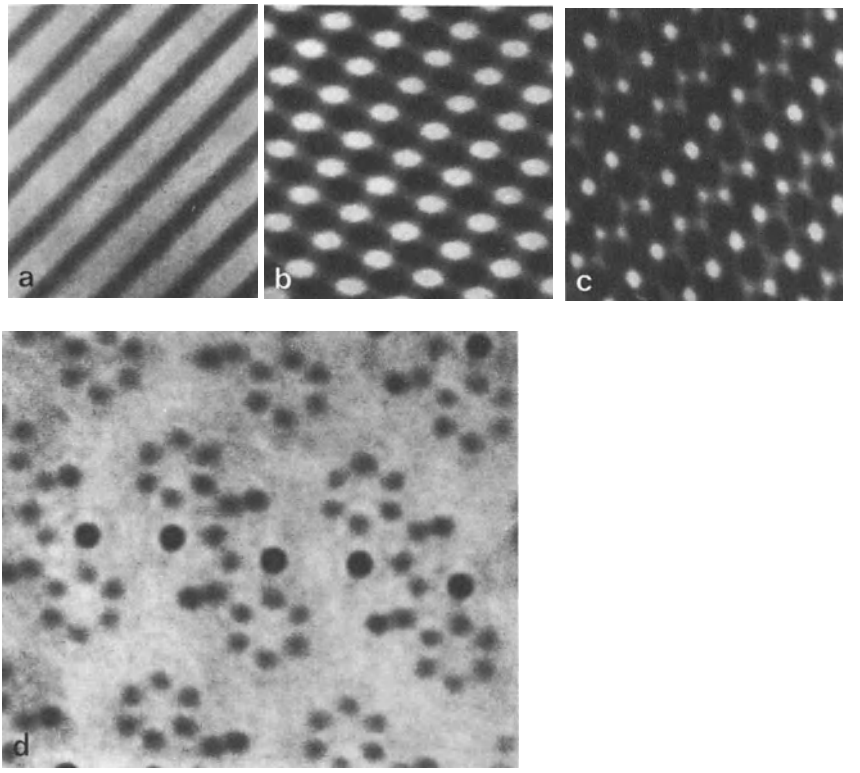

Fig. 4.67a–d. Fourier synthesis as a result of superposition of elementary harmonics F_{hkl} (two-dimensional case). Each harmonic is represented as a sinusoidal distribution of optical density (**a**). Superposition of two (**b**) or more (**c**) harmonics complicates the picture; the combination of all the harmonics – Fourier synthesis – gives the image of the structure (**d**) [4.35]

$d_{\min}$ is adopted as the measure of natural resolution of the diffraction experiment. The value of $d_{\min}$ is determined by the width of the peak of the electron density of an atom $\rho_{aT}(\boldsymbol{r})$ (4.21) in the state of thermal motion.

Therefore the resolution is determined by the decrease in function f_{aT} (4.23), and depends on the sort of an atom, i.e., on atomic number Z, on the radiation used (electrons, x-rays, neutrons – the resolution improves in this sequence), and largely on the value of the temperature factor, i.e., the quantity $\overline{u^2}$ appearing in $w(\boldsymbol{r})$ (4.24). Thus, for inorganic crystals $d_{\min}$ may reach 0.5 Å; for organic substances, $d_{\min}$ is usually $\approx$ 0.7–1.5 Å. The thermal motion smears out the electron density of the atom and individual electron shells become practically indistinguishable; in principle, they could be revealed by the x-ray method if the atoms were at rest. (Exceptions are the outermost shells; see Sect. 4.7.10.) For protein crystals $d_{\min} \approx$ 1.5–3 Å and, as a rule, atoms are not resolved on electron density maps; only their groupings are revealed.

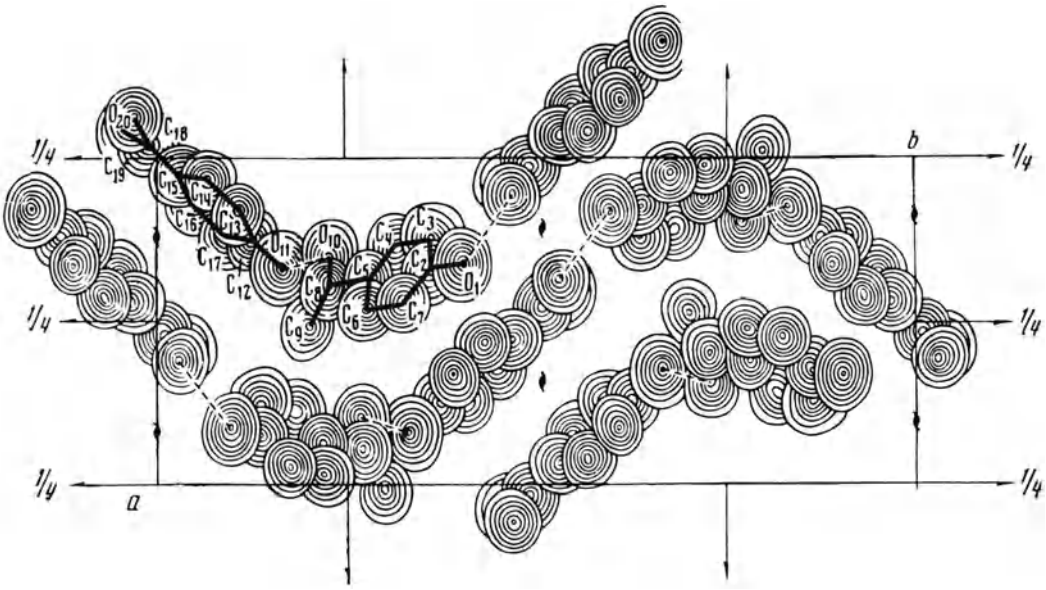

Fig. 4.68. Image of the structure of *p*-oxyacetophenone projected onto the *xy* plane as a superposition of the cross sections of the electron density of atoms obtained by constructing a three-dimensional Fourier synthesis (hydrogen atoms are not shown). The molecules are bound into a chain by the hydrogen bonds [4.36]

For these reasons, in x-ray studies of organic crystals and proteins, it is sufficient to use CuK_α radiation ($\lambda = 1.54$ Å) which permits one to record reflections with $d_{\min}$ up to 0.77 Å. This is insufficient, however, for inorganic crystals, and therefore MoK_α radiation ($\lambda = 0.71$ Å, $d_{\min} = 0.35$ Å) is used. Neutron diffraction analysis provides the highest resolution.

Sometimes it is desirable to include in Fourier series only $F_{\exp}$ with a certain limiting "artificial" $d'_{\min} > d_{\min}$. In this case the resolution is naturally defined by the quantity $d'_{\min}$. Additionally, the map obtained by Fourier synthesis will exhibit the so-called series termination waves, which distort the true distribution of scattering density around the atoms.

The moduli of the structure amplitudes $|F_H|$, which are necessary for constructing the Fourier series (4.118), are determined directly from the reflection intensities (4.47): $|F_H| \sim \sqrt{I_H}$. An experiment yields relative values of the integrated intensity, i.e., $|F_H|^2$, and hence also $|F_H|$. To express the experimentally observed values of $|F_H|$ in electron units they must be scaled to the absolute values. This can be done on the basis of (4.48) or (4.50), whose right-hand sides include the absolute values of the squares of the tabulated atomic factors $f_{j\mathrm{T}}^2$. The left-hand side contains $I_H \sim |F_H|^2$, and it is equated to the right-hand side by multiplying $|F_H|^2_{\mathrm{obs,rel}}$ and the scaling factor k, as determined from (4.48) or (4.50), so that $k\,|F_H|^2_{\mathrm{obs,rel}} = |F_H|^2_{\mathrm{obs,abs}}$. By putting the $|F_H|$ thus scaled into the series (4.118), we obtain the values of electron density $\rho(\boldsymbol{r})$ in electron units. This

makes it possible to analyze the function $\rho(\boldsymbol{r})$ quantitatively, for instance, to find the number of electrons in each peak and thereby identify a given atom, etc.

The construction of the Fourier series (4.118), however, requires a knowledge not only of the moduli $|F_H|$, but also of the phases α_H of the reflections, which are lost in the diffraction experiment. This is, in fact, the principal difficulty of structure analysis. The problem of structure determination consists essentially in finding the phases, after which the calculation of (4.118) gives the structure $\rho(\boldsymbol{r})$ at once.

All the methods for solving structures and determining phases which are used in structure analysis are computational. Experimental measurement of phases of the reflected beams involves enormous difficulties. It is possible to solve the problem in some special cases of dynamic scattering of electrons and x-rays [4.37]. Direct measurement of phases can, in principle, be carried out by using Mössbauer sources of coherent x-ray quanta. Another possibility, which has not been realized yet, consists in developing an x-ray laser and utilizing the concepts of holography.

The Fourier series (4.118) gives the three-dimensional distribution of the electron density $\rho(xyz)$. It is also possible to construct projections of the three-dimensional distribution onto coordinate or any other planes. Thus, the two-dimensional series

$$\sigma(xy) = \frac{1}{S}\sum_h \sum_k F_{hk0} \exp\left[-2\pi\mathrm{i}\left(h\frac{x}{a} + k\frac{y}{b}\right)\right] \tag{4.120}$$

represents the projection of the structure along the c^* axis and is constructed from the amplitudes F_{hk0} of the reflection zone $hk0$. According to (4.44) these amplitudes are independent of the atomic coordinates z_j. The expressions for the other two coordinate projections are similar, being constructed from F_{h0l} or F_{0kl}. There are also many other versions of construction of the Fourier series. For instance, it is possible to project, not the entire structure, but a part of it, chosen in an arbitrary way. The three-dimensional distribution (4.118) can be calculated not only within the whole volume of the unit cell, but within selected two-dimensional (plane) sections or along straight lines.

4.7.3 The Trial and Error Method. Reliability Factor

The trial and error method was the principal procedure in the early decades of the development of structure analysis. Starting from some model of a structure built according to its symmetry, chemical formula, and crystallochemical data, it is possible to calculate, from the atomic coordinates $\boldsymbol{r}_j$, the structure amplitudes F_{hkl} (4.44)

$$F_{\mathrm{calc}} = \sum_{j=1}^{N} f_j \exp[2\pi\mathrm{i}(hx_j + ky_j + lz_j)]. \tag{4.121}$$

If the trial structure is at least approximately correct, then

$$|F_H|_{\mathrm{calc}} \approx |F_H|_{\mathrm{obs}}. \tag{4.122}$$

Of importance here is the coincidence of large, by absolute value, structure amplitudes $|F_H|$. A considerable difference between calculated $|F_H|_{\text{calc}}$ and observed $|F_H|_{\text{obs}}$ shows that the model is wrong, and then other atomic arrangements are tested. As the correct solution is approached, a better agreement between $|F_H|_{\text{calc}}$ and $|F_H|_{\text{obs}}$ is achieved with small displacements of atoms. Since the coordinates x_j, y_j, z_j of the atoms are in argument of (4.121) in products with h, k, l indices, reflections with large hkl (and small d_{hkl}), are always more sensitive to the values of the coordinates. This also clearly follows from the consideration of individual harmonics (4.119) of the Fourier expansion: in higher harmonics the maxima are sharper, and they record more distinctly the possible displacements of atoms (along $\boldsymbol{H}_{hkl}$).

The trial and error method was used, as a rule, to interpret centrosymmetric structures with a small number of atoms in general positions. The large number of manual calculations made structure determination very laborious. To shorten experiments and calculations, structures were determined mostly from projections, i.e., with the use of the coordinate zones of reflections $hk0$, $0kl$, and $h0l$ only.

At present the trial and error method is hardly used at all, but its basic idea – comparing and fitting the calculated and experimental $|F|$ (4.122) – is still used widely as a criterion of the correctness of the determined structure and as a method of its refinement. As a quantitative measure of the closeness of $|F|_{\text{obs}}$ and $|F|_{\text{calc}}$ one can use the reliability factor

$$R = \frac{\sum_H ||F_H|_{\text{obs}} - |F_H|_{\text{calc}}|}{\sum_H |F_H|_{\text{obs}}} \tag{4.123}$$

or a correlation function of the general form

$$R' = \sum_H w_H (k|F_H|^{\alpha}_{\text{obs}} - |F_H|^{\alpha}_{\text{calc}})^{\beta}, \tag{4.124}$$

where w_H is a weighting factor which characterizes, for instance, the accuracy of measurement of $|F_H|_{\text{obs}}$ or the reliability of the calculation of $|F_H|_{\text{calc}}$; k is the coefficient scaling $|F_H|_{\text{obs}}$ to the absolute values, and α and β are some constants; the case $\alpha = 2$ corresponds to the consideration of intensities.

When the correct preliminary model of the structure is found, the R factor (4.123) has a value of 20–25%. Then $F_{H\text{calc}}$ can be calculated by (4.121) and the Fourier synthesis can be constructed by taking the phases α_H from this calculation and supplying them to $|F_H|_{\text{obs}}$ (4.118). In the final refinement of the structure with an allowance for the anisotropic temperature factor the R-factor reduces to 3–5%.

4.7.4 The Patterson Interatomic-Distance Function

When discussing scattering from an arbitrary object (see Sect. 4.4) we saw that the intensity is a Fourier integral of the function $Q(r)$ (4.79) of the interatomic

distances in the objects, i.e., $Q(\boldsymbol{r})$ and $I(\boldsymbol{S}) = |F(\boldsymbol{S})|^2$ are mutual Fourier transforms. For crystals, the interatomic-distance function was proposed by *Patterson* in 1935 [4.38]. We denote it by $P(\boldsymbol{r})$. Similarly to (4.80) this function has the form

$$P(\boldsymbol{r}) = \int \rho(\boldsymbol{r}')\rho(\boldsymbol{r}' - \boldsymbol{r})\,dv_{r'} = \rho(\boldsymbol{r}) * \rho(-\boldsymbol{r}), \tag{4.125}$$

i.e., $P(\boldsymbol{r})$ is a convolution of the crystal electron density $\rho(\boldsymbol{r})$ with the same, but inverse function $\rho(-\boldsymbol{r})$[5]. From the convolution theorem (4.20), as well as from the fact that intensity and $P(\boldsymbol{r})$ are mutual Fourier transforms, it follows that this function can be represented by a Fourier series with respect to the values of $|F_H|^2$

$$P(\boldsymbol{r}) = \frac{2}{\Omega} \sum_h \sum_k \sum_l |F_H|^2 \cos 2\pi(hx + ky + lz), \tag{4.126}$$

similar to the Fourier series for the electron density $\rho(\boldsymbol{r})$ (4.118). But for $P(\boldsymbol{r})$ the coefficients of the series are the values of $|F_H|^2$ found directly from experiment; they are all positive, i.e., their phases $\alpha = 0$. Indeed, as Fourier coefficients $\rho(\boldsymbol{r})$ are F_H, the Fourier coefficients of the convolution are the products of those of the initial functions, i.e., $F_H F_H^* = |F_H|^2$. Since $|F_H|^2 = |F_{\bar{H}}|^2$ (4.52), series (4.126) is constructed by the cosines.

Let us consider the properties of the Patterson function $P(\boldsymbol{r})$. The electron density of a crystal is a sum of atomic densities $\rho(\boldsymbol{r}) = \Sigma \rho_j(\boldsymbol{r} - \boldsymbol{r}_j)$ and has the highest values at the centers of atoms $\boldsymbol{r}_j$. Consequently, $P(\boldsymbol{r})$ has maxima at points $\boldsymbol{r} = \boldsymbol{r}_j - \boldsymbol{r}_k$, i.e., when the vector $\boldsymbol{r}$ is an interatomic vector. The correlation between the structure and its function of interatomic vectors is demonstrated in Fig. 4.69. The possibility of obtaining information on the set of all interatomic distances in a crystal directly from experimental data greatly simplifies the task of structure determination. Therefore the Patterson function is widely used in structure analysis.

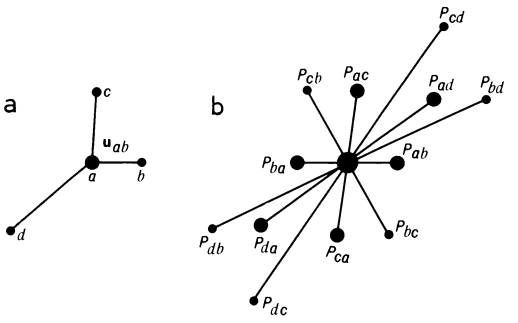

Fig. 4.69a,b. Relationship between the positions of atoms $\rho(\boldsymbol{r})$ (**a**) and the function of interatomic distances $P(\boldsymbol{u})$ (**b**)

[5] The value of $P(\boldsymbol{r})$ will not be changed for any product of ρ appearing in (4.125) if the difference of their arguments is equal to $\boldsymbol{r}$. Therefore the integrand is often written as $\rho(\boldsymbol{r}' + \boldsymbol{r})\,\rho(\boldsymbol{r}')$. It should also be noted that if ρ is centrosymmetric, then $\rho(-\boldsymbol{r}) = \rho(\boldsymbol{r})$.

The principal properties of this function are as follows:

1) The vector joining each pair of atoms a and b in $\rho(\boldsymbol{r})$ is represented in the function $P(\boldsymbol{r})$ by a peak $P_{ab}(\boldsymbol{u}_{ab})$; vector $\boldsymbol{u}_{ab}$ is drawn from the origin (Fig. 4.69);
2) the function always has a center of symmetry, i.e., $P(\boldsymbol{r}) = P(-\boldsymbol{r})$, even if the initial structure does not possess it, because, along with vector $\boldsymbol{u}_{ab}$, there is always an equal and opposite vector $\boldsymbol{u}_{ba}$. This also follows from the fact that all the harmonics in (4.126) are cosines.
3) the weight of the peak $P_{ab}(\boldsymbol{u}_{ab})$, i.e., the integral over its volume, is equal to the product of the numbers of the electrons Z_a and Z_b of atoms a and b and, if the distances $\boldsymbol{u}_{ab}$ in the structure are repeated, the product is multiplied by the number of repetitions; and
4) if $\rho(\boldsymbol{r})$ contains n atoms, then $P(\boldsymbol{r})$ contains n^2 peaks, of which n merge together at the origin, giving a peak $P(0)$ with a weight ΣZ_j^2, which represents n distances $\boldsymbol{u}_{aa}$ of atoms "to themselves", while the remaining $n(n-1)$ peaks are distributed throughout the unit cell volume.

Before we proceed to the discussion the possibilities of deriving a structure from the Patterson function it should be pointed out that this function can be analyzed in terms of the crystal symmetry. Assume, for instance, that the crystal has an axis 2 directed along the c axis. Then, to any atom with coordinates x, y, z there corresponds an atom with coordinates $\bar{x}, \bar{y}, z$, and the interatomic vector has coordinates $2x, 2y, 0$. This means that all the interatomic vectors due to the action of axis 2 arrange themselves in the zero plane perpendicular to it, i.e., as is usually said, in the cross section $P(x, y, 0)$ of the Patterson function. It is easy to see that the interatomic vectors due to the action of, say, axis 2_1 are arranged in cross section $P(x, y, 1/2)$ and those due to the action of plane m, perpendicular, say, to x, in the one-dimensional cross section $P(x, 0, 0)$, etc. Such sections are called *Harker* sections [4.39]. This information facilitates structure determination directly from the synthesis and in some cases allows us to solve the structure. The most general approach to function $P(\boldsymbol{r})$ is based on the fact that each group Φ has the regular point systems and hence the corresponding systems of interatomic vectors, which should be represented in the picture of $P(\boldsymbol{r})$.

The properties of function $P(\boldsymbol{r})$ are such that, in principle, one can pass from it directly to the electron density distribution. Integral (4.25) can be regarded as a successive shift of the structure as a whole by vector $\boldsymbol{r}$, function $\rho(\boldsymbol{r}' - \boldsymbol{r})$ being multiplied at each point by the weight assigned by $\rho(\boldsymbol{r})$.

This is particularly evident if $\rho(\boldsymbol{r})$ is represented as a set of n points (Fig. 4.70). Note that shifting ρ as a whole and placing any atom at the origin, we obtain the vectors from this atom to all the others. Hence, the shifts of the structure, with successive placement of each atom at the origin, will give all the possible distances. This is precisely function $P(\boldsymbol{r})$ in point representation.

Let us consider, on the other hand, the set of all these shifts. These are shifts of ρ by distance $-\boldsymbol{r}_j$ of a given atom with respect to the origin (since it occupies

the position $\boldsymbol{r}_j$). Consequently, all the n structures are arranged in accordance with the structure of $\rho(-\boldsymbol{r})$, which is centrosymmetric to the given structure $\rho(\boldsymbol{r})$. By marking any given atom in these n structures one can obtain the image of the inverse structure $\rho(-\boldsymbol{r})$. This is illustrated in Fig. 4.70. The simplest repetition element in a system of superimposed structures is any interatomic vector. As an example, let us take the structure depicted in Fig. 4.70a, and in its interatomic function (Fig. 4.70b) draw all the vectors which are equal, say, to vector 41 (Fig. 4.70c). Since this vector appears both in $\rho(\boldsymbol{r})$ and in $\rho(-\boldsymbol{r})$

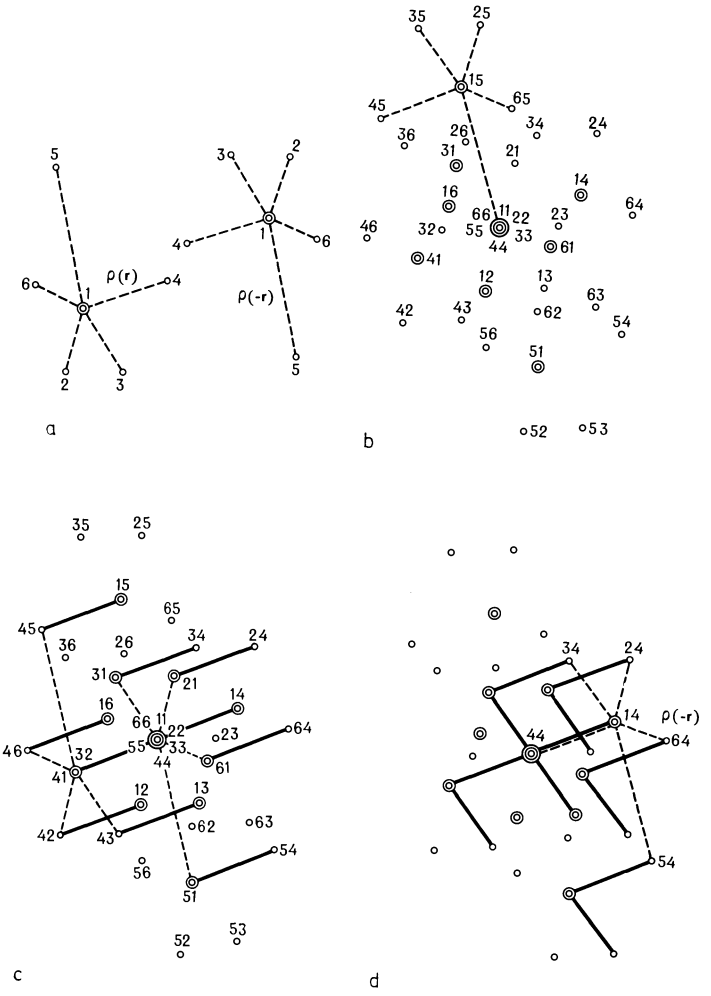

Fig. 4.70a–d. Singling out a point structure from the corresponding point Patterson function. **(a)** six-atom structure $\rho(\boldsymbol{r})$ with one "heavy" atom (denoted by the double circle) and the corresponding centrosymmetric $\rho(-\boldsymbol{r})$; **(b)** point Patterson function of this structure (one of the displaced structures is marked); **(c)** isolation of $\rho(\boldsymbol{r}) + \rho(-\boldsymbol{r})$ as a system like (left) ends of equal vectors; **(d)** isolation of $\rho(-\boldsymbol{r})$ as a system of minimal figures – "corners" [4.40]

(Fig. 4.70a), the system of its repetitions (for instance, all its left ends) is the initial structure plus its inverse $\rho(\boldsymbol{r}) + \rho(-\boldsymbol{r})$. To separate $\rho(\boldsymbol{r})$ from $\rho(-\boldsymbol{r})$ in their overall set of points, it is sufficient to repeat the same operation with another vector or with the simplest figure – a pair of vectors (Fig. 4.70d). If the structure itself has a center of symmetry, i.e., $\rho(\boldsymbol{r}) = \rho(-\boldsymbol{r})$, then the choice of the vector joining the centrosymmetric atoms as the initial one immediately singles out ρ.

Instead of drawing equal vectors we can use the principle of shift and superposition. Let us shift the $P(\boldsymbol{r})$ by the vector $\boldsymbol{u}$, which gives $P(\boldsymbol{r} - \boldsymbol{u})$, and superimpose it on the $P(\boldsymbol{r})$. If $\boldsymbol{u}$ is the interatomic vector, then $\rho(\boldsymbol{r}) + \rho(-\boldsymbol{r})$ is given by the coinciding points of $P(\boldsymbol{r})$ and $P(\boldsymbol{r} - \boldsymbol{u})$. In the centrosymmetric case the choice of the vector $\boldsymbol{u}$ between the centrosymmetric atoms produces $\rho(\boldsymbol{r})$.

The practical realization of such techniques, however, is difficult because of the spreading of the $P(\boldsymbol{r})$ peaks and their inevitable overlapping, since the number of peaks $n(n-1)$ increases rapidly with the number n of atoms in the structure.

To use this principle in practice Buerger [4.41] introduced superposition functions. With the superposition of $P(\boldsymbol{r})$ and $P(\boldsymbol{r} - \boldsymbol{u})$ such functions enhance only those peaks which coincide and remove noncoincident peaks. These requirements are met by the minimum function

$$M(\boldsymbol{r}) = \min\{P(\boldsymbol{r}),\ P(\boldsymbol{r} - \boldsymbol{u})\}, \tag{4.127}$$

in which one takes the minimum values from the superimposed pictures, and by the product function

$$\prod(\boldsymbol{r}) = P(\boldsymbol{r})P(\boldsymbol{r} - \boldsymbol{u}). \tag{4.128}$$

The product $\Pi(\boldsymbol{r})$ can be expressed analytically and represented by a Fourier series. Figure 4.71 shows the use of the M function. The result of the superposition procedure can be improved by performing it with several different vectors $\boldsymbol{u}$.

Since the picture of the structure obtained from (4.127) and (4.128) is inaccurate, it represents only an intermediate result, which yields approximate positions of the main atoms of the structure. Nevertheless it can be used as a means of calculating the phases of reflections [4.43]. The phases obtained are assigned to the values of $|F_H|_{\text{obs}}$, and then the Fourier series (4.118) is constructed. The result is shown in Fig. 4.71. Methods for improving such syntheses by successive approximations have been developed – Fourier transformation of the intermediate syntheses with "cutting off" the background in accordance with the condition of nonnegativity $\rho > 0$ and with gradual elimination of false peaks.

The above-described methods are very efficient in structure determinations and their different versions find wide application, especially in analyzing structures without a center of symmetry. For a long time, however, their drawback was the necessity of first finding, in the picture of $P(\boldsymbol{r})$, the mutual arrangement of at least three atoms (for centrosymmetric structures, two will suffice). Many procedures have been worked out for eliminating this difficulty: using strong

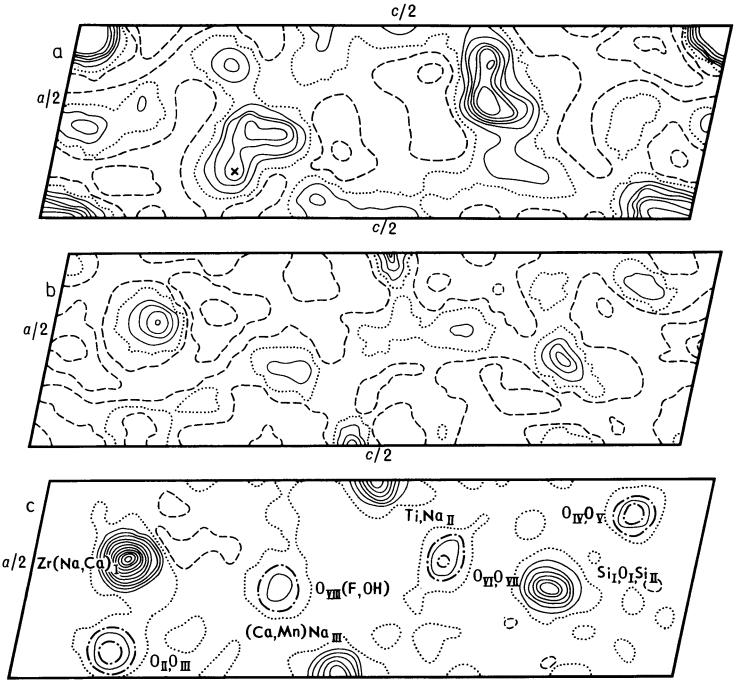

Fig. 4.71a–c. Projection $\rho(x, z)$ of the structure of Ca-seidozerite. (**a**) Patterson function, (×) position of the centrosymmetric vector between heavy atoms; (**b**) Burger function $M_2(x, z)$; (**c**) final Fourier synthesis [4.42]

"multiple" peaks which single out not one, but several structures on superposition; methods for improving the superposition functions for better calculation of the phases from them; etc. [4.44–48].

Effective algorithms for the computer search from $P(\boldsymbol{r})$ of the mutual arrangement of several heavy atoms in the structure have been developed. Such structure fragments are located by direct and complete testing of the possible arrangements. Then the fragment is used for the automatic construction of the superposition synthesis. The synthesis gives a structure model, which is refined by the least-squares method.

The interatomic distance function can be used in still another way, provided the structure of certain fragments, for instance some atomic groupings in large organic molecules, is known. Then this grouping is represented in $P(\boldsymbol{r})$ by a vector set known a priori. By finding the orientation of this set in $P(\boldsymbol{r})$ we determine the orientation of the known grouping in the structure. Another similar possibility arises if the structure contains identical molecules, but in different orientations, so that they are not related by crystallographic symmetry. Each of them has a differently oriented, but identical, set of interatomic vectors in $P(\boldsymbol{r})$ (4.125). Then, in order to find their mutual orientation, it is possible to construct a rotation function by turning $P(\boldsymbol{r})$ about point $\boldsymbol{r} = 0$ and finding its

best self-coincidence. This is achieved at rotation angles corresponding to the mutual rotation of two molecules. Such rotation can also be performed directly for the function $|F_H|^2$ in the reciprocal lattice, because it is in one-to-one correspondence with $P(\boldsymbol{r})$. This method is used in the x-ray protein crystallography.

4.7.5 Heavy-Atom Method

If a structure contains one or several atoms with a large atomic number Z or, as is customary to say, heavy atoms, which scatter x-rays strongly, while the other atoms are light, structure analysis is considerably facilitated. Indeed, in this case the f of the heavy atoms makes the basic contribution to the value of F_H (4.44, 121).

Let us consider the Patterson function for a structure having one heavy atom with Z_h and many light ones with Z_l. The height of its peaks $Z_h Z_l$ is much greater than that of the other peaks $Z_l Z_l$, and function $P(\boldsymbol{r})$ directly yields a picture of the structure with the heavy atom at the origin. True enough, if the structure $\rho(\boldsymbol{r})$ is noncentrosymmetric, a picture of $\rho(\boldsymbol{r}) + \rho(-\boldsymbol{r})$ arises, i.e., the inverse structure is also present (Fig. 4.72). The "heavy-atom" idea also lies at the basis of the method of isomorphous replacement, where two isomorphous structures are investigated [Ref. 4.3, Chap. 1], differing only in the weight Z of one atom. Then the differences $(|F_H|_I^2 - |F_H|_{II}^2)$, used as Fourier coefficients in (4.126), give the function $P(\boldsymbol{r})$, which is similar in its properties to the function with one heavy atom.

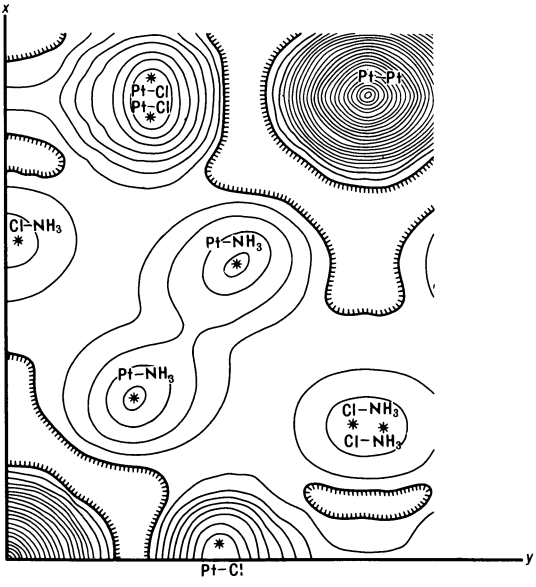

Fig. 4.72. Projection of the Patterson function for $Pt(NH_3)_2Cl_2$ [4.49]

If the structure contains several heavy atoms, their position is found from the Patterson function, and this helps to calculate the phases, since they make the major contribution to $|F_H|$ in (4.121).

The heavy-atom method is valuable in analyzing the structure of large organic and protein molecules. In this case the determination of the crystal structure is mainly a means of finding the three-dimensional structure of the molecules of which the crystal is built. The crystal structure simultaneously reveals also the structure of the constituent molecules. This procedure is used, for instance, in the structure analysis of the crystals of proteins, whose molecules contain 10^3–10^5 atoms.

In this case it is possible to obtain crystals of protein P and isomorphous crystals of $P + H$ with groups containing heavy atoms H, say, $PtCl_4$, HgY_2, etc. It is necessary to have at least two different derivatives. The crystals of proteins, like those of almost all the other natural compounds, are always non-centrosymmetric [Ref. 4.3, Chap. II, Sect. 8]; therefore, it is the phases α_H (not the signs) that are to be determined. At first, the coordinates of the heavy atoms in $P + H_1$ and $P + H_2$ are determined from the Patterson syntheses of the heavy-atom derivatives. The structure factor of the derivatives can be written

$$F_P + f_{H_1},\ F_P + f_{H_2}, \tag{4.129}$$

where F_P is the contribution from all the light atoms making up the protein molecule, and f_H is the contribution of the atom H. By obtaining the moduli $|F_P|_H$ and $|F_{PH_1}|_H = |F_P + f_{H_1}|_H$ from the experiment one can establish two possible values of α_H from the phase diagram of Fig. 4.73, and the use of $|F_{PH_2}| = |F_P + f_{H_2}|_H$ leaves only one of them. It is better to investigate more than two derivatives to eliminate experimental errors and improve the reliability of phase determination. The structure analysis of proteins is a very complicated problem because of the difficulties in obtaining isomorphous crystals of proteins

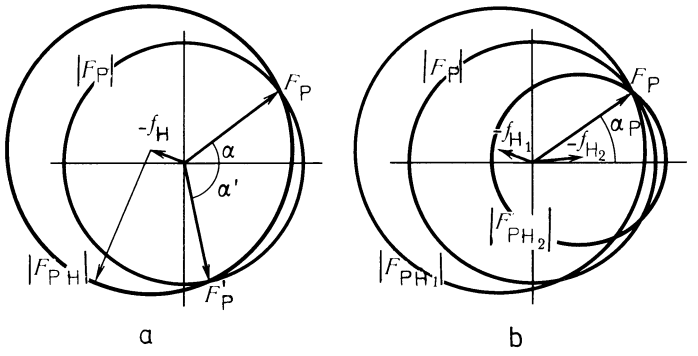

Fig. 4.73a,b. Determination of the phase of reflection in the method of isomorphous replacement [4.50].
(a) finding two possible values of phases α_P from known values of f_H, $|F_{PH}|$, $|F_P|$; **(b)** unambiguous determination of the phase by means of two derivatives with heavy atoms (in addition to the values indicated in Fig. 4.73a, f_{H_2} and $|F_{PH_2}|$ are also known)

with heavy atoms and the necessity of measuring an enormous number of reflections (10^4–10^6).

4.7.6 Direct Methods

Methods which make it possible to determine exactly or with some probability the phases α_H of reflections from a certain set of $|F_H|$ values are called direct. The existence of such methods follows from the fact that, in principle, derivation of the structure from experimental data can be carried out, for instance, using the Patterson method.

In the general case of a structure with symmetry 1 the phase α_H can take any values in the range $(0, 2\pi)$, while in the presence of a center of symmetry $\bar{1}$ it can take only two values $\alpha_H = 0$ or π, which naturally facilitates the solution of the problem. In the latter case there are two possible signs of F_H: plus or minus; the sign of F_H is designated by S_H.

Since the phases are determined by the coordinates of the atoms, unitary structure amplitudes $\hat{F}_H$ (4.56) are used, which are independent of the atomic factors

$$\hat{F}_H = F_H / \sum_{j=1}^{N} f_{\mathrm{aT}_j}. \tag{4.130a}$$

Here $|F_H|_{\mathrm{obs}}$ must be expressed in electron units by (4.48) or (4.50). So-called normalized amplitudes

$$E_H = F_H / \langle F_H^2 \rangle^{1/2}, \tag{4.130b}$$

where $\langle F_H^2 \rangle = \sum_{j=1}^{N} f_{\mathrm{aT}_j}^2$ is mean value of F^2 in the given interval of $\sin \vartheta/\lambda$, are also used.

The theory of direct method considers the phase relationships between the amplitudes, moduli of amplitudes (magnitudes), or squares of moduli of the set of reflections, whose indices are linear combinations of one another: for instance for the triplet of reflections: $h_1k_1l_1$; $h_2k_2l_2$; $(h_1 - h_2)(k_1 - k_2)(l_1 - l_2)$, or, in a short form, $\boldsymbol{H}_1, \boldsymbol{H}_2, \boldsymbol{H}_1 - \boldsymbol{H}_2$. Such combinations of indices correspond to sums or differences of the vectors $\boldsymbol{H}_1, \boldsymbol{H}_2, \ldots, \boldsymbol{H}_n$ of the reciprocal lattice and can be written in the form of a matrix

$$\begin{pmatrix} 0 & \boldsymbol{H}_1 & \boldsymbol{H}_2 & \ldots & \boldsymbol{H}_n \\ \boldsymbol{H}_1 & 0 & \boldsymbol{H}_1 - \boldsymbol{H}_2 & \ldots & \boldsymbol{H}_1 - \boldsymbol{H}_n \\ \boldsymbol{H}_2 & \boldsymbol{H}_2 - \boldsymbol{H}_1 & 0 & \ldots & \ldots \\ \ldots & \ldots & \ldots & \ldots & \ldots \\ \boldsymbol{H}_n & \boldsymbol{H}_n - \boldsymbol{H}_1 & \boldsymbol{H}_n - \boldsymbol{H}_2 & \ldots & 0 \end{pmatrix}. \tag{4.131}$$

It should be mentioned that since the phase depends on the choice of the origin,

the relations between the phases α_H must be determined, rather than their absolute values. If a center of symmetry is present, it is assumed to be the origin.

The theory of direct methods is based on some general mathematical ideas and uses the following properties of the electron-density function: its non-negativity $\rho(\boldsymbol{r}) \geqslant 0$ and its atomicity $\rho(\boldsymbol{r}) = \Sigma \rho_{aj}(\boldsymbol{r} - \boldsymbol{r}_j)$, i.e., the presence of sharply defined peaks in it.

Several approaches are used in establishing the phase relationships. The first consists in considering the trigonometric formulae, the Cauchy inequality, and the determinants. The trigonometric formulae prove that phase relationships exist. For instance, for a centrosymmetric structure with two atoms in a cell $\hat{F}_H = \cos 2\pi \boldsymbol{r}\boldsymbol{H}$ and, taking into account the equality $2\cos^2\alpha = 1 + \cos 2\alpha$, it follows that

$$\hat{F}_H^2 = \tfrac{1}{2} + \hat{F}_{2H}. \tag{4.132}$$

Other cosine formulae lead to similar relationships. The unit cell of a crystal usually contains a large number of atoms. But in this case, too, by using trigonometric formulae with combinations of F_H appearing in the matrix (4.131) and the Cauchy inequality

$$|\sum a_j b_j|^2 \leqslant \sum a_j^2 \sum b_j^2 \tag{4.133}$$

and substituting, for instance, the values $a_j = \sqrt{n_j}$, $b_j = \sqrt{n_j}\cos\alpha_j$ we obtain a number of inequalities relating $\hat{F}$ and $\hat{F}^2$. In the most general and concise form all inequalities are contained in the determinant

$$\begin{vmatrix} 1 & \hat{F}_{\bar{H}_1} & \dots & \hat{F}_{\bar{H}_n} \\ \hat{F}_{H_1} & 1 & \dots & \dots \\ \hat{F}_{H_2} & \hat{F}_{H_2 - H_1} & 1 & \dots \\ \dots & \dots & \dots & \dots \\ \hat{F}_{H_n} & \hat{F}_{H_n - H_1} & \dots & 1 \end{vmatrix} \geqslant 0, \tag{4.134}$$

which, as can be shown, is always nonnegative. One can also set $\boldsymbol{H}_i = \boldsymbol{H}_j$, etc., in it. Thus, taking a third-rank determinant with $\boldsymbol{H}_1 = \boldsymbol{H}_2$ and expanding it, we obtain, in place of (4.132) [4.51],

$$\hat{F}_H^2 \leqslant \tfrac{1}{2} + \tfrac{1}{2}\hat{F}_{2H}. \tag{4.135}$$

This simplest inequality, as well as the other inequalities, gives information on signs only at sufficiently large values of $|\hat{F}_H|$. For instance, $S_{2H} = +$ if $|\hat{F}_{2H}| = 0.5$ and $|\hat{F}_H| = 0.7$; but no answer can be obtained for small $|\hat{F}_H|$. Taking the symmetry into consideration yields additional possibilities. For instance, in the presence of axis 2

$$\hat{F}_{hkl}^2 \leqslant \tfrac{1}{2} + \tfrac{1}{2}\hat{F}_{2h0\bar{2}l}. \tag{4.136}$$

Of particular importance are the triplet relationships of amplitudes, the sums of whose indices are equal to zero: $\boldsymbol{H}_1 + \boldsymbol{H}_2 + \boldsymbol{H}_3 = 0$, i.e., $\boldsymbol{H}_3 = -\boldsymbol{H}_1 - \boldsymbol{H}_2$.

Using the condition of centrosymmetricity, one can represent $\boldsymbol{H}_3 = \boldsymbol{H}_2 \pm \boldsymbol{H}_1$ (other symmetry relationships, if any, can also be taken into account). Thus, expanding the determinant (4.134) for the triplet $\hat{F}_{\boldsymbol{H}_1}$, $\hat{F}_{\boldsymbol{H}_2}$, and $\hat{F}_{\boldsymbol{H}_2 \pm \boldsymbol{H}_1}$, we have

$$1 - \hat{F}^2_{\boldsymbol{H}_1} - \hat{F}^2_{\boldsymbol{H}_2} - \hat{F}^2_{\boldsymbol{H}_2 \pm \boldsymbol{H}_1} + 2\hat{F}_{\boldsymbol{H}_1}\hat{F}_{\boldsymbol{H}_2}\hat{F}_{\boldsymbol{H}_1 \pm \boldsymbol{H}_2} \geqslant 0, \tag{4.137}$$

whence it follows that if $\hat{F}^2_{\boldsymbol{H}_1} + \hat{F}^2_{\boldsymbol{H}_2} + F^2_{\boldsymbol{H}_2 \pm \boldsymbol{H}_1} \geqslant 1$, then

$$S_{\boldsymbol{H}_1} S_{\boldsymbol{H}_2} = S_{\boldsymbol{H}_2 \pm \boldsymbol{H}_1}. \tag{4.138}$$

Relation (4.138) implies that amplitude $\hat{F}_{\boldsymbol{H}_2 + \boldsymbol{H}_1}$ has the same sign as the product of the signs of amplitudes $\hat{F}_{\boldsymbol{H}_1}$ and $\hat{F}_{\boldsymbol{H}_2}$. It is also possible to consider the linear relationships between the amplitudes $\hat{F}_{\boldsymbol{H}}$ appearing in the matrix (4.134) [4.52]. For instance, if $|\hat{F}_{\boldsymbol{H}_1}| + |\hat{F}_{\boldsymbol{H}_2}| + |\hat{F}_{\boldsymbol{H}_1 \pm \boldsymbol{H}_2}| > 3/2$, we again arrive at (4.138). The same result can be obtained from Kitaigorodsky's theory of products: the equality (4.138) is fulfilled if $|F_{\boldsymbol{H}_1} F_{\boldsymbol{H}_2} F_{\boldsymbol{H}_1 \pm \boldsymbol{H}_2}| \geqslant 1/8$ [4.53].

Another approach consists of comparing functions $\rho(\boldsymbol{r})$ and $\rho^2(\boldsymbol{r})$ and also considering the relationship of these functions with $P(\boldsymbol{r})$. Thus, as *Sayre* [4.54] pointed out, in the case of identical atoms the function $\rho(\boldsymbol{r})$ coincides with its square $\rho^2(\boldsymbol{r})$, but the peak shapes are different. The values of F for $\rho^2(\boldsymbol{r})$ are found by the convolution theorem (4.70); then

$$F_{\boldsymbol{H}} = \frac{q_{\boldsymbol{H}}}{\Omega} \sum_{\boldsymbol{H}'} F_{\boldsymbol{H}'} F_{\boldsymbol{H} - \boldsymbol{H}'}. \tag{4.139}$$

This gives the relationship between the given and all the other amplitudes. (Factor $q_{\boldsymbol{H}}$ covers the indicated difference in peak shapes.) A similar relation (called Σ_2 formula) was obtained by *Karle* and *Hauptman* [4.55, 56]. The other consistent relationships between F's are established by analyzing the distribution functions of the probabilities of different combinations of $|F_{\boldsymbol{H}}|, |F_{\boldsymbol{H}_j}|, |F_{\boldsymbol{H}_k}|$, etc. The most general conclusion is that inequalities leading to reliable signs only at high values of the unitary structure amplitudes $|\hat{F}|$ give a statistically correct result also when applied to small amplitudes $|\hat{F}|$. Therefore a correct result is obtained by averaging over the whole *set* of $|\hat{F}|$. For instance, (4.138) can be rewritten as the statistical equality of *Cochran* [4.57] and *Zachariasen* [4.58]

$$\overline{S_{\boldsymbol{H}} S^{\boldsymbol{H}}_{\boldsymbol{H} + \boldsymbol{H}_1}} \approx S_{\boldsymbol{H}_1}. \tag{4.140}$$

Its meaning is as follows. Let us take all the pairs of $\hat{F}$ differing from each other by vector $\boldsymbol{H}_1$ in the reciprocal lattice, and form the products of their signs; the sign of the majority of the products determines the sign of the amplitude $\hat{F}_{\boldsymbol{H}_1}$. Using (4.140), it is possible to take into account the symmetric relationships between the signs of amplitudes which are characteristic of a given space group.

In the most general form the phase relationship can be written as

$$\alpha_{\boldsymbol{H}_1} + \alpha_{\boldsymbol{H}_2} + \alpha_{\boldsymbol{H}_3} \approx 2n\pi, \quad n = 0, \quad 1, 2, \ldots, \boldsymbol{H}_1 + \boldsymbol{H}_2 + \boldsymbol{H}_3 = 0. \tag{4.141}$$

From (4.141) it follows that (4.138) is a particular case of a more general formula for the noncentrosymmetric structure $\overline{\alpha_{\boldsymbol{H}} + \alpha^{\boldsymbol{H}}_{\boldsymbol{H} + \boldsymbol{H}_1}} = \alpha_{\boldsymbol{H}_1}$. The relationship

between the phases can also be expressed with the aid of the tangent formula

$$\tan \alpha_{H_1} \approx \frac{\sum_H |E_H E_{H_1 - H}| \sin(\alpha_H + \alpha_{H_1 - H})}{\sum_H |E_H E_{H_1 - H}| \cos(\alpha_H + \alpha_{H_1 - H})}. \tag{4.142}$$

Relation (4.140) can be written as the condition of the positivity of the product

$$\hat{F}_{H_1} \hat{F}_{H_2} \hat{F}_{H_2 - H_1} > 0 \tag{4.143a}$$

with a probability P^+ of the fulfillment of this inequality

$$P^+ = \frac{1}{2} + \frac{1}{2} \tanh \left\{ \left[\left(\sum_{j=1}^{N} n_j^3 \right) \left(\sum_{j=1}^{N} n_j^2 \right)^{3/2} \right] [|\hat{F}_{H_1} \hat{F}_{H_2} \hat{F}_{H_2 - H_1}|] \right\}. \tag{4.143b}$$

If the structure is composed of identical atoms, the first term under the symbol is simply equal to $N^{-1/2}$. This formula shows that the larger the product (4.143), i.e., the larger the $|\hat{F}|$ appearing in it, the higher the probability of P^+, and with particularly large $|\hat{F}|$ reliable inequalities occur. Hence it is clear that the statistical sums (4.142) and (4.144) also largely depend on the strong pairs $E_H E_{H_1 - H}$ contained in them.

The analysis of the probability distributions of phases in triplets has been extended to a larger number of amplitudes [4.59–62]. We have seen that the classical triplet can be written as one satisfying the condition $\boldsymbol{H}_1 + \boldsymbol{H}_2 + \boldsymbol{H}_3 = 0$. Similarly, it is possible to investigate quartets, quintets, and combinations containing a still larger number of amplitudes. Let us consider, for instance, the amplitude quartet $\boldsymbol{H}_1 + \boldsymbol{H}_2 + \boldsymbol{H}_3 + \boldsymbol{H}_4 = 0$, the nested neighborhood $\boldsymbol{H}_1 + \boldsymbol{H}_2, \boldsymbol{H}_2 + \boldsymbol{H}_3, \boldsymbol{H}_1 + \boldsymbol{H}_3$ and the phase $\alpha = \alpha_{H_1} + \alpha_{H_3} + \alpha_{H_3} + \alpha_{H_4}$. If the moduli of the amplitudes contained both in the quartet and in the nested neighborhood are large, the most probable value is $\alpha = 0$, but if the moduli of the amplitudes of nested neighborhood are small, the most probable value is $\alpha = \pi$. This is a significant distinction from the early theories, in which only zero values of the phase sums could be obtained.

In practical work, the phase determination is performed as follows. A group consisting of approximately ten reference amplitudes is chosen. The group includes strong amplitudes, from which many triplets (or quartets, etc.) characterized by high probabilities P^+ can be formed.

It is possible to assign arbitrarily the phases to three amplitudes (or less, depending on the space group of the crystal); this means the fixing of the coordinate origin. After that two paths are possible.

In the first, the so-called symbolic addition method, the phases of the amplitudes of the reference group are lettered and all the possible relationships between them are found. For noncentrosymmetric crystals, possible phase values are assumed to be discrete: for instance $\alpha = 0, \pi/n, 2\pi/n \ldots n \approx (8\text{–}16)$ or, more crudely, $\alpha = 0, \pi/2, \pi, 3\pi/2$. If some letters remain undetermined, different phase values are given to them, each of them should be checked [4.63].

The second, so-called multisolution method, consists in direct testing of all the variants of the phases of the amplitudes of the reference group. The method is time consuming. The phases of the several hundred strongest amplitudes are calculated for each variant (their number may reach a thousand or more). Using special criteria, the 20–30 best variants are chosen and subjected to further analysis. At this point the first and second method of solving the phase problem converge again. The analysis of a variant includes the construction of the approximate electron density function by using the established phases, localization of its maxima, and identification of the atoms of the structure with these maxima. The criteria of correctness are the number and the type of positioned atoms, the correlation of the obtained interatomic distances with crystallochemical standards, the value of the R factor, and the possibility of refining the structure model.

Since the average value of F_H is low for complicated structures the efficiency of direct methods is also limited by structure complexity. At present, they permit solving structures with up to 100–200 atoms in an asymmetric unit of the cell.

4.7.7 "Statistical-Thermodynamical" Approach to the Crystal Structure Determination

The statistical-thermodynamic approach is based on the representation of all possible distributions of atoms in the unit cell (including the true one) as statistical ensembles of states. This allows one to use thermodynamic functions to describe the states.

Let us consider a simplified model of a crystal consisting of approximately equal atoms and calculate the unitary structure factors (4.130a). Let us represent the unit cell of such a crystal as a regular net of $N = N_1 N_2 N_3$ points in which an electron density of atoms may or may not be present. The set of all possible electron-density distributions can be treated as a set of certain "states" of the thermodynamic system.

Now let us consider a generalized reliability factor, see (4.124),

$$R = \sum_H w_H [|F^2_{\text{calc}}(H)| - |F^2_{\text{exp}}(H)|]^2 .$$

The value $R = 0$ corresponds to the true structure whereas all the other electron-density distributions over the net of points ("states") correspond to various trial structures. The generalized R-factor is, in fact, a configurational Hamiltonian of the system, and the partition function $Z = \sum \exp(-R/T)$ is taken over all the "states". Now let us write the free energy $F = -T \ln Z = R - TS$, S being the entropy, and T the temperature characterizing the excitation of the system, i.e., the degree of its deviation from the true electron-density distribution. Thus the problem of the structure determination reduces to the minimization of the free energy in terms of statistical thermodynamics [4.64].

A new technique based on the use of statistical ensembles of states is the so-called Maximum Entropy (ME) method.
The configurational entropy is determined as

$$S = \sum_j p_j \log p_j$$

for a discrete set of variables $p_1, \ldots, p_N$ or as

$$S = -\int p(\boldsymbol{r}) \log p(\boldsymbol{r}) dV_r$$

for a continuous function defined in the unit cell. The entropy S can be considered as a mathematical formalization of the properties of the "maximum uniformity" or "the minimum information" contained in the $p(\boldsymbol{r})$ distribution. There are different modifications of the ME method developed for various objects.

One of the early modifications [4.65] consists of the determination of all admissible electron density distributions in the unit cell and the determination among them of the distribution $\rho(\boldsymbol{r})$ with the minimum possible entropy. An admissible electron density distribution is a distribution that correctly represents (within experimental errors) the contained information about the object, e.g., the absolute values and (partly) the phases of the structure factors. Since entropy can only be calculated for non-negative distributions, this method's modification is used, as a rule, together with the requirement of non-negativity of the sought $\rho(\boldsymbol{r})$ distribution.

In another modification of the principle [4.66] each admissible electron-density distribution $\rho(\boldsymbol{r})$ map is ascribed a certain probability $p(\rho)$ in such a way that the resulting map obtained upon averaging of a set of maps with certain weights would meet the limitations imposed on moduli and phases of the structure factors, possible values of the electron density, etc. and the requirement that the probability distribution $p(\rho)$ would possess the maximum possible entropy.

Bricogne [4.67], using an additional principle on the atomicity of the object, developed the following approach. He assumed that one can choose as a model providing the prediction of most probable unknown phases of the structure factors the structure consisting of a large number of atoms randomly distributed in the unit cell with the probability distribution $q(\boldsymbol{r})$. The latter distribution should have the maximum possible entropy.

On the other hand, one can analyze the sets of structure amplitudes corresponding to such "states", i.e., to certain atomic distributions. Thus the model of randomly distributed atoms shows a certain correlation with the joint probability distribution $p(F)$ of structure amplitudes, i.e., $F = (F_{\boldsymbol{H}_1}, F_{\boldsymbol{H}_2}, \ldots, F_{\boldsymbol{H}_n})$, each $F_{\boldsymbol{H}}$ being characterized by a modulus and a phase. It is natural that the probabilities of such distributions are different. However, since the $|F_{\boldsymbol{H}_i}|$ values are determined from the experimental intensity data, we arrive at the conditional distributions of the phases [4.67–70].

From information theory [4.71] it follows that the maximum entropy corresponds to the true electron density distribution.

Thus, as has been established [4.72], the statistical ME determination of the phases of the structure factors for randomly distributed atoms is, in fact, a certain generalization of the classical direct methods that consider a probable correlation between the absolute values $|F_{H_i}|$ of the small number of $|F_{H_i}|$ and their phases (Sect. 4.7.6).

Using the ME method, one can also take into account the errors in the $|F_{H_i}|$ determination. This method was successfully applied to the determination of rather complex structures and also to phase refinement and extension.

From the computational stand point, all the above modifications of the method reduce to the solution of various minimization problems. There are numerous publications concerning the computational schemes and testing of the above modifications on various objects.

One more additional approach to the improvement of a set of phases consists in the following. If an electron-density synthesis cannot be interpreted with sufficient reliability, it should be improved by invoking some additional information on the object. Such an additional information on the object can be obtained, e.g., by imposing various limitations on the spectrum of possible values of the electron-density distribution function. In addition to the non-negativity of $\rho(\boldsymbol{r})$, one can also require that it would be limited from the above, $\rho(\boldsymbol{r}) \leqslant \rho_{\max}$, or else that the $\rho(\boldsymbol{r})$ function would be limited inside the molecule and be equal to zero in the solvent) [4.73]. Another source of possible additional information about the object is the use of a complete set of frequencies with which different values are encountered on the electron-density maps [4.74]. Such a spectrum (a histogram) provides the information not only about possible electron-density values (i.e., the values that appear with nonzero frequencies) but also about the frequency of their appearance in the electron-density map. Special methods were developed for predicting such histograms for protein crystals and the use of the information contained in the histograms for the determination and refinement of the phases of structure factors. The most straightforward approach to the use of such histograms is the search for phases minimizing the difference

$$Q_{\text{hist}} = \sum_k (\nu_k^{\text{true}} - \nu_k^{\text{calc}})^2 \tag{4.144}$$

between the predicted values of frequencies ν_k^{true} and the frequencies ν_k^{calc} corresponding to the synthesis with the trial phase values [4.75]:

4.7.8 Nonlocal-Search Method

The formula for the structure amplitude F_H (4.44) or for its modulus $|F_H|$ can be regarded as an equation for unknowns x_j, y_j, and z_j – the atomic coordinates.

Similarly, the general formula of the R factor (4.124)

$$R = \sum w_H \left| |F_H|^{\alpha}_{\text{obs}} - |F_H|^{\alpha}_{\text{calc}} \right|^{\beta}$$

can be regarded as a function of the coordinates of all the atoms which attains a minimum if $|F_H|_{\text{calc}}$ corresponds to the true structure. For a reasonably complicated structure, however, the number of such independent coordinates, i.e., variables describing the function R, is several tens or even over hundreds, and from the computational point of view it is practically impossible to find the absolute minimum of this function.

For molecular structures, this problem is solved using the following approach [4.76, 77]. The position of a molecule in the unit cell is described by six parameters: three coordinates of its center of gravity and the three Euler angles of its orientation. The arrangement of the atoms in a molecule is often predictable reliably enough on the basis of the data on molecular stereochemistry [Ref. 2.13, Chap. 2], so that the coordinates of all the atoms (there may be up to 20–30 of them) are expressed in terms of the indicated six parameters. If there are some other degrees of freedom in the molecule, for instance the possibility of rotation about some chemical bonds (Fig. 4.74), additional parameters are introduced. If there are two independent molecules in the cell, their arrangement is already described by 12 parameters. Thus, the function R can be described by the generalized parameters $\chi_1, \chi_2, \ldots, \chi_n$, whose number $n \approx 10$–20. The struc-

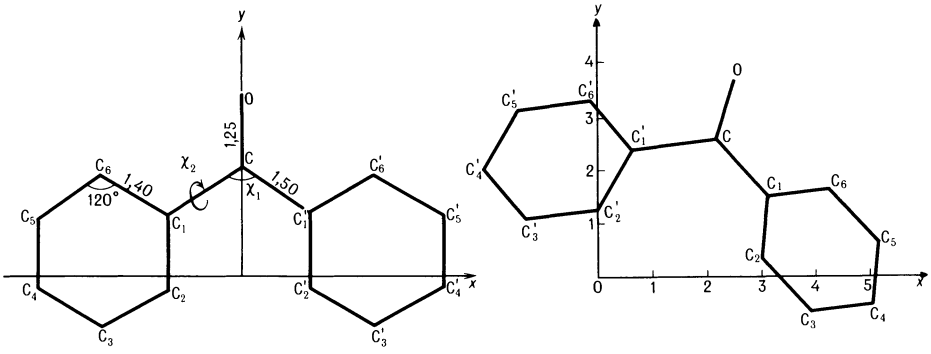

Fig. 4.74a,b. The search of the benzophenone structure. (**a**) model of the molecule; (**b**) the positions and shape of the molecule found by the nonlocal-search method. The Euler angles, molecule orientation in the cell, position of the origin of the coordinates of the molecule, and angles χ_1 and χ_2 were chosen as the generalized variables of the search [4.78]

ture of the function R in n-dimensional space is such that, in addition to the absolute minimum, it has a set of local minima, which are not so deep as the absolute. These minima are connected by "ravines" – regions of low values of R.

Imagine that a molecule is allowed to turn around and "float about" in the unit cell; this is associated with some line in R space. If this line is chosen so that we go along the "ravines" without stopping in the local minima, in the direction of decreasing R, we finally arrive at the absolute minimum. At present, methods for finding the absolute minimum have been developed for functions with $n \approx 10$–20; these methods was called methods of nonlocal (i.e., avoiding the local minima) search and are based on the idea of motion along the "ravines".

At the same time the positions of molecules about the cell is limited by one more circumstance, namely, the distances between the atoms of neighboring molecules $r_{j,k}$ must not be less than the sum of the van der Waals radii; the molecules cannot penetrate each other [Ref. 2.13, Chap. 1, Sect. 2.4]. The function of permissible intermolecular contacts M is also expressed via the generalized parameters $\chi_1, \chi_2, \ldots, \chi_n$. It has small values when the indicated condition is fulfilled, and rises abruptly if it is violated. To calculate R and M, the 100–200 highest values of $|F_H|_{obs}$ are selected. The absolute minimum of the function

$$S = R + \alpha M \tag{4.145}$$

yields the solution. Here, α is a constant, which is usually chosen as 0.1–0.2.

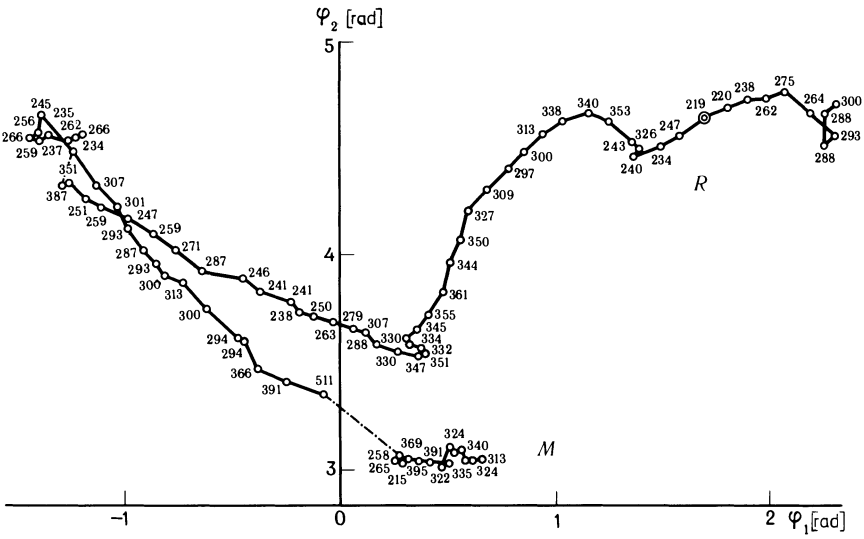

Fig. 4.75. A stage of solving the L-proline structure by the nonlocal-search method. Sequence of gradient descents of function M and ravines with respect to function R. Projection of Euler angles φ_1 and φ_2 onto a plane [4.77]

Figure 4.75 illustrates motion along a "ravine" down to the point of the solution, which corresponds to a preliminary model (the value $R \approx 20\%$) still to be refined.

4.7.9 Determination of the Absolute Configuration

Owing to Friedel's law (4.52), ordinary diffraction phenomena do not permit distinguishing between enantiomorphous forms of crystals. But there are many crystals possessing only one of the two possible absolute configurations – "right-handed" or "left-handed". They are described by the Fedorov groups Φ^I of the first kind. Almost all natural compounds form such structures. But a priori we do not know which of the two possible enantiomorphs is realized as both give identical sets of F_H, so that $F_H^r = F_H^l$.

The possibility of determining the absolute configurations arises in the so-called anomalous scattering of x-rays near their absorption edge because Friedel's law is then violated. In this case the atomic factor f_a has an additional complex component

$$f = f_a + \Delta f' + i\Delta f'' = f_a(1 + \delta_1 + i\delta_2). \tag{4.146}$$

Figure 4.76 shows the dependence of $\Delta f'$ and $\Delta f''$ on the ratio of the frequency of incident radiation ω_i to the frequency ω_e of the absorption edge of the scattering atom. If the cell has anomalously scattering atoms r along with normally scattering atoms t, the structure amplitude can be split into two components

$$F_{hkl}(F_{\bar{h}\bar{k}\bar{l}}) = A_t \pm iB_t + A_r \pm iB_r \tag{4.147}$$

(from now on the subscripts correspond to $F_{\bar{h}\bar{k}\bar{l}}$).

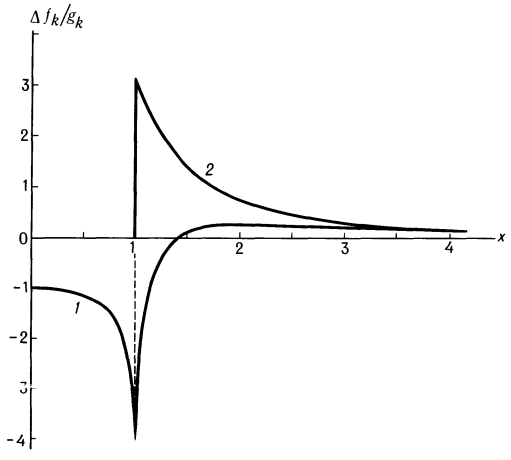

Fig. 4.76. Dependence of $\Delta f'_k/g_k$ (*Curve 1*) and $\Delta f_k g_k$ (*Curve 2*) on the frequency of incident radiation ω_i expressed in relative units $x = \omega_i/\omega_k$ (q_k: oscillator strength of K electrons, ω_k: frequency of the K edge of the absorption band) courtesy of A. N. Chekhlov)

Let us single out the anomalous component

$$F_{hkl}(F_{\bar{h}\bar{k}\bar{l}}) = A_t \pm iB_t + A_{r_0} \pm iB_{r_0} + (\delta_1 + i\delta_2)(A_{r_0} \pm iB_{r_0})$$
$$= A + iB + \delta_1(A_{r_0} \pm iB_{r_0}) + \delta_2(iA_{r_0} \mp B_{r_0}). \quad (4.148)$$

Here, A and B include the normal contributions from all the atoms, some of them being anomalous scatterers. Here A_{r_0} and B_{r_0} are the normal contributions from anomalously scattering atoms. The square of the structure amplitude is equal to

$$F^2_{hkl}(F^2_{\bar{h}\bar{k}\bar{l}}) = A^2 + B^2 + 2\delta_1(AA_{r_0} + BB_{r_0}) \pm 2\delta_2(-AB_{r_0} + A_{r_0}B)$$
$$+ (\delta_1^2 + \delta_2^2)(A^2_{r_0} + B^2_{r_0}). \quad (4.149)$$

Thus, $F_{\boldsymbol{H}} \neq F_{\bar{\boldsymbol{H}}}$, and by using (4.149) one can find the normal component from the experimental data. At the same time the difference $|F_{\boldsymbol{H}}|^2 - |F_{\bar{\boldsymbol{H}}}|^2$ due to the anomalous scattering supplies information on the absolute configuration; for enantiomorphous structures it has the opposite sign. The chirality – the "sign of the enantiomorphism" – can be established by the trial and error method, calculating the R factor for each of the enantiomorphous forms. Another way is to construct syntheses analogous to $P(\boldsymbol{r})$ (4.126), but using sine harmonics and the indicated differences as Fourier coefficients. Anomalous scattering may help in determining the phases, in particular, when investigating heavy-atom derivatives of protein crystals.

4.7.10 Structure Refinement

By finding the phases from the preliminary model, with $R \approx 15\%$ by (4.121), and using $|F|_{\text{obs}}$ the Fourier synthesis is calculated. The peak coordinates are determined, and on their basis the entire procedure of calculating F and constructing $\rho(\boldsymbol{r})$ is repeated. When the signs (phases) do not change any more, the solution is assumed to be final.

If we seek the accurate values of the atomic coordinates x_j, y_j, z_j and of the parameters of thermal vibration, the method of maximum fitting of $|F|_{\text{calc}}$ to $|F|_{\text{obs}}$ is used. To a correct preliminary model there corresponds the absolute minimum of R (4.123), and the refinement process consists in finding the lowest point of the correlation function R' (4.124) by the least-squares and gradient-descent methods. The level of complexity of the problem depends on the number of parameters minimized. They include, primarily, the coordinate parameters of atoms x_j, y_j, z_j and the average temperature factor B of the structure. Then it is possible to introduce individual isotropic (4.25) or anisotropic temperature factors, which acquire the following form in view of the different orientation of the ellipsoid axes (4.26) relative to the crystal axes:

$$T(\boldsymbol{H}) = \exp\left(-2\pi^2 \sum_{i=1}^{3} \sum_{j=1}^{3} U^{ij} h_i h_j\right), \quad (4.150)$$

where h_i and h_j are the coordinates in reciprocal space, and U^{ij} are the components of the vibrational tensor, $U^{ij} = \overline{U^2}/(\boldsymbol{a}_i^* \boldsymbol{a}_j^*)$.

At the minimum of the function R' (4.124) its derivative with respect to the refinement parameters x_i is equal to zero, and hence, finding N corrections Δx_i to the varied parameters requires the solution of a set of N equations with coefficients $a_{ij} = \sum w_H(\partial |F_{\text{calc}}|/\partial x_i)(\partial |F|/\partial x_j)$, which amounts to the inversion of a square symmetric matrix of the coefficients. If the number of parameters is large, the inversion of the entire matrix on a computer is difficult to do (N may run into the hundreds). The block-diagonal refinement can be achieved in cycles, for instance, by refining first the coordinates and then the parameters of the anisotropic thermal parameters, or else by refining N' coordinate and thermal parameters of some atomic group, then of another group, and so on. If hydrogen atoms are present, their contribution to F can also be taken into account at the final stages. When refining the structure by the least-squares method one can also introduce, if necessary, the individual weighting factors w_H, which allow for differences in the accuracy of measurements of F_H, and adjust the contribution of each of the structure amplitudes to the function being minimized.

4.7.11 Difference Fourier Syntheses

To establish the details of the electron density distribution of crystals, which are difficult to detect by means of ordinary syntheses, the Fourier difference synthesis method is used. The method consists in constructing the Fourier synthesis

$$\rho_{\text{diff}} = \frac{1}{\Omega} \sum_H \sum \sum (F_{H_{\text{obs}}} - F_{H_{\text{calc}}}) \exp[-2\pi i(\boldsymbol{rH})], \tag{4.151}$$

whose coefficients are the differences between the observed F_{obs} and calculated F_{calc} values. It is clear that ρ_{diff} will have one meaning or another, depending on which F_{calc} we subtract. If we calculate F_{calc} for part of the atoms of the structure, the other, unsubtracted atoms will remain on the map ρ_{diff}. This is used to detect hydrogen atoms in organic and other compounds. In the presence of the other, heavier (h), atoms the electron density of the hydrogen atoms ρ_{H} is hardly discernible, but the subtraction of $F_{\text{calc,h}}$ leaves only peaks of ρ_{H} (Fig. 4.77)

$$\rho_{\text{H}} = \rho_{\text{total}} - \rho_{\text{h}}. \tag{4.152}$$

A similar technique is used in x-ray crystallography of proteins, when the difference synthesis reveals small molecules added to the giant molecules of protein.

If we take F_{calc} in the approximation of the spherically symmetric temperature factor, the difference density will describe the deviations of ρ_{at} from a spherical distribution (both positive and negative) due to the anisotropy of atomic vibrations.

The method of difference syntheses is of special importance in studying the fine structure of the electron distribution due to the chemical bond between

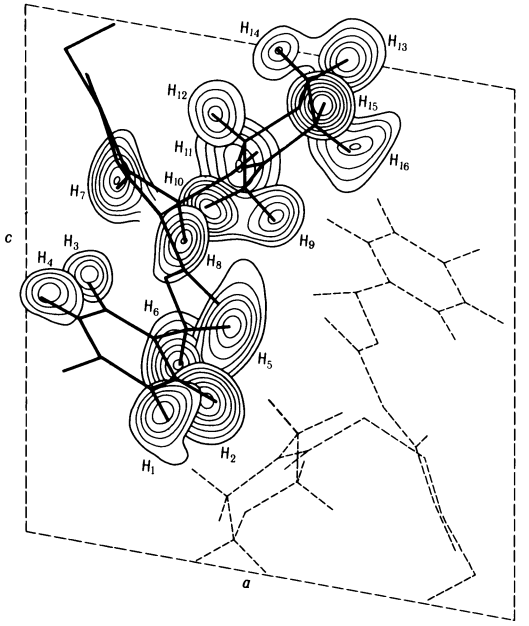

Fig. 4.77. Set of difference Fourier maps (sections) from which hydrogen atoms have been localized (the lines of equal density are drawn on an arbitrary scale) in the structure of 2H-thiopyran p-bromobenzylester [4.79]

atoms. This requires a maximum experimental precision and due allowance for corrections (absorption, etc.; see Sect. 4.5), which make it possible to obtain the most precise value of F_{obs}. In this case important information is obtained from the so-called difference deformation synthesis of the electron density

$$\rho_{def} = \frac{1}{\Omega}\sum_{H}(F_{obs} - F_{calc})\exp[-2\pi i(\boldsymbol{rH})], \tag{4.153}$$

where the F_{calc} were calculated using theoretical values of f for spherically symmetric atoms "at rest", account being taken of their positional x_i, y_i, z_i and anisotropic temperature $T(\boldsymbol{H})$ (4.150) parameters in the crystal. Such a synthesis obviously gives the picture of the redistribution of the electron density due to the chemical bond: positive peaks where the electron concentration increases (which is characteristic of the covalent bond) and negative peaks where the electron density decreases; both the increase and decrease are taken in relation to the superposition of the spherically symmetric distributions of the electron density of the isolated atoms. Such syntheses are often constructed using the positional and temperature anisotropic parameters of atoms obtained from neutron diffraction experiments (where these parameters are found most accurately; see Sect. 4.9) and theoretical values of f_a (4.14) for x-rays. An example of a difference synthesis is given in Fig. 4.77 [Ref. 4.3, Figs. 1.20, 32, 37]

Here F_{calc} can be calculated using the amplitudes f_{inn} of scattering by inner electron shells not involved in the chemical bond (Fig. 4.4b); substitution of such F into (4.153) will give ρ_{val} – the distribution of the valency electrons. This synthesis [Ref. 2.13, Fig. 1.32] is also useful, but it does not reveal as fine details

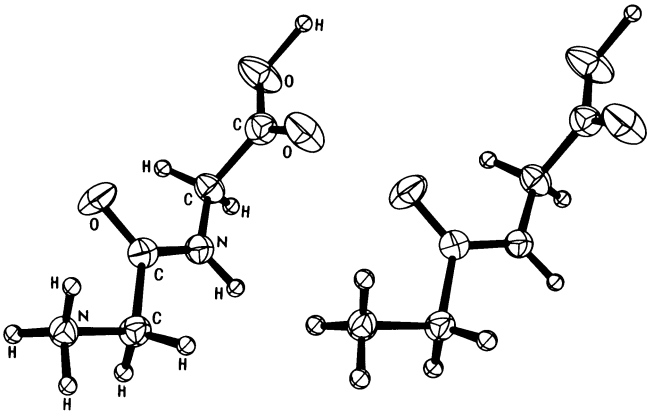

Fig. 4.78. Stereoscopic pair of images of a molecule of dipeptide glycyl-glycine. The ellipsoids of the thermal vibrations of nonhydrogen atoms are shown. The sizes of the semiaxes correspond to 50% probability of finding the atom in the ellipsoid. Hydrogen atoms are represented as spheres of radius 0.1 Å [4.80]

as ρ_{def} does (4.153). In either case it is possible to obtain both the distribution of ρ in the peaks and the number of electrons contained in them. Sometimes the electron density distribution of atoms is presented in a parametric form as linear combination of certain functions, for instance, Gaussian ones [Ref. 4.3, Sect. 1.2.7].

The structure investigation is concluded by estimating the accuracy. In present-day investigations the error in determination of the atomic coordinates is usually equal to several thousandths of an Ångstrom. In precise investigations of the electron density distribution ρ, the error in determination of its absolute values is $\Delta\rho \simeq 0.05$ e/Å^3, or better.

When completing a structure interpretation, in addition to the atomic coordinates, the data on the bond lengths and angles and on the planes or straight lines approximating the positions of some atoms are usually also given. The electron density maps in the form of lines of equal density, stereodrawings of the molecules (see, for instance, Fig. 4.78), and fragments of the structure are obtained with the aid of computer-controlled plotters and displays.

4.7.12 Automation of the Structure Analysis

The bulk of experimental and theoretical methods available to-day permits the solution of practically any structure problem. Therefore, one can speak of an automation of the structure analysis at both experimental and computational stages, with the exception, in some cases, of complex molecular or biological structures. A computer easily performs the computation of F, finding phases, computation of $\rho(\boldsymbol{r})$ at 10^5–10^6 points by summing the Fourier series over

10^3–10^6 $F's$, and – refinement of the structure, which is the most time-consuming procedure.

In modern programming techniques the organization of the F data according to their indices is routine; there are standard formats for atomic coordinates, structure amplitudes, distributions of ρ and F, and unit cell parameters. The set of programs for crystal structure analysis includes:

1) The automation of diffractometer operations, including the computation of angles, the optimization of measurements, and monitoring of position-sensitive diffractometers;
2) processing of diffractometric or densitometric data;
3) symmetry analysis, data editing, and scaling to absolute values;
4) interpretation of the Patterson function;
5) direct methods of phase determination;
6) computation of F_{hkl}, Fourier syntheses (conventional, difference, etc.);
7) structure refinement;
8) geometric structure analysis (distances, angles, planes, etc.; the least-squares method (full matrix, block-diagonal versions) with the possibility of allowing for anomalous x-ray scattering, secondary extinction, anisotropy of thermal vibrations of atoms, etc.; and
9) presentation of the results, computer graphics, the printing of various tables.

Structure analysis uses both large-memory and high-speed computers as well as personal computers that are on line with a diffractometer or densitometer and carry out both the experiment and many computations.

4.8 Electron Diffraction

4.8.1 Features of the Method

Electron motion is described by Schrödinger's wave equation

$$\nabla^2\psi + \frac{8\pi^2 m}{h^2}(E - U)\psi = 0. \tag{4.154}$$

Here, ψ is the wave function, E is the total energy and U is the potential energy. An incident wave has the form $\psi_0 = a\exp[\mathrm{i}(\boldsymbol{kr})]$. If the electrons are accelerated by a voltage V, then $E = eV$, and

$$k/2\pi = \lambda^{-1} = \sqrt{2mE}/h. \tag{4.155a}$$

Taking into account the relativistic correction we have $V^* = V[1 + (eV/2mc^2)]$ [V], and then

$$\lambda = h(2meV^*)^{-1/2} \approx 12.26V^{*-1/2}\ [\text{Å}]. \tag{4.155b}$$

Two main ranges of energy are in use: high energy electron diffraction – HEED, when $V \approx 100$ kV and $\lambda \approx 0.037$ Å, and low energy electron diffraction – LEED,

when $V \approx 10$–300 V and $\lambda \approx 4 - 1$ Å. The potential energy $U(\boldsymbol{r}) = e\varphi(\boldsymbol{r})$, where $\varphi(\boldsymbol{r})$ is the electrostatic potential.

Thus, the "scattering matter" in electron diffraction is the electrostatic potential $\varphi(\boldsymbol{r})$, which plays the same role as the electron density $\rho(\boldsymbol{r})$ does in x-ray scattering. In the kinematic approximation the scattering of the electron wave ψ_0 by the object with a distribution of potential $\varphi(\boldsymbol{r})$ is described with the aid of the general formulae of the Fourier integral (4.12), the atomic amplitude (4.15), and the structure amplitude (4.34) and (4.44). Here one should always put in the values of the potential $\varphi(\boldsymbol{r})$ and the atomic factors for electrons f_e, which are related to f by (4.17). The exact solution of Schrödinger's equation for the crystal (4.154) leads to the dynamic theory equations, which will be discussed below.

We already know that electrons interact with a substance much more intensively than x-rays (see Sect. 4.1). The basic features of the electron diffraction method are as follows. Electrons are diffracted in thin (1–10–100 nm) layers of a substance. The dependence of f_e on the atomic number of the scattering atoms is weaker than for x-rays, $f_e \sim Z^{2/3}$. Experiments are carried out in a high vacuum.

Scattering of electrons by the potential makes it possible to obtain the distribution $\varphi(\boldsymbol{r})$ from the observed structure amplitudes $\Phi_{\boldsymbol{H}}$ by constructing the Fourier series

$$\varphi(\boldsymbol{r}) = \sum_{\boldsymbol{H}} \Phi_{\boldsymbol{H}} \exp[-2\pi i(\boldsymbol{r}\cdot\boldsymbol{H})]. \tag{4.156a}$$

The potential of a crystal is, like the electron density $\rho(\boldsymbol{r})$, a three-dimensional periodic function positive everywhere; the maxima of its peaks correspond to the positions of the atomic nuclei. The value of $\varphi(\boldsymbol{r})$ can be expressed in volts by means of appropriate normalization. Because of the relatively weaker dependence on the atomic number, the peaks of light atoms in the presence of heavy atoms are revealed more clearly by the electron diffraction method than by x-ray diffraction. This is utilized, for instance, in detecting hydrogen atoms in organic compounds, carbon atoms in carbides of metals, etc. The determination of the peak heights make it possible to estimate atomic ionization, and in the case of nonstoichiometric defects, to calculate the percentage of filling by atoms of their positions.

Similar to the transition from (4.118) to (4.120), besides the three-dimensional distribution of the potential (4.156a), we can calculate the potential projection

$$\varphi'(xy) = \frac{1}{S}\sum_{hk} \Phi_{hk0} \exp\left[-2\pi i\left(h\frac{x}{a} + k\frac{y}{b}\right)\right]. \tag{4.156b}$$

4.8.2 Experimental Technique

The diagram of an electron diffraction camera ER-100 is shown in Fig. 4.79. Electrons are acclerated by an electron gun with a high voltage of 50–100 kV;

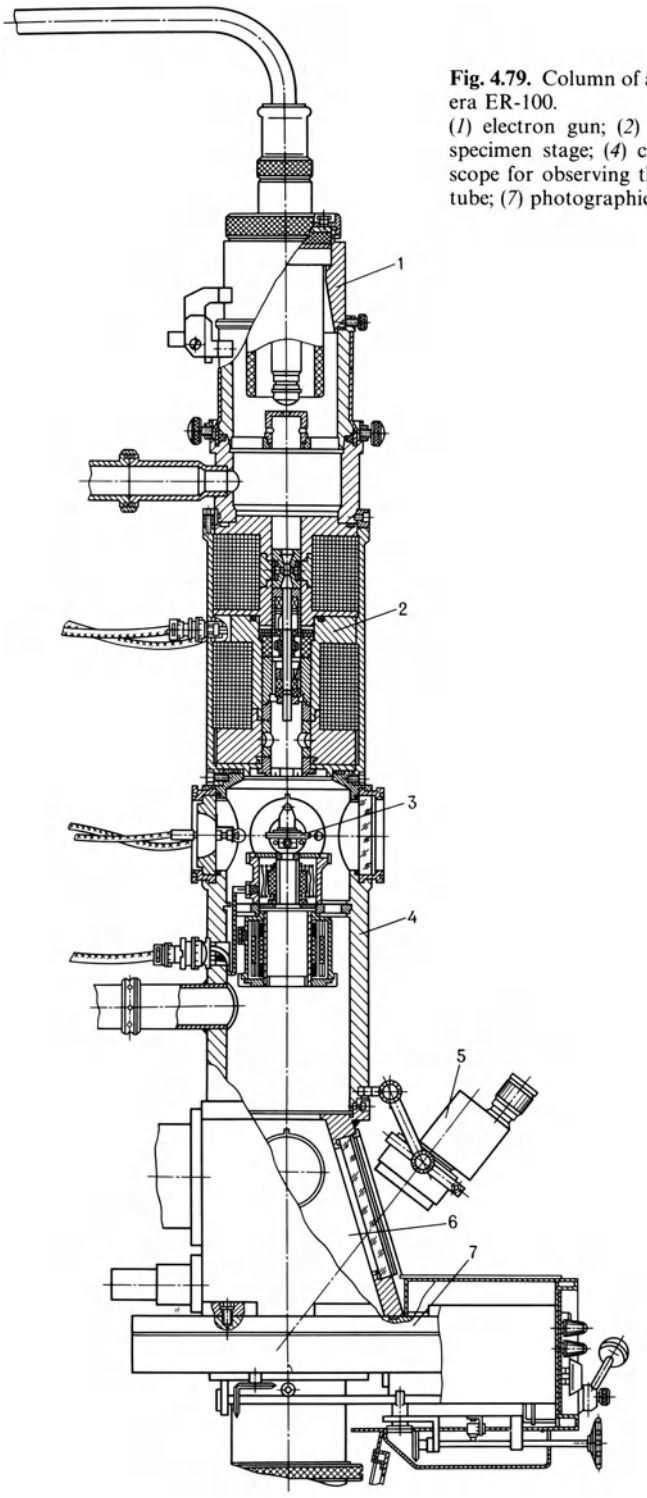

Fig. 4.79. Column of an electron-diffraction camera ER-100.
(*1*) electron gun; (*2*) electromagnetic lenses; (*3*) specimen stage; (*4*) chamber; (*5*) optical microscope for observing the image on the screen; (*6*) tube; (*7*) photographic camera

they pass through apertures, are focused by a magnetic lens, and scattered by a specimen placed on a crystal holder, which permits displacement, tilting and rotation of the object in the beam. The cross section of the beam on the specimen is about 0.2 mm^2 or less. The scattering angles do not exceed 3–5°. The specimen-screen distance L is usually 500–700 mm. The diffraction pattern is observed visually on a fluorescent screen, which is replaced by a photographic plate for recording the image. Exposures last several seconds. Recording with a counter or a Faraday cup is also possible. A counterfield is used in special instruments to study the energy distribution of the scattered electrons and particularly to remove inelastically scattered electrons upon their passage through the specimen.

The electron diffraction camera as an instrument is very close to the transmission electron microscope, although in the latter the scattered beams are transformed into an image by electron optics. A combination of the two methods offers extensive opportunities for observation of the image and selected area diffraction (microdiffraction), the formation of an image by the diffracted beams, etc. Every modern electron microscope is equipped with devices for electron diffraction studies.

Investigation of crystals with the use of various techniques of electron diffraction and electron microscopy has recently been named *electron crystallography.*

In transmission investigations the specimens from a solution or suspension are deposited on an extremely thin (down to 10^{-7} cm) organic or carbon supporting film. Specimens may be polycrystals, textures, or mosaic single crystals. This last type of specimens is obtained, as a rule, by condensation of some compound in a vacuum onto a cleaved face of an orienting single crystal (NaCl, CaF_2, or some other compound), which is usually heated, and then is transferred from it onto a substrating film. Another method is reducing the specimen thickness by etching. There are instruments with an accelerating voltage up to several hundred kilovolts; this opens up additional opportunities.

Unlike the transmission electron diffraction (TED) discussed above, reflection high-energy electron diffraction (RHEED) is used in the investigations of bulky specimen. The incident beam is directed almost parallel to the surface and experiences diffraction after penetrating to a very small depth or passing through minute protuberances of the rough surface. In this case, only half of the diffraction field is observed.

In electron diffraction investigations of free molecules in gases (GED) (Fig. 4.39d) an electron beam is directed at a thin jet of the gas or vapor of the substance under investigation.

4.8.3 Electron Diffraction Structure Analysis

The small wavelength of high-energy electrons (0.04 Å) considerably simplifies the geometric theory of electron diffraction patterns (EDP). The radius of Ewald's sphere is large, the surface practically becoming a plane (Fig. 4.14), and

the electron diffraction pattern is nothing else than an image of the central plane cross section of the reciprocal lattice. Therefore the main formula relating the distance r of the reflections in the electron diffraction pattern from the central spot with $d_{hkl} = H_{hkl}^{-1}$ is (Fig. 4.80)

$$H_{hkl}/\lambda^{-1} = r/L, \quad rd_{hkl} = L\lambda, \quad r_{hkl} = HL\lambda, \tag{4.157}$$

where L is the distance from the specimen to the photographic plate, and λ is the wavelength. In other words, the reciprocal-lattice cross section is directly represented on the electron diffraction pattern to a scale $L\lambda$. Expression (4.157) is obtained from the Bragg formula (4.3) in an approximation $\sin\theta \approx \theta$, since the electron scattering angles do not exceed 5°.

Electron diffraction patterns from a single-crystal specimen (Figs. 4.81, 82) thus reveal the reflection zone corresponding to the specimen orientation, i.e., one plane of the reciprocal lattice passing through point 000; by rotating the specimen it is possible to bring other planes into the reflecting position. In addition to the smallness of λ, the simultaneous detection of all the reflections of

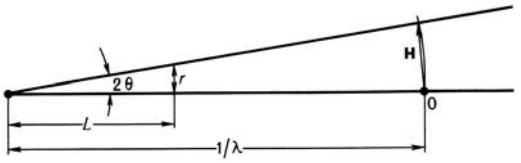

Fig. 4.80. The calculation of electron diffraction patterns

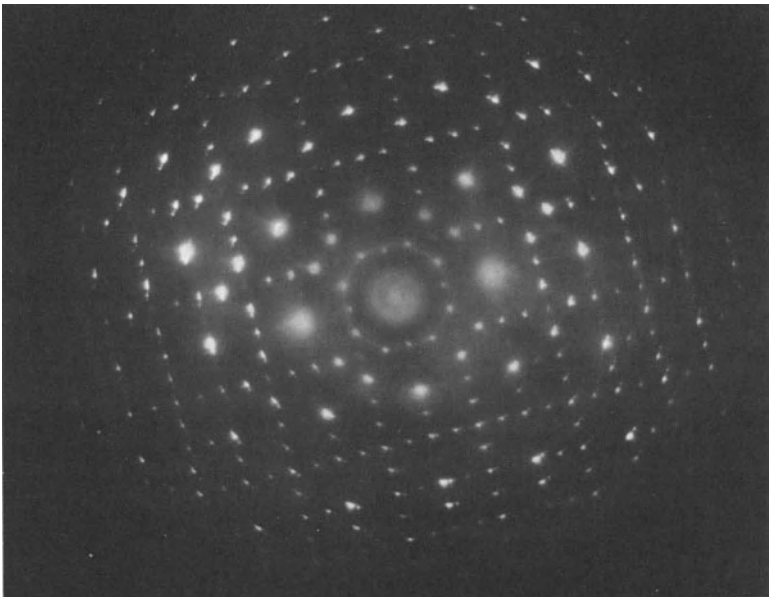

Fig. 4.81. Electron diffraction spot pattern from a mosaic crystal of $BaCl_2 \cdot H_2O$ (accelerating voltage 60 kV, L = 700 mm) [4.81]

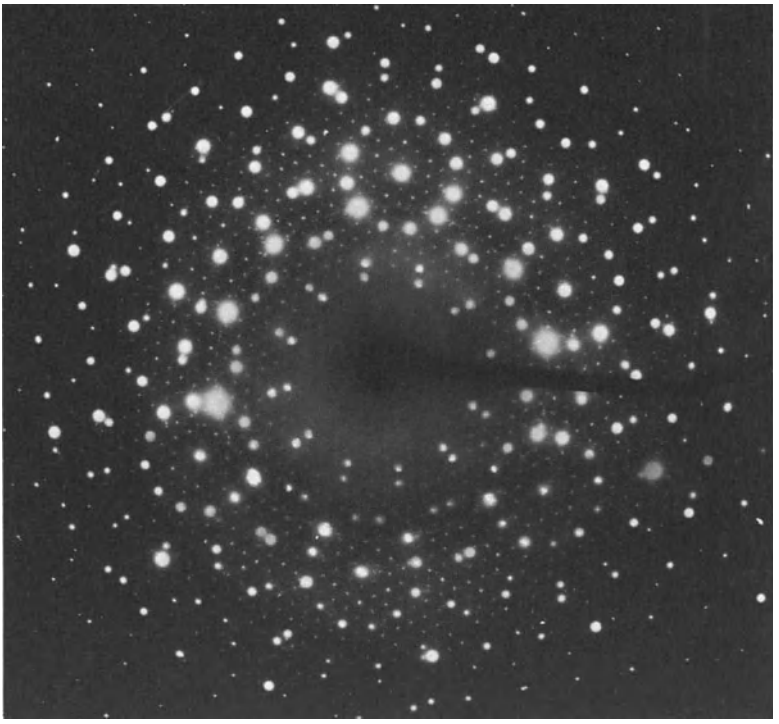

Fig. 4.82. Electron diffraction pattern of two superimposed single crystals of lizardite with secondary-scattering effects taken on an electron diffraction camera with an accelerating voltage of 400 kV [4.82]

the zone is promoted by the mosaic structure (some angular spread of the blocks) of the "single-crystal" specimen.

The interpretation of the point patterns is quite simple in the case of orthogonal lattices. If the lattice is triclinic or monoclinic the pattern of the crystal in the position with the face (001) normal to the incident beam contains no more $hk0$ reflections because the planes ab and a^*b^* do not coincide.

When changing the crystal orientation of nonorthogonal lattices it is possible to obtain the image of the a^*b^* plane containing $hk0$ reflections.

Using spot electron diffraction patterns it is easy to determine the unit cell and the Laue symmetry of the crystal.

Electron diffraction patterns from textures have gained wide use in electron diffraction studies. When small crystals are deposited on a flat substrate, they are often oriented with a definite, well-developed face parallel to it, but the azimuthal orientation is random. This is equivalent to rotation of the reciprocal lattice about an axis perpendicular to the face lying on the support. We denote this axis by c^*. Straight lines of the reciprocal lattice with constant h and k and variable l are parallel to c^*. During the above-mentioned "rotation" the nodes turn into rings lying on coaxial cylinders (Fig. 4.83). If the specimen is inclined to

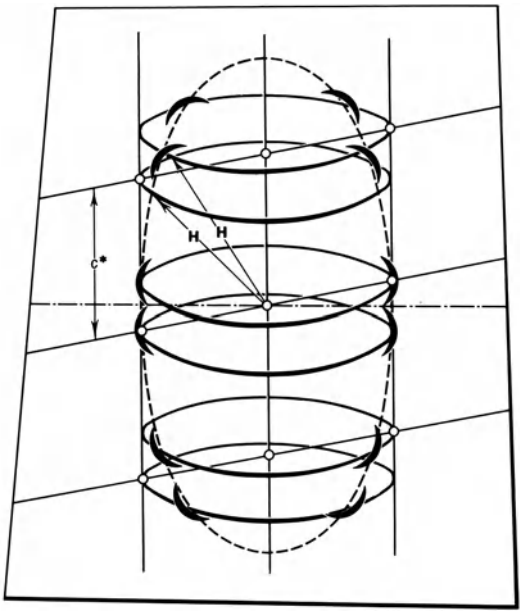

Fig. 4.83. The formation of interference curves – ellipses – in electron diffraction patterns from textures

the beam at an angle φ, the cross section of such a system will give groups of reflections arranged along ellipses, which are the most characteristic interference curves of electron diffraction patterns from textures (Fig. 4.84). If the lattice is orthogonal, all the nodes with a constant l are arranged in layer planes, to which

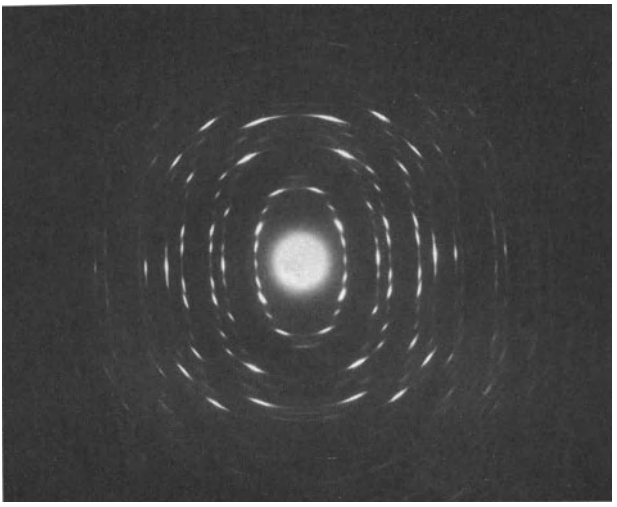

Fig. 4.84. Electron diffraction pattern of an oblique texture of the In_2Se_3 hexagonal phase. The tilt angle is 60° [4.83]

correspond layer lines in the electron diffraction patterns. There has been worked out a complete geometric theory of indexing electron diffraction patterns of oblique textures from crystals of any syngonies determination of the unit cell from them on the basis of measurement of r for reflections or the semi-minor axis of the ellipse B_{hk}, the heights of the reflections η over the zero layer line, etc.

For unit-cell determination and reflection indexing the values $d\,(02\,|\,\boldsymbol{H}|)$ are used and the reflection positions defined by the ellipses hk to which they belong, and the values η are considered. The periods a^*, b^* are directly obtained from the h_{100} and h_{010} values. The period c^*, if it is normal to the plane a^*b^* (γ^* being arbitrary), is calculated as

$$c^* = \eta/1 = (H_{hkl}^2 - H_{hk0}^2)^{1/2}/l. \tag{4.158}$$

For oblique-angled lattices

$$c^* = [(H_{l_1+l}^2 - H_{l_1-l}^2 - 2H_l^2/2]^{1/2}/l. \tag{4.159}$$

In the general case of oblique-angled lattices the coaxial cylinders hk have the radii

$$b_{hk} = (1/\sin\gamma)[(h^2/a^2) + (k^2/b^2) - (2hk\cos\gamma/ab)]^{1/2}. \tag{4.160}$$

In the texture patterns the b_{hk} and η values are represented by the lengths of the small axes of the ellipses $B_{hk} = L\lambda b_{hk}$ and the distances of the reflections hkl from the line of the small axes (equatorial line of the pattern)

$$D_{hkl} = L\lambda\eta/\sin\varphi = hp + ks + lq. \tag{4.161}$$

An analysis of the B_{hk} values gives a, b, γ, while p, s, and q are calculated from the D_{hkl} values. It is essential that the components of the normal projections c_n of the axis c on the plane ab measured in the units of a and b are

$$\begin{aligned} x_n &= (c/a)(\cos\beta - \cos\alpha\cos\gamma)/\sin^2\gamma = -p/q, \\ y_n &= (c/b)\cos\alpha - \cos\beta\cos\gamma)/\sin^2\gamma = -s/q. \end{aligned} \tag{4.162}$$

After having obtained x_n, y_n one can calculate

$$\begin{aligned} c_n &= [(x_n a)^2 + (y_n b)^2 + 2x_n y_n ab\cos\gamma]^{1/2}. \\ d_{001} &= L\lambda/q\sin\varphi, \\ c &= (c_n^2 + d_{001}^2)^{1/2}. \end{aligned} \tag{4.163}$$

The α, β values are then defined by the relations

$$\begin{aligned} \cos\alpha &= (x_n a\cos\gamma + y_n b)/c, \\ \cos\beta &= (x_n a + y_n b\cos\gamma)/c. \end{aligned} \tag{4.164}$$

Continuous rotation of single crystals around the normal to a plane tilted to the incident beam results in rotation patterns similar to the oblique texture patterns, but providing additional information [4.84] (Fig. 4.85).

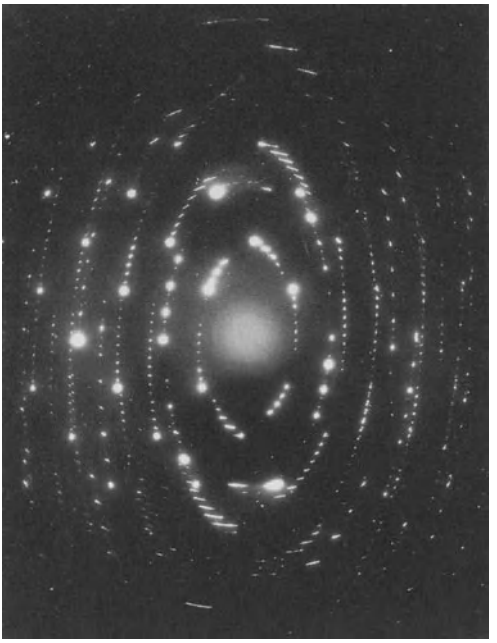

Fig. 4.85. Rotation ED pattern from a mica single crystal

Electron diffraction patterns from polycrystalline specimens are similar to x-ray Debye photographs (Fig. 4.86). They consist of a system of rings, but their interpretation is simpler because (4.157) holds. Reflection electron diffraction patterns (Figs. 4.87, 88) are used mainly for determining the phase composition and the perfection of the structure of surfaces and epitaxial films [4.86].

By using transmission pattern from amorphous solids (ASED) (Fig. 4.89), which represent a set of diffuse rings, a conclusion about the short-range order in their structure, based on the construction of the radial-distribution function (4.84), can be drawn. A similar approach can be utilized in the investigation of liquids. By employing electron diffraction patterns from gases or vapours (GED) (Fig. 4.39d) the structure of the molecules can be determined.

The intensities of scattering by a crystal are determined by the scattering amplitudes of the atoms

$$f_e^{\mathrm{abs}}(s) = 4\pi K \int \varphi(r) r^2 \frac{\sin sr}{sr} dr$$
$$\text{with} \quad K = \frac{2\pi me}{h^2} \quad \text{and} \quad f_e = K^{-1} f_e^{\mathrm{abs}}, \tag{4.165}$$

where $\varphi(r)$ is the potential of an atom, $s = 4\pi(\sin\theta)/\lambda$. In EDSA it is convenient to use f_e without K.

The atomic amplitudes f_e are connected with the amplitudes f_x of x-rays

$$f_e(s) = 4\pi K e[Z - f_x(s)]s^{-2}, \tag{4.166}$$

where Z is the nuclear charge, see also (4.17) and Fig. 4.5, 7, 8.

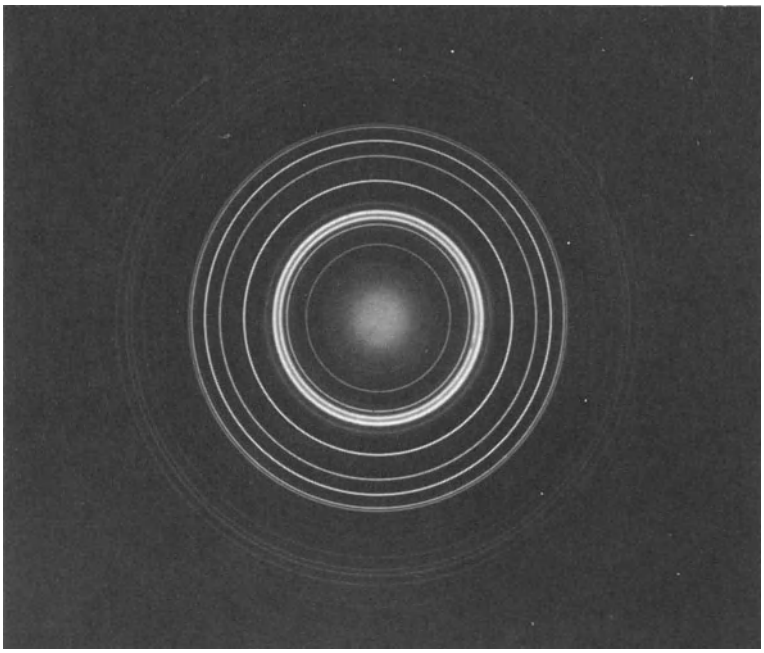

Fig. 4.86. Electron diffraction pattern from polycrystalline hexagonal nickel hydride [4.85]

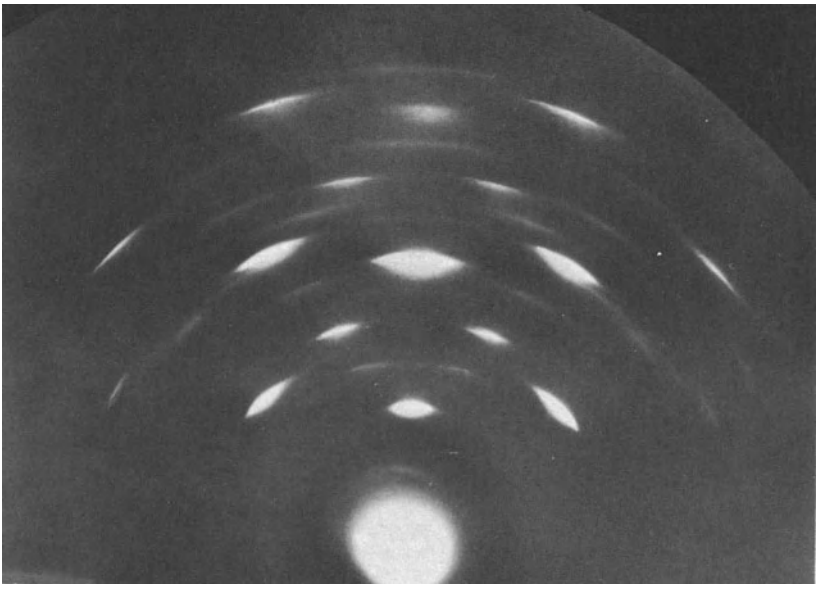

Fig. 4.87. Reflection electron diffraction pattern from a mosaic film of silver. The weak additional reflections indicate the presence of Ag_2O in the specimen

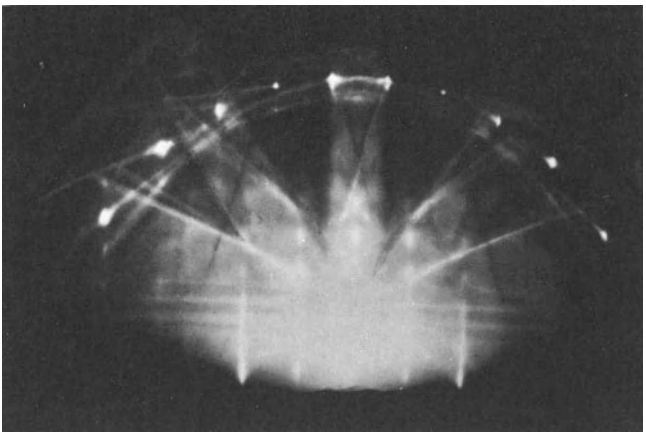

Fig. 4.88. Reflection electron diffraction pattern from a germanium single crystal. The scattering is of a dynamic nature because of the high perfection of the structure. The diffraction pattern clearly shows the Kikuchi lines and bands (courtesy of V. D. Vasiliev)

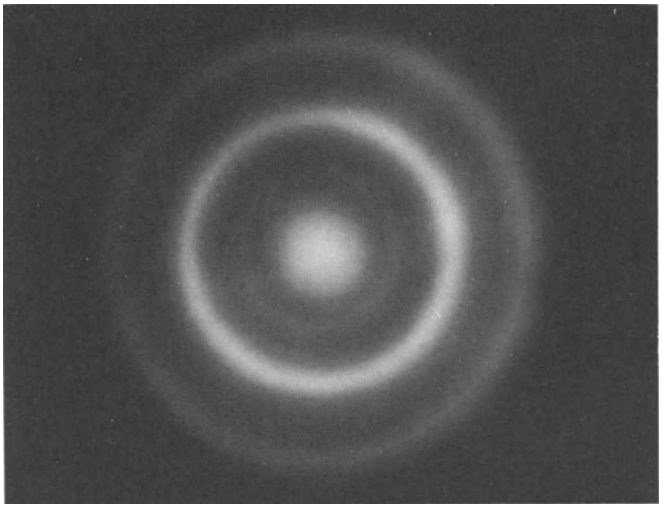

Fig. 4.89. Electron diffraction pattern from an amorphous $CuSbSe_2$ film

The intensities I_H of reflections from a crystal are determined by the square of the structure amplitude, which is calculated similarly to (4.44)

$$\Phi_{hkl} = \sum f_{je\mathrm{T}} \exp[2\pi \mathrm{i}(hx_j + ky_j + lz_j)]. \tag{4.167}$$

where $f_{e\mathrm{T}}$ is the atomic factor for the electrons with a temperature correction, see (4.23).

For mosaic, single-crystal films the integral intensity of the reflection is

$$I_h = J_0 S\lambda^2 \left|\frac{\Phi_h}{\Omega}\right|^2 \frac{td_h}{\alpha} \sim \Phi_h^2 d_h \tag{4.168}$$

and for textures

$$I_h = J_0 S\lambda^2 \left|\frac{\Phi_h}{\Omega}\right|^2 \frac{t\lambda p}{2\pi R' \sin\varphi} \sim \Phi_h^2 p/d_h R'. \tag{4.169}$$

Here J_0 is the beam density of the incident electrons, S the irradiated area and t the thickness of the specimen, α the average angular spread of mosaic blocks, R' the horizontal coordinate of the reflection in the diffraction pattern, and p the multiplicity factor.

Due to the strong interaction of the electrons with the substance the dynamic scattering phenomena are observed at comparatively small thicknesses A of the crystals. The limits of applicability of the kinematic theory are estimated from the relation

$$\mathscr{A} = \lambda \frac{|\bar{\Phi}|}{\Omega} A \lesssim 1, \tag{4.170}$$

which is similar to the expression for x-rays (4.62). Here, $\bar{\Phi}$ is the average absolute value of Φ_H (4.167).

Estimates show that for not very complicated structures composed of atoms with medium Z, $A \approx 300$–500 Å, while for simple structures made up of heavy atoms $A \approx 100$ Å. Since specimens in electron diffraction studies have thicknesses of the same order, the dynamic effects manifest themselves here more often than in x-ray diffraction. The formula for the integrated intensity of single-crystal mosaic films and textures has a form similar to (4.60) for x-rays

$$\frac{I_{hkl}}{J_0 S} = \lambda^2 \left|\frac{\Phi_{hkl}}{\Omega}\right|^2 \mathscr{L}, \tag{4.171}$$

$$\mathscr{L}_M = A\frac{d_H}{\alpha}, \quad \mathscr{L}_T = \frac{A\lambda p}{2\pi R' \sin\varphi}, \tag{4.172}$$

where S is the irradiated area of the specimen; $\mathscr{L}$ is a factor depending on the specimen type ($\mathscr{L}_M$ refers to mosaic single crystals, and $\mathscr{L}_T$, to textures); A is the specimen thickness; α is the mean angular spread of the mosaic blocks; R' is the horizontal coordinate of the reflection on the electron diffraction pattern from textures; φ is the angle of inclination of the specimen; and p is the multiplicity factor for the texture pattern (the number of nodes of the reciprocal lattice merging together in the ring).

The intensities are determined by microphotometry of electron diffraction patterns. Precision measurement of intensities is achieved both by photoregistration and by the use of scintillators, photoelectronic multipliers and charge-coupled (multi-channel) devices (the accuracy of the intensity measurements is $\sim 1\%$). Sometimes the thicknesses of the small crystals A in specimens are

greater than provided by condition (4.170) for the applicability of the kinematic theory. In the case of dynamic scattering in a mosaic single crystal or texture $I_{hkl} \sim \Phi$, i.e., the intensity is proportional to the first power of the structure amplitude. Sometimes, the scattering is of an intermediate nature. The degree of "dynamicity" of scattering can be estimated by comparing the curves of the averaged intensity $\bar{I}(\sin\theta/\lambda)$ with $\sum f_e$ or $\sum f_e^2$ in the same angular interval. Introducing the corresponding corrections, one can obtain the values of Φ_{hkl} from I_{hkl}, which will be discussed in more detail further on.

The main method in electron diffraction structure analysis is the construction of Φ^2-series which gives interatomic distance function (4.126) and subsequent construction of the Fourier synthesis of the potential (4.156) (Fig. 4.90) [4.81].

In electron diffraction studies one can also use direct methods of phase determination [4.87]. An ED pattern obtained by the method of a selected area in an electron microscope from copper phtalocyanine is depicted in Fig. 4.91a, and Fig. 4.91b is a projection of the potential of this structure. All atoms are clearly seen. Phases of the $|\Phi_{hk0}|$ structure amplitudes are determined by direct methods.

The above-described specific features of the method enable one to use it in investigating a number of important classes of objects, including those encountered only in a highly dispersed state and therefore practically inaccessible for the x-ray method. The structures of many layer ionic lattices, crystal hydrates and hydroxides, and organic and inorganic compounds containing hydrogen atoms have been studied by the electron diffraction method. Electron diffraction is widely used in analyzing layer silicates, including clay minerals. The vacuum condensation technique has proved to be convenient for studying the structure of various phases in two- and multicomponent systems (carbides and nitrides of certain metals, semiconductor compounds of elements of groups III, IV, V, VI, and some others).

From (4.17 and 166) it follows that electron scattering is less dependent on the atomic number Z than x-ray scattering. This facilitates to distinguish, in the Fourier synthesis, potentials of light atoms in the presence of the heavy ones,

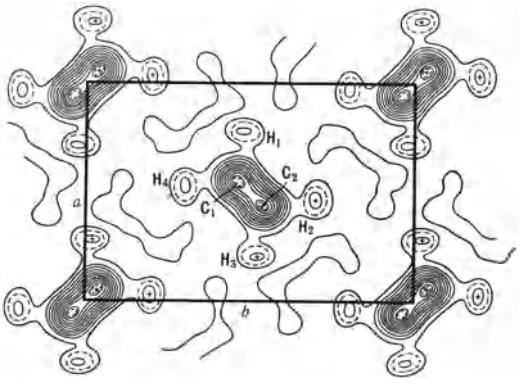

Fig. 4.90. Fourier synthesis of the potential of the structure of paraffin (projection along the axis of the chain C_nH_{2n+2}). Hydrogen atom peaks are clearly seen

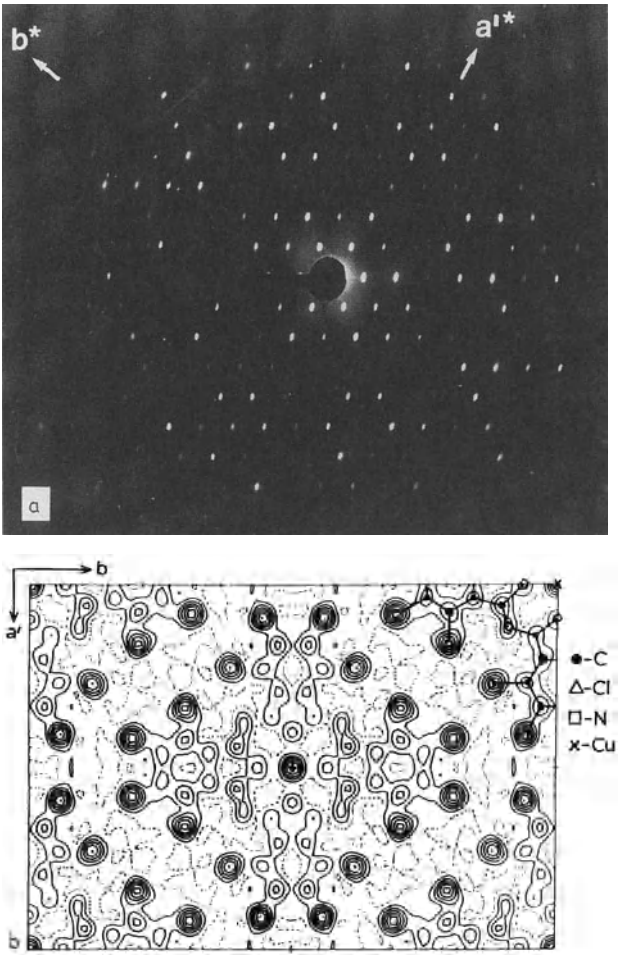

Fig. 4.91a,b. Study of copper perchlorophthalocyanine $CuCl_{16}C_{32}N_8$: electron diffraction pattern from a thin (**a**); electrostatic potential projection map (**b**) [4.87]

including hydrogen atoms (Fig. 4.90) [4.88, 89]. We should also note that, as it follows from (4.166), electron diffraction is rather sensitive to the redistribution of valence electrons in compounds during the chemical-bond formation, i.e. to the ionization of the atoms. Indeed, in this case the value of Z in (4.166) is not the charge of a neutral atom, but the charge Z' of the ion. Therefore, the values of f_e change considerably under small $s(\leqslant 0.3\ \text{Å}^{-1})$, thus allowing us to evaluate the ionization [4.90].

Passing through the sample, the diffracted beam loses some of its energy as the result of various excitation phenomena: excitation of phonons, plasmons, interbands transitions, etc. Analysis of diffraction-beam energies renders information on the chemical composition, electronic structure and the short-range atomic order of the substance. In the latter case there is a complete analogy with

the EXAFS technique of x-ray diffraction. Electron energy loss spectroscopy (EELS) has recently been applied to the investigation of the structure of thin amorphous films [4.91].

Electron diffraction structure analysis has yielded interesting results in the study of the structure of polymers, amorphous substances, and liquids. Electron diffraction study of molecules in vapors and gases is an extensive special field.

4.8.4 Dynamic Scattering of Electrons

We have already said that electrons often experience dynamic scattering in mosaic single-crystal films or textures. Scattering in large perfect single crystals can be adequately described only within the framework of the dynamic theory. In dynamic scattering all the waves, both incident and diffracted, interact with the attendant energy exchange. In addition to elastic scattering, a significant inelastic coherent and incoherent electron scattering arises.

In the dynamic scattering by perfect crystals when the thickness of specimens exceeds the value given by (4.170) the absolute intensities of reflections, especially of back reflections, increase and tend to a common level due to the multiple scattering. With the further increase of thickness the contribution of inelastic scattering becomes more significant, and the intensities of the spots are 'pumped' into the general background. It results in the appearance of the so-called Kikuchi extinction lines and bands associated with the position of reflecting planes of the crystal (Fig. 4.88).

The foundations of dynamic theory were laid down by Bethe, who considered the solution of Schrödinger's equation (4.154) for ψ in a form similar to (4.67), but with scalar waves.

The problem can be solved in the two-beam approximation by considering the interaction between the initial wave and one strong scattered wave. It is slightly less rigorous than in x-ray diffraction because the Ewald sphere, degenerated into a plane, may intersect many nodes of the reciprocal lattice or pass near them. In the two-beam approximation, similarly to (4.69),

$$(K^2 - k_0^2)\psi_0 + v_H\psi_H = 0, \quad v_H\psi_0 + (K^2 - k_H^2)\psi_H = 0, \tag{4.173}$$

where

$$k_0 = k + v_0/2k, \quad k = \sqrt{2meE/h}, \quad v_H = 4\pi|\Phi_H|/\Omega. \tag{4.174}$$

The wave field in a transparent crystal exhibits a periodic variation in the values of wave functions ψ_0 and ψ_H with the depth of penetration. Diffraction maxima for electrons have a halfwidth of the order of angular minutes, while for x-rays it is $\sim 10''$ or less. The integrated intensity is proportional to $|\Phi|$.

The effects of dynamic scattering in electron diffraction are stronger for a mosaic crystal than for polycrystalline or texture specimens. The most essential phenomenon here is the effect of extinction, i.e., the weakening of strong reflections (and their higher orders) as compared with values given by kinematic theory.

The formula for the intensity in dynamic scattering in the two-beam approximation is, cf (4.171),

$$\frac{I_H}{I_0 S} = \lambda^2 \left| \frac{\Phi_H}{\Omega} \right|^2 R(\mathscr{A}) \mathscr{L}, \quad R(\mathscr{A}) = \frac{1}{\mathscr{A} \mid A} \int_0^{\mathscr{A}} J_0(2x)\, dx. \tag{4.175}$$

The value of $\mathscr{A}$ is obtained from (4.172), and that of $\mathscr{L}$, from (4.172); J_0 is the Bessel function of zero order; the equation is similar to (4.74). Use is generally made of the graph of the function of the dynamic correction $R(\mathscr{A})$, which helps to find the value of $\mathscr{A}$ corresponding to the best agreement between the experimental and calculated intensities. Taking into account the extinction for several strong reflections, the final values of $R(\mathscr{A})$ are chosen for the averaged value of $\mathscr{A}$.

In the second Bethe approximation, the following values are used instead of $v_H = 4\pi |\Phi_H|/\Omega$ (4.174):

$$u_H = v_H - \sum_{g \neq 0, H} \frac{v_g v_{H-g}}{k^2 - k_g^2}. \tag{4.176}$$

The necessity of introducing the indicated corrections actually depends both on the accuracy of measurement of the experimental intensities and on the degree of complexity of the structure [4.86, 92].

The multiwave solution of (4.154) is more rigorous. It requires taking into consideration the matrix M of scattering and the intensity of the reflected wave is expressed by

$$I_H = \left| \left[\exp\left(\mathrm{i} \frac{A}{2k} M \right) \right]_{H^0} \right|^2. \tag{4.177}$$

The diagonal components of M are defined by the deviation from the exact value of the Bragg angle for all the possible reflections, with the crystal setting in the position for reflection $\boldsymbol{H}$.

The nondiagonal components of the matrix are formed by the interaction potentials $v_{HH'}$ of any two reflections ($\boldsymbol{H} \neq \boldsymbol{H}'$), including the zero reflection. The dynamic theory equations can also be obtained in a form similar to those of Darwin's theory.

A semiphenomenological theory of inelastic scattering, both incoherent, in the form of a general strong background, and coherent, in the form of Kikuchi lines, bands, and envelopes, has been elaborated.

4.8.5 Special Methods of Electron Diffraction

Above we have discussed the method of high-energy electron diffraction (HEED) and the main applications of EDSA. Let us now consider some other possibilities offered by this method. These are connected with the creation of various electron-optical systems for electron microscopes, and also with the registration of secondary processes on interaction of electrons with the substance.

The basic technique used for observing electron diffraction in an electron microscope is the selected area method (SAED). This technique (Fig. 4.92a) is based on the action of the intermediate lens (between the objective and the projective ones) transferring either the object image or the diffraction pattern formed by the objective lens in its conjugate and focal planes, respectively. The diffracting area is selected by the aperture in the conjugate plane (Fig. 4.93). It is no less than 1–2 μm^2, otherwise the correspondence between image and diffraction is distorted under the influence of spherical aberration. In this case the ED pattern usually presents diffraction from a monocrystalline region.

Modern electron optical systems in electron microscopes also permit to obtain micro-beam ED (MBED), scanning and rocking MB (SMBED and RMBED) and ED patterns from regions of several nm in size (nano-probe or nano-diffraction).

In the case of MBED this correspondence is close, and both the imaged and diffracting areas are limited by the cross-section of the micro-beam only and may extend over several nanometers. Both SAED and MBED suit very well the requirements for the homogeneity-inhomogeneity problems. They are also useful in structure and polytype analysis.

It is possible to realize HRED in an electron microscope by placing the specimen after the projective lens (Fig. 4.92c). However, the scale of the diffraction pattern is too small due to the short distance between specimen and screen, and the most important diffraction information gets into the background scattering area of the primary beam.

The scheme of high-dispersion ED (HDED) (Fig. 4.92d) permits to increase the scale of the ED effects in the vicinity of the primary beam. It is effective in the study of small inhomogeneities of the structure, of structure modulations and super-periodicities, epitaxial and spinoidal decomposition, incommensurate phases, short-range order in quasi-crystals and amorphous substances. HDED also permits one to investigate free particles of extremely small size (10–20 Å). Great possibilities are presented by the method of convergent-beam electron diffraction (CBED) (Fig. 4.94) [4.93]. The CBED (Fig. 4.92e) is aimed at obtaining diffracted intensity profiles with a high angular resolution. There are several forms of CBED. The term "Kossel–Möllenstedt" CBED [4.93] is used if the diffraction discs, corresponding to point reflections (or obtained with a parallel incident beam) of the usual single-crystal DP, do not overlap. If the discs overlap it is referred to as "Kossel" CBED. To perform CBED in a conventional transmission electron microscope it must operate in the micro-probe mode. If the beam is limited by a round aperture, each diffraction spot spreads into a round disc (the angular divergence of the beam in CBED equals $\approx 10^{-3}$ rad). For each angle of incidence in the convergent beam we can build the respective Ewald sphere and determine the diffraction intensities. Mutual overlapping of the discs (due to increase of the incident-beam divergence angle) creates interference effects. For example, overlapping of the discs from the incident and diffracted beams may create parallel intensity bands like the ones occurring in two-wave interaction, i.e., Kossel lines similar to those in x-ray diffraction.

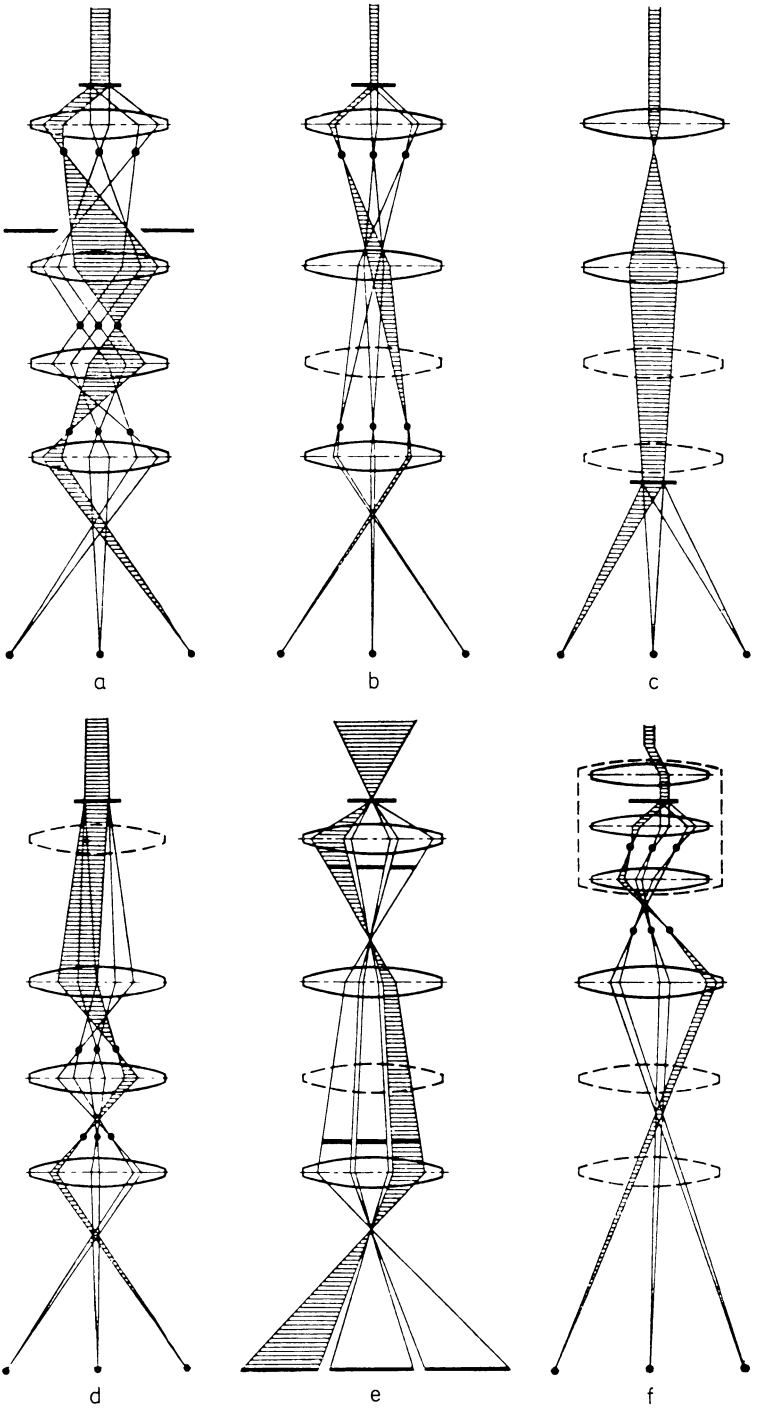
a
b
c
d
e
f

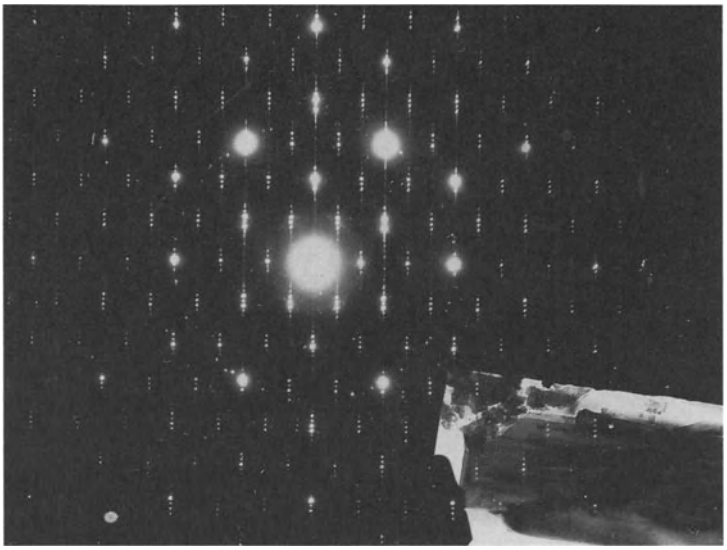

Fig. 4.93. SAED pattern from an antigarite crystal displaying superperiodicity in the *a* direction, and its image selected by the aperture

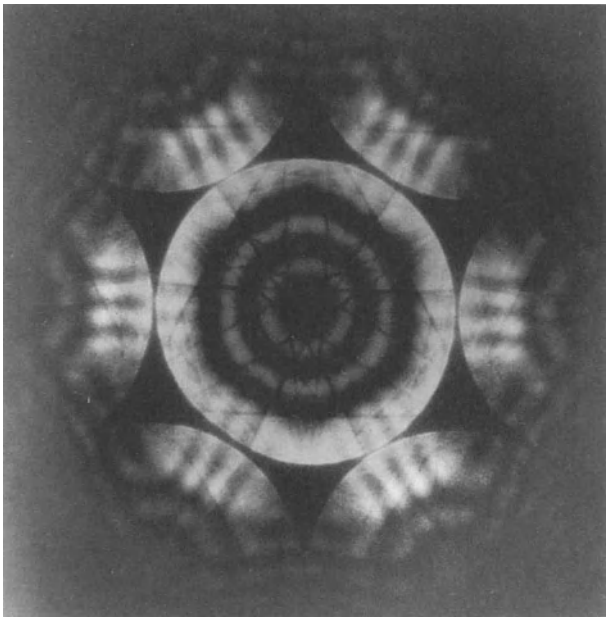

Fig. 4.94. Zone-axis CBED pattern from Si(111) crystal with non-overlapping discs. Kossel-Möllenstedt lines of high-order Laue zone (HOLZ), visualized as dark lines on the "0-th" disc, are the consequence of the intersection of the Ewald sphere with HOLZ reflections [4.93]

Fig. 4.92a–f. Optical schemes of different ED modes realized by means of EM: (**a**) SAED, (**b**) MBED, (**c**) HRED, (**d**) HDED, (**e**) CBED, (**f**) SMBED.

The geometry of Kossel-pattern formation resembles that of Kikuchi patterns as in both cases we have cones of diffracted beams which cross the screen in almost straight lines due to the short length of the wave. Both Kossel lines are equivalent and exhibit a close black-and-white contrast, while one of the Kikuchi lines is white, and the other one black and closely positioned to the central spot.

CBED is used for the high-accuracy (to 1%) determination of structural amplitudes of low-order reflections by matching the intensity profiles calculated in accordance with the multi-wave theory and those obtained experimentally. Special, large-angle (LACBED) schemes allow us to avoid overlapping of different discs-reflections and to present the intensity variation for each of them in a large-angle range. The hollow-cone method (HCED) is a CBED mode with incident electrons passing along the cone surface only.

It is also possible to determine the specimen thickness from CBED patterns. The phases of the structure amplitudes may be directly obtained from CBED.

The most important application of CBED is the possibility to determine the crystal symmetry. Unlike the x-ray diffraction technique, which can distinguish 11 Laue groups from 32 point groups, CBED based on the dynamic theory permits to distinguish polar and non-polar crystals and thus identify the point group unambiguously [4.94]. Screw axes 2_1 and gliding reflection planes are identified with the use of dynamic effects. When a crystal has such an axis or a plane, special extinction lines may appear in the discs-reflections forbidden by the kinematic theory. These lines are called *dynamical extinction lines* [4.95]. Combination of CBED patterns of reflections from zero and high-order Laue zones permits to identify any space group [4.96]. Special tables and schemes of CBED patterns for different space groups and direction of the incident beam have been calculated. They allow us to determine point and space groups of any crystal symmetry.

The EM optical system is also used for realizing the electron-channeling (EC) effects of anomalous transparency of thick samples near the Bragg-incidence angle. EC reveals some peculiarities of the distribution of atoms and their isomorphous substitutions.

In many investigations the strong interaction of electrons with the matter is taken into account by measuring the energy loss of the electrons both in the diffraction beams and between them. Under such conditions electron spectroscopic diffraction (ESD) in energy-filtering systems offers the possibility of recording ED patterns with different energy-selecting windows. It is thus possible to consider separately the contribution of elastically and inelastically scattered electrons. On the one hand, this improves the structural studies, and on the other hand, it gives information on the electron-matter interactions. The efficiency of electron-diffraction techniques and electron microscopy is enhanced by their combinations with one another and with other methods.

The combination of EM and SAED with x-ray energy dispersive spectroscopy (XEDS) has created the analytical EM revealing fine variations of structure and composition related to local areas of the objects EM image. Electron

energy loss spectroscopy (EELS) is another method which can be combined with EM and ED, to provide information on the composition and electronic state of atoms.

Summing up, all methods of electron crystallography permit to solve a wide range of problems: structure determination, polytype analysis, substance identification, homogeneity-inhomogeneity of specimens, order-disorder phenomena, defect analysis, surface analysis, study of short-range order, composition variations, phase transformations, quasi-crystals, investigations of electronic structure.

4.8.6 Low-Energy Electron Diffraction (LEED)

Since the periodic potential of the lattice terminates at the crystal surface, the arrangement of the atoms on the surface may, in principle, differ from that in the bulk. In other words, the structure of the thin surface layer may not coincide with that of the remaining part of the crystal. A the same time, the crystal surface plays an important part in such processes as electron and ion emission, adsorption and catalysis, nucleation of a new phase and diffusion (in epitaxy), ionic implantation, oxidation, etc. While adsorbing gas atoms can form two-dimensional ordered structures. Electrons with energies of 10–300 eV can penetrate into a several crystal atomic planes. Therefore LEED is an effective method for investigating the crystal surface: the arrangement of atoms on it, the nature of their thermal vibrations, etc. [4.97–99].

In LEED cameras the initial beam falls normally or at an angle of $\sim 45°$ to the specimen surface. The investigation is carried out in a vacuum of 10^{-10} $- 10^{-12}$ Torr. Elastically scattered beams forming the diffraction pattern supply information on the structure of several surface layers and, in the limit on the structure of the monoatomic surface layer.

The electron diffraction pattern geometry is determined, to a first approximation, by the two-dimensional surface lattice. Some conclusions can also be drawn from the reflection intensities. But unambiguous interpretation of electron diffraction patterns is greatly impeded by the multiple scattering of electrons. Additional information on the energy spectrum, chemical composition, and valency states is given by Auger spectroscopy of the scattered electrons.

Auger electron spectroscopy is based on the dependence of the energy spectrum of Auger electrons on the type and state of the atoms on the surface. The primary beam ($E = 10$ to 2000 eV) excites the atoms of the specimen. Auger-electrons, arising in the process of the radiationless transition of the inner atomic shells into their normal state, are emitted from the specimen surface. A modern LEED apparatus usually contains Auger spectrometers. The sensitivity of the method is sufficiently high to detect the presence of up to one atom out of a hundred in a monolayer of foreign atoms on a surface. If one needs data on impurity distribution with depth in a specimen, its surface is atomized consecutively with the aid of an ion gun.

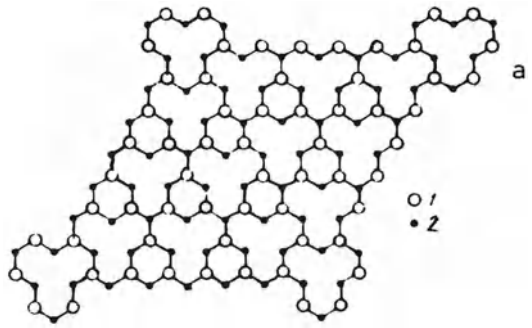

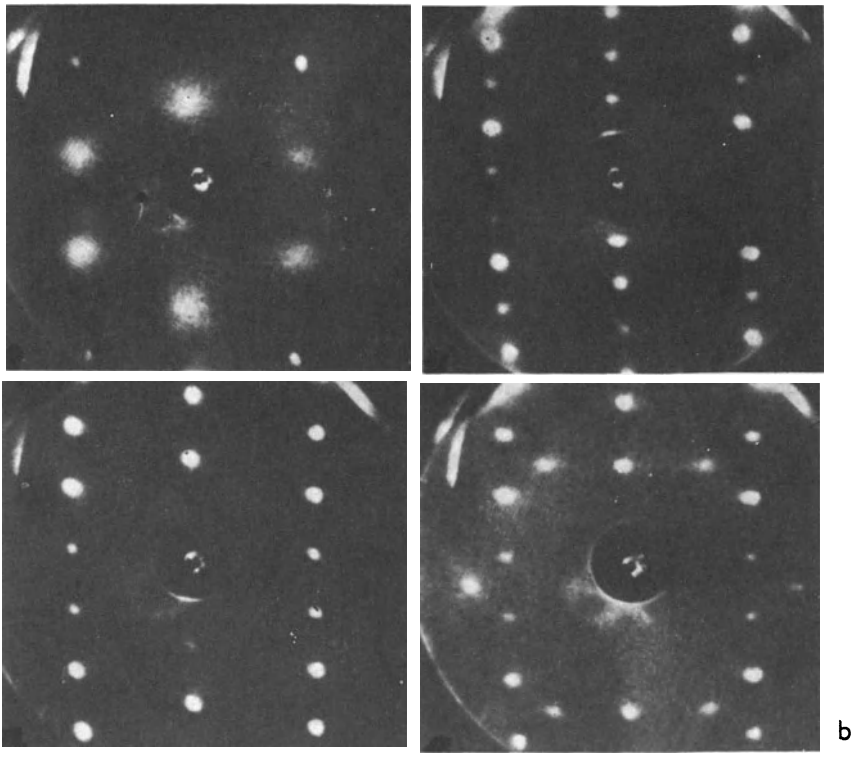

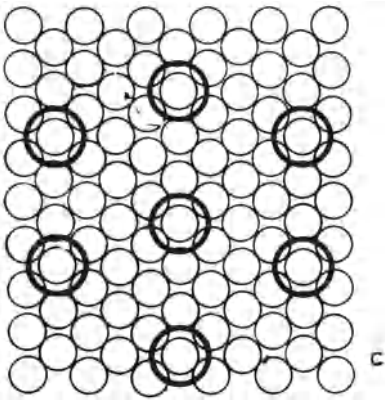

Fig. 4.95. (**a**) Model of the surface structure of Si (111) (7 × 7) [4.54]; (**b**) LEED patterns from BaO deposited on the W(110) surface; (**c**) one of the surface structures of BaO (4 × 3) on W(110) [4.100]

Many papers have been published lately on the structure of atomically pure surfaces of various crystals (Ge, Si, CdS, GaAs, W, Mo, Au, Pb, NaCl, etc.), adsorbed layers, the initial stages of growth of epitaxial films, etc.

The most interesting result of semiconductor investigations is that in the course of annealing the surface structure is changed, or rearranged, so that some superstructure is formed. It is assumed that during this rearrangement the free surface energy decreases, and the free chemical bonds become "locked".

Figure 4.95a shows the atomic structure of the Si surface, whose period exceeds by a factor of seven that of the three-dimensional lattice.

Figure 4.95b depicts the diffraction patterns of low-energy electrons recording the changes in the structure of the (110) face of tungsten during adsorption of barium oxide. As the concentration of BaO grows, various two-dimensional structures of BaO form on the indicated face. One of them (4×3) is depicted in Fig. 4.95c.

Electron diffraction patterns from the (100) faces of ionic crystals (NaCl, LiF, KCl), and also from PbS type semiconductors show no superstructure reflections, i.e., the surface structure corresponds to that of the bulk. Such a correlation also takes place for metal crystals, with the exception of Pt and Au, where the superstructure 1×5 is formed.

In the adsorption of gases, a disordered or ordered arrangement of their atoms or molecules on the surface is observed, depending on the nature of the gas and the degree of coverage of the surface by it.

In the studies of the surface structure LEED is effectively combined with scanning-tunnel and atomic-force microscopy (Sect. 4.10), field-emission scanning electron microscopy (FESEM) and Auger electron spectroscopy (AES). EC forms a happy combination with the micro-probe analysis to provide the atomic location by channeling-enhanced microanalysis.

4.9 Electron Microscopy

4.9.1 The Features of the Method

In electron microscopy an image is obtained with the aid of electrons which have passed through, have been reflected from, or emitted by, an object. Electron beams are formed by electronoptical systems with the use of lenses. The image is obtained on luminescent screens, photographic plates and films, or other electron-sensitive detectors with devices for memorizing and amplifying with displays.

The basic features of the method are as follows:

a) The possibility of obtaining very large magnification and high resolution, up to the atomic level, for the direct observation of the objects;
b) electron-optical information on the object (image) can be supplemented by a number of other chemical analytical data based on the physics of

interaction of electrons with matter, and by electron diffraction data (Sect. 4.8);

c) extensive possibilities of exerting some effects upon the object in the course of observation (heating, cooling, deformation, irradiation, etc.). The possibility of observing the dynamics of the processes and registering them by means of video recording;

d) the possibilities of observing the relief of the surface and its chemical composition, especially in scanning electron microscopy.

4.9.2 Transmission Electron Microscopy

The contemporary transmission electron microscope is one of the most complicated physical instruments (Fig. 4.96) [4.101]. The construction of its parts, especially those of the optical system, uses special materials and requires extreme accuracy. The column of the instrument must be very vibration-stable, and special foundations and suspension systems are needed for high-voltage instruments. A great stability of the accelerating potential ($\approx 10^{-6}$) and of the lens-supply current is required. The direct electron-optic magnification is as much as 800 000–1 300 000. The electron micrographs are usually further enlarged photographically by a factor of 5–20. An optical scheme of an electron microscope is illustrated in Fig. 4.97.

Electrons emitted by the cathode are accelerated by a high voltage due to the difference of the cathode and anode potentials. Then, they pass through two condensor lenses, which reduce the minimum cross section of the beam and focus it on the object. In the small space inside the objective (≈ 2 mm), miniature specimen holders are introduced having a goniometric head that enables movement and orientation of the specimen as needed, including tilting up to 60°. The specimen is placed either directly on a special microgrid or on a grid previously coated with a supporting film. Passing through the object, the electrons are scattered within some solid angle. This angle is restricted by the objective aperture. The object image formed by the objective lens is magnified by the intermediate lenses and the projecting lens.

The image is visualized on a screen or the EM picture is projected on a display and recorded photographically.

Fig. 4.96. Cross-section of the column of the electron microscope Philips CM12 [EC: emission chamber. EG: electron gun. A: anode. GA: deflection coils for electron-gun alignment. GV: valve for separately venting the emission chamber. C_1: first condenser lens. C_2: second condenser lens. BT: beam-deflection coils above the specimen. CD: condenser-diaphragm holder. TL: twin-objective lens. (The minui-condenser lens is not shown). SB: block for accommodating the "goniometer" (not shown); the goniometer permits the specimen in the specimen holder to be displaced. PT: deflection coils below the specimen. SD and SA: diaphragm holder. DL: diffraction lens. IL: intermediate lens. P_1: first projector lens. PD: partition diaphragm. P_2: second projector lens. PV: value for separately venting the projection chamber. FC: film camera. SF: fluorescent screen, for accurate focusing with a binocular magnifier. PC: plate camera. MS: fluorescent screen for observing the image through lead-glass windows in the projection chamber P. IGP: ion-getter pump]

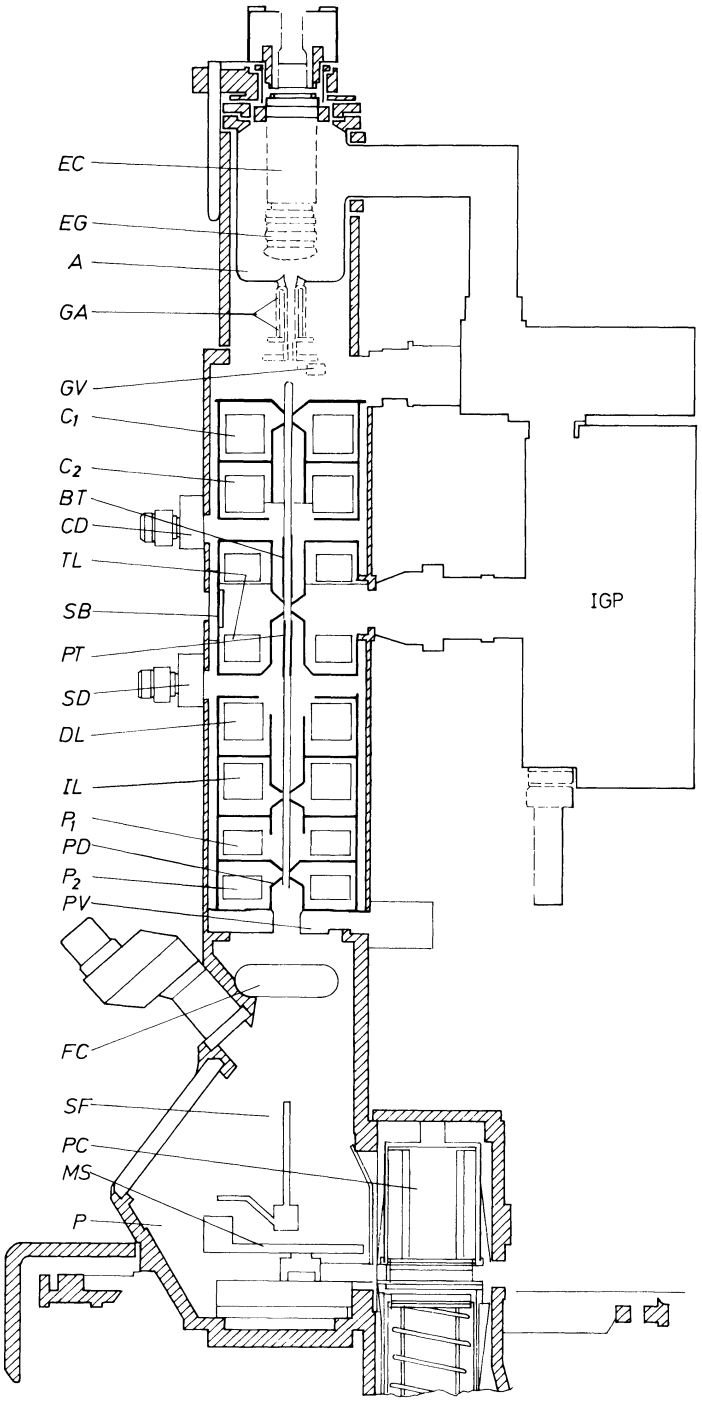
EC
EG
A
GA
GV
C1
C2
BT
CD
TL
SB
PT
SD
DL
IL
P1
PD
P2
PV
FC
SF
PC
MS
P
IGP

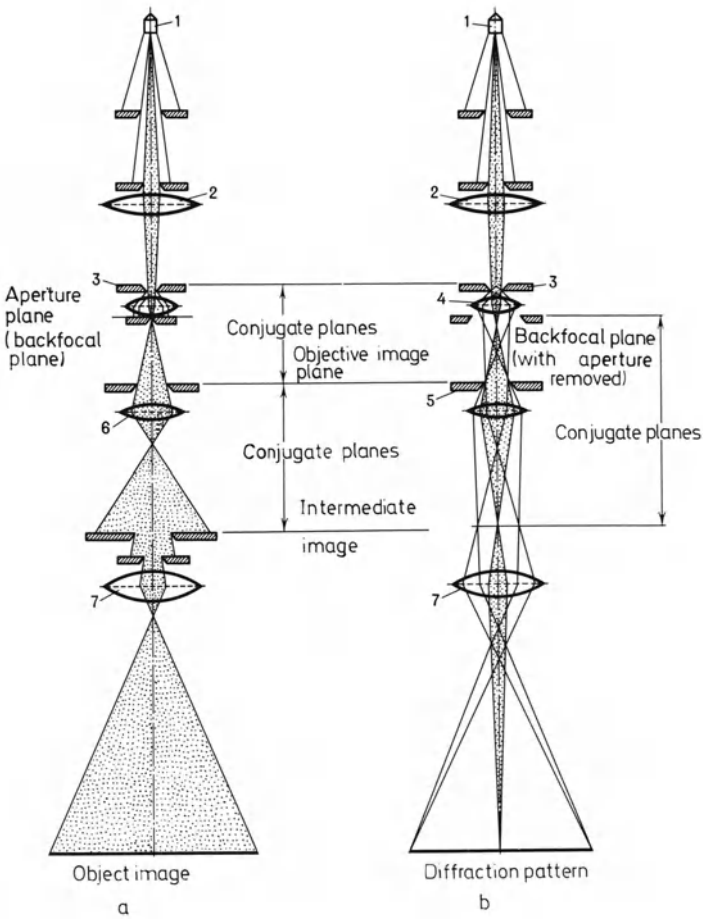

Fig. 4.97. Simplified optical scheme of a transmission electron microscope (**a**) for imaging; (**b**) for selected area electron diffraction (SAED). *1* source; *2* condenser lens; *3* object; *4* objective lens; *5* selecting area aperture; *6* intermediate lens; *7* projector lens

The vacuum system is fully automatic, capable to evacuate the microscope (down to 10^{-7} Torr) with oil-free vacuum in the specimen chamber and column. In unique instruments even superconducting lenses are used which give high lens current stability and, beside this, permit cryomicroscopy of deeply cooled specimens in ultra-high vacuum conditions (down to 10^{-9}–10^{-10} Torr) to be carried out.

Incident-beam electrons interacting with a specimen generate various phenomena such as emitting of x-rays, secondary electrons, Auger electrons, etc.. All this information could be used to obtain valuable supplementary data on the object. In the 70's scanning-transmission electron microscope (STEM) was developed. In STEM (or in TEM with a STEM accessory unit) the electron

beam scans over the specimen. The electron gun of a cathode-ray tube in the STEM is controlled by a signal from a detector, and produces an image on its screen in which the contrast is obtained by techniques different from the conventional methods. Figure 4.98 shows the detectors that are available for these techniques [4.102]. The signals from the different detectors originate from:

(1) High-energy electrons back-scattered from the specimen (BSD);
(2) low-energy electrons produced by secondary emission in the specimen (SED);
(3) x-rays emitted by excited atoms in the specimen (EDX);
(4) unscattered transmitted electrons (BFD);
(5) scattered transmitted electrons (DFD); and
(6) transmitted electrons of specific energy, selected by electron spectrometer (EELS).

Some of the signals can be used in routine "scanning electron microscopes" (SEM) (e.g., Items 1–3). In specially designed, dedicated devices Auger spectroscopy is available.

Specimen preparation is always related to thinning or fracturing of crystals or other materials. Some specimens may be prepared by grinding in a mortar or by splitting the crystal. Crystal fragments are then deposited onto a copper grid, covered by a thin carbon film. Usually the crystalline specimen is cut out from the bulk material in the desired orientation. Thereafter, the specimen is mechanically polished down to a specified thickness of 30–70 μm and then thinned chemically or by ion bombardment.

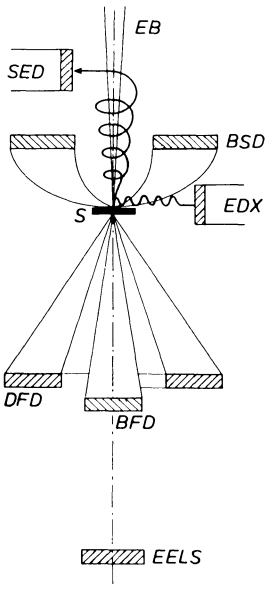

Fig. 4.98. Schematic representation of the detectors around the specimen and in the projection chamber [4.102]. The detectors are mainly used when the instrument is SEM: [EB: electron beam, SED: secondary-electron detector, BSD: back-scattered electron detector, EDX: detector for energy – dispersive x-ray analysis; BFD: bright-field detector, for nonscattered transmitted electrons), DFD: dark-field detector, for scattered transmitted electrons, EELS: electron-energy-loss spectroscopy detector, for transmitted electrons sorted by energy]

Image formation in TEM. Wavelength of electrons, λ, is determined by the accelerating voltage V. For the commonly used voltage of $V = 100\,\text{kV}$ $\lambda \approx 0.037\,\text{Å}$, for a megavolt instrument $\lambda \approx 0.008\,\text{Å}$. The resolution of any optical system is limited by the diffraction spread of the image from a point, and is equal to

$$\delta_D = 0.61\,\lambda/\alpha, \tag{4.178a}$$

where 2α is the angular aperture of the objective lens. This relation can also be interpreted in terms of the Fourier transform of the object (4.12, 118). According to the Bragg relation $n\lambda = 2d \sin\theta$, see (4.3), in our case (for $n = 1$) $2\theta \approx \alpha$, we have

$$\delta_D = 0.61d, \tag{4.178b}$$

i.e., the point-to-point resolution is determined by the minimum spacing of the diffracted beams, which are not cut off by the angular aperture of the objective lens.

A wide aperture is necessary to obtain a high resolution, but for large α the aberration, primarily the spherical aberration, of magnetic lense increases considerably. Therefore, an optimum aperture that fits these requirements has to be used, it leads to the resolution of 2.0–1.4 Å. An example of the imaging of an atomic structure is illustrated in Fig. 4.99 (see also Figs. 1.18, 21).

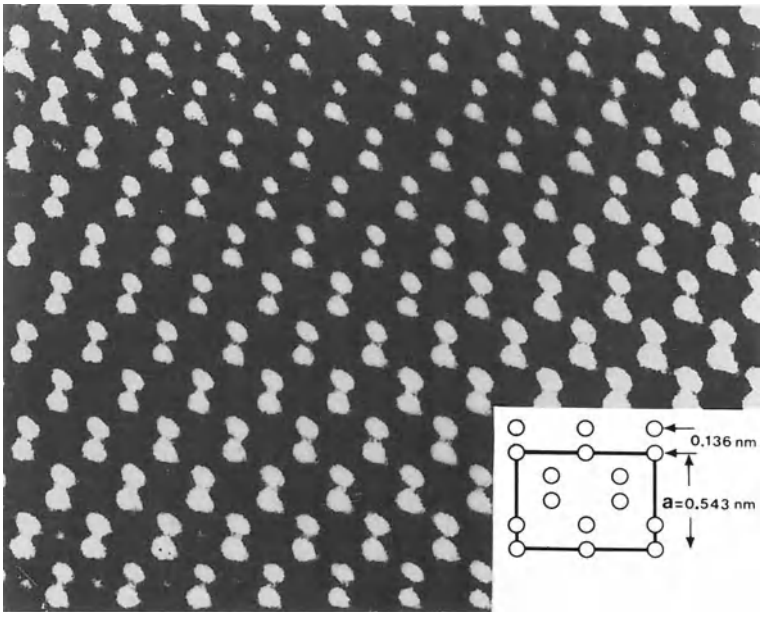

Fig. 4.99. ⟨110⟩ lattice image of Si after enhancement by photographic averaging. White spots correspond to atomic columns. Inset: projected atomic structure. (Courtesy of J. L. Hutchison)

Let us now consider the image formation in TEM (Fig. 4.97a) and the mechanism of aberration effects.

The wave function of the image ψ_I can be written as

$$\psi_I = \mathscr{F}^{-1} T \mathscr{F} q \psi_0, \tag{4.179}$$

where ψ_0 is the incident wave. The sequence of image formation is described by (4.179) in such a way that the expression should be read from right to left. Upon passing through the object, the wave ψ_0 interacts with its potential φ. Consequently, at the exit surface of the object the wave acquires the form $q\psi_0$, where q is the so-called transmission function. The scattering or diffraction of the wave $q\psi_0$ is described by the action of the Fourier operator $\mathscr{F}$ compare (4.12). This action determines the wave function in the back focal plane of the objective lens. In turn, this function is modified by the transfer function T of the lens. The transformation of the scattered wave into the image is described by the inverse Fourier transform operator $\mathscr{F}^{-1}$.

Now let us find the form of a wave at the outer surface of an object after passing through the object having the potential $\varphi(r)$. If the electron is scattered on the object without energy loss, the action of φ is to describe the phase shift of the wave, or its refraction. Such objects are called *phase objects* [4.103, 104].

The wavelength λ *in vacuo* is determined by the accelerating potential V, while λ' in the object is determined by $\varphi(r) + V$. The refractive index n is

$$\frac{\lambda}{\lambda'} = n \approx 1 + \varphi/2V. \tag{4.180}$$

On passing through a phase object of thickness A, at the exit surface the wave has the form

$$q\psi_0 = \psi_0 \exp\left[2\pi i \frac{1}{2V\lambda} \int_0^A \varphi(r)\, dz\right] = \psi_0 \exp(i\chi). \tag{4.181}$$

That is, ψ_0 acquires an extra phase shift χ determined by the potential $\varphi(xy)$ projected to within the thickness of the object A, i.e.,

$$\chi = -\sigma\varphi(xy), \quad \sigma = 2\pi me\lambda/h^2. \tag{4.182}$$

Here, σ is the interaction constant.

The shift χ is maximum when the wave passes through the centers of the atoms where the value of $\varphi(r)$, and hence of $\varphi(xy)$, is largest, and it is small when the wave passes between the atoms, where φ is close to zero. Owing to the smallness of the interaction constant σ, the absolute magnitude of the shift is small upon passing through individual atoms or thin layers of material.

As the objects used in TEM are thin, and owing to the smallness of $\sigma\varphi$ in (4.181 and 182) we can write

$$q = \exp(i\chi) \approx 1 - i\sigma\varphi(xy); \tag{4.183}$$

this is the "weak-contrast" phase-object approximation. Upon assuming that the wave incident on the object has a unit amplitude and zero phase at its

entrance surface, we obtain $q\psi_0 = q$. The amplitude of the wave at a large distance from the object is described by the two-dimensional Fourier integral

$$\mathcal{F}\, q = Q(XY) \approx \delta(XY) - \mathrm{i}\sigma\Phi(XY), \tag{4.184}$$

where X, Y are the coordinates of reciprocal space. The first terms represent the initial wave transmitted through the object in real and reciprocal space, while the second terms accounts for the scattered waves that have arisen and bear information on the structure of the object.

The expression for the contrast transfer function T (CTF) was derived by *Scherzer* [4.105]

$$T(\alpha) = \exp(\mathrm{i}\chi)\, D(\alpha)\, G(\alpha), \tag{4.185}$$

$$\chi(\alpha) = 2\pi\lambda^{-1}(\tfrac{1}{2}\Delta_f\alpha^2 - \tfrac{1}{4}C_s\alpha^4). \tag{4.186}$$

If we rewrite χ for the radial coordinate in the reciprocal space $U = \alpha\lambda^{-1}$, $(U = (x^2 + y^2)^{1/2})$, then

$$\chi(U) = \frac{\pi}{2}C_s\lambda^3 U^4 - \pi\lambda\Delta_f U^2. \tag{4.187}$$

The first term is determined by the spherical aberration C_s of the objective lens. It coincides with the corresponding formula of light optics. However, the phase shift also depends on the defocus Δ_f of the objective lens (the second term) for which the phase shift is larger in the paraxial zone of the lens. By varying Δ_f one can obtain the optimal phase shift that yields the best resolution and contrast. In case of a pure phase contrast $\exp(\mathrm{i}\chi)$ in (4.185a) equals just $\mathrm{i}\sin\chi$ (Fig. 4.100a). In thick objects scattering of electrons with energy loss and their absorption occur, while in crystals these processes are connected with collective excitation of the lattice electrons – plasmons, with phonon excitation, diffuse scattering and other phenomena. These effects can be described phenomenologically as the effective absorption $\mu(xy)$ of electrons in the object, which also contributes to the function q (4.181–183). It gives an amplitude contrast, and the corresponding part of the function T, (4.185), is $\cos\chi$. But for thin, weak-contrast phase objects this term may be neglected. $D(\alpha)$ in (4.185a) is the aperture function. For bright field imaging when the objective lens aperture is placed symmetrically around the optical axis of the microscope $D(\alpha) = \begin{cases} 1 & \text{for } \alpha \leqslant \alpha_{\max} \\ 0 & \text{for } \alpha > \alpha_{\max} \end{cases}$, $\alpha_{\max}$ being the angular size of the aperture. C_s in (4.186, 187) is the spherical aberration coefficient (usually 1–4 mm). $G(\alpha)$ is the dumping function resulting from various instrument instabilities, e.g. the lens-current and accelerating-voltage instabilities, vibrations, etc.

A plot of $\sin\chi(\alpha)$ for various Δ_f is presented in Fig. 4.100. It is an oscillating function of α (or space frequency $U = d^{-1}$), and when the sinusoidal function changes its sign, the information transfer goes in the opposite direction and the object spectrum is transmitted with the reversed sign. One should note that there is an optimum value of Δ_f (curve 2 in Fig. 4.100a) when the first zero of

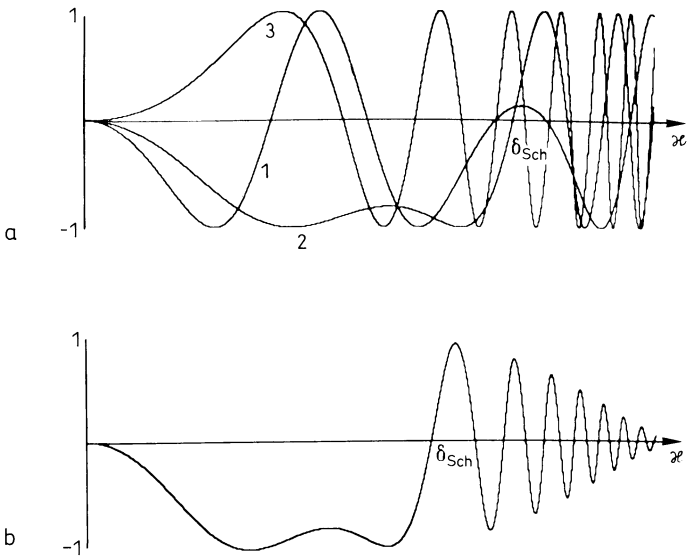

Fig. 4.100a,b. A CTF plot (sin part of CTF, in arbitrary units). (*1*) f < 0, (*2*) f: optimum (Scherzer value, (*3*) f > 0 (**a**); a CTF plot similar to (**a**), but dumping at high frequencies (**b**) [4.106]

$T(\alpha)$ and the $\sin\chi(\alpha)$ values have maximum values in this range. The function $\sin\chi$ (Fig. 4.100a) is first changing gradually, showing fast oscillation later. The first zero of (4.187) gives the value of Δ_f at the optimum Scherzer defocus

$$\Delta_{f\,\mathrm{Sch}} = (C_s\lambda)^{1/2} \tag{4.188}$$

and defines the boundary of the zone of correct contrast reproduction. Thus, the resolution is

$$\delta = U_{\max}^{-1} \approx A\,C_s^{1/4}\,\lambda^{3/4}, \tag{4.189}$$

where $A \approx 0.64$–0.70. Summing up, according to (4.179 and 184) we obtain $\mathcal{F}^{-1}TQ = \psi_n \approx 1 - i\sigma\varphi(xy) = q$, and the observed image of a weak-contrast phase object, with the accuracy down to second-order terms, has the intensity distribution

$$I \approx 1 + 2\sigma\varphi(xy), \tag{4.190}$$

i.e., owing to the phase contrast intensity represents the projected potential φ of the object (4.156b). Naturally, in image coordinates $x'y'$ the magnification should be accounted for.

In general, it should be possible to use all space frequencies of a specimen's spectrum, which the microscope is capable of transmitting. However, some kind of image processing is necessary to extract this information in a proper way. In this case the resolution is limited by the transfer function G which attenuates T values at high space frequencies because instabilities cause an effective fall-off of CTF (Fig. 4.100b). Therefore, it is possible to define an "information limit" of

the resolution as the maximum space-frequency value the microscope could transmit [4.107]

$$\delta_2 = \left(\log\frac{1}{D_L}\right)^{1/4}\left(\frac{\pi\Delta Z\lambda}{2}\right)^{1/2}, \tag{4.191}$$

where D_L is the cut-off value at which CTF is estimated, and ΔZ the defocus spread due to instrument instabilities, namely

$$\Delta Z = C_c\sqrt{\left(\frac{\Delta V}{V}\right)^2 + 4\left(\frac{\Delta I}{I}\right)^2 + \left(\frac{\Delta E}{E}\right)^2}. \tag{4.192}$$

Thus, the δ_2 value may be improved by lowering the chromatic-aberration coefficient C_c; the acceleration-voltage instability ΔV as well as the objective-lens current ΔI and the electron energy scattering ΔE instabilities.

It can be seen from (4.191) that δ_D (4.178a) value may be improved by shortening the electron wavelength λ, i.e. by increasing the accelerating voltage V. Besides, this permits to study thicker specimen, as for higher V values the electron penetration power increases. High-voltage electron microscopes (1–3 MV) are constructed for these purposes. They are mainly used in materials science for medium-resolution work and radiation-damage investigations. Recently, a new generation of high-resolution electron microscopes with "intermediate" accelerating voltages of 300–400 kV have appeared. Such an accelerating voltage improves the d_1 value to 1.65–2 Å. At the same time it is possible to preserve a small value of ΔZ and, correspondingly, to increase the information limit δ_2 to 1–1.4 Å.

We have discussed the mechanism of image formation for thin, weak-contrast phase objects in which the electron diffraction practically corresponds to the kinematic approximation. For thicker objects these approximation is not fulfilled and the dynamic theory of electron diffraction is to be used (Sect. 4.8.4). Scattering in a crystal can also be effectively described in terms of Bloch waves.

According to the Schrödinger equation (4.154) the electron wave function $\psi(r)$ for an electron moving in a periodic crystal potential can be written as $\psi(r) = \exp(ikr)u_k(r)$, $u_k(r)$ being a periodical function of r, and the periodicity coincides with that of the crystal lattice. In the reciprocal space one can use the following set of equations:

$$(k_0^2 + v_0 - k_h^2)\psi_h + \sum_g{}' v_{g-h}\psi_g = 0. \tag{4.193}$$

Here $k_0^2 = \dfrac{2mE}{h^2}$; $v(k) = \sum_g v_g\delta(k - 2\pi g)$ is the Fourier transform of $\Phi(r)$, $k_h = k_0 + 2\pi h$; k_0 is the wave vector relating to the origin of the reciprocal lattice, h and g are reciprocal lattice vectors, and $\sum'$ means summation omitting terms with $g = h$.

The ith solution of (4.193) is the ith Bloch wave $\psi^i(r)$:

$$\Psi^i(r) = \sum_h \Psi_h^i \exp(ik_h^i r). \tag{4.194}$$

The resulting electron wave function is the linear combination of different Bloch waves: $\Psi(r) = \sum_i C_i \Psi^i(r)$; C_i could be determined from the boundary conditions at the upper surface of the crystal, where only the incident electron beam is present. The image from atoms of a weak-phase, thin object usually corresponds to the first Bloch wave. In thicker objects the next Bloch waves come into action and the contrast is reversed, and later the image gets fairly difficult to interpret [4.76].

Another, called the "multi-slice" technique, was developed by *Cowley* and *Moodie* [4.108, 109]. The crystal of thickness H is considered as a set of N thin "two-dimensional" phase-amplitude objects ("slices") with distances Δz between them. For every individual slice the kinematical approximation is fulfilled.

The phase and the amplitude of the electron wave function change in these slices while the wave propagation between the slices is pure Fresnel diffraction of the wave in vacuum. Thus for electrons which have passed the n'th slice (ψ_{n+1}), a recurrence equation could be written as

$$\Psi_{n+1}(r) = [\Psi_n(r) * p_n(r, \Delta z)]\, q_n(r), \tag{4.195}$$

where $p_n(r, \Delta z) = \dfrac{\mathrm{i}}{R\lambda} \exp(-\mathrm{i}kr^2/2\Delta z)$ is the propagation function, $q_n(r)$ the transmission function, $q_n(r) = \exp(-\mathrm{i}\sigma\Phi_n(r)\Delta z - \mu_n(r)]$; the "$*$" sign means convolution. Here $\Phi_n(r) = \int_{\Delta Z} \Phi(r)\,dr$ and $\mu_n(r) = \int_{\Delta Z} \mu(r)\,dr$, μ being the absorption coefficient.

In reciprocal space, (4.195) is equivalent to

$$\Psi_{n+1}(R) = [\Psi_n(R)\, P_n(R)] * Q_n(R), \tag{4.196}$$

where Ψ_n, P_n, Q_n are Fourier transforms of ψ_n, p_n, q_n, respectively. For $n = N$ the resulting electron wave function at the bottom-specimen surface will be obtained.

To simulate real EM images, CTF of the microscope should be taken into account.

Up to this point bright-field imaging was discussed. The so-called dark-field imaging technique is also used. In this case the central (unscattered) beam in the back focal plane of the objective lens is not allowed to pass through the objective aperture. The basic idea of the dark-field technique is to use a tiny beam stopper for eliminating the powerful incident beam which in the usual bright-field technique gives a considerable constant brightness of the image intensity. The image is formed by interference of only scattered beams, instead of the scattered and unscattered ones as is the case for bright-field imaging. This leads to nonlinear contrast transfer, and a significant contribution to the amplitude contrast. Atoms and other, larger-structure inhomogeneities "sparkle" in the dark-field "background" in the absence of the incident wave, while in the bright-field imaging atoms come out as dark spots in the bright background. The dark-field technique yields high-contrast images, but their interpretation could be difficult and less straightforward than in the case of the bright-field imaging (Fig. 4.101).

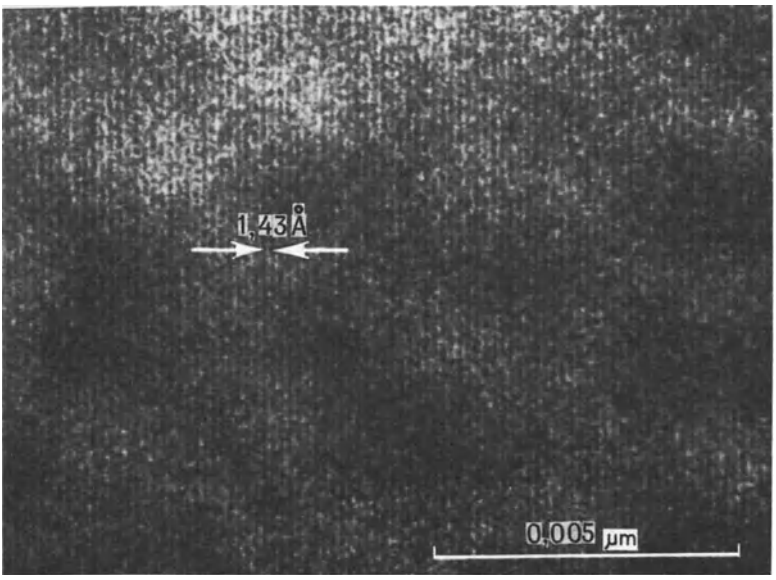

Fig. 4.101. Electron micrograph of a gold crystal: image of a system of (220) planes [4.79]

4.9.3 HREM Imaging of Atomic Structure of Crystals

Modern HREM allows to obtain a crystal-structure image, and thus HREM is often called "atomic imaging". The image is formed with the electrons scattered by the crystal having passed through the aperture. As has been stressed before, the diffraction is described as the Fourier transform of the projected potential. If the incident and only one of scattered beams are allowed to pass through the aperture, one Fourier harmonic with the corresponding interplanar distance d will appear in the image (Fig. 4.99). These pictures are conventionally called "lattice-plane images". Transmission of the whole spectrum produces a superposition of harmonics (Fig. 4.67). Such pictures present an image of a crystalline structure (Fig. 4.99). The image of a crystal structure is a projection of superimposed unit cells, i.e. the images of columns of atoms the axes of which are oriented in the direction of the beam are produced (in a thin specimen there are usually 10–30 atoms in a column).

In $\langle 110 \rangle$-oriented silicon crystals two sets of $\{111\}$ planes are aligned edge-on and are available for observation (Fig. 4.99). Single atomic columns were observed by selecting a defocus value at which the CTF transmitted 022 and 004 beams with strong and positive $\sin\chi$ [4.110]. If the atomic columns are closely spaced, they may not be resolved, as in images of silicon obtained along the [110] direction (distances between the columns 1.36 Å) (Fig. 4.99).

In the XY plane of the reciprocal space there are Φ_{hk0}-nodes of the reciprocal lattice, and all electrons scattered between the nodes, i.e., electrons which correspond to the whole $F(XY)$ transform [4.111]. Therefore, the image presents

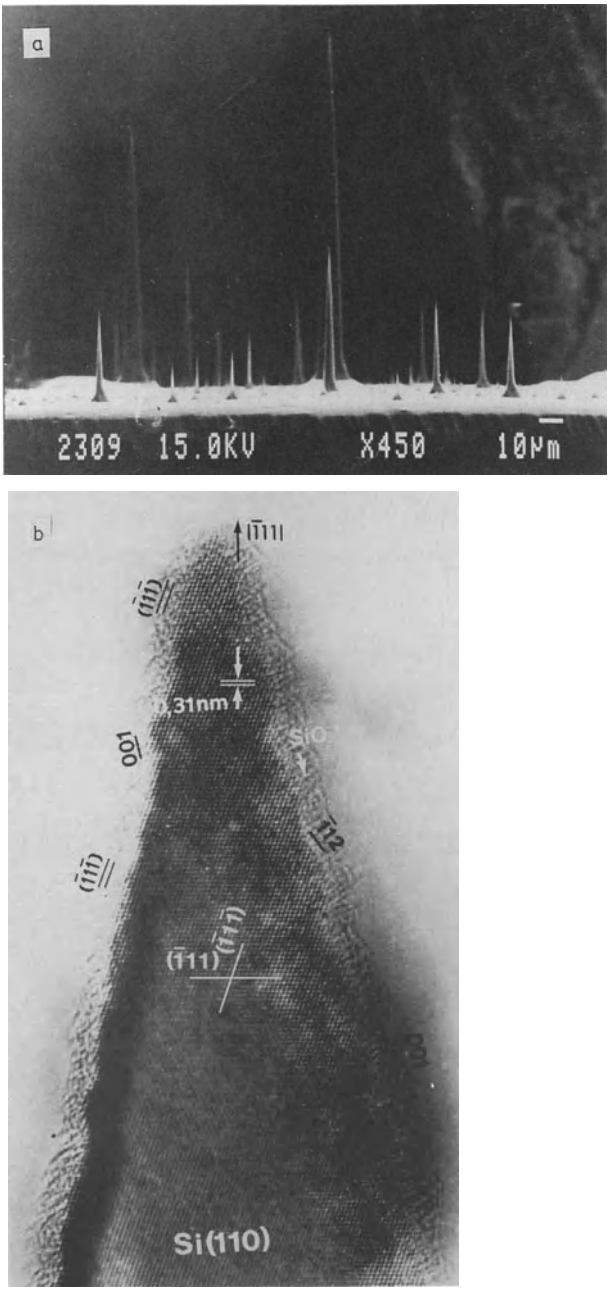

Fig. 4.102. (**a**) SEM image of silicon whiskers grown on (111) Si by VLS, obtained in secondary electrons; (**b**) ⟨110⟩ HREM image of the silicon whisker tip. The tip has a triangular cross-section. Faceting of the whisker is indicated. Left side of the whisker is almost perpendicular to the image plane. The tip is covered by a layer of SiO_2 oxide (courtesy of E. I. Givaryizov)

not only the structure of the projected unit cells but the faceting and all defects in the crystal. Figures 4.102a, b represent EM images of silicon whiskers. Whiskers were grown on ($\bar{1}11$) Si by vapor-liquid-solid (VLS) technique. Chemical etching was used for "sharpening" the whiskers (Fig. 4.102a). The crystal lattice along [110] was imaged using the incident 000 beam, four 111, two 220 and two 200 beams (Fig. 102b) Faceting of the whiskers is also shown in Fig. 4.102b. The whisker's tip is covered by a layer of SiO_2 oxide about 2 nm thick [4.112].

HREM is also employed for the investigation of epitaxial layers and interfaces.

In the case of (001) cross sections of the InAs/GaAs (001) superlattice a certain specimen thickness and objective lens defocus enables one to image GaAs and InAs differently in the lattice image motif. In the image Ga atoms are revealed as dark spots while As atomic columns – as bright ones, and in the InAs image in contrast to that both In and As atomic columns appear as bright spots (Fig. 4.103) [4.111]. The ⟨110⟩ cross-sectional lattice image of misfit Lomer dislocations along an $InAs_{0.4}Sb_{0.6}$/(001) InAs interface is exhibited in Fig. 4.104 [4.83]. The mean separation of these dislocations $\approx$ 6 nm is close to that for the degree of lattice mismatch.

Interesting results were obtained in the electron-microscopic investigation of complex oxides of heavy metals (Figs. 1.18a, 4.105, 106). An alternation of

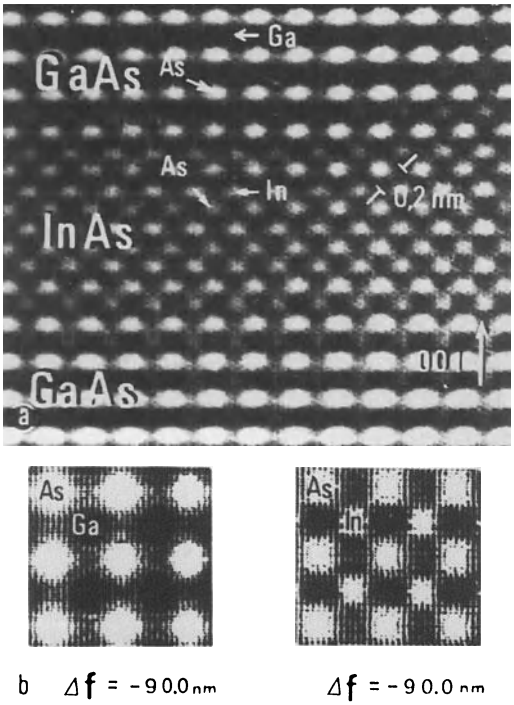

Fig. 4.103a,b. (100) cross-sectional image of an InAs/(001) GaAs superlattice selected area. (**a**) digitally filtered image; (**b**) simulated image of GaAs and InAs structures. Sample thickness is 8 nm, defocus $A_f = -90$ nm [4.111]

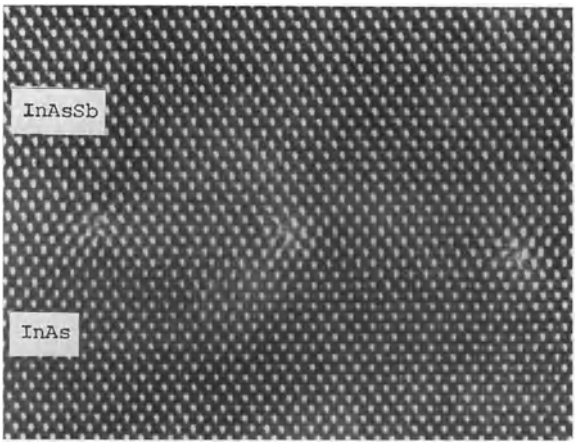

Fig. 4.104. ⟨110⟩ cross-sectional lattice image of misfit Lomer dislocations along an $InAs_{0.4}$ $Sb_{0.6}$/(001) InAs interface [4.114]

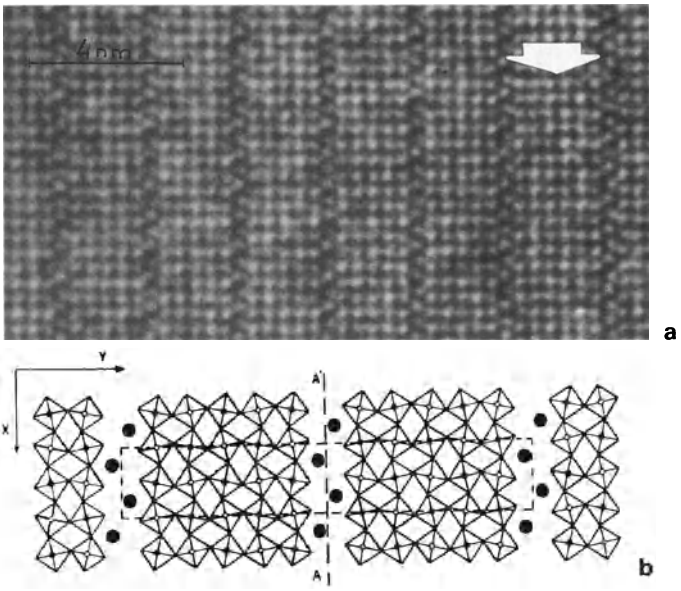

Fig. 4.105a,b. Image of the crystal structure of UW_5O_{17}. The arrow indicates an interlayer having the composition UW_6O_{20} (**a**). Diagram of the packing of octahedra, dark spots-U atoms (**b**). Only heavy atoms are seen, the "holes" between octahedra projections are light [4.115]

two-dimensional layers consisting of different combinations of octahedra were found in the structure of *U-W* oxides (Fig. 4.105) [4.115]. Similar observations were made in the study of layer silicates [4.116].

It is possible to process EM images of structures with the aid of Fourier filtration (Fig. 4.106).

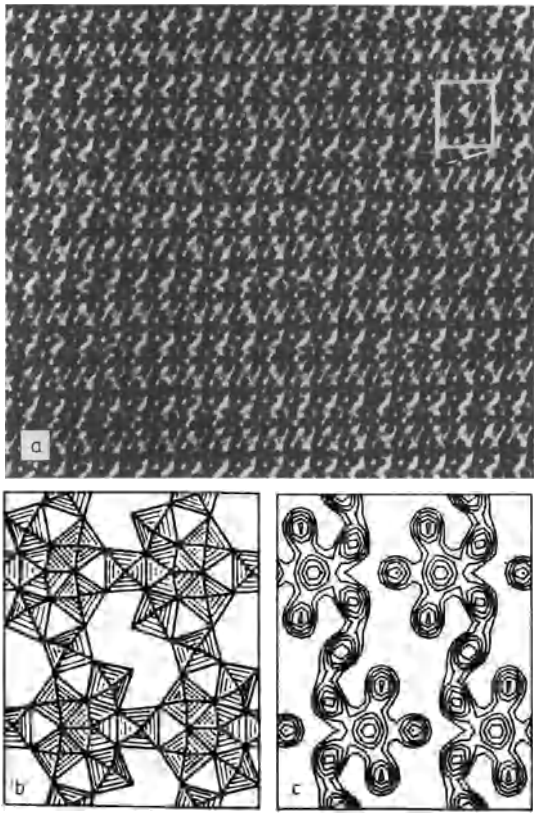

Fig. 4.106. (**a**) Electron micrograph of a thin plate of the crystal structure of $K_{8-x}Nb_{16-x}W_{12+x}O_{80}$; (**b**) diagram of the structure; MeO_6 and MeO_7 polyhedra; (**c**) processed double Fourier-transform image of the projected one unit cell of Fig. 4.106 (**a**) as a contour plot. The peaks of the densitogram yield an image of only the W and Nb atoms blurred by the apparatus functions of the microscope. Their coordinates in the projection are determined with an accuracy of 0.1 Å [4.116]

Interesting data were found with HREM on the arrangement of the atoms in the linking of domains or grains, and also in epitaxy. Real-time processes of the dynamics of atomic migration in the growth surface during crystallization of Au and other substances have been studied [4.118]. Atomic structures of quasicrystals have been investigated (Fig. 1.21).

It is of great interest to study nucleation of crystals, and in particular, microcrystalline concretions (Fig. 4.107) [4.119]. Electron microscopy is widely applied to the study of dislocations and surface structure.

Defects of the crystal structure are observed due to the change in the diffraction conditions in the vicinity of a defect [Ref. 4.120, Sect. 5.8.2]. For instance, in the area surrounding the dislocation the image intensity is redistributed, and at low resolution the image of the dislocation will appear in the bright field (Fig. 4.108).

In investigating the morphology of crystal and other surfaces, the replica and decoration techniques are widely employed [4.120, 121]. On using the TEM

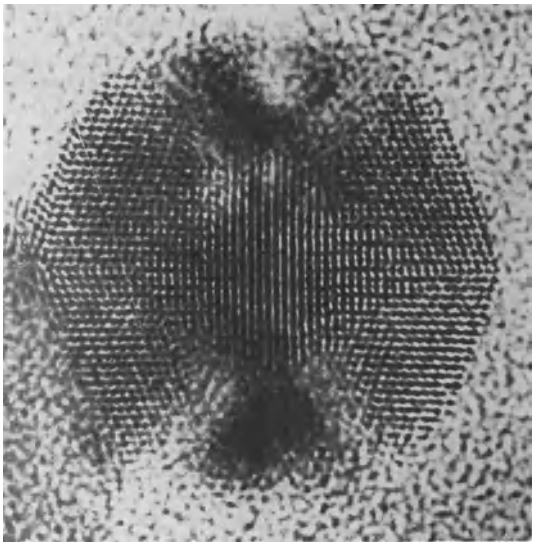

Fig. 4.107. Submicroscopic icosahedral junction of microcrystals of silver [4.120]

Fig. 4.108. Image of dislocations in a deformed silicon crystal (Yu. V. Malov, V. N. Rozhansky)

reflection mode to visualize the crystal surface one can also obtain HREM pictures of the surface relief of a crystal (Fig. 4.109) [4.123].

It was also shown by HREM that the classical view point in crystallography of the uniform filling by atoms in rational faces is not always realized (Fig. 4.110).

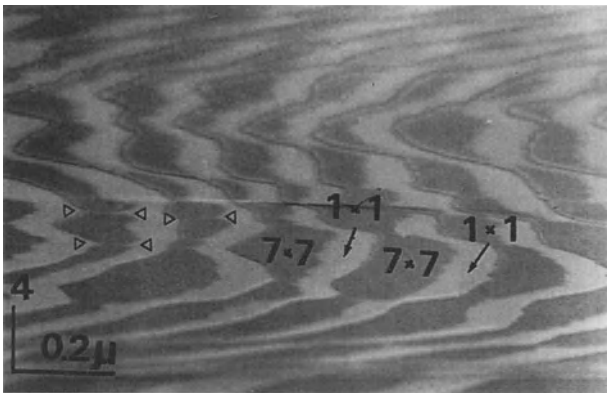

Fig. 4.109. Reflection electron microscope image of an Si (111) surface taken during the phase transition from the 1×1 high-temperature phase to the 7×7 low-temperature phase at about 830°C. The wavy lines on the left-hand side of the dark regions are surface atomic steps of unit cell height (0.31 nm); the dark and bright regions represent the 7×7 and 1×1 regions, respectively [4.121]

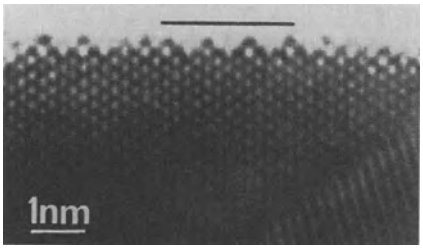

Fig. 4.110. Region of a (110) face of gold having a surface 2×1 superstructure [4.124]

4.9.4 EM in Molecular Biology. Experimental Technique

Electron microscopy is widely applied in investigations of biological crystals and individual macromolecules [4.124–125]. Biological objects can be prepared and studied in various forms such as suspensions of macromolecules (RNA, DNA, large proteins), molecular aggregates and complexes, such as ribosomes etc., and microcrystals, often in the form of two-dimensional crystalline layers.

The biological molecules *in vivo* are in a water environment and usually lose their native structure when dried in the high vacuum of the electron microscope. The molecules consist mainly of atoms with low atomic numbers, which is insufficient to get good contrast in the EM images. Thus it is necessary to enhance the contrast.

It should be mentioned that biological specimens are very sensitive to electron irradiation, and normal exposures in a electron microscopy of about $500\ e/Å^2$ result in a radiation dose to the specimen of $10^{10}-10^{11}$ rads, i.e., an enormous quantity no living matter can tolerate. So it is necessary to avoid

strong illumination of the specimens under study and to develop carefully exposed photographic material, etc., the so-called "minimum-dose technique".

All the features mentioned above demand special precautions to be taken to prevent object damageing during preparation and imaging, and to enhance image contrast. Several techniques were developed to fulfill these demands, such as metal shadowing, negative staining, freezing techniques, etc.

Negative staining may be described as immersion of the particles within an electron-dense matrix. The technique consists of depositing suspension of a specimen onto a substrate film followed by application of a stain. The stain (often it is uranil acetate) layer surrounding the particles protects them from dehydration (Fig. 4.111) and to a certain extent from radiation damage. One can see in the EM images cavities, in the stain corresponding to the shape of the object. Negatively stained specimens usually give a 20 Å resolution. The negative staining, in principle, is capable of revealing object details as fine as 8 Å in size [4.15] or even down to 5 Å in size. Object details at different z levels (z runs in the observation direction) in the resulting image are superimposed because of large depth of focus in an EM.

One of the difficulties of biological electron microscopy is the problem of combining specimens in water solutions, which are natural for biological objects with the high vacuum conditions required for the operation of an EM. One of the apparent ideas how to obtain solid specimens from biological substances is to cool and freeze them. Vitrification of the medium around the specimen makes it possible to prepare non-volatile undamaged biological object in the natural environment.

In practice, vitrification is done by rapid immersion of a small sample into an efficient cryogen. Liquid ethane or propane cooled to their melting point in liquid nitrogen can be used as a cryogen.

A relatively simple and effective enough experimental technique has been developed [4.127] which consists of a replacement of the water surrounding the specimen with a matrix of small hydrophilic molecules that highly resemble water but are non-volatile (Fig. 4.111). This permits one to improve the structure resolution considerably.

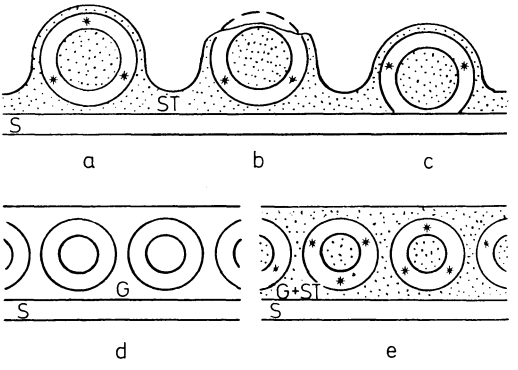

Fig. 4.111a–e. A schematic representation of negative staining and embedding in a solution of small hydrophilic molecules (e.g., glucose) (ST: stain; S: support; G: glucose; ∗: indicates possible sites of protein-stain interaction). (**a**) a rigid tubular structure, view along the axis; (**b**) tubular structure, side adjacent to substrate is stained; (**c**) side opposite to the substrate is stained; (**d**) embedding glucose; (**e**) embedding in glucose mixed with a stain

In the case of biological objects CTF can also be taken into account. True amplitude values could be measured from electron diffraction patterns. But as for the phase information, the only way to extract it properly is to process images which are in the general case disturbed by the CTF.

4.9.5 Processing of Images of Biomolecules. 3D Reconstruction

Methods of image processing are widely used in the electron microscopy of biological objects. The real electron-microscope image is subdivided into two components:

$$J(xy) = I(xy) + N(xy). \tag{4.197}$$

The main of these, $I(xy)$, is a two-dimensional image of the "ideal" object obtained in an electron microscope. However, in the process of object imaging and transfer of this information to the detector there are various sources of noise. These arise owing to emission-current and accelerating-voltage fluctuations, lens-supplying current, mechanical instabilities, etc. In addition, the specimen is also unstable; during preparation or staining and freeze-etching it may change due to chemical or some other transformations. Another source of structure perturbation is radiation damage.

It is reasonable to assume that all the deviations $\Delta I_k(xy)$ of a specimen from the "ideal" image $I_k(xy)$ are included in the noise term $N_k(xy)$.

The image enhancement involves maximum noise suppression $N(x, y)$ and hence the most accurate separation of a useful signal $I(x, y)$ from the real image $J(x, y)$. At the signal/noise ratio $I/N = \sim 5$–10 one should use a method of enhancement. This problem is usually solved by the methods of statistical processing of sets of images $J_k(k = 1, \ldots, n)$.

The image-enhancement methods are subdivided into two classes: (i) image averaging in the real space, (ii) Fourier analysis and filtration in reciprocal space.

The image can be enhanced by analog (mainly optical and photographic) methods or by computational methods for processing digitalized images in real and reciprocal space.

An image of the periodic crystal structure may be brought to self-alignment by shifting it a and b periods in a structure projection. This can be performed photographically by printing the shifted image on the same photographic paper.

EM images are also improved by using the technique of optical diffraction and filtration (Fig. 4.112). An electron micrograph of a crystal is placed in an optical diffractometer. The optical diffraction from the periodic structure is concentrated at the nodes of a reciprocal (two-dimensional) lattice (Fig. 4.112a, b, c). In the diffraction plane a screen ("mask") with holes at the points of the reciprocal lattice is placed (Fig. 4.112c). Then only beams passing through the holes from the image $I(x, y)$, thereby eliminating aperiodic components, i.e., the "noises" $N(x, y)$ in the periodic structure. This is optical filtration of the electron micrograph (Fig. 4.112d).

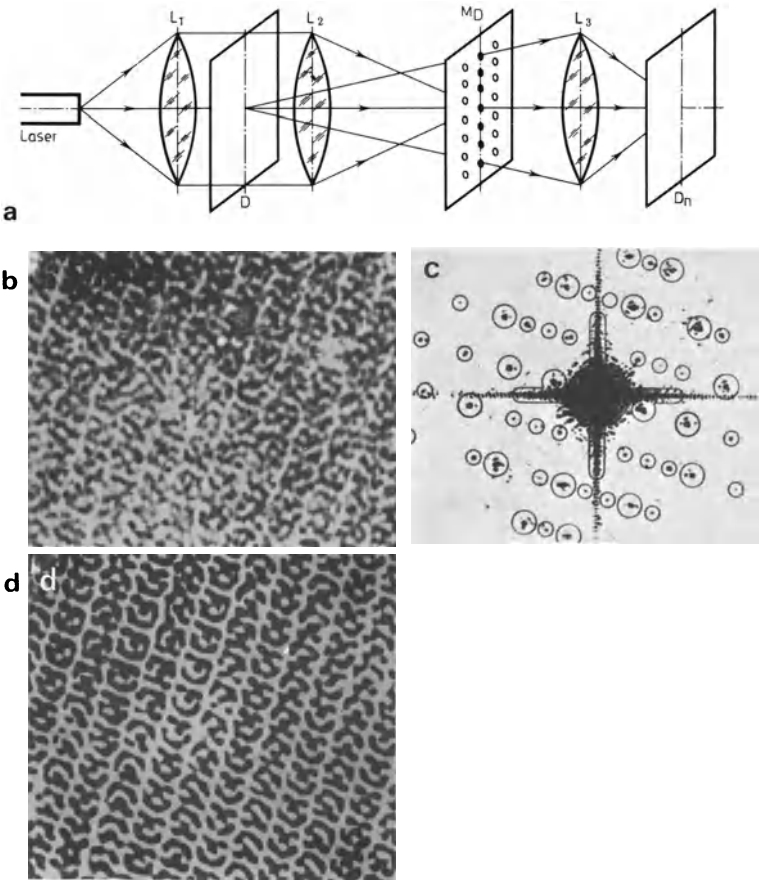

Fig. 4.112a–d. Optical diffraction and filtration of electron micrographs. (**a**) diagram of an optical diffractometer [(L_1, L_2, L_3) lenses of the optical system; D: object (an electron micrograph); M: the diffraction plane and a mask, which transmits only the beams corresponding to the periodic component; D_n: plane of the filtered image]; (**b**) electron micrograph of the two-dimensional crystalline layer of the protein phosphorylase B; (**c**) diffraction from it (the circles correspond to the holes in the mask); (**d**) filtered image compare [4.128]

In practice, this is now done with the aid of a computer when the micrograph is first scanned by densitometer, and the filtration process and Fourier transformations are performed by the computer.

If the object itself, and consequently its projection, have a rotational N-fold axis of symmetry, the structure coincides with itself on rotation through the angle $2\pi/N$. If the image is rotated through arbitrary angles and is aligned photographically with the initial image, then the best density coincidence will take place as a rotation through $\alpha = (k2\pi/N)$ $(k = 1, \ldots, N)$. This gives the enhanced structure image with the $\sqrt{N}$ times reduced background.

Rotational filtering can be performed also on the basis of the Fourier expansion of an image in polar coordinates over the angles.

In the case of asymmetric images a set of images is processed by computational or analog methods. The initial selection of images involves the fulfillment of the maximum similarity condition.

The averaging of n images in real space gives

$$I_{\text{enh}} = \frac{1}{n} \sum_{k=1} J_k(x, y) = \langle I_k \rangle (x, y) + \frac{1}{n} \sum N_k(x, y). \tag{4.198}$$

The signal/noise ratio of an average image is $\sqrt{n}$ times enhanced.

The degree of similarity and the accuracy of superposition of two images on account of both the translational and angular shifts is estimated by a cross-correlation function of the two selected images J_1 and J_2:

$$k(x') = J_1 * J_2 = \int J_1(x) J_2(x + x') dx. \tag{4.199}$$

The calculation of a correlation function is performed by means of a Fourier transformation on the basis of the convolution theorem. The so-called "maximum likelihood method" [4.129] and some other techniques are used for image analysis.

Multivariate statistical analysis (MSA) [4.130, 131] is nowadays the main tool in image processing. In up-to-date studies single-particle images are usually subdivided first of all into several classes so that images which belong to a class highly resemble each other, or differ with one another. The variance inside a class should be minimum while it should have a maximum value between the classes.

The fundamental limitation of an electron-microscopic image is its two-dimensionality, i.e. it is just a magnified projection of the object. But various projections of a three-dimensional object permit to reproduce its space structure mathematically. Such methods are called *three-dimensional reconstruction* methods; they are finding ever-increasing application, especially in the analysis of biological structures.

The two-dimensional image $\varphi_2(x_\tau)$ is the projection of a three-dimensional object $\varphi_3(\boldsymbol{r})$

$$\varphi_2(x_\tau) = \int \varphi_3(\boldsymbol{r}) d\tau \quad \text{with} \quad \tau \perp x. \tag{4.200}$$

The projection direction is defined by the unit vector τ and the projection is formed on the plane x perpendicular to τ. So, the problem of a three-dimensional reconstruction may be represented as

$$\text{set } \varphi_2(x_{\tau,i}) \rightarrow \varphi_3(\boldsymbol{r}). \tag{4.201}$$

By tilting the specimen in the electron microscope, i.e. by changing the projection direction τ_i various projections can be obtained. Sometimes individual particles arrange themselves on the substrate in different orientations and then the in orientations have to be determined with the aid of special techniques developed for this purpose [4.132]. If the object is symmetrical (helical, as bacteriophage tails, or icosahedral, like spherical viruses), then even one projec-

tion is equivalent, owing to symmetry operations, to a set of projections from which the three-dimensional structure can be reconstructed.

All modern reconstruction techniques could be subdivided into two groups: series expansion techniques and methods of integral-equation solving [4.133, 134]. The former group includes iterative techniques, spherical function and Legendre and Chebyshev polynomial series expansions. Convolution and Fourier-transform-based techniques could be attributed to the latter.

Thus, in the method of projected functions [4.133, 135] each projection is modified with the aid of the so-called Radon operator R, and the summation of

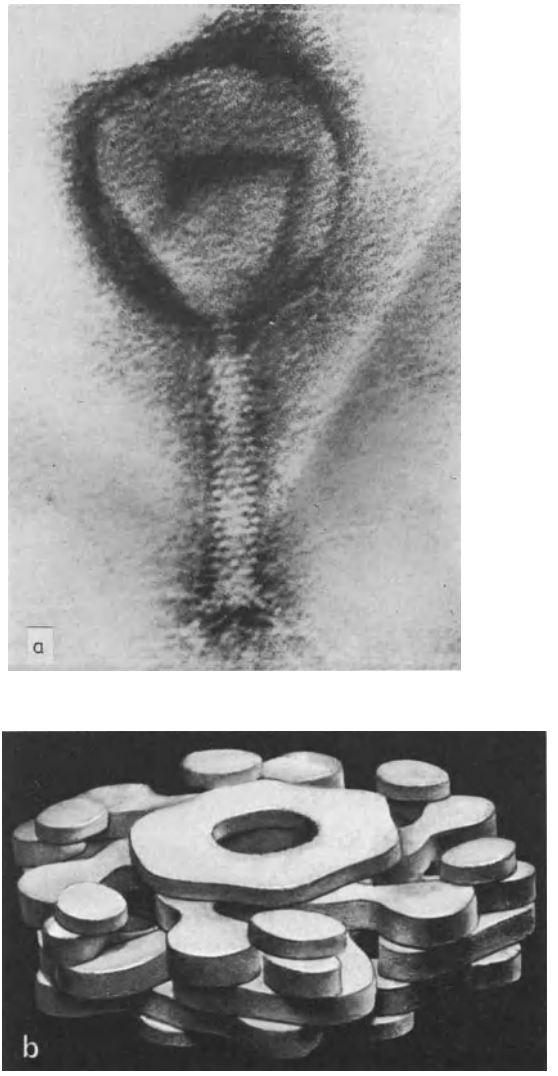

Fig. 4.113. (**a**) Electron micrograph of a bacteriophage T6 (× 550000); (**b**) structure of a single disc of the tail obtained by three-dimensional reconstruction [4.136]

modified functions gives the three-dimensional structure:

$$\varphi_3(\boldsymbol{r}) = \sum_i R\varphi_{2,\tau_i}(x_i). \tag{4.202}$$

The Fourier method makes use of the fact that the Fourier transform $\mathscr{F}_{2i} = \Phi(\boldsymbol{X})$ of projection $\varphi_2(x_{\tau_i})$ is the central cross-section of the three-dimensional transform $\mathscr{F}_3(\varphi_2) \equiv \Phi(X_i)$, where X_i is the two-dimensional coordinate in the reciprocal-space plane $X_i \perp \tau$. From a set of two-dimensional cross-sections one can obtain the three-dimensional transform $\Phi(X, Y, Z)$, and then $\varphi_3(\boldsymbol{r})$. Schematically this reconstruction can be presented as

$$\text{set } \varphi_2(x_{\tau i}) \rightarrow \text{set } \Phi_2(X_i) \rightarrow \Phi_3(X, Y, Z) \rightarrow \mathscr{F}^{-1}(\Phi_3) = \varphi_3(\boldsymbol{r}). \tag{4.203}$$

Figure 4.113a displays an electron micrograph of bacteriophage T6 and Fig. 4.113b exhibits the three-dimensional reconstruction of a single disc of the bacteriophage tail.

4.9.6 Two-Dimensional Biocrystals

Many biological particles, e.g., proteins or even large molecular complexes like ribosomes, can form crystals; some of them could form thin (down to one-molecule thick) two-dimensional crystalline layers. Figure 4.112, b gives an example of a two-dimensional crystal (phosphorylase B). Membrane proteins can also be regularly arranged within lipid membranes. Two-dimensional crystals are suitable for obtaining their three-dimensional structure. Their 3D transform consists of a number of one-dimensional rods in the Z direction with hk-indices, which are normal to the layer plane. So, by tilting the specimen it is possible to obtain continuous $|F(h, k, Z)|$ structure factor which will represent most of the full 3D transform. Then, according to scheme (4.203) the Fourier synthesis of the structure can be calculated.

In this way a moderate-resolution (20 Å in the plane of the crystal and 40 Å perpendicular to it) structure of bacterial hydrogenase from *Thiocapsa roseopersicina* was obtained. The 2D crystals were negatively stained by uranylacetate (Fig. 4.114a) and a number of tilted projections were obtained. The three-dimensional Fourier synthesis resulted in the model shown in Fig. 4.114b [4.137]. The packing unit of the crystal is a double-layered twisted cylinder with 12 distinct domains. This is the hexamer of hydrogenase molecules, individual molecules are supposed to be "dumb-bell" shaped.

Additional possibilities arise in the joint analysis of electron micrographs and electron-diffraction patterns from one and the same specimen. It is possible to use the former for calculating the phases from the image, and the latter for

measuring intensities in reflection and obtaining $|F_{hkZ}|$. Combining these data, the Fourier synthesis can be calculated [4.138].

The most spectacular example of this approach is the investigation of bacteriorhodopsin by Henderson and collaborators [4.139–141]. At the initial stage of this study the information was extracted by processing EM images and electron-diffraction patterns. The CTF correction, the correlation averaging of a large number of unit cells, etc., were used. Later stages included phases calculation for electron-diffraction structure amplitudes with the aid of protein crystallography techniques [Ref. 4.120, Sect. 2.9.4 and Chap. 6]. Not only the α-helices packing was determined, but also data was obtained on the position of polypeptide chain and side amino acid residues (Fig. 4.115).

In the investigation of two-dimensional crystals of catalase [4.142] and ribosomes [4.143], the phases calculated from the EM images were related to x-ray diffraction data to obtain 3D images at 30–40 Å resolution.

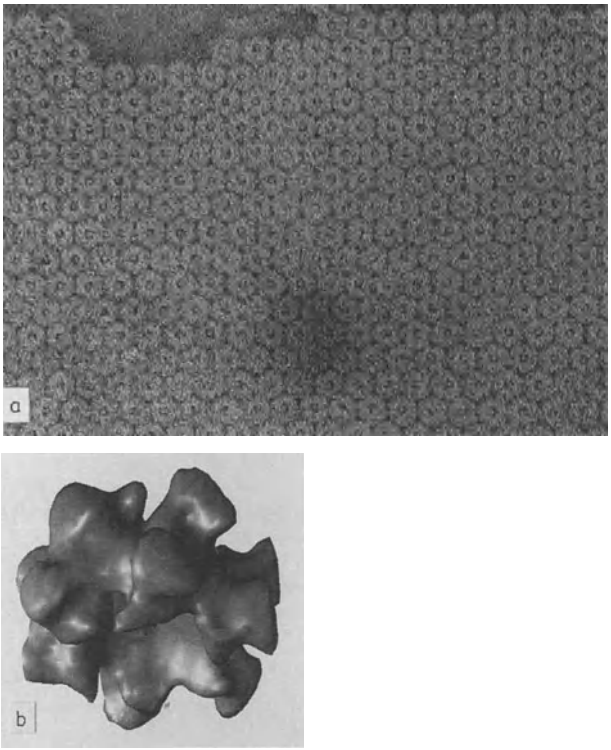

Fig. 4.114. Hydrogenase 2D-crystal, negatively stained with 2% uranyl acetate. Space group is P321, period a = 122 Å (**a**); 3D-model of hydrogenase hexamer (**b**) [4.137]

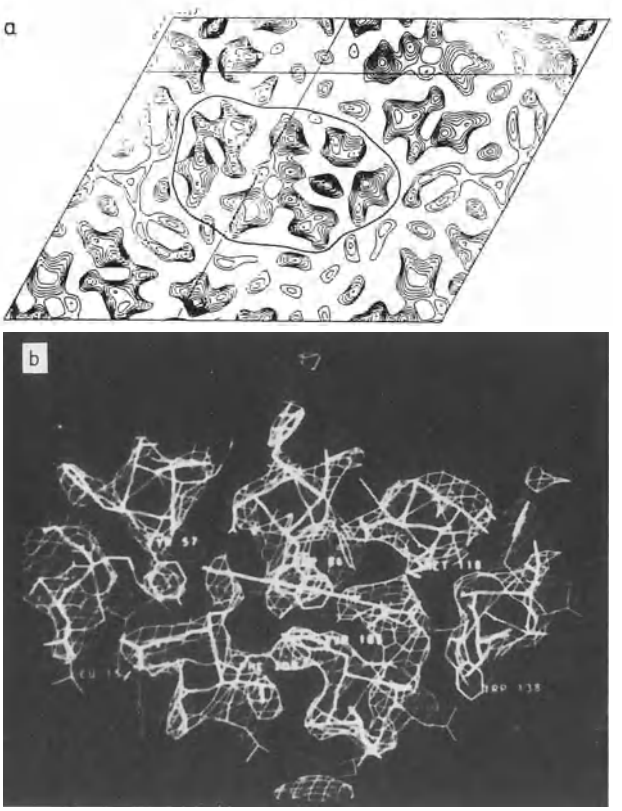

Fig. 4.115a,b. Bacteriorhodopsin structure at 3,5 Å resolution. **(a)** a section through the map parallel to the membrane plane at the level of the retinal; **(b)** a 7 Å thick slice through the map with the atomic model superimposed [4.139]

4.9.7 TEM of Single Bioparticles

The typical image resolution of single particles in routine work is about 20–25 Å. Individual particles are mainly studied by the negative staining technique, but recently the vitrification technique has become popular in this field, too. The problem comes up of how to locate the particles and align them, and afterwards how to select those that match one another (Sect. 4.9.2). To classify the images of particles in different orientations, statistical methods of data processing are required. To suppress noise substantially, several thousands or even tens of thousands of particle images should be processed, so multivariate statistics is used in the data processing.

One of the present-day ideas of data acquisition and processing is the "conical tilt reconstruction" [4.144]. Few different tilts of the specimen will yield a sufficient number of images required for the 3D reconstruction. The relative orientation of different particles in tilted images could easily be determined from the zero-tilt image, say, by cross-correlation. Figure 4.116 gives an example of a structure determination by this technique: the structure of 50S ribosome from *E. coli* subunits [4.145]. Computational methods for determining the orientation of particles in various projections have also been developed [4.131, 132].

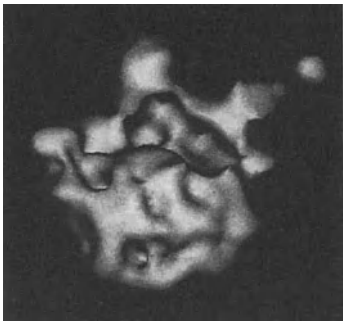

Fig. 4.116. 3D model of 50S ribosomal subunit, calculated by cone-tilt reconstruction [4.146]

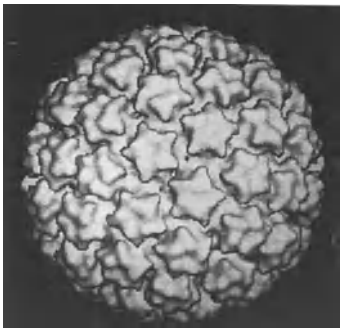

Fig. 4.117. 3D structure of unstained, vitrified Rhesus rotavirus

In case of spherical viruses their icosahedral 532 point-group symmetry makes one picture equivalent to 20–60 different views of the particle. Recently, a new technique has been developed, which takes into account data on several different virus particles to increase the number of projections used [4.147, 148]. Figure 4.117 shows a 3D reconstruction of the Rhesus virus [4.148].

4.9.8 Scanning Electron Microscopy (SEM) of Solids

In TEM the image is formed by transmission of electrons simultaneously through all the points of the specimen [4.101]; the crossover of the electron beam is then larger than the size of the specimen. But another principle is also possible: a condensor system focuses a very fine electron beam on a small area – a "point" of the specimen surface (both in the case of transmission and reflection). A special deflecting system scans the surface of the specimen with an electron beam. Thus, the image is formed by successive recording of its different areas. The "response" with any kind of radiation from a given microregion of the specimen is recorded, and the response from a "point" is presented in the corresponding point of the image. The resolution depends on the diameter of the beam. In the transmission version (TEM) a resolution of about 2–5 Å was achieved in unique investigations. In the best commercial, reflecting SEM apparatus it is 15–30 Å. Special detectors record transmitted or secondary electrons (the most widely used registration mode), cathodoluminescence, x-rays, Auger electrons, etc. In SEM the image is observed on the screen of

a cathode-ray tube [4.149]. The beam in it is controlled by a detector and scans the screen synchronously with the beam falling on the object. At the same time several screens can be used to show the "usual" EM picture, the distribution pattern of any chemical element in the specimen or its chemical composition in any local point.

SEM is the most efficient instrument for investigating the morphology and microrelief of a bulk single crystal. The depth of focus in the scanning microscope greatly exceeds that of optical microscopes, which permits observation of three-dimensional structures with a deep relief (Figs. 4.102a, 118).

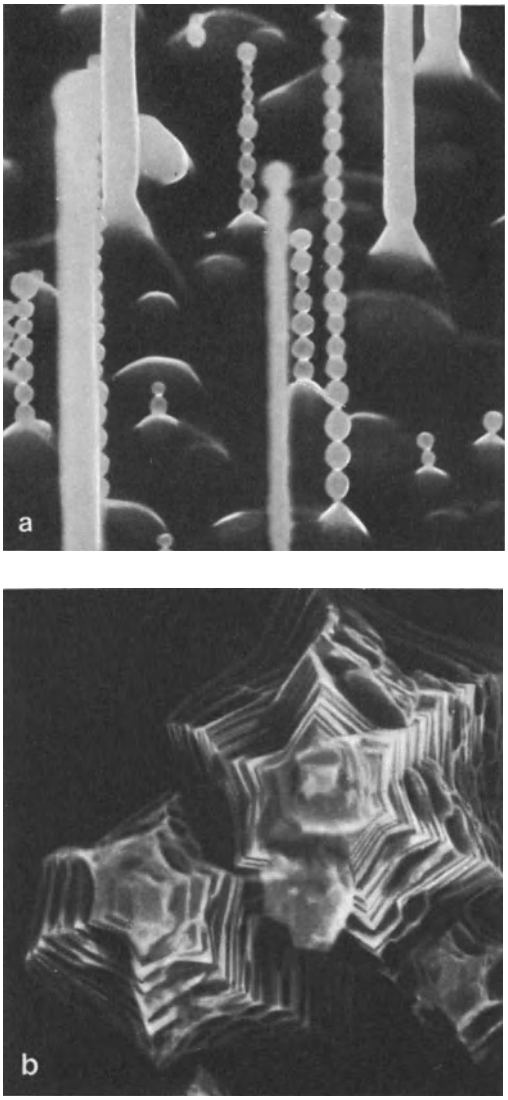

Fig. 4.118a,b. Electron micrographs obtained in a reflecting scanning microscope. (**a**) whiskers of silicon crystals demonstrating the periodic instability of their growth (×20.000)[4.150]; (**b**) mineral millerite (×7.000) [4.150]

The most important feature of SEM and STEM is that both are analytical methods, i.e. they permit determination of the chemical composition of specimen. Characteristic x-ray radiation excited at local points of the surface by the incident scanning beam registered with the aid of crystal analyzers makes it possible to observe distribution of any chemical element on the surface of a specimen. The same possibility is presented by an analysis of Auger spectra of electrons.

Many STEM are equipped with special devices for the operation in reflection and transmission scanning modes, for chemical microanalysis and other measurements. They are also equipped with a computer, which processes the image and automatically gives information on the particle size and shape distribution, the distribution of the chemical elements, etc.

Apart from these basic types of instruments, emission and mirror microscopes are used. In an emission microscope the electrons are emitted by the specimen under the effect of heating or ultra-violet radiation. An electrooptical system projects the electrons onto a fluorescent screen, forming the image of the object. Under special conditions the emission microscope gives an image at the atomic level (Fig. 1.19).

In a mirror electron microscope the specimen is subjected to the potential that hinders movement of the electrons. The electron beam does not reach the surface but close to it, it is deflected in the opposite direction into the electrooptical system which forms the image of the object on the screen.

4.10 Scanning Tunneling Microscopy

Scanning tunneling microscopy (STM) is a very powerful, nondestructive technique for studying the structure of crystal surfaces, adsorption layers and thin films, solid-liquid interfaces, etc. It operates mainly with surfaces of conductive crystals although there are several modifications of the technique which allow dielectric surfaces to be investigated as well. STM provides a real-space imaging with atomic resolution of the spatial distribution of the electron density at a surface. It has been developed by *Binning* and *Rohrer* in 1986 [4.151] and at present STM is a quickly developing field of both the structure analysis and nanotechnology [4.152].

4.10.1 Principle of Operation

STM is based on a pure quantum-mechanical phenomenon of electron tunneling between two conductive media separated by a sufficiently thin, insulating layer (e.g., vacuum). The latter form a potential barrier for an electron with the effective height $\varphi^* = (\varphi_1 + \varphi_2)/2$ where φ_1 and φ_2 are the work functions of the two media. If a dc potential difference $V \ll \varphi^*$ is applied to two parallel flat plates separated with a gap d (Fig. 4.119a,b) the tunneling current I is spatially

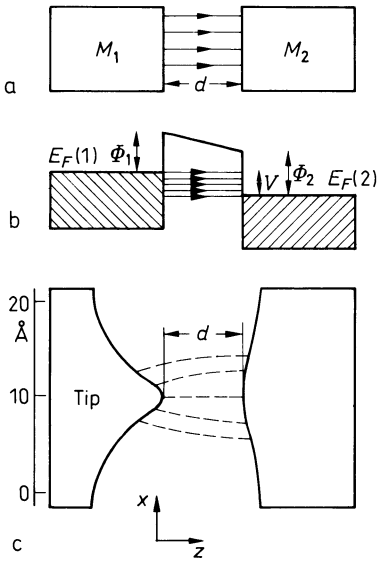

Fig. 4.119. Tunnelling in the metal-insulator-metal system. (**a**) spatially uniform tunnelling current between two planar electrodes made of different metals; (**b**) energy barrier of the above system; (**c**) tunnel current between a metal tip and the corrugated conductive surface [4.151]

uniform and depends exponentially on the gap width

$$I = (2\pi e^2/h)\cdot(k_0/4\pi^2 d)\cdot V\cdot\exp(-2k_0 d). \tag{4.204}$$

In the above formula e and h are the electron charge and the Planck constant, respectively, and k_0 is the inverse decay length of the wave-function density outside the surface, that is under the barrier. All the information about the substance is contained in k_0 which is proportional to the square root of the effective height of the barrier:

$$k_0 = h^{-1}(2m\varphi^*)^{1/2}, \tag{4.205}$$

where m is the electron mass. At higher voltages, the effective barrier height in (4.205) becomes a function of V. The constant φ^* depends on the density of the electronic states on both sides of the tunneling barrier. In fact, only the states between the Fermi levels $E_F(1)$ and $E_F(2)$ contribute to the tunneling current (Fig. 4.119b). For typical φ^* values of about 4–5 eV k_0 is of about 1 Å and a tunneling current of $I \sim 10^{-9}$ A ($V \sim 10$ mV, $d \sim 10$ Å) can be easily measured.

Now, let us consider the example where a sharp metal tip is separated by a small distance d from a corrugated surface of another conductive medium (Fig. 4.119c). In the case of non-free electrons and non-planar barriers, the total current I can no longer be expressed in the simplest form (4.204). However, what is of great importance, the exponential dependence of I on some effective tip-surface distance and the barrier height is still conserved. The electrons close to the Fermi level $E_F(1)$ tunneling to the empty states $E_F(2) + V$ contribute most effectively to the total tunneling current since they face the smallest effective barrier gap. It is evident that, in its major part, the current is provided by the

atoms at the very apex of the tip (separated by the distance d from the opposite surface), although some effective tip-surface distance $d^* > d$ must be introduced.

When the tip is moving along the corrugated surface with the average distance between them being kept constant, the amplitude of the tunneling current is modulated according to the change in the tunneling gap $d(x)$. The current is confined to a filament between the apex of the tip and the object under study. Basic to the operation of the scanning tunneling microscope (STM) is the extreme sensitivity of the current to the tunneling gap. Its amplitude decreases roughly by an order of magnitude for a distance increment of 1 Å. The effective diameter of the current filament for a pointed-tip can be extremely small, down to an atomic size. The latter determines the spatial resolution of the technique. Using vacuum, gas or a liquid as a tunneling barrier the filament of the current can be scanned along the surface without any damage.

4.10.2 Basic Construction of an STM

The operation of an STM is shown schematically in Fig. 4.120. The principal elements of its design are a metal tip (T) and three piezoelectric drivers which can move the tip along three coordinate axis x, y, and z with a very high precision. In fact, the drivers form a tripod for fine-tip positioning the rough positioner L brings the sample S within reach of the tripod. The system P protects the instrument from external vibrations.

The device can operate in two modes. When the voltage applied to the Z driver is fixed, the scanning of the tip along the x and y axes results in a variation of the tunneling current due to the change in the tunneling gap ("constant distance" mode). It is used to attain the atomic resolution. The other, constant current mode, is preferrable when a rough structure of the surface is investigated. In the latter case, during the x, y-scanning an electronic feedback system maintains the current at a constant level changing the tip-surface distance with controlling voltage across the Z piezodriver. In the constant-current mode the trace of the tip (e.g., along the y axis) almost follows the surface topography, although any electronic inhomogeneities, e.g. charged atoms, also form a structure in the tip trace.

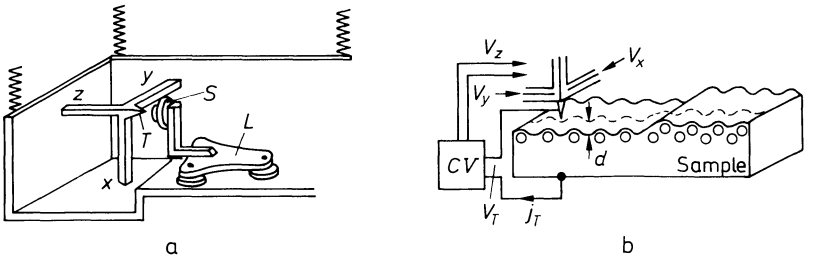

Fig. 4.120. The schematic of an STM. (**a**) design of the microscope; (**b**) illustrating the operation in the constant-current mode [4.153]

4.10.3 Specific Features of Scanning Tunneling Microscopy

Now we can summarize the basic features of scanning tunneling microscopy following from the very principle of the device operation. First of all it is a high-resolution non-destructive technique operating in real space. As the tunnel current is independent of temperature, the STM can operate in a very wide temperature range, from the liquid-helium temperature up to hundreds of degrees of centigrade. The device can also work in liquids. The relatively high scanning speed allows imaging of a surface within several minutes or even faster. Thus, such dynamic processes as adsorption, diffusion, etching or other chemical reactions at the surface can be studied *in situ*. Computer processing data allows a three-dimensional displaying of the surface relief.

In the simplest approach, the spatial resolution of an STM is limited mainly by the diameter L_{eff} of the current filament mentioned above. In turn, this diameter is determined by three characteristic distances involved in the tunneling process, namely, the curvature radius R of a tip, the tunneling-gap width d and the decay length of wave-function density k_0^{-1}. More precisely, the minimum periodicity $\lambda_{\min}$ of a resolvable, sinusoidal surface corrugation with the amplitude a_s is

$$\lambda_{\min} = (\pi/\ln A)^{-1/2} \cdot L_{\text{eff}} \sim \pi(\ln A)^{-1/2} \cdot [(R + d)k_0^{-1}]^{1/2}. \tag{4.206}$$

The logarithmic factor in (4.206) $A = a_s/a_d$, takes into account the gap-width instability parameter a_d. For a typical tip curvature (about 10 Å) and a barrier height (which determines k_0) of the order of a few electron-volts, the resolution lies within the range of 10 Å, although with some improvements it may reach 2 Å.

Despite a very high resolution of STM there are some principal difficulties in the interpretation of the images obtained. Since the tunneling current depends on properties of both the conductive media participating in the process, the image of the surface under investigation is a convolution of its electronic properties with those of a tip. If the geometry, the structure and the electronic properties of the tip are known, the image of the electron density at the surface can be calculated using some mathematical procedures. Image processing (e.g., spatial filtering) can also be applied to improve the pattern.

Figure 4.119b shows that by increasing an external voltage one can probe electronic states of the medium well below the Fermi level. In this case, the voltage-current curve reflects the spectrum of the density of electronic states. In fact, the curve itself is called the *tunneling spectrum*. When the tunneling gap is filled with a liquid, electrons are tunneling inelastically and their energy losses can affect the shape of the current-voltage curve. Thus an STM provides the unique possibility to perform *local* spectral analysis of the surface with atomic resolution. Scanning the surface at various voltages V between the tip and a surface, one obtains different *spectroscopic images* related to different depth in the energy scale. Scanning tunneling spectroscopy (STS) opens up new prospects for studying matter

4.10.4 Atomic Force Microscope

As follows from the principle of operation, the application of STM is limited to the surfaces of conductive solids. However, this disadvantage has been overcome with a novel device using the spatial distribution of atomic forces. It is well known that interatomic and intermolecular interactions include contributions from the attractive Van-der-Waals and repulsive steric forces. They depend on distance in accordance with the Lenard-Jones potential:

$$U(r) = A/r^{12} - B/r^6. \tag{4.207}$$

Thus, scanning a surface with a fine probe sensitive to these forces, we can study the surface relief irrespective of the electric conductivity of the matter. Although, in this case, the decay of the forces with distance is not exponential, it is still sharp enough to provide sufficient sensitivity of the method.

The probe can be designed in the following way. A small piece of a diamond crystal with a sharp edge or a small single crystal of Al_2O_3 (*1*), Fig. 4.121, is glued to a cantilever (*2*) which is a spring with a very low value of the elastic constant K. A change in the atomic force ΔF results in a weak deviation of the cantilever end, $\Delta d = \Delta F/K$. This small deviation (of the order of several Ångstroms) may be measured with an STM recording the tunnel current between the conductive cantilever and a metal tip (*3*). The sample (*4*) is positioned with a piezoceramic X, Y, Z-tripod (*5*). The device can work using either short-range repulsive forces (distances d less than 2 Å, the force $F > 10^{-8}$ N) or long-range attractive forces ($d > 4$ Å, $F \sim 10^{-10} - 10^{-12}$ N). In the former case the resolution is higher but scanning could be destructive for the surfaces. The latter mode is non-destructive but requires higher sensitivity of the equipment detecting the deviation of the cantilever. Perhaps, the best solution here is the use of a laser interferometer.

When a cantilever is supplied with a sensor made of a small piece of a magnetic material, a microscope becomes sensitive to the magnetic structure of a surface. Such devices are especially useful for studying magnetization, domain structure and other properties of ferro- and ferri-magnetic materials.

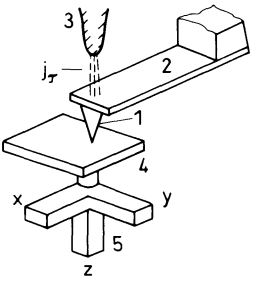

Fig. 4.121. The schematic of the atomic force microscope [4.155]

4.10.5 Several Examples of Surface Images

Figure 4.122 shows a typical STM image of the atomic surface of a silicone single crystal with resolved Si atoms. When the Si surface is exposed to hydrogen, the chemisorption results in blurring the image (Fig. 4.123). The STM image of the graphite surface with an atomic resolution is depicted in Fig. 4.124. A small cluster of gold atoms on the surface is also resolved. An image obtained with an atomic-force microscope is demonstrated in Fig. 4.125a. Atoms on the

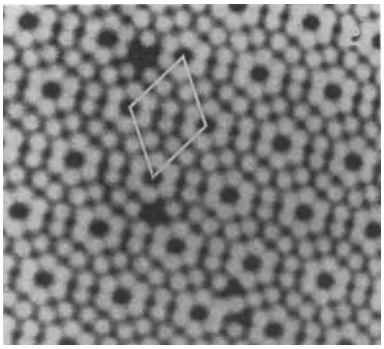

Fig. 4.122. STM image of the clean Si (111) 7×7 surface with atomic resolution [4.156]

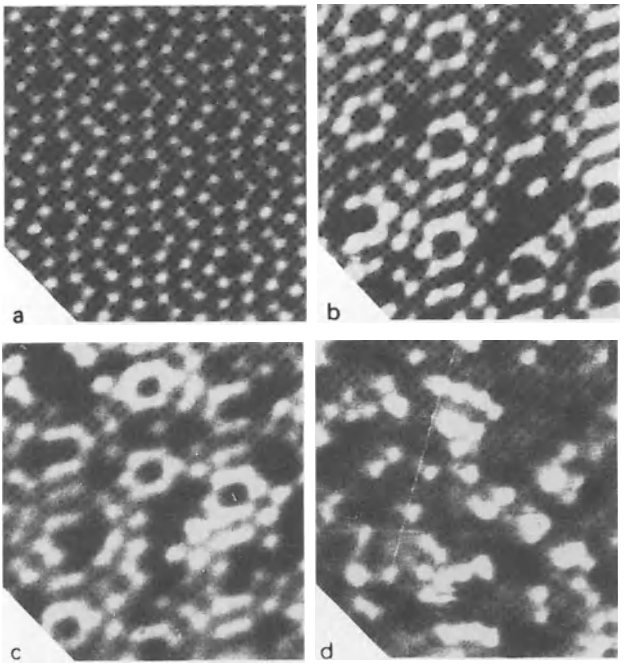

Fig. 4.123. Chemisorption of hydrogen on Si. STM images of unoccupied states of the Si (111) 7×7 surface as a function of H exposure; (**a**) 0; (**b**) 0.1; (**c**) 0.25; (**d**) 0.7 of a monolayer [4.157]

Fig. 4.125. Comparing AFM (**a**) and STM (**b**) images of the $TaSe_2$ surface. Periodicity in (**a**) relates to the atomic lattice constant, periodicity in (**b**) corresponds to the $\sqrt{13} \times \sqrt{13}$ superlattice due to charge density wave states [4.159]

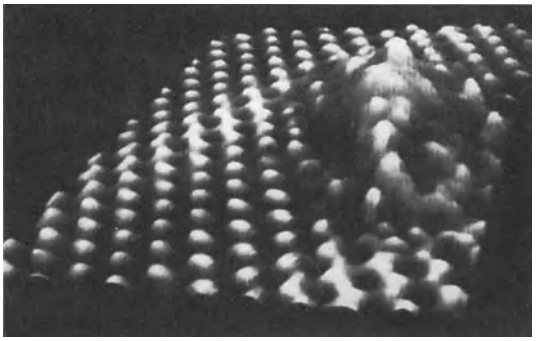

Fig. 4.124. STM image of an isolated gold cluster 12 Å in size and two atomic layers high on graphite [4.158]

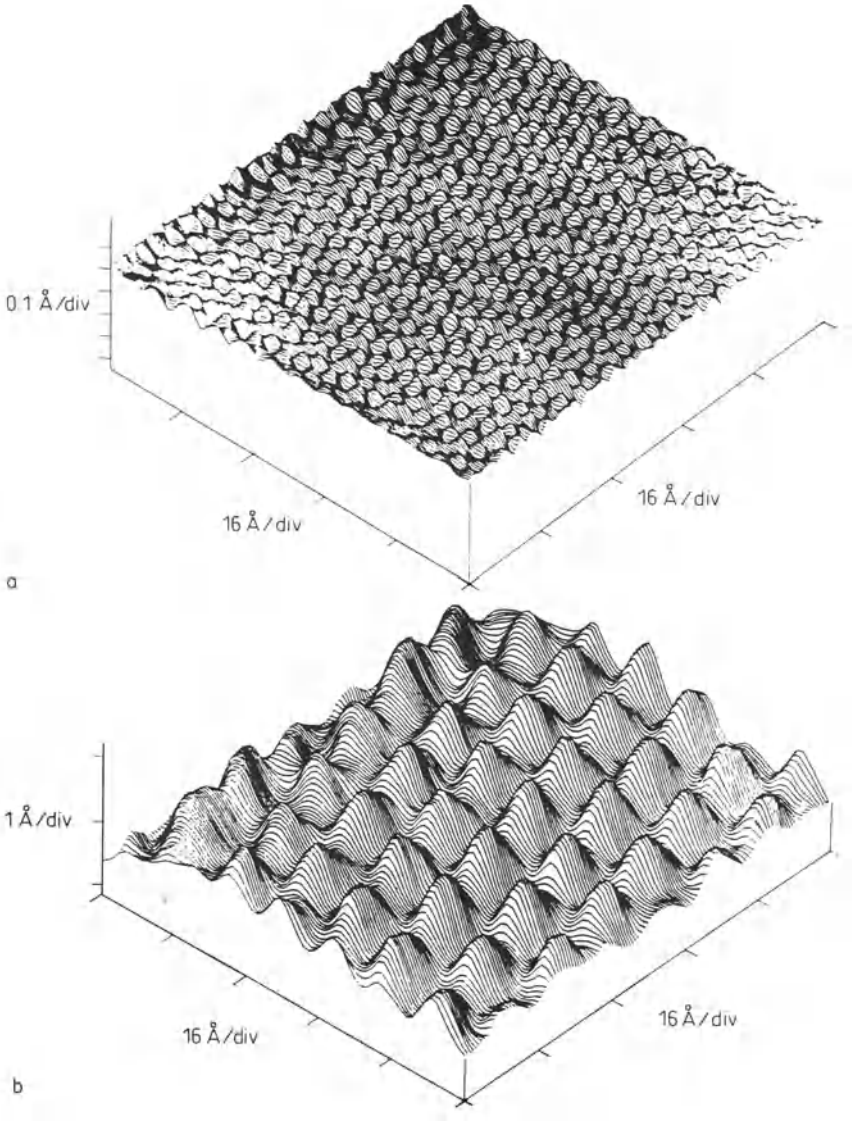

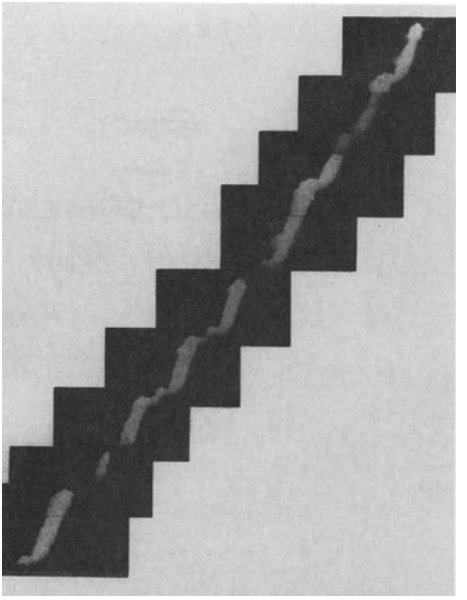

Fig. 4.126. Single-molecule of laurylmethyl cellulose on graphite. Characteristic single and double kinks are seen. The width of a single STM image is 9.5 nm [4.161]

crystalline $TaSe_2$ surface are clearly seen. The same surface analysed with an STM shows a larger periodicity due to the charge-density wave forming a superlattice in the crystal. In contrast to AFM, the STM "feels" charged points and visualizes the wave. The structure of individual organic molecules, in particular, of polymers adsorbed at the conductive surface can be studied by STM (Fig. 4.126).

4.11 Neutron Diffraction, Mössbauer Diffraction, and Scattering of Nuclear Particles in Crystals

4.11.1 Principles and Techniques of the Neutron Diffraction Method

A neutron is a heavy particle with a mass of 1.009 Daltons, a spin of 1/2, and a magnetic moment of 1.91319 nuclear magnetons. In neutron diffraction, the wave properties of these particles are used.

Neutron diffraction investigations require powerful neutron sources. This purpose is served by high-flux, slow-neutron nuclear reactors; pulsed reactors can also be used. In nuclear reactors the neutrons are in thermal equilibrium with the moderator atoms. According to de Broglie's equation the wavelength is

$$\lambda = \frac{h}{mv} = \frac{h}{\sqrt{3mkT}}, \tag{4.208}$$

where m is the mass of the neutrons, v is its velocity, h and k are Planck's and Boltzmann's constants, respectively, and T is the absolute temperature. The spectrum of the neutron beam channeled from the reactor is continuous ("white"), because of the Maxwellian velocity distribution; its maximum at 100°C corresponds to $\lambda \approx 1.3$ Å.

When it is necessary to use long-wave neutrons (5–30 Å), the entire spectrum can be shifted with respect to energies by passing the reactor neutrons through cooling filters. These may take the form of chambers filled with liquid helium, hydrogen, or another moderator (e.g., beryllium) cooled to helium temperatures.

In modern research reactors, a thermal-neutron flux of about 10^{15} $cm^{-2} \cdot s^{-1}$ is maintained in the core. But the collimated flux of monochromatic neutrons that hits the specimen has a substantially lower intensity. Figure 4.127 is a schematic representation of a neutron diffraction unit. A neutron beam with a "white" spectrum passes through the reactor shielding along a channel terminating in a monochromator. Primary collimation is performed in the channel. Large single crystals of Cu, Zn, Pb, or other metals, or pyrolytic graphite plates usually serve as monochromators. The intensity of the resulting monochromatic beam strongly depends on the quality of the monochromator and also on the collimation; in good units the monochromatic neutron flux is 10^{7}–10^{8} $cm^{-2} \cdot s^{-1}$. New possibilities for condensed-matter research are opened by the use of powerful sources of pulsed neutrons. In the spallation process, neutrons are generated in the bombardment of a heavy-element (e.g., uranium) target by protons accelerated in a proton synchrotron. Such sources provide high-resolution neutron diffraction patterns (Fig. 5.29 below) and allow the conduction of various investigations by neutron techniques [4.160].

Diffractometric units are similar in their principle and design to x-ray devices, but they are usually larger because the detector must have a thick radiation shielding. Proportional gas counters filled with ^{3}He or $^{10}BF_3$ are generally used as detectors. For polycrystalline specimens it is sufficient to have a one-circle diffractometer, while for single crystals the four-circle design is most convenient. The devices are either fully automated or remote controlled. When required, various attachments are used: for cooling and heating of specimens, their magnetization, uniform compression etc. Since the initial flux and the neutron scattering cross section are less than for x-rays, the objects under investigation are larger than in x-ray investigations – several millimeters. In the polychromatic version, neutron diffraction can be used by analogy with the Laue x-ray method. Then, with the detector fixed and the crystal rotating, the reflected neutron beams with different λ can be measured by the time-of-flight method.

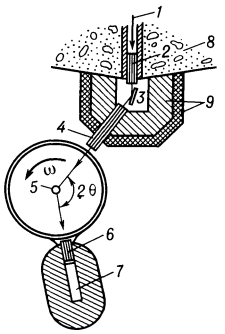

Fig. 4.127. Neutron diffractometer.
(*1*) neutron beam from a reactor; (*2*) primary collimator; (*3*) monochromator; (*4*) secondary collimator; (*5*) specimen; (*6*) collimator in front of the detector; (*7*) neutron detector; (*8*) reactor shielding; (*9*) neutron and γ radiation shields

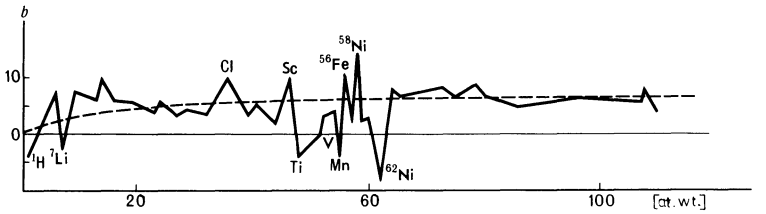

Fig. 4.128. Dependence of the amplitude of coherent nuclear scattering of neutrons on the atomic weight of the elements (- - -) scattering on the nuclear potential [4.162]

We are already familiar with the interaction of neutrons with matter (Sect. 4.1). Nuclear interaction is described by the amplitudes of nuclear scattering b, which are of the order of 10^{-12} cm and are measured in Fermi units $f(f = 10^{-13}$ cm). The values of b vary nonmonotonically with the atomic number Z (Fig. 4.128). Isotopes of one and the same element have different values of b; for some isotopes the value of b is negative because of the presence of resonance levels in their nuclei (this is not the case in either x-ray or electron scattering). Thus, for hydrogen ^{1}H$b = -3.74$, for deuterium ^{2}D$b = 6.57$ for carbon ^{12}C $b = +6.6$, for nitrogen ^{14}N $b = +9.4$, and for manganese ^{55}Mn $b = -3.7f$. Since the size of a nucleus is small (10^{-13} cm) as compared with the wavelength $\lambda \sim 10^{-8}$ cm, the values of b do not decrease with increasing scattering angle, i.e. they are constant for all $\sin\theta/\lambda$. Atoms or ions which have a nonzero spin and/or orbital magnetic moment exhibit an additional interaction with the magnetic moment of the neutron, which is of the same order of magnitude as the nuclear interaction. The atomic amplitude f_M of magnetic scattering depends on the shape of the relevant electron shell and decreases with increasing $\sin\theta/\lambda$. The temperature factor is taken into account in the same way as for x-rays, see (4.22–27). Besides, the effects of absorption, and inelastic coherent and incoherent scattering take place.

The intensity of coherent elastic scattering of nonpolarized neutrons by a crystal is determined by the sum of the squares of the structure amplitudes

$$|F_{nH}|^2 = |\sum_{j=1}^{N} b_j f_T \exp[2\pi i\,(\boldsymbol{r}_j \boldsymbol{H})]|^2 + q^2 |\sum_{j'=1}^{N'} f_{j'mT} \exp[2\pi i(\boldsymbol{r}_{j'} \boldsymbol{H})]|^2, \quad (4.209)$$

where $f_{j'mT}$ refers exclusively to N' magnetically scattering atoms, if they are present in the structure, and q is the product of the unit vectors of the normal to reflection plane by the beam vector. The integrated intensity formulae are similar to (4.77 and 4.103).

4.11.2 Investigation of the Atomic Structure

Neutron diffraction analysis is used predominantly for refining or obtaining additional information on structures studied by the x-ray method. Investigation is often conducted simultaneously with x-ray studies, and thus data on the

unit cell, symmetry, and positions of most of the atoms are already available. Then the calculation of phases (4.46) permits construction of the Fourier synthesis of nuclear density

$$n(\boldsymbol{r}) = \sum_{H} F_{nH} \exp\left[-2\pi i(\boldsymbol{rH})\right] \cdot \tag{4.210}$$

In the absence of magnetic scattering the peaks of this synthesis give time-average distribution of the nuclei due to the thermal motion; the peak heights are proportional to the scattering amplitudes b of the corresponding nuclei and, if b is negative, the peak is negative as well, i.e., it shows the atom as a "pit" on the Fourier synthesis (Fig. 4.129). In refining the position of the nuclei, use is made of difference synthesis and also of the least-squares method with anisotropic temperature factors. Neutron diffraction data are especially suitable for the latter method because, as indicated above, the values of b are constant and the intensity decrease is due solely to the thermal motion.

The advantages offered by neutron diffraction structure analysis are due to the previously described features of nuclear amplitudes b. These include, in the first place, a better (as compared with x-ray analysis) possibility for determining the position of light atoms in the presence of heavy ones. A significant advantage is the detection of hydrogen atoms in crystals of different compounds. Hydrogen atoms can be replaced, completely or partly, by deuterium, which provides additional information. The H peaks in the Fourier synthesis maps are negative and those of D positive, in accordance with the sign of the amplitude of scattering.

Various modifications of ordinary and heavy ice, a number of crystal hydrates, many organic and inorganic compounds, including metal hydrides,

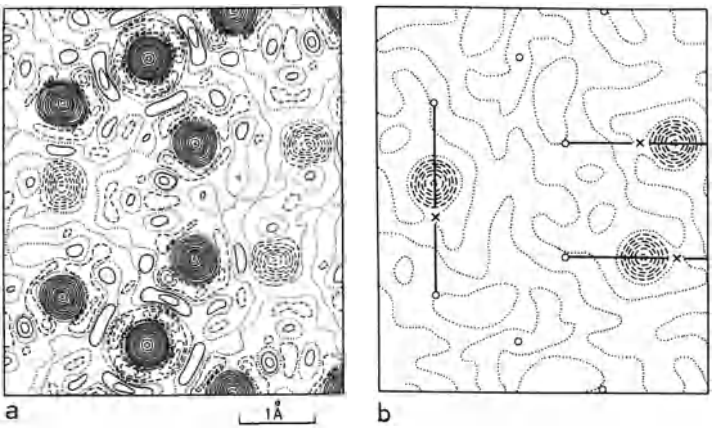

Fig. 4.129a,b. Structure of KH_2PO_4 in the ferroelectric state at $-180°C$. (**a**) Fourier projection of the nuclear density onto the (001) plane; (**b**) projection of the difference synthesis on which H atoms are clearly visible (when the sign of the external electric field is reserved, the H atoms shift to the positions marked with crosses) [4.163]

hydrogen-containing ferroelectrics, and phase transitions in them were studied in this way (Figs. 4.130, 131). Other examples of investigated structures with atoms differing drastically in their atomic numbers Z include nitrides, carbides, oxides of heavy metals, etc.

Another advantage of neutron-diffraction studies consists of the possibility of investigating structures containing atoms with close Z, which are almost indistinguishable by the x-ray method. Examples are Fe, Ni, Co, and Cr alloys and their compounds, for instance, ferrospinels, complicated oxides, and silicates containing Mg and Al. The amplitudes b for such atoms or their isotopes differ widely enough for the individual positions of these atoms to be determined. The

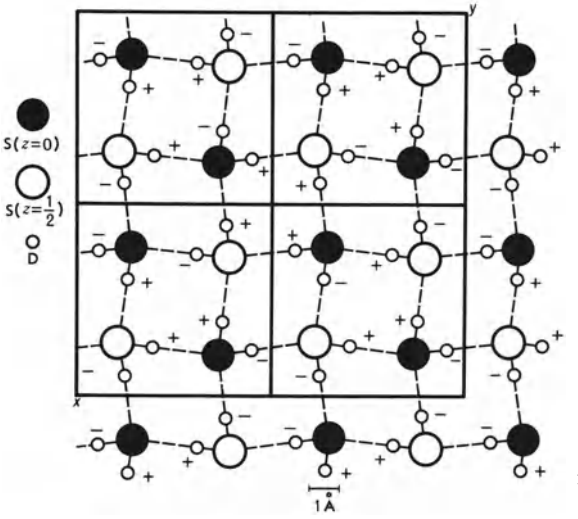

Fig. 4.130. Structure of solid D_2S at 102 K. Projection onto the (001) plane. (– – –) hydrogen bonds forming zigzag chains parallel to the [100] and [010] axes [4.164]

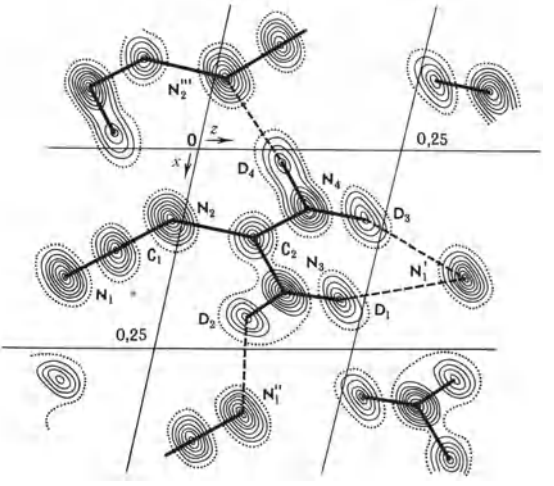

Fig. 4.131. Projection of the nuclear density of the crystalline structure of deuterated dicyandiamide $C_2N_4D_4$. Dashed lines join the hydrogen-bonded atoms [4.165]

difference in b for isotopes of a given element makes it possible, in principle, to investigate the ordering of isotopic nuclei in crystalline structures.

Since the values of b are independent on the scattering angle, the decrease in structure amplitudes F_{nH} (4.209) with increasing $|\boldsymbol{H}|$ depends exclusively on the temperature factor. Therefore the neutron structure amplitudes can be measured up to higher values of $\sin\theta/\lambda$, i.e., higher hkl (lower d_{hkl}) than in x-ray or can give both the positional and thermal motion parameters with an accuracy higher than in x-ray diffraction. This is used, in particular, when constructing difference x-ray – neutron diffraction syntheses, see (4.153).

Neutron diffraction studies open up additional opportunities for determining crystal structures involving comparison of F_x and F_n. As the x-ray and neutron atomic (nuclear) amplitudes of individual atoms appearing in the structure-amplitude equation are different, such a comparison is equivalent to isomorphous replacement. In addition, for neutrons there is an effect similar to anomalous x-ray scattering; such "anomalous" nuclei are, for some λ, ^{113}Cd and ^{149}Sm, among others. By changing the wavelength we also change the b and hence F_{nH} (4.168) of the given structure; thus we can determine the position of the anomalously scattering atoms.

In some cases the "zero" matrix method, i.e., the use of isotopes or different atoms with opposite signs of b, may prove to be highly sensitive. If their nuclei occupy equivalent positions of the unit cell, such positions can be "left out" of diffraction by an appropriate choice of concentrations. Thus, only diffraction from other atoms takes place.

The most complicated compounds investigated by neutron diffraction are vitamin B_{12} (refinement of the structure investigated by x-rays with a resolution of 1 Å) and protein myoglobin.

4.11.3 Investigation of the Magnetic Structure

In such studies the neutron diffraction method yields unique information [4.166]. Various kinds of spin ordering of magnetic atoms (transition metals, rare-earth elements, and actinides) with a parallel (ferromagnetics), antiparallel (antiferromagnetics), inclined, conical, helical, etc., spin orientation [Ref. 4.3, Chap. 1, Sect. 2.11] affect the amplitude of scattering by magnetic structures.

Different versions of ordering of atomic magnetic spins are possible. In one case it is achieved within the ordinary crystallographic, i.e., "chemical" unit cell of a given compound, which is determined by x-rays. Then the "magnetic" cell coincides with the "chemical", and the magnetic contribution to the intensities (4.209) is represented together with the nuclear, so that the nuclear contribution must be subtracted to determine the magnetic structure.

In another case the magnetic structure is described by a unit cell exceeding the ordinary "chemical" cell by some multiple, and the cell is superstructural with respect to the ordinary cell (Fig. 4.132). Then the magnetic contribution to scattering is manifested in the appearance of additional, purely "magnetic",

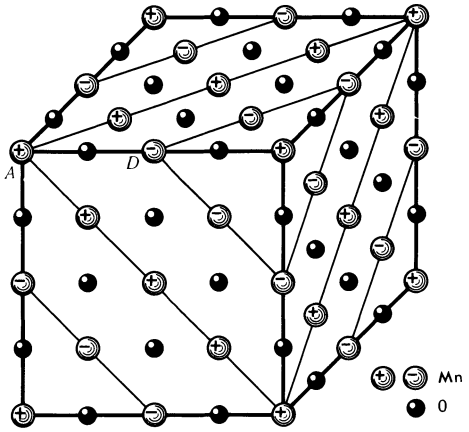

Fig. 4.132. Model of the magnetic structure of MnO. Magnetic moments of Mn atoms in positions A(+) and D(−) are antiparallel and lie in planes perpendicular to the [111] axis of the crystal. The linear dimensions of the magnetic cell are twice as large as those of the "chemical" one [4.167]

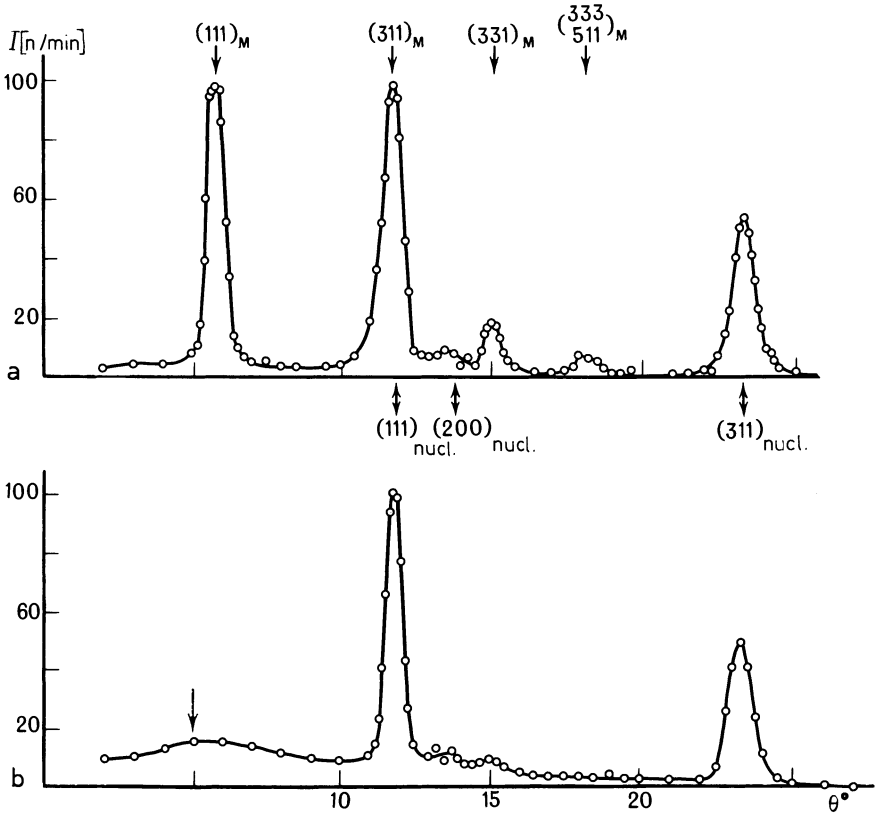

Fig. 4.133a,b. Neutron diffraction patterns from MnO powder at 80 (**a**) and 293 K (**b**) (below and above the Curie point). The low-temperature neutron diffraction pattern shows reflections due to neutron scattering by an increased unit cell (compared with the "chemical" one). The arrow indicates the effect on diffraction of the short-range residual magnetic ordering [4.167]

reflections due to the large magnetic cell and may be absent in the nuclear-scattering maxima (Fig. 4.133). In both cases when describing the magnetic symmetry, it is possible to use the space groups of antisymmetry $\Phi' \equiv \text{III}$ or color symmetry $\Phi^{(c)}$ and $\Phi^{(q)}$ (see Sect. 2.9) associated with the group Φ of the chemical structure.

Finally, in some kinds of helical ordering the period of the helix may not be commensurate with that of the "chemical" structure; then there is no correlation of ordinary symmetry Φ and the magnetic symmetry, which belongs to the type G_1^3. In this case the relevant magnetic reflections appear along the reciprocal space axis which corresponds to the axis of the helical magnetic ordering (Fig. 4.134).

Additional opportunites are created by using a beam of polarized monochromatic neutrons, which can be obtained by reflecting the primary beam from some magnetized ferromagnetic single crystals. Then the magnetic and nuclear contributions are separated more distinctly, and the details of the magnetic structure are revealed better than for nonpolarized neutrons.

Many classes of magnetic structures, phase transformations in them, the behaviour of spins near the Curie point, etc., have been studied with the aid of neutron diffraction analysis of magnetic materials [4.34].

The computation of the Fourier synthesis using the F_M of magnetic scattering gives the distribution of the spin density of the magnetic atoms. Figure 4.135 depicts such a pattern for a body-centered structure of α-Fe after the subtraction

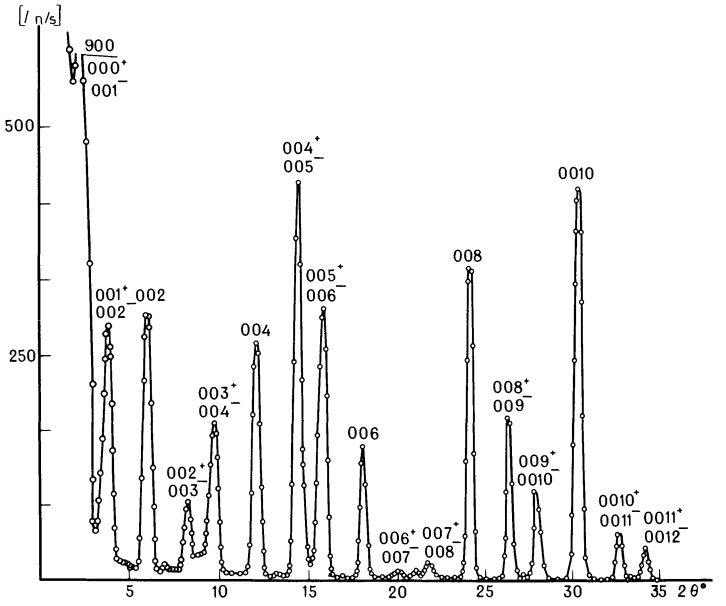

Fig. 4.134. Neutron diffraction pattern (reflections 00*l*) from a single crystal of $BaSc_{1.5}Fe_{10.5}O_{19}$ at 4.2 K, $\lambda = 1.22$ Å. The signs $^+$ and $^-$ mark the satellite magnetic reflections [4.168]

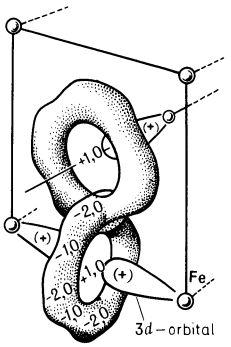

Fig. 4.135. Spin density distribution in α-Fe [4.169]

of the spherical component. The electrons of the shell of the Fe atom with an uncompensated spin in the α phase are distributed in a complicated manner. In addition to the positive areas due to 3*d* electrons, three-dimensional chains of annular regions of negative magnetization were revealed, which have not yet been interpreted unambiguously. Similar investigations were conducted for some other metals. As we see, they supply information on the distribution of the magnetic-shell electrons.

Inelastic coherent magnetic scattering of neutrons, which is similar to x-ray scattering by phonons, enables one to investigate magnons, i.e., spin waves in crystals.

4.11.4 Other Possibilities Offered by the Neutron-Diffraction Method

The energies of a thermal neutrons and of a lattice vibrations (phonons) are close to one another; therefore, an energy exchange between neutrons and the lattice, i.e., their inelastic scattering, takes place [4.170]. In the neutron-phonon interaction, energy can be transferred both from neutron to lattice and vice versa. Investigation into the angular and energy distribution of scattered neutrons is called neutron spectroscopy. Measurement of coherent inelastic scattering of neutrons from single crystals is an efficient tool in studying the phonon spectrum of a crystal and hence the atomic interaction forces responsible for this spectrum. Similar data can be obtained from inelastic incoherent scattering.

Neutron diffraction analysis, like the other diffraction methods, can be used for studying the structure of noncrystalline objects. When investigating amorphous solids, glasses, and liquids, the possibility of obtaining the scattering curves up to large values of $\sin\theta/\lambda$ is extremely valuable, because the drop of the curves is due only to the temperature factor, while the nuclear amplitudes b are constant. Therefore it is possible to obtain curves of the radial distribution for a given substance with a high accuracy.

New opportunities also open up for the use of small-angle neutron scattering. Changes in wavelength from 1 to 30 Å enable one to study nonuniformities of different sizes. The small-angle method helps to obtain data on the decomposition of metallic solid solutions of the iron group (of atoms with close

Z) and the formation of new phases in them, and also on the structure of glasses, the dislocation structure of metals, and the structure of polymers and biological objects.

In neutron scattering dynamic effects are also observed and used.

4.11.5 Diffraction of Mössbauer Radiation

Some nuclei, namely ^{57}Fe, ^{119}Sn, ^{125}Te, and others are sources of Mössbauer γ-radiation with an energy of 1–100 keV and, accordingly, wavelenghts λ from several to tenths of an angstrom. These are precisely the wavelengths that are used in classical x-ray analysis, and therefore diffraction of Mössbauer radiation from crystals can be used [4.171].

Mössbauer diffraction has a number of specific features. They are based primarily on the extremely small energy width of γ-quanta, about 10^{-8} eV (for the ordinary characteristic radiation of an x-ray tube this is about 1 eV). Therefore, along with the scattering by electrons of atomic shells, which is usual for x-rays, resonance scattering from nuclei is of no less importance. If a crystal contains Mössbauer nuclei, the phenomenon of excitation by the incident radiation of their respective levels and subsequent emission of γ quanta, which is actually resonance scattering, occurs with a time and space correlation unobtainable in other methods. The conditions of exact resonance may be disturbed by moving a source or a detector. Then observation of the Doppler effect makes it possible to determine the scattering amplitudes and phases experimentally (Fig. 4.136).

In distinction from ordinary x-ray scattering, where atomic amplitudes are scalar quantities depending on the electron density $\rho(\boldsymbol{r})$ of the atom and on the scattering angle, in Mössbauer diffraction the atomic amplitude f_M

$$f_M(\boldsymbol{k}, \boldsymbol{P}, \boldsymbol{k}_0, \boldsymbol{P}_0) = f_e(\boldsymbol{k}, \boldsymbol{P}, \boldsymbol{k}_0, \boldsymbol{P}_0) + f_R(\boldsymbol{k}, \boldsymbol{P}, \boldsymbol{k}_0, \boldsymbol{P}_0) \tag{4.211}$$

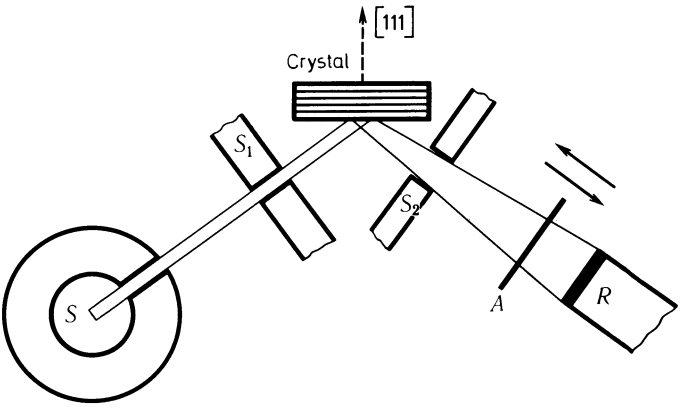

Fig. 4.136. Scheme of a setup for Mössbauer diffraction. (S) Mössbauer source; (S_1) and (S_2) collimators; (A) vibrating resonance absorber for measuring the Doppler effect; (R) detector

consists of an electron, f_e, and nuclear, f_n, components, which depend on the wave vectors $\boldsymbol{k}_0$ and $\boldsymbol{k}$ of the incident and scattered waves as well as on their polarization vectors $\boldsymbol{P}_0$ and $\boldsymbol{P}$ and are, in the general case, matrix quantities. The nucleus in a crystal is in the electric and magnetic fields of the surrounding atoms; its energy levels are thus split, which change f_n and hence f_M. The equations of diffraction from a crystal in the kinematic approximation acquire a very complicated form, and consideration of the dynamic effects is still more complicated. At the same time, owing to these specific features, a number of remarkable phenomena arise, which find ever-increasing application in the study of crystals. The potentialities of the method are, unfortunately, limited by the relatively weak intensity of Mössbauer sources (only tens of quanta per minute have to be counted) and their relatively short lifetime (the half-life of the sources is less than a year). Another limitation is the fact that the crystal under investigation must contain Mössbauer nuclei.

Thus the basic features of Mössbauer diffraction are as follows:

1) The possibility of experimental determination of the phases of structure amplitudes by observing $f_M = f_e + f_n$ at different (at least three) Doppler shifts. This has been done for the simplest structures, but similar projects are under way for more complicated structures, including proteins.
2) The possibility of studying the magnetic structure of crystals (which may supplement or replace neutron diffraction investigations), because f_n depends on the magnetic fields at the nucleus and the orientation of the atomic magnetic moment.
3) The dependence of Mössbauer scattering on the gradients of the electric field at the nuclei makes it possible to study these fine phenomena as well and determine, in particular, the different orientation of the tensors of this gradient at the crystal lattice points indistinguishable (equivalent) from the standpoint of ordinary symmetry. This can be described with the aid of color symmetry.

The collective interaction of crystal nuclei with the incident and scattered waves of Mössbauer radiation gives rise to a number of specific features, and the amplitudes of scattering from nuclei in the crystal become different in their energy characteristics from those for free nuclei. It turns out that interactions remain effective only in elastic scattering, whereas they are suppressed in inelastic scattering [4.172]. Therefore dynamic scattering at Bragg angles is accompanied by an anomalously high transmission, a γ-nuclear effect similar to the Borrmann effect in x-ray diffraction.

In scattering from crystals it is possible, by using the high energy resolution of Mössbauer detectors, to separate the elastic from inelastic components of the diffracted beams and use the latter to obtain information on lattice dynamics. This can be done even for crystals containing no Mössbauer nuclei.

Phenomena of coherent scattering of γ quanta also exhibit the effects of birefringence and optical activity.

Thus, the Mössbauer method is a promising line of crystal structure analysis. However, its wide application is still hindered by the scarcity of effective sources and by a number of experimental difficulties.

In conclusion, we wish to emphasize once more that all the diffraction methods, namely x-ray, electron and neutron analysis, and also the Mössbauer method, are very similar in regard to the essence of the phenomenon utilized – scattering of short waves in crystals or in noncrystalline substances – and the mathematical devices of the theory. But due to the differences in the physical nature of interaction with matter each method has its own field of application. In principle, all these methods are independent and each can be used separately for solving almost any structure problem, but in fact they often complement each other. One must naturally also take into consideration the differences in experimental realization, because each method has its own advantages and limitations. With due regard for all these features, one should choose the proper way to solve the problem at hand.

4.11.6 Particle Channeling and the Shadow Effect

Under certain conditions, the passage of heavy charged particles – protons, α-particles, and ions – through crystals with a simple structure is accompanied by phenomena which do not require wave treatment and are interpreted simply from the standpoint of classical mechanics [4.173]. If we inspect a crystal with a simple, e.g., close-packed structure, we see that the crystallographic planes in it are clearly defined physically; there are parallel planes which are occupied by atomic nuclei and the central parts of electron shells; they alternate with parallel "empty" regions with a low or zero electron density corresponding to the periphery of the atoms (Fig. 4.137). Obviously, both the "populated" and "empty" planes are most clearly evident at the small crystallographic indices, i.e., large spacings. Similarly, there are vacant "channels" and dense one-dimensional rows of atoms in radial directions with small axial indices.

The channeling phenomenon actually consists in the classical transmission of charged particles through a crystal along its vacant planes or axes, hence the terms "plane" and "axial" channeling. The atoms disposed on both sides of each vacant plane (or surrounding the axial channel) promote, by means of their electrostatic field, the passage of the particles precisely in these directions. The

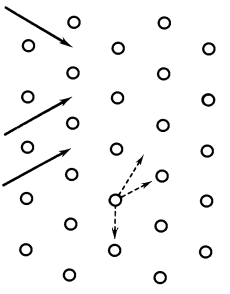

Fig. 4.137. Two-dimensional scheme of channeling and shadow phenomena. The atoms are denoted by circles. In channeling (*solid arrows*) the particles "slip" between the atoms. In the shadow effect (*dashed arrows*) the rational atomic rows impede the particle motion

particles can pass through the channels only if the angle of their entry into the channel does not exceed a certain value (of the order of 1°), which depends on the momentum, the atomic number ratio, and the interplanar distance.

The channeled particles, "slipping" along the periphery of atoms, interact with them only weakly. At the same time the unchanneled particles, which follow arbitrary directions, have much stronger interaction (nuclear or electron) with the atoms of a crystal.

Crystal defects hinder the channeling, and therefore this phenomenon can be used for their investigation.

The shadow effect can be regarded as the "negative" of the channeling. In this case the centers of emission of fast charged particles – protons, deuterons, and heavy ions-are the atoms of the crystal structure themselves. This effect can be achieved either by introducing α-radioactive nuclei into the lattice or by exciting nuclear reactions in the lattice atoms with the use of appropriate radiation. Since the atom (nucleus) itself is at the center of "populated" crystallographic planes, the particles emitted from it, encountering the greatest number of atoms along precisely these planes and other rational crystallographic planes and axial directions, cannot penetrate through them, and deflect from them. Thus, the angular distribution of particles leaving a single crystal will have sharp minima – "shadows" – along the emergences of crystallographic planes and axes with small indices. The shadow intensity is then equal to about 1% of the average intensity in the other directions. The shadow pattern recorded on a photographic plate (Fig. 4.138) (sometimes such patterns are called proton or ion pattern) is nothing else than a gnomonic projection of the crystal.

The shadow effect can be used for determining the orientation of crystals and thin single-crystal films, for studying lattice defects, and also for nuclear physics investigations.

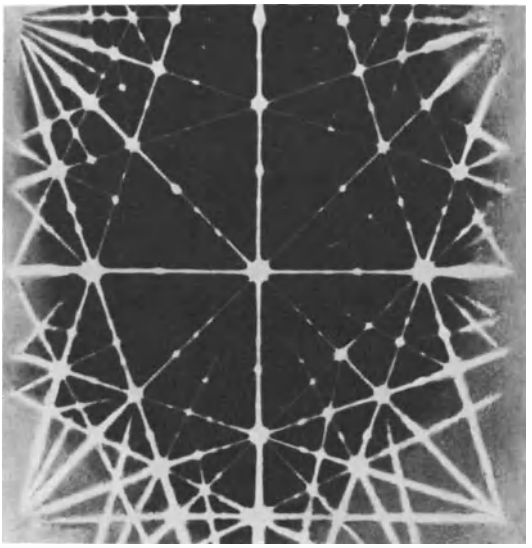

Fig. 4.138. Ion shadow pattern of a tungsten crystal (courtesy of A. F. Tulinov)

5. New Developments in Crystallography

5.1 Quasicrystals

5.1.1 The Discovery of Quasicrystals

In 1984 *Shechtman* et al. [5.1] investigated the structure of the rapidly cooled $Al_{86}M_{14}$ alloy by the method of electron diffraction. The diffraction patterns (Fig. 5.1) presented a system of reflections which, in reciprocal space, had an icosahedral $m\bar{5}m$ symmetry. This indicated that the structure of the alloy also had an icosahedral point symmetry.

For the majority of crystallographers the discovery was a complete surprise, as in the classical theory of crystal symmetry 5-fold rotation axes, being incompatible with the 3-dimensional translation symmetry of crystal structure, are forbidden; a fact that had been proved by hundreds of thousands of experiments.

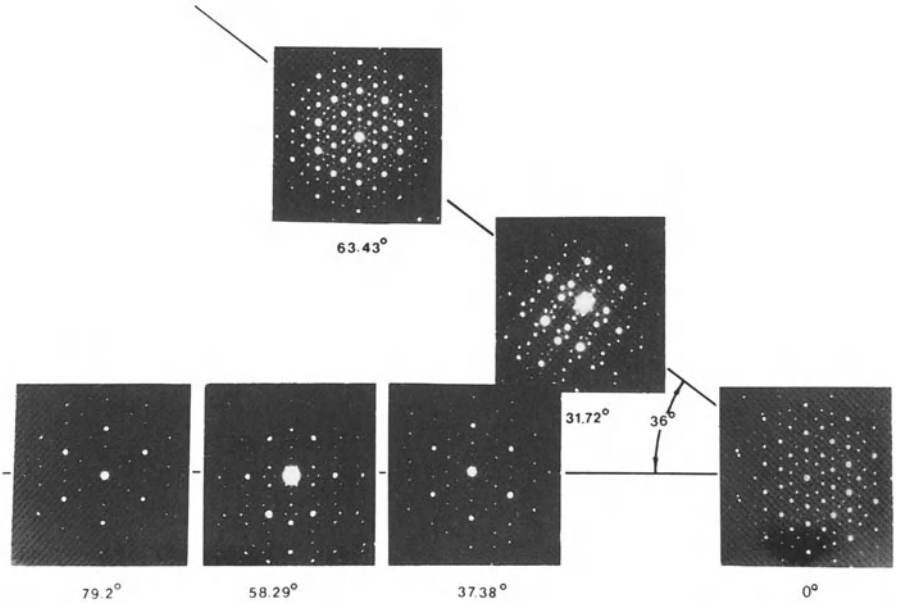

Fig. 5.1. Selected-area electron diffraction patterns taken from a single grain of the icosahedral phase at different angles of inclination. The initial (0°) and (63.43°) electron diffraction patterns indicate presence of 5-fold symmetry axes (see also Fig. 5.6)

Therefore, it became immediately clear that the observed structure could not possess a 3-dimensional translational symmetry, but at the same time had a high degree of ordering, as the observed Bragg reflections were rather sharp.

This structure, and similar structures of a number of other alloys studied later, was called a "quasicrystal". The discovery of quasicrystals caused the scientists to recall the remarkable work by *Penrose* [5.2] on a plane tiling with 5-fold axes of symmetry (Fig. 5.2a). This mosaic of Penrose is built of two rhombs (Fig. 5.2b) and has a specific quasiperiodicity and long-range order.

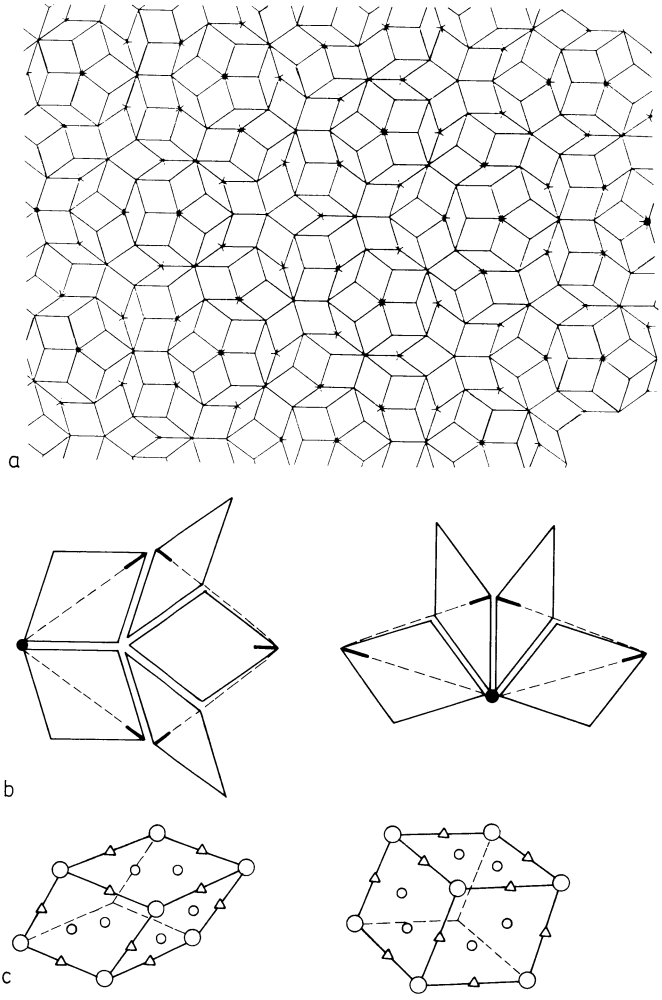

Fig. 5.2. Two-dimensional Penrose tiling (**a**) which is built of two rhombs marked by a dash (**b**) [5.3]; the dashes are needed for the local matching rules. Three-dimensional Penrose lattice can be built of two Ammann rhombohedra – acute and obtuse (**c**). Possible atomic sites in the rhombohedra [5.4] are marked with large circles (Mn atoms) and with triangles and small circles (Al atoms of different types)

Mackay [5.3, 5, 6] foresaw the possibility of a 5-fold symmetry in the atomic structure of matter. He used the 3-dimensional analogs of *Penrose*'s rhombus – two rhombohedra (Fig. 5.2c) acute and obtuse, discovered by Ammann, which fill the 3-dimensional space without gaps (3-dimensional tiling) with 5-fold symmetry (a rhombic triacontahedron – a polyhedron possessing 5-fold (see below Fig. 5.9) symmetry with 30 faces, 32 vertices and 60 edges – could be built with such rhombohedra (ten of each type)) to build a crystal-like structure and showed that diffraction from the Penrose tiling consisted of sharp spots.

After the article of Shechtman and co-workers, along with many alloys with icosahedral symmetry, uniaxial structures with 8-, 10-, and 12-fold axes were observed.

The discovery of a quasicrystalline state of matter caused crystallographers, mathematicians and physicists to change their traditional concepts of the structure of solids. An avalanche of experimental and theoretical investigations followed. Now the situation is stable and a continuous acquisition of knowledge is proceeding, many reviews and books have been written [5.5–10] and, though several major problems remain unsolved, we can already speak of the birth of a new paradigm—the quasicrystalline state of matter.

Let us consider the main concepts in the present-day theory of the quasicrystalline state, which, as it turns out, can be built on the basis of projections of n-dimensional periodic space onto a space of lower dimension.

5.1.2 The Non-Traditional Symmetry of Aperiodic Objects

Symmetry operations in infinite figures can work in a rather unusual way. The founding fathers of crystallography probably suspected this, as E. S. Fedorov in his famous work devoted to the derivation of the 230 space groups wrote: "... I shall not derive all types of symmetry of infinite figures, but only for those of them which are called 'regular systems of figures'" [5.11]. This approach gave rise to the traditional translation symmetry – the three-dimensional periodicity of crystals. But, as we have already seen in the example of the Penrose pattern, the existence of aperiodic infinite structures with a certain translation ordering is possible, in the sense that a certain law exists according to which structure elements are positioned in space.

Particular cases of aperiodic objects are provided by those objects which can be described by the almost periodic functions introduced in 1924 by *Bohr* [5.14]. A spatially-continuous function $F(x)$ (so far only one-dimensional objects are being considered) is called almost periodic if it can be described by the following infinite series (but not by a Fourier integral, as is the case for arbitrary aperiodic functions):

$$F(x) = \sum_n f_n \exp(2\pi i x \lambda_n), \tag{5.1}$$

where an infinite set of arbitrary real numbers λ_n (the Fourier spectrum of the function $F(x)$) is a countable set. For an almost periodic function $F(x)$ instead of

translation invariance, see (2.2), there is the requirement for the smallest possible changes during translation. That is, for any smallest possible value ε there is a final translation t such that for all points x

$$|F(x') - F(x)| \leqslant \varepsilon, \tag{5.2}$$

where $x' = x + t$. From a physical viewpoint it is clear that for almost periodic objects diffraction will produce a discrete system of reflections in accordance with the discrete character of the Fourier spectrum λ_n. Particular cases of almost periodic functions are the periodic functions for which the set λ_n is a simple set of integer numbers.

Of still greater importance is the case of the so-called *quasiperiodic functions* for which each λ_n of the infinite Fourier spectrum can be represented as a superposition of a finite number of irrational numbers $\alpha_k (k = 1, 2, \ldots N)$ with integer coefficients p_{nk}:

$$\lambda_n = \sum_{k=1}^{N} p_{nk}\alpha_k. \tag{5.3}$$

In this case instead of (5.1) a periodic function $\varkappa(x_1, x_2, \ldots x_n)$ in an N-dimensional space we can introduce:

$$\varkappa(x_1, x_2, \ldots x_N) = \sum_n f_n \exp\left[2\pi i(x_1 p_{n1} + x_2 p_{n2} + \cdots + x_N p_{nN})\right]. \tag{5.4}$$

The numbers p_{nk} can be regarded as Miller indices. The quasiperiodic function $F(x)$ appears as a cross-section of the periodic function $\varkappa(x_1, x_2, \ldots x_N)$ by a straight line $x_1 = \alpha_1 x$, $x_2 = \alpha_2 x$, $\ldots$, $x_N = \alpha_N x$ in a N-dimensional space:

$$F(x) = \varkappa(\alpha_1 x, \alpha_2 x, \ldots \alpha_N x). \tag{5.5}$$

Therefore, quasiperiodic functions are naturally connected with periodic functions in a higher-dimensional space (the latter is called the superspace).

After these definitions have been introduced, it is natural to consider their possible generalization and modification. First we can make a cut through N-dimensional space by a space of any dimensionality $d < N$ and produce d-dimensional quasiperiodic structures (let us assume that $d = 1, 2, 3$ to obtain structures which could be realized in our 3-dimensional space). In this case the cutting subspace is called a parallel space ($d_\parallel = d$), and the orthogonal subspace – a perpendicular space ($d_\perp = N - d_\parallel$). In 2- and 3-dimensional quasiperiodic objects, rotational elements of symmetry are also possible, i.e., in a general case the inequality (5.2) can be meaningful at $\boldsymbol{x}' = g\boldsymbol{x} + \boldsymbol{t}$, g being the rotation matrix for the angle $2\pi/m$. It is important that in quasiperiodic structures m can assume any value, and not only the integers 1, 2, 3, 4, 6, as would be the case for crystals.

Besides continuous quasiperiodic functions, their discrete analogs of different dimensionality can be considered. These are called tilings or quasilattices. In this case during translation and/or rotation operations of symmetry instead of (5.2), a condition is introduced that $F(\boldsymbol{x}')$ and $F(\boldsymbol{x})$ should coincide almost everywhere, that is, the relative number of points where $F(\boldsymbol{x}')$ and $F(\boldsymbol{x})$ do not

coincide should be less than ε. To produce tilings or quasilattices the so-called "strip" (or cut-projection) method is used. In the strip method a region in N-dimensional space is selected, which is limited by perpendicular space, and the points of the N-dimensional lattice which fall within the strip are projected onto the parallel space. As a result, in the parallel space there appears a quasiperiodic lattice where the density of the points depends on the strip size in perpendicular space. There are other techniques for generating quasiperiodic structures, which do not involve operations with multidimensional space. For example, the classification of space groups of quasicrystals can be carried out with the use of the symmetry of Fourier harmonics and Fourier spectra of the quasicrystal density $\rho(\boldsymbol{x})$.

5.1.3 The One-Dimensional Quasicrystal (d = 1, N = 2)

A simple 1-dimensional model allows us to demonstrate, in a complete and clear manner, many peculiarities of those quasicrystal structures which exist in 2 or 3 dimensions. A 1-dimensional quasicrystal can be described by a projection onto physical axis $x_{\parallel}$ of those points of a 2-dimensional square lattice (Fig. 5.3) which fall within a band ("strip") with an irrational slope of the lines. In Fig. 5.3 the tangent of the slope strip measured with respect to the axis x_2 equals the golden mean $\tau = (1 + \sqrt{5})/2 = 1.618034\ldots$, and the strip width corresponds to the size of the unit cell of the square lattice. After projection (shown for one

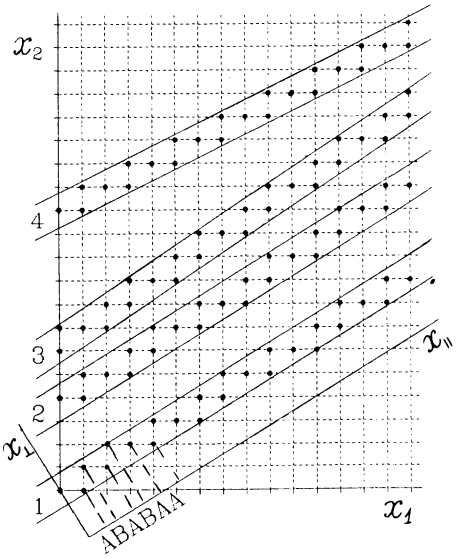

4 – ABAABAABAABAABAABAABAABA
3 – BAABABAABABAABABAABABAAB
2 – ABAABABAABAABABAABABAABA
1 – ABABAABAABABAABAABABAABA

Fig. 5.3. One-dimensional quasiperiodic lattices (1 and 2) and their rational (periodic) approximants (3 and 4) obtained as the projections from two-dimensional square lattice

case only) onto the axis $x_{\parallel}$, there appears a quasiperiodic sequence of long and short linear sections A and B forming the Fibonacci sequence (Fibonacci discussed the propagation of adult and baby rabbits generation by generation).

First of all let us note that by moving the strip along $x_{\perp}$ (as the bands 1, 2 in Fig. 5.3) we can generate an infinite number of different quasiperiodic sequences. Such a movement is called a uniform phasonic shift. But, if we adhere to the definition of translation invariance given above, all these sequences should be regarded as similar. Indeed, it can be shown that for any two sequences there is a physical translation (i.e., a translation along the x_{φ} axis) after which the density of points in which these sequences do not coincide can be infinitely small.

On a uniform phasonic shift there occurs a replacement of neighbouring sections of A and B in an infinite number of points; the shift decreases with a decrease of the point density. Still, at present there are models in which the atoms are not replaced during phasonic shift but are continuously changing their positions.

Besides translation symmetry, the quasicrystal sequences possess scale invariance, i.e. similarity symmetry. In fact, a substitution of sections A by A′B′, and sections B by A′ results in quasiperiodic sequence of sections A′ and B′ which are τ times shorter than A and B. It is clear that such replacement can be carried out many times both to make sections A and B longer or shorter (such transformations are called inflation and deflation). A single section (e.g., A) can thus give rise to a whole quasicrystalline sequence after an infinite number of transformations of the type $A \rightarrow AB$, $B \rightarrow A$. Therefore, we can conclude that quasicrystals can be invariant under inflation and deflation, and appear identical in different scale (the latter property is characteristic of the so-called fractal structures). It should be noted that unlike the traditional similarity system (Sect. 2.9.6), quasicrystals do not have, generally speaking, a special point, and inflation (or deflation) occurs uniformly in the whole space.

The sequences shown in Fig. 5.3 have centres of inversion. Structure 1 has in point $x_{\parallel} = 0$ an inversion centre in the traditional crystallographic sense (that is because the centre of strip 1 coincides with the point (0, 0)). Evidently, such a true inversion centre should disappear after an infinitesimal phasonic shift of the strip, and quasicrystal sequences generally have an infinite number of inversion centres, in the same sense as in the case of translations, see (5.2).

Apart from global symmetry, quasicrystal sequences exhibit local symmetry. That is, if an arbitrary section of length L is selected in this sequence, we shall find an infinite number of such sections, the nearest being at a distance not exceeding L.

5.1.4 Fourier Transform of Quasiperiodic Sequences

To obtain a Fourier spectrum we must calculate the transform for the 2-dimensional crystal limited by a strip (for periodic structures this has been discussed in Sect. 4.2.1), and project all reciprocal lattice vectors onto the axis $x_{\parallel}$.

Evidently all points of the reciprocal lattice in 2-dimensional space will appear as infinitely narrow (of δ-function type) in the $x_{\|}$ direction, and in the $x_{\perp}$ direction will have a width inverse to that of the strip. Projection onto the axis x_{φ} of any reciprocal lattice vector will give

$$k_{\varphi} = \frac{(h'\tau + h)}{a\sqrt{1 + \tau^2}}, \tag{5.6}$$

where a is the unit-cell size of the 2-dimensional lattice, and h' and h are the Miller indices for the 2-dimensional reciprocal lattice. Naturally, (5.6) is an analog of (5.3) with $N = 2$. Numbers of the type (5.6) densely fill the whole axis, i.e. any real number can be approximated by (5.6) with infinite accuracy, but usually in quasicrystals only reflections with relatively small h' and h have noticeable intensity, and the experiments produce a discrete system of reflections of the type (5.6). Thus, using two integers, any vector in the reciprocal lattice can be indexed, but in quasicrystal structures such indexing is essentially ambiguous, as a result of scale invariance of such structures. In fact, in space $x_{\|}$ we do not a priori know the size of the unit cell in 2-dimensional space; should we choose it, e.g. τ times larger than in (5.6) ($a_1 = \tau a$), then $k_{\|}$ can be written as

$$k_{\|} = \frac{(m'\tau + m)}{(a_1\sqrt{1 + \tau^2})}, \tag{5.7}$$

where m' and m are related to h' and h as $m' = h' + h, m = h'$. Another peculiarity of quasicrystals is the change of phases of the structure amplitudes $F_{h'h}$ during the phasonic shift x_1 of the strip:

$$F_{h'h} \rightarrow F_{h'h} \exp(\mathrm{i}k_{\perp}x_{\perp}), \tag{5.8}$$

where the perpendicular component of wave vector $k_{\perp}$ is:

$$k_{\perp} = \frac{(h' - \tau h)}{(a\sqrt{1 + \tau^2})}. \tag{5.9}$$

Thus the phase problem of quasicrystals is less trivial than that of crystals.

Apart from a uniform phasonic shift, it is interesting to see the consequences of a non-uniform displacement, i.e. one depending on the $x_{\|}$ coordinate; in this case it is called phason deformation. The simplest example of a phason deformation is the change in the strip slope (i.e., $x_{\perp}$ in proportion to $x_{\|}$). If the slope tangent is irrational (but not equal to τ), we obtain a quasiperiodic structure without scale invariance. If it is rational, we obtain periodic structures (possibly with a very large period). These structures are called crystal approximants or just approximants, as they closely approximate quasiperiodic structures. Especially useful approximants (n-order Fibonacci approximants) arise if the slope tangent equals the ratio of Fibonacci numbers, F_{n+1}/F_n (see strips 3, 4 in Fig. 5.3). Fibonacci numbers are generated by the recurrence relation $F_{n+1} = F_n + F_{n-1}$, where $F_1 = 1$ and $F_2 = 1$ give the Fibonacci sequence ($F_i = 1, 1, 2, 3, 5, 8, 13, 21, 34, \ldots$.). The ratio of Fibonacci numbers, F_{n+1}/F_n,

approximates τ better than other rational numbers with a comparable denominator value, and therefore Fibonacci approximants are close to quasicrystals in their local structure. For example, any n-order approximant coincides with some part of the quasicrystal sequence for the length of more than two periods (approximately F_{n+4} elements of A and B). On the scale transformation A → AB, B → A, the order of approximants increases by a step. Thus a quasicrystal can be regarded as a limit to an infinite number of such transformations.

In the three-dimensional case there is a number of crystals approximants. This explains a great number of works in which the structure of a quasicrystal under study is treated like that of an ordinary 3-dimensional crystal with a large unit cell. This approach certainly promotes the understanding of the structure of real quasicrystals.

5.1.5 Two-Dimensional Quasicrystals and Their Symmetry (d = 2, N = 3, 4, 5, . . .)

As compared with 1-dimensional quasicrystals, in 2-dimensional space only the possibility of having rotation elements of symmetry is added. It is the existence of non-crystallographic rotation axes in 2-dimensional and 3-dimensional cases, however, that was most unexpected from the viewpoint of traditional crystallography. In 2-dimensional quasicrystals any rotation axes of symmetry can exist; Fig. 5.2a gives an example of a 2-dimensional crystal lattice (Penrose tiling), another example is given in Fig. 5.4.

At present there is evidently no complete theory of the possible space groups of symmetry in 2-dimensional quasicrystals, but *Rokhsar* and co-workers [5.16, 17] have developed a classification of 2-dimensional quasicrystal lattices (analogs of the 2-dimensional Bravais lattices) and the corresponding 2-dimensional space groups with practically all orders of rotation axes.

First of all, there are lattices with non-periodicity arising from point-group symmetry (5-, 7-fold axes, etc.). If we invoke this restriction, then the number of basic vectors necessary for indexing should be a minimum for a given point group, such lattices will be called quasicrystalline. Other non-periodic lattices which can be regarded as superpositions of quasicrystal and/or periodic lattices (and these structures are quite numerous) are called "incommensurately modulated structures".

The proposed classification of 2-dimensional groups is not based on the concepts of multidimensional crystallography, but evolves from the analysis of symmetry in diffraction patterns and reciprocal space. First, a 2-dimensional "standard lattice" with N-fold rotation symmetry is introduced, presenting a set of all possible linear combinations (with integer coefficients) of N basic vectors of equal length divided by angles $2\pi/N$. With non-crystallographic numbers $N = 5, 7, 8, \ldots$ such a lattice densely covers the 2-dimensional plane, but this is of no importance in the reciprocal space as (unlike in real space) it does not demand a minimum distance between the lattice points. If we present the points of a 2-dimensional lattice as points belonging to such a complex plane, the

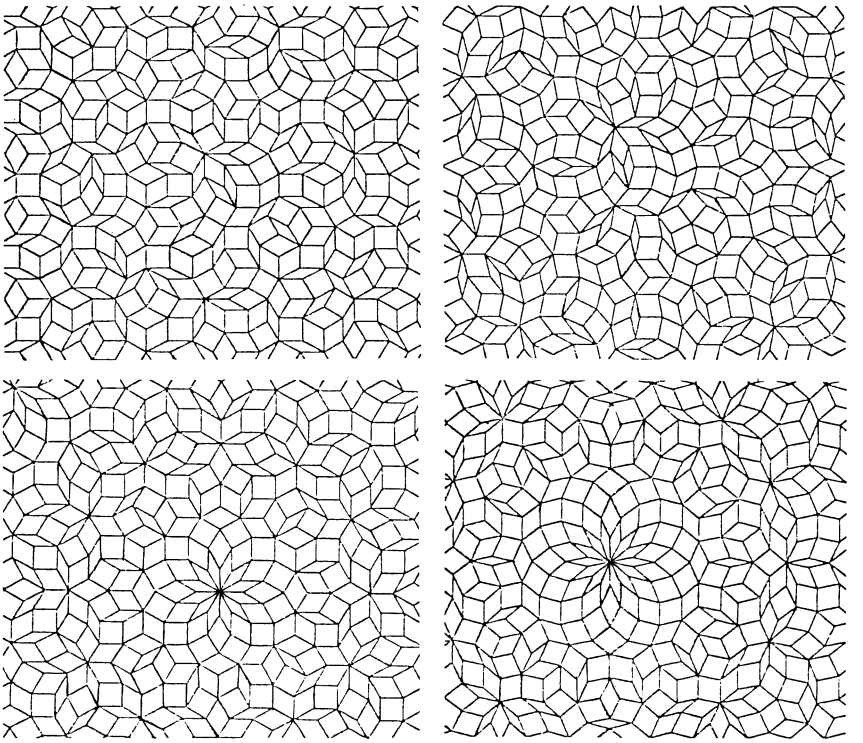

Fig. 5.4. Two-dimensional quasiperiodic tilings with 12-fold symmetry (left side) and 14-fold symmetry (right side). Upper and lower parts correspond to different types of projections from high-dimensional lattices [5.15]

standard lattice will be equivalent to the set Z_N of all linear combinations (with integer coefficients) of N-power roots of 1; in particular, Z_3 and Z_6 are equivalent to square and hexagonal Bravais lattices 4*mm* and 6*mm*. This equivalence allows us to apply methods of the algebraic theory of numbers, which is used to prove that with $N < 46$ any 2-dimensional lattice is equivalent to a standard one (or, if $N > 46$ – to several lattices). Further analysis of space groups is carried out only for structures with standard lattices, with the order of the rotation axes in the space groups $N < 23$ (as with odd values of N the lattice has a $2n$-fold axis). Still, this analysis takes care of all the most important cases.

The spatial distribution of density of any (quasi)crystal structure can be written as Fourier series, see. (5.1), of the vectors $\boldsymbol{k}$ of the standard reciprocal lattice:

$$\rho(\boldsymbol{r}) = \sum_{\boldsymbol{k}} \rho(\boldsymbol{k}) \exp(2\pi i \boldsymbol{k}\boldsymbol{r}). \tag{5.10}$$

If the function $\rho(\boldsymbol{k})$ is invariant relative to crystallographic space group (i.e., $\rho(g\boldsymbol{r} + \boldsymbol{t}_g) = \rho(\boldsymbol{r})$, where g is the symmetry operation of the point group, and

is t_g the corresponding translation) the Fourier components $\rho(k)$ will satisfy the relation

$$\rho(kg) = \rho(k)\exp[2\pi i(kgt_g)]. \tag{5.11}$$

Point group symmetry provides for the equality of reflection intensities, but not of the phases of the Fourier harmonics $\rho(kg)$ and $\rho(k)$, and therefore in non-periodic structures another equation is generally used:

$$\rho(kg) = \rho(k)\exp[-2\pi i\Phi_g(k)], \tag{5.12}$$

where $\Phi_g(k)$ is called the phase function. Further analysis of the space groups presents the analysis of all possible phase functions. This approach has been known for a long time for Fedorov groups [5.18]. It turns out that with a certain gauge transformation all the phases Φ_g can be reduced to zero for all rotation elements of symmetry ($\Phi_r = 0$), whereas for the reflection elements (if they are present in the space group) we can obtain $\Phi_m = 0$ or $\Phi_m = 1/2$. In multidimensional terms such gauge transformation includes both translation in physical space and the uniform phasonic shift (roughly speaking, after transformation the strip is placed in the most symmetrical way). For example, in a quasiperiodic structure 1 (Fig. 5.3) we have $\Phi_m = 0$ for inversion relative to the point $x_{\parallel} = 0$, while in structure 2 such a point is absent. The value of $\Phi_m = 1/2$ is possible only when $N = 2^j$; in this case there are two groups – symmorphic ($pNmm$) and non-symmorphic ($pNgm$) (Fig. 5.5), the same as for the square Bravais lattice ($N = 2^2$) where there are the groups $p4mm$ and $p4gm$ (Fig. 2.56). Naturally, in non-symmorphic groups $pNgm$, a systematic extinction of the reflections is observed. A list of two-dimensional space groups with $N < 23$ is given in Table 5.1.

Though a description of 2-dimensional quasicrystals with the help of standard lattices is fairly convenient for their classification, it is not minimal and we can always find a basis with a number of vectors less than N. In a general case

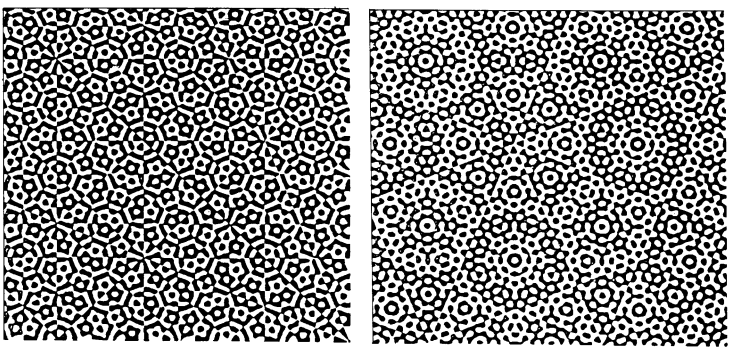

Fig. 5.5a,b. Two-dimensional quasicrystal structures with symmorphic (**a**) and non-symmorphic (**b**) space groups $p8mm$ and $p8gm$, respectively [5.16]

Table 5.1. Two-dimensional space groups of quasicrystals (Rokhsar et al.) [5.16]

	Point group	Lattice	Space group	Φ_r	Φ_m
N even	N	Z_N	pN	0	—
	Nmm	Z_N	$pNmm$	0	0
$N = 2^j$	Nmm	Z_N	$pNgm$	0	1/2
N odd	N	Z_{2N}	pN	0	—
$N \neq p^s$	Nm	Z_{2N}	pNm	0	0
$N = p^s$	$Nm1$	Z_{2N}	$pNm1$	0	0
$N = p^s$	$N1m$	Z_{2N}	$pN1m$	0	0

the minimal basis contains $\phi(N)$ vectors, where Euler's function $\phi(N)$ equals the number of integers from 1 to $N-1$ which are mutually prime to N. In multidimensional terms it means that the minimal dimensionality of the superspace in which a periodic Bravais lattice is compatible with N-fold rotation axis equals $\phi(N)$ [5.19]. It is interesting to note that for all observed 2-dimensional quasilattices (octagonal $N = 8$, decagonal $N = 10$, and dodecagonal $N = 12$) the value of $\phi(N)$ is the same: $\phi(8) = \phi(10) = \phi(12) = 4$, and they can therefore be obtained as projections of 4-d periodic lattices. For indexing reflections $\phi(N)$ Miller indices are sufficient, but a more symmetrical indexing with N indices is usually chosen.

5.1.6 Three-Dimensional Quasicrystals (d = 3, N = 4, 5, 6, . . .)

It is reasonable to distinguish quasicrystals, as has been done for the 2-dimensional case, from the whole multitude of quasiperiodic structures. (As quasicrystals we classify only those structures the non-periodicity of which is conditioned by a non-crystallographic point group). In the 3-dimensional case quasicrystals have either a monoaxial structure with 5-, 7- or higher-fold axes and can be described as various stackings of tiles of 2-dimensional crystals [5.17], or the icosahedral point group. The latter case is most interesting and a great number of publications is devoted to it. This is the case we will consider below.

The icosahedral point groups 532-Y and $m\bar{5}m$-Y_h contain rotation 5-, 3-, and 2-fold axes, and Y_h also has the mirror planes m; the positions of symmetry elements in the group $m\bar{5}m$ are shown in Fig. 5.6 (see also Fig. 2.1). These groups are non-crystallographic and therefore the long-range order in such a point group can only be quasiperiodic.

We must note that in quasicrystals – both 2- and 3-dimensional, there exists a rigid long-range orientation order. It is defined as the similar orientation of geometrical structure elements like, e.g., Penrose rhombs that fill the 2-dimensional space, or rhombohedra in 3-dimensional space. There are, in accordance with $5m$ symmetry of 2-dimensional space, 10 orientations for each of the two kinds of rhombs, and only these orientations are repeated everywhere, with all decahedra having the same orientation (Fig. 5.2a). In 3-dimensional space

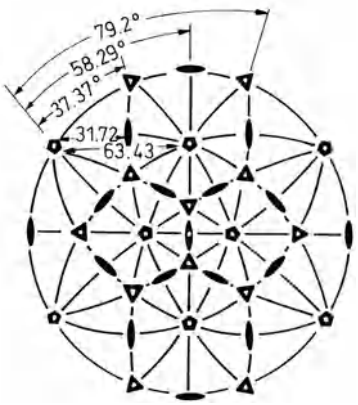

Fig. 5.6. Stereographic projection of the symmetry elements of the icosahedral point group [5.1]

with $m\bar{5}m$ symmetry there are 60 orientations for each of the two kinds of rhombohedra which are repeated everywhere. In this sense, the long-range orientation order is realised by mutual orientation of atoms in 3-dimensional quasicrystals, e.g., on "decoration" with atoms filling the rhombohedra space, as is shown in Fig. 5.2b. The existence of pseudoperiodic, rigid, long-range orientational order is proved by the regular habit of the observed quasicrystal grains (Fig. 5.7). It is interesting to note that long-range orientation order is also observed in a different class of ordered condensed substances, the so-called hexatic liquid crystals [Ref. 5.20, Sect 6.9].

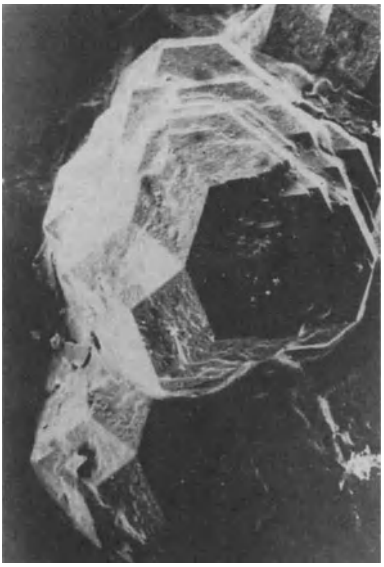

Fig. 5.7. Single grain of icosahedral quasicrystal [5.20]

Different approaches were used by *Janssen* [5.22], *Levitov* and *Rhyner* [5.19], and *Rokhsar* et al. [5.23] to determine the possible space groups of icosahedral symmetry. It turned out that quasicrystals with point symmetry Y and Y_h can have Bravais lattices of three types (primitive, body-centered and face-centered) and relatively few (only 11) non-equivalent space groups.

The minimum dimensionality of the space in which a periodic lattice is compatible with icosahedral point symmetry is six; therefore, at least six basic vectors and six Miller indices are required for indexing reflections in electron diffraction patterns. Six rational independent vectors directed along 5-fold axes, i.e. towards icosahedra vertices, are usually chosen for basic vectors (Fig. 5.8). Still, it is possible to use six rationally independent vectors directed along 3-fold axes (i.e., towards dodecahedra vertices) or 2-fold axes. The vectors $\boldsymbol{e}_1, \ldots, \boldsymbol{e}_6$ shown in Fig. 5.8 have the Miller indices (100000), . . . , (000001), and in the Cartesian system of coordinates are written as

$$\boldsymbol{e}_1 = A(0, -1, \tau); \quad \boldsymbol{e}_2 = A(0, 1, \tau); \quad \boldsymbol{e}_3 = A(-\tau, 0, 1);$$

$$\boldsymbol{e}_4 = A(-1, -\tau, 0); \quad \boldsymbol{e}_5 = A(1, -\tau, 0); \quad \boldsymbol{e}_6 = A(\tau, 0, 1). \tag{5.13}$$

The length of the vectors $\boldsymbol{e}_i$ is determined by the interplanar distance d_0 of the corresponding reflections ($|\boldsymbol{e}_i| = A\sqrt{1+\tau^2} = 2\pi/d_0$) and can be expressed through the unit-cell size of a 6-dimensional cube (the choice of the latter, as we shall see below, is ambiguous).

Using the basic vectors $\boldsymbol{e}_1, \ldots, \boldsymbol{e}_6$, it is easy to write the matrices A_5 and A_3 of the icosahedral point group which correspond to rotations by 5- and

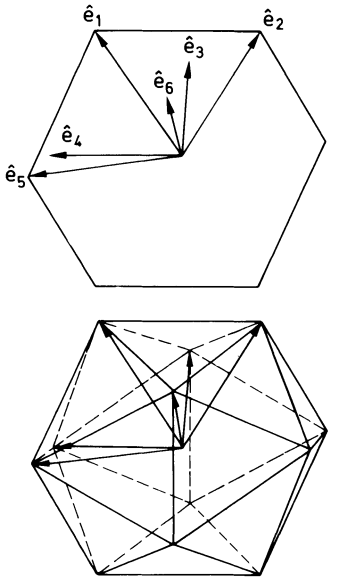

Fig. 5.8. A possible set of basic vectors in icosahedral quasicrystals [5.17]

3-fold axes (compare with 3-dimensional case, Table 2.5):

$$A_5 = \begin{vmatrix} 1 & 0 & 0 & 0 & 0 & 0 \\ 0 & 0 & 0 & 0 & 0 & 1 \\ 0 & 1 & 0 & 0 & 0 & 0 \\ 0 & 0 & 1 & 0 & 0 & 0 \\ 0 & 0 & 0 & 1 & 0 & 0 \\ 0 & 0 & 0 & 0 & 1 & 0 \end{vmatrix} \quad A_3 = \begin{vmatrix} 0 & 0 & 1 & 0 & 0 & 0 \\ 1 & 0 & 0 & 0 & 0 & 0 \\ 0 & 1 & 0 & 0 & 0 & 0 \\ 0 & 0 & 0 & 0 & -1 & 0 \\ 0 & 0 & 0 & 0 & 0 & -1 \\ 0 & 0 & 0 & 1 & 0 & 0 \end{vmatrix}. \tag{5.14}$$

Any vector of the quasicrystal reciprocal lattice is a superposition of basic vectors with integer coefficients (6-d Miller indices):

$$\boldsymbol{h} = (h_1, h_2, h_3, h_4, h_5, h_6) = \sum_{i=1}^{6} h_i \boldsymbol{e}_i. \tag{5.15}$$

If the lattice is primitive, then h_i denotes any integer. If it is body-centered, then $\sum h_i$ is an even number, and in a face-centered lattice all h_i in (5.15) have similar parity. Besides systematic extinctions connected with centering of the lattices, extinctions which are connected with screw axes and gliding planes are also possible.

As for 1- and 2-dimensional crystals, there occur inflation and deflation similarity symmetry and positions of reflections, with the similarity coefficient being equal to τ^n if $\sum h_i$ is even, and τ^{3n} if it is odd, n being any integer (the latter case can evidently exist only in a primitive lattice). The similarity symmetry τ^n is clearly seen in Fig. 5.1.

Indexing of icosahedral reflections should be done with care as, e.g., the reflections (101000) and (010100) are non-equivalent in 3-dimensional space and have different lengths. Moreover, different scientists select different directions for the basic vectors. Besides, similarity symmetry provides some freedom in the selection of the length of basic vectors, as in the 1-dimensional case discussed earlier (Fig. 5.1 gives only one way of indexing).

Space groups of quasicrystals with icosahedral symmetry can be symmorphic and non-symmorphic; if the point group is Y, then non-symmorphic groups contain 5-fold screw axes (2- and 3-fold screw axes are absent); if the point group is Y_h, then its non-symmorphic character is determined by the existence of glide planes.

In the derivation of the full set of possible space groups with icosahedral symmetry the problem of their abstract equivalence—isomorphism—is of great importance. It has been shown by *Levitov* and *Rhyner* [5.19], and *Rokhsar* et al. [5.23] that beside equivalence of enantio-isomorphous pairs (i.e., structures transforming into one another by mirror reflection) usual in crystallography, in quasicrystals space groups can be isomorphous as the result of scale transformations (inflation and deflation). As a result, groups with the screw axes $5_1, 5_2, 5_3, 5_4$ are abstractly isomorphous, and the list of such groups can be rather short (see Table 5.2, in which the corresponding extinction rules are given).

Table 5.2. The list of the three-dimensional icosahedral space groups for the two icosahedral point groups $Y(532)$ and $Y_h(\bar{5}\bar{3}m)$ [5.23]. The symbols P^*, F^*, and I^* refer to the primitive, face-centered, and body-centered lattices, where the asterisk indicates that the lattices are in wave-vector space. The notation $2/q$ indicates the presence of (quasi-) glide planes perpendicular to the twofold axes.

Point group	Space group	Phase functions of generators	Indices of extinct points
532	P^*532	$\phi_u = \phi_t = 0$	
	P^*5_132	$\phi_u = (00\frac{4}{5}\frac{4}{5}0\,\frac{1}{5})$, $\phi_t = (\frac{1}{5}\,00000)$	$(hkk\,kkk)$, $h \neq 5n$
	F^*532	$\phi_u = \phi_t = 0$	
	F^*5_132	$\phi_u = (\frac{1}{5}\,0\,\frac{1}{5}\,\frac{1}{5}\,00)$, $\phi_t = (\frac{1}{5}\,00\,000)$	$(hkk\,kkk)$, $h \neq 5n$
	I^*532	$\phi_u = \phi_t = 0$	
	I^*5_132	$\phi_u = (\frac{4}{5}\,0\,\frac{3}{5}\,\frac{3}{5}\,0\,\frac{2}{5})$, $\phi_t = (\frac{1}{5}\,00\,000)$	$(hkk\,kkk)$, $h \neq 5n$
$\bar{5}\bar{3}^2_m$ $(\bar{5}\bar{3}m)$	$P^*\bar{5}\bar{3}^2_m$	$\phi_u = \phi_t = 0$	
	$P^*\bar{5}\bar{3}^2_q$	$\phi_u = (000\,\frac{1}{2}\,\frac{1}{2}\,0)$, $\phi_r = 0$	$(h\bar{h}k,\ lm\bar{k})$, $1 + m$ odd
	$F^*\bar{5}\bar{3}^2_m$	$\phi_u = \phi_t = 0$	
	$I^*\bar{5}\bar{3}^2_m$	$\phi_u = \phi_t = 0$	
	$I^*\bar{5}\bar{3}^2_q$	$\phi_u = (0\,\frac{1}{2}\,0\,000)$, $\phi_t = 0$	$(h, \bar{h}, \bar{h} + k, l, m, \bar{k})$, h odd

Still, as in the theory of crystallographic groups, enantiomorphous pairs are geometrically different (though abstractly isomorphous), for quasicrystals it is reasonable to distinguish structures with the screw axes 5_1, 5_2, 5_3, 5_4, e.g., by standardising a set of basic vectors. This is also important because such structures could also be differentiated by their physical properties (e.g., by the sign and rotation of the plane of polarization, or their polarization properties for x-ray and Mössbauer reflections).

5.1.7 Structure Analysis of Quasicrystals

The problem of constructing non-periodic tilings and quasilattices with real atoms and molecules had been discussed by *Penrose* [5.2] and *Mackay* [5.3, 5] long before the discovery of quasicrystals.

From an experimental viewpoint, the methods of investigating quasicrystals are at present the same as those used for the study of ordinary crystals. Electron diffraction (especially microdiffraction, with the use of which quasicrystals have been discovered) is used for the determination of the symmetry of quasicrystals, their deformation and defects. X-ray and neutron diffraction are used to determine atomic coordinates, which became possible only after fairly perfect quasicrystals (with sizes up to 0.1 mm or even 1 mm) had been obtained. Besides these main methods, EXAFS spectra, Mössbauer spectra and NMR have been applied for the investigation of local structure. Research on the physical properties of large quasicrystals (magnetic, elastic, etc.) has started.

Still, the basic difference from classical methods of structural analysis lies in the fact that to describe the structure of quasicrystals one cannot use the usual and convenient concept of a "unit cell" in 3-dimensional reciprocal space, but

has to look for means of describing the structure in general. In this case the method of crystallographic approximants is helpful.

At present three main approaches, based on the concept of pseudo-periodicity, that mutually complement one another are used in the definition and modelling of the quasicrystal structure of alloys. The simplest consists in decorating with atoms those geometrical elements which form Penrose lattices (e.g., atoms decorate rhombs in 2-dimensional space and rhombohedra in 3-dimensional, Fig. 5.2). Such decoration takes into account crystallochemical information on the size of the atoms, their possible coordination, etc. More complex building blocks are also used, such as icosahedra or other combinations of rhombohedra (Fig. 5.9).

The second approach consists of the use of crystal approximants already mentioned above, i.e. periodic structures which are close in their composition to quasicrystals. Such approximants can contain hundreds or thousands of atoms, and their atomic ordering differs from quasicrystalline only at distances exceeding the size of the unit cell [5.24–27].

The third and the most rigid but complicated approach consists of regarding the quasicrystal as a 3-dimensional cross-section of the periodic 6-dimensional

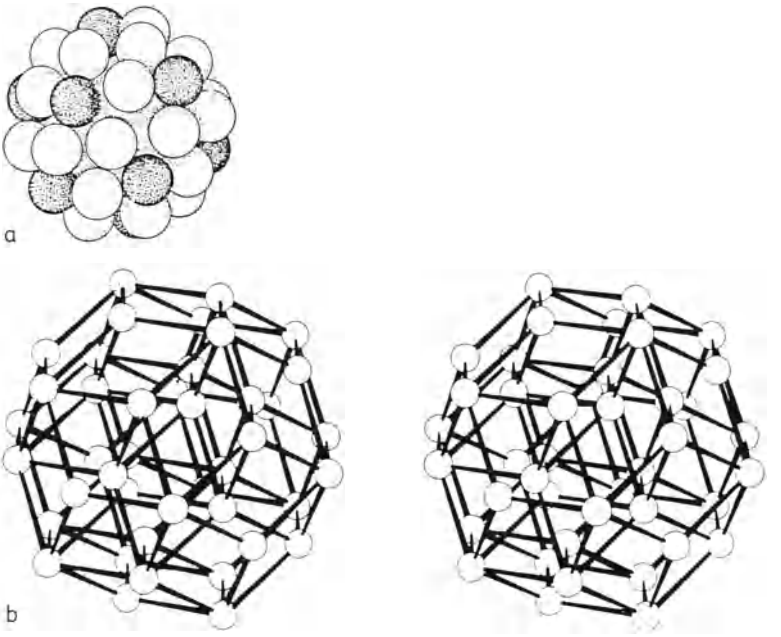

Fig. 5.9a,b. Atomic clusters with icosahedral symmetry. (**a**) The 54-atom Mackay icosahedron which may be a structure unit in AlMnSi quasicrystals and in α-AlMnSi crystal approximant [5.24]; the dark atoms are Mn; only outer shell is shown. (**b**) Rhombic triacontahedron which is the building block of three-dimensional Penrose pattern (Mackay, 1981) [5.5]; it may be considered as a superposition of acute and obtuse rhombohedra shown in Fig. 5.2. This cluster appears as a structure unit in AlLiCu quasicrystals and in the R-AlLiCu crystal approximant

space. Thus by performing 6-dimensional indexing (5.15) of the diffraction data, we can obtain the 6-dimensional Patterson function:

$$P_6(x_1, x_2, x_3, x_4, x_5, x_6) =$$
$$\sum_h |F_h|^2 \cos [2\pi(h_1x_1 + h_2x_2 + h_3x_3 + h_4x_4 + h_5x_5 + h_6x_6)], \qquad (5.16)$$

where $|F_h|^2$ denotes the experimental diffraction squares of the moduli of the structure amplitudes, see (4.126), and produce 3-dimensional sections. We may perform similar operations for the Fourier synthesis of the scattering density, if it is possible to obtain the phases.

The first and sometimes the third approach make use of the knowledge of the structure of the approximants.

An example of the simplest approximant is presented by a slightly idealized structure of a cubic MnSi crystal [5.27]: $a = 4.6$ Å; space group $P2_1\,3$; 8 atoms per unit cell in 4a positions (Fig. 5.10).

The Mn and Si atoms of such an idealized structure have the coordinates (x, x, x) with $x_{Mn} = (\tau - 1)/4 \cong 0.155$ and $x_{Si} = 1 - x \cong 0.845$. As a result, each Mn atom is surrounded by seven Si atoms positioned in the vertices of a dodecahedron, and vice versa. Parts of Mackay icosahedra are also observed (the unit cell being too small to house a whole one). Even such a simple structure produces a system of Bragg reflections similar to those observed in true icosahedral quasicrystals. The MnSi structure contains both parts of higher- (α-Al-Mn-Si and R-Al_5Li_3Cu), and lower-order approximants; the approximant of lower order presents a standard body-centered lattice, and therefore in MnSi one can find 8-atom clusters of the body-centered lattice with atoms in (000), (001), (100), (010), $(\frac{1}{2}, \frac{1}{2}, \frac{1}{2})$, $(-\frac{1}{2}, \frac{1}{2}, \frac{1}{2})$ $(\frac{1}{2}, \frac{1}{2}, -\frac{1}{2})$, $(\frac{1}{2}, -\frac{1}{2}, \frac{1}{2})$ positions.

The MnSi structure can be obtained by projecting the points of a 6-dimensional cubic lattice with one atom per unit cell. In this case the central atom of the dodecahedron in Fig. 5.10 is projected from the point (000000), the nearest six atoms – from (100000), . . . (000001), the seventh atom is a projection of the point (000111); the next six atoms are projected from points of (000011) type. If the strip in the 6-dimensional space is selected in a suitable way, the resulting

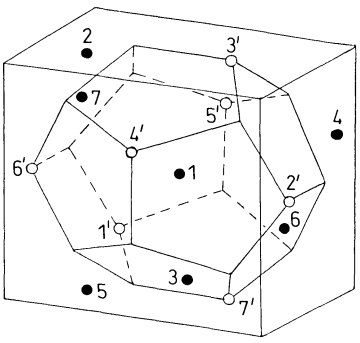

Fig. 5.10. The idealized structure of one of the simplest approximant – MnSi cubic crystal [5.27]

structure will be periodic; other positions of the strip generate higher-order approximants and quasicrystals.

Useful approximants are that of α-Al-Mn-Si with cubic $Pm\bar{3}$ structure similar to $Im\bar{3}$: lattice period $a = 12.625$ Å, 136 atoms per unit cell; T-$Mg_{31}(AlZn)_{49}$ and its isomorph – the R-Al_5Li_3Cu alloy ($Im\bar{3}$, $a = 14$ Å, 160 atoms per unit cell) (Fig. 5.11). Many approximants with non-cubic symmetry are known (see the review by Shoemaker and Shoemaker [5.25]).

In Al-Mn-Si alloys a sequence of cubic approximants with the unit cell dimensions 4.6 Å, 12.6 Å, 33.1 Å, 86.6 Å have been observed; the unit-cell size ratios are close to τ^2.

An example of the 6d → 3d cut-projection approach is presented by an investigation of the $Al_{5.70}Cu_{1.08}Li_{3.22}$ alloy by neutron diffraction (x-ray data were also used) [5.21]. In this case a cubic 6-dimensional lattice is primitive P. For the phase determination, an isotopic replacement—an analog of isomorphous replacement in x-ray diffraction—was utilized, as, i.e. ^6Li and ^7Li, as isotopes of this element have different scattering amplitudes with opposite signs. It turned out that Al and Cu atoms occupy statistically similar positions, while Li atoms occupy the positions that are different. Thus the structure could be regarded as a pseudo-binary alloy (Al, Cu)Li. The scattering density (nuclear – as neutron diffraction was used) of (Al, Cu) is presented in the example of a 2-dimensional cut through the 6-dimensional density (Fig. 5.12a), of Li atoms (Fig. 5.12b); Fig. 5.13a,b gives respective projections on 3-dimensional perpendicular space. The third in the series of figures (Fig. 5.14a,b) shows the averaged schemes of the (Al, Cu) and Li atoms positions in the fragment of 3-dimensional tiling.

Comparison of this quasicrystal structure with its cubic crystal approximant, which has a slightly different ideal composition, namely Al_5Li_3Cu (Fig. 5.11),

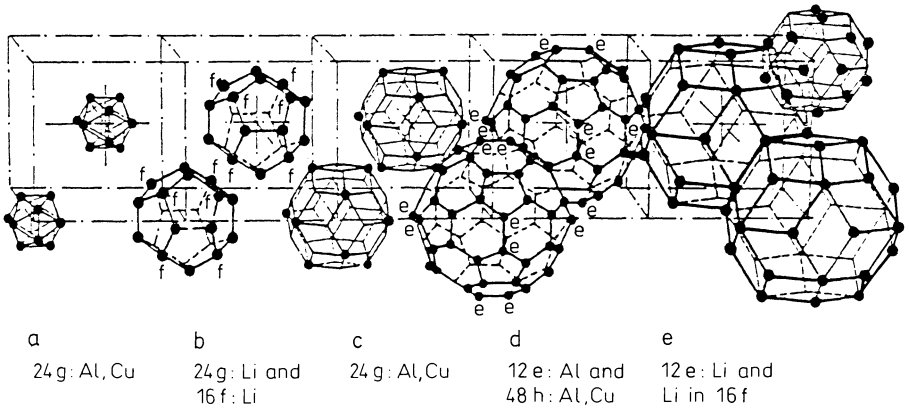

Fig. 5.11a–d. The body-centred cubic structure of R-Al_5Li_3Cu approximant [5.25]: (**a**) small empty icosahedra centered at 000 and $\frac{1}{2}\frac{1}{2}\frac{1}{2}$; (**b**) dodecahedra; (**c**) the addition of icosahedra to the previous dodecahedra forms the small triacontahedra; (**d**) "soccer-balls" and (**e**) large triacontahedra

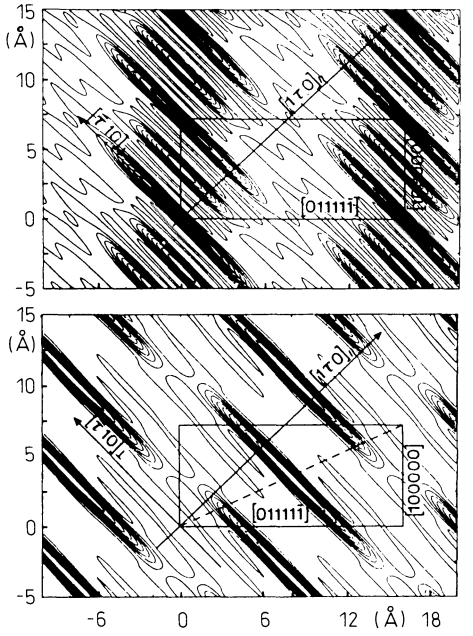

Fig. 5.12. Examples of 2-dimensional slices of the experimentally determined 6-dimensional density for an AlLiCu quasicrystal; for Al + Cu sublattice (upper) and for the Li sublattice (lower). The slices are taken along five-fold axes, one in physical space, the other in the perpendicular space. Atom positions are given by the intersection of physical five-fold axis with the density features [5.21]

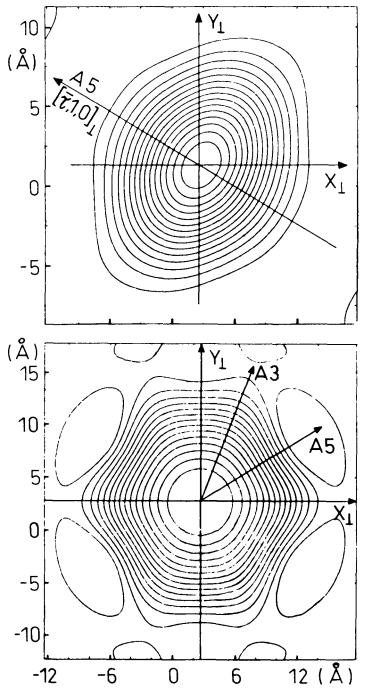

Fig. 5.13. Projection onto the 3-dimensional perpendicular space of atomic volumes corresponding to the density features shown in Fig. 5.12: Al + Cu atoms (upper); Li atoms (lower) [5.21]

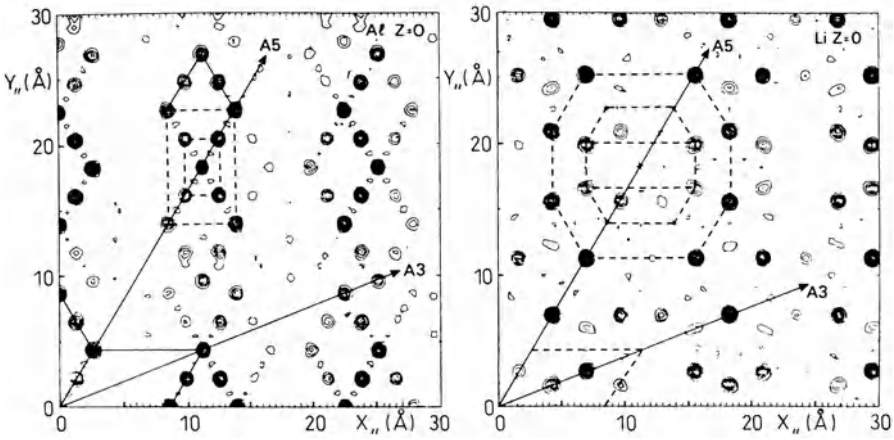

Fig. 5.14. Examples of 2-dimensional slices of the physical 3-dimensional density for the AlLiCu quasicrystal, as deduced from a cut of the 6-dimensional structure. Mid edge and vertex decoration of 3-dimensional Penrose tiling are shown for Al + Cu atoms (left); diagonal sites appear for Li atoms (right) [5.21]

reveals many common features in the packing of atoms. Naturally, our "three-dimensional" imagination visualizes the crystal model of the approximants with more ease, but the latter can still be the basis for an understanding of the structure of quasicrystals.

5.1.8 Order and Disorder in the Structure of Quasicrystals

The discovery and study of quasicrystals has not only widened our concepts of the ordered state of matter, but has also proved the universal character of the ideas. They can be applied to the description of a great variety of structures—from the simplest crystals to the components of living cells.

The concept of three-dimensional crystal ordering is based on the principle of a rigid spatial symmetry. This is also proved by the thermodynamic view of the possible agreement between the uniform local order and long-range correlation being symmetric over the whole space. It has been proved geometrically that the space-limited local 3-dimensionally periodic ordering leads to a periodicity over the infinite 3-dimensional atomic system (for local conditions of spatial symmetry, see Sect. 2.8.13).

The ideas proposed by Penrose [5.2], the discovery and investigation of quasicrystals have shown that the local ordering with 5-fold symmetry which the crystallographers found so unusual, leads to a further ordering of the whole space, which is not periodic, but is quasiperiodic in character. In fact, the packing itself – 2-dimensional tiling by Penrose rhombs – requires quasiperiodicity. The situation is similar in the 3-dimensional space. But what

produces icosahedral packing of atoms? As was mentioned in Sect. 1.2.3, in microclusters of several substances icosahedral atomic configurations are observed, they are also known to exist in several macroscopic structures of metallic glasses and, finally, in a number of crystal structures, including the structures of crystal approximants of quasicrystals. From the viewpoint of crystal chemistry, the formation of local icosahedral or "partly icosahedral" configurations could be promoted by the appropriate sizes (radii) of the atoms. If such configurations are stable enough, they will find their place in a suitable 3-dimensionally periodic crystal structure, or, being especially rigid, will form quasicrystals without 3-dimensional periodicity, but with the specific local icosahedral symmetry.

The approach to quasicrystals and quasiperiodic structures described above has now become standard, but it is open to new ideas. Besides the possible phason disordering mentioned above, we must note that ideal quasicrystalline long-range order is unlikely to exist over the whole of space. This presents an analogy with the "idealized" periodicity of the real crystal which, in fact, consists of mosaic blocs. We can therefore speak of the mosaic blocs of real quasicrystals. They can also have various types of disordering like dislocations, superposition of blocs and various point defects. A certain disordering in the structure of quasicrystals is also revealed in some of their physical properties.

As we have mentioned above, the observed diffraction patterns from quasicrystals are as a rule characterized by sharp Bragg reflections. Still, for some quasicrystals smeared-out reflections are observed. To explain this phenomenon a number of researchers have proposed a model of quasicrystal as "icosahedral glass" in which, unlike regular Penrose tiling, icosahedral regions are blocked randomly with empty gaps – frustrations – in between.

Another model of quasicrystals is that of a dense random tiling. It is an intermediate model between those of "ideal" quasicrystal and icosahedral glass (Fig. 5.15). This model produces sharp diffraction peaks.

In this connection it is reasonable to turn to the geometrical problem of space population (division). In classical crystallography (Sect. 2.8.14) the model is based on the concept of stereohedra, parallelohedra, and, in a general case, of stereons, each of which "works" with a 3-dimensional periodicity. The quasicrystalline approach of Penrose, Mackay and other scientists has shown that it is possible to divide the space into several fundamental regions (of different kinds) in such a way that the periodicity condition is not fulfilled. This presents a substantial contribution of the quasicrystals paradigm to the understanding of the geometry of our 3- and 2-dimensional spaces and its relation to n-dimensional geometry.

A different problem is presented by the mechanism for the occurrence of frustrations. A model of such structure – random tiling – is shown in Fig. 5.15 for the 2-dimensional case as a packing of regular pentagons. If we try to place them densely, we are immediately faced with the necessity either to superimpose the figures, or leave gaps between them. Frustrations of this kind are the result of the properties of our space and of order parameters. This is also true for

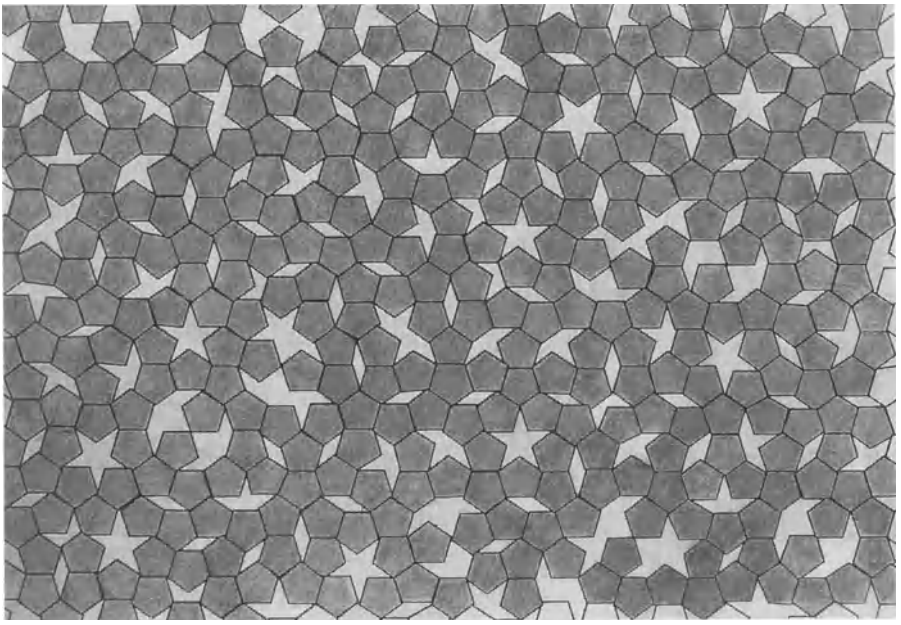

Fig. 5.15. Two-dimensional random tiling model for the structure of quasicrystals which produces sharp diffraction peaks surrounded by faint halos [5.28]

dodecahedra in the 3-dimensional space. In reality, frustrations are filled by irregular configurations of atoms.

Other complex systems are, in fact, the results of frustrations as well, since even the relatively simple mechanism of local ordering, if it is spread over the whole volume, will inevitably lead to the faulty packing of some elements and to the formation of various defects. These defects are present in many complex structures, where they can be distributed either periodically (Frank–Kasper metal phases, blue phases in liquid crystals, cubic lyotropic crystals), or quasiperiodically, or according to some other complex law.

Until today another important problem has not been solved – are the quasicrystals thermodynamically in equilibrium or metastable phases? The solution is hindered by the fact that little is known of the quasicrystal growth mechanism.

The process of rapid cooling used by Shechtman gave fine quasicrystal grains. It turned out that heating of such quasicrystals (Al-Mn type) lead to irreversible transformation into ordinary crystals, i.e. these quasicrystals were metastable. Still, other quasicrystals investigated in recent years, were grown slowly like ordinary crystals. These remained stable on heating up to the melting point. This indicates that such alloys are equilibrium thermodynamic phases. Therefore, quasicrystal phases can appear both as metastable and as equilibrium phases.

5.2 Incommensurately Modulated Structures

The multidimensional crystallography considered above with respect to the structure of quasicrystals, can successfully be applied to the description of incommensurate modulated structures [Ref. 2.14]. The multidimensional approach is rather effective in a description of the symmetry of incommensurate structures, which are a particular case of quasiperiodic structures [5.22, 30]. Incommensurate modulation of crystal properties (e.g., atomic displacements, site population numbers, the magnetic-momentum direction, etc.) can proceed by different physical mechanisms, mainly caused by the competition of two or several modes of ordering. As the point symmetry of incommensurate phases does not disagree with their periodicity, basic commensurate (crystal) structure, which is subjected to modulation, is usually present. The diffraction patterns reveal reflections from periodic, basic structure and satellite reflections arise from the incommensurate modulation.

When incommensurate modulation takes place in only one direction, a description of the symmetry of all possible structures can be limited to four-dimensional [(3 + 1)-dimensional] superspace. A complete list of such (3 + 1)-dimensional space groups had been made by De Wolff et al. [5.31]. This list does not include all 4-dimensional space groups, as several different 4-dimensional groups can correspond to one type of 3-dimensional crystal modulation.

Multidimensional space groups are also extremely useful for the description of such phenomena as phase transitions in incommensurate phases.

5.3 Development of Experimental Technique for X-Ray Structure Analysis

5.3.1 Powerful Sources of X-Ray Radiation

The use of powerful sources of x-ray radiation and fast diffraction-data collection are important for many purposes, e.g., for studying very small crystals such as inclusions in minerals or superconducting single crystals, for high-pressure investigations with the use of diamond anvils and for diffraction studies of thin films that give very weak diffraction patterns. Powerful sources are especially important for recording a large number (10^5–10^6) of reflections in x-ray crystallography of proteins and viruses. They can also be used for the detection of weak x-ray scattering by a magnetic structure.

In some cases fast recording of diffraction data is necessary to reduce the errors caused by meagre statistics and to increase the accuracy of intensity measurements. Thus, high speed of data collection is necessary in investigation of dopants in laser crystals, in studies of small structural changes caused by the action of various physical factors, e.g., by laser pumping, application of electric or magnetic fields, etc.

High-speed recording of diffraction data is also important in the investigation of the kinetics of nonstationary and fast structural changes (e.g., phase transformations in inorganic crystals and metal alloys) or in studies of biological macromolecules.

Higher rates of crystallographic-data collection can be achieved by enhancement of the x-ray source brilliance. In recent years, ever-increasing importance has been given to the development of synchrotron-radiation sources that provide an x-ray-radiation source brilliance exceeding by six-seven orders of magnitude that of conventional tubes with rotating anodes, namely 10^{16} photons/sec · mm^2 · mrad^2 · mA · O,1% BW (second-generation SR sources). In the near future, the brilliance of such sources is expected to be increased even more – by three to four orders of magnitude up to 10^{20} (third-generation SR sources, undulators).

Another way to increase the rate of intensity measurements is the use of the so-called parallel measurements of diffraction intensities in diffractometers with two-dimensional position-sensitive detectors. Such diffractometers provide a double increase of the rate of data collection, e.g., for protein single crystals, in comparison with conventional single-channel diffractometers. Figure 5.16 illustrates the schematics of the x-ray analysis with the use of a SR from the wiggler of the technological storage ring (Moscow) with focusing of the primary beam and a two-coordinate detector.

Finally, the third way to increase the rate of intensity measurements is the use of a comparatively wide range of the white spectrum of the radiation source instead of monochromatic radiation, i.e., the so-called Laue method.

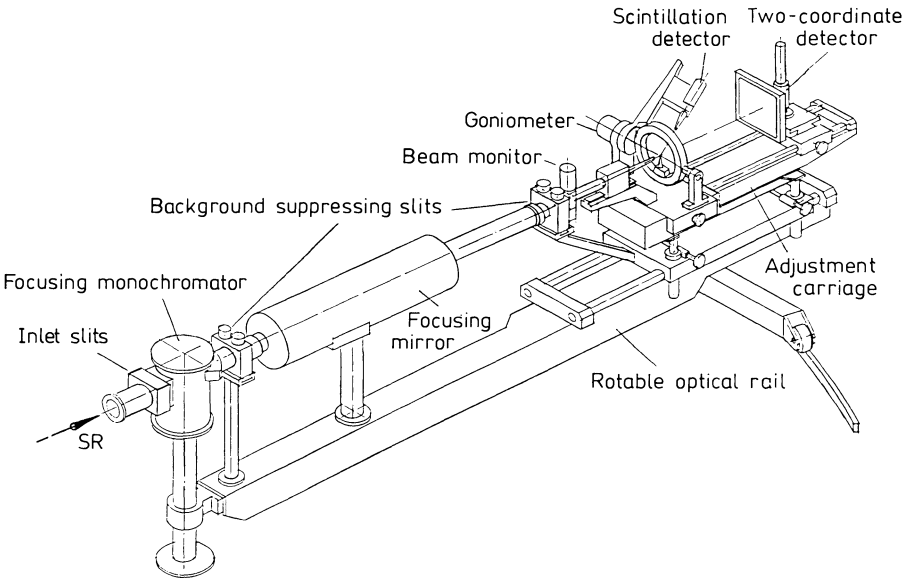

Fig. 5.16. BL-W1A station for x-ray structure analysis

5.3.2 The Synchrotron Radiation Sources

Synchrotron radiation (SR) is generated upon electron (or positron) motion along a circular orbit in magnetic fields of synchrotrons or storage rings with the velocity close to the light velocity. SR is directed along the tangent to the orbit and only slightly deviates from the orbit plane.

It should be emphasized that the first studies with the use of SR were carried out in the seventies on synchrotrons built for needs of high-energy physics (the so-called first-generation SR sources). However, soon it became clear that it is necessary to design special SR sources with high intensity, stability and beam lifetime. At present, the third-generation SR sources is ready to appear. These sources are characterized by high brightness, small dimensions of a radiating bunch, and a wide use of wigglers and undulators.

Circulation of electron bunches in a storage ring provides the temporal SR structure. The temporal length of a bunch, as a rule, is from 50 ps to 1 ns. Thus, a beam is the sequence of short flushes, the interval between which (from several nanoseconds up to several microseconds) is determined by the number of bunches and the period of revolution.

A wide spectrum range allows the use of a longer wavelength range in the Laue method. In order to use anomal scattering, it is also possible to choose wavelengths close to the absorption edge. The extended high-intensity radiation spectrum provides a high rate of data collection in energy-dispersive diffractometers. Polarized SR is employed for topographic studies. New results in structure studies can be obtained with the use of a more rigid (30–300 keV) x-ray radiation [5.32].

At present the following storage rings are utilized for structural investigations: LURE (Orsay, France), DESY (Hamburg, Germany), SRS (Daresbury England), NSLS (Brookhaven, USA), CHESS (Ithaca, USA), SPEAR and PEP (Stanford, USA), Photon Factory (Tsukuba, Japan), VEPP-2 and VEPP-3 (Novosibirsk, USSR). New projects are under construction: ESRF (Grenoble, France), APS (Argonne, USA), ALS (Berkeley, USA), ELETTRA (Trieste, Italy), a new NTK storage ring in Japan, SR sources in Moscow and Zelenograd (Russia).

5.3.3 Characteristics of Synchrotron Radiation

The SR spectrum depends on the electron energy E and the density of the magnetic-flux rotating electrons with the wavelength

$$\lambda_c = 186.4/E^2B = 5.59(R/E^3),$$

where λ_c is the wavelength separating the SR spectrum into two parts with equal integral intensity, $R = 33.3\ E/B$ is the orbital radius (λ is measured in Å, E in GeV, B in kG, and R in m). The spectral intensity rapidly decreases towards short wavelengths and is rather extended towards long wavelengths (Fig. 5.17).

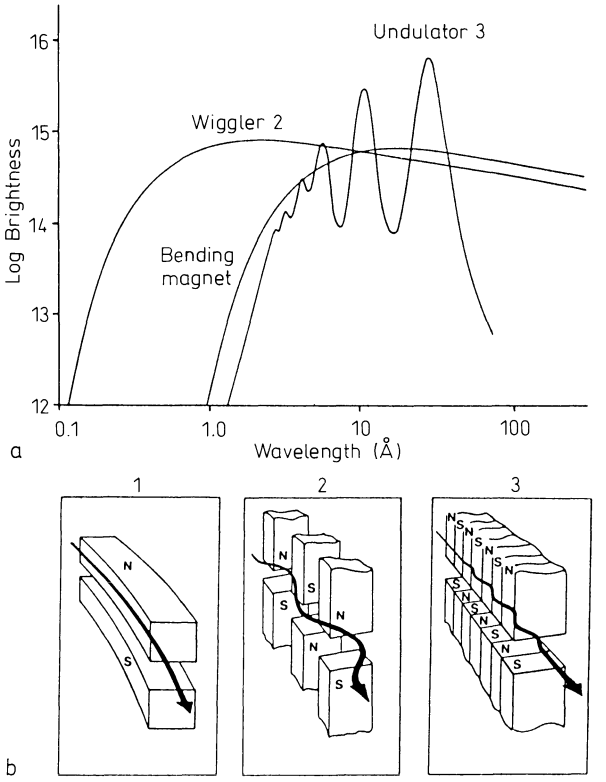

Fig. 5.17a,b. Synchrotron radiation spectra (**a**) emitted from (*1*) bending magnet, (*2*) wiggler, (*3*) undulator (**b**) [5.33]

The wavelength corresponding to the intensity maximum is

$$\lambda_m = 2.38\lambda.$$

If superconducting magnets with $B = 45\,\mathrm{kG}$ are used, the spectrum shifts towards short wavelengths: $\lambda_c = 1.04\,\text{Å}$, $\lambda_m = 2.5\text{–}2.0\,\text{Å}$.

For many applications, an important characteristic is the spectral distribution of the source intensity determined by the number of photons in the narrow spectral range emitted per second into the unit angle θ in the ring plane. For $\lambda > \lambda_c$, such a distribution is described by the expression

$$N[\text{photons/s}\cdot\text{eV}\cdot\text{mA}\cdot\text{mrad}] = 4.5\times 10^{12}\, j\,[\text{mA}](R[\text{m}])^{1/3}(\varepsilon[\text{eV}])^{-2/3}.$$

In modern storage rings the current j is about 100–300 mA. A typical energy spectrum of SR is exhibited in Fig. 5.17.

The synchrotron radiation can strictly be polarized solely in the ring plane, small deviations from this plane result in the appearance of a vertically polarized component. Thus the polarization is closer to linear, the smaller the vertical divergence of the SR beam. The spectrum and the intensity of the synchrotron radiation can be changed by special devices, e.g., wigglers and undulators, built into the rectilinear portions of the storage ring. A wiggler consists of several

strong, e.g., superconducting magnets that direct the electrons (positrons) along the trajectories with small radii. In this case the spectrum shifts towards more rigid radiation. If there are several periods of electron (positron) rotations, the intensities of all the periods are summed up and the radiation intensity increases. An undulator is a multipole wiggler with moderately strong magnets. In undulators electrons (positrons) only slightly deviate from the rectilinear track.

5.3.4 The Primary SR Beam

The primary SR beam is formed by monochromators. A SR beam converging into the storage-ring plane within several milliradians is focused by an asymmetric 150 mm-long bent Si(111) or Ge(111) monochromator crystals with the cut angle $\alpha = 8^\circ$ onto the surface or the input slit of the detector, $\Delta\lambda/\lambda$ being 10^{-3}–10^{-4}. A beam divergent with about 0.5 mrad in the perpendicular plane is focused onto the surface or the inlet slit of the detector with the aid of a segmented quartz-glass mirror providing the total external reflection and excluding the $\lambda/2$, $\lambda/3$, . . . harmonics from the monochromator. Eight 200 mm-long plane segments reduce the vertical dimensions of the focused beam from 8 to 1 mm at a distance of 20 m from the source. Thus the density of the photon beam increases by a factor of eight. The monochromator and the mirror are adjusted by a computer with the aid of a step motor.

An increase of the SR intensity results in heating of the monochromator and mirror. Therefore, mirrors are manufactured from thermally stable silicon carbide (SiC), and the monochromator is cooled by running water or melted metals.

In experiments with time separation it is necessary to use high-speed, mechanical beam-choppers with a signal duration up to 2 μs). Photoreactions and temperature jumps are initiated by lasers.

The intensities of the diffraction patterns are recorded on photographic films by two-dimensional position-sensitive integrating detectors (more than 10^6 photons/s). Photographic recording of the diffraction intensities from protein single crystals is often performed by employing of the Arndt-Wonnacott camera. Image plate technique is also widely used.

5.3.5 Laue Method for Crystallographic Data Acquisition from Single Crystals

In contrast to the radiation spectrum from an x-ray tube, the synchrotron-radiation spectrum is homogeneous over a wide wavelength range. This dictates the application of the Laue method in which integrated diffraction intensities are measured from a fixed crystal irradiated with a polychromatic beam. The Ewald construction (Fig. 5.18) shows that many points of the reciprocal lattice lying in the region limited by two Ewald spheres with radii $1/\lambda_{max}$ and $1/\lambda_{min}$ and the sphere of limiting resolution, turn out to be in the reflecting position at the same time. The complete set of intensities is collected from one to three x-ray diffraction patterns instead of tens of oscillation diffraction patterns necessary in case of a monochromatic beam. As a result, the set of integral intensities in a polychromatic beam can be obtained within about 10^{-1}–10^{-3} seconds. In

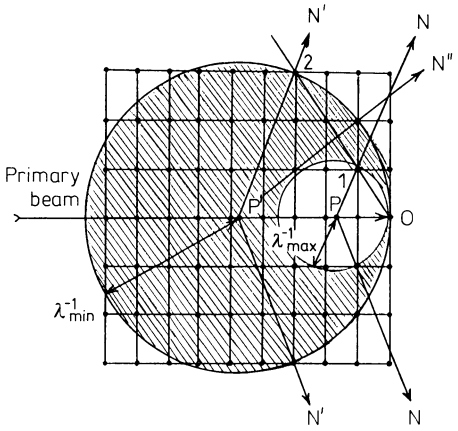

Fig. 5.18. Scheme of the Laue method in the reciprocal space. Points in the dashed region between the Ewald spheres of radii λ_{max} and λ_{min} (e.g., points N, N', N") provide x-ray reflections. Points 1 and 2 lying on the same nodal line passing through the initial point O provide reflection in one direction (reflected rays PN and P'N')

third-generation storage rings such a set of diffraction intensities would be obtained presumably within the time-of-flight of an electron bunch ($\simeq$ 10 s). The use of the Laue technique requires the solution of some problems:

1. *Harmonic Overlaps (Multiplets).* Radiation of wavelengths λ, $\lambda/2$, $\lambda/3$, . . . is reflected by the planes with the spacings d, $d/2$, $d/3$, . . . at the same angle 2θ, and therefore all the respective reflections will superimpose in one diffraction spot (beams 1 and 2 in Fig. 5.18). But if λ_{min} and λ_{max} are not limited by reflection from the mirror and transmission through the filters, the number of such superimposed reflections will not exceed 17% of the total number. In reality (λ = 0.5–1.6 Å), it will be even less.
2. *Spatial Overlaps.* X-ray diffraction patterns contain a lot of too closely located or overlapping reflections. The methods of integral intensity measurements by fitting profiles provide separate intensity measurements of the reflections spaced by 0.1 mm.
3. *Wavelength Normalization.* The intensities of various reflections are measured at different wavelengths. Therefore it is necessary to take into account the intensity of the primary beam, its interaction with the crystal, and the efficiency of the detector recording.

5.3.6 Some Results Obtained with Synchrotron Radiation Sources

X-ray diffraction patterns were obtained in a Laue camera from a diamond crystal ten times smaller than conventional specimens. Diffraction patterns were recorded on image plates at an exposure of about one hour.

The synchrotron radiation is used to study the kinetics of structural transitions. In this case, the intensity of a monochromatic beam on the specimen was increased not with the aid of a crystal monochromator but with a monochromator based on a layer structure with $\Delta\lambda/\lambda = 10^{-2}$ (E = 5–8 keV). Diffraction patterns were recorded by a linear photodiode detector simultaneously at

1024 points each 17 ms in time. The use of diamond anvils and systems with energy-dispersive recording provided the observation of phase transitions with a 10 s resolution under pressures up to $\simeq 10$ GPa at temperatures up to 1500 °C [5.34].

5.3.7 Diffractometers with Two-Dimensional Position-Sensitive Detectors

Instruments with position-sensitive detectors are widely used in x-ray diffraction analysis of proteins. Large unit cell parameters of protein crystals ($\geqslant 100$ Å) require the intensity measurement of tens and thousands and, for viruses, even millions of reflections. Of great importance now are high-resolution studies of complicated proteins with large molecular masses and investigation of their functions. Large unit cells of proteins give rise to simultaneous formation of tens and hundreds of reflections recorded in parallel by a two-dimensional detector. Such parallel measurements drastically decrease the time of data collection and, consequently, also the irradiation dose. Parallel measurements are carried out in screen-free oscillation and precession x-ray cameras and Weissenberg goniometers.

Low film sensitivity, small dynamical range, low accuracy of measurements accuracy, the necessity of chemical treatment of the film, and, hence, the absence of the feedback and control in the real time scale impose some restrictions on the application of the photographic method.

The sensitivity of the film is limited by the chemical veil equivalent to the recording of 10^4 photons on a 0.3 mm × 0.3 mm diffraction area. The dynamic range (the ratio of the maximum to minimum intensity) is 10:1, for a set of three films it is 100:1. The error in photographic intensity measurements is of about 5%. The method of parallel recording of the diffraction intensities in diffractometers with area electronic detectors combine the advantages of photon counters with the two-dimensional recording on photographic films. As area electronic detectors, one often uses proportional chambers with numerous wires [5.30, 35] proportional chamber with spherical drift gaps [5.35, 36], the television type scintillation counters [5.37], and films based on photostimulated luminescence-image plates [5.38].

A proportional chamber consists of anode wires located in one plane and cathode wires located in two other mutually perpendicular planes normal to the plane of anode wires.

A proportional chamber is filled with xenon and quenching additives. Absorption of x-ray photons by xenon atoms provides the formation of a primary-ionization electron cloud. Under the action of the electric field this cloud moves towards the anode wires and forms an avalanche of shock ionization. The negative charge on the anode wires induces a positive charge on several closely located cathode wires in both planes. The center of gravity of the positive charge determines the X and Z coordinates of the recorded photon. The X and Z coordinates are determined with the aid of the delay lines normal to the Z and X

wires. The number of pixels is 256×256. The proper camera background on the diffraction spot < 1 pulse/min, the dynamic range is 10^7:1, the precision of intensity measurements is 1–2%. Of use are also the chambers with spherical drift gaps located before the proportional camera. The spatial resolution is improved by an order of magnitude (up to 0.2–0.3 mm), the number of pixels is 512×512.

A two-dimensional Scintillation Counter consists of a thin layer of crystal phosphor (e.g. Gd_2O_2S) applied onto a fiber-optical slab connected with an electronic-optical brightness amplifier whose output, in turn, is connected with the input of a transmitting television tube. The television-tube sweep is synchronized with readdressing of the fast operative memory. An analog TV signal is transformed into a digital form and is stored in the respective memory cell. The number of pixels is $150–300 \times 200–400$. The dynamic range is 10^2:1, and the counter speed is very high.

The image plate detector is based on the phenomenon of photostimulated luminescence. The x-ray quanta incident onto a BaFBr (Eu^{2+})-based image-plate detector provide the formation of a latent image and the x-ray diffraction pattern stored as a F-center distribution. Such a latent image is read as a photostimulated luminescence pattern when the film is scanned with a narrow helium-neon laser beam ($\lambda = 632.8$ nm). The luminescence pattern ($\lambda = 390$ nm) is recorded by a photoelectron multiplier and then is stored in a computer. The film can be repeatedly (up to 10000 times) used, the time of the diffraction pattern reading in a computer is 2–8 minutes, the detector background is 300 times lower than that of the film, the dynamical range is 10^5:1. The main parameters of two-dimensional detectors are listed in Table 5.3.

Consider the schematic of a KARD-diffractometer with a two-dimensional proportional chamber [5.39] shown in Fig. 5.19. The computer-controlled diffractometer consists of a two-dimensional proportional chamber with 256×256 fast delay lines, an electronic circuit for data collection, a special device for visualization, intermediate memory, a multiple-circle goniometric device, a stabilized high-voltage source with a sealed-off x-ray tube with the 0.4×0.4 mm^2 focus projection, and a graphite monochromator. The detector is preceeded by a special helium buffer. A KARD goniometer provides the rotation of the primary beam about two mutually perpendicular μ and Υ axes, whereas the detector with a variable crystal-detector distance is immobile. The crystal is automatically rotated about the three Euler axes, ω, χ, and φ.

The X and Z coordinates of the diffraction spots are related to the angles Υ and ν by the following relationships

$$\begin{aligned} X &= R \tan(\Upsilon - \Upsilon_o) + X_o, \\ Z &= R \frac{\tan \nu}{\cos(\Upsilon - \Upsilon_o)} + Z_o, \end{aligned} \tag{5.17}$$

where R is the crystal-detector distance. Using formulae (4.100) and (4.101) from Ch. 4, it is possible to determine the cylindrical coordinates of the reciprocal

Table 5.3. Main parameters of two-dimensional detectors

	Photofilm with micro-densitometer	Proportional chamber	Proportional chamber with spherical drift gap	Scintilation TV counter	Film with photo-stimulated luminescence and laser reading device
Number of pixels	$2{\cdot}10^3 \times 2{\cdot}10^3$	256×256	512×512	300×400	$2{\cdot}10^3 \times 2{\cdot}10^3$
Pixel dimension	0, 05	1, 3	0, 2	0, 15	0, 1
Dynamical range	10:1	10^7:1	10^7:1	100:1	10^5:1
Detector background of the diffraction reflection area, photon	10^4	1 per min	1 per min	dark current	30
High speed	Almost unlimited	$2, 5{\cdot}10^5$	$6{\cdot}10^4$	Almost unlimited	Almost unlimited
Efficiency CuK_α	60	70	80	70	100

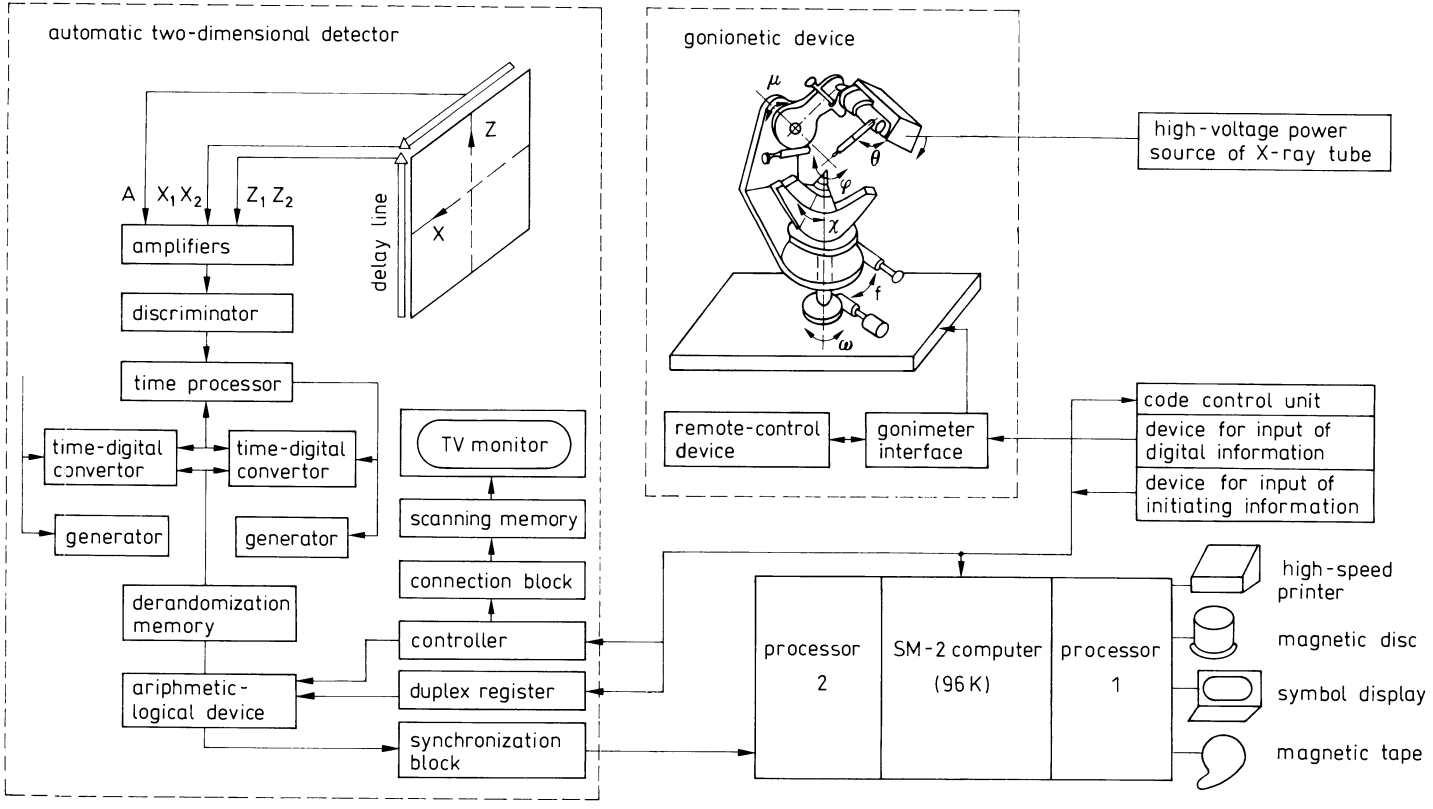

Fig. 5.19. Block scheme of a KARD-4 coordinate diffractometer based on a two-dimensional proportional chamber. (*1*) automatic two-dimensional detector; (*2*) amplifiers; (*3*) discriminator; (*4*) time processor; (*5*) time-digital convertor; (*6*) time-digital convertor; (*7*) generator; (*8*) generator; (*9*) derandomization memory; (*10*) arithmetic-logical device; (*11*) delay line; (*12*) TV monitor; (*13*) scanning memory; (*14*) connection block; (*15*) controller; (*16*) duplex register; (*17*) goniometric device; (*18*) remote-control device; (*19*) goniometer interface; (*20*) pocessor 2; (*21*) SM-2 computer (96 K); (*22*) processor 1; (*23*) high-voltage power source of x-ray tube; (*24*) code control unit; (*25*) device for input of digital information; (*26*) device for input of initiating information; (*27*) high-speed printer; (*28*) magnetic disk; (*29*) symbol display; (*30*) magnetic tape; (*31*) synchronization block

lattice point, the orthogonal coordinates by formula (4.102), and then to determine and refine the orientation matrix. In turn, knowing the orientation matrix (α_{ik}) and indices h_k, it is possible to determine the orthogonal coordinates of the points in the reciprocal space by formula (3.42) and, thus also angles ν, Υ and ω. In the general case of inclined geometry we have

$$\begin{aligned}
\nu &= \sin^{-1}(\lambda Z^* + \sin\mu_o), \\
\Upsilon &= \cos^{-1}\frac{\cos^2\nu + \cos\mu_o - \lambda^2(X^{*2} + Y^{*2})}{2\cos\nu\cos\mu_o}, \\
\omega &= \sin^{-1}\frac{\cos^2\mu_o - \cos^2\nu + \lambda^2(X^{*2} + Y^{*2})}{2\lambda\sqrt{X^{*2} + Y^{*2}}\cos\mu_o} + \tan^{-1}\frac{Y^*}{X^*}.
\end{aligned} \tag{5.18}$$

Then it is also possible to calculate from (1) the diffraction pattern recorded on a two-dimensional detector for the given value of the rotation angle ω of the crystal.

The investigation of a crystal structure in a diffractometer with a two-dimensional detector is carried out in three stages.

The preliminary first stage is devoted to indexing and rough crystal orientation by partly or fully automated methods. At this stage the crystal orientation and unit cell parameters are refined automatically, and the absorption curves and the intensities of the reference reflections are determined.

The second stage is the data collection proper. The buffer memory collects and stores the diffraction pattern in the running $\delta\omega$ range. The computer also provides the list of reflection indices, reflection intervals, spot dimensions, summation of the photons in the diffraction spot, the intensities of diffraction peaks and the background, and statistical errors.

The third stage reduces to the primary processing of the diffraction data obtained, introduction of the correction for drift, Lorentz, polarization, and absorption factors. The symmetry-related reflections are averaged, the reliability factors and the moduli of structure amplitude are calculated.

Moving the area detector relative to the crystal and varying the crystal-detector distance R at which the neighboring reflections can still be resolved, it is possible to attain the optimum experimental resolution.

High-speed performance of the proportional chambers allows experiments with a sealed-off x-ray tube and a tube with the rotating anode. But it is insufficient for experiments with a synchrotron radiation. In case of SR the diffractometers with photostimulated-luminescence sensitive films are used.

Such diffractometers can be of several types: the first type is a chamber analogous to the conventional Arndt-Wonnacott or Weissenberg camera with photorecording combined with an independent device for laser reading of information. The second type of diffractometers has a device with either one plane plate or a system of two plates sensitive to photostimulated luminescence and a laser reading device. The third type of diffractometers provides the fast mechanical change of the plates for time-resolved investigations.

The advantage of the first type of diffractometers consists in the use of only one reading device for several cameras. The shortcoming of these devices is the necessity of manual installation of the film-detector into the reading device.

The advantage of the second-type diffractometers is the fully automated data collection and their transmission to the computer memory (a large number of frames for quite a long time) without intervention of a crystallographer and the possibility of introducing the correction for inhomogeneous detector efficiency over the area. But the shortcoming consists in the necessity of interrupting the exposure for reading the diffraction pattern and using several reading systems for a series of diffractometers.

Another way for reducing the time of exposure break is the use of two-plate blocks in integrating schemes (Fig. 5.20). One plate is read whereas the other is exposed. The exposure is not interrupted if it is longer than the reading time.

Diffractometers with photostimulated-luminescence plates can be successfully used also in the combination with conventional sources of x-ray radiation, since, in comparison with the x-ray photographic films, they possess higher sensitivity, dynamical range, and the efficiency in recording a short-wavelength radiation.

In time-resolved studies, it is also convenient to use devices with fast mechanical plate replacement (forty 100×108 mm^2 plates 0.2 s) and devices with photographing of linear x-ray patterns along the generatrix of a cylinder on which the image plate is located. Another type of time-resolved photographing is the chopped displacement of the plate-detector during its exposure.

For all the devices with two-dimensional detectors the reliability factor for symmetry-related integral intensities is 4–8%, i.e., two times lower than for photographic methods. In addition to the structural determinations of macromolecular crystals the diffractometers with two-dimensional detectors can be used for crystal orientation and for structural investigations of polymers, fibers, liquid crystals, and amorphous materials, etc.

5.4 X-Ray Studies of Crystal Surface

In the recent decade the wide recognition was gained by x-ray studies of crystal surfaces and the processes occurring there [5.40]. Of great scientific interest and practical importance are surface phase transitions, adsorption and desorption, the initial stages of epitaxial growth, reconstruction and relaxation. In such processes, structural rearrangements occur only within several surface atomic layers. Therefore the study of such structural transformations by the x-ray technique requires the separation of the signal from the surface atoms and that from the bulk atomic layers. Almost all such studies became possible due to the use of synchrotron radiation possessing high spectral brightness.

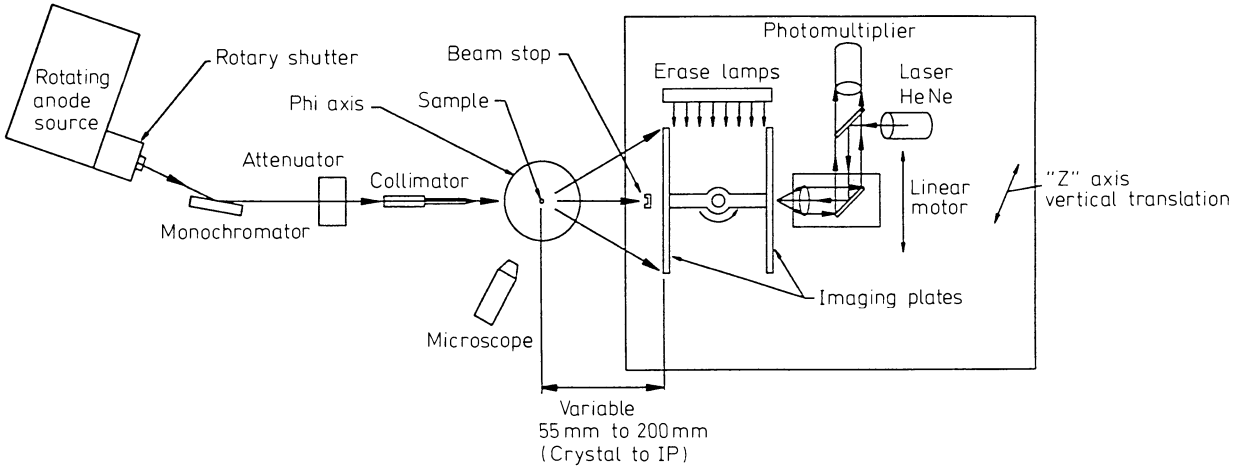

Fig. 5.20. Schematic of a diffractometric device based on two imaging plates for photostimulated luminescence and a built-in HeNe laser [5.39]

5.4.1 Surface Diffraction

The method of surface diffraction [5.40] is based on the phenomenon of the total external reflection of x-rays from the surface of a solid. The refraction index n of x-rays with the wavelength λ is expressed as follows

$$n = 1 - \lambda^2 e^2 F(0)/2\pi mc^2 v, \tag{5.19}$$

where c is the velocity of light, m and e are the electron mass and charge, respectively, v is the unit cell volume, and $F(0)$ is the structure amplitude in the direction of the incident beam. Neglecting the absorption, we obtain

$$n = 1 - \delta = 1 - 2.701 \times 10^{-6} (\sum_j Z_j / \sum_j A_j) p\lambda^2, \tag{5.20}$$

where Z_j and A_j are the atomic charge and mass, respectively (summation is carried out over the whole unit cell), p is the density in g/cm^3, and λ is the wavelength in Å. It is seen that the refraction index is smaller by $\simeq 10^{-5}$ than unity. The typical values of the critical angle of the total external reflection, $a_c = \sqrt{2\delta}$, for wavelengths of the order of 1.5 Å are within the range 0.2°–0.6°.

The total external reflection of x-rays is characterized by the exponential attenuation of the refracted wave. For the incidence angles $\alpha_i < \alpha_c$ the penetration depth is

$$L_i = (2k\sqrt{\alpha_c^2 - \alpha_i^2})^{-1}, \tag{5.21}$$

where k is the absolute value of the wave vector of the incident wave. In the range of the total external reflection, x-rays penetrate into a depth of 10–30 Å. This makes it possible to use this phenomenon for studying the surface structure. Figure 5.21 illustrates the geometry of the experiment. Varying the incidence angle α_i (or the angle α_f of the diffracted beam exit), it is possible to vary also the penetration depth and to perform the layer analysis.

One of the first studies by the method of surface diffraction [5.41] had the aim to investigate the structure perfection of thin crystalline aluminum layers grown on the GaAs substrate by the molecular beam epitaxy. In particular, it was revealed that the structure of the first atomic aluminum layers is determined

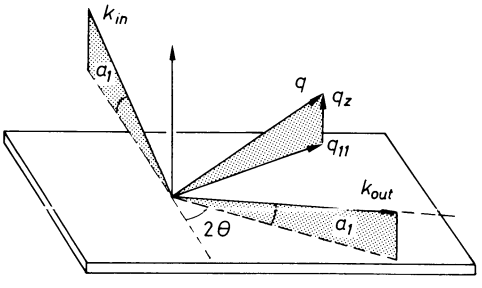

Fig. 5.21. The schematic of surface diffraction; k_{in} and k_{out} are the wave vectors of the incident and diffracted waves, respectively, $q_{||}$ and q_z are the pulses applied parallel and normal to the surface, respectively

by the substrate structure. Further deposition of aluminum results in the linear dependence of the aluminum lattice constant on the layer thickness. Upon deposition of about 25 atomic layers of aluminum the structure undergoes the phase transition to the structure of single crystalline aluminum.

The method of surface diffraction can be efficiently used for studying the order-disorder surface transitions. Thus the phase transitions on the (111) and (100) faces of Cu_3Au single crystals were studied in [5.42, 43]. A Cu_3Au single crystal is an ordered fcc alloy [Ref. 5.29, Fig. 2.9b]. Below the phase transitions temperature ($T_0 = 663$ K), gold atoms occupy the sites at the unit cell vertices whereas copper atoms occupy the face centers. Above T_0, both gold and copper atoms are distributed randomly. The study of disordering on the surface is of great interest for thermodynamics of the first-order phase transitions in semi-infinite systems.

These studies showed the formation of a thin ($\simeq 20$ Å) surface ordered layer whereas deeper (100–600 Å) layers remained to be disordered.

Most studies by the method of surface diffraction were performed on atomically clean surfaces. The experimental equipment for such studies should provide ultrahigh vacuum, precision angular rotation of a specimen, and incident-beam monochromatization and focusing. A diffractometer for such studies should provide the specimen rotation (ω), it is also necessary to set the detector angles ($2\theta_B$), the angles of incidence and exit, (α_i and α_f) and all the necessary adjusting translations and tilting angles. A position-sensitive detector allows one to record the diffracted radiation at different angles. The surface preparation and its investigation by the traditional techniques such as LEED, RHEED, and Auger spectroscopy are made in an evacuated camera outside the synchrotron radiation source. Then the specimen in a ultrahigh vacuum camera is placed into another portable ultrahigh vacuum camera and is mounted on a diffractometer. The circular berillium window provides the choice of any necessary diffraction angle.

In many laboratories, ultrahigh-vacuum setups have been designed that can be placed directly before the SR sources and provide *in situ* surface diffraction studies.

The physical foundations of x-ray surface analysis are similar to those for the conventional x-ray structure analysis of bulk crystals. It should be emphasized that the physical and geometrical features of diffraction occurring in a two-dimensional layer are similar to those in low-energy electron diffraction (LEED). Let p_s be the projection of the electron density of surface atomic layers onto the crystal surface. Then

$$p_s(x, y) = \int p(r)\, dr_z = (1/A) \sum_{hk} F_{hk} \exp[-2\pi i(hx + ky)], \tag{5.22}$$

where A is the area of the unit cell face. Since the two-dimensional structure amplitude F_{hk} is expressed as

$$F_{hk} = |F_{hk}| \exp(i\alpha_{hk}),$$

then

$$p_s(x, y) = 1/A \sum_{hk} |F_{hk}| \cos[2\pi(hx + ky) - i\alpha_{hk}]. \tag{5.23}$$

In most cases the structure is determined with the use of the Patterson function and the construction of $P(xy)$ series. The surface investigations are characterized by the following: whereas the three dimensional reciprocal lattice of a bulk crystal is a set of points, the two dimensional reciprocal lattice of a surface is a set of rods extended along the surface normal (the so-called Bragg rods of two-dimensional diffraction). The integral intensities of two-dimensional reflections are obtained by intensity integration over the rod cross-sections. The integral intensity is described by the following expression

$$I_{hk}(qz) = (I_o/\Omega)(a\lambda^2 P/A \sin 2\theta)(e^4/m^2c^4)|F_{hk}|^2(\lambda/2\pi)\Delta q_Z, \tag{5.24}$$

where I_o is the incident beam intensity, Ω is the angular scanning velocity, P is the polarization factor, a is the area of the surface participating in diffraction, and Δq_Z is the detector resolution along the Bragg rod, cf. (4.63). In most experiments the angles α_i and α_f are so small that it is possible to take $q_Z = 0$. Then the scattering plane is normal to the Bragg rod

$$(\lambda/2\pi)\Delta q_Z = L/R, \tag{5.25}$$

where L is the detector dimension in the direction normal to the scattering plane and R is the specimen-detector distance. The intensity distribution along the Bragg rods contains the information about the structural changes along the surface normal.

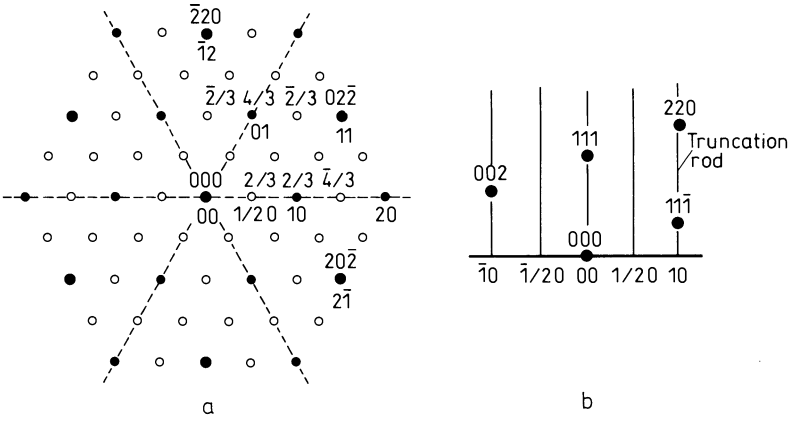

Fig. 5.22a,b. The reciprocal lattice of the (111) 2×2 surface of a crystal with the zinc blende structure. (**a**) The (111) plane is parallel to the crystal surface. The reciprocal-lattice points in the crystal bulk are depicted by black circles, the Bragg rods with the fractional indices due to surface reconstruction are indicated by light circles. (**b**) The $(220)_c$ plane normal to the surface and including the $(10)_h$ direction

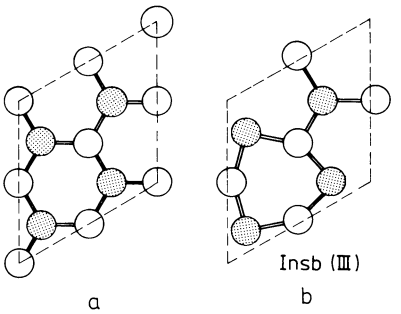

Fig. 5.23a, b. Unreconstructed (**a**) and reconstructed (**b**) InSb (111) 2 × 2 surface. The dashed circles represent the atoms of group V

Consider the two-dimensional unit cell on the (111) surface of crystals with the zinc blende structure. Similar to LEED, the unit cell in the surface x-ray diffraction studies is based on the vectors $\boldsymbol{a}_1$ and $\boldsymbol{a}_2$ parallel to the surface with the vector $\boldsymbol{a}_3$ being normal to the surface. The reciprocal lattice for a reconstructed (2 × 2) surface with the parameters $2\boldsymbol{a}_1$ and $2\boldsymbol{a}_2$ is shown in Fig. 5.22. The multiple increase of lattice parameters provides the formation of h, k reflections with fractional indices. Such reflections yield the information on the structure of the surface superlattice. Figure 5.23 shows the unit cell of the reconstructed InSb(2 × 2) surface [5.44]. The surface diffraction studies provided the determination of the variations in interatomic bond lengths and valence angles in the upper reconstructed atomic layer. The method of surface diffraction has already been successfully applied for the studies of (2 × 2)GaAs, (2 × 2)InSb, (2 × 2)GaSb, (7 × 7)Si, and (7 × 7)Ge surfaces. Under progress are the studies of adsorption on atomically clean germanium, silicon and other surfaces [5.45].

5.4.2 The Method of X-Ray Standing Waves

X-ray standing waves are generated in the lattice of a perfect single crystal due to the superposition of the incident and diffracted plane waves under the conditions of dynamical diffraction [5.46]. The intensity of the standing wave field is described by the expression

$$I(r) = |E_o|^2 + |E_h|^2 + 2|E_h||E_o|\cos(hr + \alpha), \tag{5.26}$$

where h is the reciprocal lattice vector, and $|E_o|$ and $|E_h|$ are the amplitudes of the incident and diffracted waves, respectively, and α is the phase of the complex E_h/E_o ratio. The period of the standing wave is equal to or smaller by an integer factor than the spacing for the system of reflecting planes under consideration, whereas the intensity of the field is constant in the plane parallel to the reflecting planes of the crystal. The $|E_h|/|E_o|$ ratio and α depend on the experimental conditions, in particular, on the diffraction geometry and the deviation of the incidence angle from the exact value of the Bragg angle. Thus for the most widespread Bragg geometry $|E_h| = |E_o|$ under the conditions of total diffraction reflection. In this region the phase varies from 0 to π. The latter fact results in the

displacement of the antinode of the standing wave by a half of the spacing [5.47].

Generation of standing waves is accompanied by inelastic scattering of x-rays, i.e., by photoelectric absorption and the Compton and thermal diffuse scattering. They manifest themselves in anomalous angular curves of photoemission, fluorescence, Compton quanta yield, etc. Figure 5.24 shows the angular curves of the x-ray reflection coefficient $P_r = |E_h|^2/|E_o|^2$, phase α and the field intensities on the atomic planes. Figure 5.25 shows the angular variation of fluorescence from the atomic monolayer on the crystal surface. For the ordered arrangement of atoms in the layer at distances equal to the spacing d, the character of the angular dependence of the fluorescence yield is analogous to curve (3) in Fig. 5.24. If the layer is displaced by $d/2$, the position of the antinode

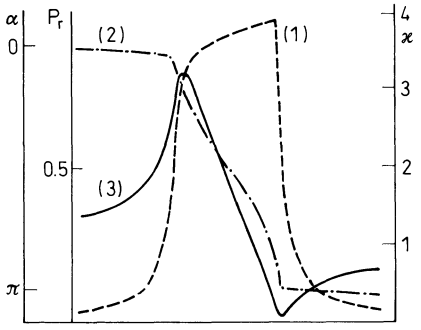

Fig. 5.24. The angular curves of the reflection coefficient for x-rays (*1*), phases α(*2*), and the field intensity at atoms (*3*) in the vicinity of the total external reflection

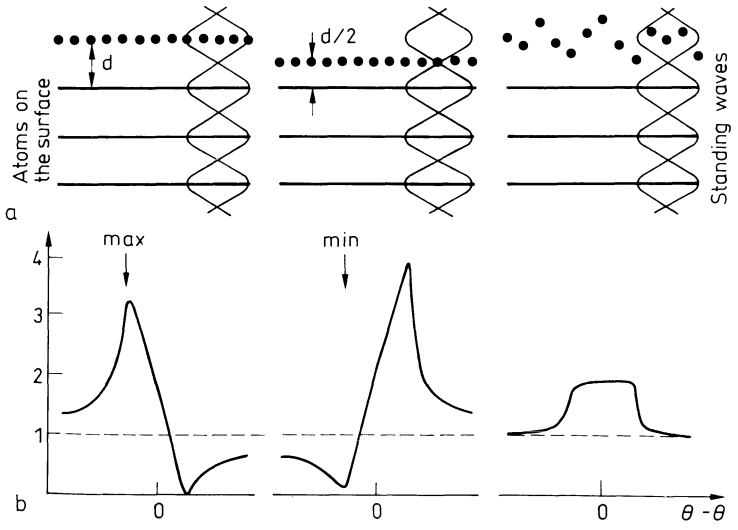

Fig. 5.25. Illustrating the structural information provided by the method of x-ray standing waves. (**a**) standing waves and the atoms on the surface; (**b**) the respective curve of fluorescence yield

of the standing wave relative to the matrix atoms corresponds to the node position relative to the monolayer atoms and vice versa. This results in the appearance of an additional phase π in (5.26) and the change in the mutual arrangement of the minimum and maximum of the angular curve of the fluorescence yield. If a monolayer is disordered, the equal number of atoms correspond to the nodes and antinodes of the standing wave. Upon averaging over the atomic coordinates of the layer the interference term for the field intensity in (5.26) becomes zero and the angular curve acquires the shape of the reflection curve.

The main objects of XRSW experiments with the use of SR are monoatomic layers of adsorbed atoms on atomically clean surfaces [5.48]. The method allows one to determine the average position of the layer relative to the diffracting planes generating standing wave (the so-called coherent position) and the degree of atomic order in this layer (the so-called coherent fraction). In most experiments the use is made of symmetric reflections (the reciprocal-lattice vector is normal to the surface) and therefore the positions of atoms with respect to the surface can be measured. Thus the methods of x-ray standing waves complements the method of surface diffraction that provides the information on the positions of atoms along the surface.

The fluorescence radiation of adsorbed atoms is recorded with the aid of a solid state detector. The use of modern powerful SR sources provides the localization of very small (0.01–0.10 monolayer) number of atoms. Adsorbed atoms were first localized by the x-ray standing wave technique in [5.49]. The authors studied the fluorescence yield of bromine atoms chemisorbed on the Si(220) surface. The measurements were made in air. The determined coherent position (1.73 ± 0.07 Å) confirmed the covalent nature of the Si-Br bond.

In other experiments the use was made of portable high-vacuum cameras. Thus gallium arsenide structure on the Si(111) surface in ultrahigh vacuum (8×10^{-11} torr) was studied in [5.50]. Annealing at 850° C provided the formation of the 7×7 surface which was studied by the LEED and Auger spectroscopy techniques. At the substrate temperature 600° C, a half of the GaAs monolayer was deposited onto the Si(111) surface. In the course of the experiment, the angular fluorescence curves for AsK_α and GaK_α were measured simultaneously. It has been established that As atoms are located only in the upper part of the (111) bilayer whereas Ga-atoms occupy the lower part of it. Thus at the interface solely As-Si bonds are present; the GaAs single crystal growing at the silicon surface has the B-type polarity.

In order to obtain the data on the structure of the adsorbed layer not only symmetric reflections can be used. Thus in [5.51] chemisorption was studied with the use of the (111) reflection and also the reflection from the (220) planes inclined to the surface. The simultaneous structure characterization in several directions can be implemented if x-ray standing waves are excited under the conditions of multibeam diffraction. The x-ray optical scheme of such experiments is shown in Fig. 5.26 [5.52]. Angular curves of photoelectron yield were measured under the conditions of multibeam 111/220 diffraction from a Si

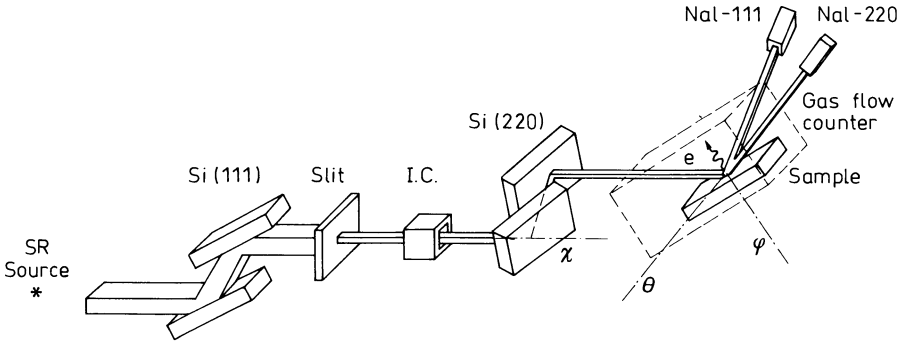

Fig. 5.26. X-ray optics scheme for x-ray standing-wave experiments under the conditions of multibeam diffraction

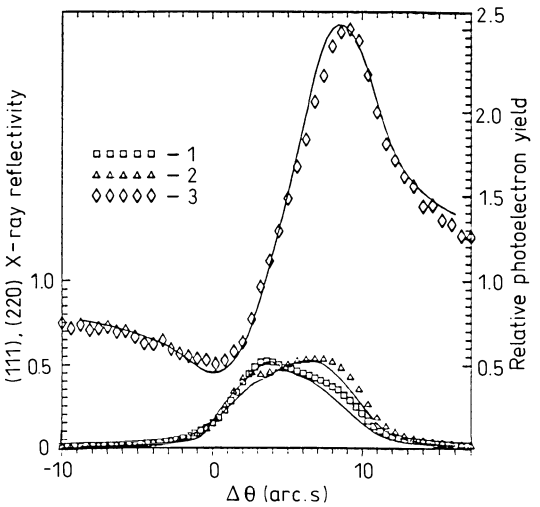

Fig. 5.27. The experimental angular dependence of the photoelectron yield under the conditions of multibeam diffraction in the angular range of strong multibeam interaction

crystal. The curve shown in Fig. 5.27 measured in the angular range of the multibeam interaction resulted from the superposition of two systems of standing waves along the (111) and (220) directions.

5.5 Methods for Analysis of Powder Diffraction Patterns

The wide spread of powder diffractometry for the solution of qualitative and special problems such as the determination of the crystalline phases in mixtures, the studies of surface and bulk textures, microstresses on the surface and in the bulk, etc. is explained by relative simplicity of the experimental implementation

of the method and availability of fine crystalline or polycrystalline specimens. But structural information obtained by powder diffractometry was relatively scarce since the angular resolution of the method was substantially lower than that of single crystal techniques, whereas powder diffraction patterns include, as a rule, several groups of almost unresolved overlapped Bragg peaks whose number depends on the angular dispersion of the instrument (the so-called instrumental function).

Since it was believed that the structural information is contained in the integral intensity, i.e., in a Bragg peak as a whole, it was natural to consider the groups of unresolved peaks separately. But such a division was always rather arbitrary and yielded, even in the most favorable cases, only semiqualitative results. The main difficulty met in the determination of the integral intensities was the impossibility of the unique analytical description of the Bragg line profile, the instrumental function of the apparatus, and the errors in the determination of the background line for the groups of unresolved reflections.

In 1967, *Rietveld* [5.53] suggested a new approach to the analysis of powder diffraction patterns. Since then the method has been widely used in the x-ray analysis and neutron powder diffraction and has become the main method for structural studies by neutrons. At the same time, scientists have already had in their possession rather powerful computers. Owing to insufficiently strong monochromatic neutron beams on the specimen used in structural investigations, it was possible to use diffractometers with low or moderate resolution. Therefore the profiles of Bragg peaks had, in fact, a pure Gaussian shape with the angular dispersion (the total peak width at the half-height) described by the expression

$$A^{1/2} = (U \tan^2 \theta + V \tan \theta + Z), \tag{5.27}$$

where θ is the scattering angle, and U, V, and Z are free parameters. Since the peak profile on the diffraction pattern is a linear combination of the convolution of the spectral (W), instrumental (G) and diffraction (S) functions and the background,

$$Y(2\theta) = (W * G * S) + \text{background}, \tag{5.28}$$

Rietveld suggested to use in the least squares refinement the whole diffraction pattern upon preliminary refinement of the background from the background-free areas between the peaks. The instrumental parameters entered the refinement procedure as those to be refined. As the criterion of the refinement merit the well known R-factors and the difference between the experimental and calculated diffraction patterns were used. The latter comparison was taken to be a necessary figure of merit. In addition, the following fitting parameter was introduced

$$\chi = R_{wp}/R_{exp}, \tag{5.29}$$

where R_{wp} is the weighted profile R-factor and R_{exp} is the expected R-factor. For a correctly designed experiment and correctly chosen model, χ tends to unity,

$\chi \to 1$, in other words, χ also indicates the quality of the experiment and the sufficiency of the given experimental set (necessary number of parameters) for the refinement. Already the first refinements proved the method efficiency. The obtained positional parameters were in good agreement with the results of the single crystal x-ray studies, the mean square errors of the obtained values being substantially lower.

The application of the Rietveld technique to the structure refinement by the powder diffraction data was so successful that the method was recognized as a method for the full-profile analysis. Numerous computer programs for the method are an essential part of powder diffraction software [5.54]. At present, the most well known program is that written by *Young* and *Wills* [5.55] and its modifications for the analysis of multiphase systems. Figures 5.28 and 5.29 show the results of the full-profile analysis obtained for ceolite [5.56], a structure of a moderate complexity, and one of the organic compounds [5.57]

Despite all the successes of the full profile analysis in the refinement of the positional parameters, the extraction of information on atomic thermal vibrations in the crystal lattice remained rather problematic even in the isotropic harmonic approximation. The main problem was the correct background line for large scattering angles where the effects of the thermal vibrations are most pronounced and the groups of unresolved reflections are located. This dictated the improvement of the angular resolution of experimental setups at the simultaneous preservation, or even increase, of the diffractometer luminocity due to the application of focusing monochromators and coordinate detectors. But with a decrease of the angular dispersion and an increase in the resolution of experimental setups, the Bragg peak profiles start deviating from the Gaussian shape both due to the instrumental effects in convolution (1) and due to

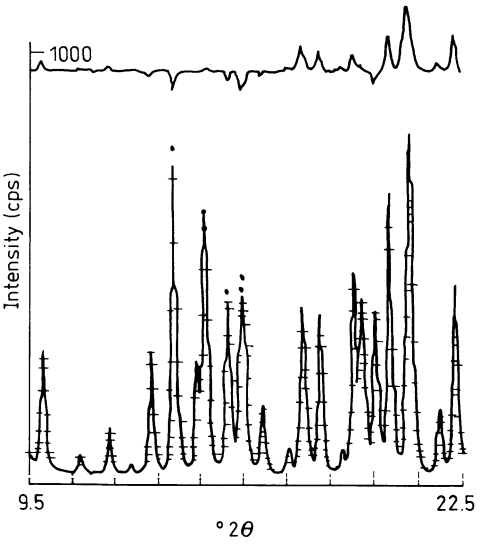

Fig. 5.28. Full profile analysis of x-ray diffraction pattern of ceolite B.ZSM-5 with sorbed pyridine.
Solid line denotes experimental data, (—) represent calculated data, the difference curve is shown above [5.56]

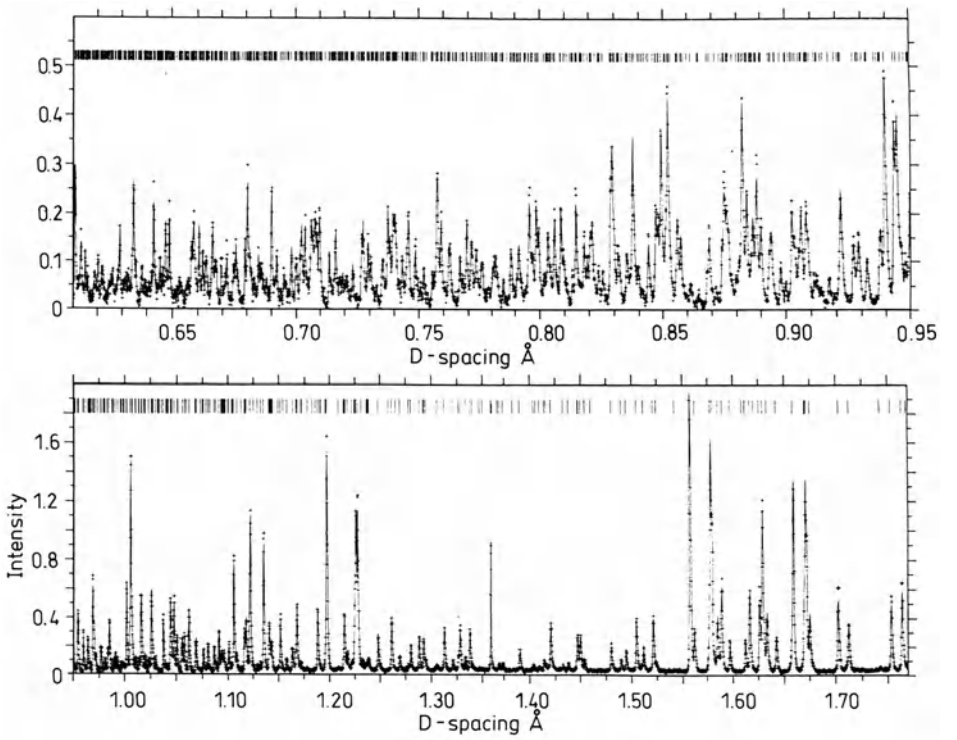

Fig. 5.29. Full profile analysis of time-of-flight neutron diffraction pattern of benzene obtained on a HRPD, ISIS high-resolution diffractometer.
Solid line denotes experimental data, + represent calculated data, the position of Bragg reflections is shown above these lines [5.57]

structurally independent effects such as the grain size, microstresses, etc. The attempts to improve the situation by the introduction into the refinement programs of a set of profile analytical functions (at present, seven-eight functions [5.55]) that are the combinations of various Gaussians and Lorentzians were only of a limited success. But such a work gave rise to numerous investigations of physics of the Gaussian profile distortions and resulted in the creation of various methods and programs for taking into account also the grain size and microstresses [5.54]. This allowed not only the extraction of the structural information but also the information on the grain size and microstresses from the powder diffraction patterns.

But the problem of obtaining the correct values of thermal parameters and mean-square errors in the profile analysis has not been solved. It was suggested [5.58] that the mean-square errors in the Rietveld method are underestimated due to good fitting of the profile and not of the structural model and that the use of integral intensities would be more correct. The latter study gave rise to a new

direction in the powder diffraction analysis – the so-called profile fitting technique [5.59]. The method reduces to the deconvolution of convolution (5.28):

$$Y(2\theta) = (W * G) * S + \text{background} \tag{5.30}$$

with separate fitting of the expression in brackets in the right-hand side, first without the invocation of the structural model and the extraction of the integral intensities. At the second stage, the obtained integral intensities are refined by any known least-squares technique. The efficiency of the profile fitting is illustrated by Fig. 5.30.

The final reliability factors reduce down to 0.7% for the correct mean square errors and thermal vibration parameters. According to [6], this indicates the obvious advantages of the profile analysis over the full-profile technique. But the suggested new method requires the creation of a bank of profile data for a series of standard specimens which then can be used for the selection of the convolution $(W * G)$ for different areas of experimental diffraction patterns. Moreover, it also requires a careful choice of specimens to avoid possible texture effects.

In the process of the further development of the two-stage method [5.56] it was also suggested [5.60] to refine experimental profiles of various portions of

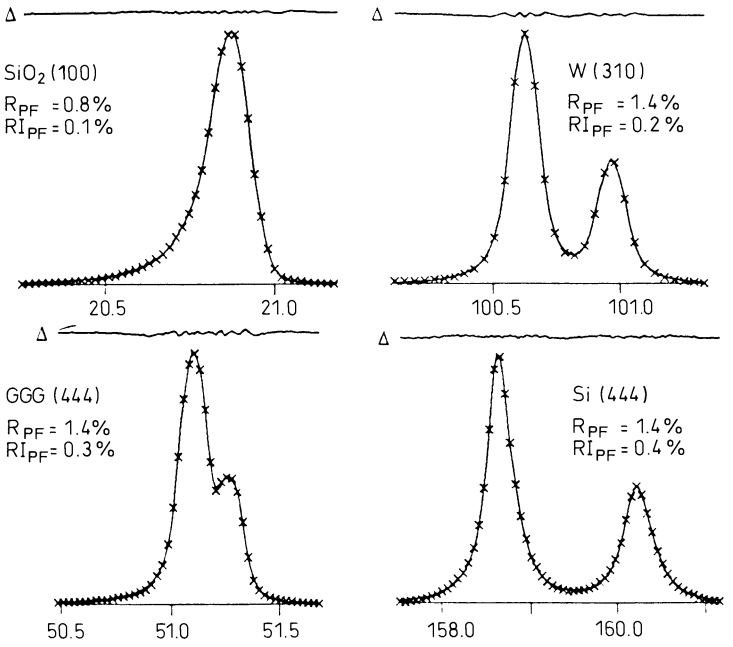

Fig. 5.30. Four typical profiles for *hkl* series and CuK_α doublets for the determination of the instrumental function $W * G$.
Solid line denotes the calculated data, × represents the experimental data (intermediate points are omitted), Δ gives the difference (above), all the data on the same intensity scale; R_{PF} is the profile factor, RI_{PF} is the integral profile factor, SiO_2: quartz, GGG: galium-gadolinium garnet [5.58]

diffraction patterns in individual least-squares procedures with no invocation of the profiles of standard specimens.

Despite a series of shortcomings, the method of the full-profile analysis remains to be the most popular method for the treatment of powder diffraction patterns because of its relative simplicity, efficiency and moderate time-consuming. This method lies in the basis of most programs for the structure determinations from the powder diffraction data [5.61].

The methods for the analysis of powder diffraction patterns are being further developed. The following problems are still waiting for their solution: the correlation of the refined parameters, the introduction of the correction for thermal diffuse scattering, the determination of the background for obtaining not only harmonic but also anharmonic parameters of thermal vibrations, etc.

5.6 EXAFS Spectroscopy

From the mid seventies a new analytical method for the investigation of the structure of local atomic environment of a chemical element has gained general acceptance – the study of extended x-ray absorption fine structure (EXAFS). The method allows the investigation of the structure of noncrystalline materials and supplements the x-ray structure analysis of crystals providing the local investigation of small specimen regions. The method also gives the radial distribution curve of the local environment of each of the specimen under investigation. The radial distribution curve allows the determination of interatomic distances and coordination numbers and also the identification of the kinds of atoms in the vicinity of the atom under study [5.62].

5.6.1 The Fundamentals of the EXAFS Theory

An x-ray radiation passing though a material is weakened due to its interaction with the material atoms. For radiation wavelength $\lambda \cong 1$–10 Å, the main role in absorption is played by the photoelectric effect. X-ray absorption in a layer of thickness L is expressed as

$$I_o = I \exp(-\mu L), \tag{5.30}$$

where I_o and I are the intensities of the primary and transmitted beam, respectively, and μ is the linear absorption coefficient depending on the nature of an absorbing atom ($\cong Z^3$). For the most part of the spectrum μ monotonically increases with the wavelength as $\cong \lambda^3$. But in the x-ray spectrum range with $\lambda = \lambda_q$ (where λ_q are the wavelengths corresponding to the quantum energy $E_q = hc/\lambda_q$ giving rise to ionization of atomic K, L_{I} and L_{II} levels) μ experiences a drastic increase (absorption jump). In such ranges the dependence of the absorption coefficient on λ is rather complicated which is schematically illustrated in Fig. 5.31. A sharp increase of μ is called the absorption edge; the fluctuations of $\mu(E)$ in the 20–30 eV range adjacent to the absorption edge from

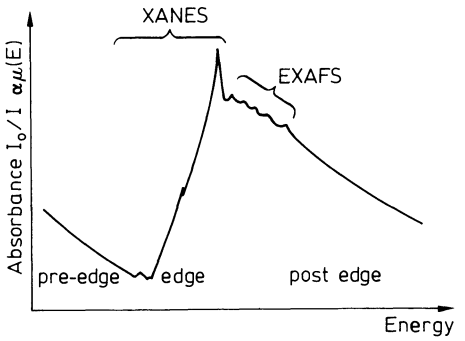

Fig. 5.31. Schematic of the absorption cross-section in vicinity of an elemental absorption edge showing the EXAFS and XANES

the side of high energies is called a x-ray absorption near edge structure (XANES). Relatively weak $\mu(E)$ oscillations in the 50–1000 eV range above the absorption edge are called an extended x-ray absorption fine structure (EXAFS).

The formation of an EXAFS is due to the environment of an ionized atom and phenomenologically can be described in the following way. Photoelectric absorption occurs when a bound electron (e.g., at the K-level is excited by an incident photon with the energy hc/λ higher than the binding energy of this level, E_q. For $hc/1 < E_q$, no excitation is possible (pre-edge). For $hc/\lambda > E_q$, an emitted electron has the energy $hc/\lambda - E_q$ and can be considered as a spherical wave with the wavelength $\lambda_e = 2\pi/k$ and $k = (2m(hc/1 - E_q)/\hbar)^{1/2}$. Such wave is scattered in the backward direction by the nearest atoms surrounding the ionized one. The backward scattered wave interacts with the primary wave. As a result of interference, the primary wave is either enhanced or weakened depending on the wave phase shift. In turn, the phase shift is determined by λ_e and the mutual arrangement of the atom emitting a photoelectron and the atoms participating in scattering. Since μ is determined in terms of the wave functions of the initial ψ_q and final ψ_j states of the photoelectron, the enhancement of ψ_j due to interference should result in stronger absorption.

EXAFS is formed by the atoms of the nearest environment spaced by 3–5 Å, in other words, by the atoms of the first two coordination spheres (the effects of multiple scattering can be neglected). EXAFS is independent of the long-range order and therefore can be used for the investigation of the local atomic structure of any material – amorphous or crystalline. The only requirement here is a sufficient amount of the material and a sufficient concentration of excited atoms for the reliable signal-background ratio.

5.6.2 Structure Information Extracted from EXAFS Spectra

The analysis of EXAFS spectra yields the information on the local neighbours of an excited atom thus providing the determination of the number, distances, and the type of neighboring atoms. An EXAFS spectrum is the oscillating part of the absorption coefficient normalized to the absorption coefficient

$$\chi(k) = (\mu - \mu_0)/\mu_0 = \Delta\mu/\mu_0, \tag{5.31}$$

where μ_0 is the absorption coefficient in the absence of the EXAFS and $\mu = -(1/L)\,1m\,I/I_o$. A simplified expression for EXAFS-oscillations in a single-electron plane-wave approximation is written as

$$\chi(k) = -\sum_j (N_j/kR_j^2)|f_j(k,\pi)|\exp(-2\sigma_j k^2)^2 \exp(-2R_j\gamma)\sin(2kR_j + \phi_j(k)), \tag{5.32}$$

where

N_j is the number of atoms scattering at distance R_j.

$|f_j(k,n)|$ is the amplitude of photoelectron scattering in the backward direction by the jth atom (π-change of the phase),

$\exp(-2\sigma_j k^2)$ is the Debye-Waller factor due to thermal vibrations and statistical disorder of atoms, σ is the disordering amplitude,

$\exp(-2R_j\gamma)$ is the factor that takes account of losses in inelastic scattering of photoelectrons, γ is the electron free path,

$\phi_j(k)$ is the phase variation for a photoelectron occurring in its emission and scattering.

In most cases EXAFS oscillations are studied with the aid of the Fourier-analysis of spectra. The Fourier transformation $\chi(k)$ yields the curve that allows the determination of the radial distribution curve for atoms around the absorbing atom. The positions of maxima on such curve correlate with interatomic distances, their amplitudes correlate with the coordination numbers, and the half-widths with the amplitude of the atomic thermal vibrations (Fig. 5.32).

The other methods of the analysis are based on the direct solution of the equation describing the EXAFS-oscillations for a certain model. There are two such models. In the first one, the environment of each atom is represented by a number of coordination spheres set by their radii, coordination number and the Debye-Waller factor. In this case the EXAFS-oscillations are the sum of the contributions from a finite number of such spheres. The second model reduces to

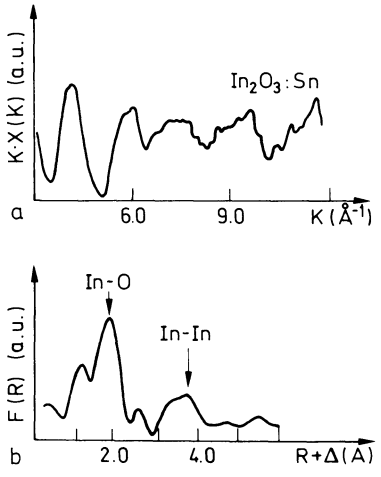

Fig. 5.32a,b. EXAFS spectrum from a thin In_2O_3 film on a Sn substrate (**a**), and the radial distribution function obtained from this spectrum (**b**) [5.63]

the introduction of a correlation function and the solution of an integral equation.

5.6.3 Experimental Methods and Apparatus

EXAFS spectroscopy is associated with the advent of sources of synchrotron radiation (SR). Directional synchrotron radiation having a high intensity and continuous spectrum in the wide energy range is almost ideal for obtaining EXAFS spectra.

The traditional method for obtaining EXAFS spectra is the transmission technique based on the measurements of the intensity ratio of the incident and transmitted radiation. As a rule, for a monochromatic radiation the use is made of a double crystal monochromators of various types made of silicon or germanium single crystals. Monochromators provide rather a high degree of radiation monochromatization $\Delta\lambda/\lambda$ (of the order of 10^{-4}) and a smooth variation of the wavelength without substantial change of the beam position in the space. To cut off high-order reflections and to focus the beam on a specimen one uses mirrors of complete external reflection of x-rays. The incident and transmitted radiation are recorded by high-precision ionization cameras with different absorption coefficients. The apparatus also includes collimation slits and specimen holders. The measurements are made in the automatic mode and controlled by a computer.

To reduce the time of spectrum recording, methods for simultaneous recording of the whole transmission spectrum are being developed. This can be attained by sweeping the spectrum into a line over radiation energy with the aid of a focusing monochromator and recording the transmitted beam by a linear detector.

In addition to the transmission method there also exist a series of experimental techniques based on the measuring the yield of secondary processes of the exciting-radiation interaction with the material of the system under study, i.e., x-ray fluorescence, Auger-electrons, total or partial photocurrent, and ions desorbed from the surface. These methods widen the class of substances and materials suitable for the study, change the character and the volume of the obtainable information and allow the investigation of the near edge structure not only in the bulk but also in thin surface layers including monolayers.

EXAFS spectroscopy can also be implemented with the aid of conventional x-ray tubes in combination with the high-luminosity focusing x-ray optics.

References

Chapter 1

1.1 B.K. Vainshtein, V.V. Barynin, G.V. Gurskaya, V.Ya. Nikitin: Kristallografiya **12**, 860 (1967) [English transl.: Sov. Phys. – Crystallogr. **12**, 750 (1968)

1.2 A.A. Urusovskaya, R. Tyaagaradzhan, M.V. Klassen-Neklyudova: Kristallografiya **8**, 625 (1963) [English transl.: Sov. Phys. – Crystallogr. **8**, 501 (1964)

1.3 V.G. Govorkov, E.P. Kozlovskaya, Kh.S. Bagdasarov, N.N. Voinova, E.A. Fedorov: Kristallografiya **17**, 599 (1972) [English transl.: Sov. Phys. – Crystallogr. **17**, 518 (1972)

1.4 E. Kaldis, N. Petelev, A. Simanovskis: J. Cryst. Growth **40**, 298 (1977)

1.5 M.V. Lomonosov: *Polnoye sobraniye sochineniy*. T.2. Trudy po fizike i khimii 1747-1752 (Complete works, Vol.2, Investigations on physics and chemistry, 1747-1752) (Izd-vo Akad. Nauk SSSR, Moscow 1951) p.275 (in Russian)

1.6 R.-J. Haüy: *Struktura kristallov. Izbrannye trudy* (Structure of crystals. Selected works) (Izd-vo Akad. Nauk SSSR, Leningrad 1962) (in Russian)

1.7 W. Friedrich, P. Knipping, M. Laue: Ann. Phys. N.Y. **41**, 971 (1913)

1.8 V.N. Rozhansky, N.D. Zakharov: *Issledovaniye tochechnykh defektov i ikh kompleksov metodom diffraktionnoi elektronnoi mikroskopii*. Trudy Shkoly po metodam issledovaniya tochechnykh defektov, Bukuriani, Fevral' 1976 (Institut fiziki AN GSSR, Tbilisi 1977)

1.9 C.L. Hannay, P. Fitz-James: Can. J. Microbiol. **1**, 694 (1955)

1.10 O. Nishikawa, E.W. Muller: J. Appl. Phys. **35**, 2806 (1964)

1.11 D. Schechtman, I. Blech, D. Gratias, J.W. Cahn: Phys. Rev. Lett. **53**, 1951 (1984)

1.12 M. Audier: Microsc. Microanal. Microstruct. **1**, 405 (1990)

1.13 A.F. Skryshevsky: *Strukturnyi analiz zhidkostei* (Rentgenografiya, neitrono-, elektronografiya) (Structure Analysis of Liquids, X-Ray, Neutron and Electron Diffraction) (Vysshaya shkola, Moscow 1971) (in Russian)
S. Iijima, Y.G. Alpress: Acta Crystallogr. A **30**, 22 (1974)

Chapter 2

2.1 E.S. Fedorov: *Kurs kristallografii* (A Course of Crystallography) (Rikker, St. Petersburg 1901) (in Russian)

2.2 B.N. Deloné, et al.: Dokl. Akad. Nauk SSSR **209**, 25 (1974)

2.3 B.N. Deloné, R.V. Galiulin, M.I. Shtogrin: Teoriya Brave i ee obobschcheniye na trekhmernyje reshotki (Bravai' theory and its generalization for three-dimensional lattices), in *Bravé O. Izbrannye trudy* (O. Bravais' selected works) (Nauka, Leningrad 1974) p.333 (in Russian)

2.4 B.N. Deloné, M.I. Shtogrin: Dokl. Akad. Nauk SSSR **219**, 95 (1974)

2.5 M.I. Shtogrin: Tr. Mat. Inst. Akad. Nauk SSSR **213**, 3 (1973)

2.6 M.I. Shtogrin: Dokl. Akad. Nauk SSSR **218**, 528 (1974)

2.7 A.V. Shubnikov: Kristallografiya **5**, 489 (1960) [English transl.: Sov. Phys. – Crystallogr. **5**, 469 (1961)
2.8 A.V. Shubnikov, N.V. Belov: *Coloured Symmetry* (Pergamon, Oxford 1964)
2.9 C.H. MacGillavry: *Symmetry Aspects of M.C. Escher's Periodic Drawings* (Oostoek, Utrecht 1965)
2.10 J.F.C. Hessel: *Krystallometrie, oder Krystallonomie und Krystallographie*, Gehler's physikalisches Wörterbuch, Bd.5 (Schwichert, Leipzig 1830)
2.11 A. Gadolin: *Abhandlung über die Herleitung aller krystallographischer Systeme mit ihren Unterabteilungen aus einem einzigen Prinzip*, ed. by P. Groth (Engelmann, Leipzig 1896)
2.12 J. Donohue: *The Structure of the Elements* (Wiley, New York 1974)
2.13 B.K. Vainshtein, V.M. Fridkin, V.I. Indenbom: *Sovremennaya Kristallografiya*. T. 2. Struktura kristallov, ed. by B.K. Vainshtein (Nauka, Moscow 1979) [English transl.: *Modern Crystallography II*, Structure of Crystals, ed. by B.K. Vainshtein, Springer Ser. Solid-State Sci., Vol.21 (Springer, Berlin, Heidelberg 1981)
2.14 L.A. Shuvalov, A.A. Urusovskaya, I.S. Zheludev, A.V. Zalesskii, B.N. Grechushnikov, I.G. Chystyakov, S.A. Semiletov: *Sovremennya Kristallografiya*. T. 4. Fizicheskije svoistva kristallov, ed. by B.K. Vainshtein (Nauka, Moscow 1981) [English transl.: *Modern Crystallography IV*, Physical Properties of Crystals, ed. by L.A. Shuvalov, Springer Ser. Solid-State Sci., Vol.37 (Springer, Berlin, Heidelberg 1988)]
2.15 A.V. Shubnikov, V.A. Koptsik: *Simmetriya v nauke i iskusstve* (Nauka, Moscow 1972) [English transl.: *Symmetry in Science and Art* (Plenum, New York 1974)
2.16 M.J. Buerger: *Elementary Crystallography* (Wiley, New York 1956)
2.17 A.L. Mackay: Chemia **23**, 433 (1969)
2.18 B.K. Vainshtein: Kristallografiya **4**, 842 (1959) [English transl.: Sov. Phys. – Crystallogr. **4**, 801 (1960)
2.19 N.A. Kiselev, F.Ya. Lerner: J. Mol. Biol. **86**, 587 (1974)
2.20 E. Alexander: Z. Kristallogr. Kristallgeom. Kristallphys. Kristallchem. **70**, 367 (1929)
2.21 E. Alexander, K. Herrmann: Z. Kristallogr. Kristallgeom. Kristallphys. Kristallchem. **70**, 328 (1929)
2.22 L. Weber: Z. Kristallogr. Kristallgeom. Kristallphys. Kristallchem. **70**, 309 (1929)
2.23 L. Sohncke: *Entwicklung einer Theorie der Kristallstruktur* (Engelmann, Leipzig 1879)
2.24 V.A. Koptsik: *Shubnikovskiye gruppy* (Shubnikov Groups) (Izd-vo MGU, Moscow 1966) (in Russian)
2.25 H. Zassenhaus: Comment. Math. Helv. **21**, 117 (1948)
2.26 R.V. Galiulin: *Matrichno-vektornyi sposob vyvoda fedorovskikh grupp* (Matrix-vector method for deriving Fedorov groups) (VINITI, Moscow 1969) (in Russian)
2.27 *International Tables for X-Ray Crystallography*, Vol.1, Symmetry Groups, ed. by N.F.M. Henry, K. Lonsdale (1952); Vol.2, Mathematical Tables, ed. by J.S. Kasper, K. Lonsdale (1959); Vol.3, Physical and Chemical Tables, ed. by C.H. MacGillavry, G.D. Rieck (1962); Vol.4 Revised and Supplementary Tables to Vols.2 and 3, ed. by J.A. Ibers, W.C. Hamilton (1974)

2.28 *Internationale Tabellen zur Bestimmung von Kristallstrukturen*, Bd.1. Gruppentheoretische Tafeln (Gebr. Borntraeger, Berlin 1935)
2.29 *International Tables for Crystallography*, Vol.A: Space Group Symmetry, ed. by Th. Hahn, 3rd edn. (Kluwer, Dordrecht 1992)
2.30 N.V. Belov: Tr. Inst. Kristallogr. Akad. Nauk SSSR **6**, 25 (1951)
2.31 B.N. Deloné, N.P. Dolbilin, M.I. Shtogrin, R.V. Galiulin: Dopkl. Akad. Nauk SSSR **227**, 19 (1976)
2.32 N.M. Bashkirov: Kristallografiya **4**, 466 (1959) [English transl.: Sov. Phys. – Crystallogr. **4**, 442 (1960)
2.33 B.N. Deloné, N. Padurov, A. Aleksandrov: *Matematicheskiye osnovy strukturnogo analiza kristallov* (Mathematical Foundations of Structure Analasis of Crystals) (Gostekhizdat, Moscow 1934) (in Russian)
2.34 B.N. Deloné: Usp. Mat. Nauk **3**, 16 (1937); **4**, 102 (1938)
2.35 B.K. Vainshtein: Kristallografiya **5**, 341 (1960) [English transl.: Sov. Phys. – Crystallogr. **5**, 323 (1960)]
2.36 B.K. Vainshtein, B.B. Zvyagin: Kristallografiya **8**, 147 (1963) [English transl.: Sov. Phys. – Crystallogr. **8**, 107 (1963)
2.37 H. Heesch: Z. Kristallogr. Kristallgeom. Kristallphys. Kristallchem. **73**, 325 (1930)
2.38 H. Heesch: Z. Kristallogr. Kristallgeom. Kristallphys. Kristallchem. **71**, 95 (1929)
2.39 V.A. Koptsik: Krist. Tech. **10**, 231 (1975)
2.40 A. Niggli: Z. Kristallogr. Kristallgeom. Kristallphys. Kristallchem. **111**, 288 (1959)
2.41 A. Niggli, H. Wondratschek: Z. Kristallogr. Kristallgeom. Kristallphys. Kristallchem. **114**, 215 (1960); **115**, 1 (1961)
2.42 B.A. Tavger, V.M. Zaitsev: Zh. Eksp. Teor. Fiz. **30**, 564 (1956)
2.43 A.M. Zamorzaev: Kristallografiya **2**, 15 (1957) [English transl.: Sov. Phys. – Crystallogr. **2**, 10 (1957)
2.44 B.L. van der Waerden, J.J. Burkhardt: Z. Kristallogr. Kristallgeom. Kristallphys. Kristallchem. **115**, 231 (1961)
2.45 M.C. Escher: *The Graphic Work* (Oldbourne, London 1960)
2.46 N.V. Belov, T.N. Tarkhova: Kristallografiya **1**, 4, 615, 619 (1956); ibid. **3**, 618 (1958) [English transl.: Sov. Phys. – Crystallogr. **3**, 625 (1959)]
2.47 N.V. Belov, E.N. Belova: Kristallografiya **2**, 21 (1957) [English transl.: Sov. Phys. – Crystallogr. **2**, 16 (1957)]
2.48 A.V. Shubnikov: *Simmetriya i antisimmetriya konechnykh figur* (Symmetry and antisymmetry of finite figures) (Izd-vo Akad. Nauk SSSR, Moscow 1951) (in Russian)
2.49 D. Harker: Acta Crystallogr. A**32**, 133 (1976)
2.50 V.L. Indenbom: Kristallografiya **4**, 619 (1959) [English transl.: Sov. Phys. – Crystallogr. **4**, 578 (1960)
2.51 L.A. Shuvalov: Kristallografiya **7**, 520 (1962) [English transl.: Sov. Phys. – Crystallogr. **7**, 418 (1963)]
2.52 V.L. Indenbom, N.V. Belov, N.N. Neronova: Kristallografiya **5**, 497 (1960) [English transl.: Sov. Phys. – Crystallogr. **5**, 477 (1961)]
2.53 O. Wittke: Z. Kristallogr. Kristallgeom. Kristallphys. Kristallchem. **117**, 153 (1962)
2.54 O. Wittke, J. Garrido: Bull. Soc. Fr. Mineral. Cristallogr. **82**, 223 (1959)

2.55 N.N. Neronova, N.V. Belov: Kristallografiya **6**, 3 (1961) [English transl.: Sov. Phys. – Crystallogr. **6**, 1 (1961)]
2.56 A.L. Machay, G.S. Powley: Acta Crystallogr. **16**, 11 (1963)
2.57 N.V. Belov, N.N. Neronova, T.S. Smirnova: Tr. Inst. Kristallogr. Akad. Nauk SSSR, **11**, 33 (1955); Kristallografiya **2**, 315 (1957) [English transl.: Sov. Phys. – Crystallogr. **2**, 311 (1957)
2.58 A.M. Zamorzajev, E.I. Galyazskij, A.F. Palistrant: *Tsvetnaja simmetriya, obobshcheniya i prilozheniya* (Colour symmetry, its generalization and application) (Shtiintsa, Kishinev 1978) (in Russian)
2.59 K. Dornberger-Schiff: *Lerhgang über OD-Strukturen* (Akademie, Berlin 1966)
2.60 K. Fichtner: Krist. Tech. **12**, 1263 (1977)

Chapter 3

3.1 A.A. Chernov, E.I. Givargizov, K.S. Bagdasarov, V.A. Kuznetsov, L.N. Demyanets, A.N. Lobachev: *Sovremennaya Kristallografiya*, T. 3. Obrazovanije kristallov, ed. by B.K. Vainshtein (Nauka, Moscow 1980) [English transl.: A.A. Chernov: *Modern Crystallography III, Crystal Growth*, Springer Ser. Solid-State Sci., Vol.36 (Springer, Berlin, Heidelberg 1984)
3.2 A.I. Glazow: Bull. USSR Miner. Soc. **104**, 486 (1975)
3.3 B.N. Deloné, N. Padurov, A. Aleksandrov: *Matematicheskiye osnovy strukturnogo analiza kristallov* (Mathematical foundations of structure analasis of crystals) (Gostekhizdat, Moscow 1934) (in Russian)
3.4 B.N. Deloné, et al.: Dokl. Akad. Nauk SSSR **209**, 25 (1974)
3.5 B.N. Deloné, R.V. Galiulin, M.I. Shtogrin: Teoriya Brave i ee obobschcheniye na trekhmernyje reshotki (Bravai' theory and its generalization for three-dimensional lattices), in *Bravé O. Izbrannye trudy* (O. Bravais' selected works) (Nauka, Leningrad 1974) p.333 (in Russian)
3.6 B.N. Deloné, M.I. Shtogrin: Dokl. Akad. Nauk SSSR **219**, 95 (1974)

Chapter 4

4.1 W.L. Bragg: Proc. Cambridge Phil. Soc. **17**, 43 (1913)
4.2 G. Wulff: Phys. Z **14**, 217 (1913)
4.3 B.K. Vainshtein, V.M. Fridkin, V.I. Indenbom: *Sovremennaya Kristallografiya*. T. 2. Struktura kristallov, ed. by B.K. Vainshtein (Nauka, Moscow 1979) [English transl.: *Structure of Crystals*, Modern Crystallography, Vol.2 (Springer, Berlin, Heidelberg 1995)
4.4 *International Tables for X-Ray Crystallography*, Vol.1, Symmetry Groups, ed. by N.F.M. Henry, K. Lonsdale (1952); Vol.2, Mathematical Tables, ed. by J.S. Kasper, K. Lonsdale (1959); Vol.3, Physical and Chemical Tables, ed. by C.H. MacGillavry, G.D. Rieck (1962); Vol.4 Revised and Supplementary Tables to Vols.2 and 3, ed. by J.A. Ibers, W.C. Hamilton (1974)
4.5 R.C. McWeeny: Acta Crystallogr. **4**, 513 (1951); **5**, 463 (1952)
4.6 P.A. Doyle, P.S. Turner: Acta Crystallogra. A **24**, 390 (1968)
4.7 R.F. Stewart: J. Chem. Phys. **51**, 4569 (1969)
4.8 Y. Wang, P. Coppens: Inorg. Chem. **15**, 1122 (1976)

4.9 L.A. Muradyan, M.I. Sirota, I.P. Makarova, V.I. Simonov: Kristallografiya **30**, 258 (1985) [English transl.: Sov. Phys. – Crystallogr. **30**, 148 (1985)
4.10 U.H. Zucker, E. Perenthaler, W.F. Kuns, R. Bachmann, H. Schulz: J. Appl. Crystallogr. **16**, 358 (1983)
4.11 G.B. Boky: *Kristallokhimiya* (Crystal chemistry) (Nauka, Moscow 1971) (in Russian)
4.12 W.L. Bragg, E.R. Howells, M.F. Perutz: Acta Crystallogr. **5**, 136 (1952)
4.13 A. Hargreaves, H.C. Watson: Acta Crystallogr. **10**, 368 (1957)
4.14 H. Hashimoto, A. Howie, M.J. Whelan: Proc. R. Soc. London A **269**, 79 (1962)
4.15 P.N.T. Unwin: Electron Microscopy, Vol.1, 5th Europ. Cong. Electron Microscopy, Manchester (1972) p.232
4.16 W.H. Zachariasen: Acta Crystallogr. **23**, 558 (1967)
4.17 P.J. Becker, P. Coppens: Acta Crystallogr. A **30**, 129 (1947)
4.18 W.H. Zachariasen: *Theory of X-Ray Diffraction in Crystals* (Wiley, New York 1945)
4.19 G. Borrman, W. Hartwig: Z. Kristallogr. Kristallgeom. Kristallphys. Kristallchem. **121**, 401 (1965)
4.20 A. Authier: Bull. Soc. Fr. Mineral. Cristallogr. **84**, 51 (1961)
4.21 R.W. James: *The Dynamical Theory of X-Ray Diffraction*. Solid State Physics, Vol.15 (Academic, London 1963) p.53
4.22 M. Lefeld-Sosnovska, E. Zielinska-Rohosinska: Acta Phys. Pol. **21**, 329 (1962)
4.23 P.B. Hirsch, G.H. Ramachandran: Acta Crystallogr. **3**, 187 (1950)
4.24 N. Kato: Acta Crystallogr. A**25**, 119 (1969)
4.25 Z.G. Pinsker: *Dinamicheskoye rasseyaniye rentgenovskikh luchei v ideal'nykh kristallakh* (Nauka, Moscow 1974) [English transl.: *Dynamical Scattering of X-Rays in Crystals*, Springer Ser. in Solid-State Sci., Vol.3 (Springer, Berlin, Heidelberg 1978)
4.26 M. Hart: Sci. Prog. London **56**, 429 (1968)
4.27 J. Bradler, A.R. Lang: Acta Crystallogr. A **24**, 246 (1968)
4.28 H.B. Stuhrman: Acta Crystallogr. A **26**, 297 (1970)
4.29 D.I. Svergun, L.A. Feigin, B.M. Schedrin: Acta Crystallogr. A **38**, 827 (1982)
4.30 F. de Bergevin, M. Brunel: Phys. Lett. A **39**, 141 (1972)
4.31 C.C. Tang, W.G. Stirling, D.L. Jones, C.C. Wilson, P.W. Haycock, A.J. Rollason, A.H. Thomas, D. Fort: J. Magn. Mag. Mater. **103**, 86 (1992)
4.32 D. Gibbs, D.R. Harshman, E.D. Isaacs, D.B. McWhan, D. Mils, C. Vettier: Phys. Rev. Lett. **61**, 1241 (1988)
4.33 D.M. Kheiker: Kristallografiya **23**, 1288 (1978) [English transl.: Sov. Phys. – Crystallogr. **23**, 729 (1978)
4.34 L.A. Shuvalov, A.A. Urusovskaya, I.S. Zheludev, A.V. Zalesskii, B.N. Grechushnikov, I.G. Chystyakov, S.A. Semiletov: *Sovremennya Kristallografiya*. T. 4. Fizicheskije svoistva kristallov, ed. by B.K. Vainshtein (Nauka, Moscow 1981) [English transl.: *Modern Crystallography IV*, Physical Properties of Crystals, ed. by L.A. Shuvalov, Springer Ser. Solid-State Sci., Vol.37 (Springer, Berlin, Heidelberg 1988)]
4.35 A. Guinier, G. von Eller: Les méthodes expérimentales des déterminations de structures cristallines par rayons X, *Handbuch der Physik*, Bd.32, T.1 (Springer, Berlin, Heidelberg 1957)

4.36 B.K. Vainshtein, G.M. Lobanova, G.V. Gurskaya: Kristallografiya **19**, 531 (1974) [English trans.: Sov. Phys. – Crystallogr. **19**, 329 (1974)]
4.37 B. Post: Acta Crystallogr. A **35**, 17 (1979)
4.38 A.L. Patterson: Z. Kristallogr. Kristallgeom. Kristallphys. Kristallchem. A **90** 517 (1935)
4.39 D. Harker: J. Chem. Phys. **4**, 381 (1936)
4.40 B.K. Vainshtein: Tr. Inst. Kristallogr. Akad. Nauk SSSR **7**, 15 (1952)
4.41 M.J. Buerger: *Vector Space and Its Application in Crystal-Structure Investigation* (Wiley, New York 1959)
4.42 M.I. Sirota, V.I. Simonov: Kristallografiya **15**, 681 (1970) [English transl.: Sov. Phys. – Crystallogr. **15**, 589 (1970)
4.43 V.I. Simonov: Acta Crystallogr. B **25**, 1 (1969)
4.44 S.V. Borisov: Kristallografiya **9**, 515 (1965) [English transl.: Sov. Phys. – Crystallogr. **9**, 603 (1965)
4.45 S.V. Borisov, V.P. Golovatchev, V.V. Ilyukhin, E.A. Kuz'min, N.V. Belov: Zh. Strukt. Khim. **18**, 175 (1972)
4.46 V.V. Ilyukhin, S.V. Borisov, A.N. Chernov, I.V. Belov: Kristallografiya **17**, 269 (1972) [English transl.: Sov. Phys. – Crystallogr. **17**, 227 (1972)]
4.47 L.V. Bukvetskaya, T.G. Shishova, V.I. Andrianov, V.I. Simonov: Kristallografiya **22**, 494 (1977) [English transl.: Sov. Phys. – Crystallogr. **22**, 282 (1977)]
4.48 E.A. Kuz'min, S.V. Borisov, V.P. Golovachev, V.I. Iljukhin, L.N. Solovijeva, A.N. Chernov: *Sistematicheskij analiz funktsii Pattersona na osnovye simmetrii kristalla* (A systemativ analysis of Patterson's function on the basis of crystal symmetry) (Isz-vo Akad. Nauk SSSR, Khabarovsk 1974) (in Russian)
4.49 M.A. Porai-Koshits: Tr. Inst. Kristallogr. Akad. Nauk SSSR **9**, 229 (1954)
4.50 D. Harker: Acta Crystallogr **9**, 1 (1956)
4.51 D. Harker, J.S. Kasper: Acta Crystallogr. **1**, 70 (1948)
4.52 B.K. Vainshtein: Kristallografiya **9**, 7 (1964) [English transl.: Sov. Phys. – Crystallogr. **9**, 5 (1964)]
4.53 A.I. Kitaigorodsky: *Teoriya strukteurnogo analiza* (Theory of structure analysis) (Izd-vo Akad. Nauk SSSR, Moscow 1957) (in Russian)
4.54 D. Sayre: Acta Crystallogr. **5**, 60 (1952)
4.55 J. Karle, H. Hauptman: Acta Crystallogr. **6**, 131 (1953)
4.56 H. Hauptman, J. Karle: *The Solution of the Phase Problem* I. The Centrosymmetric Crystal, American Crystallographic Association Monograph, No.3 (Edwards Brothers, Ann Arbor, MI 1953)
4.57 W.A. Cochran: Acta Crystallogr. **5**, 65 (1952)
4.58 W.H. Zachariasen: Acta Crystallogr. **5**, 68 (1952)
4.59 H. Hauptman: *Crystal Structure Determination. The Role of the Cosine Semivariants* (Plenum, New York 1972)
4.60 H.A. Hauptman: Acta Crystallogr. A **31**, 529 (1975)
4.61 J. Karle, I.L. Karle: Acta Crystallogr. **21**, 849 (1966)
4.62 G.A. Tsourcaris: Acta Crystallogr. A **26**, 492 (1970)
4.63 M.M. Woolfson: Rep. Prog. Phys. **34**, 369 (1971)
4.64 M. Toda, R. Kubo, N. Saito: *Statistical Physics I, Equilibrium Statistical Mechanics*, 2nd edn., Springer Ser. Solid-State Sci., Vol.30 (Springer, Berlin, Heidelberg 1992)

R. Kubo, M. Toda, N. Hashitsume: *Statistical Physics II, Nonequilibrium Statistical Mechanics*, 2nd edn., Springer Ser. Solid-State Sci., Vol.31 (Springer, Berlin, Heidelberg 1991)
4.65 A.G. Khachaturyan, S.V. Semenovskaya, B.K. Vainshtein: Sov. Phys. – Crystallogr. **24**, 519 (1979)
4.66 S.F. Gull, G.J. Daniell: Nature **272**, 686 (1978)
4.67 A.D. Podjarny, D. Moras, J. Navaza, P.M. Alzary: Acta Crystallogr. A **44**, 545 (1988)
4.68 G. Bricogne: Acta Crystallogr. A **40**, 410 (1984)
4.69 A. Klug: Acta Crystallogr. **11**, 515 (1958)
4.70 G. Bricogne: Acta Crystallogr. A **40**, 410 (984)
4.71 A.D. McLachlan: Gazzetta Chimica Italiana **117**, 11 (1987)
4.72 J. Skilling, S.F. Gull: In *Maximum-Entropy and Bayesian Methods in Inverse Problems*, ed. by C.R. Smith, W.T. Grandy (Reidel, Dordrecht 1985) p.83
4.73 V.I. Simonov: *Crystollogr. Computing Techniques*, ed. by F.R. Ahmed, K. Huml, B. Sedlacek (Munksgaard, Copenhagen 1976) p.138
4.74 V.Yu. Lunin: Acta Crystallogr. A **44**, 144 (1988)
4.75 V.Yu. Lunin, E.A. Veroslova: Acta Crystallogr. A **47**, 238 (1991)
4.76 B.K. Vainshtein, I.M. Gel'fand, R.L. Kayushina, Yu.G. Fedorov: Dokl. Akad. Nauk SSSR **153**, 93 (1963)
4.77 I.M. Gel'fand, E.B. Vul, S.L. Ginzburg, Yu.G. Fedorov: *Metod ovragov v zadachakh rentgenostrukturnogo analiza* (Ravine method in problems of X-ray structure analysis) (Nauka, Moscow 1966) (in Russian)
4.78 E.B. Vul, G.M. Lobanova: Kristallografiya **12**, 411 (1967) (in Russian)
4.79 A.E. Smith, R. Kalish, E.J. Smuiny: Acta Crystallogr. B **28**, 3494 (1972)
4.80 G.R. Freeman, R.A. Hearn, C.E. Bugg: Acta Crystallogr. B **28**, 2906 (1972)
4.81 B.K. Vainshtein: Adv. Struct. Res. Diffr. Methods **1**, 24 (1964)
4.82 B.B. Zvyagin: *Elektronografiy i strukturnaya kristallografiya glinistykh mineralov* (Nauka, Moscow 1964) [English transl.: *Electron Diffraction Analysis of Clay Mineral Structures* (Plenum, New York 1967)]
4.83 S.A. Semiletov: Dokl. Akad. Nauk SSSR **137**, 584 (1961)
4.84 B.B. Zvyagin, A.P. Zhuchlistov, M.G. Kyazumov, A.M. Fominenkov: Kristallografiya **35**, 602 (1990)
4.85 Yu.P. Khodyrev, R.V. Baranova, S.A. Semiletov: Izv. Akad. Nauk SSSR Met. **2**, 2226 (1977)
4.86 R.M. Imamov, V.V. Udalova: Kristallografiya **21**, 907 (1976)
4.87 D.L. Dorset, W.F. Tivol, J.N. Turner: Ultramicroscopy **38**, 41 (1991)
4.88 B.K. Vainshtein: *Structure Analysis by Electron Diffraction* (Pergamon, Oxford 1964)
4.89 D.L. Dorset: Ultramicroscopy **38**, 23 (1991)
4.90 V.F. Dvoryankin, B.K. Vainshtein: Kristallografiya **1**, 626 (1956)
4.91 R.F. Egerton: *Electron Energy-Loss Spectroscopy in the Electron Microscope* (Plenum, New York 1986)
4.92 R.A. Goodman: Acta Crystallogr. A **31**, 804 (1973)
4.93 M. Tanaka, M. Terauchi: Convergent Beam Electron Diffraction. JEOL Ltd (1985)
4.94 B.F. Baxton, J.A. Eades, J.W. Steeds, G.M. Rackham: Phys. Trans. Roy. Soc. (London) **281**, 171 (1976)
4.95 J. Gjonnes, A.F. Moodie: Acta Crystallogr. **19**, 65 (1965)

4.96 M. Tanaka, H. Sekii, T. Nagasawa: Acta Crystallogr. A **39**, 825 (1983)
4.97 J.J. Lander: *Low-Energy Electron Diffraction and Surface Structural Chemistry*, Prog. Solid-State Chem. Vol.2 (Pergamon, Oxford 1965) p.26
4.98 M.A. Van Hove, W.H. Weinberg, C.-M. Chan: *Low-Energy Electron Diffraction*, Springer Ser. Surf. Sci., Vol.6 (Springer, Berlin, Heidelberg 1986)
4.99 M.C. Desjonquères, D. Spanjaard: *Concepts in Surface Physics*, 2nd edn. (Springer, Berlin, Heidelberg 1996)
4.100 D.A. Gorodetsky, Yu.P. Mel'nik, V.K. Shklyar: Kristallografiya **23**, 1093 (1978) [English transl.: Sov. Phys. – Crystallogr. **23**, 620 (1978)
4.101 L. Reimer: *Transmission Electron Microscopy*, 3rd edn., Springer Ser. Opt. Sci., Vol.36 (Springer, Berlin, Heidelberg 1993)
4.102 Philips Tech. Rev. **43**, 275 (1987)
4.103 B.K. Vainshtein: Sov. Phys. Usp. **30**, 393 (1987)
4.104 J.M. Cowley: *Diffraction Physics* (North-Holland, Amsterdam 1975)
4.105 O. Scherzer: J. Appl. Phys. **20**, 20 (1949)
4.106 J.C.H. Spence: *Experimental High-Resolution Electron Microscopy* (Clarendon, Oxford 1981)
4.107 K. Kambe: Ultramicroscopy **10**, 223 (1982)
4.108 J.M. Cowley, A.F. Moodie: Acta Crystallogr. **10**, 609 (1957)
4.109 J.M. Cowley, A.F. Moodie: Proc. Roy. Soc. (London) A **76**, 3378 (1960)
4.110 H. Hashimoto, E. Endoh, Y. Takai, H. Tomioka, Y. Yokota: Chem. Scripta **14**, 23 (1978-1979)
4.111 J.L. Hutchison, T. Honda, E.D. Boyes: JEOL news, E **24**, 9 (1986)
4.112 V.L. Karasev, N.A. Kiselev, E.V. Orlova, M.A. Gribelyuk, A.K. Gutakovsky, Yu.O. Kanter, S.M. Pintus, S.V. Rubanov, S.I. Stenin, A.A. Fedorov: Ultramicroscopy **35**, 11 (1991)
4.113 M.P.A. Vieqers, A.F. De Yong, M.R. Leys: Spectrochem. Acta B **40**, 835 (1985)
4.114 J.L. Hutchison: JEOL news, E **28**, 4 (1990)
4.115 N.D. Zakharov, M.A. Gribeluk, B.K. Vainshtein, O.N. Rozanova, K. Ushida, S. Horinehi: Acta Crystallogr. B **39**, 575 (1983)
4.116 S. Hovmoller, A.Sjogren, G. Farrants, M. Sundserg, B.O. Marinder: Nature **311**, 238 (1984)
4.117 V.A. Drits, N.D. Zakharov, I.P. Khadzhi: Izv. Akad. Nauk SSSR, Ser. Geol. N **11**, 82 (1979)
4.118 R. Sinelair, F.A. Ponce, T. Yamashita, D.J. Smith, R.A. Camps, L.A. Freeman, S.J. Erasmus, W.C. Nixon, K.C.A. Smith, C.J.D. Catto: Nature **298**, 127 (1982)
4.119 L.D. Mark: Ultramicroscopy **18**, 445 (1985)
4.120 D.Y. Smith, L.D. Mark: Ultramicroscopy **16**, 101 (1985)
4.121 H. Bethge, W. Keller: Optik **23**, 462 (1965/1966)
4.122 G.I. Distler: Izv. Akad. Nauk SSSR Ser. Fiz.Mat. **36**, 1846 (1972)
4.123 K. Yagi: *Advances in Optical and Electron Microscopy* (Academic, London 1989) p.57
4.124 B.K. Vainshtein: *Adv. Optical and Electron Microscopy*, Vol.7 (Academic, London 1978) p.94
4.125 P.W. Haskes, U. Valdre (eds.): *Biophysical Electron Microscopy* (Academic, London 1990)
4.126 N.A. Kiselev, D.J. De Rosier, A. Klug: J. Mol. Biol. **35**, 561 (1968)

4.127 P.N.T. Unwin, R. Henderson: J. Mol. Biol. **94**, 425 (1975)
4.128 G.I. Kosourov, I.E. Lifshits, N.A. Kiselev: Kristallografiya, **16**, 813 (1971)
4.129 V.P. Kosykh, A.I. Pustovskikh, V.S. Kirichuk, T. Kuhne, E.V. Orlova, V.L. Tsuprun, N.A. Kiselev: Kristallography **28**, 1982 (1983) [English transl.: Sov. Phys. – Crystallogr. **28**, 637 (1983)
4.130 M. van Heel, J. Frank: Ultramicroscopy **6**, 187 (1981)
4.131 M. van Heel: Optik **82**, 114 (1989)
4.132 A.B. Goncharov, B.K. Vainshtein, A.I. Ryskin, A.A. Vagin: Sov. Phys. – Crystallogr. **32**, 504 (1987)
4.133 J. Radon: Ber. Saechs. Acad. Wiss, Leipzig, Math.-Phys. Kl., Acad. Wissen. Leipzig **69**, 262 (1917)
4.134 W. Baumeister, W. Fogell (eds.): *Electron Microscopy at Molecular Dimensions* (Springer, Berlin, Heidelberg 1980)
4.135 B.K. Vainsthein, S.S. Orlov: Kristallografiya **17**, 253 (1972) [English transl.: Sov. Phys. – Crystallogr. **17**, 214 (1972)]
4.136 A.M. Mikhailov, B.K. Vainshtein: Kristallografiya **16**, 505 (1971) [English transl.: Sov. Phys. – Crystallogr. **16**, 428 (1971)
4.137 M.B. Sherman, E.V. Orlova, S. Hovmoller, E.A. Smirnova, N.A. Zorin: J. Bacterol. **173**, 2576 (1991)
4.138 H. Hoshimoto, M. Mannami, T. Naiku: Philos. Trans. Roy. Soc. (London) **253**, 459 (1961)
4.139 R. Henderson, J.M. Baldwin, T.A. Ceska, F. Zemlin, E. Beckmann, K.H. Downing: J. Mol. Biol. **213**, 899 (1990)
4.140 R. Henderson, J.W. Baldwin, K.H. Downing, J. Lepault, F. Zemlin: Ultramicroscopy **19**, 147 (1986)
4.141 J.W. Baldwin, R. Henderson, E. Beckman, F. Zemlin: J. Mol. Biol. **202** 585 (1988)
4.142 B.K. Vainshtein, G.V. Gurskaya, V.V. Barynin: Kristallografiya **16**, 751 (1971)
4.143 Y. Yonath, H.G. Wittmann: Trends in Biochemical Sci. **14**, 329 (1989)
4.144 M. Radermacher, W. Hoppe: Proc. 10th Int'l. Cong. on Electron Microscopy (1978) p.218
M. Radermacher: J. Electron Microsc. Techn. **9**, 359 (1988)
4.145 M. Radermacher, T. Wagenknecht, A. Vershoor, J. Frank: J. Microsc. **146**, 113 (1987)
4.146 A. Klug, D.J. de Rosier: Nature (London) **212**, 29 (1966)
4.147 R.A. Growther, D.J. de Rosier, A. Klug: Proc. Roy. Soc. (London) A **317**, 319 (1970)
4.148 M. Yeager, K.A. Dryden, N.H. Olson, H.B. Greeberg, T.S. Baker: J. Cell. Biol. **110**, 2133 (1990)
T.S. Baker, W.W. Newcomb, F.P. Booy, J.C. Brown, A.C. Steven: American Soc. for Microbiology **64**, 563 (1990)
4.149 L. Reimer: *Scanning Electron Microscopy*, Springer Ser. Opt. Sci., Vol.45 (Springer, Berlin, Heidelberg 1985)
4.150 E.I. Givargizov: J. Cryst. Growth **20**, 217 (1973)
G.S. Gritsayenko, M.I. Ilyin: Izv. Akad. Nauk, SSSR Ser. Geol. **17**, 21 (1975)
4.151 G. Binnig, H. Rohrer: IBM J. Res. Develop. **30**, 355 (1986)
4.152 H.-J. Güntherodt, R. Wiesendanger (eds.): *Scanning Tunneling Microscopy I*, 2nd edn., Springer Ser. Surf. Sci., Vol.20 (Springer, Berlin, Heidelberg 1994)

R. Wiesendanger, H.-J. Güntherodt (eds.): *Scanning Tunneling Microscopy II*, 2nd edn., Springer Ser. Surf. Sci., Vol.28 (Springer, Berlin, Heidelberg 1995)
R. Wiesendanger, H.-J. Güntherodt (eds.): *Scanning Tunneling Microscopy III*, 2nd edn., Springer Ser. Surf. Sci., Vol.29 (Springer, Berlin, Heidelberg 1996)
4.153 S.I. Vasil'yev, Yu.N. Moiseyev, N.I. Nikitin, S.V. Savinov, I.V. Yaminsky: Elektron. Promyshl. **3**, 36 (1991)
4.154 Chunli Bai: *Scanning Tunneling Microscopy and its Application*, Springer Ser. Surf. Sci., Vol.32 (Springer, Berlin, Heidelberg 1995)
4.155 Yu.N. Moiseyev, V.I. Panov, S.V. Savinov; I.V. Yaminsky: Elektron. Promyshl. **3**, 39 (1991)
4.156 F. Besenbacher, K. Mortensen: Europhys. News **21**, 68 (1990)
4.157 T. Sakurai et al.: J. Vac. Sci. Technol. **8**, 251 (1990)
4.158 A. Humbert et al.: J. Vac. Sci. Technol. **8**, 311 (1990)
4.159 E. Meyer et al.: J. Vac. Sci. Technol. **8**, 495 (1990)
4.160 C.C. Wilson: Neutron News **1**, 14 (1990)
4.161 J.R. Rabe et al.: J. Vac. Sci. Technol. **8**, 679 (1990)
4.162 G.E. Bacon: *Neutron Diffraction*, 2nd edn. (Clarendon, Oxford 1962)
4.163 G.E. Bacon, R.S. Pease: Proc. Roy. Soc. (London) A **230**, 359 (1955)
4.164 E. Sandor, S.O. Ogunade: Nature (London) **224**, 905 (1969)
4.165 N.V. Rannev, R.P. Ozerov, I.D. Datt, A.N. Kshynyakina: Kristallografiya **11**, 175 (1966) [English transl.: Sov. Phys. – Crystallogr. **11**, 177 (1966)]
4.166 D.E. Cox: IEEE Trans. MAG-**8**, 161 (1972)
4.167 C.G. Shull, W.A. Stauser, E.O. Wollan: Phys. Rev. **83**, 333 (1951)
4.168 O.P. Aleshko-Ozhevsky, I.I. Yamzin: Zh. Eksp. Teor. Fiz. **56**, 1217 (1969)
4.169 C.G. Shull, H.A. Mook: Phys. Rev. Lett. **16**, 184 (1966)
4.170 G.L. Squires: *Introduction to the Theory of Thermal Neutron Scattering* (Cambridge Univ. Press, Cambridge 1978)
4.171 R.N. Kuz'min, A.V. Kolpakov, G.S. Zhdanov: Kristallografiya **11**, 511 (1966) [English transl.: Sov. Phys. – Crystallogr. **11**, 457 (1967)]
4.172 A.M. Afanasiev, Yu.M. Kagan: Zh. Eksp. Teor. Fiz. **48**, 327 (1965)
4.173 A.F. Tulinov, Yu.V. Melikov: Priroda Moscow **10**, 39 (1974)

Chapter 5

5.1 D. Schechtman, I. Blech, D. Gratias, J.W. Cahn: Phys. Rev. Lett. **53**, 1951 (1984)
5.2 R. Penrose: Math. Intell. **2**, 32 (1979)
5.3 A.L. Mackay: Physica A **114**, 609 (1982)
5.4 A. Yamamoto, K. Hiraga: Phys. Rev. B **37**, 6207 (1988)
5.5 Y.L. Mackay: Kristallografiya. **26**, 910 (1981) [English transl.: Sov. Phys. – Crystallogr. **26**, 517 (1981)]
5.6 A.L. Mackay: Computers and Math. with Applications **128**, 21 (1986)
5.7 D.R. Nelson, B.I. Halperin: Science **229**, 233 (1985)
5.8 M.V. Jaric' (ed.): *Aperiodicity and Order*, Vol.1. Introduction to the mathematics of quasicrystals. Vol.3. Extended icosahedral structures (Academic, Orlando, FL 1989)
5.9 T. Janssen: Phys. Rep. **168**, 55 (1988)

5.10 C.H. Janot, J.M. Dubois (eds.): *Quasicrystalline Materials* (World Scientific, Singapore 1988)
5.11 E.S. Fedorov: *Symmetry of Crystals* (American Crystallographic Association, New York 1971)
5.12 H. Bohr: Acta Math. **45**, 29 (1924)
5.13 H. Bohr: Acta Math. **46**, 101 (1925)
5.14 H. Bohr: Acta Math. **47**, 237 (1927)
5.15 D. Gratias: Physica Scripta **129**, 38 (1989)
5.16 D.S. Rokhsar, D.C. Wright, N.D. Mermin: Acta Crystallogr. A **44**, 197 (1988)
5.17 D.A. Rabson, N.D. Mermin, D.S. Rokhsar, D.C. Wright: Rev. Mod. Phys. **63**, 699 (1991)
5.18 A. Bienenstock, P.P. Ewald: Acta Crystallogr. **15**, 1253 (1962)
5.19 L.S. Levitov, J. Rhyner: J. de Physique **49**, 1835 (1988)
5.20 B.K. Vainshtein, V.M. Fridkin, V.I. Indenbom: *Sovremennaya Kristallografiya*. T. 2. Struktura kristallov, ed. by B.K. Vainshtein (Nauka, Moscow 1979) [English transl.: *Structure of Crystals*, Modern Crystallography, Vol.2 (Springer, Berlin, Heidelberg 1995)
5.21 C. Janot: Europhys. News **21**, 23 (1990)
5.22 T. Janssen: Acta Crystallogr. A **42**, 261 (1986)
5.23 D.S. Rokhsar, D.C. Wright, N.D. Mermin: Phys. Rev. B **37**, 8145 (1988)
5.24 V. Elser, C.L. Henley: Phys. Rev. Lett. **55**, 2883 (1985)
5.25 M. Audier, J. Pannetier, M. Leblane, C. Janot, J.M. Lang, B. Dubost: Physica. B **153**, 136 (1988)
5.26 D.P. Shoemaker, C.B. Shoemaker: Introduction to quasicrystals, *Icosahedral Coordination in Metal Crystals, Aperiodicity and Order*, ed. by M.V. Jaric (1988) Vol.1, p.1
5.27 V.E. Dmitrienko: J. de Physique **51**, 2717 (1990)
5.28 P.W. Stephens, A.I. Goldman: Scientific American **264**, 44 (April 1991)
5.29 L.A. Shuvalov, A.A. Urusovskaya, I.S. Zheludev, A.V. Zalesskii, B.N. Grechushnikov, I.G. Chystyakov, S.A. Semiletov: *Sovremennya Kristallografiya*. T. 4. Fizicheskije svoistva kristallov, ed. by B.K. Vainshtein (Nauka, Moscow 1981) [English transl.: *Modern Crystallography IV, Physical Properties of Crystals*, ed. by L.A. Shuvalov, Springer Ser. Solid-State Sci., Vol.37 (Springer, Berlin, Heidelberg 1988)]
5.30 P.M. De Wolff: Acta Crystallogr. A **30**, 777 (1974)
5.31 P.M. De Wolff, T. Janssen, A. Janner: Acta Crystallogr. A **37**, 625 (1981)
5.32 M. Hart: Workshop on "Applications of High Energy X-Ray Scattering at European Synchrotron Radiation Facilities. Proc. ESRF (1988) p.165
5.33 H. Wiedemann: *Particle Accelerator Physics I, II* (Springer, Berlin, Heidelberg 1993,1995)
5.34 N.H. Xuong, S.T. Freer, R. Hamlin, et al.: Acta Crystallogr. A **34**, 239 (1978)
5.35 M.E. Andrianova, D.M. Kheiker, A.N. Popov, V.I. Simonov, Y.S. Anisimov, S.P. Chirnenko, A.B. Ivanov, S.A. Movchan, V.D. Peshekhonov, Y.V. Zanevsky: J. Appl. Crystallogr. **15**, 626 (1982)
5.36 R. Kohn, R. Fourme, R. Bosshard, et al.: Nuclear Instrum. Methods **201**, 203 (1982)
5.37 U.W. Arndt, D.J. Gilmore: J. Appl. Crystallogra. **12**, 1 (1979)
5.38 J. Myahara, K. Takahashi: Nuclear Instrum. Methods. **179**, 503 (1981)
5.39 R-AXIS II. Rigaku Automated X-Ray Imaging System. Rigaku Denki Booklet

5.40 R.L. Johnson, J.H. Fock, I.K. Robinson, J. Bohr, R. Feidenhans'l, J. Als-Nielsen, M. Nielsen, M. Toney: In *The Structure of Surfaces*, ed. by M.A. Van Hove, S.Y. Tong, Springer Ser. Surf. Sci., Vol.2 (Springer, Berlin, Heidelberg 1985)
5.41 W.C. Marra, P. Eisenberger, A.Y. Cho: J. Appl. Phys. **50**, 6927 (1979)
5.42 X.M. Zhu, R. Feidenhansl's, H. Zabel, Als. Nielsen, R. Du, C.P. Flynn, F. Grey: Phys. Rev. B **37**, 7157 (1988)
5.43 H. Dosch, L. Mailander, A. Lied, J. Peisl, F. Grey, R.L. Johnson, S. Krummacher: Phys. Rev. Lett. **60**, 2382 (1988)
5.44 J. Bohr, F. Feidenhansl's, M. Nielsen, M. Toney, R.L. Johnson, I.K. Kobinson: Phys. Rev. Lett. **12**, 1275 (1985)
5.45 R. Feidenhanl's: Surf. Sci. Rep. **10**, 105 (1989)
5.46 B.W. Battermam: Appl. Phys. Lett. **1**, 68 (1962)
5.47 A.M. Afanas'ev, V.G. Kon: Zh. Eksper. Techn. Fiz. **74**, 300 (1978)
5.48 M.V. Koval'chuck, V.G. Kon: Usp. Fiz. Nauk. **149**, 69 (1986)
5.49 P.L. Cowen, J.A. Golovchenko, M.F. Robbinson: Phys. Rev. Lett. **44**, 1680 (1980)
5.50 J.R. Patel, P.E. Freeland, M.S. Hybersten, D.C. Jacobson, L.A. Golovchenko: Phys. Rev. Lett. **59**, 2180 (1987)
5.51 L.A. Golovchenko, J.R. Patel, D.R. Kaplan, P.L. Cowan, M.S. Bedzyk: Phys. Rev. Lett. **49**, 560 (1982)
5.52 A.Yu. Kazimirov, M.V. Koval'chuk, I.Yu. Kharitonov, L.V. Samoilova, T. Ishikawa, S. Kikuta: Proc. 4th Int'l Conf. on Synchrotron Radiation Instrum., Chester (1991)
5.53 H.M. Rietveld: Acta Crystallogr. **24**, 151 (1967)
5.54 D.K. Smith, S. Gorter: J. Appl. Crystallogr. **24**, 369 (1991)
5.55 R.A. Young, D.B. Willes: Adv. X-Ray Analy. **24**, 1 (1981)
5.56 B.F. Mehtzen: J. Appl. Crystallogr. **22**, 100 (1989)
5.57 C.C. Wilson: Neutron News **1**, 14 (1990)
5.58 M.J. Coopker, K.D. Rouse, M. Sakata: Z. Krystallogr. **157**, 101 (1981)
5.59 G. Will, W. Parrish, T.C. Huang: Z. Appl. Crystallogr. **16**, 611 (1983)
5.60 H. Toraya: J. Appl. Crystallogr. **23**, 485 (1990)
5.61 R. Phil, A. Clearfield: Acta Crystallogr. B **41**, 418 (1985)
5.62 J. Stöhr: *NEXAFS Spectroscopy*, Springer Ser. Surf. Sci., Vol.25 (Springer, Berlin, Heidelberg 1992)
5.63 V. Bets, T. Zamozdiks, A. Lusis, et al.: Nuclear Instrum. Methods. A **261** 173 (1987)

Bibliography

General

Altman S.: *Rotations, Quaternions and Double Groups* (Clarendon, Oxford 1986)

Arndt U.W., A.J. Wonnacott (eds.): *Rotation Method in Crystallography*. Data Collection from Macromolecular Crystals (North-Holland, Amsterdam 1977)

Azaroff L.V. M.J. Buerger: *The Powder Method in X-Ray Crystallography* (McGraw-Hill, New York 1958)

Azaroff L.V. R. Kaplow, N. Kato, R.J. Weiss, A.J.C. Wilson, R.A. Young: *X-ray Diffraction* (McGraw-Hill, New York 1974)

Bacon G.E.: *Neutron Scattering in Chemistry* (Butterworths, London 1977)

Baumeister, W., W. Fogell (eds.): *Electron Microsopy at Molecular Dimensions* (Springer, Berlin, Heidelberg 1980)

Belov N.V.: *Ocherki po strukturnoi kristallografii i fedorovskim gruppam simmetrii* (Essays on structural crystallography and the Fedorov symmetry groups) (Nauka, Moscow 1986)

Bernal J.D., C.H. Carlisle: The range of generalized crystallography. Kristallografiya **13**, 927 (1969) [English transl.: Sov. Phys. – Crystallogr. **13**, 811 (1969)]

Bhagavantam S., T. Venkatarayudu: *Theory of Groups and Its Application to Physical Problems*, 2nd edn. (Andhra University, Waltair 1951)

Bhagavantam S.: *Crystal Symmetry and Physical Properties* (Academic, London 1966)

Bogomolov S.A.: *Vyvod pravil'nykh sistem po methodu Fedorova* (Derivation of regular systems by Fedorov's method) (ONTI-Leningrad 1932, 1934) Vols.1,2

Bokii G.B.: Kristallokhimiya (Nauka, Moscow 1971)

Borchardt-Ott W.: *Kristallographie*. Eine Einführung für Naturwissenschaftler (Springer, Berlin, Heidelberg 1976)

Bradley C.I., A.P. Cracknell: *The Mathematical Theory of Symmetry in Solids: Representation Theory for Point Groups and Space Groups* (Clarendon, Oxford 1971)

Bragg L.: *The Development of X-Ray Analysis* (Hafner, New York 1975)

Bragg W.L.: *The Crystalline State* (Bell, London 1933)

Bravais A.: Mémoire sur les systémes formés par des points distribués réguliérement sur un plan ou dans l'espace. Etudes Cristallographiques **128**, 101 (1850-51) (J. de l'Ecole polytechnique. Cahier **33-34**, t. 19-20)

Bravais A.: Etudes cristallographiques. Extrait des Comptes rendus de l'Académie des Sciences **32**, 284 (1851)

Buerger M.J.: *The Precession Method in X-Ray Crystallography* (Wiley, New York, 1964)

Buerger M.J.: *Contemporary Crystallography* (McGraw-Hill, New York 1970)

Burckhardt J.J.: *Die Bewegungsgruppen der Kristallographie*, 2. Aufl. (Birkhäuser, Basel 1966)

Burckhardt J.J.: *Die Symmetrie der Kristalle*. Von Rene-Just Haug zur kristallographischen Schule in Zürich (Birkhäuser, Basel 1988)

Buseck P.R., J.M. Cowley, L. Eyring (eds.): *High-Resolution Transmission Electron Microscopy and Associated Techniques* (Oxford Univ. Press, Oxford 1988)

Cowley J.M.: *Diffraction Physics*, 2nd edn. (North-Holland, Amsterdam 1981)
Cowley J.M. (ed.): *Electron Diffraction Techniques* (Oxford Univ. Press, Oxford 1992)

Dachs H. (ed.): *Neutron Diffraction*, Topics Curr. Phys., Vol.6 (Springer, Berlin, Heidelberg 1978)
Deloné B.N., N. Padurov, A. Aleksandrov: *Matematicheskie osnovy strukturnogo analiza kristallov* (Mathematical foundations of structure analysis of crystals) (Gostekhizdat, Moscow 1934)
Dornberge-Schiff K.: *Grundzüge einer Theorie der OD-Strukturen aus Schichten* (Akademie-Verlag, Berlin 1964)
Drits V.A.: *Electron Diffraction and High-Resolution Electron Microscopy of Mineral Structures* (Springer, Berlin, Heidelberg 1987)
Engel P.: *Geometric Crystallography: an Axiomatic Introduction to Crystallography* (Reidel, Dordrecht 1986)

Ewald P.P. (ed.): *Fifty Years of X-Ray Diffraction* (Oosthoek, Utrecht 1962)
Evarestov R.A., V.P. Smirnov: *Metody teorii grupp v kvantovoi khimii tverdogo tela* (Group theory methods in solid quantum chemistry) (Izd-vo LGU Leningrad 1987)
Evarestov R.A., V.P. Smirnov: *Site Symmetry in Crystals*, 2nd edn., Springer Ser. Solid-State Sci., Vol.108 (Springer, Berlin, Heidelberg 1996)

Fadeyev D.K.: *Tablitsy osnovnykh unitarnykh predstavlenij fedorovskikh grupp* (Tables of unitary representations of Fedorov groups) (Izd-vo Akad. Nauk SSSR, Moscow 1961)
Fedorov E.S.: *Nachala ucheniya o figurakh* (Elements of the Science of Figures) (Izd-vo Akad. Nauk SSSR, Moscow 1953)
Fedorov E.S.: *Simmetriya i struktura kristallov* (Symmetry and Structure of Crystals) (Izd-vo Akad. Nauk SSSR, Moscow 1949)
Fedorov E.S.: *Symmetry of Crystals* (Americal Crystallographic Association 1971)
Fedorov E.S.: *Pravil'noye delenie ploskosti i prstranstva* (Regular divisions of plane and space) (Nauka, Leningrad 1979)
Feigin L.A., D.I. Svergun: *Structure Analysis by Small-Angle X-Ray and Neutron Scattering* (Plenum, New York 1987)

Gadolin A.: *Abhandlung über die Herleitung aller krystallographischer Systeme mit ihren Unterabteilungen aus einem einzigen Prinzip*, ed. by P. Groth (Engelman, Leipzig 1896)
Galiulin R.V.: *Kristallograficheskay geometriya* (Crystallographic geometry) (Nauka, Moscow 1984)
Giacovazzo C.: *Direct Methods in Crystallography* (Academic, London 1988)
Giacovazzo C. (ed.): *Fundamentsl of Crystallography* (Int'l Union of Crystallography and Oxford Univ. Press, Oxford 1991)
Glasser L.S.: *Crystallography and its Application* (Van Nostrand-Reinhold, Wokingham 1977)

Glusker J.P., B.K. Patterson, M. Rossi (eds.): *Patterson and Pattersons. Fifty years of the Patterson Function* (Int'l Union of Crystallography and Oxford Univ. Press, Oxford 1991)

Goodman P. (ed.): *Fifty Years of Electron Diffraction* (Reidel, Dordrecht 1981)

Groth P.: *Physikalische Kristallographie und Einleitung in die kristallographische Kenntnis der wichtigsten Substanzen* (Engelmann, Leipzig 1905)

Groth P.: *Chemische Kristallographie* (Engelmann, Leipzig 1906-1919) Bde.1-5

Guinier A.: *Théorie et technique de la radiocristallographie*, 2nd edn. (Dunod, Paris 1956)

Guinier A., R. Jullien: *The Solid State: From Superconductors to Superalloys* (Int'l Union of Crystallography and Oxford Univ. Press, Oxford 1991)

Gurman S.J.: *Synchrotron Radiation and Biophysics*, ed. by S.S. Hasnain (Chichester 1990)

Hargittai I. (ed.): *Symmetry. Unifying Human Understanding* (Pergamon, New York 1986)

Hargittai I., B.K. Vainshtein (eds.): *Crystal Symmetries*. Shubnikov Centennial Papers (Pergamon, Oxford 1988)

Hauy M., l'Abbé: *Essai d'une théorie sur la structure des cristaux, appliquée a plusieurs genres de substances cristallisées* (Gogué et Née de la Rochelle, Libraires, Paris 1784)

Hawkes P.W.: *Electron Optics and Electron Microscopy* (Taylor & Francis, London 1972)

Helliwell J.R.: *Macromolecular Crystallography with Synchrotron Radiation* (Cambridge Univ. Press, Cambridge 1992)

Hessel I.F.Ch.: *Krystallometrie, oder Krystallonomie und Krystallographie*, Gehler's physikalisches Wörterbuch, Bd.5 (Schwichert, Leipzig 1830)

Hirsch P.B., A. Howie, P.B. Nickolson, D.W. Pashley, J.J. Whelan: *Electron Microscopy of Thin Crystals*, 2nd edn. (Kreiger, New York 1977)

Hove M.A. Van, S.Y. Tong: *Surface Crystallography by LEED*, Springer Ser. Chem. Phys., Vol.2 (Springer, Berlin, Heidelberg 1979)

Internationale Tabellen zur Bestimmung von Kristallstrukturen, Bd.1. Gruppentheoretische Tafeln (Borntträger, Berlin 1935)

International Tables for X-Ray Crystallography, Vol.1, Symmetry Groups, ed. by N.F.M. Henry, K. Lonsdale (1952); Vol.2, Mathematical Tables, ed. by J.S. Kasper, K. Lonsdale (1959); Vol.3, Physical and Chemical Tables, ed. by C.H. MacGilavry, G.D. Rieck (1962); Vol.4, Revised and Supplementary Tables to Vols.2 and 3, ed. by J.A. Ibers, W.C. Hamilton (1974); 2nd edn. Vol.A, Spase Group Symmetry, ed. by Th. Hahn (Kluwer, Dordrecht 1989); 3rd edn. Vol.A (1992)

Inui T, Y. Tanabe, Y. Onodera: *Group Theory and its Applications in Physics*, 2nd edn., Springer Ser. Solid-State Sci., Vol.78 (Springer, Berlin, Heidelberg 1996)

Isaacs N.W., M.R. Taylor (eds.): *Crystallographic Computing. 4: Techniques and New Technologies* (Int'l Union of Crystallography and Oxford Univ. Press, Oxford 1989)

Izymov Yu.A., R.P. Ozerov: *Magnitnaya neitronografiya* (Nauka, Moscow 1966) [English transl.: *Magnetic Neutron Diffraction* (Plenum, New York 1970)]

James R.W.: *The Optical Principles of the Diffraction of X-Rays* (Bell, London 1950)
Janot C., J.M. Dubois (eds.): *Quasicrystalline Materials* (World Scientific, Singapore 1988)

Jaric M.V. (ed.): *Aperiodicity and Order*, Vol.1. Introduction to quasicrystals. Vol.2. Introduction to the mathematics of quasicrystals. Vol.3 Extended icosahedral structures (Academic, London 1989)
Jaswon M.A., M.A. Ros: *Crystal Symmetry: Theory of Colour Crystallography* (Ellis Horwood, Chichester 1983)

Kleber W.: *Einführung in die Kristallographie* (Technik, Berlin 1971)
Knox R.S., A. Gold (eds.): *Symmetry in the Solid State* (Benjamin, New York 1964)
Koptsik V.A.: *Shubnikovskie gruppy* (Shubnikov groups) (Izd-vo MGU, Moscow 1966)
Kovalev O.V.: *Neprivodimye i indutsirovannye predstavleniya i kopredstavleniya fedorovskikh grupp* (Irreducible and induced representations and corepresentations of the Fedorov groups) (Nauka, Moscow 1986)
Krivoglaz, M.A.: *Difraktsiya rentgenovskikh luchei i neitronov v neidealnikh kristallakh* (Naukova Dumka, Kiev 1983)

Ladd M.F.C.: *Symmetry in Molecular and Crystals* (Wiley, Chichester 1989)
Ladd M.F.C., R.A. Palmer: *Theory and Practice of Direct Methods in Crystallography* (Plenum, New York 1980)
Ladd M.F.C., R.A. Palmer: *Structure Determination by X-Ray Crystallography* 2nd edn. (Plenunm, New York 1985)
Landau L.D., E.M. Lifshits: *Kurs teoreticheskoi fiziki*. T.3. Kvantovaya mekhanika. Nerelyativistskaya teoriya (Fizmatgiz, Moscow 1963) [English transl: *Course of Theoretical Physics*, Vol.3 *Quantum Mechanicals. Nonrelativistic Theory* (Plenum, Oxford 1977)]
Laue M.: *Materiewellen und ihre Interferenzen* (Geest & Protig, Leipzig 1948)
Laue M.: *Röntgenstrahl-Interferenzen* (Geest & Portig, Frankfurt/Main 1960)
Lipson, H., Cochran, W.: *The Determination of Crystal Structures* (Bell, London 1953)
Lipson H., C.A. Taylor: *Fourier Transform and X-Ray Diffraction* (Bell, London 1958)
Lipson H., H. Steeple: *Interpretation of X-Ray Powder Diffraction Patterns* (MacMillan, London 1970)
Lomonosov M.V.: Polnoe sobranie sochinenii. T.2. Trudy po fizike i khimii 1747-1752 (Complete works, Vol.2, Invesigations on physics and chemistry 1747-1752) (Izd-vo Akad. Nauk SSSR, Moscow 1951)
Ludwig W., C. Falter: *Symmetries in Physics*, 2nd edn., Springer Ser. Solid-State Sci. Vol.64 (Springer, Berlin, Heidelberg 1996)
Luybarskij G.Ya.: *Teoriya grupp i ee primenenie v fizike* (Gostekhizdat, Moscow 1957)

Mackay A.L.: *Generalized Crystallography*. Computers and Math. with Applications. Part B. 12, 21 (1986)
McKie D., C. McKie: *Essentials in Crystallography* (Blackwell, Oxford 1986)

Moras D., A.D. Podjarny, J.C. Thierry (eds.): *Crystallographic Computing 5: From Chemistry to Biology* (Int'l Union of Crystallography and Oxford Univ. Press, Oxford 1991)

Nozik Yu.Z., R.P. Ozerov, K. Hennig: *Neitrony i tverdoe telo* (Neutrons and a solid), Vol.1 *Structural Neutron Diffraction Analysis* (Atomizdat, Moscow 1979)

Paufler P.: *Physikalische Kristallographie* (Akademie-Verlag, Berlin 1986)

Pinsker Z.G.: *Electron Diffraction* (Butterworths, London 1952)

Pinsker Z.G.: *Dynamical Scattering of X-Ray in Crystals*, Springer Ser. Solid-State Sci., Vol.3 (Springer, Berlin, Heidelberg 1978)

Porai-Koshits M.A.: *Prakticheskij kurs rentgenostrukturnogo analiza* (Practical course of X-Ray structure analysis), Vol.2 (Izd-vo MGU, Moscow 1960)

Porai-Koshits M.A.: *Osnovy strukturnogo analiza khimikcheskikh soedineniy* (Fundamentals of the structure analysis of chemical compounds) (Vysshaya Shkola, Moscow 1982)

Problemy kristallografii (Problems of crystallography) (A.V. Shubnikov Centennial Papers) (Nauka, Moscow 1987) [English transl.: Modern Crystallography, ed. by B.K. Vainshtein, A.A. Chernov (Nova Science, New York 1988)]

Ramachandran G.N. R. Srinivasan: *Fourier Methods in Crystallography* (Wiley, New York 1970)

Schneer C.J. (ed.): *Crystal Form and Structure* (Wiley, Chichester 1977)

Schönflies A.: *Kristallsysteme und Kristallstrukturen* (Teubner, Leipzig 1891)

Shafranovksy I.I.: *Istoriya kristallografii s drevneishikh vremen do nashikh dneij* (The history of crystallography from ancient times to this day) (Nauka, Leningrad 1978)

Shafranovsky I.I.: *Istoriya kristallografii. XIX vek* (History of crystallography, century XIX) (Nauka, Leningrad 1980)

Shafranovsky I.I.: *Simmetriya v prirode* (Symmetry in nature) (Nedra, Leningrad 1985)

Shubnikov A.V., E.E. Flint, G.B. Bokii: *Osnovy kristalloggrafii* (Fundamentals of crystallography) (Izd-vo Akad. Nauk SSSR, Moscow 1940)

Shubnikov A.V.: *Simmetriya i antisimmetriya konechnykh figur* (Symmetry and antisymmetry of finite figures) (Izd-vo Akad. Nauk SSSR, Moscow 1951)

Shubnikov A.V., N.V. Belov: *Coloured Symmetry* (Pergamon, Oxford 1964)

Shubnikov A.V.: *U istokov kristallografii* (At the source of crystallography) (Nauka, Moscow 1972)

Shubnikov A.V., V.A. Koptsik: *Symmetry in Science and Art* (Plenum, New York 1974)

Sirotin Yu.I., M.P. Shaskol'skaya: *Osnovy kristallofiziki* (Fundamentals of crystal physcis) (Nauka, Moscow 1979)

Sohncke L.: *Entwicklung einer Theorie der Kristallstruktur* (Engelmann, Leipzig 1879)

Spence J.C.H.: *Experimental High-Resolution Electron Microscopy* (Clarendon, Oxford 1981)

Steeds J.W.: *Convergent Beam Electron Diffraction* (Edizione Enea, Roma 1986)

Streitwolf H.-W.: *Gruppentheorie in der Festkörperphysik* (Geest & Portig, Leipzig 1967)

Tanaka M., M. Teranchi: *Convergent-Beam Electron Diffraction* (Jeol, Tokyo 1985) Vol.1

Tanaka M., M. Teranchi, T. Kaneyana: *Convergent-Beam Electron Diffraction* (Jeol, Tokyo 1988) Vol.2

Tanner B.K.: *X-ray Diffraction Topography* (Pergamon, Oxford 1976)

Thomas C., M.Y. Goringe: *Transmission Electron Microscopy of Materials* (Wiley, New York 1979)

Tulinov A.F.: Effect of the crystal lattice on some atomic and nuclear processes. Sov. Phys. – Usp. **8**, 864 (1966)

Vainshtein B.K.: *Strukturnaya elektronographiya* (Izd-vo Akad. Nauk SSSR, Moscow 1956) [English transl.: *Structure Analysis by Electron Diffraction* (Pergamon, Oxford 1964)]

Vainstein B.K.: *Difraktsiya rentgenovykh luchei na tsepnykh molekulakh* (Izd-vo Akad. Nauk SSSR, Moscow 1963) [English transl.: *Diffraction of X-rays by Chain Molecules* (Elsevier, Amsterdam 1966)]

Vainstein B.K.: *Electron Microscopical Analysis of the Three-Dimensional Structure of Biological Macromolecules*, Adv. Optical and Electron Microscopy, Vol.7 (Academic, London 1978)

Vainstein B.K., V.I. Simonov (eds.): *Metody strukturnogo analiza* (Ser. Problemy sovremennoi kristallografii) (Methods of structural analysis) (Nauka, Moscow 1989)

Vainshtein B.K., V.I. Simonov (eds.): *Structural Crystallography: Centennial of the Birth of Acad. N.V. Belov* (Nauka, Moscow 1992)

Vainshtein B.K. (ed.): *Space Groups: Centennial of their Derivation* (Nauka, Moscow 1992)

Vainshtein B.K., L.A. Shuvalov (eds.): *Physical Crystallography* (Nauka, Moscow 1992)

Verma A.R., O.N. Srivastava: *Crystallography for Solid State Physics* (Halsted, New York 1982)

Vigner E.P.: *Symmetry and Reflections* (Indiana Univ. Press, Indiana 1970)

Weyl H.: *The Classical Groups, Their Invariants and Representations* (Princeton Univ. Press, Princeton, NJ 1939)

Weyl H.: *Symmetry* (Princeton Univ. Press, Princeton 1952)

Wigner E.P.: Events, laws of nature and invariance principle. Science **145**, 995 (1964)

Willis B.T.M., A.M. Pryor: *Thermal Vibrations in Crystallography* (Cambridge Univ. Press, Cambridge 1975)

Woolfson M.M.: *An Introduction to X-Ray Crystallography* (Cambridge Univ. Press, Cambridge 1978)

Wooster W.A.: *Diffuse X-Ray Reflections from Crystals* (Clarendon, Oxford 1962)

Wooster W.A.: *Tensors and Group Theory for the Physical Properties of Crystals* (Clarendon, Oxford 1973)

Wulff Yu.V.: *Izbrannye raboty po kristallofizike i kristallografii* (Selected works on crystal physics and crystallography) (Gostekhizdat, Moscow 1952)

Zamorzajev A.M.: *Teoriya antisimmetrii i razlichnye ee obobshcheniya* (Antisymmetry theory and its various generalizations) (Shtiintsa, Kishinev 1976)
Zamorzajev A.M., E.I. Galyarskij, A.F. Palistrant: *Tsvetnaja simmetriya, obobshcheniya i prilozheniya* (Colour symmetry, its generalization and application) (Shtiintsa, Kishinev 1978)
Zhdanov G.S.: *Fizika tverdogo tela* (Solid State Physics) (Izd-vo MGU, Moscow 1961)
Zhidomirov G.M. (ed.): *X-ray Method for Study Structure of Amorphous Solids (EXAFS spectroscopy)* (Nauka, Novosibirsk 1988)
Zholudev I.S.: *Simmetriya i ee prilozheniya* (Symmetry and its applications) (Atomizdat, Moscow 1976)
Zvyagin B.B.: *Electrografiya i struktyrnaya kristallografiya glinistykh mineralov* (Nauka, Moscow 1964) [English Transl.: *Electron Diffraction Analysis of Clay Mineral Structures* (Plenum, New York 1967)]
Zvyagin B.B. (ed.): *Sovremennaya elektronnaya mikroskopiya v issledovanii veschestva* (Modern electron microscopy for materials study) (Nauka, Moscow 1982)

Crystallographic Journals

Acta Crystallographica, published since 1948, divided into: Sections A and B in 1968; Sections A,B and C in 1983; Sections A,B,C and D in 1992
Acta Crystallographica, Sect.A: Foundations of Crystallography
Acta Crystallographica, Sect.B: Structural Science
Acta Crystallographica, Sect.C: Crystal Structure Communications
Acta Crystallographica, Sect.D: Biological Crystallography
American Mineralogist (Am. Mineral.), published since 1916

Bulletin de la Societe Francaise de Mineralogie et de Cristallographie (Bull. Soc. Fr. Mineral. Cristallogr.), published since 1878

Crystal Lattice Defects (Cryst. Lattice Defects), published since 1969
Crystal Structure Communications (Cryst. Struct. Commun.), published since 1972
Crystal Research and Technology (Cryst. Res. and Technology), published since 1966
Crystallography Reviews (Cryst. Rev.), published since 1987

Doklady Akademii Nauk SSSR (Dokl. Akad. Nauk SSSR), published since 1933

Fizika Metallov i Metallovedeniye (Fiz. Met. Metalloved.) [Metal Physics and Physical Metallurgy], published since 1955
Fizika Tverdogo Tela (Fiz. Tverd. Tela) [Solid state physics], published since 1953

Izvesiya Akademii Nauk SSSR, Seriya Fizicheskaya (Izv. Akad. Nauk SSSR Ser. Fiz) [Physical series], published since 1936

J. Applied Crystallography (J. Appl. Crystallogr.), published since 1968
J. Cluster Science, published since 1990
J. Crystal Growth (J. Cryst. Growth), published since 1967
J. Crystal and Molecular Structure, published since 1971
J. Crystallographic and Spectrosopic Research, published since 1971

J. Materials Science (J. Mater. Sci.), published since 1966
J. Materials Research, published since 1986
J. Physics C: Solid Physics (J. Phys. C), published since 1968
J. Physics and Chemistry of Solids (J. Phys. Chem. Solids), published since 1956
J. Solid State Chemistry (J. Solid State Chem.), published since 1969

Koordinatsionnaya Khimiya (Koord. Khim.) [Coordination Chemistry], published since 1975
Kristall and Technik (Krist. Tech.), published since 1966
Kristallografiya (Kristallografiya), published since 1956 [English transl.: by Am. Inst. of Phys.: Soviet Physics – Crystallography (Sov. Phys. – Crystallogr.)]

Microscopy, Microanalysis, Microstructures, published since 1990
Molecular Crystals and Liquid Crystals (Mol. Cryst. Liq. Cryst.), published since 1966

Physica Status Solidi (Phys. Status Solidi), published since 1961
Physical Review [Section] B: Solid State (Phys. Rev. B), published since 1893
Poverkhnost': Fisika, Khimiya, Mekhanika (Surface: Physics, Chemistry, Mechanics), published since 1982

Solid State Communications, published since 1963
Structure Reports (Struct. Rep.), Vol.8 and following, published since 1956
Strukturbericht, Vols.1-7, published from 1936 to 1943
Sverchprovodomost': Phisika, Khimiya, Technika (Superconductivity: Physics, Chemistry, Technique), published since 1987

Thin Solid Films, published since 1967

Uspekhi Fizicheskikh Nauk (Usp. Fiz. Nauk) [Advances of physical sciences], published since 1918 [English transl.: Soviet Physics – Uspekhi (Sov. Phys. – Usp.)]

Zeitschrift für Kristallographie, Kristallogeometrie, Kristallphysik, Kristallchemie (Z. Kristallogr. Kristallgeom. Kristallphys. Kristallchem.), published since 1877
Zhurnal Strukturnoi Khimii (Zh. Struk. Khim.) [Journal of structural chemistry], published since 1959

Subject Index

Accuracy of structure determination 334
Amorphous solids 24, 273, 343
Amplitude of scattering 224, 271
- crystal shape 237
Anisotropy 7
Anomalous transmission 263
Antisymmetry 157, 159, 171
- multiple 171
Aperiodic object 407
Approximant 421
Asymmetric object 79
Atomic amplitude (factor) 227, 330
- electrons 229, 336
- neutrons 229, 393
- x-rays 227
Auger electron spectroscopy 355, 357
Automation of structure analysis 334
Axis of symmetry
- inversion-rotation 66
- mirror-rotation 67
- rotation 65, 96
- - non-crystallographic 24, 405, 412
- screw 68, 246
- of zone 194

Borrmann effect 263
Bragg case of diffraction 257
Bragg-Wulff (equation) 15, 224, 237,
- 280, 339
Bravais group 123, 128
Bravais lattice 123, 128
Buerger (superposition) function 317
Bundle of normals and edges 182

Camera (x-ray)
- Arndt-Wonacott 289, 435, 437
- Buerger (precession) 293
- Debye-Scherrer 300
- De Jong-Bouman 292
- Weissenberg 291, 437
Cauchy inequality 322
Cayley's square 46, 100
Cell
- angles 219-221
- body-centered 216
- face-centered 216
- hexagonal 127, 216
- periods 220-221
- primitive 215
- reciprocal 215
- reduced (unique) 216
- rhombohedral 127, 216
- unit 63, 121
Channeling
- electron 354
- particles 403
Character of representation 52, 102
Chasles center 34
Chasles' theorem 34
Chirality 79
Classes
(crystallographic) 83, 96, 189, 191
Close packing 19
Cluster 420
Condensed state 24, 27
Constancy of angles law 11, 180
Contrast of image
- amplitude 364
- phase 364
Contrast transfer function (CTF) 464
Convolution theorem 232
Crystal blocks 253, 258
Crystal grains 3
Crystal setting 196, 197
Crystal-surface investigation
- x-ray 438, 440
- - standing wave 443
- LEED 441, 445
- photoelectron 446
- RHEED 441
Crystal system 97, 122, 134
Crystalline state 1, 3
Crystallites 3
Curie principle 100

Darwin theory 257
Debye photograph 300, 303
Decoration method 372
Delone variants (parallelohedra) 153, 219
Densitometer 294
Determinant of structure amplitudes 322
Difference synthesis Fourier 332
- deformation 333
- valence 333
Diffraction
- Bethe approximation 350
- chain molecules 274
- crystals 234
- dynamic theory 252, 256, 271, 349
- electron 229, 335
- - high energy (HEED) 335, 350
- - - reflection(RHEED) 343
- - low energy (LEED) 348
- kinematic theory 252, 346
- Mössbauer radiation 401
- neutron 230, 392
- one-dimensional lattice 234
- pattern symmetry 244
- powder 300, 446
- row of points 234
- - surface 440
- three-dimensional lattice 236
- x-ray 223, 229, 256
Diffractometer
- four-circle 295
- neutron 393
- x-ray for polycrystals 304
- x-ray for single crystals 295, 438
- - with position-sensitive detectors
- - 296, 436
Dirichlet construction 148, 151
Dirichlet region 152
Discreteness 21, 53
- sphere 54, 147
Displacement screw 111
Dynamic scattering
- Darwin's treatment 257
- of electrons 346, 349
- Laue-Ewald treatment 258
- x-rays 256, 266, 271

Edge of crystal 181, 194
- indices 183
Electron crystallography 338
Electron density 226
- atom 226
- cell 242
- crystal 227, 242, 309
- quasicrystal 413
Electron diffraction
- camera 337
- convergent beam (CBED) 351, 354
- - large angle (LACBED) 354
- high dispersion (HDED) 351
- high energy (HEED) 335, 351
- - reflection (RHEED) 338, 341
- high resolution (HRED) 351, 368
- low energy (LEED) 335, 355
- microbeam (MBED) 351
- - rocking (RMBED) 351
- - scanning (SMBED) 351
- microdiffraction 338
- pattern 338
- - polycrystal 341
- - reflection 343
- - rotation 343
- - spot 339, 405
- - texture 341
- selected area
(SAED) 338, 351, 360, 405
- spectroscopic (ESD) 354
- theory
- - dynamic 349
- - - two-beam approximation 349
- - - multi-slice method 367
- - geometric 338
- - kinematic 346
Electron energy loss spectroscopy
(EELS) 349
Electron microscope 359
- emission 385
- high resolution (HREM) 23, 368
- scanning (SEM) 361, 383
- - field emission (FESEM) 357
- - transmission (STEM) 360, 385
- transmission (TEM) 358, 382
Electron microscopy 357
- decoration method 372
- image 362
- optical system 352
- replica method 372
- resolution 362, 368
- staining method 375
- micrograph 17, 368, 372, 379
- - optical filtration 377

- three-dimensional reconstruction 378
- two-dimensional 381
Electrostatic potential
- atom 229
- crystal 336
- - projection 336
Elements of symmetry 64-70
Ellipsoid of thermal vibration 233
Enantiomorphism 79, 82
Enantiomorphous
forms 79, 188, 330, 419
Equality 33
- congruent 33
- mirror 33
Euler's equation 193
Euler's theorem 42
Ewalid's construction 239, 285
Ewald-Laue theory 258
Ewald sphere 240, 259, 339, 349
Extinction 245, 248
- coefficient 255
- length 260
- primary 255, 258
- secondary 256

Face of crystal 179, 182, 203
- corresponding 180
- habitus 179, 183
- indices 183, 202
- unit 181, 196, 197, 202
Factor (amplitude)
- atomic 227, 330, 343
- - temperature 232, 242
- Lorentz 255, 294
- phase 242
- polarization 255
- reliability 313, 325
- structure 241, 275, 330, 345
- - normalized 321
- - unitary 250, 321, 325
- temperature 231, 345
- - anisotropic 331
- - isotropic 331
- transmission 255
Families of point group 86
Fedorov (space) group 15, 120, 139
Fibonacci sequence 410
Filtration optical 376
Focusing of x-ray
- Bragg-Brentano 302
- Preston 301
- Zeeman-Bolin 301

Forms of crystal
- closed 183
- general 189
- ideal 193
- simple 183, 188
- - combinations 192
Fourier
- coefficients (terms) 235, 243
- integral 227, 308
- operator 227
- series 243, 309, 336
- synthesis 308
- - difference 332
- - electron density 242, 309
- - nuclear density 395
- - potential 336
- transform 237, 308
Friedel's law 245, 330
Fullerene 94
Fundamental (independent) region 54, 74

Goniometer
- contact-type one-circle 199
- optical 199
- photogoniometer 200
- reflecting two-circle (of theodolite)
- 199
- x-ray 291
Goniometric calculations 200
Goniometry 179, 194
Group, symmetry 10, 44
- abstract 46, 101
- antisymmetry 159, 171, 399
- asymmorphous 136
- black-and-white 167, 171
- of borders 107
- Bravais 123, 127, 131
- - three-dimensional 120, 124
- - two-dimensional 110
- color 168
- crystallographic 60, 82, 91, 96
- cyclic 47
- cylindrical (helical) 110, 115
- extension 48
- Fedorov 15, 120, 131, 137
- - nomenclature 138
- first-kind 56, 96

- generalized 157
- generator 47
- grey 171
- hemisymmorphous 136
- holohedral 97
- homology 176
- homomorphism 47, 129
- icosahedral 91, 418
- inversion 96
- isomorphism 46
- layer 56, 116
- limiting 63, 85, 93, 96, 170
- *m*-dimensional 157
- mirror 96
- motion 123
- noncrystallographic 415
- nonsymmorphous 110, 136, 414, 418
- one-dimensional 57
- orbit 72
- permutations 77, 79
- - multiplication 77
- plane twice-periodic 108
- point 56, 82, 95, 182, 244
- - antisymmetry 159
- - color 168
- - crystallographic 82, 85, 91, 95, 101
- - families 86-93
- - icosahedral 416, 419
- product
- - external direct 49
- - semidirect 49
- quasicrystallographic 415
- quasiperiodic 415
- ribbon 116
- representation 53, 101, 106
- - character 102
- rod 56
- rotation 96
- second-kind 56, 81, 96
- Shubnikov 171
- similarity 175
- single-colored 171
- space 15, 56, 129, 131
- - antisymmetry 171
- - color 171
- - multiple antisymmetry 171
- symmetry 10, 30
- - operations 44
- symmorphous 110, 131, 414, 418
- three-dimensional 61, 120
- two-dimensional 58
- x-ray 249
Groupoids 177

Habit of crystal 11, 97, 180, 182, 203
Harker sections 315
Haüy law 11, 180
"Hedgehogs" construction 147
Hemihedry 192
Holohedry 192
Homogeneity 5, 10, 53
- discrete 53
- macroscopic 5, 6, 22
- microscopic 21, 53
- sphere 54, 147

Imaging
- in electron microscopy 362, 369
- atomic 368
- bright-field 367
- dark-field 367
- lattice-plane 368
- processing 376
Independent (fundamental) region 54, 74
Indexing of Debye photographs 303
Indicatrice suffaces 8
Indices
- of axes 182
- of edges 183
- of face 183, 191, 202
- hexagonal 192
- lattice 212
- of line, row 206
- Miller 181, 207
- of plane 207
- of point 206
- Weiss 181, 206
Inhomogeneity 53
Integrated reflection coefficient 254
Intensity
- diffraction peak 305, 346
- distribution 251
- integrated 253, 255, 294
- law of conservation 243
- reflection 242, 298, 346, 350
- - polycrystal 305
- statistical distribution 251
Interatomic distances 220, 221, 271
Interatomic distances
- function 251, 272, 314, 318
- - cylindrical symmetry 275
- - spherical symmetry 275

Interferometry of x-ray 269
Interplanar spacing 208
Interplanar distances 209, 220, 221
Inversion 37
Isogon 72, 146
Isomorphism of groups 46
Isotropic substance 7

Kikuchi lines and bands 349, 354
Kinematic scattering
- electrons 346
- x-rays 252

Lattice
- atomic 120, 211, 219, 248
- base-centered 124
- body-centered 125
- Bravais 123, 128
- cubic 221
- direct 211, 219, 248
- face-centered 125
- hexagonal 221
- monoclinic 220
- net 206
- one-dimensional 234
- orthorhombic 221
- primitive 125
- reciprocal 211, 219, 234, 248
- - vector 211
- rhombohedral 221
- row 206
- side-centered 124
- space 15, 121, 211
- tetragonal 221
- three-dimensional 15, 120, 235
- triclinic 220
- two-dimensional 124
Laue
- case of diffraction 257, 432
- classes of symmetry 245, 287, 340
- conditions 234
- photographs 286
Laue-Ewald theory 258
Limitation sphere 240
Liquid 24, 274
Liquid crystal 26, 274
Lorentz factor 255, 294

Magnetic scattering
- neutrons 230
- x-rays 283
Magnetic structure 175, 397
Maximum enthropy method 326
Mesomorphic phases 26
Methods of determination of atomic
- structure
- direct 321
- - multisolution 325
- - symbolic addition 324
- heavy atom 319
- isomorphous replacement 319
- nonlocal search 327
- Patterson function 314
- trial and error 313
Methods of recording of x-ray patterns
- Arndt-Wonacott 289
- Buerger's precession 293
- Debye-Scherrer 300
- De Jong-Bouman 292
- diffractometer 295, 304
- Laue 285
- moving crystal and film 291
- oscillation 287
- rotation 287
- Weissenberg's equi-inclination 291
Metric chracteristics 219-221
Microdensitometer 295
Microhomogeneity 21, 53
Microscopy
- atomic force 357, 389
- electron 357
- - field-emission scanning 357
- scanning tunneling (STM) 357, 385
Miller indices 181, 183, 207
Modulated structure
- commensurate 23
- incommensurate 23, 427
Moiré method 269
Monochromator, crystal 281, 431
Mosaic crystal 253, 258, 340
Moseley's law 280
Mössbauer diffraction 401
Motions
- improper 34
- proper 34

Neutron diffractometer 393
Neutron scattering
- magnetic 230, 394
- nuclear 230, 394
- time-of-flight method 449
Nuclear density 395

Operation of symmetry 10
- first kind 34, 110
- multiplication 45
- second kind 36, 110
- unit 44
Order
- long-range 24
- short-range 24, 25
Orientation of crystal 297

Parallelepiped
- repeat 63
- unit (primitive) 13, 124
- primitive 121, 124
- - empty 121
Parallelogon 77
Parallelohedron 151, 152
- sorts by Delone 153
Parameters of unit cell 181, 216
Patterson function 272, 314, 318, 421
Pendellössung fringes 265
Phase analysis 305
Phase diagram 320
Phase object 363
Phase problem 308, 312
- determinant of structure amplitudes 322
- solving 327
- - direct methods 321
- - - Cauchy inequality 322
- - - Karle and Hauptman 323
- - - Sayre 323
- - - tangent formula 324
- - - Zachariasen-Cochran 323
Phases
- of reflections 312
- - determination 312, 324
- - structure amplitudes 312, 347
- - relationships 321
Plane of symmetry
- glide-reflection 68, 246
- - diamond 69
- mirror 66
Planigon 76
Planion 76
Polarity 71
Polarization factor 255
- coefficient 283
Pole figure 306
Polycrystalline solid 1, 299
Polygon 148
Polyhedron 148
- color 168
- crystalline 182
- icosahedral 420
Polymer 25, 274
Potential of crystal 336
Powder pattern 446
Principle of maximum and minimum symmetry 100
Programs for crystal structure analysis 335
Projection
- radial 113
- spherical 83
- stereographic 83
- of structure, two-dimensional 312

Quasicrystal 23, 405
- approximant 421
- icosahedral 416
- one-dimensional 409
- Penrose tiling 24, 406, 415
- reciprocal lattice 418
- six-dimensional 422
- structure analysis 419
- three-dimensional 415, 426
- two-dimensional 412, 426
- unit cell 419
Quasiperiodic function 408
- Fourier transform 410

Radial distribution function 25, 274, 453
- cylindrical symmetry 275
- spherical symmetry 275
Radius of gyration 277
Rational parameters law 11, 180
Reciprocal lattice 211, 219, 237, 248, 442
- vector 155, 210, 236, 248, 339
Reciprocal space 155, 227, 236, 271
Reconstruction, three-dimensional 378
Reduction algorithm 216
Refinement of crystal structure 331
- Rietveld technique 305, 448
Reflection, integrated coefficient 254
Reflection sphere 239, 285, 339
Region (unit) asymmetric 54, 80
Regular point system (RPS) 72, 145, 246
Replica method 372
Representation of group 51, 53
- character, 52, 102, 104
- irreducible 52, 155, 166

- point group 101, 104
- reducible 52
- unitary 52, 103, 105
- vector 101
Resolution
- electron microscopy 362, 368
- structure determination 310
R-factor (reliability factor) 313, 327
Rotation function 319
Rotation
- inversion 37
- mirror 36, 38
- screw 35
Row of points 234
(r,R)-condition 54, 147

Scanning tunneling microscopy (STM) - 385
- image
- - spectroscopic 388
- - surface 390
- microscope 387
Scattering *see also* Diffraction
- anomalous 229, 245, 330
- of electrons 364
- by non-crystalline substances 271
- small-angle 276
- by spherically symmetric systems 272
- thermal diffusion 244
Scattering amplitude 224, 242
- neutrons
- - magnetic 394
- - nuclear 394
- x-rays 225, 271
Schönflies' theorem 55, 59, 62
Schrödinger's equation 335, 349 - 366
Screw displacement 111
Secondary waves 224, 234
Setting of crystal 196-197
Shadow effect 404
Shape of crystalline polyhedron
- ideal (perfect) 182
Shape function 276
Shubnikov (antisymmetric) group 171
Simple form of crystal 183, 188
- closed 183
- combinations 192
- open 183
Single crystal 3, 182
Singular direction 110, 116
Singular (special) point 39
Small-angle scattering 276
Sorts Delone (of lattice) 153, 218
Sphere
- discreteness 54, 147
- Ewald 240, 259, 339, 349
- homogeneity 54, 147
- limitation 240
- reflection 239, 285, 339
Spin density 400
Staining method 375
Statistical distribution (of intensity) 251
Statistical-thermodynamical approach - 325
Stenon's law 11, 180
Stereohedron 148
Stereon 54, 74, 79, 148, 153
Structure amplitude (structural factor) - 241, 246, 275, 330, 336, 345, 394
- normalized 321
- unitary 321
Structure refinement 331
Subgroup 48, 144, 168
Sublattice 146
Symmetric object 29
Symmetry 9, 28
- antisymmetry 158, 164
- axis 66
- center 66
- color 157, 171
- cylindrical 275
- of diffraction pattern 244
- elements 64-70
- generalized 156, 170
- helical 113
- icosahedral 24, 94, 405
- layer 56, 116
- local 75
- magnetic 399
- operation 10, 20, 29, 64
- - unit 44
- partial 177
- plane 68
- point 39, 56, 182, 244
- rod 56
- of similarity 175
- space 30, 56, 120, 157
- spherical 275
- statistical 177
- transformation 29, 32
- - first kind 41, 110

- - second kind 41, 110
- translational 14, 21, 177
Synchrotron radiation 429, 432
Syngony 97, 122, 134

Temperature factor 231
- anisotropic 232, 331
- isotropic 331
Tetartohedry 192
Texture 305, 338
- oblique 341
Thermal vibrations 232
- anisotropic 232
- ellipsoid 233
Transformation
- countervariant 213
- covariant 213
- orthogonal 40
- symmetry 29, 31
- - first kind 34, 110
- - isometric 32, 40
- - second kind 34, 110
Translation 13, 21, 130, 206

Unit cell 13, 63, 121, 212, 297, 342
- edges 181
- parameters 217
- periods 219
- primitive 121
- reciprocal 214
Unit face 196-197, 203
Unitary parameters 181

Vector
- of atomic lattice 123, 209
- basic 121
- of reciprocal lattice 209, 259

Wave function 226, 335, 363, 367
Wave, secondary 224, 234
Waves, interference 222, 252
Weiss indices 181, 183, 206
Weiss' zone law 194
Wigner-Seitz cell 152
Wulff's net 202

X-ray
- detector 433
- diffractometer 296, 436
- EXAFS 451
- groups (of symmetry) 249
- interferometry 269
- moiré 269
- phase analysis 305
- photograph
- - Debye 300
- - Laue 285
- - oscillation 289
- - precession 241
- - rotation 289
- source 427
- topography 267
- tube 278
X-rays 222, 228, 278
- focusing
- - Bragg-Brentano 302
- - Preston 301
- - Zeeman-Bolin 301
- polarization 283

Zone 193
- axis 193
- development 203
- law 194, 208
Zone of reflections 312, 339